

# INDIAN JOURNAL OF PHYSICS

VOL. 28

AND

PROCEEDINGS

OF THE

*Indian Association for the Cultivation of Science, Vol. 37*

*(Published in Collaboration with the Indian Physical Society)*

( With Thirty Plates )

Printed by Sibendranath Kanjilal, Superintendent Calcutta University Press,  
48, Hazra Road, Ballygunge, Calcutta and published by the Registrar.  
Indian Association for the Cultivation of Science.

Jadavpur, Calcutta 32

1954

Price Rs. 20 cr & 2

## BOARD OF EDITORS

R. K. ASUNDI	S. K. MITRA
K. BANERJEE	P. RAY
D. M. BOSE	K. R. RAO
S. N. BOSE	M. N. SAHA
K. R. DIXIT	B. N. SRIVASTAVA

S. C. SIKKAR (*Secretary*)

## EDITORIAL COLLABORATORS

DR. D. BASU, PH.D.

DR. N. N. DASGUPTA, M.Sc., PH.D.

PROF. G. P. DUBE, M.Sc.

PROF. P. S. GILL, PH.D.

DR. S. R. KHASTGIR, D.Sc., F.N.I.,  
F.R.S.F

PROF. P. K. KICHLU, D.Sc. F.N.I.

PROF. D. S. KOTHARI, D.Sc., F.N.I.

DR. K. S. KRISHNAN, D.Sc., F.R.S.

PROF. P. C. MAHANTI, D.Sc., F.N.I.

PROF. B. D. NAG CHOWDHURY, PH.D.

PROF. S. R. PALIT, D.Sc., F.N.I.

DR. S. PARTHASARATHY, D.Sc., F.N.I.

DR. H. RAKSHIT, D.Sc., F.N.I.

DR. R. GOPALAMURTY RAO.

DR. VIKRAM A. SARABHAI, M.A., PH.D.

PROF. N. R. SEN, D.Sc., F.N.I.

## ASSISTANT EDITOR

MR. A. N. BANERJEE, M.Sc.

## NOTICE TO INTENDING AUTHORS

Manuscripts for publication should be sent to Mr. A. N. Banerjee, Assistant Editor, 2 & 3, Lady Willingdon Road, Jadavpur, Calcutta 32.

The manuscript of each paper should contain in the beginning a short abstract of the paper.

All references to published papers should be given in the text by quoting the surname of the authors followed by the year of publication within braces, *e.g.*, Sen (1912). The actual references should be given in a list at the end of the paper according to the following specimen :

Sen, B. K., 1912, *Ind. J. Phys.*, **16**, 320.

The references should be arranged alphabetically in the list.

All diagrams should be drawn on thick white paper in Indian ink, and letters and numbers in the diagrams should be written neatly in capital type in Indian ink. The size of the diagrams should be at least three times that of the intended size of the actual figure.

## Annual Subscription—

Inland Rs. 20

Foreign £. 2



# INDIAN JOURNAL OF PHYSICS VOL. 28, 1954

## CONTENTS

### No. 1. January

	Page
1. A Demountable All-Metal Hot-Cathode Vacuum Ionisation Gauge—By P. K. Dutt ... ..	1
2. Hardness of Metals and Alloys—By G. P. Chatterjee ... ..	9
3. The Ultraviolet Absorption Spectra of $\alpha$ -Chloronaphthalene and $\alpha$ -Bromonaphthalene in Different States—By A. R. Deb ... ..	21
4. Effect of Steepness of Rise and Fall of the Input Pulse on the Response of Pulse Amplifiers. Part I.—By Bimal Krishna Bhattacharyya ... ..	31
5. Intensity Formulae for Bands involving High Multiplicity Terms. Part III. ${}^6\Pi - {}^6\Sigma$ and ${}^6\Pi - {}^6\Pi$ Transitions—By D. Premaswarup ... ..	48

### No. 2. February

6. Ionization Distribution in the F-Region—By B. Chatterjee ... ..	53
7. A Reactance Tube Controlled Oscillator of unusually Wide Frequency Sweep—By B. M. Banerjee ... ..	67
8. An Instrument for Direct Measurements of Capacitance and Power Factor—By J. C. Bhattacharya ... ..	75
9. Raman Spectra of Ortho and Para Chlorophenol in the Solid State at Low Temperatures—By D. C. Biswas ... ..	85
10. An Instrument for measuring the Decay of Mu Mesons—By H. S. Hans ... ..	93

### No. 3. March

11. Spectroscopic Constants of Molecules. I. On the Ground State Frequencies of Diatoms of the type XX—By K. Majumdar and Y. P. Varshni ... ..	103
12. Ionosphere and Nature of Fading Patterns of received Radio Signals—By R. N. Singh ... ..	109
13. On Born's Approximation and its connection with Covariant Perturbation Theory—By S. N. Biswas ... ..	119
14. An X-ray study of <i>o</i> -Phthalic Acid—By D. M. Chakrabartty ... ..	129
15. A Rigid Curvilinear Polygonal Core in an Infinite Plate under Tension at Infinity and Shear—By B. Karunes ... ..	133
16. Effect of Background Intensity on Resolution—By Mahendra Singh Sodha ... ..	141

	Page
1. The Effect of Chain Transfer on the Distribution of Molecular Weights in High Polymers. Part I. Combination—By Santi R. Palit and Kesab Chandra Majumdar ... ..	1
<b>No. 4. April</b>	
17. Observation of Scatter Echoes on High Power Pulsed Transmissions—By S. N. Mitra and V. C. Iyengar ... ..	147
18. On the Production of Charged Meson Pairs by Neutral Particles in Cosmic Rays—By S. B. Roy and R. Chakravarti ... ..	167
19. On the Validity of Semi-Empirical Atomic Mass-formula in the region of Rare-Earth Nuclides—By G. P. Dube and Lal Saheb Singh ... ..	177
20. A New Electrodynamic Method of measuring Magnetic Fields—By S. K. Dutta Roy ... ..	183
21. On the Time of Relaxation of some Organic Molecules in pure Liquid State—By Dilip Kumar Ghosh ... ..	191
<b>No. 5. May</b>	
22. Pseudoscalar Interaction and Proton-Proton Scattering—By D. Basu ... ..	201
23. On the Raman Spectra of Ethylene Dichloride in solutions of different strengths—By Sukhendu Bikash Banerjee ... ..	205
24. Spectroscopic Constants of Molecules. II. On the Vibration Frequency of Diatoms of the type XX—By K. Majumdar and Y. P. Varshni ... ..	209
25. Force Constants and Thermodynamic Properties of $TiCl_4$ —By D. Tirumalesa and V. Ramakrishna Rao ... ..	216
26. Proton-Proton Scattering at 340 Mev—By C. C. Banerjee ... ..	227
27. On the Kinetic Energy of Fission-Fragments from $U^{235}$ —By G. P. Dube and Lal Saheb Singh ... ..	227
28. Electron Capture by Ions passing through Gases—By N. C. Sil ... ..	252
29. Accurate Determination of the Magnetic Anisotropies of the Hydrated Salts of some Elements of the Iron Group—By Sunilkumar Datta ... ..	239
<b>No. 6. June</b>	
30. Peak Amplitude Recorder for Investigation on Fading—By S. C. Mazumder and S. N. Mitra ... ..	251
31. Calculation of Perturbations in certain Molecular Electronic Terms Part I. — By D. Premaswarup ... ..	256
32. Distortion in Electron Lens—By M. L. De and D. K. Saha ... ..	263
33. Atomic Nitrogen as a Constituent for Region $F_1$ —By A. P. Mitra ... ..	269
34. Multiplet Separation Factors in the Spectrum of Chromium II—By V. Suryanarayana and V. Ramakrishna Rao ... ..	285

	Page
35 On the Raman Spectra of Acetyl Chloride and Chloroacetyl Chloride in the Vapour state—By Monomohan Mazumder ... ..	297

No. 7. July

36. The Raman Spectra of <i>m</i> - and <i>p</i> -Xylene in the Solid State at different low Temperatures—By D. C. Biswas ... ..	303
37. Electrical Conductivity of Single Crystals of Graphite along the Basal Plane and a New and Simple Method of measuring Electrical Conductivities—By Ajit Kumar Dutta and Amalendu Chowdhury ... ..	312
38. Molecular Orbital Theory and the Reactivity of Polyphenyls—By Sadhan Basu ... ..	319
39. Theoretical Calculation of Shifts in Substituted Benzenes—By S. Ramamurty ... ..	325
40. On the Intensity-Distribution in the Wing of the Rayleigh Line due to Liquid Oxygen—By G. S. Kastha ... ..	329
41. The Lead Absorption of Cosmic Rays—By P. S. Gill ... ..	335
42. A Table for the Calculation of Surface Tension from measurements of Sessile Drops—By N. R. Tawde and K. G. Parvatikar ... ..	345

*Proceedings of the Indian Association for the Cultivation of Science*

2. The Effect of Chain Transfer on the Distribution of Molecular Weights in High Polymers. Part II. Termination by Disproportionation—By Kesab Chandra Majumdar and Santi R. Palit ... ..	19
---	----

No. 8. August.

43. Electron Optical Treatment of Current Division in Radio Valves—By S. Deb ... ..	349
44. On the Raman Spectra of Styrene and Polystyrene at $-180^{\circ}\text{C}$ —By N. K. Roy ... ..	365
45. Effect of Steepness of Rise and Fall of the Input Pulse on the Response of Pulse Amplifiers. Part II—By Bimal Krishna Bhattacharyya ... ..	371
46. Relative Cross-section of $(n, p)$ -Reactions in $\text{Al}^{27}$ and $\text{Mg}^{24}$ —By S. K. Nandi and N. K. Saha ... ..	396

No. 9. September

47. Analysis of the Ultraviolet Fluorescence Spectra of $\text{I}_2$ Molecule—By C. V. Narayana Rao and V. Ramakrishna Rao ... ..	403
48. Raman and Fluorescence Spectra of Ortho- and Para Bromotoluene in the Solid State at Low Temperatures—By D. C. Biswas ... ..	423
49. Mean Life of Decay of Muons in the absence of Matter—By N. N. Biswas ... ..	431
50. On Dependence of Resolving Power of Prism, Grating and Reflecting Echelon on Stage of Resolution and Detecting Instrument—By Om Prakash Sharma and Mahendra Singh Sodha ... ..	437

	Page
51. A Study of Air Absorption of some Liquids—By G. L. De and P. C. Mahanti	441
<i>Proceeding of the Indian Association for the Cultivation of Science.</i>	
3. Proceedings of the High Polymer Symposium held in the Association in March 1954	29

### No. 10. October

52. Pulse Slope Modulation—A New Method of Modulating Video Pulses and its possible Application on Line Circuits—By Jayneswar Das ...	449
53. Force Constants for Methyl Cyanide and Methyl Isocyanide—By S. L. N. G. Krishnamachari ...	463
54. Study of Hulbert-Hirschfelder $U(r)$ Function in $C_2$ (Swan) System—By N. R. Tawde and K. Gopalakrishnan ...	469
55. Synthesis of a Network for a prescribed Time-function—By Nirmal Baran Chakrabarty ...	473
56. Absorption of 3.18 cm Microwaves in some Aromatic and Aliphatic Compounds in the Liquid State—By Dilip Kumar Ghosh ...	485

### No. 11. November

57. Interpretation of the Near Ultraviolet Absorption Spectrum of Acetaldehyde Molecule as due to a Single Electronic Transition—By V. Ramakrishna Rao and I. Achyuta Rao ...	491
58. Molecular Orbital Calculation on Phthalocyanine—By Sadhan Basu ...	511
59. On the Resolving Power of Compound Fabry-Perot Etalon—By Madhukar Kashinath Machwe and Mahendra Singh Sodha ...	522
60. Band Spectrum of CrF Molecule—By Mrs. B. Kanaka Durgavathi and V. Ramakrishna Rao ...	525
61. Analysis of the Relaxation Period of a Multivibrator—By D. C. Sarkar and Rais Ahmed ...	533

### No. 12. December

62. On Dependence of Resolving Power of Fabry-Perot Etalon, Lummer-Gehrcke plate and Transmission Echelon on Stage of Resolution—By Shashanka Shekhar Mitra ...	543
63. The Band Spectrum of Tellurium in the Visible region—By N. Durga Prasad and P. Tiruvenganna Rao ...	549
64. Effect of Solar Activity on Ionosphere and Earth's Magnetic Field—By S. N. Mitra and S. C. Mazumdar ...	563

55. Calculation of Perturbations in certain Molecular Electronic Terms. Part II.  
 $^2\Pi - ^4\Sigma$ ,  $^2\Pi - ^4\Pi$ ,  $^4\Sigma - ^4\Pi$  and  $^4\Pi - ^4\Pi$  Perturbations—By D. Premaswarup 581

*Proceedings of the Indian Association for the Cultivation of Science*

4. Studies in Chain-Transfer. Phenylazotriphenyl Methane Catalysed Polymeri-  
 sation of Styrene in Toluene—By R. N. Chadha and G. S. Misra ... 37
5. Studies on Macromolecules. The Spreading Properties of Rubber and its  
 derivatives—By N. H. Sivaramakrishnan and M. R. A. Rao ... 41



# A DEMOUNTABLE ALL METAL HOT-CATHODE VACUUM IONISATION GAUGE\*

BY P. K. DUTT

INSTITUTE OF NUCLEAR PHYSICS, CALCUTTA UNIVERSITY  
92, UPPER CIRCULAR ROAD, CALCUTTA

*(Received for publication, December 7, 1953)*

**ABSTRACT** An all metal demountable hot-cathode vacuum ion-gauge has been constructed whose filament can be changed any number of times without a change in the operational characteristics. The characteristic curves of the gauge have been given. Some points towards the constructional improvements have been discussed which might account for better sensitiveness.

A hot-cathode demountable type sturdy metal ion-gauge has been developed, the filament of which can be changed within a short time any number of times after it is poisoned or burnt out, without a change in the characteristics of the gauge operation. This gauge has been constructed out of the materials readily available in the laboratory store. Though not so sensitive like the modern glass envelope types, it is suitable particularly for a dynamic metal vacuum system. It is well known that the greatest disadvantage for a hot-cathode ion-gauge is the life of the cathode. The cathode is likely to be poisoned, if not destroyed by gases like oxygen and hydro-carbon vapours, etc., (Dushman, 1949) which are very difficult to get rid of in a vacuum system; many vacuum operations necessitate the introduction of air from time to time, each time the ion-gauge has to be re-exhausted and the gases absorbed by the electrodes while in presence of air have to be removed, which is usually done by increasing the electron emission from the cathode more than the normal rating for a little time. This also causes shortening of the cathode life.

The average life of each filament used in this gauge is of the order of that of the tungsten filament of the commercial type ion-gauges with glass envelopes, e. g. R. C. A. 1950. So, economically it has one advantage over the commercial type, whose filament, if once loses its emissive properties has to be rejected permanently.

Attempts have been made to incorporate the desirable features found in the previous designs (Buckley, 1916; Dushman and Found, 1921; Morse & Bowie, 1940), e. g. reliability, high insulation for the ion-collector, long filament life etc.

The gauge envelope has been represented pictorially in figure 1 and figure 2 shows the photograph to the filament and the grid-structure.

\* Communicated by Prof. B. D. Nag.

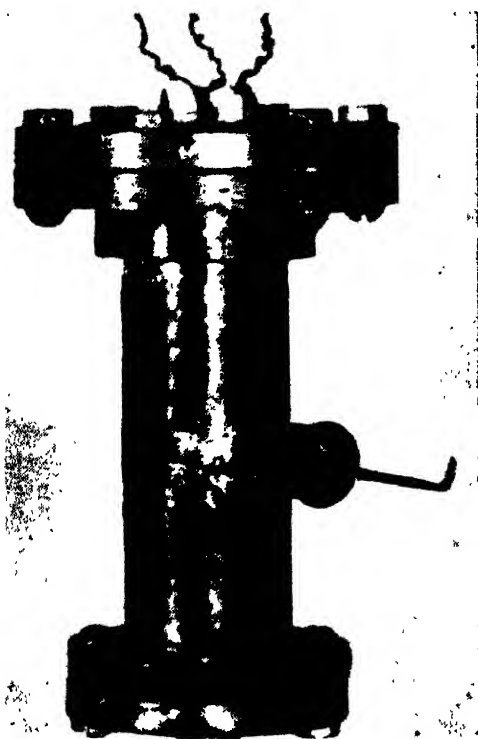


FIG. 1

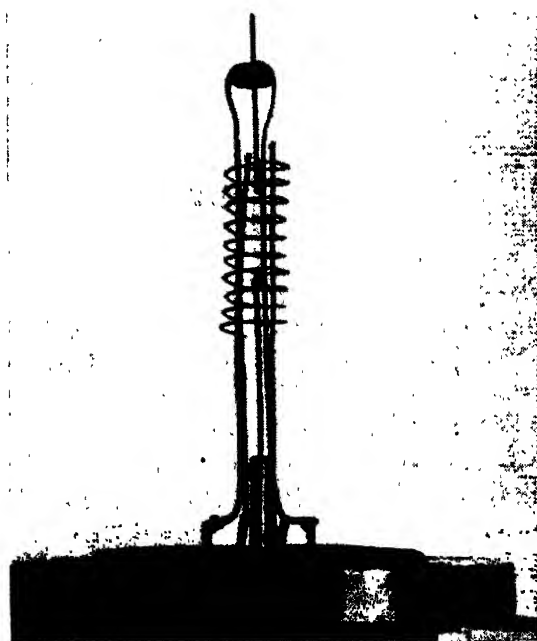


FIG. 2



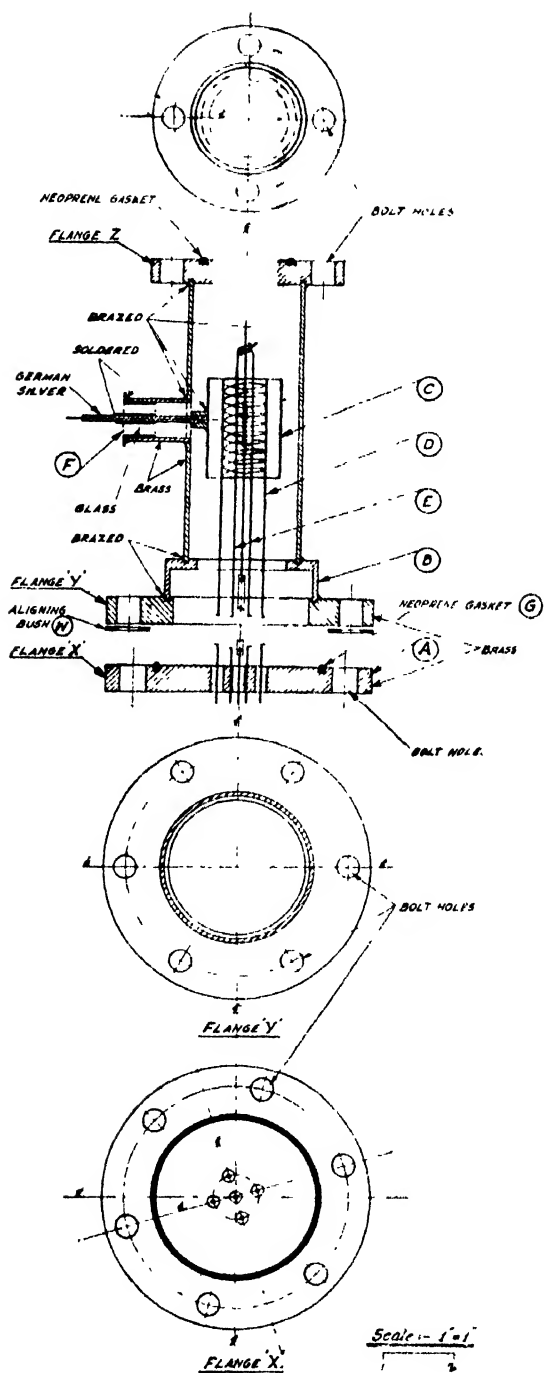


FIG. 3

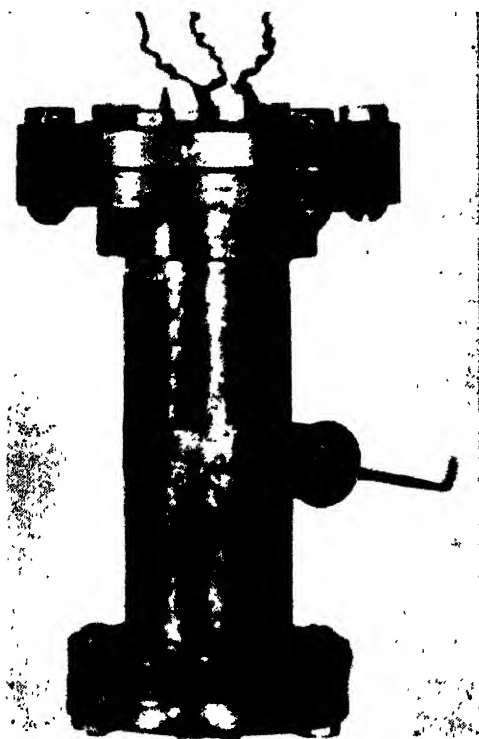


FIG. 1

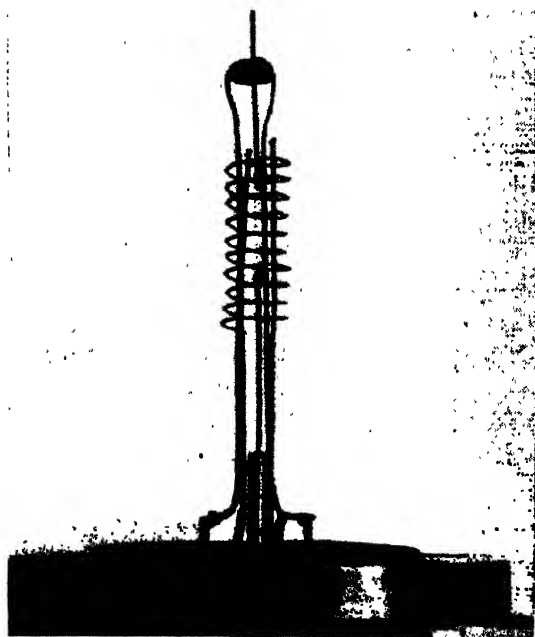


FIG. 2

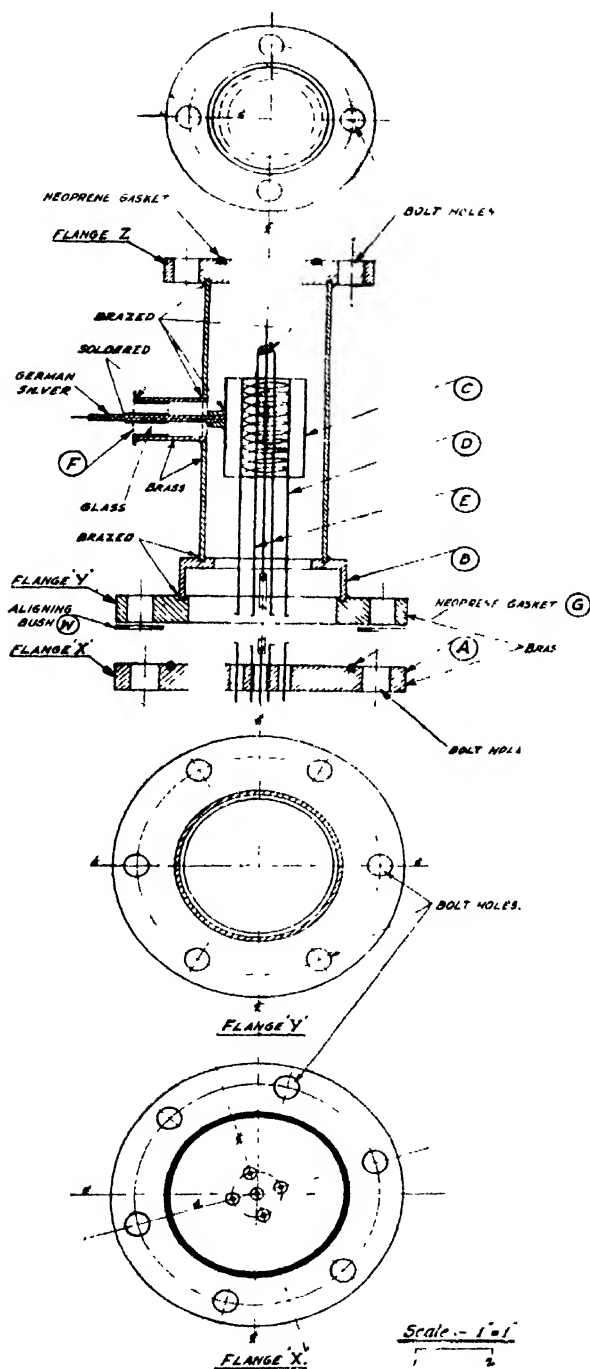


FIG. 3

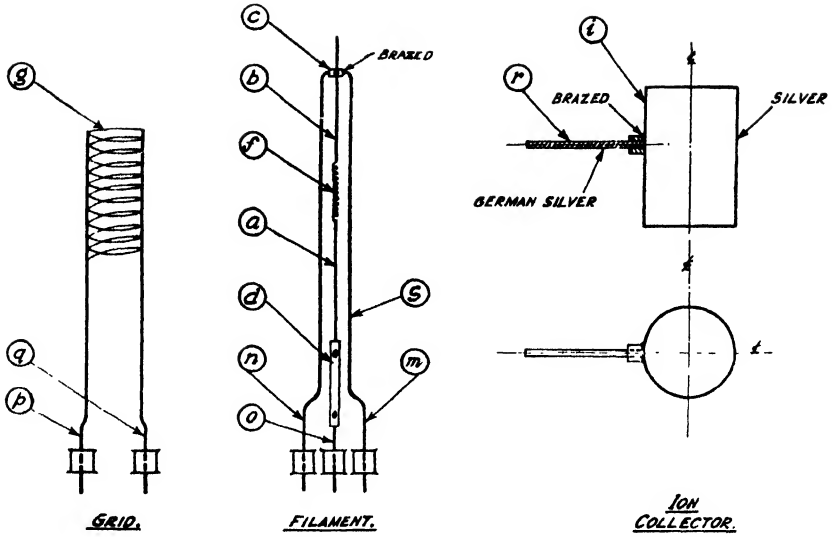


FIG. 4

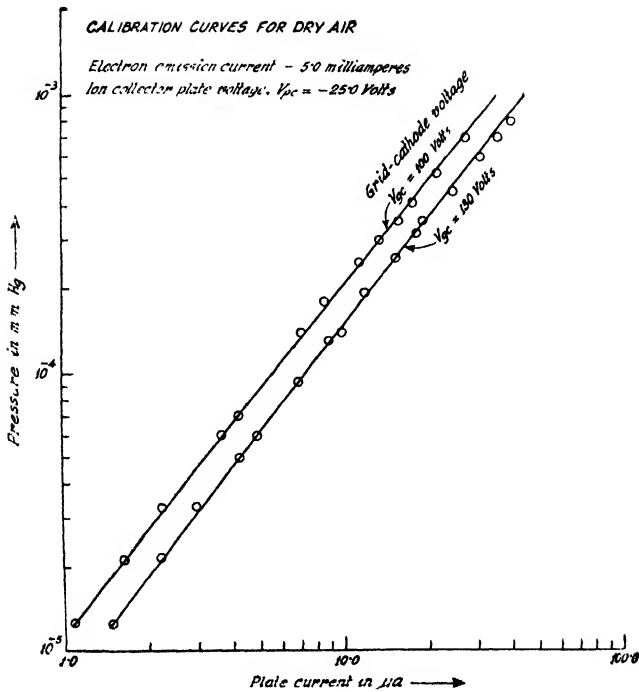


FIG. 5

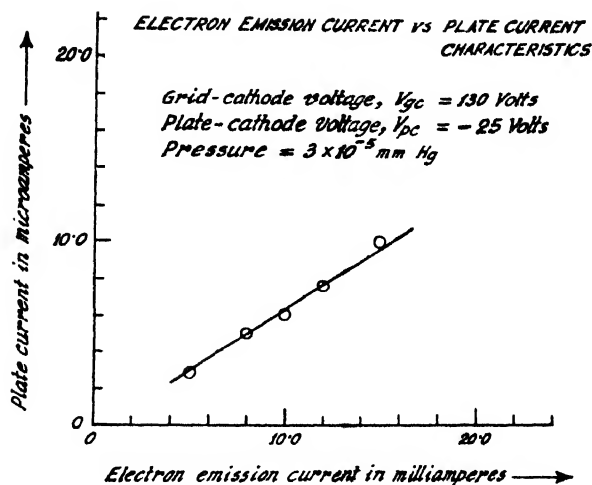


FIG. 6

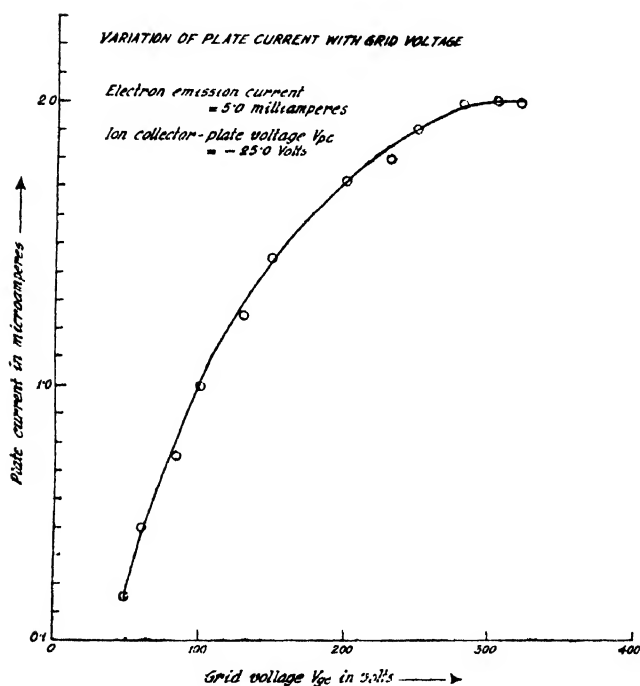


FIG. 7

The construction of the gauge can be understood from figure 3. The gauge body is made of brass. The portions *A* and *B* which are originally attached to each other when in operation with the Neoprene gasket *G* and nut bolts through the flanges *X* and *Y* can be separated whenever it is required to change the filament. Alignment between them during each assembly, is done by an 'index' mark and the aligning

bush *W*. The gauge is connected to the vacuum system with the flange *Z*. The structures of the plate *C*, grid *D* and the filament *E* have been shown separately in figure 4.

The filament *f* is a 6 mil. tungsten wire, 2 inch in length, coiled on a 50 mil. mandrel, the coil length being about  $\frac{3}{4}$ th inch. The two ends of the filament are spot-welded (via nickel medium) with two short tungsten wires *a*, *b* of 40 mil. diameter which are inserted into two small brass-holders *c*, *d* and held by set screws. The upper holder *c* is brazed to the 40 mil. tungsten wire support *s* of the filament structure and the lower one *d* is clamped to the terminal of the Kovar-glass seal *o*, soldered to the metal flange *X*. For a change of the filament the unit *a b f* can be taken out as a whole by loosening the screws on *c d* and a new unit can be put in. For normal operation, as shown in the calibration curve (figure 5), the filament requires about 3.0 amps. of current at 6.5 volts.

The grid *g* is a 10 turn spiral of 15 mil. molybdenum wire (wound on a  $\frac{1}{2}$  inch. cylindrical mandrel). Each turn of the spiral being spot-welded to the two supporting 40 mil. nickel wires. The nickel wires were again spot-welded to the Kovar-glass seal terminals *p* and *q* on the metal flange *X*. The coil length of the grid spiral was  $1\frac{3}{8}$  inch and the relative distance between each turn of the spiral was  $\frac{1}{8}$  inch.

The ion collector *i*, was a hollow silver cylinder 6 mil. thick,  $1\frac{1}{2}$  inch. in length, its inside diameter being 1 inch. It was supported by a German silver wire 60 mil. thick lead in through the Kovar-glass seal *F*, as shown in figure 3, soldered to the gauge metal wall.

In the present design outgassing of the electrodes was difficult, and required longer time than that required for the commercial types of gauges, e.g., RCA 1950, complete outgassing being hardly possible. The only means of degassing the plate and grid structures in this present gauge is by electron bombardment. Moreover, the inner wall of the metal gauge-body was a constant source of gassing. So another metal demountable type of gauge with a glass envelope round the inner wall of the gauge body to minimize the metal surface exposed to the operation as far as possible, has been designed. It has a thin ion collecting electrode made of nickel, and the grid structure is helical; provision has been made to heat the grid to sufficient temperature for better outgassing by passing current through it.

With "External Control" type circuit arrangement the observed characteristic curves have been given in figures 5, 6, and 7.

For comparison, the characteristics of a commercial type ion-gauge with glass envelope, RCA 1950 are given along with it, in figure 8, taken from the R C A Tube Manual—9205—6818.

Kelly (1950) has described an all metal ion-gauge, on which he has used water coils for cooling the gauge body. In this present gauge no such cooling device has been used, as it was thought that it would make it complicated and inconvenient to use. The gauge, though worked at a

temperature 2 to 3°C higher than the room temperature due to the heat dissipated from the filament and the other electrodes, gave consistent readings

## CALIBRATION CURVES FOR THE GAUGE RCA. 1950.

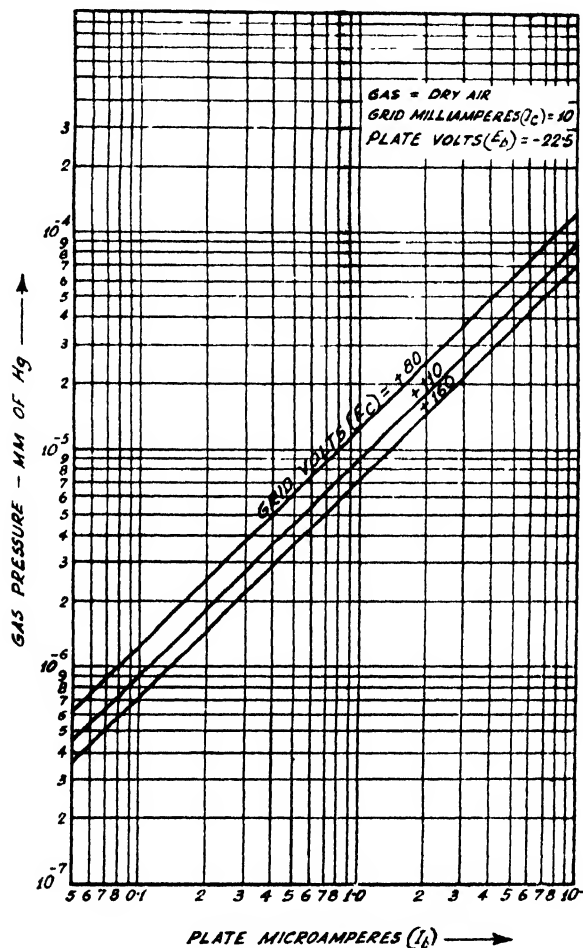


FIG. 8

when compared and calibrated against the gauge RCA 1950, on different occasions under different conditions for a pressure range of  $1 \times 10^{-3}$  mm. to  $8 \times 10^{-6}$  mm. Hg.

It can conveniently be used for hunting leaks without any great care for the safety of the filament, as it can be replaced readily and easily without dismantling the gauge envelope. The gauge has been tested on the vacuum system of the 38 inch cyclotron of the Institute of Nuclear Physics, Calcutta University. It has the added advantage that it has practically no r.f. pick up from the cyclotron oscillator without any extra shielding arrangement.

## ACKNOWLEDGMENTS

The author is indebted to Prof. M. N. Saha, F. R. S., Director of the Institute of Nuclear Physics, Calcutta University for his kind interest and encouragement in the work and wishes to thank Prof. B. D. Nag for helpful suggestions and guidance.

## REFERENCES

- Buckley, O. E. 1916, *Proc. Nat. Acad. Sci. U. S.* **2**, 683.  
Dushman, S. 1949, 'Scientific foundation of Vacuum Technique', John Wiley & Sons, Inc, New York, p p 344  
Dushman, S. and Found C. G., 1931, *Phys. Rev.*, **17**, 7.  
Kelly, F. M. 1950, *Rev. Sci. Instr.*, **21**, 675.  
Morse, R. S. and Bowie R. M. 1940, *Rev. Sci. Instr.*, **11**, 91.



# HARDNESS OF METALS AND ALLOYS

By G. P. CHATTERJEE

BENGAL ENGINEERING COLLEGE, HOWRAH

(Received for publication, December 11, 1955)

**ABSTRACT.** While tensile strength and other mechanical or physical properties of metals and alloys can be well defined and expressed in terms of the fundamental units of mass, length and time, it is difficult to define hardness and express it in terms of those units. An attempt has been made in this paper to define hardness  $H$  as the work done per unit volume of indentation in a static ball indentation test. On this basis and on the basis of Meyer's Law,  $L = ad^n$ , where  $L$  is the load,  $d$  is the diameter of indentation and  $a$  and  $n$  are constants, it has been found that

$$H = \frac{p c \beta n}{[2 - \cos \theta (\sin^2 \theta + 2)]}$$

where  $p$  and  $\beta$  are constants and  $\theta$  is the angle of indentation. For a given value of  $\theta$  it has been shown that  $H$  may be expressed by the simple equation

$$H = a/f_n$$

where the factor  $f_n$  is a known function of  $n$ . Thus the determination of  $H$  merely involves the determination of the values of  $a$  and  $n$ . The values of  $H$  expressed as Kgmm<sup>2</sup>/mm<sup>3</sup> compares well with those of the Brinell hardness number  $H_B$  for different metals and alloys under different treatments. Considering the completely different approach to the concept of hardness  $H$  and the different method adopted in measuring  $H$ , the agreement between  $H$  and  $H_B$  values appears to be quite satisfactory. The advantages and limitations of the method have also been indicated.

## 1. INTRODUCTION

Pure metals are comparatively soft. But when alloyed or given different treatments—thermal or mechanical—they become harder. Hardness, like tensile strength, is a structure-sensitive property. But while tensile strength and other mechanical or physical properties can be well defined and expressed in terms of the fundamental units of mass, length and time, it is rather difficult to define hardness or to express it in terms of these units. As early as 1925, Tuckermann (1925) remarked in this connection that "hardness in common parlance represents a hazily conceived conglomeration or aggregate of properties" like "resistance to abrasion, scratching or cutting, resistance to plastic deformation, high modulus of elasticity, high yield point, high strength" and so on. Various methods, both static and dynamic, have been proposed to measure hardness. But in all the proposed methods the distribution of stress actually applied is not of a simple nature (Nadai, 1937). For example, in the static indentation test, as in the Brinell or Vicker's hardness test, the hardness  $N$  is defined as  $N = L/A$ , where  $L$  is

In equations (8a) and (8b), the indentation angle  $\theta$  and the so-called "hardenability index"  $n$  are both variable. And  $n$  in general is not an integer.

Suppose 
$$\frac{1}{2} \int_0^\theta \sin^{n+1} \theta d\theta = F(n) \quad \dots (9)$$

where  $F(n)$  is some function of  $n$  for a given value of  $\theta$ .

If  $F(\theta)$  and  $G(\theta)$  be two independent functions of  $\theta$ , then

$$\int_0^\theta F(\theta)G(\theta)d\theta \bigg/ \int_0^\theta F(\theta)d\theta = f(\theta) \quad \dots (10)$$

where  $f(\theta)$  is another function of  $\theta$  defined by equation (10).

Substituting  $\sin^{n+1} \theta$  for  $F(\theta)$  and  $\log_e \sin \theta$  for  $G(\theta)$ , one gets

$$\frac{1}{2} \int_0^\theta \sin^{n+1} \theta \log_e \sin \theta d\theta = f(\theta) \frac{1}{2} \int_0^\theta \sin^{n+1} \theta d\theta \quad \dots (11)$$

From equation (9) it is obvious that

$$\frac{dF(n)}{dn} = \frac{1}{2} \int_0^\theta \sin^{n+1} \theta \log_e \sin \theta d\theta \quad \dots (12)$$

Combining equations (9), (11) and (12) one gets

$$\frac{dF(n)}{dn} = f(\theta) F(n) \quad \dots (13a)$$

Let 
$$\beta = f(\theta) \quad \dots (13b)$$

Then, 
$$\frac{1}{F(n)} \cdot \frac{dF(n)}{dn} = \beta \quad \dots (13c)$$

and, 
$$F(n) = \alpha e^{\beta n} \quad \dots (14)$$

It may be noted from equation (13b) that  $\beta$  is a function of  $\theta$  but is independent of  $n$ . Hence, for a given value of  $\theta$ ,  $\beta$  may be taken as constant independent of the nature of the material.

From equation (14) it is obvious that

$$\log_e F(n) = \beta n + \log_e \alpha \quad \dots (15)$$

$\log_e F(n)$  is thus a linear function of  $n$ . How far this is true will be evident from figure 2, where  $\log_e F(n)$  has been plotted as function of  $n$  for different values of  $\theta$ . It is easy to find out the values of  $\alpha$  and  $\beta$  from the intercepts and slopes of these lines. For example, for  $\theta = 30^\circ$ , it has been found that

$$\alpha = 0.0525$$

$$\beta = 0.9076$$

Combining equations (8b), (9) and (14), one gets

$$W = A 2^3 R^3 \alpha e^{\beta n} \quad \dots (16)$$

From equations (3), (7a) and (7b) the volume  $V$  of the indentation may be expressed as

$$V = \frac{\pi R^3}{3} [2 - \cos \theta (\sin^2 \theta + 2)] \quad \dots (17)$$

Combining equations (16) and (17), hardness  $H$ , defined as work done per unit volume of indentation, may be expressed as

$$H = \frac{W}{V} = \frac{A 24 \pi e^{\beta n}}{\pi [2 - \cos \theta (\sin^2 \theta + 2)]} \quad \dots (18a)$$

$$= \frac{p e^{\beta n}}{[2 - \cos \theta (\sin^2 \theta + 2)]} \quad \dots (18b)$$

where  $p$  stands for  $(A 24 \alpha / \pi)$ .

It has been indicated before that for  $\theta = 30^\circ$ ,  $\alpha = 0.0525$  and  $\beta = -0.9076$ . Substituting these values in equation (18a) one gets

$$H = 17.79 e^{-0.9076n} \quad \dots (19)$$

If the diameter  $D$  of the ball be 10 mm, one gets from equations (6b) and (19)

$$H = a(10^{-2} \times 7.79 e^{-0.9076n}) \text{ mm}^{n-2} \quad \dots (20a)$$

$$= a f_n \text{ mm}^{n-2} \quad \dots (20b)$$

where  $f_n = 10^{n-2} \times 7.79 e^{-0.9076n} \quad \dots (21)$

$f_n$  as function of  $n$  is plotted in figure 3.

#### 4. THE HARDNESS MEASUREMENTS

Since  $f_n$  is a known function of  $n$ , expressed by equation (21) it will be evident from equation (20b) that the determination of the values of  $H$

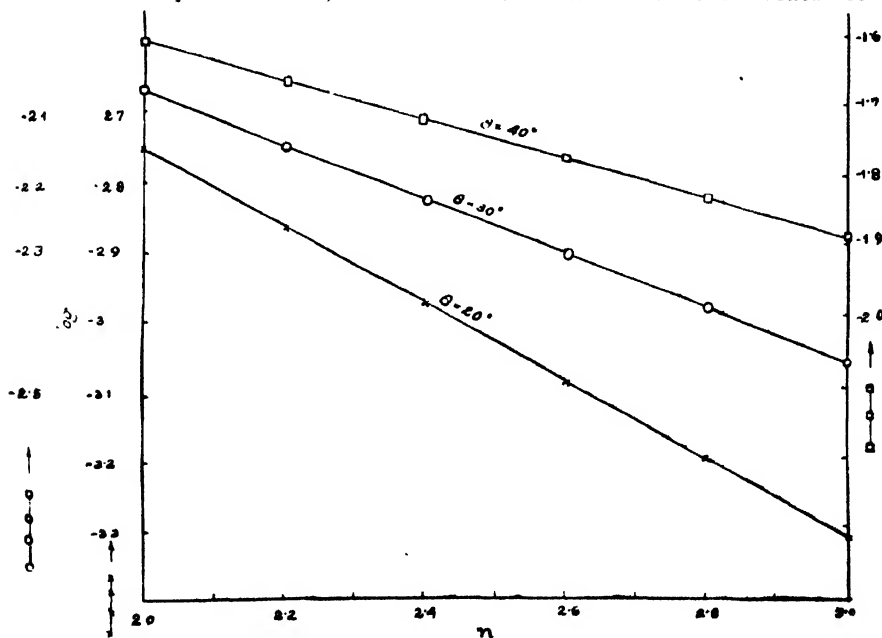


FIG. 2

Log  $F_n$  as function of  $n$  for different values of  $\theta$

involves merely the determination of the values of  $a$  and  $n$ . From equation (6a) it may be shown that

$$n = \log \frac{L_1}{L_2} / \log \frac{d_1}{d_2} \quad (22)$$

Thus the measurement of the indentation diameters  $d_1$  and  $d_2$  corresponding to loads  $L_1$  and  $L_2$  gives the value of  $n$  from equation (22). Once the value of  $n$  is known, the value of  $a$  may be obtained from equation (6a) and that of  $f_n$  from equation (21) or more easily from figure 3. The value of  $H$  may then be easily computed from equation (20b). The values of  $a$  and  $n$  were determined for different metals and alloys taking note of the range of validity of Meyer's law as discussed by Meyer (1908) and Tabor (1951) and briefly indicated in Section 6 of this paper. The time of loading was 30 seconds in all cases. The Brinell hardness  $H_B$  values were also determined for all the specimens with the usual precautions.

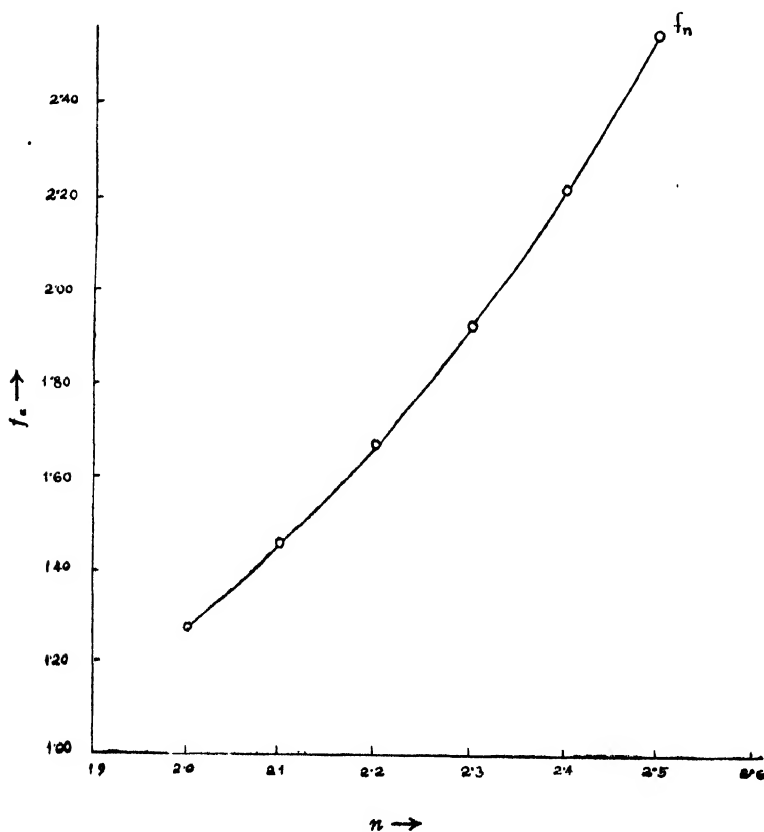


FIG. 3

Graph showing  $f_n$  as function of Meyer index  $n$

In the measurement of indentation diameters it is essential that the load comes in equilibrium with the specimen. This usually occurs in about 10 to 20 seconds. Although for diamond indentors the variation of hardness

beyond the time of loading of 10 seconds is very small (Lea, 1936), it may not be so for other indentors.

As a hard steel ball of Brinell hardness number 1000 was used in this investigation, it was necessary to check the effect of increased time of loading on the values of  $H$ . It was found that on increasing the time of loading from 30 to 100 seconds, the values of  $H$  decreased by about 6 per cent. for softer materials (like bismuth) and about 4 per cent. for harder ones (like cobalt). These corrections have been incorporated in the values

TABLE I  
Values of  $n$ ,  $a$ ,  $H$  and  $H_B$  for some common metals

Metal	$n$	$a$	$H$ Kgm-mm/mm <sup>2</sup>	$H_B$
Lead	2.09	2.60	3.5	3.5
Tin	2.20	2.51	4.3	4.0
Bismuth	1.96	6.8	7.9	7.8
Cadmium	2.02	16.0	19.2	19.3
Aluminium	2.27	12.6	21.6	21.4
Magnesium	2.18	21.9	33.5	33.9
Copper	2.40	17.0	34.4	36.2
Zinc	2.15	27.8	37.0	41.7
Antimony	2.04	34.7	43.3	44.9
Nickel	2.38	34.9	69.9	66.4
Iron	2.30	47.6	85.7	28.0
Cobalt	2.33	70.3	134.0	180.0

TABLE II  
Values of  $n$ ,  $a$ ,  $H$  and  $H_B$  for normalised carbon steels with different carbon contents

%C	$n$	$a$	$H$ Kgm-mm/mm <sup>2</sup>	$H_B$
0.12	2.16	89	122.2	120.0
0.26	2.18	98	150.9	147.2
0.41	2.19	112	174.7	169.3
0.49	2.20	126	199.1	195.8
0.68	2.25	140	235.9	229.6
0.81	2.27	149	256.0	249.0
1.01	2.30	154	278.3	270.1

of  $H$  in Tables I and II. On increasing the time of loading from 100 to 200 seconds, further variations in hardness values were negligibly small except for very soft metals like lead undergoing appreciable creep at ordinary temperatures (Norbury, 1923). In such a case a smaller load for a longer time is preferable to create appreciable indentation diameters and also to minimise the effects of creep.

The load in this investigation varied from 300 gm. for soft metals like lead to 3000 kgm for comparatively harder materials like steel (Tabor, 1951).

## 5. EXPERIMENTAL RESULTS AND DISCUSSIONS

The values of  $a$ ,  $n$ ,  $H$  and  $H_B$  for some common metals are shown in Table I and the values of  $H$  and  $H_B$  are plotted in figure 4. Considering the entirely different approach to the concept of hardness, *viz.*, the work done per unit volume of indentation and also the different method of measuring  $H$ , it is indeed surprising that values of  $H$  and  $H_B$  for many of the common pure metals are nearly of the same magnitude.

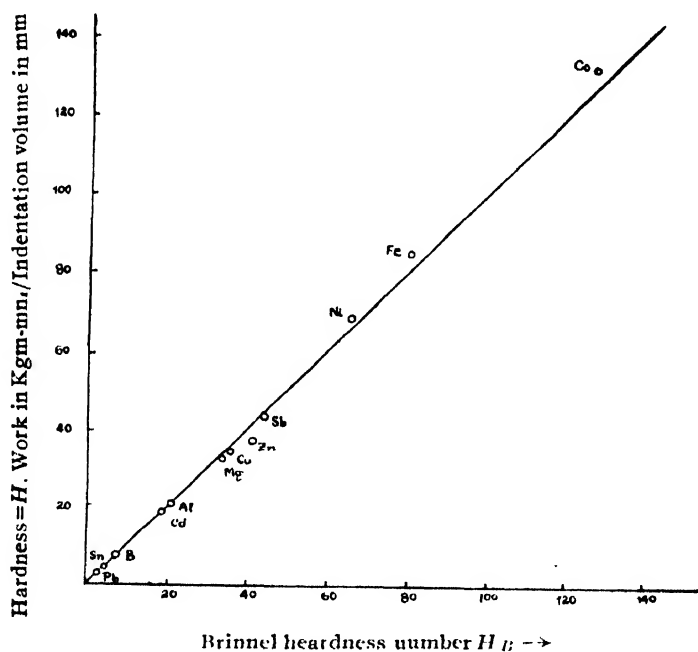


FIG. 4

Graph showing the relation between  $H$  and  $H_B$  values

It is known that cold working and in some cases quenching increase hardness but do not very much affect compressibility. On the other hand alloying increases hardness and also decreases compressibility. In the method of measurement of two indentation diameters  $d_1$  and  $d_2$  under two different loads  $L_1$  and  $L_2$ , the specimen is subjected to different maximum compressive stresses. It is necessary, therefore, to compare the  $H$  and  $H_B$

values of metals and alloys under different treatments—thermal or mechanical—and also as a function of increasing alloying elements. For this purpose copper and aluminium were given different degrees of cold reduction and at each stage, both  $H$  and  $H_B$  values were measured. The results are shown in figure 5. In figure 6, the values of  $H$  and  $H_B$  are plotted from the data in Table II as function of % carbon of several normalised specimens of steel. In both cases the values of  $H$  are nearly of the same magnitude as those of  $H_B$ .

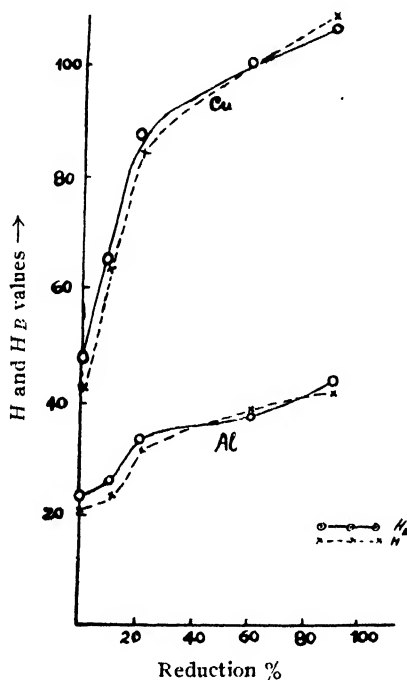


FIG. 5

$H$  and  $H_B$  values as function of cold reduction % for copper and aluminium

The question may be asked here, "If hardness is to be recognised as the amount of work done per unit volume of indentation, how does the energy lost in the form of heat or the energy remaining latent as potential energy in the stressed material affect the result?" In this connection it may be said that when a metal is subjected to plastic deformation, most of the work done,  $W$ , is dissipated in the form of heat  $Q$  and a small proportion of energy  $q$  remains latent in the deformed metal.

Thus,

$$W = Q + q$$

The magnitude of  $q$  has been determined by various authors (Rosenhein and Scott, 1933; Taylor and Quinney, 1934; Clarebrough, Hargreaves and others, 1952). Taylor (1934), for example, finds that for mild steel annealed in vacuo, when the work done  $W$  is 6.75 calories/gm.,  $Q = 5.99$  calories/gm. and  $q = W - Q = 0.76$  calories/gm. For decarbonised mild steel when

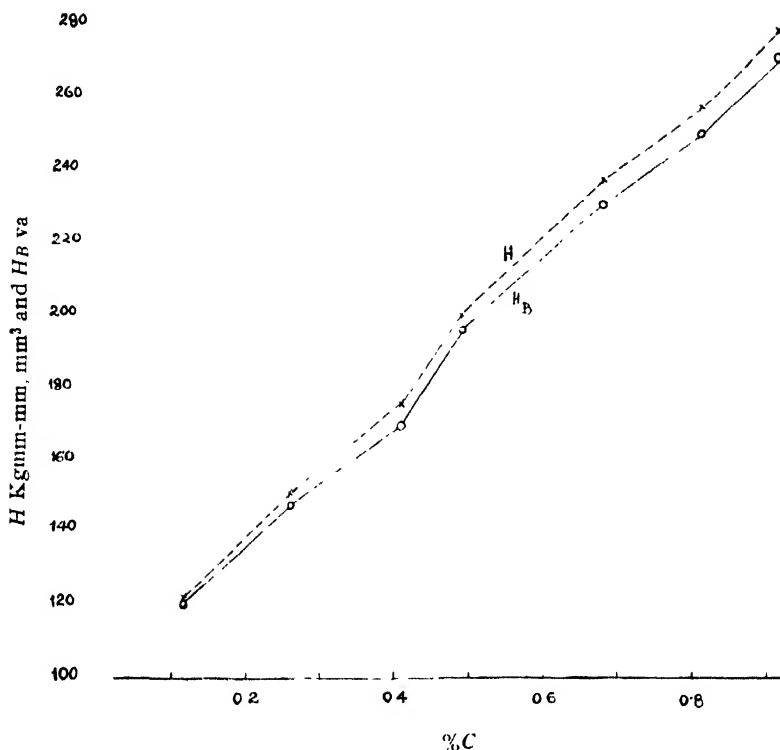


FIG. 6

$H$  and  $H_B$  values as function of %C for several normalised specimens of carbon steels

$W=7.92$  calories/gm.,  $Q=7.25$  calories/gm. and  $q=0.67$  calories/gm. Clarebrough and others (1952) found that for copper, when  $W=3.84$  calories/gm.,  $q=0.1$  calories/gm. and when  $W=34.3$  calories/gm.,  $q=0.331$  calories/gm. Thus, the major portion of the work done  $W$  is dissipated in the form of heat  $Q$  and a very small proportion  $q$  of the energy remains latent. Nevertheless, in considering hardness  $H$  as work done per unit volume of indentation, it is the mechanical work  $W$  which is taken into consideration. Obviously,  $W$ , being the sum of heat evolved  $Q$  and the latent energy  $q$ , takes into consideration both these factors and hence the results remain unaffected.

## 6. LIMITATIONS AND ADVANTAGES

Since the calculation of the work done  $W$  has been based on Meyer's Law, the range of validity of the hardness number  $H$  depends on the range of validity of Meyer's Law. The following points (O'Neill, 1934; Tabor, 1951) may be noted in this connection :



(i) For very small and very large loads Meyer's law fails.

(a) For very small loads, *i.e.* for very small values of indentation diameter  $d$ , the plots of  $\log L$  as function of  $\log d$  give rather high  $n$  values. Meyer (1908) has put the lower limit to  $d/D = 0.1$ .

(b) For very large loads the indenter itself undergoes appreciable deformation. The indenter should be two and half times harder (Tabor, 1951) than the specimen. If the indenter has a Brinell hardness number of 1000, metals of Brinell number greater than 400 should not be used.

A method to compute the approximate values of load for which Meyer's law is valid for different metals and alloys has been indicated by Tabor (1951).

(ii) Meyer's analysis fails if there is large creep. Because, the load should come in equilibrium, which does not occur if plastic flow continues. Creep usually reduces the values of  $n$  and sometimes values less than 2 are considered to be due to creep (Norbury, 1923).

The measurement of hardness  $H_B$  by the Brinell method has its disadvantages and limitations (O'Neill, 1934). Similarly, the measurement of hardness  $H$  based on work done per unit volume of indentation has also its limitations being based on Meyer's law. The question may then be asked, "What advantages are obtained by adopting this method in favour of the Brinell method which is so simple?" The advantages are:

(i) This method introduces a fundamental physical concept in the definition of hardness, *viz.* the amount of work done in  $\text{kgm-mm.}$  per unit volume of indentation in  $\text{mm}^3$ . The Brinell method does not provide a satisfactory physical concept (Tabor, 1951).

(ii) This method is based on a constant angle of indentation, *i.e.* on indentations of similar geometrical shape—a condition which certainly offers better comparable hardness values than when the angle is made variable as in the Brinell test (O'Neill, 1934; Lea, 1936; Tabor, 1951).

(iii) The method takes into consideration the hardness-level  $a$  and the hardenability index  $n$  of metals and alloys at two different loads and hence in principle takes into consideration two points of the hardness-load diagram, compared with only one such point taken into consideration in the Brinell method.

The simplicity of a particular test like the Brinell or the Vicker's test should not obscure the need for a fundamental investigation into the concept of hardness. An attempt has been made in the present paper to indicate some physical concept underlying the meaning of hardness of metals and alloys.

## 7. CONCLUSIONS

1(a) The hardness value  $H$  defined as the work done per unit volume of indentation in a static ball indentation test may be expressed as

$$H = \frac{24A\alpha e^{\beta n}}{\pi[2 - \cos\theta(\sin^2\theta + 2)]}$$

where  $\alpha$  and  $\beta$  are constants independent of the nature of the material,  $n$  is the so-called Meyer index,  $\theta$  is the angle of indentation and  $A$  is a constant given by  $A = aD^{n-2}$ , where  $D$  is the ball diameter.

(b) for  $\theta = 30^\circ$ , it has been found that  $\alpha = 0.0525$  and  $\beta = -0.9076$ . Hence, if the ball diameter  $D$  be 10 mm.,  $H$  is given by the simple formula

$$H = af_n$$

where

$$f_n = 7.79 \times 10^{n-2} e^{-0.9076n}$$

Hence, the determination of  $H$  merely involves the determination of the values of  $n$  and  $a$ .

2. The values of  $H$  compare quite well with those of the Brinell hardness number  $H_B$  for different metals and alloys under different treatments.

3. Hardness values  $H$  have some potential usefulness because it is based on a constant angle of indentation, i.e. comparisons of  $H$  are made on geometrically similar indentations—a condition which offers better comparable hardness values than when the angle is made variable as in the Brinell test.

4. Unlike other hardness numbers, the hardness value  $H$  defined as the work done per unit volume of indentation has a definite physical concept and also a definite unit, viz. Kgmm/mm<sup>3</sup>.

## ACKNOWLEDGMENTS

The author is grateful to Dr. M. N. Saha, F. R. S., for his continuous encouragement and wishes to acknowledge the help of Mr. K. C. Shome, the Research Scholar of this College, for drawing the figures and checking up several data and computations.

## REFERENCES

- Chatterjee, G. P., 1951, *Trans. Ind. Inst. Metals*, **V**, 245.  
 Clarebrough, L. M., Hargreaves, M. E. and others, 1952, *Proc. Roy. Soc. A*, **216**, 507.  
 Lea, F. C., 1936, *Hardness of Metals*, Charles Griffin and Co., London.  
 Matsumura, T., 1932, *Eng. Memos. Kyoto Univ.*, **7**, 48.  
 Meyer, E., 1908, *ZVDI*, **52**, 654-2, **31**, 49-55, **144**, 250.  
 Nadai, A., 1937, *Plasticity*, Mc-Graw Hill Book Co.  
 Norbury, A. L., 1923, *Trans. Farad. Soc.*, **19**, 140-220, 221.  
 O'Neill, H., 1934, *The Hardness of Metals and its Measurement*, Chapman and Hall.  
 Rosenheim, W. and Scott, V. H., 1933, *Proc. Roy. Soc. A*, **140**, 9.  
 Tabor, D., 1951, *The Hardness of Metals*, Clarendon Press, Oxford.  
 Taylor, G. I. and Quinney, H., 1934, *Proc. Roy. Soc. A*, **143**, 307.  
 Tuckermann, L. B., 1925, *Hardness and Hardness Testing*, Mech. Eng., 147.

# THE ULTRAVIOLET ABSORPTION SPECTRA OF $\alpha$ -CHLORO- AND $\alpha$ -BROMONAPHTHALENE IN DIFFERENT STATES \*

By A. R. DEB

OPTICS DEPARTMENT, INDIAN ASSOCIATION FOR THE CULTIVATION OF SCIENCE, CALCUTTA 32

(Received for publication, December 15, 1953)

**ABSTRACT.** The near ultraviolet absorption spectra of  $\alpha$ -chloronaphthalene and  $\alpha$ -bromonaphthalene in the vapour, liquid and solid states have been photographed, using very thin films of the substances in the case of liquid and solid states.

In the vapour state  $\alpha$ -chloronaphthalene yields 17 bands between 2896 Å and 2495 Å. The first band on the longer wavelength side at 34520  $\text{cm}^{-1}$ , has been assigned as the  $\nu_0$  band. The other bands correspond to vibrational frequencies 273, 50<sup>0</sup>, 1401 and 1505  $\text{cm}^{-1}$  and their progressions, the frequency 1401  $\text{cm}^{-1}$  being the most prominent. In the liquid state the  $\nu_0$  band shifts by 1135  $\text{cm}^{-1}$  towards longer wavelengths and only four broad bands are observed. The distance between the centres of these successive bands is 1375  $\text{cm}^{-1}$ . In the solid state at  $-180^\circ\text{C}$ , the  $\nu_0$  band further shifts towards longer wavelengths by 337  $\text{cm}^{-1}$ , and the vibrational frequency 1375  $\text{cm}^{-1}$  of the liquid state is changed to about 1424  $\text{cm}^{-1}$ .

In the case of  $\alpha$ -bromonaphthalene in the vapour state eleven bands have been observed with the  $\nu_0$  band at 34528  $\text{cm}^{-1}$  and progressions of two vibrational frequencies 496 and 1380  $\text{cm}^{-1}$ . In the liquid state at room temperature the  $\nu_0$  band is shifted towards longer wavelengths by 1321  $\text{cm}^{-1}$  and only four broad bands, corresponding to vibrational frequency 1343  $\text{cm}^{-1}$  are observed. At  $-180^\circ\text{C}$  in the solid state the  $\nu_0$  band further shifts towards longer wavelengths by 355  $\text{cm}^{-1}$  and the vibrational frequency 1343  $\text{cm}^{-1}$  of the liquid state is changed to about 1400  $\text{cm}^{-1}$ . The  $\nu_0$  band becomes appreciably sharper at  $-180^\circ\text{C}$ , though other bands do not show any sharpening.

Both the substances in the liquid and solid states show some very feeble bands in the region between 3250 Å and 3050 Å, when films of thickness about 0.1 mm. are used. The positions of these bands shift slightly towards longer wavelengths with solidification of the substances and lowering of temperature to  $-180^\circ\text{C}$ . All these results have been discussed.

## INTRODUCTION

The results of investigation on the ultraviolet absorption spectra of organic substances in different states carried out in this laboratory (Deb, 1951a, 1951b, 1953a; Swamy, 1952, 1953) have shown that the influence of intermolecular field on the electronic state of the molecules in the liquid and solid states is different for different molecules, and it depends on the structure and chemical composition of the molecules. Only substituted benzene compounds were studied before, as these show bands in the near ultraviolet region. Substituted naphthalene compounds also show such bands and it was thought worthwhile to extend the investigations to a few such compounds. The present paper deals with the results obtained in the case of  $\alpha$ -chloro and  $\alpha$ -bromonaphthalene in different states and at different temperatures.

\* Communicated by Prof. S. C. Sirkar

## EXPERIMENTAL

The liquids used were of chemically pure quality and  $\alpha$ -chloronaphthalene was supplied by B. D. H., the other liquid being obtained from Fisher Scientific Co., U.S.A. They were distilled under reduced pressure in sealed double bulbs of Pyrex glass before use. The technique used was the same as that described in an earlier paper (Deb, 1951a). The thicknesses used in the case of the solid and liquid phases were of the order of a few microns. Thicker films (0.1 mm. thick) showed new feeble bands on the longer wavelength side of the main system in both the cases. Microphotometric records of the spectrograms were taken with a Kipp and Zonen type self-recording microphotometer.

The absorption spectra of the vapours were studied by introducing the vapours in absorption tubes, 44 cm in length at their saturation pressures at 30°C in the case of  $\alpha$ -chloronaphthalene and at about 50°C in the other case. The latter temperature was maintained in the absorption tube by slightly heating the tube.

## RESULTS

The microphotometric records of the absorption spectra are reproduced in figures 1-4. The frequencies in  $\text{cm}^{-1}$  of the bands are given in Tables I and II in which the assignments are also given.

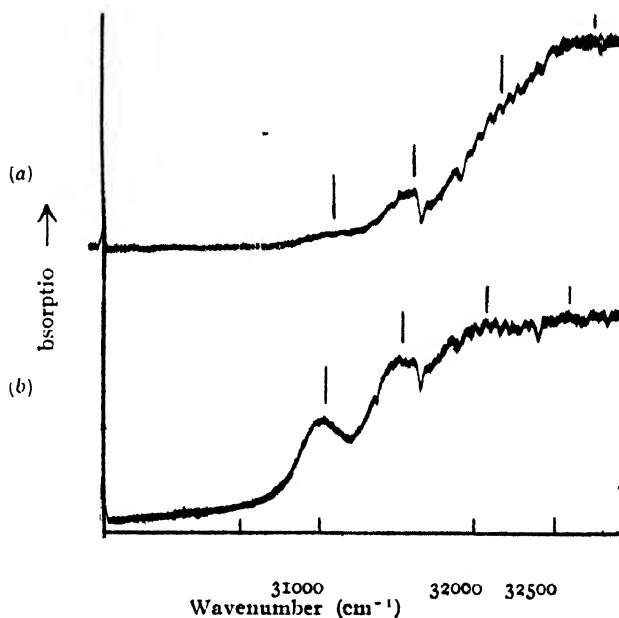


FIG. 1

Microphotometric records of the ultraviolet absorption spectra  
of  $\alpha$ -chloronaphthalene (First system)

(a) Liquid at 32°C;                      (b) Solid at -180°C

The positions of the bands have been indicated by vertical lines.

TABLE I

 Ultraviolet absorption bands of  $\alpha$ -chloronaphthalene

Vapour at 30°C		Liquid at 30°C		Solid at -180°C	
Wavenumber (cm <sup>-1</sup> ) and Int.	Assignment	Wavenumber (cm <sup>-1</sup> ) and Int.	Assign- ment	Wavenumber (cm <sup>-1</sup> ) and Int.	Assignment
1st system					
		31114 (vw)	$\nu_0$	31056 (s)	$\nu_0$
		31658 (vw)	$\nu_0 + 544$	31572 (s)	$\nu_0 + 516$
		32207 (vw)	$\nu_0 + 2 \times 544$	32203 (w)	$\nu_0 + 2 \times 516$
		32744	$\nu_0 + 3 \times 544$	32592 (w)	$\nu_0 + 3 \times 516$
2nd system			2nd system		
34520 (vw)	$\nu_0$	33385 (m)	$\nu_0$	33048 (m)	$\nu_0$
34793 (m)	$\nu_0 + 273$				
35028 (m)	$\nu_0 + 508$				
35065 (m)	$\nu_0 + 2 \times 273$				
35538 (vw)	$\nu_0 + 2 \times 508$				
35921 (vw)	$\nu_0 + 1401$	34760 (vs)	$\nu_0 + 1375$	34472 (vs)	$\nu_0 + 1424$
36025 (s)	$\nu_0 + 1515$				
36190 (ms)	$\nu_0 + 1401 + 273$				
36412 (vs)	$\nu_0 + 1401 + 508$				
36545 (w)	$\nu_0 + 1505 + 508$				
36943 (s)	$\nu_0 + 1401 + 2 \times 508$				
37330 (vv)	$\nu_0 + 2 \times 1401$	36116 (s)	$\nu_0 + 2 \times 1375$	35896 (s)	$\nu_0 + 2 \times 1424$
37838 (vs)	$\nu_0 + 2 \times 1401 + 508$				
38346 (m)	$\nu_0 + 2 \times 1401 + 2 \times 508$				
38733 (ms)	$\nu_0 + 3 \times 1401$	37498 (w)	$\nu_0 + 3 \times 1375$	37302 (m)	$\nu_0 + 3 \times 1424$
39265 (m)	$\nu_0 + 3 \times 1401 + 508$				
39749 (vw)	$\nu_0 + 3 \times 1401 + 2 \times 508$				
40116 (vvv)	$\nu_0 + 4 \times 1401$				

## DISCUSSION

It is seen from figures 1-4 as well as from Tables I and II that the near ultraviolet absorption spectra of both the substances consist of two groups of bands, which were called by de Laszlo (1926) as Part I and Part II, the feeble group on the longer wavelength side being called Part I. The microphotometric records reproduced show that bands of Part I are extremely feeble compared to those of the other part.

From a consideration of the relative intensities of the bands in the two parts it is evident that they do not belong to the same system of bands. Bands of Part II, therefore, have been assumed to constitute a separate and the main system of bands, called in this paper as the second system, and assignments have been made accordingly.

Microphotometric records of the ultraviolet absorption spectra of  $\alpha$  chloronaphthalene (Second system).

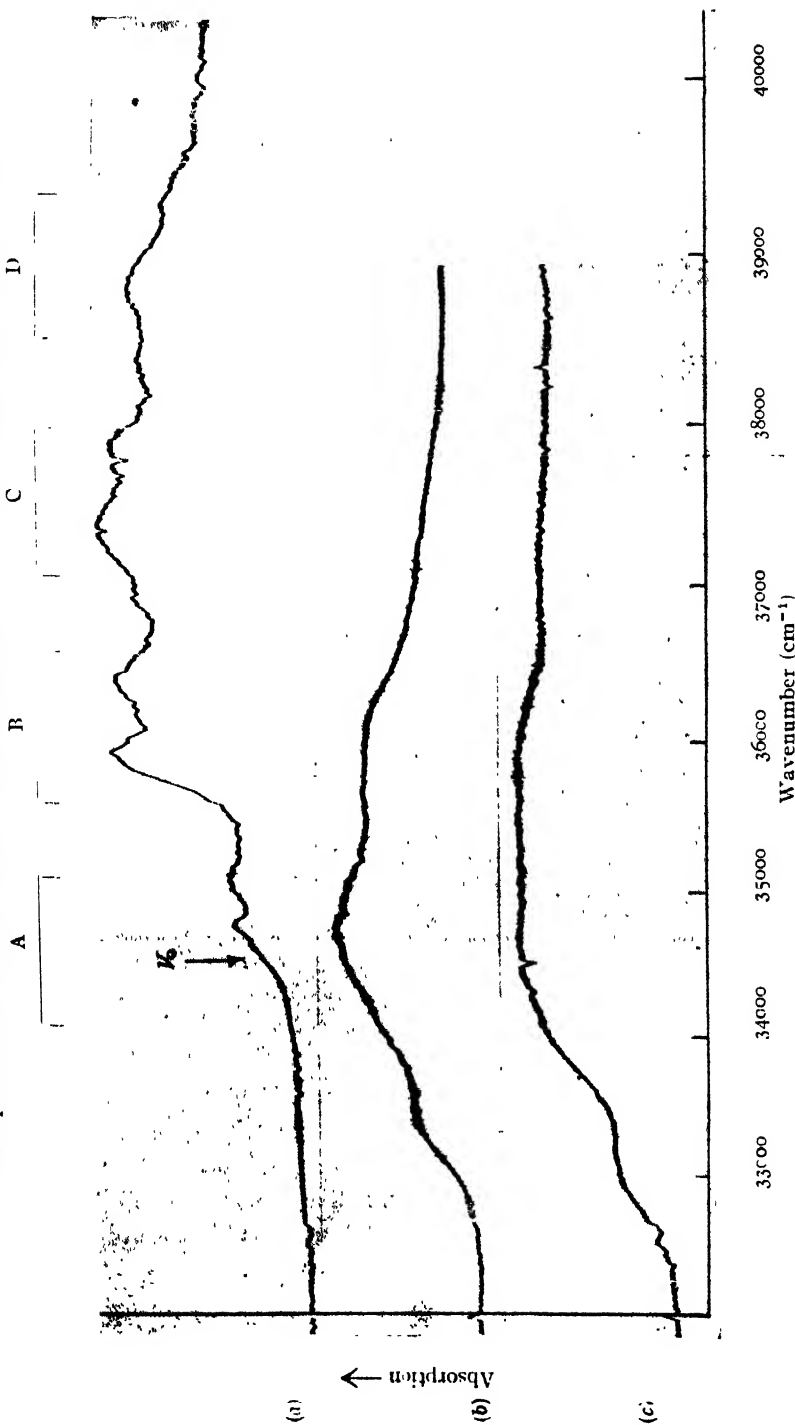


FIG. 2

(a) Vapour at  $30^\circ\text{C}$ ; (b) Liquid at  $30^\circ\text{C}$ ; (c) Solid at  $-180^\circ\text{C}$

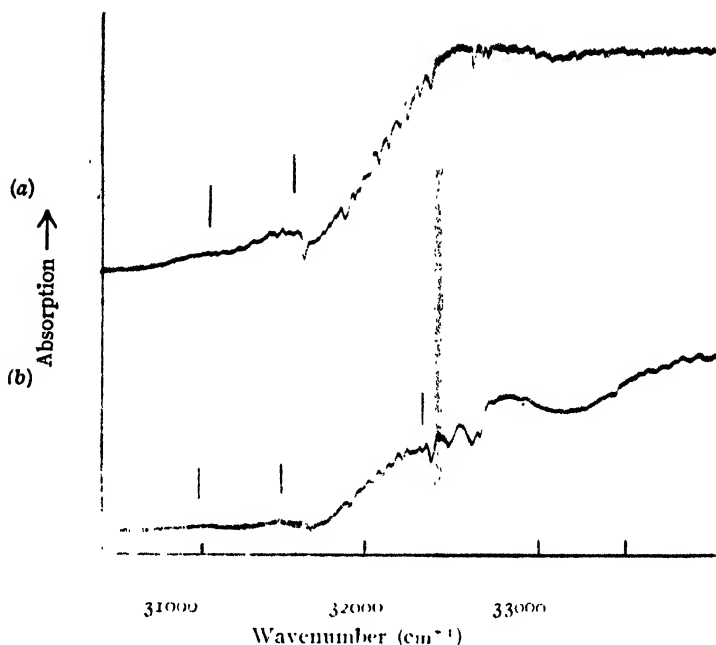


FIG. 3

Microphotometric records of the ultraviolet absorption spectra of  $\alpha$ -bromonaphthalene (First system)

(a) Liquid at  $32^{\circ}\text{C}$ ,

(b) Solid at  $-180^{\circ}\text{C}$

The bands have been marked by vertical lines. The strong band below  $33000\text{ cm}^{-1}$  is the first band of the second system.

#### (a) BANDS OF THE SECOND SYSTEM

It is seen from figures 2 and 4 that in the case of the vapour state of both the substances, the first group of bands marked A on the extreme longer wavelength side of the second system is much weaker than the next group of bands on the shorter wavelength side. These weak bands, however, persist with almost same relative intensities even at  $-180^{\circ}\text{C}$ , though they merge into one another to form one broad band. These bands cannot, therefore, be due to transitions from excited vibrational levels in the electronic ground state, because in that case they would have disappeared at  $-180^{\circ}\text{C}$ . The band on the extreme longer wavelength side has been, therefore, assigned as the  $\nu_0$  band in each case.

$\alpha$ -Chloronaphthalene: The  $\nu_0$  band of second system in the vapour state of this substance is a very weak band at  $34520\text{ cm}^{-1}$ . Sixteen more bands have been observed corresponding to vibrational frequencies 273, 508, 1401 and  $1505\text{ cm}^{-1}$ . The bands corresponding to the frequency  $1401\text{ cm}^{-1}$  are the most prominent ones. In the case of the liquid state at  $30^{\circ}\text{C}$  the several bands in each of the groups marked A, B, C, D in figure 2 merge into one band. The  $\nu_0$  band is taken at  $33385\text{ cm}^{-1}$ , the C. G. of

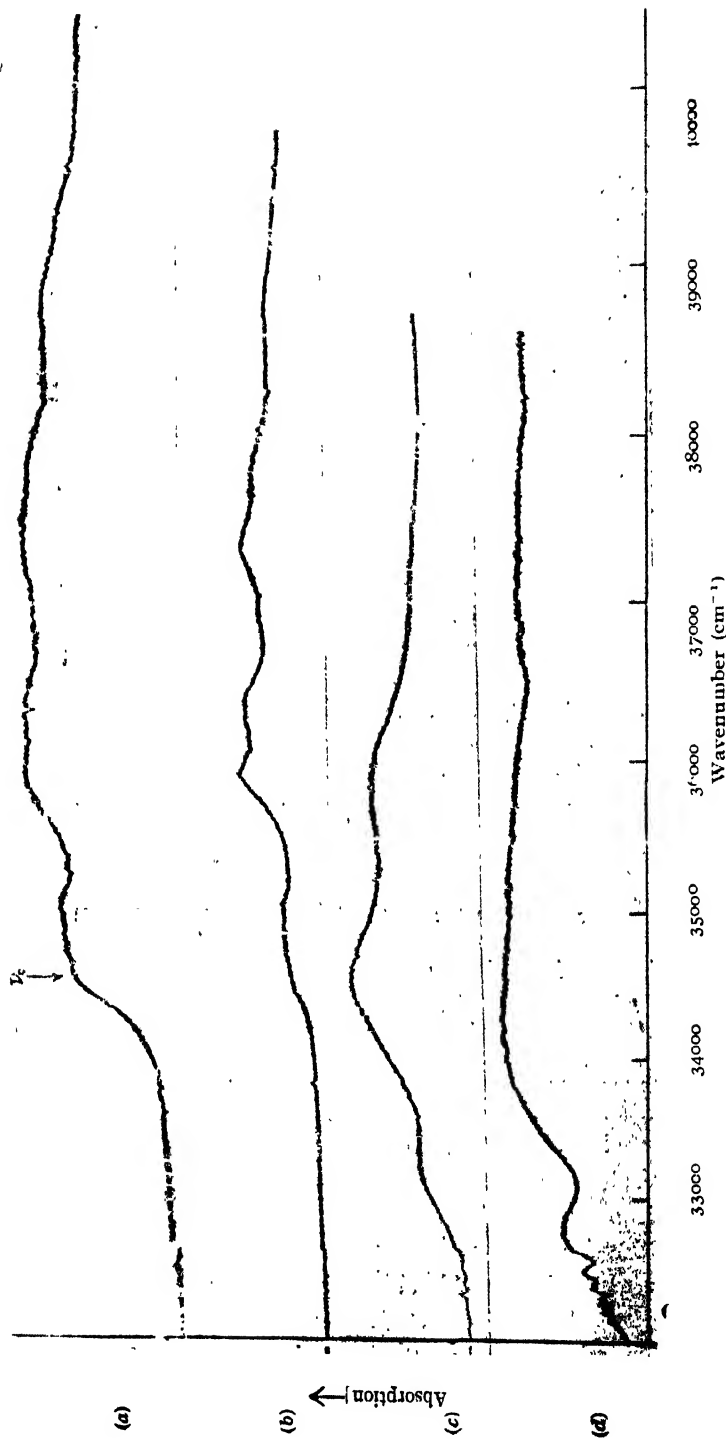
Microphotometric records of the ultraviolet absorption spectra of  $\alpha$ -bromonaphthalene (Second system)

FIG. 4

(a) Vapour at about  $50^\circ\text{C}$ .  
 (b) " at room temp ( $30^\circ\text{C}$ )

(c) Liquid at  $30^\circ\text{C}$   
 (d) Solid at  $-180^\circ\text{C}$



TABLE II

 Ultraviolet absorption bands of  $\alpha$ -bromonaphthalene

Vapour			Liquid at 30°C		Solid at -180°C	
(de Laszlo, 1926)	(Present author)					
$\nu$ (cm <sup>-1</sup> )	$\nu$ (cm <sup>-1</sup> ) and Int.	Assignment	$\nu$ (cm <sup>-1</sup> ) and Int.	Assignment	$\nu$ (cm <sup>-1</sup> ) and Int.	Assignment
1st system			1st system			
31143			31037(vw)	$\nu_0$		
31414					30380(vw)	
31666			31556(vw)	$\nu_0 + 510$	31477(vw)	$\nu_0 + 488$
32000					32363(vw)	$\nu_0 + 1374$
32248						
32405						
...						
...						
2nd system			2nd system			
34472	34528(m)	$\nu_0$	33207(m)	$\nu_0$	32852(s)	
34967	35024(m)	$\nu_0 + 496$				
35052						
35703						
35908	35908(vs)	$\nu_0 + 1380$	34550(vs)	$\nu_0 + 1343$	34253(vs)	$\nu_0 + 1401$
36221	36405(s)	$\nu_0 + 1380 + 496$				
36298						
	36603(ms)	$\nu_0 + 1380 + 2 \times 496$				
37163	37288(vs)	$\nu_0 + 2 \times 1380$	35889(vs)	$\nu_0 + 2 \times 1343$	35665(vs)	$\nu_0 + 2 \times 1401$
37172						
37710	37781(ms)	$\nu_0 + 2 \times 1380 + 496$				
37910						
	38302(vw)	$\nu_0 + 2 \times 1380 + 2 \times 496$				
38568	38673(s)	$\nu_0 + 3 \times 1380$	37232(w)	$\nu_0 + 3 \times 1343$	37067(w)	$\nu_0 + 3 \times 1401$
38823						
	39157(vw)	$\nu_0 + 3 \times 1380 + 496$				
	40052(vw)	$\nu_0 + 4 \times 1380$				

the first group and the bands indicate a progression of vibrational frequency 1375 cm<sup>-1</sup>. In the investigation reported by de Laszlo (1926), the author only mentioned the wavenumbers of the bands and their molecular absorption co-efficients, and he did not analyse the bands. From a study of several naphthalene derivatives he concluded that in hexane solution the absorption spectra are shifted towards the red with respect to the vapour spectra, and that this red shift is greater for part II bands than for part I. In the present case a shift of the  $\nu_0$  band of the 2nd system as large as 1135 cm<sup>-1</sup> with liquifaction of the vapour is observed. It is, therefore, evident that in this compound also, as in substituted benzenes, the influence of the intermolecular field lowers the excited state electronic energy level when the substance is liquified from vapour phase, with the difference that

the lowering in this case is much larger than in most of the substituted benzenes. All the bands in the liquid state are very broad which shows that the electronic energy levels are themselves broadened due to fluctuation of the intermolecular field, this fluctuation being caused probably by thermal fluctuation of density.

At low temperatures in the solid state the broad bands are further shifted towards longer wavelengths, the shift of the  $\nu_0$  band being  $337\text{ cm}^{-1}$ . The vibrational frequency increases from  $1375\text{ cm}^{-1}$  in the liquid state to  $1424\text{ cm}^{-1}$  in the solid state at  $-180^\circ\text{C}$ . That the bands are broad even at  $-180^\circ\text{C}$ , probably shows that both the angular oscillation of the molecules and the excitation of vibrational modes disturb the intermolecular field and broaden the electronic energy level. The fact that the  $\nu_0$  band is sharper than the other bands shows that the influence of both these causes are present. There may be some angular oscillations of small amplitude even at  $-180^\circ\text{C}$  and such oscillations might produce a fluctuation in the intermolecular field and might thereby broaden the bands. It is interesting to note that an intense line at  $1375\text{ cm}^{-1}$  is observed in the Raman spectrum of this liquid (Magat, 1934). This shows that this frequency is the same for the excited and ground states.

*$\alpha$ -Bromonaphthalene*: The  $\nu_0$  band of the second system of this substance in the vapour state is at  $31528\text{ cm}^{-1}$  and 10 more bands corresponding to vibrational frequencies 496 and  $1380\text{ cm}^{-1}$  are present in the spectrum. In the liquid state at room temperature these bands are replaced by 4 broad bands with the  $\nu_0$  band at  $33207\text{ cm}^{-1}$  and the centres of other bands roughly corresponding to a vibrational frequency  $1343\text{ cm}^{-1}$ . The shift of the  $\nu_0$  band towards longer wavelength side in this case is  $1321\text{ cm}^{-1}$ , which indicates a stronger influence of the intermolecular field on the electronic energy levels than that observed in the case of  $\alpha$ -chloronaphthalene. In the case of the solid state at  $-180^\circ\text{C}$ , the bands appear to have undergone changes which are similar to those observed in the case of  $\alpha$ -chloronaphthalene. The  $\nu_0$  band shifts by  $355\text{ cm}^{-1}$  towards longer wavelengths, and the vibrational frequency is changed to about  $1401\text{ cm}^{-1}$ . In this case, however, one remarkable feature is observed. The  $\nu_0$  band in the solid state at  $-180^\circ\text{C}$  becomes appreciably sharper than the corresponding band in the liquid state though the other bands do not show any such sharpening. This shows that when transitions take place between the electronic levels not associated with any vibrational level, the levels themselves are not perturbed very much, but association of any vibrational transition with electronic transition makes the electronic levels broad. Such a phenomenon was observed also in the case of diphenylmethane (Deb, 1953a) where the  $\nu_0$  band in the liquid state was much sharper than the other bands. This phenomenon also shows that in these cases, the angular oscillation of the molecules is not mainly responsible for the width of the bands.

(b) BANDS OF THE FIRST SYSTEM

This system is produced when the thickness of the absorbing layer in the case of solid and liquid states is about 0.1 mm. which is many times that used for obtaining the second system. In the vapour state de Laszlo (1926) obtained these bands at a high temperature (120°C for the bromo compound). The work in the vapour state has not been repeated for this system.

*$\alpha$ -Chloronaphthalene*: In this case four bands have been observed both in the liquid and solid states. In each case the first band on the longer wavelength side has been assigned as the  $\nu_0$  band. In the case of the liquid state it is at  $31114\text{ cm}^{-1}$  and in the case of the solid state, at  $31056\text{ cm}^{-1}$ . There is thus a shift towards longer wavelengths by  $58\text{ cm}^{-1}$ . The other bands in the liquid state are at distances 544, 1093 and  $1630\text{ cm}^{-1}$  from the  $\nu_0$  band. Probably they correspond to a vibrational frequency  $544\text{ cm}^{-1}$  which in the solid state changes to  $516\text{ cm}^{-1}$ .

*$\alpha$ -Bromonaphthalene*: In this case only three bands of this system have been observed. The  $\nu_0$  band due to the liquid state is at  $31037\text{ cm}^{-1}$  and that due to the solid state is at  $30989\text{ cm}^{-1}$ . In the case of the vapour state the first band of this part reported by de Laszlo (1926) is at  $31143\text{ cm}^{-1}$ . Taking this to be the  $\nu_0$  band, its shift is found to be towards longer wavelengths both with liquifaction of the vapour and solidification of the liquid. It is thus seen that electronic energy levels of the excited states responsible for these bands are lowered by intermolecular forces both with liquifaction of vapour and solidification of the liquid, as is the case with the first system.

In the case of naphthalene vapour also there is a group of bands in this region besides the other group on the shorter wavelength side (de Laszlo, 1924). Tsujikawa and Kanda (1950) have recorded 9 bands in this region for naphthalene in the solid state, which become sharper on lowering of temperature. According to them these bands owe their origin to the superposition of molecular vibration of symmetry  $B_{2g}$  upon electronic transition. In a recent investigation (Deb, 1953b) it has been shown that in the case of diphenyl a group of very feeble bands is observed in this region in the solid state in addition to the main group below  $2800\text{ \AA}$ . These bands are not observed in the case of the liquid state, but they become sharper at low temperatures. It was suggested that this group of bands on the longer wavelength side of the main system, owes its origin to transitions taking place in one ring when the other ring is in an excited state. The energy level of one of the rings may be lowered by the influence of the adjacent ring in an excited state and the bands produced by transitions in the first ring may lie on the longer wavelength side of the main system produced by excitation of only one of rings. The probability of such simultaneous excitation of the two rings is very low, and this may explain the very low intensity of the observed bands of the first system compared to that of the other group.

Such an explanation is applicable in the case of compounds under present investigation also. The difference, as regards this feeble group of bands between diphenyl on the one hand and naphthalene and its derivatives on the other is that in the former case these bands are not observed in the liquid or vapour state. This may be due to the facts that in diphenyl one of the phenyl groups has freedom of rotational oscillation about C—C bond, while in naphthalene molecule no such freedom is present and that such oscillations may broaden the energy level so much in the case of the liquid and vapour states that they disappear in the background owing to their diffuseness.

#### ACKNOWLEDGMENT

The author wishes to express his grateful thanks to Professor S. C. Sirkar, D. Sc., F. N. I., for this kind guidance throughout the progress of the work.

#### REFERENCES

- De Laszlo, H. G., 1924, *Proc. Roy. Soc.*, **A**, 108, 622.  
" " 1926, *ibid*, **A**, 111, 355.  
Deb, A. R., 1951a, *Ind. J. Phys.*, **25**, 233.  
" " 1951b, *ibid*, **25**, 433.  
" " 1953a, *ibid*, **27**, 183.  
" " 1953b, *ibid*, **27**, 305.  
Magat, M., 1934, Table of constants, p. 73.  
Swamy. H. N., 1952, *Ind. J. Phys.*, **26**, 119, 233, 445.  
" " 1953, *ibid*, **27**, 55, 119.  
Tsujiikawa, I. and Kanda, E., 1950, *Sci Rep. Res. Inst., Tohoku Univ. Ser A.*, **2**, 420.

# EFFECT OF STEEPNESS OF RISE AND FALL OF THE INPUT PULSE ON THE RESPONSE OF PULSE AMPLIFIERS (PART I)\*

By BIMAL KRISHNA BHATTACHARYYA

INSTITUTE OF NUCLEAR PHYSICS, 92, UPPER CIRCULAR ROAD, CALCUTTA-9

(Received for publication, December 7, 1953)

**ABSTRACT.** The effect of steepness of pulse-fronts on the response characteristics of RC-coupled pulse amplifiers has been studied. The analytical expressions of the responses of the amplifier to pulses of the following types have been derived : (i) Ramp function input pulse. (ii) A pulse with linear rise and fall and (iii) a saw-tooth pulse. In the case of a ramp function input pulse expressions have been deduced relating the rise and delay times of the reproduced pulse with the rise time of the input pulse. In the cases of pulses having sharp rise and fall, formulae have been derived for the maximum output voltage obtainable and the time corresponding to this maximum, as a function of times of rise and fall of the input pulse. The response characteristics for all the interesting cases have been plotted.

## INTRODUCTION

Pulse amplifiers are used not only in various branches of electronics but also in almost every work of nuclear physics where it is necessary to amplify the signal coming out of a detector, e.g., the ionisation chamber, proportional counters, etc. In various types of work, specially in experimental problems of nuclear physics, pulse amplifiers are meant only to reproduce the leading edge of the incoming pulse faithfully. The leading edge of the pulse is generally assumed to rise in a very short time and it is desired that the rise time and delay time of the pulse amplifier be very small.

Since all this information about the pulse amplifier is desirable before the start of the actual experiment, the response characteristics of the pulse amplifier to a step-function input pulse (figure 1) which rises from its initial to final value instantaneously, have been obtained theoretically and are available in standard text-books on pulse amplifiers (Valley and Wallman, 1948). An actual pulse can never have such an abrupt rise. The pulse from an ionisation chamber or other types of detector in nuclear physics requires a finite build-up time. So the response of a pulse amplifier calculated by assuming the input voltage to be a step function, does not always demonstrate physically accurate pictures.

To get a correct idea about the output of the pulse amplifier, it is necessary for the purpose of theoretical computations to assume such an

\* Communicated by Prof. M. N. Saha, F.R.S.

input pulse that is a very good approximation to the actual pulse. A sharply rising pulse front may be well represented by a linearly rising pulse in practically all the cases. So the input pulse can be assumed to be one that rises linearly to its final value and then flattens out (figure 2). Such a type of pulse is called a ramp function. It is also easy to express this ramp function pulse analytically as given below :

$$e(t) = K \left[ \frac{t}{t_1} u(t) - \frac{(t-t_1)}{t_1} \cdot u(t-t_1) \right] \quad \dots (1)$$

where  $K$  represents the height of the pulse and  $u(t)$  and  $u(t-t_1)$  are unit step functions beginning at times  $t=0$  and  $t=t_1$  respectively.

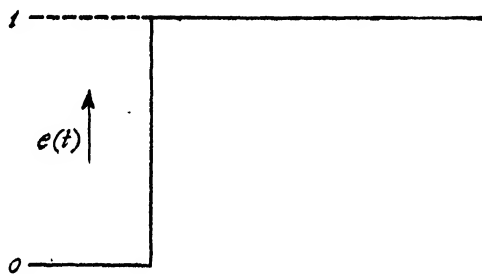


FIG. 1 A step function input pulse.

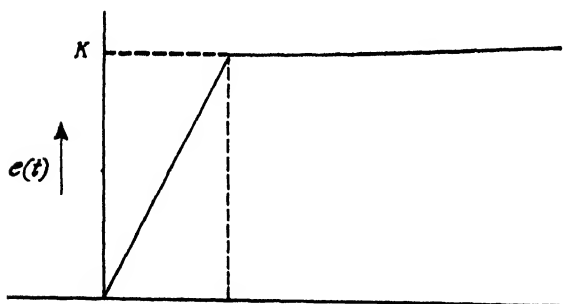


FIG. 2 A ramp function input pulse.

In many cases the incoming pulses are not flattened at the top but begin to fall sharply after reaching the final amplitude. The fall can be taken to be linear in many cases (figure 3). Even when the fall is exponential, the initial portion of the decay is practically linear in most of the cases. This pulse can be represented by the expression :

$$e(t) = K \left[ \frac{t}{t_1} u(t) - \frac{t_2}{t_1} \cdot \frac{(t-t_1)}{(t_2-t_1)} u(t-t_1) + \frac{(t-t_2)}{(t_2-t_1)} \cdot u(t-t_2) \right] \quad \dots (2)$$

When  $t_1 = t_2$ , the pulse shown in figure 3 takes the form of a saw-tooth pulse (figure 4). This pulse is expressed by the following analytical relation :

$$e(t) = K \frac{t}{t_1} [u(t) - u(t - t_1)] \quad (3)$$

The subject of study in this paper is to determine the response functions of typical RC-coupled pulse amplifiers (figure 5) to these types of commonly-occurring pulses. Attention has been concentrated mainly on the effect of variation of steepness in the case of ramp function input pulse on the shape of the output voltage and the rise time and delay time of reproduced pulse. When the pulse does not flatten out at the top (figures 3 and 4), main consideration is given to the determination of the maximum output voltage obtainable, the time at which this maximum occurs and the faithfulness with which the input pulse is reproduced.

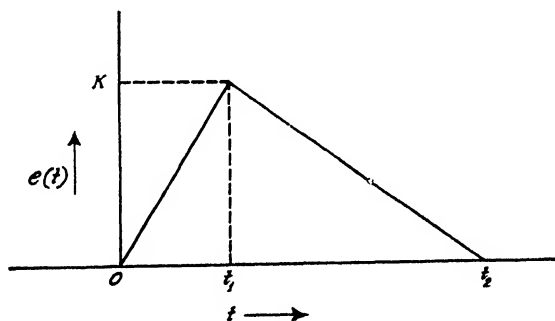


Fig. 3. A pulse with linear rise and fall.

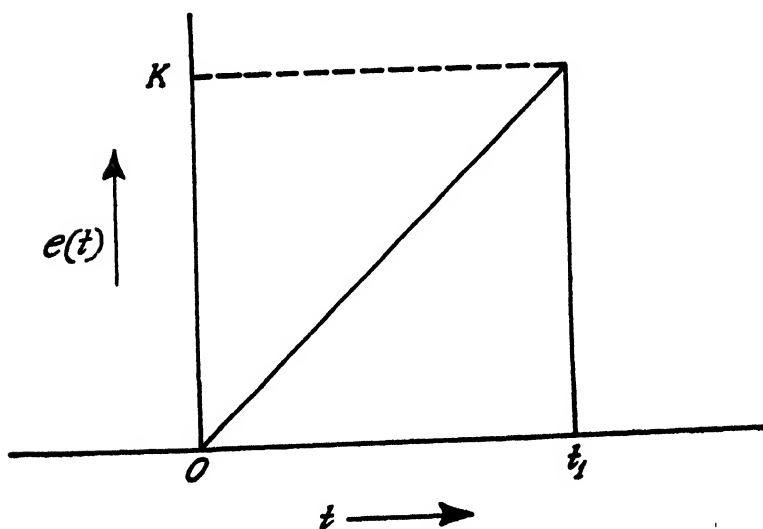


Fig. 4. A saw-tooth pulse.

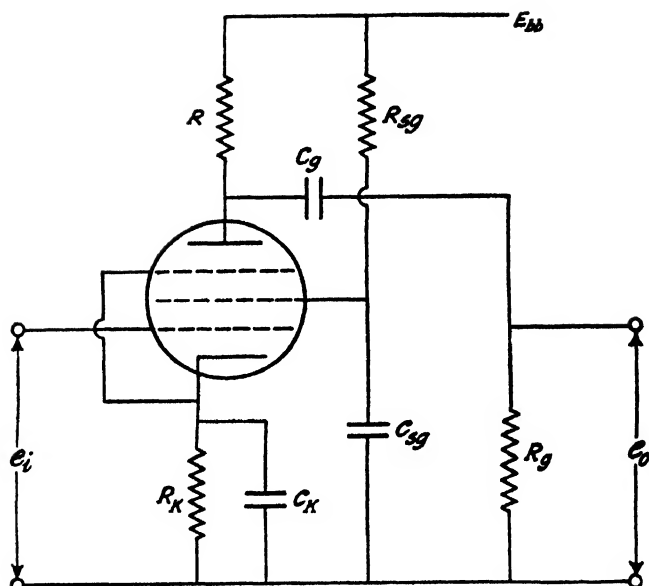


Fig. 5. An RC-coupled pulse amplifier.

## RESPONSE TO A RAMP FUNCTION INPUT PULSE

We shall assume that only the high frequency equivalent circuit requires consideration in determining the reproduced output of the leading edge.

In the following analysis we shall always denote the Laplace transform of the voltage  $e(t)$  by  $e(p)$ .

The high frequency equivalent circuit of the RC-coupled pulse amplifier is shown in figure 6, where  $R$  is the load resistance,  $C$  is the combination of stray and wiring capacitances and  $g_m$  denotes the mutual transconductance of the vacuum tube.

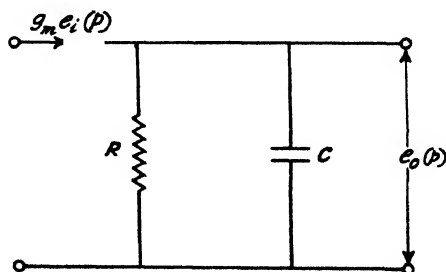


Fig. 6. High frequency equivalent circuit of the amplifier.

If  $e_o(p)$  is the output voltage of the amplifier, we have

$$e_o(p) = g_m e_i(p) \cdot \frac{R}{1 + pCR} \quad \dots (4)$$



From equation (1) we obtain the Laplace transform of the input voltage

$$e_i(p) = K \frac{1}{p^2 t_1} e^{-pt_1} \quad \dots (5)$$

If the resulting equation obtained by putting (5) into (4) be normalized with the substitution  $t = t/RC$  and  $e_0(t) = \frac{e_0(t)}{g_m K R}$ , we have

$$e_0(p) = \frac{1}{t_r} \cdot \frac{(1 - e^{-pt_r})}{(1 + p)^2 p^2} \quad (6)$$

where

$$t_r = t_1/RC$$

The inverse Laplace transform of (6) gives

$$e_0(t) = \frac{1}{t_r} (\epsilon^{-t} + t - 1), \quad 0 < t \leq t_r$$

and (7)

$$e_0(t) = \frac{1}{t_r} [\epsilon^{-t} (1 - \epsilon^{t_r}) + t_r], \quad t \geq t_r$$

Thus the response of a single stage  $RC$  amplifier is obtained for the case of a ramp function input pulse.

Now, the problem is to find out the voltage response of a chain of amplifiers, as shown in figure 7, to a ramp function. It will be assumed

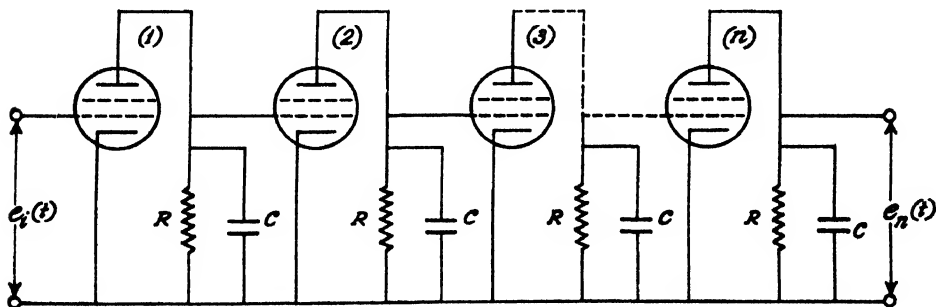


Fig. 7. A chain of identical  $RC$ -coupled amplifiers.

that all the stages are identical.

It is easy to show that the transform of the voltage developed across the  $n$ th tube is given by

$$e_n(p) = \frac{(g_m R)^n}{(1 + pCR)^n} e_i(p) \quad \dots (8)$$

where  $e_n(p)$  is the voltage developed across the load resistance of the  $n$ th

## B. K. Bhattacharyya

tube. Normalizing by the substitution  $t = t_r RC$  and  $e_n(t) = e_n(t) / (g_m R)^n$ , we have

$$n(p) = \frac{1}{p} \left[ \frac{1}{p^2(1+p)^n} - \frac{e^{-pt_r}}{p^2(1+p)^n} \right] \quad \dots (9)$$

By evaluating the transform of (9), we obtain

$$n(t) = \frac{1}{t_r} \left[ (t-n) + \frac{1}{(n-1)!} \cdot e^{-t} \left\{ \sum_{r=0}^{(n-1)} \frac{(n-1)!}{C_r(r+1)!} t^{(n-r-1)} \right\} \right], \quad 0 \leq t \leq t_r \quad \dots (10)$$

and

$$e_n(t) = 1 + \frac{1}{t_r(n-1)!} \left[ \left\{ \sum_{r=0}^{(n-1)} \frac{(n-1)!}{C_r t^{(n-r-1)}(r+1)!} \right\} - e^{-t_r} \left\{ \sum_{r=0}^{(n-1)} \frac{(n-1)!}{C_r} \right\} \right] (t-t_r)^{n-r-1} \cdot (r+1)! \left\{ \right\}, \quad t \geq t_r \quad \dots (11)$$

With the help of (10) and (11) we can find the output voltage after any number of stages. Figures 8-11 show the responses of RC-coupled amplifiers to a ramp function input with different rise times, *e.g.*, (i) 0.5, (ii) 1.0, (iii) 1.5 and (iv) 5.0.

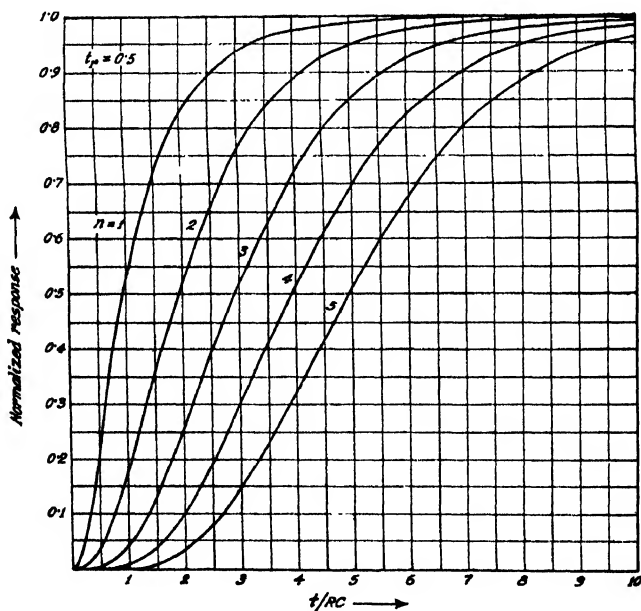


Fig. 8. Response of a RC-coupled pulse amplifier to a ramp function with rise time  $t_r = 0.5$

That the response to a ramp function with a very sharp rise, *e.g.*, 0.1 in terms of  $RC$ , is practically identical with that to a step function, is obvious

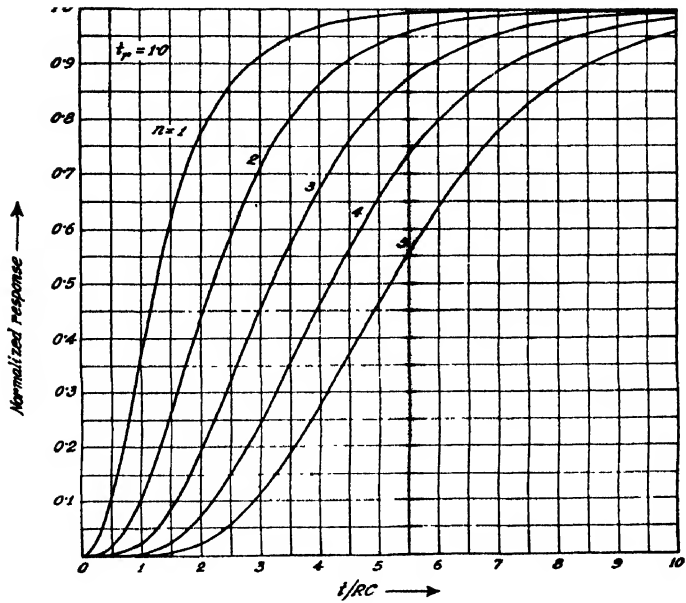


Fig. 9. Response of an RC-coupled pulse amplifier to a ramp function with a rise time  $t_r = 1.0$ .

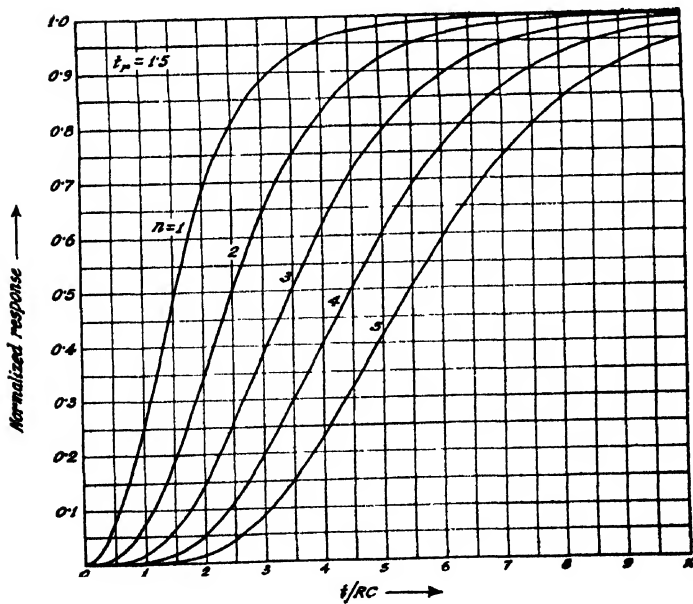


Fig. 10. Response of an RC-coupled pulse amplifier to a ramp function with a rise time  $t_r = 1.5$ .

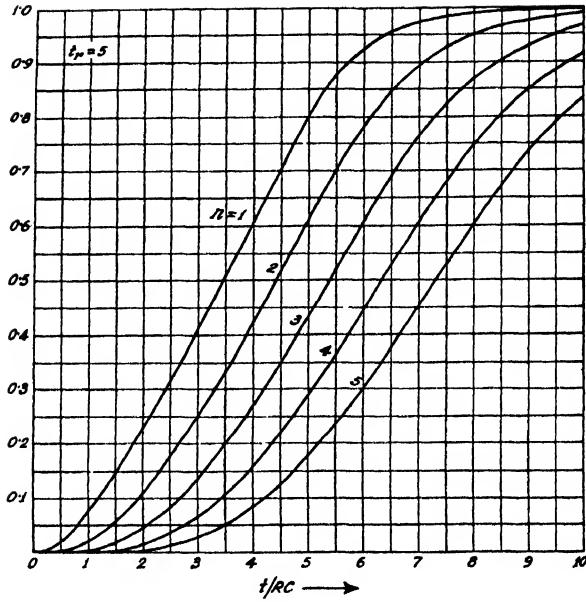


Fig. 11. Response of an RC-coupled pulse amplifier to a ramp function with rise time  $t_r = 5.0$ .

when we study figures 12 and 13. The response functions of RC-coupled pulse amplifiers to a step function input is well known and can be found in standard text-books on pulse technique.

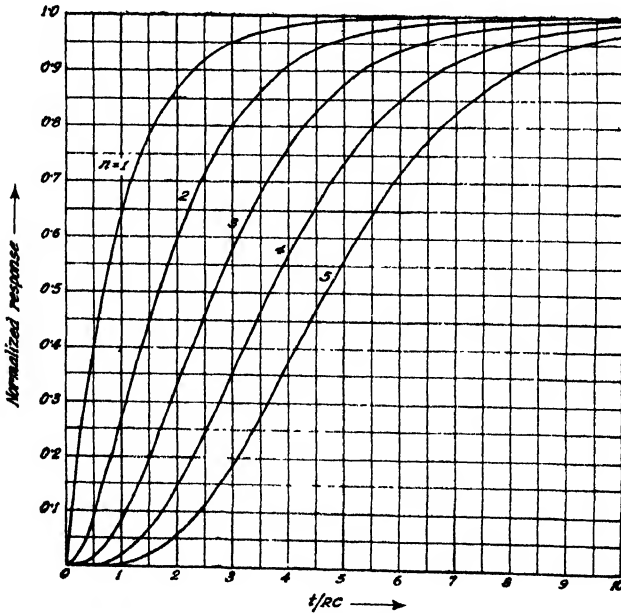


Fig. 12. Response of an RC-coupled pulse amplifier to a step function input.

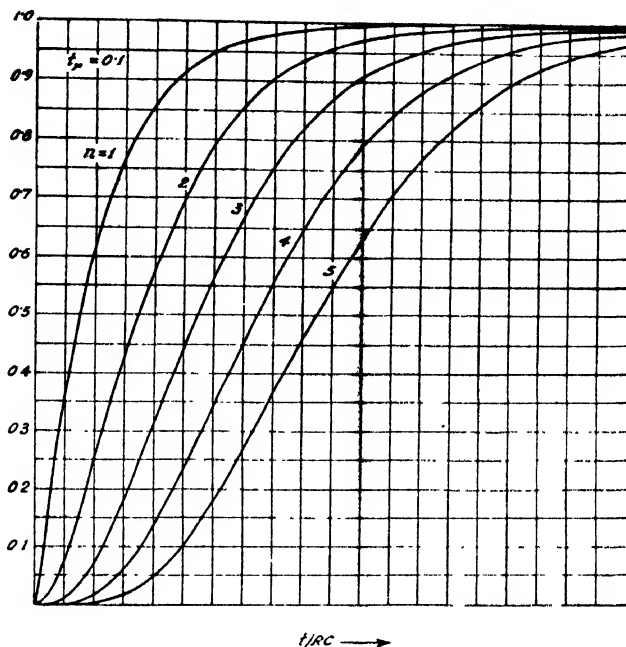


Fig. 13. Response of an RC-coupled pulse amplifier to a ramp function with a rise time  $t_r = 0.1$ .

#### RISE AND DELAY TIMES OF THE OUTPUT PULSE

If we follow the conventional definitions of rise and delay times of the pulse amplifier in this case also, we have :

$$\text{Rise time} = t_u - t_l = T_r$$

$$\text{Delay time} = t_d$$

where  $t_u$ ,  $t_l$  and  $t_d$  correspond to the times at which the normalized response assumes the values 0.9, 0.1 and 0.5 respectively. The input pulse has finite rise and delay times of its own which are given by the expressions :

10 to 90 per cent. rise times of the input pulse  $= 0.8 t_r$  and delay time  $= 0.5 t_r$ .

So the actual contribution of the pulse amplifier to the increase of rise time and delay time of the output response is determined by the expressions  $(T_r - 0.8 t_r)$  and  $(t_d - 0.5 t_r)$  respectively.

We shall now derive expressions relating all the three parameters,  $t_u$ ,  $t_l$  and  $t_d$  with the rise time  $t_r$  of the input pulse for a single stage RC amplifier.

If  $t_u \geq t_r$ , we have

$$t_u = \log_{10} \frac{10(e^{t_r} - 1)}{t_r} \quad \dots (12)$$

When  $t_r$  tends to zero in the limit (step function input),

$$t_u = \log_{10} 10 = 2.302585$$

When  $t_u \leq t_r$ ,  $t_u$  is related to  $t_r$  by the expression

$$t_r = \frac{10}{9}(\epsilon t_u + t_u - 1) \quad \dots (13)$$

If  $t_u = t_r$ , we obtain the relation

$$\epsilon - t_u = 1 - 0.1 t_u \quad \dots (14)$$

Similarly,  $t_l$  is expressed in terms of  $t_r$  by the following equations

$$t_r = 10(\epsilon - t_l + t_l - 1), \quad t_l \leq t_r \quad \dots (15)$$

$$t_l = \log_e \frac{10(\epsilon t_l - 1)}{9 t_l}, \quad t_l \geq t_r \quad \dots (16)$$

In the case of step-function response ( $t_r = 0$ ), we have from (16),

$$\lim_{t_r \rightarrow 0} [t_l] = 0.105360$$

When  $t_l = t_r$ ,

$$\epsilon - t_l = 1 - 0.9 t_l \quad \dots (17)$$

Solving (17) numerically, we obtain the corresponding value of  $t_l$  to be 0.214559. In figure 14 we have plotted  $t_u$ ,  $t_l$  and  $T_r$  against rise time  $t_r$  of the input pulse. In the same figure we have drawn the curve  $(T_r - 0.8 t_r)$  versus  $t_r$  to show clearly the contribution of the pulse amplifier to the increase of rise time of the reproduced pulse. It is found that the increase of rise time is significant at small values of  $t_r$ . When  $t_r \geq 9.0$ ,  $(T_r - 0.8 t_r)$  is less than 0.2. This shows that with the decrease of steepness of pulse-fronts the faithfulness of amplification improves to a large extent.

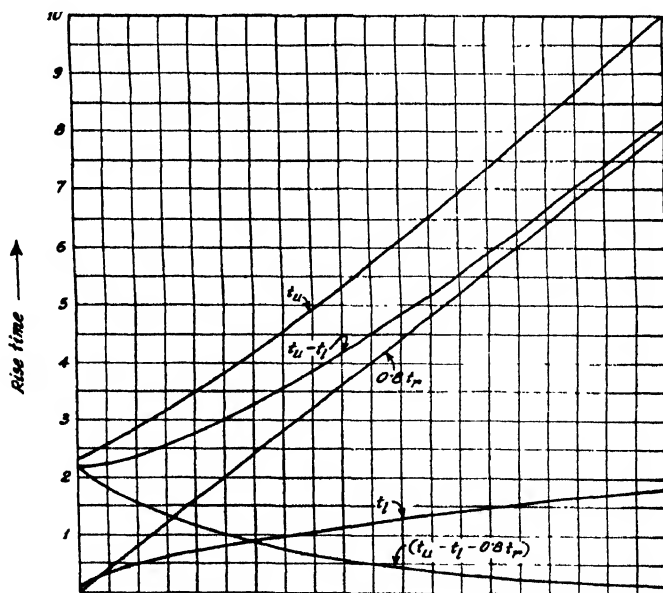


Fig. 14. A plot of rise time of the output pulse as a function of  $t_r$ .

The delay time  $t_d$  is related to the rise time  $t_r$  of the input pulse by the expressions :

$$t_r = 2(e^{-t_d} + t_d - 1), \quad t_d \leq t_r \quad (18)$$

and

$$t_d = \log_e \frac{2(e^{t_r} - 1)}{t_r} \quad t_d \geq t_r \quad (19)$$

When  $t_r$  tends to zero, we can find out  $t_d$  with the help of (19).

Thus,

$$\lim_{t_r \rightarrow 0} [t_d] = \log_e 2 = 0.693147 \quad \dots (20)$$

which is the expression of the delay time in the case of step function input.

When  $t_d = t_r$ , both (18) and (19) lead to the equation

$$e^{-t_d} = 1 - 0.5 t_d \quad \dots (21)$$

Solving (21) numerically we obtain this particular value of  $t_d$  to be

$$t_d = 1.593624 = t_r$$

A plot of delay time  $t_d$  versus  $t_r$  is given in figure 15. In the same figure the curve of  $(t_d - 0.5 t_r)$  against  $t_r$  is also drawn. The delay of reproduction caused by the pulse amplifier is practically constant and nearly equal to one in terms of  $RC$  when  $t_r > 5$ . At smaller values of  $t_r$  the delay curve slightly drops to assume the limiting value 0.6931 in the case of step-function response ( $t_r = 0$ ). So we can conclude that while the steepness of pulse fronts decreases the delay introduced by the amplifier does not increase appreciably. It increases from its value 0.6931 at  $t_r = 0$  (step-function input) to 0.910203 at  $t_r = 3$  and increases slowly to approach unity asymptotically as  $t_r$  increases beyond this value.

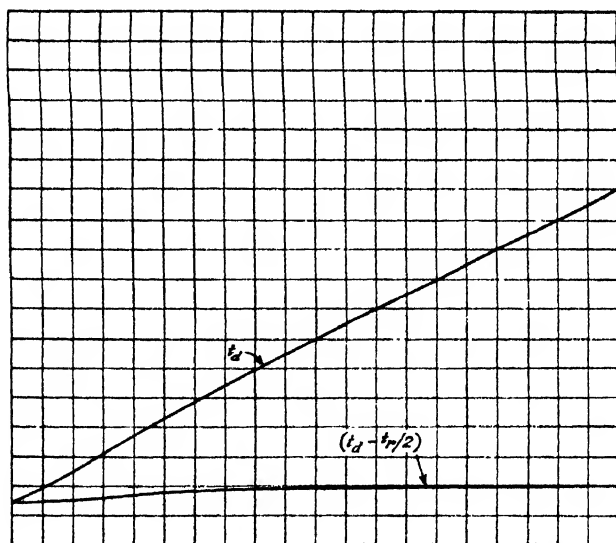


Fig. 15. A plot of delay time of the output pulse as a function of  $t_r$ .

## RESPONSE TO A PULSE WITH LINEAR RISE AND FALL

It will be assumed that for the purpose of finding out the response it is sufficient to consider only the high frequency equivalent circuit of the amplifier (figure 6).

The output voltage  $e_o(p)$  is given by the expression

$$e_o(p) = \frac{g_m R}{1 + pCR} \left[ \frac{1}{p^2 t_1} - \frac{t_2}{t_1(t_2 - t_1)} \cdot \frac{e^{-pt_1}}{p^2} + \frac{1}{(t_2 - t_1)} \cdot \frac{e^{-pt_2}}{p^2} \right] \dots (22)$$

If we normalize (22) by substituting  $t = t/RC$  and  $e_o(t) = e_o(t) 'g_m R$ , we have

$$e_o(p) = \frac{1}{(1+p)} \left[ \frac{1}{p^2 t_r} - \frac{t_f}{t_r(t_f - t_r)} \cdot \frac{e^{-pt}}{p^2} + \frac{1}{(t_f - t_r)} \cdot \frac{e^{-pt_f}}{p^2} \right] \dots (23)$$

where

$$t_r = t_1/RC \text{ and } t_f = t_2/RC.$$

Taking the inverse Laplace transform of (23), we obtain

$$e_o(t) = \frac{e^{-t} + (t-1)}{t_r}, \quad 0 \leq t \leq t_r, \quad \dots (24)$$

$$e_o(t) = \frac{e^{-t}}{t_r} \left[ 1 - \frac{t_f}{t_f - t_r} \cdot e^{t_r} \right] - \frac{t - t_f - 1}{t_f - t_r} e^{-t}, \quad t_r \leq t \leq t_f \quad \dots (25)$$

$$\text{and} \quad e_o(t) = \frac{e^{-t}}{t_r} \left[ 1 - \frac{t_f e^{t_r} - t_r e^{t_f}}{(t_f - t_r)} \right], \quad t \geq t_f \quad \dots (26)$$

The nature of the response is illustrated in figures 16-20, where the effect of variation of  $t_r$  and  $t_f$  is shown clearly.

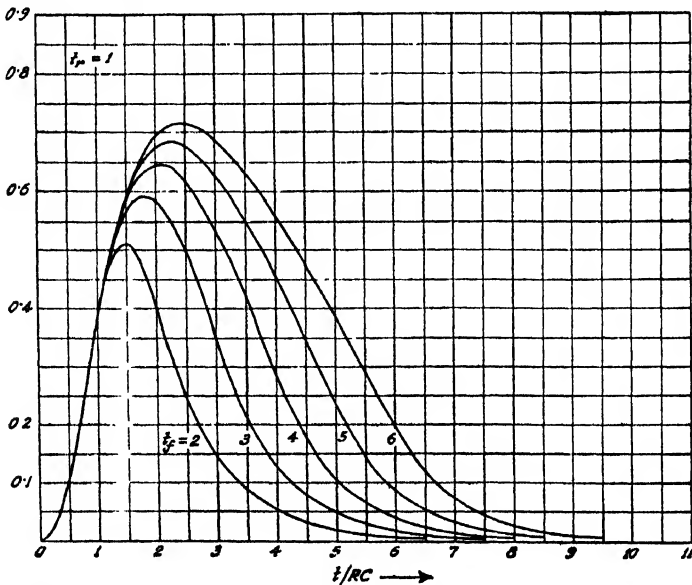


Fig. 16. Response of an RC-coupled pulse amplifier to a pulse with linear rise and fall (rise time =  $RC$ ),



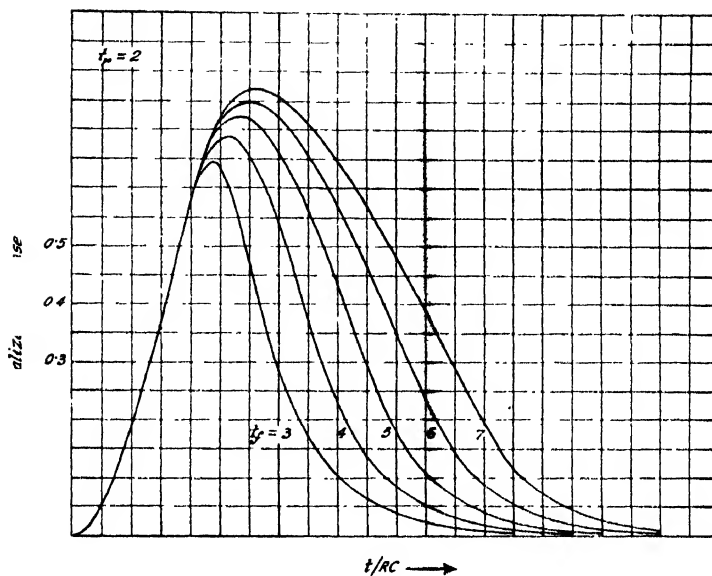


Fig. 17. Response of an  $RC$ -coupled pulse amplifier to a pulse with linear rise and fall (rise time  $= 2RC$ ).

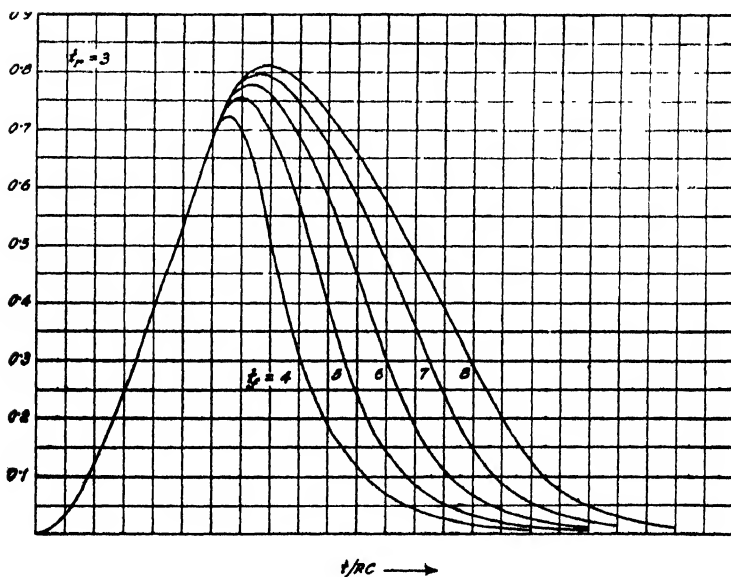


Fig. 18. Response of an  $RC$ -coupled pulse amplifier to a pulse with linear rise and fall (rise time  $= 3RC$ ).

It is interesting to note that the maximum amplitude gradually increases as the steepness of fall is reduced for a constant time of rise. The maximum amplitude of the output voltage occurs at a time which lies in the interval  $t_r \leq t_m \leq t_f$ . So  $t_m$  can be determined by solving the equation obtained by

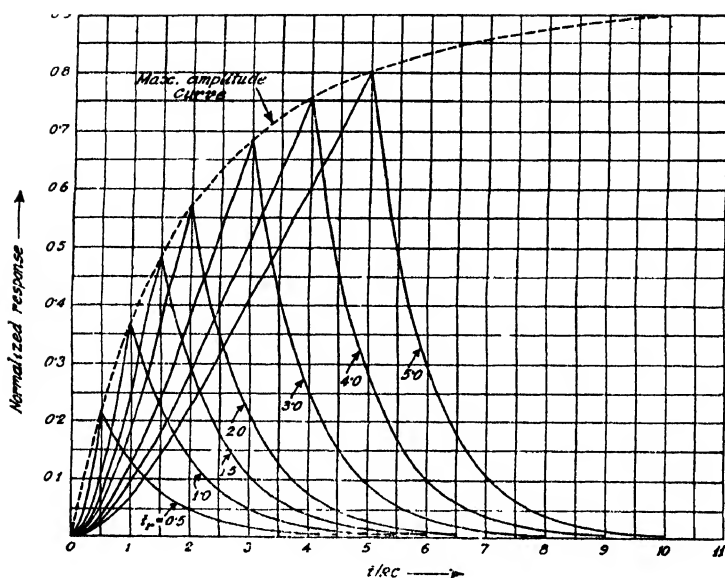


Fig. 22. Response of an RC-coupled pulse amplifier to a saw-tooth pulse with variable rise time. The maximum amplitude versus  $t_r$  curve is shown in dotted lines.

It is evident from the plot that the maximum output occurs at  $t = t_r$ . The maximum amplitude curve as a function of  $t_r$  is given by the equation

$$e_0(t_r) = \frac{e^{-t_r} + (t_r - 1)}{t_r} \quad (32)$$

The maximum amplitude curve is shown in dotted line in figure 22.

### CONCLUSION

The object of this paper is to show the changes of response characteristics with the variation of steepness of pulse fronts. It has been shown that a resistance-coupled pulse amplifier does not increase the rise time of the reproduced pulse appreciably if the input pulse has a rise time much greater than  $RC$  (e.g.,  $t_1 = 9RC$ ). It has a major contribution only if the steepness of the input pulse front is very great (e.g.,  $t_1 = 0.2$  or  $0.5 RC$ ). The additional delay introduced by the amplifier to reproduce the input pulse has a value practically equal to  $RC$  when  $t_1 > 5RC$ . It has a minimum value in the case of a step function input pulse. Figure 15 will furnish a ready information about the exact delay time corresponding to a specified  $t_r$ .

In the case of pulses with linear rise and fall, it has been noted that the maximum amplitude of the output pulse and the time which corresponds to this maximum, are directly related to times of both rise and fall.

Though the nature of the responses in every case may be drawn from physical principles, a mathematical treatment of the response characteristics of pulse amplifiers to various types of input is necessary for accurate assump-

tions regarding the design and performance of amplifiers. In this paper we have only discussed about the responses of a simple resistance-coupled amplifier. In a future communication we shall make an attempt to give a detailed analysis regarding the effects of negative feed-back and shunt-compensation on the response characteristics.

#### ACKNOWLEDGMENTS

The author is deeply indebted to Prof. M. N. Saha, D.Sc., F.R.S. and Prof. B. D. Nag, Ph.D., for their kind interest in the work. He also wishes to express his gratefulness to Mr. B. M. Banerjee for his valuable advice and suggestions during the progress of the work.

#### REFERENCES

- Bhattacharyya, B. K., 1953, *Ind. J. Phys.*, **27**, 209.  
Gardner, M. F. and Barnes, J. L., 1948, *Transients in Linear Systems*, Vol. 1, Wiley, New York.  
Gillespie, A. B., 1947, *A. E. R. E. Report, G/R 118*, August.  
*Ibid*, **168**, February.  
Moskowitz, S. and Racker J., 1951, *Pulse Techniques*, Prentice-Hall, Inc., New York.  
Valley, G. E., and Wallman, H., 1949, *Vacuum Tube Amplifiers*, McGraw-Hill Book Co., Inc., New York.

# INTENSITY FORMULAE FOR BANDS INVOLVING HIGH MULTIPLICITY TERMS. PART III. ${}^6\Pi - {}^6\Sigma$ AND ${}^6\Pi - {}^6\Pi$ TRANSITIONS

By D. PREMASWARUP

DEPARTMENT OF PHYSICS, ANDHRA UNIVERSITY, WALTAIR

(Received for publication, November 6, 1953)

**ABSTRACT.** In continuation of the author's previous work on bands involving high multiplicity terms, intensity formulae have been derived for bands due to the transitions  ${}^6\Pi - {}^6\Sigma$  and  ${}^6\Pi - {}^6\Pi$ .

This paper presents the results of the calculations on the intensity distribution in the different rotational branches of bands belonging to  ${}^6\Pi - {}^6\Sigma$  and  ${}^6\Pi - {}^6\Pi$  transitions. The relevant methods adopted and the necessary formulae were given in the earlier communications (Parts I and II of this series) by the author. The calculated intensity factors are given in Tables I and II respectively. As in the previous papers, here too the intensity factors are given only for the two limiting cases of coupling, (a) and (b) of the upper and lower states. Further, these factors are shown only for a limited number of branches, namely, all those for which  $\Delta K = \Delta J = 0, \pm 1$ , i.e., the main branches, while among branches for which  $\Delta K$  has other values, only one representative branch is included for each  $\Delta K$  value, the others being omitted for the sake of brevity.

From a study of the tables, conclusions that can be drawn are similar to those applying for quintet and lower multiplicity transitions. Thus in  ${}^6\Pi - {}^6\Sigma$  transition if the two states belong to the same coupling case the main branches (with  $\Delta K = \Delta J = 0, \pm 1$ ) will be the most intense with the  $Q$ -branches twice as intense as the  $P$ - or  $R$ - branches, and satellite branches with  $\Delta K = 0, \pm 1$ , less intense and rapidly falling in intensity with increasing  $J$ ; while if the two states belong to different coupling cases all the branches (108 in number) will be equally intense. Another interesting conclusion is that in the main branches the intensities of the six components (either the  $P$ -,  $Q$ - or  $R$ -branches) are in the ratio 1 : 9 : 4 : 4 : 9 : 1 when both states belong to different coupling cases while they are of equal intensities if both states belong to the same coupling case. In practical cases, however, where the  $\Pi$  state belongs to an intermediate state of coupling between (a) and (b), the main branches will be the most intense (with the  $Q$ - branch more intense than either  $P$ - or  $R$ -) and the satellite branches (which are very much less intense than the main branches) decrease in intensity with increasing value of  $|\Delta K|$  and cannot be observed beyond a value of about 3 for  $|\Delta K|$ .

TABLE I

Intensity factors for  ${}^6\Pi-{}^6\Sigma$  bands

Branches		Intensity factors	
${}^6\Pi \rightarrow {}^6\Sigma$	${}^6\Sigma \rightarrow {}^6\Pi$	${}^6\Pi(a)$	${}^6\Pi(b)$
$P_1(J)$	$R_1(J-1)$	$\frac{(2J+5)^2(2J+3)^2}{128J^2(J-1)}$	$\frac{(2J+1)(2J-7)}{(J-2)}$
$Q_1(J)$	$Q_1(J)$	$\frac{(2J+5)^2(2J+3)(2J+1)(2J-3)}{128(J+1)J^2(J-1)}$	$\frac{4(J+1)(2J+1)(2J-5)}{J(2J-3)}$
$R_1(J)$	$P_1(J+1)$	$\frac{(2J+5)(2J+3)(2J-1)(2J-3)}{128(J+1)J(J-1)}$	$\frac{(2J+3)(2J-1)}{(J-1)}$
$P_2(J)$	$R_2(J-1)$	$\frac{9(2J+3)^2(2J+1)(2J-3)}{128(J+1)J^2}$	$\frac{(J+1)(2J+1)(2J-5)^2}{J(J-1)(2J-3)}$
$Q_2(J)$	$Q_2(J)$	$\frac{9(2J+3)^2(2J+1)(2J-1)(2J-3)}{128(J+1)J^2J^2}$	$\frac{4(2J+1)(2J^2-J-8)^2}{(J+1)J(2J-1)(2J-3)}$
$R_2(J)$	$P_2(J+1)$	$\frac{9(2J+3)(2J+1)(2J-1)(2J-3)}{128(J+1)J^2}$	$\frac{(J+2)(2J+3)(2J+1)(2J-3)}{(J+1)J(2J-1)}$
$P_3(J)$	$R_3(J-1)$	$\frac{(2J+3)(2J+1)(2J-1)^2}{32(J+1)J(J-1)}$	$\frac{(2J+3)(J+1)(2J-3)^2(J-2)}{J^2(2J-1)(J-1)}$
$Q_3(J)$	$Q_3(J)$	$\frac{(2J+3)(2J+1)^3(2J-1)}{32(J+1)^2J(J-1)}$	$\frac{4(2J^2+J-9)^2}{(J+1)J(2J-1)}$
$R_3(J)$	$P_3(J+1)$	$\frac{(2J+3)^2(2J+1)(2J-1)}{32(J+1)^2(J-1)}$	$\frac{(2J+5)(J+2)(2J+3)(2J-1)(J-1)}{(J+1)^2(2J+1)J}$
$P_4(J)$	$R_4(J-1)$	$\frac{(2J+3)(2J-1)^2(2J-3)}{32(J+2)J^2}$	$\frac{(J+2)(2J+3)(2J-1)(J-1)(2J-3)}{(J+1)(2J+1)J^2}$
$Q_4(J)$	$Q_4(J)$	$\frac{(2J+3)^2(2J+1)(2J-1)^2}{32(J+2)(J+1)J^2}$	$\frac{4(2J^2+3J-8)^2}{(2J+3)(J+1)J}$
$R_4(J)$	$P_4(J+1)$	$\frac{(2J+5)(2J+3)^2(2J-1)}{32(J+2)(J+1)J}$	$\frac{(J+3)(2J+5)^2J(2J-1)}{(J+2)(2J+3)(J+1)^2}$
$P_5(J)$	$R_5(J-1)$	$\frac{9(2J+5)(2J-1)(2J-3)(2J-5)}{128(J+1)J^2}$	$\frac{(2J+5)(2J+1)(2J-1)(J-1)}{(2J+3)(J+1)J}$
$Q_5(J)$	$Q_5(J)$	$\frac{9(2J+5)^2(2J+1)(2J-1)(2J-3)}{128(J+1)^2J^2}$	$\frac{4(2J+1)(2J^2+5J-5)^2}{(2J+5)(2J+3)(J+1)J}$
$R_5(J)$	$P_5(J+1)$	$\frac{9(2J+7)(2J+5)^2(2J-1)}{128(J+1)^2J}$	$\frac{(2J+7)^2(2J+1)J}{(2J+5)(J+2)(J+1)}$
$P_6(J)$	$R_6(J-1)$	$\frac{(2J-1)(2J-3)(2J-5)(2J-7)}{128(J+2)(J+1)J}$	$\frac{(2J+3)(2J-1)}{(J+2)}$
$Q_6(J)$	$Q_6(J)$	$\frac{(2J+7)(2J+1)(2J-1)(2J-3)(2J-5)}{128(J+2)(J+1)^2J}$	$\frac{4(2J+1)J(2J+7)}{(2J+5)(J+1)}$
$R_6(J)$	$P_6(J+1)$	$\frac{(2J+9)(2J+7)(2J-1)(2J-3)}{128(J+2)(J+1)^2}$	$\frac{(2J+9)(2J+1)}{(J+3)}$
${}^K P_{16}(J)$	${}^W R_{61}(J-1)$	$\frac{(2J+5)(2J+3)(2J-1)(2J-3)}{128(J+2)(J+1)J}$	

TABLE I (contd)

Branches		Intensity factors	
${}^6\Pi \rightarrow {}^6\Sigma$	${}^6\Sigma \rightarrow {}^6\Pi$	${}^6\Pi(a)$	${}^6\Pi(b)$
${}^6P_{26}(f)$	${}^6R_{62}(f-1)$	$\frac{5(2f+5)(2f+3)(2f+1)(2f-1)}{128(f+2)(f+1)f}$	0
${}^6P_{16}(f)$	${}^6P_{63}(f-1)$	$\frac{5(2f+5)(2f+3)(2f+1)(2f-1)}{64(f+2)(f+1)f}$	0
${}^6P_{36}(f)$	${}^6R_{61}(f-1)$	$\frac{5(2f+5)(2f+3)(f-1)(2f-3)}{64(f+2)(f+1)f}$	0
${}^6P_{56}(f)$	${}^6R_{65}(f-1)$	$\frac{5(2f+5)(2f-1)(2f-3)(2f-5)}{128(f+2)(f+1)f}$	0
${}^6Q_{66}(f)$	${}^6Q_{65}(f)$	$\frac{5(2f+5)^2(2f+1)(2f-1)(2f-3)}{128(f+2)(f+1)^2f}$	$\frac{5(2f+3)(2f+1)}{(2f+5)(f+2)(f+1)}$
${}^6Q_{21}(f)$	${}^6Q_{12}(f)$	$\frac{5(2f+3)^2(2f+1)(2f-1)(2f-3)}{128(f+1)f^2(f-1)}$	$\frac{5(2f+1)(2f-1)}{f(f-1)(2f-3)}$
${}^6R_{21}(f)$	${}^6P_{12}(f+1)$	$\frac{5(2f+3)(2f+1)(2f-1)(2f-3)}{128(f+1)f(f-1)}$	0
${}^6R_{31}(f)$	${}^6P_{13}(f+1)$	$\frac{5(2f+3)(2f+1)(2f-1)(2f-3)}{64(f+1)(f-1)}$	0
${}^6R_{41}(f)$	${}^6P_{14}(f+1)$	$\frac{5(2f+5)(2f+3)(2f-1)(2f-3)}{64(f+1)f(f-1)}$	0
${}^6R_{51}(f)$	${}^6P_{15}(f+1)$	$\frac{5(2f+7)(2f+5)(2f+3)(2f-3)}{128(f+1)f(f-1)}$	0
${}^6R_{61}(f)$	${}^6P_{16}(f+1)$	$\frac{(2f+6)(2f+7)(2f+5)(2f+3)}{128(f+1)f(f-1)}$	0

TABLE II  
Intensity factors for  $\Pi^6 - {}^6\Pi$  bands

Branch	${}^6\Pi(a) \rightarrow {}^6\Pi(a)$	${}^6\Pi(a) \rightarrow {}^6\Pi(b)$	${}^6\Pi(a) \rightarrow {}^6\Pi(b)$
$P_1(f)$	$\frac{(2f+3)(2f-3)}{f}$	$\frac{(2f+3)^2(2f-3)(2f-5)}{128f^2(f-1)}$	$\frac{(2f+1)(2f-3)(2f-7)}{(f-2)(2f-5)}$
$Q_1(f)$	$\frac{9(2f+1)}{(f+1)f}$	$\frac{9(2f+3)(2f+1)(2f-5)}{128(f+1)f^2(f-1)}$	$\frac{16(f+1)(2f+1)}{f(2f-3)^2}$
$R_1(f)$	$\frac{(2f+5)(2f-1)}{(f+1)}$	$\frac{(2f+5)(2f+3)(2f-1)(2f-5)}{128(f+1)f(f-1)}$	$\frac{(2f+3)(2f-1)(2f-5)}{(f-1)(2f-3)}$
$P_2(f)$	$\frac{(2f+1)(2f-1)}{f}$	$\frac{(6f+1)^2(2f+1)(2f-1)}{128(f+1)f^2}$	$\frac{(f+1)(2f+1)(2f-1)(2f-5)^2}{f(f-1)(2f-3)^2}$
$Q_2(f)$	$\frac{(2f+1)}{(f+1)f}$	$\frac{(6f+1)^2(2f+1)}{128(f+1)^2f^2}$	$\frac{16(2f+1)(2f^2-f-8)^2}{(f+1)f(2f-1)^2(2f-3)^2}$
$R_2(f)$	$\frac{(2f+3)(2f+1)}{(f+1)}$	$\frac{(6f+1)^2(2f+3)(2f+1)}{128(f+1)^2f}$	$\frac{(f+2)(2f+3)(2f+1)(2f-3)^2}{(f+1)f(2f-1)^2}$
$P_3(f)$	$\frac{(2f+1)(2f-1)}{f}$	$\frac{(2f+3)(2f-1)(2f-5)^2}{32(f+1)f(f-1)}$	$\frac{(2f+3)(f+1)(2f+1)(2f-3)^2(f-2)}{f^2(2f-1)^2(f-1)}$

TABLE II (contd.).

Branch	${}^6\Pi(a) \rightarrow {}^6\Pi(a)$	${}^6\Pi(a) \rightarrow {}^6\Pi(b)$	${}^6\Pi(a) \rightarrow {}^6\Pi(b)$
$Q_4(f)$	$\frac{(2f+1)}{(f+1)f}$	$\frac{(2f+3)(2f-5)^2}{32(f+1)^2(f-1)}$	$\frac{15(2f^2+7-5)^2}{(f+1)(f+1)f(2f-1)^2}$
$R_3(f)$	$\frac{(2f+3)(2f+1)}{(f+1)}$	$\frac{(2f+3)^2(2f-5)^2}{32(f+1)^2(f-1)}$	$\frac{(f+5)(f+2)(2f+3)(2f-1)^2(f-1)}{(f+1)^2(2f+1)^2(f+1)}$
$P_4(f)$	$\frac{(2f+3)(2f-3)}{f}$	$\frac{(2f-3)(4f^2-4f-39)^2}{32(f+2)(2f+1)f^2}$	$\frac{(f+2)(2f+3)^2(2f-1)(f-1)(2f-3)}{(f+1)(f+1)^2f^2}$
$Q_4(f)$	$\frac{9(2f+1)}{(f+1)f}$	$\frac{9(1f^2-1f-39)^2}{32(f+2)(2f+3)(f+1)f^2}$	$\frac{15(2f^2+3f-8)^2}{(2f+3)^2(f+1)(2f+1)f}$
$R_4(f)$	$\frac{(2f+5)(2f-1)}{(f+1)}$	$\frac{(2f+5)(2f-1)(4f^2-4f-39)^2}{32(f+2)(2f+3)(f+1)(2f+1)f}$	$\frac{(f+3)(2f+5)^2(2f+1)(2f-1)}{(f+2)(2f+3)^2(f+1)^2}$
$P_5(f)$	$\frac{(2f+5)(2f-5)}{f}$	$\frac{(6f+25)^2(2f-1)(2f-3)(2f-5)}{128(2f+3)(f+1)f^2}$	$\frac{(2f+5)^2(2f+1)(2f-1)(f-1)}{(2f+3)^2(f+1)f}$
$Q_5(f)$	$\frac{25(2f+1)}{(f+1)f}$	$\frac{25(6f+25)^2(2f+1)(f-1)(2f-3)}{128(2f+5)(2f+3)(f+1)^2f^2}$	$\frac{15(2f+1)(2f^2+5f-5)^2}{(2f+5)^2(f+3)^2(f+1)f}$
$R_5(f)$	$\frac{(2f+7)(2f-3)}{(f+1)}$	$\frac{(6f+25)^2(2f+7)(2f-1)(2f-3)^2}{128(2f+5)(2f+3)(f+1)^2f}$	$\frac{(2f+7)^2(2f+5)(2f+1)f}{(2f+5)^2(f+2)(f+1)}$
$P_6(f)$	$\frac{(2f+7)(2f-7)}{f}$	$\frac{(2f+7)(2f-1)(2f-3)(2f-5)(2f-7)}{128(2f+5)(f+2)(f+1)f}$	$\frac{(2f+7)(2f+3)(2f-1)}{(2f+5)(f+2)}$
$Q_6(f)$	$\frac{49(2f+1)}{(f+1)f}$	$\frac{49(2f+1)(2f-1)(2f-3)(2f-5)}{128(2f+5)(f+2)(f+1)^2f}$	$\frac{16(2f+1)f}{(2f+5)^2(f+1)}$
$R_6(f)$	$\frac{(2f+9)(2f-5)}{(f+1)}$	$\frac{(2f+9)(2f+1)(2f-3)(2f-5)^2}{128(2f+5)(f+2)(f+1)^2}$	$\frac{(2f+9)(2f+5)(2f+1)}{(2f+7)(f+3)}$
$KP_{16}(f)$	0	$\frac{(2f+7)(2f+3)(2f-1)(2f-3)}{128(f+2)(f+1)f}$	0
$LP_{26}(f)$	0	$\frac{5(2f+7)(2f+3)(2f+1)(2f-1)}{128(f+2)(f+1)f}$	0
$VP_{36}(f)$	0	$\frac{5(2f+7)(2f+3)(2f+1)(2f-1)}{64(f+2)(f+1)f}$	0
$VP_{46}(f)$	0	$\frac{5(2f+7)(2f+3)(2f-1)(2f-3)}{64(f+2)(f+1)f}$	0
$VP_{56}(f)$	0	$\frac{5(2f+7)(2f-1)(2f-3)(2f-5)}{128(f+2)(f+1)f}$	0
$PQ_{56}(f)$	0	$\frac{125(2f+7)(2f+1)(2f-1)(2f-3)}{128(2f+5)(f+2)(f+1)^2f}$	$\frac{5(2f+7)(2f+3)(2f+1)}{(2f+5)^2(f+2)(f+1)}$
$RQ_{21}(f)$	0	$\frac{5(2f+1)(2f-1)(2f-5)}{128(f+1)f^2(f-1)}$	$\frac{5(2f+1)(2f-1)(2f-5)}{f(f-1)(2f-3)^2}$
$SR_{21}(f)$	0	$\frac{5(2f+3)(2f+1)(2f-1)(2f-5)}{128(f+1)f(f-1)}$	0
$TR_{31}(f)$	0	$\frac{5(2f+3)(2f+1)(2f-1)(2f-5)}{64(f+1)f(f-1)}$	0
$VR_{41}(f)$	0	$\frac{5(2f+5)(2f+3)(2f-1)(2f-5)}{64(f+1)f(f-1)}$	0
$VR_{51}(f)$	0	$\frac{5(2f+7)(2f+5)(2f+3)(2f-5)}{128(f+1)f(f-1)}$	0
$WR_{61}(f)$	0	$\frac{(2f+9)(2f+7)(2f+5)(2f+3)(2f-5)}{128(f+1)f(f-1)(2f-3)}$	0

For  ${}^6\Pi - {}^6\Pi$  transition also exactly similar considerations hold good except that the  $Q$ - branches are here weaker than the  $P$ - or  $R$ - branches and fall very rapidly in intensity with increasing  $J$  unlike the  $P$ - or  $R$ - branches which increase in intensity with increasing  $J$  attaining a maximum and then falling off in intensity with increasing  $J$ .

#### ACKNOWLEDGMENT

The author wishes to acknowledge his deep indebtedness to Prof. K. R. Rao for his invaluable guidance in carrying out this work.

#### REFERENCES

- Premaswarup, D., 1953, *Ind. J. Phys.*, **27**, 415.  
Premaswarup, D., 1953, *Ind. J. Phys.*, **27**, 578.



# IONIZATION DISTRIBUTION IN THE F-REGION

By B. CHATTERJEE\*

INSTITUTE OF RADIO PHYSICS AND ELECTRONICS, UNIVERSITY OF CALCUTTA

(Received for publication, January 12, 1951)

**ABSTRACT.** The height distribution of ionization in the composite F-region is calculated on the assumptions that the scale height (*i.e.*, the temperature) increases and the recombination coefficient decreases with height in this region. The recombination coefficient is assumed to vary in terms of the reduced height, that is the height (above  $F_1 \text{ max}$ ) measured in terms of the scale height and not in terms of the actual height as had been done earlier by A. P. Mitra in making similar calculations. The present assumption automatically takes into account the effect of rising temperature on the value of the recombination coefficient. Height distribution curves for high and low latitude stations are drawn for typical summer and winter conditions in the high atmosphere in the F-region. It is found that when the possible effects of ionospheric tidal drifts are taken into account, the forms of the distribution curves, as also the separation between the  $F_1$  and  $F_2$ -layers, agree with those deduced from observational data. The investigation lends support to the hypothesis that the ionospheric regions  $F_1$  and  $F_2$  belong to a common bank of ionization produced by a common ionizing radiation from the sun.

## 1. INTRODUCTION

According to current ideas, the higher regions of the ionosphere,  $F_1$  and  $F_2$ , owe their ionizations to a common ionizing radiation from the sun (the radiation ionizing O atom at its first ionization potential). It is supposed that owing to the peculiar physical characteristics of the atmosphere prevailing in these high regions and/or due to air motions resulting from tidal forces, two ionization maxima, instead of the usual single one due to the Chapman process, are produced in a single bank of ionization. The physical characteristics that lead to this double maxima are two-fold, namely, increase of temperature (*i.e.*, scale height) and rapid decrease of recombination coefficient with height from above the  $F_1$ -maximum. These may be compared to the two opposite effects, *viz.* decreasing intensity of ionizing radiation and increasing density of ionizable particles with depth of penetration of the solar rays which lead to the production of the Chapman maximum of ionization. This idea regarding the process of bifurcation of the F-region into  $F_1$  and  $F_2$  was first suggested by Mohler (1940) and was later extended by Bates and Massey (1946).

The tidal hypothesis for the production of the double maxima was put forward by Martyn (1947). According to this hypothesis the  $F_2$ -maximum is produced above the normal  $F_1$ -maximum by the vertical motion of ions under the influence of geomagnetic field. However, though the effects of

\* Communicated by Prof. S. K. Mitra.

tides is considered to be significant in modifying the parameters of the  $F_2$ -region, it does not appear to be large enough to produce the two maxima.

As a test of the first hypothesis one may examine quantitatively if the observed rates of decrease of recombination coefficient and increase of temperature with height do actually lead to the bifurcation process. A closer test would be to see if the various phenomena associated with bifurcation *e.g.*, diurnal, seasonal and latitudinal variations of the  $F_1$ - $F_2$  separation follow as necessary consequences of the probable height variation of these two parameters. The simpler first-mentioned test was carried out by A. P. Mitra (1952). He made a detailed study of the doubling process of the  $F$ -region by taking the effects of the changing scale height and changing recombination coefficient into account. His formula, however, gave a steady increase of ionization density with height in the  $F_2$ -region under equilibrium condition (*i.e.*, for  $dN/dt=0$ ). He, therefore, argued that the equilibrium condition is seldom attained in this region and introduced a correction factor for the same. When this was done, a second ionization maximum corresponding to the  $F_2$ -layer was obtained.

In the present paper the hypothesis is examined anew with a somewhat modified assumption regarding the nature of the height variation of the recombination coefficient ( $\alpha$ ). It is assumed that  $\alpha$  is a function of the reduced height  $z \left( = \frac{h-h_0}{H} \right)$  rather than simply of the height  $h$  as assumed by A. P. Mitra. This assumption makes the initial rate of fall of  $\alpha$  with height much sharper and automatically takes into account the effects of varying temperature. Further, it is found that when the possible effects of ionospheric tidal drifts are superposed, the forms of the distributions, as also the observed variations of the  $F_1$ - $F_2$  separation, agree with the observed data.

The assumptions made regarding the variations of temperature and recombination coefficient with height are based on observed data and discussed in the following section.

## 2. ASSUMPTIONS MADE REGARDING THE PHYSICAL PROPERTIES OF THE UPPER ATMOSPHERE AT THE $F$ -REGION HEIGHT

Evidences, partly direct and partly indirect *e.g.*, works of Martyn and Pulley (1936) and rocket data (Mitra, 1952, p. 549) indicate that the upper atmospheric temperature begins to rise from a height of about 85 km, and that the rise continues up to about 400 km, after which the temperature falls gradually with height, to merge itself with the interstellar temperature. The exact nature of the temperature rise with height is not known but it is generally assumed to be linear, *e.g.*, the standard temperature distribution adopted by the National Advisory Committee for Aeronautics, U.S.A. and

the temperature distribution in the 'model atmosphere' as assumed by Gerson (1951). Of course, all the methods of temperature determination in the F<sub>2</sub>-region are indirect and the conclusion of Maeda and Fukada, "It, therefore, seems that the theory involving the temperature of the F<sub>2</sub>-region is unnatural", can hardly be refuted. But in the present state of our knowledge and technique we have to be satisfied with these results.

We may, therefore, write, for the temperature  $T$  at any height  $h$  as,

$$T = T_0 + bh$$

where  $T_0$  is the temperature at the reference level ( $h=0$ ) and  $b$  is the height gradient.

Since the scale height is defined by  $H = KT/mg$ , one may also write,

$$H = K(T_0 + bh)/mg = H_0 + \beta h, \quad \dots (1)$$

where

$$H_0 = KT_0/mg$$

and  $\beta$  is the scale height gradient (The variation of  $g$  with height is neglected).  $T_0$  and  $b$  vary with the hour of the day and the season of the year and we shall adopt the distributions as given by Gerson. It may be mentioned in this connection that the value of  $T$  (and hence of  $H$ ), as adopted in the model atmosphere of Gerson, was obtained not only from electron concentration but also from collisional frequency and luminosity curves and filter photographs of northern aurorae. Thus one is justified in assuming these values for finding the electron distribution in the F-region.

Regarding the variation of recombination coefficient in the F-region, ionospheric observations show that it is much less (about one order) in the F<sub>2</sub>-region than in the F<sub>1</sub>-region. It is also satisfactory to note that according to the theoretical expressions for the recombination coefficient, or rather the effective recombination coefficient ( $\alpha$ ) that have been suggested  $\alpha$  will decrease with height. For example, we have two expressions for  $\alpha$ , both due to Bates and Massey (1946, 1950).

$$\alpha = \alpha_r + \lambda \alpha_i$$

where

$$\lambda = \frac{Bn}{\gamma_1 B + \alpha_i N_e}$$

and

$$\alpha = \frac{\alpha(d)n(O)}{N_e}$$

In the above expressions,

$B$  = coefficient of attachment of electrons to neutral atoms and molecules ;

$n$  = number density of neutral particles ;

$N_e$  = number density of electrons ;

$BN - \gamma_1$  = rate of loss of negative ions due to photo-detachment of electrons ;

$\alpha_i$  = coefficient of mutual neutralisation of positive and negative ions ;

$\alpha(d)$  = coefficient of dissociative recombination ;

$n(O)$  = number density of oxygen atoms.

It is seen that according to the first expression,  $\alpha$  diminishes with height

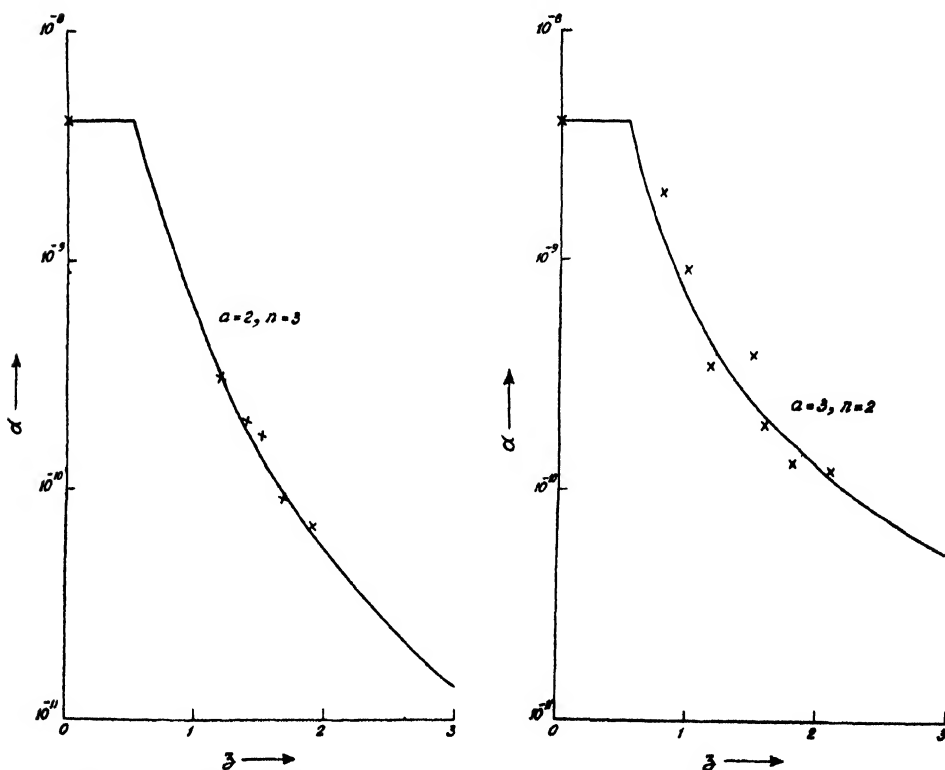
because  $n$  decreases and  $N_e$  increases with height in the  $F_2$ -region. The same is also true for the second expression because  $n(0)$  decreases and  $N_e$  increases with height.

It may also be mentioned that according to some investigators, the variation of  $\alpha$  in the  $F_2$ -region may be attributed to the height variations of temperature and pressure in this region (Baral and Mitra, 1951)

On account of these complicating factors, it is not possible, in the present state of our knowledge, to give any law of height variation of  $\alpha$  that may be strictly acceptable on theoretical grounds. One has, therefore, to be satisfied with empirical relations as may be considered to represent best the observed facts of height variation. We have adopted in our calculation the relation

$$\alpha = \frac{\alpha_0}{(1 + az)^n}$$

where  $\alpha_0$  is the value of  $\alpha$  in the  $F_1$ -region where it is known to be sensibly constant with height. The multiplication factor  $a$  and the power index  $n$  are so chosen as to yield approximately the observed variation of  $\alpha$  with height. It may be mentioned that A. P. Mitra also took a similar power law of varia-



Figs. 1(a) and (b). Variations of  $\alpha$  with  $z$  for high and low latitude stations as assumed in the calculations. The crosses indicate the observed values: (a) for low latitude station, Calcutta and (b) for high latitude station, Slough. It will be noticed that the curve for the assumed parameter values, namely,  $a=2, n=3$ , for curve (a) and  $a=3, n=2$  for curve (b) approximately pass through the mean positions of the observed values.

tion in his calculations, the exponent ( $n$ ) being assumed by him to lie between 2 and 3. In our calculations, we have taken  $n=3$  and  $a=2$  for low latitude stations and  $n=2$  and  $a=3$  for high latitude stations. The calculated height variation of  $\alpha$  with these values of  $a$  and  $n$ , resemble approximately the mean observed variation of  $\alpha$  in the regions concerned. This is shown in figures 1 (a) and 1 (b). The observed values of the parameters used in calculating the experimental points in the graphs are shown in Tables I(a) and I(b).

Calcutta (low latitude) data

Month and year	$\alpha$	$h_m$	$H$	$z$
January, 1953	$2 \times 10^{-10}$	300	70	1.4
February, 1953	$1.7 \times 10^{-10}$	330	87	1.5
August, 1946	$7 \times 10^{-11}$	388	100	1.88
September, 1946	$9.2 \times 10^{-11}$	365	97	1.7
November, 1952	$3 \times 10^{-10}$	300	84	1.2

TABLE I(b)

Slough (high latitude) data

Month and year	$\alpha$	$h_m$	$H$	$z$
February, 1951	$3.5 \times 10^{-10}$	275	63	1.18
April, 1951	$3.9 \times 10^{-10}$	290	60	1.
May, 1951	$2 \times 10^{-10}$	315	72	1.6
June, 1951	$1.35 \times 10^{-10}$	360	84	1.91
July, 1951	$1.25 \times 10^{-10}$	365	80	2.10
September, 1951	$3.9 \times 10^{-10}$	275	62.5	1.2
October, 1951	$9 \times 10^{-10}$	255	54	1.01
December, 1951	$2 \times 10^{-9}$	235	43	0.8

$\alpha$  for 200 km has been taken as  $4 \times 10^{-9}$  (Mitra, 1952, p 291). Cases for which  $h_m$ , the height of maximum ionization density is less than 400 km have only been considered. The simplified relation, as used in the calculations, does not hold good for  $h_m > 400$  km, due to the fall of temperature above this height

The calculations for the Slough data and some of the Calcutta data have been done by the author using the well known method of Appleton. Other data of Calcutta have been taken from the calculations of Baral and Mitra (1951) In Appleton's methods of calculation we have,

$$q = \frac{N_B^2 \frac{dN_A}{dt} - N_A^2 \frac{dN_B}{dt}}{N_B^2 - N_A^2}$$

for values of  $q$  for hours, equally spaced on the two sides of local noon. The subscripts  $A$  and  $B$  give the values for these two equally spaced hours.

Knowing the zenith angle of the sun, the value of  $q$  for noon is calculated and then  $\alpha$  for noon is obtained from the formula,

$$\alpha = \frac{q - \frac{dN}{dt}}{N^2}$$

Now if we assume that  $z_0$  is the height up to which the  $F_1$ -region condition prevails, (i.e.  $\alpha$  remains sensibly constant) we get,

$$\left. \begin{aligned} \alpha &= \alpha_0 ; [ \text{for } z < z_0 ] \\ \alpha &= \frac{\alpha_0}{[1 + a(z - z_0)]^n} ; [ \text{for } z > z_0 ] \end{aligned} \right\} \quad \dots (2)$$

In the analysis to follow, only the noon-time condition (for  $dN/dt = 0$ ) has been considered. This is because analytical solution is possible for this case only. Analysis for the general case has not been attempted because the calculations would have been too laborious, involving successive approximation. This study has been reserved for a future communication.

### 3. STRUCTURE OF THE COMPOSITE F-REGION

In the ideal case of an isothermal atmosphere with constant recombination coefficient and monochromatic ionizing radiation, the distribution of ionization with height under equilibrium condition is given by the well known Chapman (1931) formula,

$$N = N_0 e^{\frac{1}{2}(1 - \sec \chi - \sec \chi_0)} \quad \dots (3)$$

where  $N_0$  = maximum ionization density (for  $z = \chi = 0$ ) formed at a height  $h_0$ .

$N$  = ionization density at any height  $h$ , measured from the reference level.

$\chi$  = solar zenith angle.

This formula, however, is not applicable to regions above the E-region because both scale height (i.e. temperature) and recombination coefficient vary with height.

In the major portion of the  $F_1$ -region, though  $H$  varies appreciably with height, the recombination coefficient does not do so. In this case if  $\alpha$  is regarded as constant, we can write the variation of  $N$  with height, after Nicolet (1951) as

$$N = N_0 e^{\frac{1+\beta}{2}(1 - \sec \chi - \sec \chi_0)} \quad \dots (4)$$

Now, the time rate of change of ionization, when the tidal effect is neglected, is given by

$$\frac{dN}{dt} = q - \alpha N^2 \quad \dots (5)$$

where,  $q$  = the rate of ion production at a height  $h$ , the variation of which with height is (according to Nicolet)

$$q = q_0 e^{(1+\beta)(1-e^{-\alpha z})} \quad (6)$$

For equilibrium condition (near noon)  $\frac{dN}{dt} = 0$ . Hence,  $N = \sqrt{q/\alpha}$ .

Substituting the values of  $q$  from (6) and  $\alpha$  from (2) (for  $z > z_0$ ), in the above expression,

$$N = \sqrt{\frac{q_0}{\alpha_0} [1 + a(z - z_0)]^n} \cdot e^{\frac{1+\beta}{2}(1-e^{-\alpha_0 z})}$$

$$= N_0 [1 + a(z - z_0)]^{n/2} \cdot e^{\frac{1+\beta}{2}(1-e^{-\alpha_0 z})}$$

where,

$$N_0 = \sqrt{q_0/\alpha_0}$$

$$\text{Or} \quad \frac{N}{N_0} = [1 + a(z - z_0)]^{n/2} \cdot e^{\frac{1+\beta}{2}(1-e^{-\alpha_0 z})} \quad \dots (7)$$

Hence, for the ionization distribution of the composite F-region,

$$\frac{N}{N_0} = e^{\frac{1+\beta}{2}(1-e^{-\alpha_0 z})} ; \text{ [for } z < z_0 \text{]} \quad \dots (8a)$$

$$\text{and} \quad \frac{N}{N_0} = [1 + a(z - z_0)]^{n/2} \cdot e^{\frac{1+\beta}{2}(1-e^{-\alpha_0 z})} ; \text{ [for } z > z_0 \text{]} \quad \dots (8b)$$

The actual value of  $z_0$  is a matter of guess-work. It must be positive i.e. above normal  $F_1$ -maximum level ( $h_0$ ) but cannot be very large; for, we know from experimental observations that the  $F_2$ -region conditions begin from only a little distance above  $h_0$ . Considering these,  $z_0$  has been taken as 0.5, which is quite reasonable.

In plotting the ionization distribution curve with height ( $h$ ), it is to be noted that,

$$z = \frac{h - h_0}{H} = \frac{h - h_0}{H_0 + \beta h}$$

For simplifying the calculations, let the reference level be at  $h_0$ , from which the height is to be measured i.e. let us put  $h_0 = 0$ .

$$\text{Then,} \quad z = \frac{h}{H_0 + \beta h} ; \text{ or } h = \frac{H_0 z}{1 - \beta z}$$

where  $H_0$  is the scale height at  $h_0$ .

As  $h_0$  is at  $F_1$  max,  $z$  represents height in terms of scale height measured from the maximum of  $F_1$ . Now, the  $F_1$ -maximum is formed at height of about 200 km and from experimental observations it is known that the value of  $\alpha$  (Mitra, 1952, page 553) at 200 km (i.e.  $H_0$ ) is about 50 in summer and 35 in winter. With these data the height variation of ionization can be represented directly in terms of  $h$ , as has been done in figures 2-5.

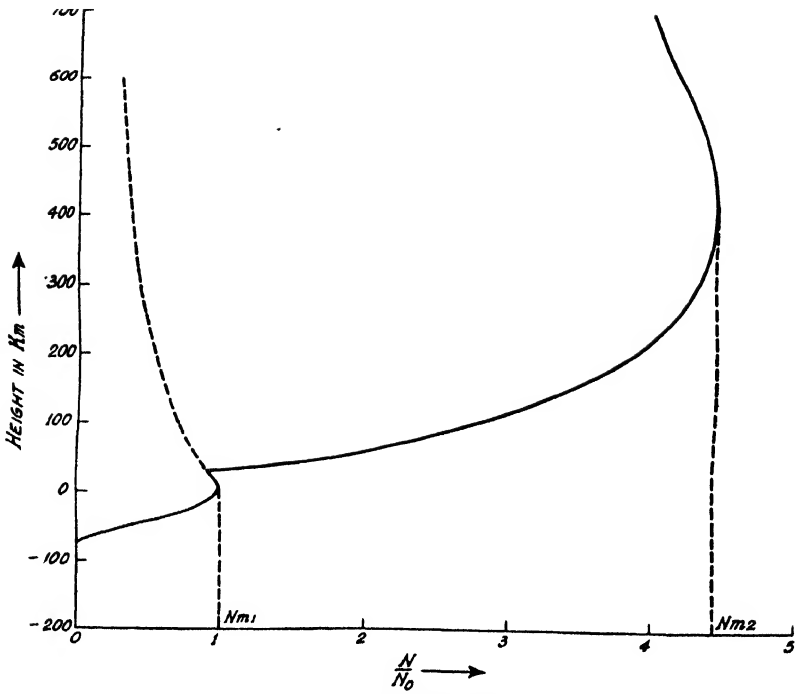


Fig. 2 Variation of ionization density with height as obtained by putting  $H_0=50$  km,  $\beta=0.25$ ,  $a=2$ ,  $n=3$  in Eqs. (8a) and 8(b). The curve represents a typical ionization distribution at high latitudes in summer noon.

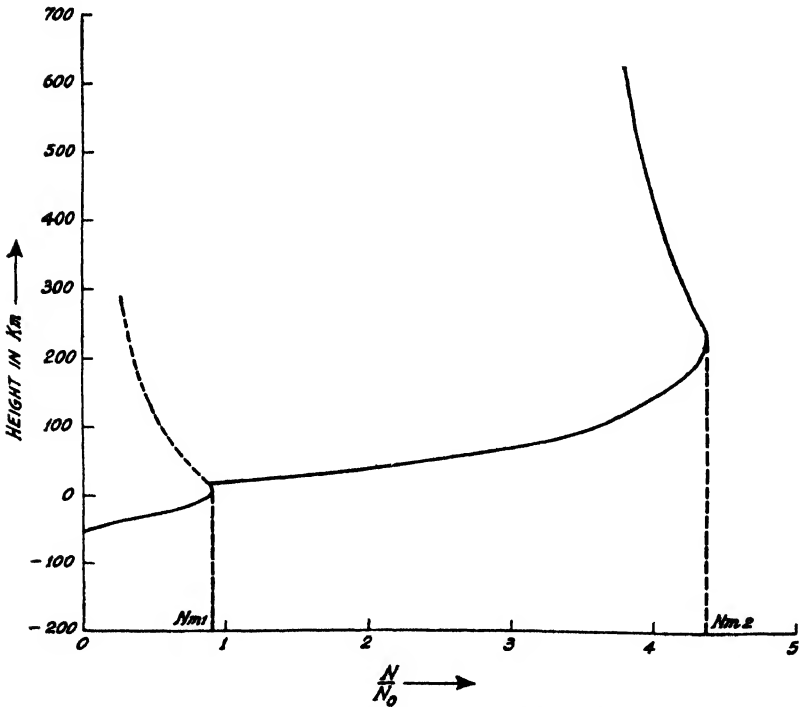


Fig. 3. Variation of ionization density with height as obtained by putting  $H_0=35$  km,  $\beta=0.2$ ,  $a=2$ ,  $n=3$  in Eqs. (8a) and 8(b). The curve represents a typical ionization distribution at high latitudes in winter noon.



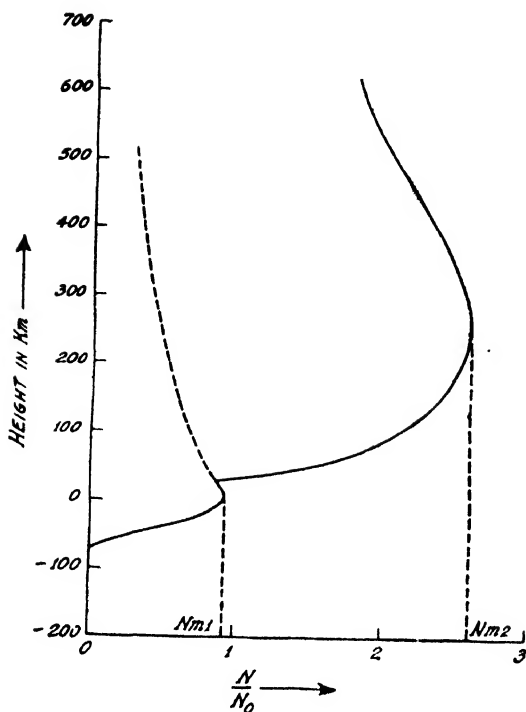


Fig. 4 Variation of ionization density with height as obtained by putting  $H_0=50$  km,  $\beta=0.25$ ,  $a=3$ ,  $n=2$  in Eqs. (8a) and (8b). The curve represents a typical ionization distribution at low latitudes in summer noon.

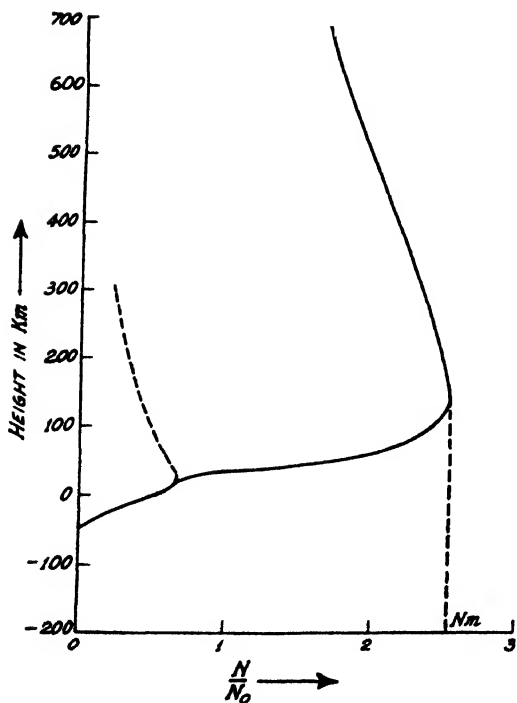


Fig. 5. Variation of ionization density with height as obtained by putting  $H_0=35$  km,  $\beta=0.2$ ,  $a=3$ ,  $n=2$  in Eqs. (8a) and (8b). The curve represents a typical ionization distribution at low latitudes in winter noon.

## 4. IONIZATION DISTRIBUTION WITH HEIGHT

## 1. For low latitudes :

(a) *Summer noon condition*,  $\chi = 0^\circ$  (figure 2). We assume the value of  $\beta$  to be 0.25. For the adjustable parameters  $a$  and  $n$ , we assume values  $a=2$ ,  $n=3$ . As already mentioned these values of  $a$  and  $n$  are chosen to suit approximately the observed height variation of  $\alpha$  at low latitude stations. The figure shows two distinct maxima of ionization. The  $F_2$ -layer has a very large semi-thickness and the  $F_{2\max}$  is situated at a height of about 400 km from the  $F_{1\max}$ . The results correspond well with experimental observation, particularly when the tidal effects are taken into account.

(b) *Winter noon condition*,  $\chi = 30^\circ$  (figure 3). In this case the values of  $a$  and  $n$  are kept the same as in figure 2. Only a lower value of  $\beta$  ( $=0.20$ ) is taken, as the temperature gradient is lower in winter. In this case also two distinct maxima in ionization distribution are observed. But the semi-thickness of the  $F_2$ -region has become much smaller— $F_{2\max}$  being situated at a height of about 200 km from the  $F_{1\max}$ . This lowered height of  $F_{2\max}$  is due to decreased temperature in winter. It is also to be noted that the winter height of the  $F_1$ -maximum is situated about 10 km above the summer height. Thus we see that though the height of  $F_{2\max}$  changes by a large amount from summer to winter that of  $F_{1\max}$  remains practically the same. The ionization density ratio  $\frac{N_{m2}}{N_{m1}}$  is, however, much larger in winter

than is shown in the figure. This large value of  $N_{m2}$  in winter is due to tidal effects as explained qualitatively in the next section.

## 2. For middle and high latitudes :

(a) *Summer noon condition*,  $\chi = 20^\circ$  (figure 4). The value of  $\beta$  is assumed to be equal to 0.25 as in figure 2. The value of  $a$  and  $n$  are, however, taken respectively to be 3 and 2. This makes the height variation of recombination co-efficient slightly less sharp than its value in low latitudes, as is supposed to be the case. Here also the  $F_2$ -region is very thick, and the

$F_{2\max}$  is formed at a height of about 250 km above  $F_{1\max}$ .  $\frac{N_{m2}}{N_{m1}}$  is 2.8. All

these results agree well with the experimental observations in middle and slightly higher latitudes, specially when the tidal corrections are made.

(b) *Winter noon condition*;  $\chi = 60^\circ$  (figure 5). As in the case of low latitude stations, the value of  $\beta$  is taken to be 0.2, a little lower than that of the summer noon value. The values of  $a$  and  $n$  are taken to be the same. It is to be noted that the normal  $F_1$ -maximum (under the condition of constant recombination coefficient) lies above the point  $z_0$  due to the large value of  $\chi$ . There is only one maximum in the ionization distribution curve of the composite F-region formed at a height of about 140 km above  $h_0$ . This is what is observed in high latitude stations in winter. From this it

may be concluded that if the solar zenith angle is larger than a certain given value, so that the normal  $F_1$ -maximum occurs above the point  $z_0$ , the actual value of  $z_0$  depending on local conditions—then there will be a single maximum in the F-region at noon i.e. there is no bifurcation.

The ionization distribution in the very high latitude stations and in the auroral zones is largely governed by ionizations caused by impact of charged particles and hence it cannot be represented by equations. (8a) and (8b). Also, on the magnetic equator (e.g. at Huancayo), the ionization distribution is rendered complicated by the strong current system (electro-jet) flowing over it. Excepting these special regions, equations (8a) and (8b) give for other parts of the globe, the noon time ionization distribution more or less correctly, subject to the tidal influences which are discussed below.

#### 5. MODIFICATION IN THE IONIZATION DISTRIBUTION DUE TO TIDAL EFFECTS

According to Martyn (1947) equation (5) is modified as follows in presence of tidal effects :

$$-\frac{dN}{dt} = q - \alpha N^2 + \frac{d}{dz}(Nv) \quad \dots (9)$$

where  $v$  is the vertical ionic drift velocity, measured positively downwards.

For conditions in the  $F_2$ -region, Martyn solved this equation with the approximation that  $(q - \alpha N^2)$  is negligible compared to  $\frac{d}{dz}(Nv)$ . A. P. Mitra (1951) has made an accurate analysis for the night time condition i.e. for  $q=0$ ; and recently Weiss (1953) has made a generalised analysis of Eq. (9) under the condition of a constant recombination co-efficient. All these calculations show that tidal effects modify the ionization distribution in the  $F_2$ -region, as deduced from Eqs. (8a) and (8b); and that the modifications are such as to make them more in accord with the observed results.

It is to be noted that, on account of the high recombination co-efficient at lower heights, the ionization density of the undisturbed  $F_2$ -region will decrease when the drift velocity is downwards and will increase when it is upwards. The separation between the two layers ( $F_1$  and  $F_2$ ) will thus always increase for downward drift and generally decrease for upward drift. We have used 'generally' for the latter, because if the gradient of drift is steep in the upper part of the  $F_2$ -region, then an upward drift may cause an increase of separation.

Now, calculations by Martyn show that for low latitude stations in summer, the drift is downwards at noon. As a result of this, the maximum ionization density of the  $F_2$ -region is decreased, and the separation between  $F_1$  and  $F_2$ , which is already large, increases further. At such latitudes in winter, there is a reversal of phase of the drift velocity somewhere between the  $F_1$  and  $F_2$ -layers. At the level of reversal the amplitude of  $v$  must be

very small. As such, there is very little modification in the maximum ionization density at this level. The separation between the two regions, however, increases considerably in the winter due to the large downward drift of ions in the upper part of the  $F_2$ -region.

For high latitudes in summer, the drift velocity is found to be downwards in the forenoon, though, the magnitude of the drift is not very large. This causes some decrease in the maximum ionization density of  $F_2$  and increases further the already large separation between  $F_1$  and  $F_2$ . Further, in such latitudes, in winter, there is a small upward drift at noon. This increases the maximum ionization density of  $F_2$  and helps the merging together of the two regions, decreasing their separation, if any.

We thus see that as a result of contribution by the tidal drifts, the separation between  $F_1$  and  $F_2$  at low latitudes is large both in summer and in winter (the summer separation being relatively large due to increased temperature); but at middle and high latitudes it is large only in summer (Ghosh, 1953). In winter, the separation is small at middle latitudes. This further diminishes with increase of latitude and ultimately vanishes in high latitudes where the two regions merge together.

## 6. DISCUSSION

Simple inspection of the curves in figures 2-5 shows that when the recombination co-efficient is decreasing and the scale height is increasing with height, then, if the solar zenith angle is not very large, a secondary maximum is produced above the normal  $F_1$ -maximum. But, if the solar zenith angle is very large (as in winter at high latitude stations) only a single maximum is produced in the  $F$ -region. It is formed slightly above the height where the normal  $F_1$ -maximum would have been, and has a larger ionization density.

The above results at once explain the diurnal variation of  $F_1$ - $F_2$ -separation when and where such separation exists. In the morning, as the solar zenith angle is very large, the  $F_{1\max}$  is formed above  $z_0$  and hence there is no bifurcation, only one maximum being formed. As the sun moves up in the sky,  $F_{1\max}$  comes down (below  $z_0$ ) and two distinct maxima are formed. As the solar zenith angle decreases further with the approach of noon, the height of  $F_{1\max}$  goes down further and due to the increase in the temperature above,  $F_{2\max}$  moves up (at a much faster rate). Thus, with advance of the day,  $F_1$ - $F_2$  separation increases, being maximum at about noon. The reverse process takes place in the afternoon hours when the solar zenith angle increases. Near sunset,  $F_{1\max}$  moves up above  $z_0$  and the two layers merge together.

The slight irregularities observed in the diurnal variation of  $F_{1\max}$  are also explained by Eq. (8a). From experimental observations it is known that in low and middle latitude stations, the diurnal variation of  $F_1$ -region critical frequency is approximately given by  $(\cos \chi)^{0.8}$ , instead of by

$(\cos \chi)^{0.25}$ , as given by the Chapman law. This is explained by Eq. (8a), according to which the diurnal variation should be given by  $(\cos \chi)^{1+\beta}$ , which, for  $\beta=0.2$  (as taken), is  $(\cos \chi)^{0.3}$ .

In discussing the results of calculations it should be noted that the curves drawn in figures. 2—5 are only illustrative and not representative of actual conditions prevailing in any particular station. It is also to be mentioned that the effect of fall of temperature with height above 400 km has not been considered in our simplified calculations. The calculated heights of  $F_2$  max, which are above 400 km, are to be reduced to certain extent due to the effect of this negative temperature gradient. At very low latitudes (near the equator) both  $H_0$  and  $\beta$  are high throughout the year. As such, the ionization distribution (neglecting the tidal corrections) should be almost the same throughout the year, analogous to that in figure 2. The seasonal variation of ionization densities and  $F_1$ - $F_2$  separations in these stations, as observed, are mainly due to tidal effects as explained in the paragraph 4 of the previous section. As pointed out in that paragraph, the tidal effect causes the maximum ionization density of the  $F_2$ -region to decrease in summer and the  $F_1$ - $F_2$  separation to increase in both the summer and winter solstices. Also, at high latitudes in winter,  $H_0$  is much smaller and  $h_0$  is at a lower height. Hence, the single ionization maximum in the F-region is produced at a much lower height, being just above the height where the normal summer-time  $F_1$  max would have been. This lowering is further helped by a small upward tidal drift as discussed in the paragraph 5 of the previous section.

During periods of high solar activity the enhanced solar ionizing radiation increases the rate of ion production ( $q$ ) and raises the temperature level (both  $H_0$  and  $\beta$ ) in the F-region throughout the globe (excepting at high latitude stations in winter). As a result, there is increased ionization and increased separation between the  $F_1$  and  $F_2$ -layers during such periods (Ghosh, 1953). (In winter at high latitudes, due to very large zenith angle of the sun and very small daylight hours, the upper atmospheric temperature, in so far as it is controlled by the absorption of solar radiations, is very little affected by solar activity).

It thus appears that Eqs. (8a) and (8b) derived on the hypothesis that  $F_1$  and  $F_2$  belong to a common bank of ionization can explain all the so-called 'anomalous' behaviours of the  $F_2$ -region when proper values of the parameters  $H_0$ ,  $\beta$ ,  $a$  and  $n$  are introduced in Eqs. (8a) and (8b) and account is taken of the relevant tidal effects. The equations are applicable to the  $F_1$  cum  $F_2$  conditions at all points on the globe, excepting over the auroral regions and over the magnetic equator, for reasons already explained.

#### ACKNOWLEDGMENTS

The author wishes to express his grateful thanks to Prof. S. K. Mitra for his constant guidance, help and encouragement throughout the progress

of the work. Thanks are also due to the Scientific Man Power Committee, Government of India, for financial help.

#### REFERENCES

- Baral, S. S. and Mitra, A. P., 1951, *Jour. Atoms. Terr. Phys.*, **1**, 95.  
 Bates, D. R., 1950, *Phys. Rev.*, **78**, 492.  
 Bates, D. R. and Massey, H. S. W., 1946, *Proc. Roy. Soc. A.*, **187**, 24.  
 Chapman, S., 1931, *Proc. Phys. Soc.*, **43**, 26.  
 Gerson, N. C., 1951, *Rep. Prog. Phys. Soc. Lond.*, **14**, 316.  
 Ghosh, Mrinmayee, 1953, *Ind. Jour. Phys.*, **27**, 421.  
 Martyn, D. F., 1947, *Proc. Roy. Soc. A.*, **189**, 241.  
 Martyn, D. F. and Pulley, O. O., 1935, *Proc. Roy. Soc. A.*, **154**, 455.  
 Mitra, A. P., 1952, *Ind. Jour. Phys.*, **26**, 79.  
 Mitra, A. P., 1951, *Jour. Atoms. Terr. Phys.*, **1**, 286.  
 Mitra, S. K., 1952, *The Upper Atmosphere* (2nd Edition), p. 313.  
 Mohler, F. L., 1940, *Bur. Std. Jour. Res.*, **25**, 507.  
 Nicolet, M., 1951, *Jour. Atoms. Terr. Phys.*, **1**, 141.  
 Weiss, A. A., 1953, *Jour. Atoms. Terr. Phys.*, **3**, 30.

# A REACTANCE TUBE CONTROLLED OSCILLATOR OF UNUSUALLY WIDE FREQUENCY SWEEP

By B. M. BANERJEE

INSTITUTE OF NUCLEAR PHYSICS, 92, UPPER CIRCULAR ROAD, CALCUTTA-9

(Received for publication, December 11, 1953)

**ABSTRACT.** A reactance tube oscillator producing an unusually wide frequency sweep has been described.

## INTRODUCTION

Reactance tube controlled oscillators are utilized in the automatic frequency control systems of superheterodyne receivers and in reactance tube modulators of simple types of frequency modulation transmitters. A wide range of frequency sweep is advantageous in both applications. Commonly, however, this sweep is of the order of a few tens or hundreds of kilocycles. The need for a wider range of sweep was actually felt in connection with the development of automatic frequency control systems of the receiver of an ionospheric sounding equipment (Banerjee and Roy, 1952). Reactance tube oscillators of conventional design (Reich, Young and Beck, 1949, Hund and others) could not provide a sweep greater than a megacycle. In the modified design described here, sweeps as great as 16 megacycles were obtained.

A reactance tube oscillator may be broken up functionally into the parts shown in the block diagrams given below (figure 1).

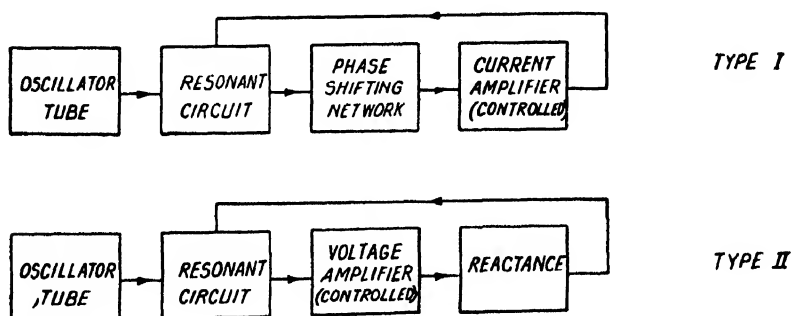


FIG. 1 Block diagram of reactance tube oscillator.

Type I alone is suitable for producing a wide frequency sweep in high frequency oscillators. The difficulty in obtaining amplification with a phase shift close to zero or 180 degrees limits application of type II mainly to the audio-frequency region.

To produce a frequency change in an oscillator, the reactive elements of the frequency controlling resonant circuit is varied. As the frequency of oscillation is given by the expression,

$$f = \frac{1}{2\pi\sqrt{LC}}$$

the change in frequency is given by

$$\Delta f = -\frac{f}{2} \cdot \frac{\Delta C}{C} = -\frac{f}{2} \left( \frac{\Delta X_c}{X_c} \right).$$

Now  $X_c$  may be written as

$$X_c = E/I_c$$

where

$E$  = voltage across the capacity

and  $I_c$  = charging current through this capacity, so that

$$\left| \frac{\Delta f}{f} \right| = \frac{1}{2} \frac{\Delta I_c}{I_c}$$

where  $\Delta I_c$  is the reactive current taken by the reactance tube, which thus behaves as a reactance element and produces the frequency change  $\Delta f$ , and  $I_c$  is the charging current through the actual reactance.

The current  $\Delta I_c$  through the reactance tube is limited to a peak value nearly equal to the *d. c.* anode current passed by this tube. This cannot be increased indefinitely. To obtain a large value of  $\frac{\Delta f}{f}$ , one has to arrange

circuit conditions such that the maximum r. f. current through the reactance tube is obtained for a minimum charging current in the actual reactance. This is accomplished by reducing the unavoidable capacitances in the resonant circuit to a minimum value, so that the charging current of the actual reactance has the minimum value for a given resonant circuit voltage. A further reduction of the charging current is possible, if the resonant circuit r. f. voltage is reduced, while a full modulation of the reactance tube current is retained, so that  $\Delta I_c$  has the maximum value obtainable. In the conventional arrangement, the phase shifting network introduces an amplitude reduction of three to ten times (Reich), so that even if a high transconductance tube is utilized in the current amplifier position, a fairly large r. f. voltage must remain on the resonant circuit to secure full modulation of its current. In the arrangement described here (figures 2 and 3), an amplifier is interposed between the resonant circuit and the current amplifier, in such a manner that its associated coupling elements naturally secure the necessary 90° phase shift, while giving an amplification of the resonant circuit voltage. A great reduction of the resonant circuit operating voltage is thus permissible, with a corresponding increase in the frequency sweep.



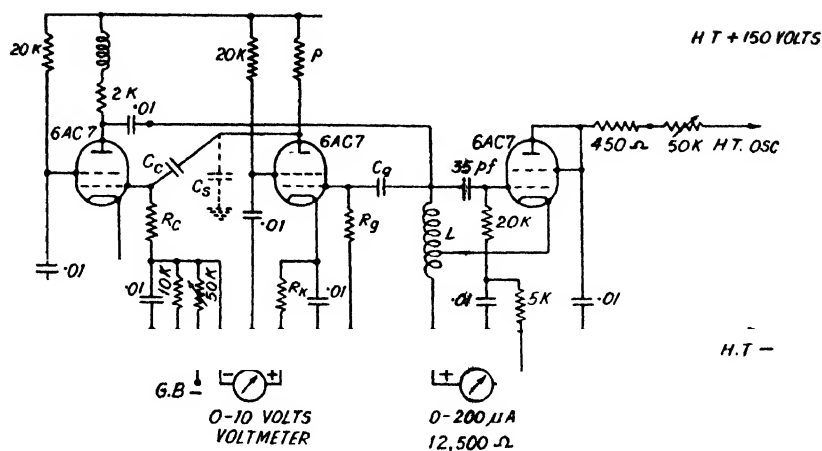


FIG. 2 Improved reactance tube oscillator utilizing 6AC7 tubes. Suitable for frequencies below 30 Mc/s.

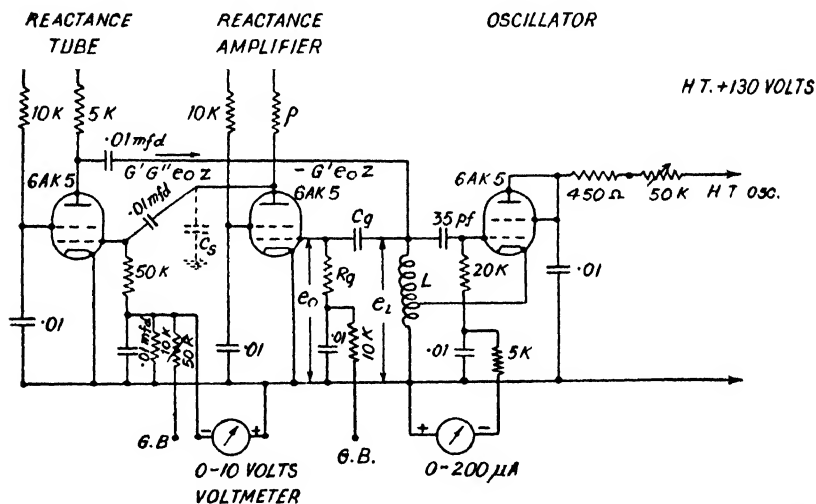


FIG. 3 Improved reactance tube oscillator utilizing 6AK5 tubes. Suitable for operation above 30 Mc/s.

### THE CIRCUIT

The circuits developed have the forms shown in the figures 2 and 3. They consist of an oscillator, a reactance amplifier and the reactance tube. Radio-frequency oscillations, generated by the Hartley type oscillator circuit, are developed across the resonant circuit inductance  $L$ , which has as the tuning capacity, the input capacities of the oscillator and reactance amplifier and the output capacity of the reactance tube, besides the component and wiring capacities to ground. The oscillator anode voltage, controlled by the 50K adjustable resistance, sets the amplitude of the r. f. oscillations to the optimum value. The r. f. oscillation across  $L$  is applied through a  $C_g R_g$  coupling network to the grid of the reactance amplifier. The reactance

amplifier is a resistance coupled wide-band amplifier. The amplified voltage is applied to the grid of the reactance tube through another  $C_g R_g$  network. The output current of the reactance tube is made to pass through the oscillator resonant circuit, and is controlled as usual by varying the grid bias. The  $90^\circ$  phase shift needed between the output current of the reactance tube and the voltage across the resonant circuit, is obtained automatically, when the component values of the  $C_g R_g$  coupling networks and  $C_g \rho$  network of the reactance amplifier are suitably proportioned. In that condition, the frequency of oscillations generated by the arrangement changes over a range of several megacycles as the grid bias of the reactance tube is varied while the amplitude of the oscillations remain sensibly constant. This is indicated by the oscillator grid current meter. When the component values are such that the phase shift deviates considerably from  $90^\circ$ , the in-phase or out-of-phase component of the reactance tube current produces a powerful degenerative or regenerative action. As a result, as the grid bias of the reactance tube is diminished, so as to allow greater current flow through the reactance tube, the oscillator grid current decreases, leading ultimately to cessation of oscillations or increases leading ultimately to squegging. When the values of these components, the value of  $\rho$  particularly, are adjusted to optimum, the frequency sweep obtained is a maximum, squegging is removed and there is a small variation of the oscillator grid current with reactance tube grid bias.

When the operating frequency is below 30 Mc/s, the gain available from the reactance amplifier is substantial. The large gain in the feedback loop then makes it impossible to avoid squegging even with critical adjustments\* of the value of  $\rho$ .

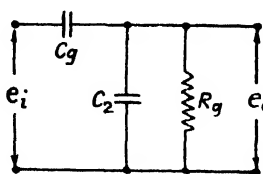


FIG. 4

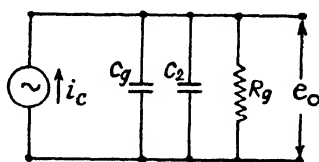


FIG. 5

$e_i$  = Voltage at input of  $C_g R_g$  network.

$e_o$  = Voltage at output of  $C_g R_g$  network.

$C_g$  = Coupling capacity, e.g., capacity between resonant circuit to reactance amplifier grid.

$i_c$  = Current through  $C_g$  when the output terminals, i.e.,  $e_o$  is short-circuited in figure 4.

$$= e_o / \omega C_g.$$

$C_2$  = Shunting capacity to ground at the output terminals of the  $C_g R_g$  network, e.g., reactance amplifier input capacity.

$R_g$  = Resistive component across the output terminals, e.g., grid leak of the reactance amplifier; at high frequencies, input resistance of the reactance amplifier grid circuit—that due to transit time effects.

\* It will be appreciated from the phase diagrams that are given later, that there will be movement in the output current phase when the frequency sweep is a good fraction the operating frequency.

It is then judicious to throw off some loop gain by reducing the coupling capacity between the resonant circuit and the reactance amplifier.

The phase diagrams are given in the figures 4, 5 and 6. In figures 4, 5 and 6 the phase shift  $\epsilon$  between the input and output voltages of a  $C_g R_g$  coupling network is calculated. It is positive—the output phase leads the input. The system is conveniently analysed by application of Norton's theorem.\*  $i_c$  is the current through  $C_g$  when the output terminals are short-circuited. The resultant output voltage is, therefore, equal to the voltage developed due to  $i_c$  flowing through the parallel combination of  $C_g$ ,  $C_2$  and  $R_g$ .

In figure 3,  $Z$  represents the impedance of the parallel combination of  $\rho$  and  $C_s$ , the reactance amplifier anode load and shunting capacity. This has an amplitude

$$|Z| = \frac{\rho}{\sqrt{1 + \omega^2 C_s^2 \rho^2}}$$

and phase  $\theta$  given by

$$\tan \theta = -\omega C_s \rho$$

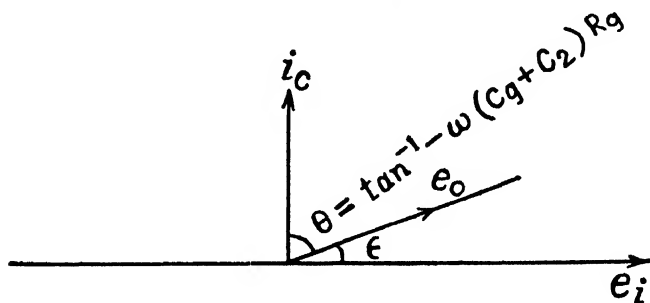


FIG. 6. Phase diagram of a  $C_g R_g$  coupling network.

The resultant phase diagram of the circuit, therefore, is of the nature given in figure 7.  $\phi_1$  and  $\phi_2$  represent the angles due to transit time delays in the reactance amplifier and reactance tubes. With 6AC7 tubes,  $\phi_1$  and  $\phi_2$  are not negligible at 30 Mc/s.

#### PERFORMANCE

The performance of several typical circuit combinations are presented in the curves of figures 8, 9, 10, and 11. They were obtained with two different circuit arrangements, figures 2 and 3, one utilizing 6AC7 tubes and the other 6AK5. Transit time effects make it desirable to utilize the 6AK5 circuit above 30 Mc/s. Compared to the conventional reactance tube circuits, oscillation is secured more readily in this new type of circuit. The phase-shifting  $R$ - $C$  combination in the conventional reactance tube circuit introduces a large damping on the oscillator resonant circuit. This is avoided in the newly developed circuit. When the operating frequency is high ( $> 30$  Mc/s), this factor assumes considerable importance.

\* Everitt—Communication Engineering—p. 48.

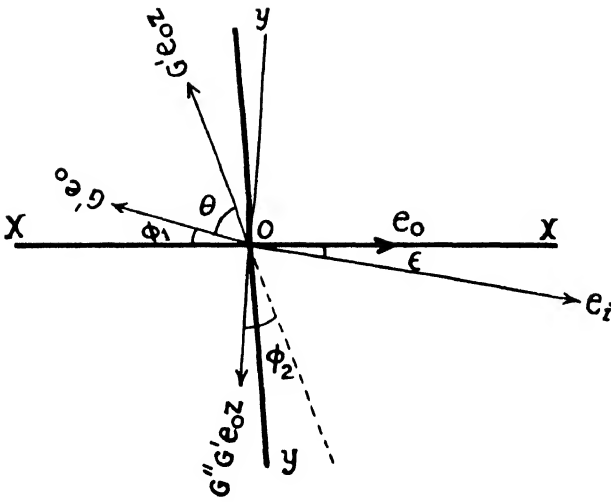


FIG. 7

Phase diagram of the reactance tube current. Resultant phase difference between output current and resonant circuit voltage  $= \epsilon + (180^\circ - \phi_1 - \theta) + (180^\circ - \phi_2) = 360^\circ - (\theta + \phi_1 + \phi_2 - \epsilon)$ .

$\epsilon$  = Phase shift between the input and output voltages of a  $C, R$ , network.

$\phi_1, \phi_2$  = Phase lag due to transit time delays in the reactance amplifier and reactance tube.  $\theta$  = Phase lag between the output current and voltage  $G'e_oZ$  of the reactance amplifier.  $(\theta + \phi_1 + \phi_2 - \epsilon)$  should be close to  $90^\circ$ : degenerative when greater than  $90^\circ$  and regenerative when less than  $90^\circ$ ; degenerative when  $\rho$  is greater than optimum and regenerative when  $\rho$  is less than optimum.

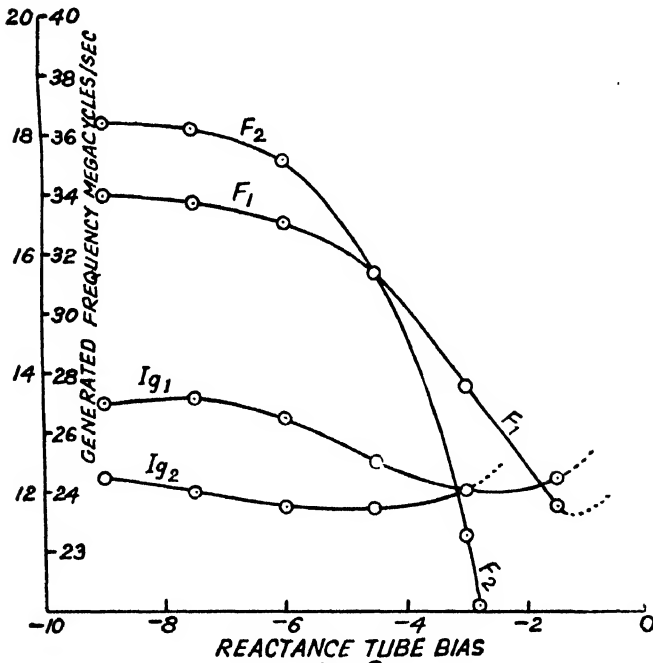
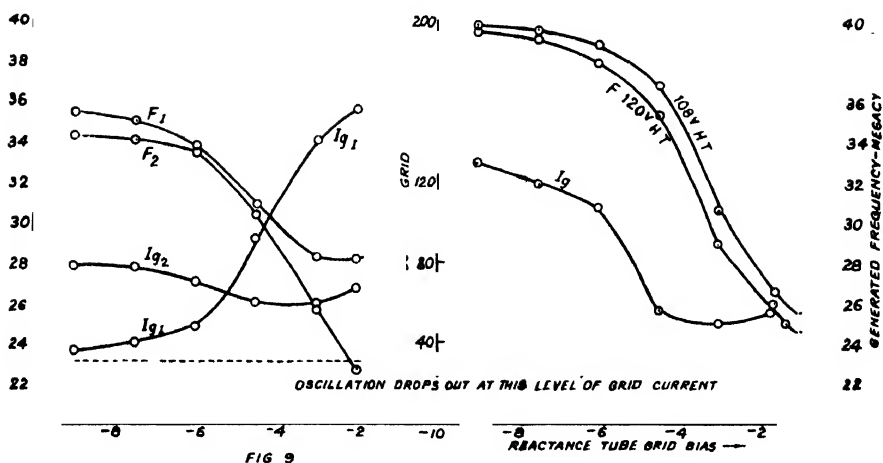


FIG. 8.

Characteristics of a wide sweep reactance tube oscillator utilizing circuit of figure 2. The curves marked  $F$  give the variation of frequency with reactance tube grid bias voltage, while curves marked  $I_g$  show the variation of oscillator grid current with reactance tube grid bias. Curves with suffix 1 were obtained with  $\rho = 500$  ohms:  $R_s = 50$  K;  $R_p = 2$  K;  $C_s = .01$  mfd;  $C_p = 11$  pf.; curves with suffix 2 with  $\rho = 500$  ohms:  $R_s = R_p = 50$  K;  $C_s = C_p = 11$  pf.; the resonant circuit had a measured stray capacity of 32 pf across it. Suffix 1 corresponds to the frequency range 20-40 Mc/s; Suffix 2 for 10-20 Mc/s. The minimum frequency reached in the first arrangement is 21.3 Mc/s. It was obtained when the oscillator H. T. was reduced to 14 volts from the normal value of 40 volts. Reduction of reactance tube bias beyond  $-2.8$  volts in arrangement 2 caused squegging. Frequencies were measured with calibrated receivers. (Hammarlund BC 779; Hallicrafter S-27).



Characteristics of a reactance tube oscillator utilizing circuit of figure 3. Curves with suffix 1 utilized  $\rho = 1000$  ohms;  $R_r = R_q = 50$  K;  $C_c = .01$  mfd;  $C_g = 7.5$  pf; Osc. H. T. +24 volts; Reactance amplifier bias -1.5 volts; oscillation frequency = 36 Mc/s with no H. T. on reactance amplifier and reactance tube; squegging completely removed. Curves with suffix 2 utilized  $\rho = 3000$  ohms;  $C_c = C_g = 15$  pf;  $R_r = R_q = 50$  K; Osc. H. T. +24 volts; R. A. bias -1.5 volts; R. A. and R. T. anode supply reduced to 108 volts to avoid squegging. Minimum frequency of 21.8 Mc/s reached when oscillator H. T. is reduced to zero. Maximum frequency of 34.6 mc/s is obtained when R. A. and R. T. H. T. is zero.

Characteristics of reactance tube oscillator utilizing circuit of figure 3.  $\rho = 3000$  ohms;  $C_c = C_g = 15$  pf.  $R_r = R_q = 50$  K; Osc. H. T. +24 volts; R. A. bias -1.5 volts; oscillation frequency = 40 Mc/s with no H. T. on R. A. and R. T. Minimum oscillation frequency of 23.7 Mc/s reached when oscillator H. T. was reduced to zero

When the frequency sweep required is a good fraction of the operating frequency, the arrangement becomes very susceptible to squegging, at certain values of the reactance tube bias. To minimize this tendency to generate interrupted oscillations, it is not enough to reduce the grid condenser and grid leak values. It is also desirable to have a separate low-internal resistance source for the oscillator high tension.

It is to be noted that as the grid bias is reduced, the generated frequency diminishes up to a certain limit, beyond which it again tends to increase.

It must not be forgotten that wide frequency sweep is obtained at the cost of the amplitude of generated oscillations. In applications, where amplitude of the generated oscillations (R.F.) is important, a suitable compromise must be made in the actual design. Wide-band amplifiers are to be incorporated, in case where such compromise would not satisfy requirements.

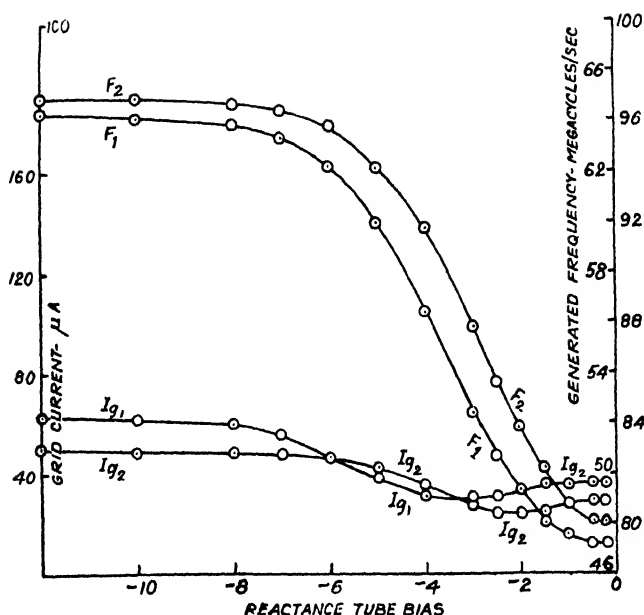


FIG. 11. Characteristics of reactance tube oscillators utilizing circuit of figure 3. Curves with suffix 1 utilized a centre tapped 5 turn coil of  $1/2$  inch diameter (frequency scale 46-66 mc/s);  $\rho=1,000$  ohms;  $R_c=R_g=50$  K  $\Omega$ ,  $C_c=C_g=15$  pf; oscillator H. T. +36 volts; reactance amplifier grid bias = -1.5 volts; maximum frequency of 64.9 Mc/s reached when R. A. and R. T. H. T. is zero; no squegging.

Curves with suffix 2, utilized a 5 turn centre tapped coil of  $1/4$  inch diameter; frequency scale 80-100 Mc/s;  $\rho=310$  ohms;  $R_c=R_g=50$  K  $\Omega$ ,  $C_c=C_g=15$  pf; oscillator H. T. +30 volts; Reactance amplifier bias = -0.5 volts; maximum frequency = 93.3 Mc/s reached when oscillator H. T. is reduced; no squegging.

#### ACKNOWLEDGMENTS

The author is indebted to Prof. M. N. Saha, F. R. S., M. P., Director of the Institute of Nuclear Physics, for his kind interest.

#### REFERENCES

- Banerjee, B. M. and Roy, R., 1952, *Ind. J. Phys.*, **28**, 473.  
 Foster, D. E. and Seeley, S. W., 1937, *Proc. I. R. E.*, **25**, 289.  
 Hund, August, Frequency Modulation, First Edition, 155-174, Mc Graw-Hill Book Co.  
 Reich, H. J., Theory and Application of Electron Tubes, Second Edition, 213, Mc Graw-Hill Book Co.  
 Schaeffer, C. F., 1940, *Proc. I. R. E.*, **28**, 166.  
 Young, J. D. and Beck, H. M., 1949, *Proc. I. R. E.*, **37**, 1078.  
 Weel, A. Van, 1953, *Brit. I. R. E.*, **13**, 315.

# AN INSTRUMENT FOR DIRECT MEASUREMENTS OF CAPACITANCE AND POWER FACTOR \*

BY J. C. BHATTACHARYA

INSTITUTE OF RADIO PHYSICS AND ELECTRONICS, CALCUTTA UNIVERSITY

(Received for publication, January 12, 1954)

**ABSTRACT.** The paper gives the design details of a new type of capacitance meter by which the capacitances and power factors of small condensers (maximum value  $0.02 \mu F$ ) can be directly measured on two calibrated meters, no adjustment or calculation being necessary. The design is based on the principle that when a small condenser (the test capacitor) is connected across the tuned circuit of an oscillator, both its frequency and magnification factor change. The change in frequency is indicated by a frequency-discriminator. This gives the value of the added capacitance. The change in magnification factor gives the power factor. By suitable discriminator and computer circuits, the meter readings are made proportional to capacitances and power factors.

## 1. INTRODUCTION

Various methods are employed for the determination of the capacitance and the power factor of a condenser. For the static condition the capacitance can be measured by charging the condenser to a given voltage and then discharging it through a leak resistance of high value. From the rate of fall of the voltage and the value of the leak resistance ( $R$ ), the capacitance ( $C$ ) can be calculated. The power factor ( $P$ ) at any frequency

( $\omega/2\pi$ ) is obtained from the value of  $\frac{I}{\sqrt{1 + \omega^2 C^2 R^2}}$ . At audio frequencies the

two quantities are usually determined by a bridge circuit. By inserting a parallel combination of a resistor and a capacitor in one of the arms of the bridge and adjusting it for balance, both the capacitance and the leak resistance can be calculated. In some types of impedance bridge, the resistance

dial is calibrated in decrement  $D$  (which is  $\frac{I}{\omega C R}$ ) and, from the reading of

this, the power factor is calculated. At radio frequencies, the capacitor value and the leak resistance (and hence the power factor) can also be measured by the so-called substitution method. In all these methods, however, several adjustments and/or computations are needed. And, when quick measurements, as in commercial tests are needed, these methods fail to satisfy the need. It is to be noted that the value of  $C$  can be measured directly by a frequency discriminator circuit. But any method by which  $P$  can be determined without making adjustments for balancing etc. is still

\* Communicated by Prof. S. K. Mitra

unknown. In the present communication an instrument is described by which both capacitance and power factor of the test capacitor can be determined directly, no adjustment or calculation being necessary. By merely connecting the test capacitor across two terminals of the instrument provided for the purpose, the values of the capacitance and power factor are obtained from the readings of two meters mounted on the panel.

## 2. THE METHOD OF MEASUREMENT

Figure 1 shows schematically the method of working of the instrument for direct measurements of capacitance and power factor of a condenser.

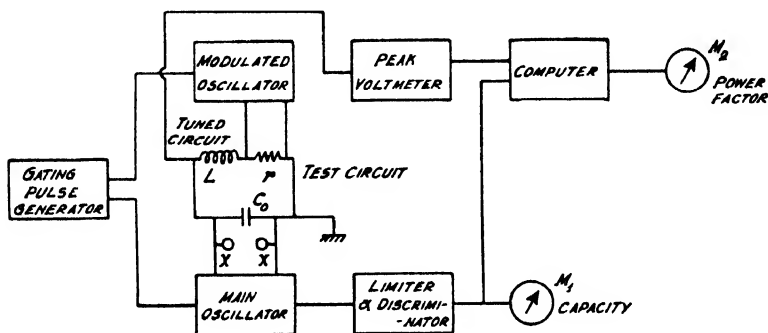


Fig. 1. Schematic diagram of the instrument which measures the value and power factor of capacitor automatically; XX are the points where the test capacitor is connected. The value of the capacitor is indicated by meter  $M_1$  and the power factor by meter  $M_2$ .

### (i) Measurement of $C$ .

The  $LC_0$  oscillatory circuit shown is the frequency determining network. When a test capacitor  $C$  (small compared to  $C_0$ ) is connected across the terminals (XX), the oscillation frequency changes by  $\Delta f$ , given by

$$\Delta f = \frac{f_0}{C_0} \cdot C \quad (1)$$

where  $f_0 = \frac{1}{2\pi\sqrt{LC_0}}$  is the original resonant frequency of the circuit. As  $\frac{f_0}{2C_0}$

is a constant for the oscillator used, the test capacitor  $C$  is directly proportional to  $\Delta f$ .  $\Delta f$  is measured by means of a Foster-Sceley type discriminator as follows :

The centre frequency of the discriminator is set at  $f_0$ , so that when the capacitor is not connected the discriminator has zero output. This output is recorded in a meter directly calibrated to give the capacitance value.

### (ii) Measurement of power factor.

The power factor of the test capacitor is obtained as follows: Let the magnification factor of the tuned circuit  $LC_0$  be  $Q_0$ . When the test capacitor



$C$  is connected across the terminals, let the new magnification factor of the circuit be  $Q$ . The power factor of the capacitor  $C$  is then given by

$$P = \frac{C_0}{C} \cdot \frac{Q_0 - Q}{Q_0 Q} \quad (2)$$

Here  $C_0$  and  $Q_0$  are constants. Hence,

$$P = K \cdot \frac{Q_0 - Q}{CQ} \quad (3)$$

where  $K = \frac{C_0}{Q_0}$  is a known constant and  $C$  is also known from discriminator output as indicated above. To determine  $Q$ , an r.f. voltage (of varying frequency) is injected across the resistance  $r$ , the frequency sweeping over the entire range of possible resonant frequency of the circuit. When the frequency of the injected voltage coincides with the actual resonant frequency (with the test capacitor connected), the instantaneous voltage developed across the circuit is  $Q$  times the input voltage. The voltage which is proportional to  $Q$  is measured by means of a peak voltmeter and is fed into a subtractor circuit, the output of which gives a voltage proportional to  $(Q_0 - Q)$ . Since the discriminator output is proportional to  $C$ , one can obtain by means of a multiplier and divider, a voltage proportional to  $Q_0 - Q/QC$  which, in its turn, is proportional to the required power factor. The computer output is calibrated to read the power factors directly.

Gating of the various stages is necessary, because, during measurements of  $Q$ , the oscillator has to be shut off, and during measurements of  $C$ , the peak voltmeter should be inactive. This is done by measuring these two quantities alternately at the rate of 50 c/s.

### 3. THE DESIGN OF THE INSTRUMENT

The oscillator circuit  $LC\tau$  is the test circuit of the instrument (figure 1).  $L$  is an air-core coil of a few turns of thick wire tuned to a frequency of about 1 Mc/s by means of a high grade mica condenser of value 2000  $\mu\mu\text{F}$ . The diagram of the oscillator circuit is shown in figure 2. The small

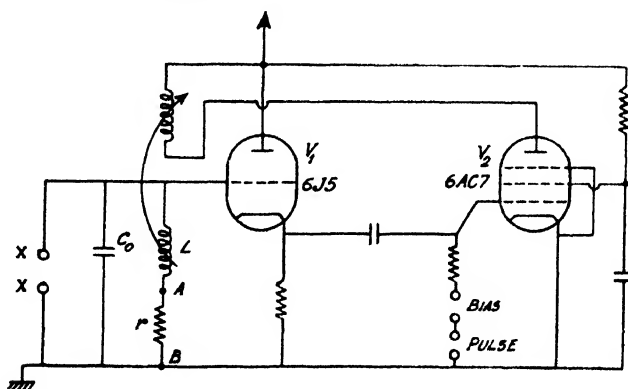


Fig. 2. The detail circuit diagram of the main oscillator.

resistance  $r$ , introduced in series with the coil is for injecting an r. f. voltage of constant amplitude in the circuit.

The oscillator assembly is slightly different from the conventional feedback type. It consists of two valves. To the grid of the first valve is connected one end of the tuned circuit; the other end is earthed. The first valve ( $V_1$ ) acts as a cathode follower with resistive load. The output of this valve is amplified by the second valve ( $V_2$ ) which has an inductive load. For oscillator, the final output is fed back in proper phase to the tuned circuit by mutual inductive coupling. If the amplifier tube is biased to cut-off, the oscillation stops without any fraction of the bias voltage appearing across the tuned circuit (Whitehead and Rueggaberg, 1949). The oscillator is switched on and off by applying suitable pulses to the second tube ( $V_2$ ). The repetition frequency of the pulse is 50 c/s and the pulse width is approximately 6 milliseconds. These pulses or bias voltages do not appear in the tuned circuit, and this is necessary as pointed out later. Normally, the bias of  $V_2$  is such that the system does not oscillate. When positive pulses of suitable amplitude are applied, oscillation occurs, the frequency being controlled by the tuned circuit.

The oscillator voltage is fed into a limiter followed by a Foster Seeley type discriminator, the circuit diagram of which is shown in figure 3. The

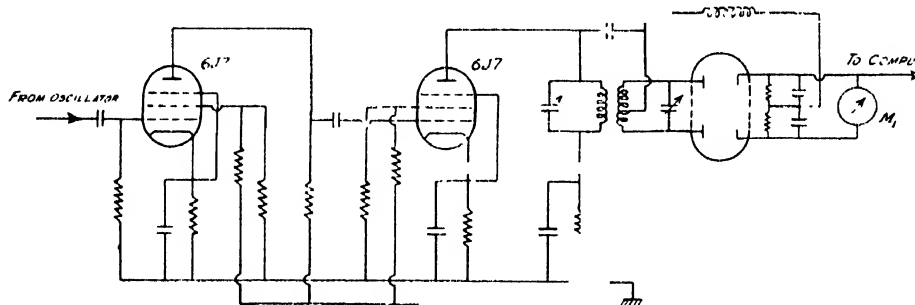


Fig. 3. The circuit diagram of the limiter and discriminator

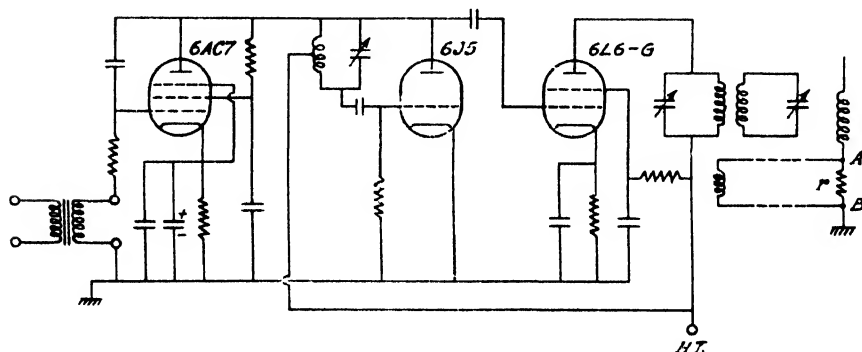


Fig. 4. The circuit diagram of the frequency-modulated oscillator and the amplifier for injecting constant voltage at variable frequency across the points AB (figure 2).

discriminator output is measured by a sensitive voltmeter which is calibrated directly in terms of capacity value. The output voltage is also fed into a computer system to be described later.

A separate auxiliary oscillator (figure 4) with a power amplifier is used to inject r. f. voltage of variable frequency across  $r$ , the points  $AB$  in figure 2. The oscillator is frequency-modulated by means of a reactance tube. The modulating signal to the reactance tube is obtained from the 50 c/s mains. The oscillator voltage is fed into a wide band power amplifier which is designed so as to give constant voltage across the load ( $r$ ), over the entire frequency range at which the test circuit may be at resonance.

The power amplifier is gated by 50 c/s pulses with a duty cycle of 300 milliseconds. The gating pulses are obtained from the 50 c/s mains and the power amplifier is operated at the positive half cycles. Since the test circuit oscillator operates during the negative half cycles, the r. f. voltage across  $r$  is injected only when the oscillator is not working. During this period the effect of  $V_1$  (figure 2) on the tuned circuit is equivalent to that of a fixed small capacitance, since the cathode of  $V_1$  is at a constant voltage (Jones and Ward, 1950).

The voltage across the tuning condenser appears twice in a full cycle of 50 c/s signal. During the negative half cycle the oscillator operates and r. f. voltage is developed across the tuned circuit. During the positive half cycle the frequency-modulated signal is applied across the small series resistance  $r$  in the tuned circuit, and when the frequency of injected voltage coincides with the resonant frequency of the tuned circuit, a magnified voltage ( $Q$  times the injected voltage) is produced across it. This voltage is measured by a vacuum tube peak-voltmeter. The voltmeter connections are so arranged that it is inoperative when the main oscillator (in the test circuit) operates and is operative only during the positive half cycle when the r. f. voltage is being injected across the resistance  $r$ . The circuit diagram of this arrangement is shown in figure 5.

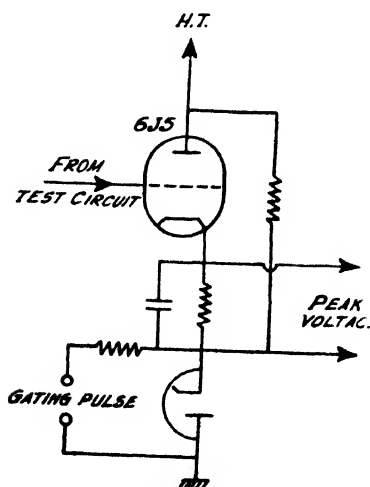


Fig. 5. The circuit diagram of the gated peak voltmeter which measures the voltage across the tuned circuit due to injection of voltage across  $AB$  (figure 2). The peak voltmeter is inoperative when the main oscillator is working.

The voltage at the cathode of the detector tube is maintained at such a value that during the positive half cycle, the tube is biased to exact cut-off. During this time any small voltage applied to the grid makes the tube conducting. During the negative cycle the tube is biased far beyond cut-off and the detector becomes inoperative. No output is, therefore, obtained from the detector when the main oscillator operates.

Since the voltage injected across the series resistance  $r$  is maintained constant (for all the frequencies), the peak voltmeter reading is a direct measure of the effective magnification factor of the circuit. When the test capacitor is included, the magnification factor of the circuit is reduced to a value, say  $Q$ , from the unloaded value  $Q_0$ . From the reduction of this magnification factor ( $Q_0 - Q$ ), the power factor of the test capacitor is calculated by means of the computer.

#### *The Computer :*

The purpose of the computer is to obtain from the two voltages, e. g. the output voltages of the peak voltmeter and of the discriminator, meter readings proportional to the power factor of the test capacitor. The schematic diagram of the computer circuit is given in figure 6. It consists of the multiplier, the subtractor and the divider.

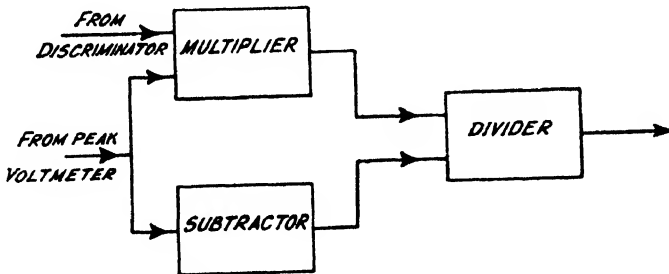


Fig. 6 Schematic diagram of the computer which produces a voltage proportional to the power factor of the capacitor.

(i) *The Multiplier*—It is known that when a multigrid tube is properly adjusted, its plate current varies linearly with the voltage injected in the control grid when the signal grid is kept at a constant voltage and vice versa. So, when both control grid and the signal grid voltages vary, the variation of plate current is proportional to the product of the two voltages injected in the two grids (Chauce, et al).

This fact forms the basis of the design of the multiplier circuit. The plate current *versus* signal and control grid voltage characteristics were first studied with different voltages applied to the other electrodes of a pentagrid tube (1A7-GT) and the optimum condition for linear characteristics determined. It was found that with the given supply voltages to the plates and the electrodes  $G_2$ ,  $G_3$  and  $G_5$ , the plate current was proportional to the product of the voltages applied to the control ( $G_1$ ) and signal ( $G_4$ ) grids when the bias applied to these two grids were  $-14.0$  and  $-4.5$  volts respectively.

A resistance, small compared to the plate resistance of the tube, is included in the plate circuit. The output voltage appears across this resistance as shown in figure 7.

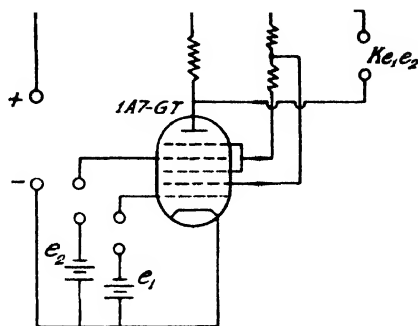


Fig. 7 Circuit diagram of the multiplier.

(ii) *The Subtractor.* For a triode with resistive load, operating in the linear portion of its grid voltage plate current characteristics, the drop in plate voltage for a voltage  $c$  applied to the grid is  $kc$ , where  $k$  is a constant depending on the plate current and the load value. Thus, if  $E_0$  be the initial plate voltage, then the plate voltage when a signal  $c$  is applied to the grid is

$$E_0 - kc = k(c_0 - c)$$

where  $E_0$  is equal to  $ke_0$ ,  $e_0$  being another constant.

In our case, the value of  $e_0$  is made proportional to  $Q_0$  and that of  $c$  to  $Q$  and thus the subtraction is effected (figure 8).

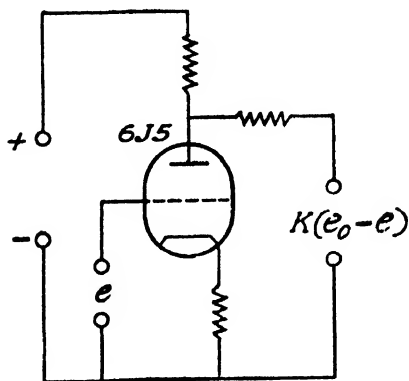


Fig. 8. Circuit diagram of the subtractor.

(iii) *The Divider.* Division is accomplished by first determining a quantity proportional to the reciprocal of the divisor and then multiplying it with the dividend. The principle of determining the inverse quantity of a given voltage is as follows :

If a voltage  $E$  is applied to the two resistances  $R_1$  and  $R_2$  in series, then the voltage  $e'$  across  $R_2$  is given by

$$e' = E \cdot \frac{R_2}{R_1 + R_2}$$

If  $R_2 \ll R_1$ , then,

$$e' \approx E \cdot \frac{R_2}{R_1}$$

Now, if  $R_1$  be such that it can be varied linearly with any input voltage, i.e.,  $R_1 = K e_1$  then,

$$e' = E \cdot \frac{R_2}{K e_1} = K_1 \cdot \frac{1}{e_1}$$

where

$$K_1 = \frac{E R_2}{K}$$

Now, ordinary triodes and pentodes do not show linear variation of plate resistance with grid voltage throughout their characteristics but do so only over very small ranges. This range, however, can be increased by using some sort of feed back. In our case, the pentode is used as the variable resistance whose screen voltage is controlled by another triode which in its turn is controlled by the voltage  $e_1$ .

Such a circuit used in conjunction with a multiplier circuit will give in its output a quantity proportional to the quotient of the two quantities. The circuit is shown schematically in figure 10. All interstage couplings used here are direct, and, therefore, the cathodes of succeeding tubes in the chain have to be maintained at higher and higher potentials.

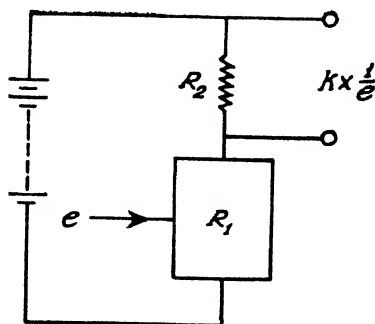


Fig. 9. Circuit for obtaining inverse voltage of a d.c. voltage

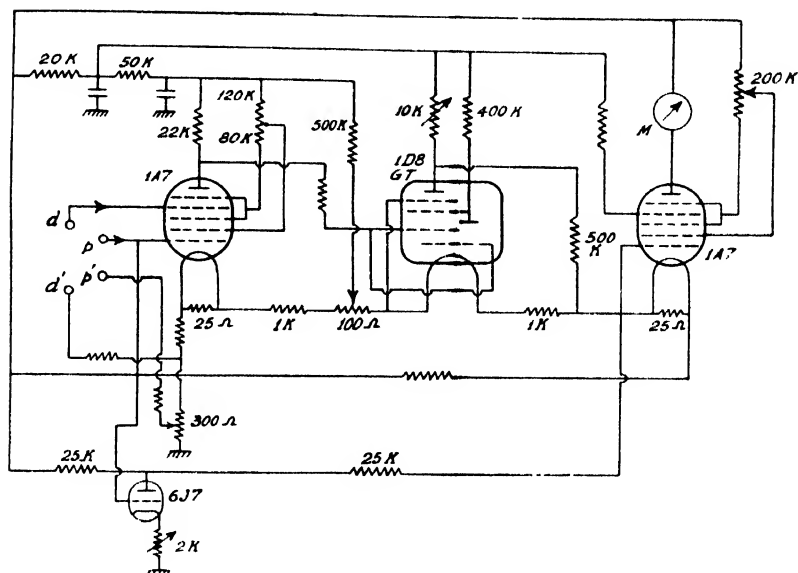


Fig. 10. Circuit diagram of the computer for calculating the power factor. It has two inputs. (1) The points  $pp'$  where the peak voltmeter output (figure 5) is fed and (2) the points  $dd'$  where the output of the discriminator is fed. The meter  $M$  reads the power factor

#### 4. RESULTS OF MEASUREMENTS : CONCLUDING REMARKS

The capacitances and power factors of a number of condensers were measured by means of the instrument constructed and the values were also determined with the help of a  $Q$ -meter. The two sets of results are shown in Tables I and II for comparison.

TABLE I

Nominal value $\pm 10\%$	Measured by $Q$ -meter	Measured by the instrument ( $100\mu\text{V} = 0.95$ volts)
$10\text{ pF}$ (or $\mu\text{F}$ )	9.5 pF	10.0 pF
10 "	10.5 "	10.5 "
30 "	31.0 "	30.5 "
30 "	30.0 "	30.0 "
52 "	54.0 "	54.0 "
52 "	55.0 "	55.0 "
82 "	82.0 "	82.0 "
82 "	82.5 "	82.5 "
130 "	127 "	126 "
130 "	128 "	127 "
170 "	170 "	167 "
170 "	168 "	165 "
220 "	220 "	215 "
220 "	222 "	218 "

TABLE II

Capacity (nominal value)	Calculated power factor	Measured power factor (.01 = 26 $\mu$ A)
80 pF	.0004	.0004
	.0011	.0011
	.0040	.0039
	.0073	.0073
	.0105	.0104
120 pF	.0013	.0013
	.0037	.0037
	.0065	.0064
	.0089	.0089

The apparatus is designed for measurements of condensers of small values (maximum 0.02  $\mu$ F) with power factors not exceeding 0.02. The accuracy of the measured values as obtained from direct readings of this instrument, is comparable to that obtained with any standard instrument for the purpose. It is possible to increase the ranges of both the values, but with some loss in accuracy. The instrument can also be modified to measure the inductance and  $Q$  values of coils at the working frequency of the instrument. With a little modification, measurement at other frequencies is also possible. Introduction of tuned circuits, tuned to different frequencies serves the purpose. By ganging them together, it is possible to switch over to other frequencies with a single control.

## ACKNOWLEDGMENTS

The author expresses his indebtedness to Mr. J. S. Chatterjee for suggesting the work and to Professor S. K. Mitra for many helpful discussions.

## REFERENCES

- Chance *et al*, Waveforms, Radiation Laboratory Series (Vol. 19), M. I. T., p. 669.  
 Jones, D. M. and Ward, J. F., 1950, *Proc. I. R. E.*, **97**, 645.  
 Whitehead and Rueggeber, 1949, *Trans. Arcm. Inst. Elec. Eng. Part 1*, **68**, 520.



# RAMAN SPECTRA OF ORTHO- AND PARA CHLOROPHENOL IN THE SOLID STATE AT LOW TEMPERATURES \*

BY D. C. BISWAS

OPTICS DEPARTMENT, INDIAN ASSOCIATION FOR THE CULTIVATION OF SCIENCE,  
JADAVPUR, CALCUTTA 32

(Received for publication, January 9, 1954)

Plates IA-D

**ABSTRACT.** The Raman spectra of ortho- and para chlorophenol in the liquid state and in the solid state at different temperatures have been recorded and compared with each other. Polarisation of the Raman lines of the two liquids has also been studied. Both the liquids have yielded a few feeble extra Raman lines not reported by previous workers. The changes in the position and intensities of the Raman lines which take place with solidification of the liquids are more spectacular in the case of the ortho-compound than in the case of the para compound. The lines  $379\text{ cm}^{-1}$  and  $499\text{ cm}^{-1}$  shift respectively to  $388\text{ cm}^{-1}$  and  $510\text{ cm}^{-1}$  with solidification of the ortho compound.

Three new lines appear in low frequency region with the solidification of ortho chlorophenol, while six such lines appear in the case of the para compound. In the former case when the polycrystalline masses are cooled to  $-180^{\circ}\text{C}$ , the intensity of the new line  $26\text{ cm}^{-1}$  increases while that of the other two new lines remain constant. In the case of para chlorophenol on the other hand, the intensity of the line  $98\text{ cm}^{-1}$  increases and a new line at  $155\text{ cm}^{-1}$  appears as the crystalline mass is cooled to  $-180^{\circ}\text{C}$ . The probable causes for these changes have been discussed.

## INTRODUCTION

The Raman spectra of benzene and substituted benzenes in the solid state have been investigated by several previous workers with a view to explaining the origin of the low frequency Raman lines which appear with the solidification of these substances. It was first pointed out by Sirkar (1936) that the intensity and positions of such low frequency Raman lines of crystals of naphthalene change considerably as the crystals are cooled to  $-180^{\circ}\text{C}$  and that these changes cannot be explained by assuming the contraction of the lattice at the low temperature, K stler and Rousset (1941) and also Bhagavantam (1941) put forward a theory to explain the origin of these lines. According to this theory the new lines are due to angular oscillations of the molecules about three axes, one perpendicular to the plane of the molecule and the other two lying in the plane of the molecule. It was

\* Communicated by Prof. S. C. Sirkar

phenol have frequency-shifts 415 (o), 442 (1), 554 (1), 600 (o), 623 (1), 650 (o), 710 (1), 764 (o), 822 (1), 884 (o), 935 (o), 974 (o), 1195 (ob), 1545 (o) and 3080 (2)  $\text{cm}^{-1}$ . In the case of the para compound such lines are at 164 (1b), 271 (1), 498 (o) and 1608 (2)  $\text{cm}^{-1}$ . As these lines are all equally weak, they cannot be due to any impurity, because in that case at least some of these extra lines would have much higher intensities than the other extra lines. Probably the spectrograms obtained in the present investigation are denser than those obtained by previous workers and, therefore, these weak lines did not appear in the latter spectrogram. The presence of

TABLE I

*o*-Chlorophenol ( $\text{ClC}_6\text{H}_4\text{OH}$ ) ;  $\Delta\bar{\nu}$  in  $\text{cm}^{-1}$ .

Liquid		Solid (present author)	
Kohlrausch and Pomgratz (1935)	Present author	-30°C	-180°C
174 (10b)	176 (8), $\pm$ c; D	51 (1), e, k	56 (2), e, k
268 (6b) d	260 (1) e; D	63 (o), e, k	69 (o), e, k
	270 (6) $\pm$ c, $\pm$ k; D	94 (1b), e, k	94 (1b) e, k
378 (6)	379 (6) $\pm$ e; P	176 (3), $\pm$ e	176 (2) e
	415 (o) e; P	273 (2), e, k	275 (1), e, k
	442 (1), e, k; P	388 (1), e, k	388 (1), e, k
498 (4)	499 (3), $\pm$ e, k; P	510 (1), e, k	512 (1), e, k
	554 (1), e, k; P		
561 (6)	563 (6), $\pm$ e, k; P	564 (1), e, k	564 (1), e, k
	600 (o), e; P		
	623 (1), e; P		
	650 (o), e; P		
678 (8)	680 (8), $\pm$ e, k, i; P	684 (4), e, k	684 (4), e, k
	710 (1), e, k; P		
750 (1)	750 (2), e, k; P		
	764 (o), e; P		
	822 (1), e; P		
833 (7)	832 (8), $\pm$ e, k, i; P	832 (2), e, k	832 (2), e, k
	884 (o), e; P		
	935 (o), e; P		
1000 (o)	974 (o), e; P		
	995 (o), e; P		
1030 (10)	1023 (15), $\pm$ e, k, i; P	1027 (5), e, k	1027 (4), e, k
1124 (3)	1123 (3), e, k; P	1123 (1), e, k	1123 (1), e, k
1154 (3)	1158 (4), e, k; P	1160 (2), e, k	1160 (2), e, k
	1195 (ob) e; P		
1246 (6)	1254 (5), e, k; P	1254 (2), k	1258 (2), e, k
1290 (3)	1287 (3), k; P	1287 (1), k	1287 (1), k
1337 (o)			
1456 (o)	1463 (1), e; P		
	1545 (o), e; P		
1588 (7b)	1595 (10), e; D	1596 (8), e	1596 (2), e, k
3068 (12b)	3068 (6), e, k, i; P	3070 (6), e, k, i	3073 (5), e, k
3177 (3)	3080 (2), e, k; P		
	3180 (2), e, k; P	3175 (1), k	3175 (1), k
3516 (1b)	3533 (ob), k; P	3533 (ob), k	3533 (ob), k

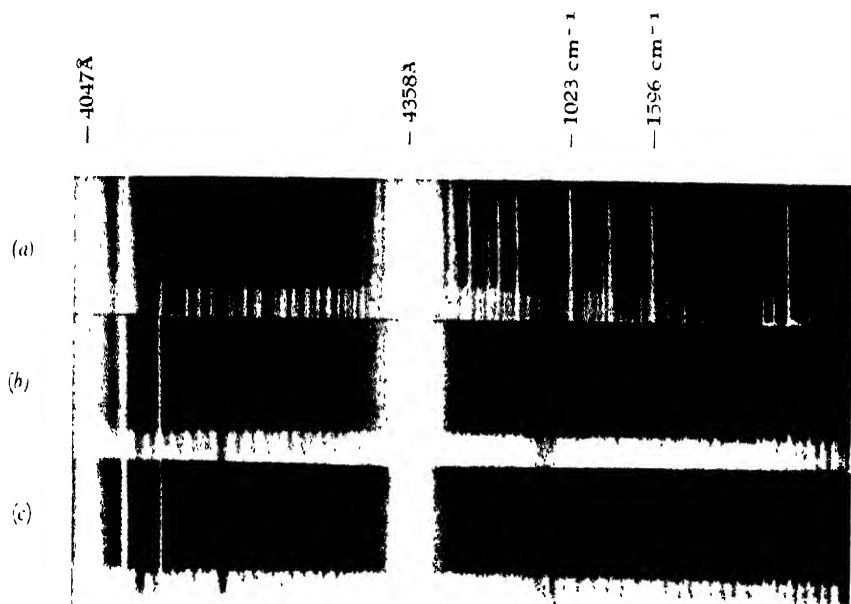


Fig. 1

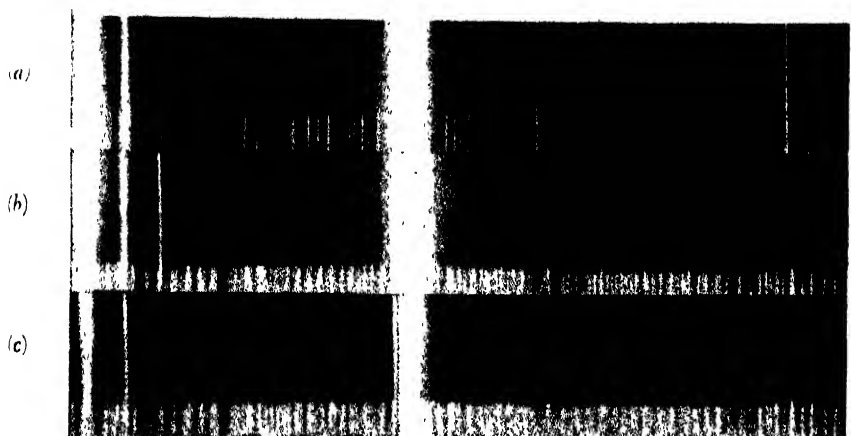


Fig. 2

## Raman spectra

Fig. 1. Ortho chlorophenol

- (a) Liquid at  $28^\circ\text{C}$
- (b) Solid at  $-30^\circ\text{C}$
- (c) " "  $-180^\circ\text{C}$

Fig. 2. Para chlorophenol

- (a) Liquid at  $28^\circ\text{C}$
- (b) Solid at  $-30^\circ\text{C}$
- (c) " "  $-180^\circ\text{C}$

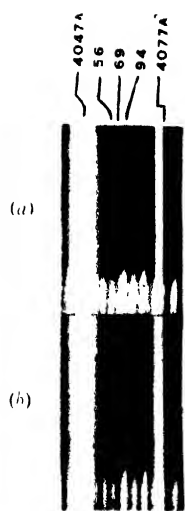


Fig. 3



Fig. 4

Raman spectra (enlarged)

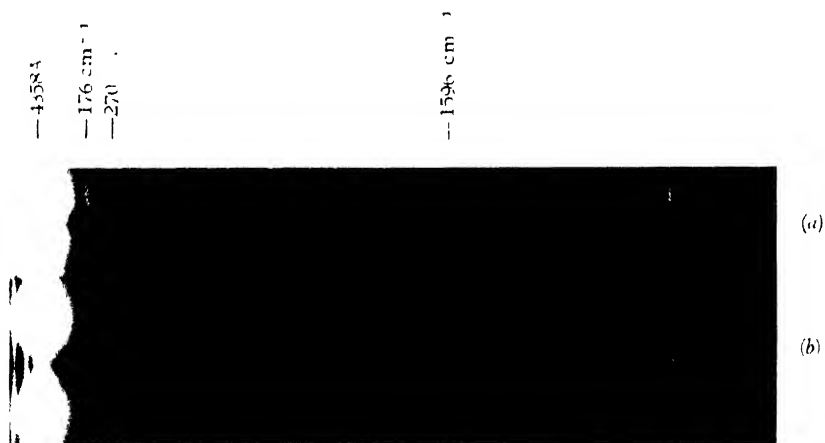
Fig. 3. *o*-Chlorophenol(a) Solid at  $-180^{\circ}\text{C}$ (b) " "  $30^{\circ}\text{C}$ Fig. 4. *p*-Chlorophenol(a) Solid at  $-180^{\circ}\text{C}$ (b) " "  $30^{\circ}\text{C}$ 

Fig. 5

Polarisation of Raman lines in liquid state

(a) *Ortho* chlorophenol(b) *Para* chlorophenol

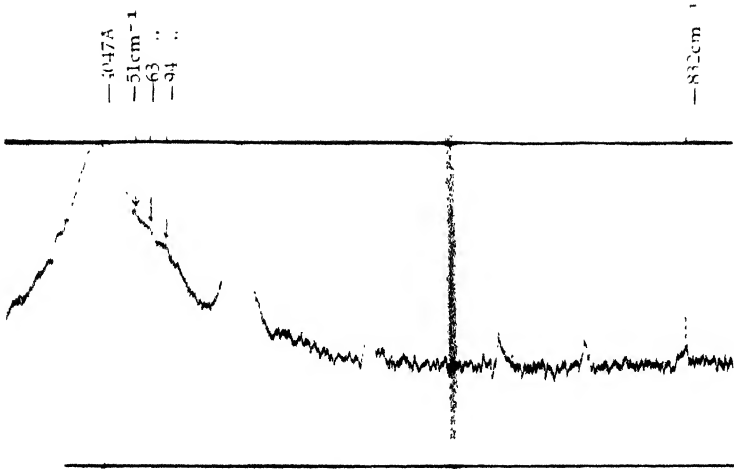


Fig 6

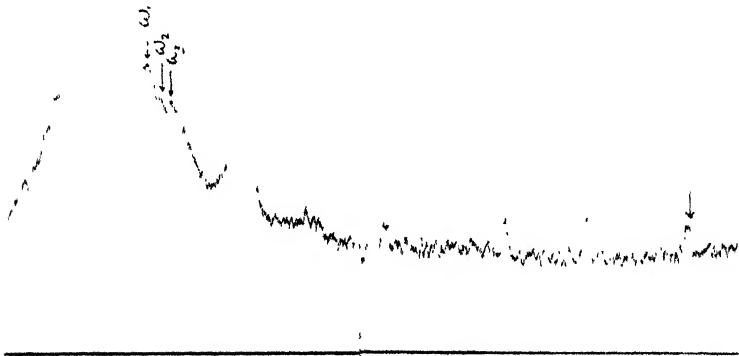
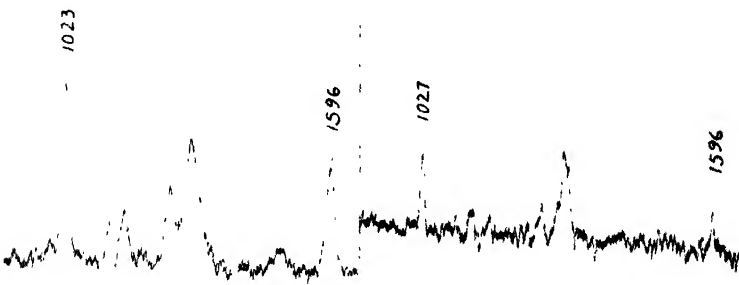


Fig 7



(a) Fig 8 (b)

Microphotometric records

Fig. 6. Ortho chlorophenol, solid at -30°C

Fig. 7. " " solid at -180°C  
(  $\omega_1=56\text{cm}^{-1}$ ,  $\omega_2=69\text{cm}^{-1}$ ,  $\omega_3=94\text{cm}^{-1}$  )

Fig. 8 (a). Ortho chlorophenol, liquid at 28°C

Fig. 8 (b). " " , solid at -180°C

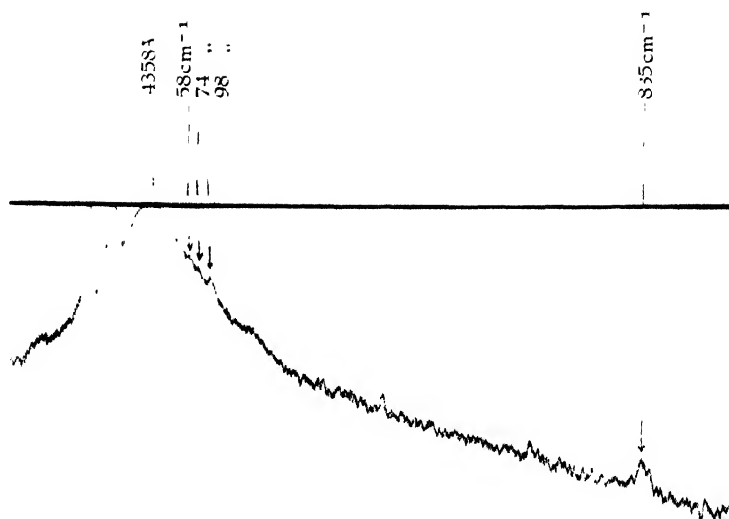


Fig. 9

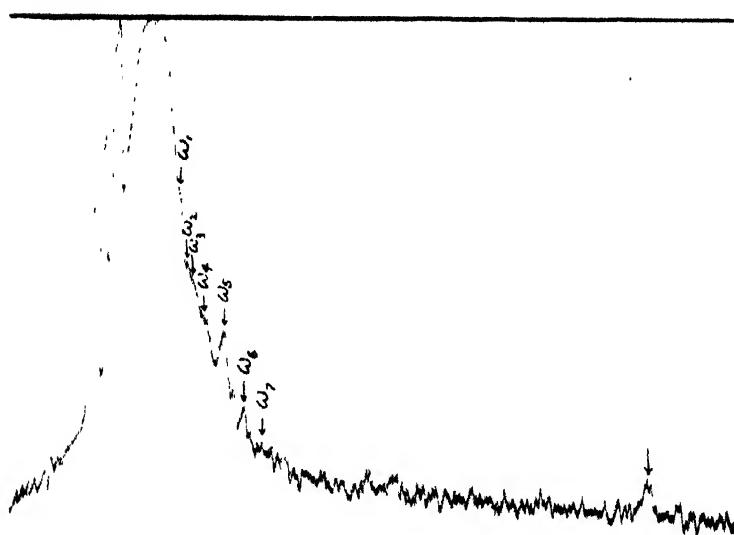


Fig. 10

## Microphotometric records

Fig. 9. Para-chlorophenol, solid at  $30^{\circ}\text{C}$ Fig. 10. " " " " at  $-180^{\circ}\text{C}$ 

(  $\omega_1 = 20\text{cm}^{-1}$ ,  $\omega_2 = 40\text{cm}^{-1}$ ,  $\omega_3 = 58\text{cm}^{-1}$ ,  $\omega_4 = 74\text{cm}^{-1}$ ,  
 $\omega_5 = 98\text{cm}^{-1}$ ,  $\omega_6 = 132\text{cm}^{-1}$ ,  $\omega_7 = 155\text{cm}^{-1}$  )

the three lines 164, 271 and 498  $\text{cm}^{-1}$  is not improbable, because the ortho compound shows lines in these regions. Some of the very strong lines of the ortho compound are not present in the spectrogram due to the para compound and therefore, the three lines mentioned above cannot be due to the presence of small percentage of ortho chlorophenol in the liquid used as para chlorophenol. Some of the lines due to both these liquids reported as broad by the previous authors have been found to be split up into pairs of lines in the present investigation. The lines 268  $\text{cm}^{-1}$  and 3068  $\text{cm}^{-1}$  are split up respectively into the pairs 260, 270  $\text{cm}^{-1}$  and 3068, 3080  $\text{cm}^{-1}$ .

TABLE II

*p*-Chlorophenol. ( $\text{ClC}_6\text{H}_4\text{OH}$ ) ;  $\Delta\nu$  in  $\text{cm}^{-1}$

Liquid		Solid		
Kohlrausch and Pongratz (1935)	Present author	Korshunov (1952)	Present author	
			-30°C	-180°C
		21 (9)	20 (2) ? k	20 (2) ? k
		29 (3)		
		36 (10)	40 (3), e, k	40 (2), e, k
		57 (10)	58 (3), e, k	58 (2), e, k
		73 (6)	74 (2), e, k	71 (1), e, k
		78 (6)		
		96 (7)	96 (4), e, k	98 (4), e, k
		118 (7)	124 (1b), e, k	132 (ob), e, k
		155 (5)		155 (1), e, k
		176 (1)	170 (1), e	170 (0), e
		196 (0)		
	164 (1b), e; D			
	271 (1), $\pm$ e, k; D			
331 (5)	333 (5), $\pm$ e, k, i; D		337 (1), e	337 (1), e
381 (6)	386 (7), $\pm$ e, k, i; P		386 (2), e	386 (2), e
	498 (0), e; P			
635 (4)	638 (4), e, k; P		640 (2), e, k	640 (1), e, k
817 (8)	828 (8), $\pm$ e, k; P		835 (3), e, k	835 (3), e, k
832 (5)	847 (3), $\pm$ e, k; P		845 (1), e, k	840 (0), e, k
928 (00)				
1001 (1)	983 (2), e; P			
1092 (8)	1092 (10), e, k; P		1092 (5), e, k	1092 (4), e, k
1165 (2)	1170 (3), $\pm$ e, k; P		1173 (1), e, k	1173 (0), e, k
1251 (3)	1258 (3), $\pm$ e, k; P		1263 (0), e, k	1263 (0), e, k
1342 (00)				
1590 (5b)	1592 (4), e; D		1592 (1), e	1592 (1), e
	1608 (2), e; D		1608 (0), e	
3068 (5)	3070 (10), e, k, i; P		3073 (8), e, k, i	3073 (5), e, k, i
3535 (00) ?	3533 (od), k; P			

Some of the lines due to both the liquids are totally depolarised. Of these the line 1596  $\text{cm}^{-1}$  due to ortho chlorophenol and the line 1592  $\text{cm}^{-1}$  due to para chlorophenol can be assigned to  $\nu_{16}$  and it appears that it is the

symmetry of the carbon ring and not of the whole molecule that determines the polarisation character of this line.

(b) *Solid phase :*

It can be seen from Tables I and II that although only three new lines appear in the low frequency region in the case of ortho chlorophenol in the solid state at  $-30^{\circ}\text{C}$ , in the case of the para compound the number of such lines is six. The dependence of intensities and position of these lines on temperature is also quite different in the two cases. In the case of the ortho compound the lines  $51\text{ cm}^{-1}$  and  $63\text{ cm}^{-1}$  shift respectively to  $56\text{ cm}^{-1}$  and  $69\text{ cm}^{-1}$  with change of temperature from  $-30^{\circ}\text{C}$  to  $-180^{\circ}\text{C}$  and the first line becomes stronger at the lower temperature. The third line at  $94\text{ cm}^{-1}$  remains in the same position with the same width and intensity with the lowering of temperature mentioned above. In the case of the para compound on the other hand, five of the six new lines in the low frequency region observed at  $-30^{\circ}\text{C}$  remain in the same position at  $-180^{\circ}\text{C}$ , while the line  $124\text{ cm}^{-1}$  shifts to  $132\text{ cm}^{-1}$  and becomes broader at  $-180^{\circ}\text{C}$ . An extra line appears at  $155\text{ cm}^{-1}$  at  $-180^{\circ}\text{C}$ . Korshunov (1952) observed this line even at a temperature probably much above  $-30^{\circ}\text{C}$ , but it could not be detected on the spectrogram for the crystal at  $-30^{\circ}\text{C}$  in the present investigation although it was observed at  $-180^{\circ}\text{C}$ . This shows that the intensity of this line increases with lowering of temperature. The line  $29\text{ cm}^{-1}$  reported by Korshunov (1952) was not found on the spectrogram for any of the two low temperatures and the line  $78\text{ cm}^{-1}$  could not possibly be resolved on the spectrogram obtained in the present investigation. The line  $74\text{ cm}^{-1}$  seems to weaken a little with lowering of temperature.

Besides these changes in the positions and intensities of the new lines in the low frequency region changes in relative intensities and positions of some of the lines due to intramolecular oscillations are also observed with solidification of the liquid and lowering of temperature of the solid in both the cases. In the case of the ortho compound the lines  $379$ ,  $499$  and  $680\text{ cm}^{-1}$  shift respectively to  $388$ ,  $510$  and  $684\text{ cm}^{-1}$ .

As regards the origin of the new lines in the low frequency region, the theory put forward by Kastler and Rousset (1941) and Bhagavantam (1941) ascribe them to angular oscillations of the molecules about their axes in the lattice field. There are two criteria by which such a theory can be tested. First, if all these lines were due to angular oscillations their intensities would diminish with lowering of temperature, because it has been observed by Swamy (1953) that in the case of both these chlorophenols the absorption bands in the ultraviolet region become sharper with lowering of temperature of the solid to  $-180^{\circ}\text{C}$ , and this sharpening is due to diminution in the amplitude of angular oscillations with lowering of temperature of the crystals. As the intensity of the new Raman lines in



the low-frequency region does not diminish with lowering of temperature and at least in the case of some of them it increases, all these lines cannot be due to angular oscillations. Such a conclusion has been arrived at also in the case of benzene by Ichishima and Mizushima (1950). Secondly, the phenomenon of angular oscillation presupposes the existence of a restoring force. Question now arises whether this restoring force is of the same order of magnitude in the lattice as in the liquid phase. In the case of molecules in the liquid phase their angular motion is restricted by viscous forces and if the molecule possesses a permanent electric moment, the time of relaxation derived from the theory put forward by Debye (1929) gives the order of the frequency of angular oscillation of the molecules in the liquid. It was first pointed out by Sirkar and Sen (1949) that the time of relaxation observed in the case of some polar molecules in the liquid state would lead to a frequency of the angular oscillation of the order of a fraction of a wave number, while the new Raman lines in the solid state have frequencies ranging from  $20\text{ cm}^{-1}$  up to  $180\text{ cm}^{-1}$ . It was also pointed out by Sirkar (1951) that even in the case of the nonpolar benzene molecule in the solid state the restoring force calculated on the assumption of some of the lines to be due to vibration of two molecules against each other is of the order of  $10^{-4}$  dynes/cm, which is many times stronger than Van der Waals' forces. As pointed out by Ichishima and Mizushima (1950) at least one of the new lines due to solid benzene is due to translational oscillation. Thus the existence of such strong restoring forces in solid benzene is proved beyond doubt. Such forces appear in the solid state evidently due to formation of virtual bonds among neighbouring molecules and in the case of chlorophenols studied in the present investigation the fact that no changes in the intensity of the line  $1596\text{ cm}^{-1}$  take place with solidification of the liquid as can be seen from Plates IC-D, indicates the formation of such bonds not at the expense of some of the C=C bonds in the molecule but through some other electrons.

In the case of *p*-chlorophenol the line  $176\text{ cm}^{-1}$  reported by Korshunov (1952) as one of the new lines due to the solid, in fact, corresponds to a broad band at  $164\text{ cm}^{-1}$  in the case of the liquid. The changes in the positions of the line due to intramolecular vibrations are less conspicuous in this case than in the case of the ortho compound, probably because the permanent electric moment is larger in the latter case. The broadening of the new line  $132\text{ cm}^{-1}$  at lower temperatures is probably due to the fact that the lattice contracts and influence of distant neighbours is perceptible at temperatures near about  $-180^{\circ}\text{C}$ .

#### ACKNOWLEDGMENT

The author is indebted to Prof. S. C. Sirkar, D. Sc., F. N. I., for his kind interest and continued guidance throughout the progress of the work.

## REFERENCES

- Bhagavantam, S., 1941, *Proc. Ind. Acad. Sci.*, **13A**, 543.  
 Biswas, D. C. 1953, *Ind. J. Phys.*, **27**, 379.  
 Debye, P., 1929, Polar molecule.  
 Fruhling, A., 1950, *J. Chem. Phys.*, **18**, 1119.  
 Hibben, J. H., 1937, *J. Chem. Phys.*, **5**, 704.  
 Ichishima, I. and Mizushima, S., 1950, *J. Chem. Phys.*, **18**, 1686.  
 Kastler, A. and Rousset, A., 1941, *Comptes Rendus*, **218**, 998.  
 Kohlrausch, K. W. F. and Pongratz, A., 3935, *Monatsch*, **65**, 199.  
 Korshunov, A. V., 1952, *Doklady Acad. Nauk. S. S. S. R.*, **86**, 695.  
 Ray, A. K., 1950, *Ind. J. Phys.*, **24**, 112.  
 „ 1951a, *Ind. J. Phys.*, **25**, 131.  
 „ 1951b, *Ind. J. Phys.*, **25**, 459.  
 Roy, N. K., 1953, *Ind. J. Phys.*, **27**, 167.  
 Sirkar, S. C., 1936, *Ind. J. Phys.*, **10**, 189.  
 „ 1951, *J. Chem. Phys.*, **19**, 256.  
 Sirkar, S. C. and Ray, A. K., 1950, *Ind. J. Phys.*, **24**, 189.  
 Sirkar, S. C. and Sen, S. N., 1949, *Nature*, **164**, 1048.  
 Swamy, H. N., 1951, *Ind. J. Phys.*, **25**, 119.  
 „ 1952a, *Ind. J. Phys.*, **26**, 233.  
 „ 1952b, *Ind. J. Phys.*, **26**, 445.  
 „ 1953a, *Ind. J. Phys.*, **27**, 55.  
 „ 1953b, *Ind. J. Phys.*, **27**, 119.

# AN INSTRUMENT FOR MEASURING THE DECAY OF $\mu$ -MESONS\*

BY H. S. HANS

DEPARTMENT OF PHYSICS, MUSLIM UNIVERSITY, ALIGARH

(Received for publication, November 6, 1953)

**ABSTRACT.** An electronic instrument designed to study many problems connected with the decay of  $\mu$ -mesons is discussed in detail. Special coincidence circuits, which differ from ordinary coincidence circuits in the fact that the output pulse from the special coincidence corresponds to the first input pulse, rather than to the last one, are used for recording the incoming mesons and the decay electrons. Many channels of delayed coincidences are used so that several points on the decay curve can be obtained simultaneously.

## INTRODUCTION

An electronic instrument is described which can be used for measuring the life time of  $\mu$ -mesons. The instrument was designed to study many problems connected with the decay of  $\mu$ -mesons. The main features of the instrument are as follows :

1. Special coincidence circuits are used for recording the incoming mesons and the decay electrons.
2. Many channels of delayed coincidences are used so that several points on the decay curve can be obtained simultaneously.

Several circuits have been previously reported by Benade and Sard (1949), Rossi and Nereson (1943), Ticho and Schein (1947), and Hincks and Pontecorvo (1950). The present paper discusses in considerable details the new features introduced.

## ARRANGEMENT OF G-M COUNTERS

The block diagram of the arrangement of G-M counter tubes, absorbers, and the circuit is given in figure 1. As is evident from the figure, the first three trays  $A_1$ ,  $A_2$ ,  $A_3$  consisting of twelve G-M counters each, receive the incoming charged particles of the cosmic rays. The lead absorbers having a thickness of 8 cm or more filter out most of the soft component. Absorber  $I$  serves as a source of decay electrons. Those mesons which are of such energy that they can pass through first three

\* Communicated by Prof. P. S. Gill

trays, but cannot penetrate absorber *I*, will stop in it and give rise to decay electrons. The lower three trays *B*<sub>1</sub>, *B*<sub>2</sub> and *B*<sub>3</sub> consisting of 18 G-M

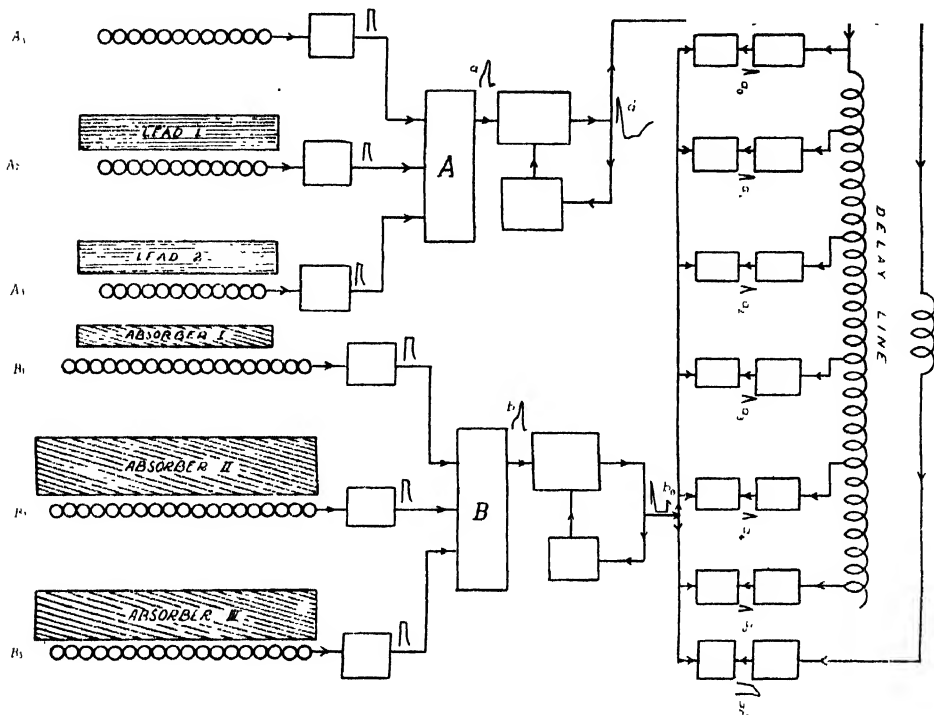


Fig. 1. Block diagram of counter arrangement, absorbers and the circuit.

counters each receive some of those decay electrons, which go through the solid angle defined by these three trays. Absorbers *II* and *III* may be used for determining the spectrum of decay electrons.

#### ELECTRONIC CIRCUITRY

*General Description:* The pulses from each of the six trays are fed to three staged amplifiers which give out positive pulses of about 20 volts, of nearly square shape, ten microseconds broad. A minimum negative input pulse of half a volt is required to saturate the amplifiers. The amplifiers, along with one cathode follower attached to each amplifier, are mounted just next to their respective trays on the frame itself.

The pulses from cathode followers of each amplifier are fed to the main electronic instrument by long leads from 1.5 metres to 2.5 metres in length. Due to the cathode followers, the pulses do not suffer any change in shape or size, in traversing these long leads. The pulses from the first three amplifiers are fed to a special coincidence circuit *A*; and similarly, pulses from the other three amplifiers are fed to another exactly similar special coincidence circuit *B*. Pulse from circuit *A*, will be referred to as pulse *a* and that from circuit *B* will be referred to as pulse *b*.

These special coincidence circuits differ from ordinary coincidence circuits in the fact that the output pulse from the special coincidence corresponds to the first input pulse, rather than to the last one. In fact it comes  $t$  microseconds after the earliest pulse ( $t=1.1$  microseconds in this case). Time  $t$  is kept nearly equal to the maximum time lag expected in the counter. This feature of the special coincidence technique is meant to reduce the fluctuation of time lags of the discharges in G-M counters as explained below.

There is a time lag between the time of the passing of an ionising particle through the G-M counter and the appearance of the pulse (Sands and Sard, 1947). This delay depends on the distance where ions are formed with respect to the central wire. If the ions are formed close to the wire, this delay will be less. But if they are formed farther off, it takes some time before the ions reach the wire and the charge spreads, thus causing delay in the appearance of the pulse with respect to the time of the passing of the particle. The time delay varies according to Gaussian distribution, (Sands and Sard, 1947; Corson and Wilson, 1948), and its value may, in certain cases, be as much as one microsecond which causes an uncertainty in the time measurements. The probability of the maximum time lag is about one in  $10^4$  in a single counter (Sands and Sard, 1947). But if a particle passes through three counters in succession, the probability of this delay in all the three counters at one time is reduced to one in  $10^6$ . It will mean that if the earliest of the pulses from the three counter trays initiates the coincidence pulse, the time lag will be reduced to a minimum value.

Pulses  $a$  and  $b$  are fed to two sharpener-cum-feed-back circuits, which serve to sharpen the pulses, and also paralyse the circuit for ten to fifteen microseconds after the passage of the pulse. While pulse  $a$  is changed to a positive pulse  $a'$  of width 1.5 microseconds followed by a negative gate of 10 microseconds, the pulse  $b$  is changed to a sharp positive pulse  $b_0$  of an effective width  $\leq 0.3$  microseconds followed by a negative gate of 10 microseconds. The negative gate in both channels serves the same purpose as the anti-coincidence feature in the circuit of Ticho and Schein (Ticho, 1947). It can easily be seen that a particle passing through all the six trays will never be counted as a decay electron.

Pulse  $a'$  is fed to a delay line which consists of many sections, each section having a delay of about 0.3 microseconds. From six different points of this delay line pulses are taken and fed to equaliser circuits which give out positive pulses of nearly equal size and width, each being about one microsecond at the base. These will be referred to as  $a_0, a_1, a_2, a_3, a_4$  and  $a_5$ . Pulse  $a_0$  has practically no delay with respect to  $b_0$ , while pulses  $a_1, a_2, a_3, a_4$  and  $a_5$  are delayed by 1.1, 2.7, 4.2, 5.8 and 7.3 microseconds respectively with respect to pulse  $a_0$ . The exact relative positions and shapes of the pulses are shown in figure 2(a).

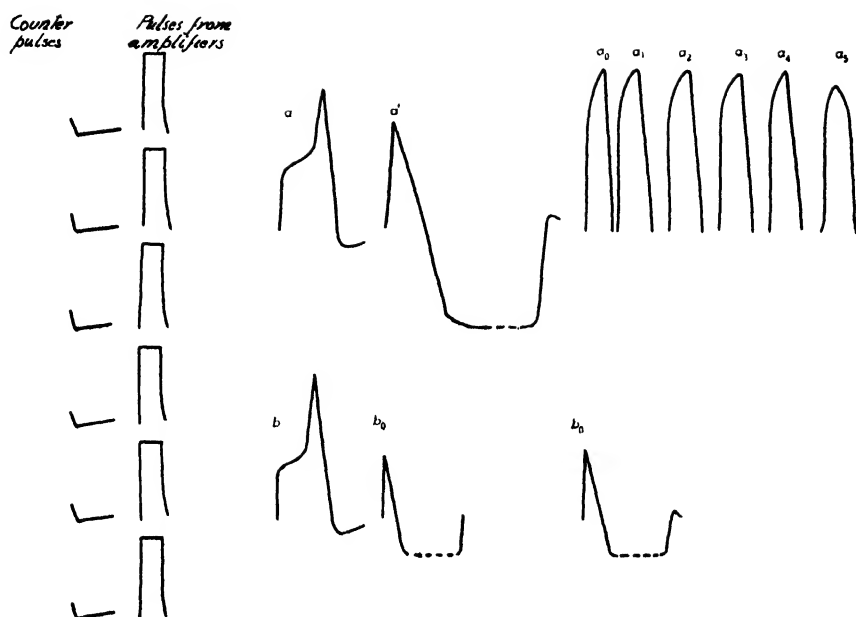


Fig. 2(a). Relative positions and shapes of the pulses in different parts of the circuit.

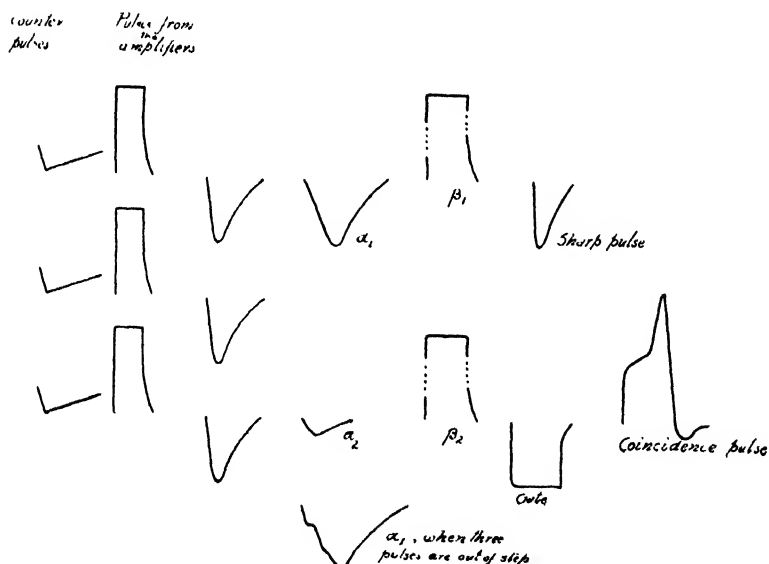


Fig. 2(b). Relative positions and shapes of pulses of different points of special coincidence circuit.

Each pulse  $a_0, a_1, a_2, a_3, a_4$  and  $a_5$  is fed to its corresponding input of the six double coincidence tubes, while pulse  $b_0$  which is  $\leq 0.3$  microseconds in effective width is fed to the other input of the double coincidence tubes. The coincidence, between  $a_0$  and  $b_0$  is prompt coincidence, while others will be delayed coincidences. The relationship between different

pulses in the whole circuit shows that the prompt coincidence occurs when pulse  $b_0$  appears 0.3 microseconds or less before and one microsecond or less after the  $a_0$  pulse. Similarly for the other pulses, the effective interval in which coincidences can occur are :

- 1st channel (coincidence between  $a_1$  and  $b_0$ )  
when pulse  $b_0$  appears within 0.8 and 1.8 microseconds after  $a_0$ .
- 2nd channel (coincidence between  $a_2$  and  $b_0$ )  
when pulse  $b_0$  appears within 2.4 and 3.4 microseconds after  $a_0$ .
- 3rd channel (coincidence between  $a_3$  and  $b_0$ )  
when pulse  $b_0$  appears within 3.9 and 4.8 microseconds after  $a_0$ .
- 4th channel (coincidence between  $a_4$  and  $b_0$ )  
when pulse  $b_0$  appears within 5.5 and 6.5 microseconds after  $a_0$ .
- 5th channel (coincidence between  $a_5$  and  $b_0$ )  
when pulse  $b_0$  appears within 7.0 and 8.0 microseconds after  $a_0$ .

Another channel was added which recorded a delayed coincidence between pulse  $b_0$  and a delayed gate of a variable width, which was opened by the pulse  $a'$ . This channel recorded delayed coincidences when  $b_0$  came between one microsecond to six microseconds after  $a_0$ .

Each of the delayed coincidence pulses was recorded by a univibrator of large time constant which made a neon bulb glow. The flashes of the neon bulbs connected to appropriate channels were recorded on a moving film.

#### DETAILED DESCRIPTION

**Amplifiers :** The circuit is shown in figure 3. The first tube 6AU6 is biased to near cut off point so that it is saturated with small pulses. Other

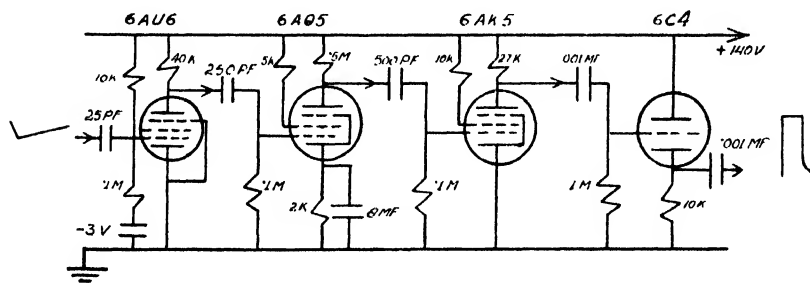


Fig. 3. Three staged amplifier for counter pulses

two tubes 6AQ5 and 6AK5 are sharp cut off pentodes giving out a positive pulse of a sharp first edge and a flat top. Tube 6C4 serves as a cathode follower.

**Special Coincidence Circuit :** Its detailed diagram is shown in figure 4. Each of the three positive pulses from the amplifiers is fed to a cathode coupled univibrator through a small capacity of 25 PF. The univibrator

gives out a sharp negative pulse, the size of which can be changed by adjusting the potentiometer  $R_1$ . The three negative pulses are added

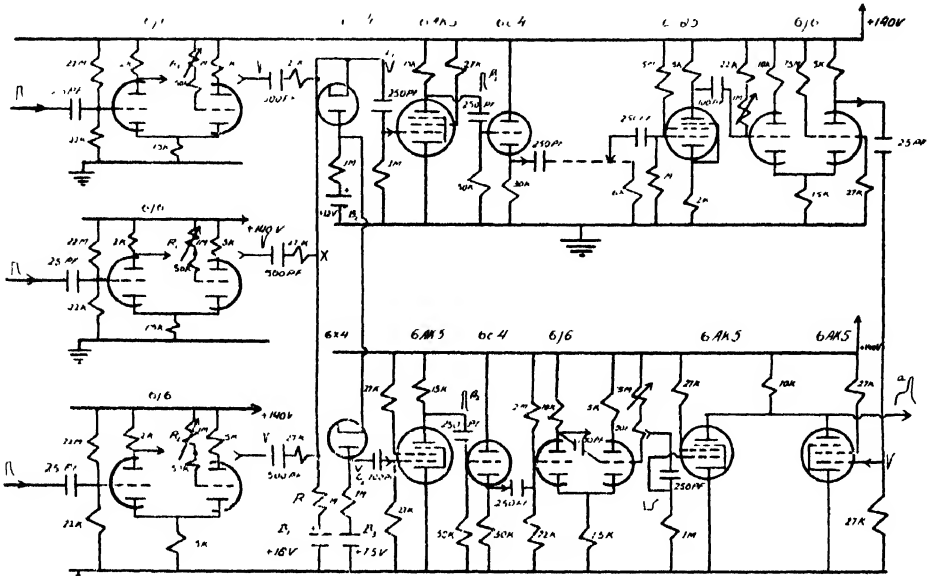


Fig. 4. Detailed diagram of special coincidence circuit

together over a resistance  $R_2$ . If three pulses come at the same time the resultant pulse at point  $X$  will be a triangular pulse; but if in the extreme case the three come after one another, the pulse  $\alpha_1$  will have the shape shown in figure 2(b). Pulse  $\alpha_1$  is fed to a set of two diode discriminators in series. Due to the positive biases, the pulses can pass through the diodes only if their size is more than a given minimum, determined by the biases. The biases are adjusted such that the pulse passes the second diode only if the pulse  $z_1$  is due to the sum of three pulses. Naturally the pulse  $\alpha_2$  at the plate of second diode will be a coincidence pulse, while the first edge of the pulse  $z_1$  at the cathode of the first diode will correspond to the earliest input pulse. Both pulses  $\alpha_1$  and  $\alpha_2$  are fed to amplifier tubes 6AK5. The first edge of the pulse  $\alpha_1$  saturates its amplifying tube, while the pulse  $\alpha_2$  saturates the other tube. Pulse  $\beta_1$  at the end of the first amplifier corresponds to the earliest of the pulses and pulse  $\beta_2$  at the end of the second amplifier corresponds to the latest. Pulse  $\beta_1$  after a cathode follower is fed to a delay line which delays it for 1.1 microsecond. After amplifying and sharpening this pulse with two tubes, it is fed to one input of a double coincidence. On the other hand, pulse  $\beta_2$  is fed to a gating univibrator which gives out a negative gate of nearly two microseconds. The gate is fed to the other input of the double coincidence. The resultant coincidence pulse is shown in figure 2(b). The upper left edge of the coincidence pulse is due to the earliest pulse and as is clear from the previous description: this edge will always appear after a fixed time interval



of 1.1 microsecond after the earliest pulse. Coincidence occurs only if the last pulse comes within 1.1 microsecond after the earliest pulse.

#### Sharpener-cum-Feed-Back :

Diagram of the circuit to which pulse *a* is fed is shown in figure 5. The first tube 6J6 acts as a *discriminator*. The potentiometer  $P_1$  is set at such a value that the tube is triggered **only** by the upper left edge of the coincidence pulse. The negative output is applied to one of the grids of a 6J6 tube which works as an anti-coincidence tube. As the other grid of the tube is biased beyond cut-off, a positive pulse comes out which is applied to a cathode follower. This positive pulse, after being inverted is applied to a gating circuit which gives out a fifteen microsecond positive pulse. This gate is fed to the biased grid of the anti-coincidence tube. The result is a sharp positive pulse followed by a negative gate. The sharpness of the pulse can be increased by reducing the bias of the anti-coincidence tube.

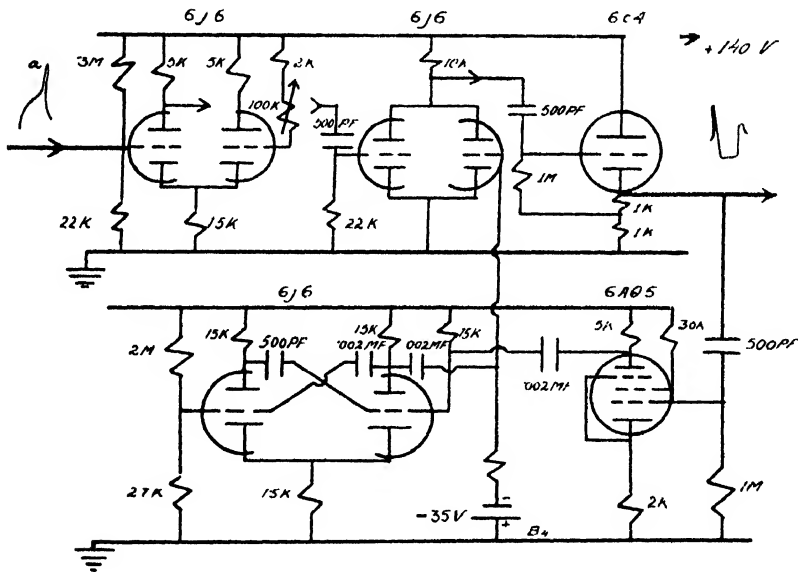


Fig. 5. Detailed diagram of sharpener-cum-feed-back .

The second coincidence pulse *b* is also applied to an exactly similar circuit described above, except that the constants of the first tube are changed to secure a sharp pulse of fast rise time. The bias voltage is also kept less than that in the above case for the same reason.

It was tested that the change of frequency of input pulses upto 20,000 per second did not in any way affect the output pulses  $a'$  and  $b_0$ .

#### Delayed Coincidence :

The delay line to which pulse  $a'$  is fed was made in the laboratory, and consists of large number of ebonite cored inductances of nearly equal value, different points of which were grounded through condensers, making it a

## REFERENCES

- Benade, A. H. and Sard, R. D., 1949, *Phys. Rev.*, **76**, 488.  
Corson, D. L. and Wilson, R. R., 1948, *Rev. Sc. Inst.*, **19**, 207.  
Hincks, R. and Pontecorvo, B., 1950, *Phys. Rev.*, **77**, 120.  
Rossi, B. and Nereson, N., 1913, *Phys. Rev.*, **64**, 199.  
Sands, M. L. and Sard, R. F., 1947, *Phys. Rev.*, **72**, 10.  
Ticho, H. K., M., 1947, *Rev. Sc. Inst.*, **18**, 271.

# SPECTROSCOPIC CONSTANTS OF MOLECULES I ON THE GROUND STATE FREQUENCIES OF DIATOMS OF THE TYPE XX

By K. MAJUMDAR AND Y. P. VARSHNI  
DEPARTMENT OF PHYSICS, ALLAHABAD UNIVERSITY, ALLAHABAD

(Received for publication, December 19, 1953)

**ABSTRACT.** The theoretical evaluation of the spectroscopic constants of molecules by quantum mechanics has been retarded due to the difficulties in calculations. In the present and the succeeding papers the authors propose to discuss the existing relations and to suggest new ones—empirical or semi-theoretical—between the spectroscopic constants of molecules. A new unit for “ $10^3$  dynes/cm.” viz. “Des.” after the pioneer worker Deslandre is proposed.

An improved form of Matuyama-Clark relation connecting the ground state frequencies of diatoms (diatomic molecules) formed of the same element has been suggested. The relation is  $\log \omega_e = g - h \log n^{2I}$ , where  $n$  is the total quantum number of the valence electrons,  $V$  the ionisation potential and  $g$  and  $h$  are constants for each group. Values for FrFr, GeGe, SnSn, PoPo and AtAt have been predicted.

## GENERAL INTRODUCTION

The explanation of hydrogen molecule on wave mechanics by Heitler and London (1927), and the refinements by later workers, placed the valence theories on a solid foundation and it became possible to calculate theoretically the spectroscopic constants of  $H_2$ . However, except for the simplest cases the theoretical discussion of molecules deals with the problem of a system consisting of rather large number of particles (electrons and nuclei). There is hardly any possibility of solving such problems rigorously. To arrive at an approximate solution various factors have to be neglected. According to the type of approximation used, we are led to different valence theories. Often the approximations are very questionable and the results obtained can only be called ‘daring approximations’. So far as numerical magnitudes are concerned, the calculations are almost hopelessly complicated for the heavier molecules. As Coulson (1952) remarks “It has laughingly been said that calculating the dissociation energy of a heavy molecule is like weighing the captain of a ship by determining the difference in displacement of his ship when he is, or is not, on board.”

Attempts have been made in the past to obtain empirical correlations between different molecular constants, such as force constant, internuclear distance etc. Some of the well-known empirical formulae are due to Brige (1925), Mecke (1925), Morse (1929), Clark and his collaborators (1934-1952),

Allen and Longair (1935), Badger (1934, 1935), Huggins (1935, 1936), Sutherland (1938, 1940), Linnett (1940, 1942), Gordy (1946), Guggenheimer (1946), Wu and Chao (1947) and others.

It is the purpose of the present and the succeeding papers to discuss the existing relations and to suggest new ones—empirical or semi-theoretical. The methods will be applied to the prediction of undetermined constants wherever possible.

It is expected that the present method of approaching the problem of spectroscopic constants may prove useful, in encouraging experimental and theoretical developments. From the practical standpoint, some incentive may be given to the task of verification or otherwise of predicted values. Further, a more careful determination of such constants which are found to be empirically anomalous would be advisable (e.g. vibration frequencies of  $\text{FF}$ ,  $\text{PN}$ ,  $\text{AsN}$  etc.) It is interesting to note that often two independent empirical methods lead to the same results.

On the theoretical side, as mentioned above, progress by the rigorous methods of quantum mechanics has been retarded by difficulties of calculation, and empirical methods may, therefore, be useful. The present trend indicates that the theory will advance more along a semi-empirical, rather than a purely theoretical approach. Some of the empirical relations may serve as hand holds by which the theoretician can climb to more commanding positions.

#### NOTATION AND SYMBOLS

Clark (1935 *b*) has suggested the use of the term “di-atom” as a short form of the somewhat cumbersome “diatomic molecule” and he has advanced several reasons in support of his suggestion. Though his suggestion has not gained general currency, it is found that it is very convenient and will be used.

Similarly following Clark a homonuclear diatomic molecule will be denoted by  $\text{XX}$  instead of the conventional  $\text{X}_2$ . Walsh (1951) has also used the same symbol.

Clark has divided the molecules into ‘periods’ which are designated as  $\text{KK}$ ,  $\text{KL}$ ,  $\text{KM}$ ,  $\text{LL}$ ,  $\text{LM}$  etc., the letters indicating the closed electronic shells of the component atoms. Thus  $\text{CO}$  is  $(\text{KK})$ ,  $\text{AlO}$  is  $(\text{KL})$  etc. This notation has since been followed by several authors and it will also be followed here.

The symbols used for the molecular constants are usually those which have been used by Herzberg in his well-known book “Molecular Spectra and Molecular Structure” Part I (1950).

$\omega_e$ ,  $\omega_e x_e$  and  $\omega_e y_e$  are defined by

$$G(v) = \omega_e(v + \frac{1}{2}) - \omega_e x_e(v + \frac{1}{2})^2 + \omega_e y_e(v + \frac{1}{2})^3$$

$r_e$ —internuclear distance at equilibrium

$\mu_A$ —reduced mass in atomic weight units

$$k_e = 4\pi^2 \mu c^2 \omega_e^2 = 5.888 \times 10^{-2} \mu_A \omega_e^2 \text{ dynes/cm.}$$

$D_0$ —dissociation energy for the ground state

( )—constants and symbols in parentheses are uncertain.

The new unit :

The force constant  $k_e$  is usually expressed in terms of  $10^5$  dynes/cm. It seems better to have some short symbol for this unit as the force constant is used very frequently. The authors suggest the symbol "Des", after-Deslandre, the pioneer worker in Molecular Spectra. It is hoped that the suggestion will meet the approval of other workers in the field.

#### D A T A

The data has been taken in most cases from the following sources :

1. G. Herzberg : "Molecular Spectra and Molecular Structure" Part I, 1950, (D. Van Nostrand Co. Inc., New York).
2. G. Herzberg : "Atomic Spectra and Atomic Structure", 1944 (Dover Publications, New York).
3. A. G. Gaydon : "Dissociation Energies and Spectra of Diatomic Molecules", 1950 (Dover Publications Inc., New York).
4. B. Rosen (editor) : "Donnees Spectroscopiques Concernant les Molecules Diatomiques", 1951 (Hermann and Cie, Depositaires, Paris V c)
5. W. Jevons : "Report on Band-Spectra of Diatomic Molecules" (Appendix II), 1932 (Cambridge University Press).
6. C. D. Hodgman (editor) : "Handbook of Chemistry and Physics", 1951 (Chemical Rubber Publishing Co., Ohio).
7. C. E. Moore : "Atomic Energy Levels", 1949 (Washington).

#### I N T R O D U C T I O N

Matuyama (1934) proposed that the logarithms of the ground state vibrational frequencies of diatoms XX formed of the same element were linear with the logarithms of the atomic weights of X for each group in the Periodic Table. The relation may be expressed as

$$\log \omega_e + p \log A = \text{a constant} \quad \dots (1)$$

where  $p$  is a constant ( $\sim 1$ ) for a given group. It was found however, that discrepancies occurred in the LL period, containing NaNa, PP, SS, ClCl. It may be added that this cannot hold for the different isotopes, because, for the isotopes  $k_e$  is constant *i.e.*

$$4\pi^2 \frac{A}{2} c^2 \omega_e^2 = \text{constant}$$

or,

$$\log \omega_e + \frac{1}{2} \log A = \text{constant}$$

while in (1),  $p \sim 1$ .

Clark (1937) modified the above relation as follows :

$$\log \omega_e = p - n \log 2Z \quad \dots (2)$$

where  $n$  and  $p$  are constants and  $2Z$  is the number of extra-nuclear electrons (twice the nuclear charge) of XX. He showed that equation (2) was more successful than Matuyama's, though the anomalies persisted in LL period.

A similar relation is found to hold good if, instead of  $zZ$ , the effective charge  $Z_e$ , defined as follows, is used.

$$V' = \frac{RZ_e^2}{n^2} \text{ or } Z_e^2 = \frac{n^2 V}{R}$$

where  $V$  is the ionisation potential of  $X$ ,  $n$  the total quantum number of the valence electrons, and  $R$  the Rydberg constant. We can write the final relation as

$$\log \omega_e = g - h \log n^2 V \qquad \dots (3)$$

where  $g$  and  $h$  are constants for each group. The relationship is shown graphically figure 1. To avoid overlapping the ordinates of the points of the fourth in fifth groups have been decreased by .6. The values of the constants  $g$  and  $h$  for the various groups are given in Table I.

TABLE I

Group	$g$	$h$
I	4.0594	1.1349
IV	4.9401	1.0431
V	6.4827	1.7338
V and VII	5.2353	1.2015

The results are tabulated in Table II.  $\omega_e(3)$  represents the values calculated from equation (3) and  $\omega_e(2)$  from the Matuyama-Clark relation (2).

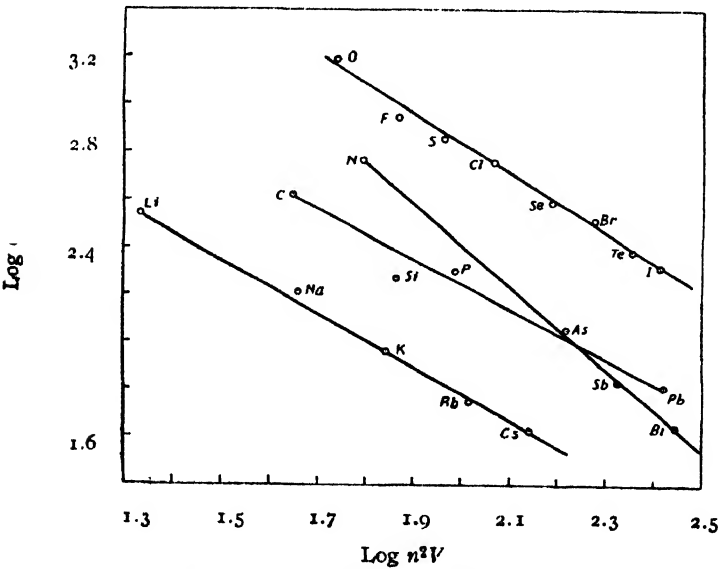


Fig. 1. The  $\log \omega_e$  values for the fourth and fifth groups have been decreased by .6 to avoid overlapping

Experimental data for the ionisation potentials of Francium, Polonium and Astatine are available. However, Finkelberg and Stern (1950) and Kohlrausch (1949) have estimated them by semi-empirical methods. The ionisation potential of Bi has been taken from Richtmyer and Kennard (1947). Other data have been taken from general references.

TABLE II

Group	Molecule	<i>n</i>	<i>V</i> in volt	$\omega_c$ (3)	$\omega_c$ (2)	$\omega_c$ observed
I	LiLi	2	5.390	351.4	351.4	351.4
	NaNa	3	5.138	147.9	136	159.2
	KK	4	4.31	93.1	91.2	92.6
	RbRb	5	4.176	58.0	56.1	57.3
	CsCs	6	3.893	42	42	42
	FrFr	7	$4.0 \pm 1^b$	30.7 $\pm 1.2$	30.1	
IV	CC	2	11.465	1611.3		1641.3 (750)
	SiSi	3	8.119	987		
	GeGe	4	8.106	543		
	SnSn	5	7.332	380		
	PbPb	6	7.115	250.5		256.5
V	NN	2	15.545	2359.6	2359.6	2359.6
	PP	3	10.977	1257	1026	780.4
	AsAs	4	10.5	420.9	431.5	429.4
	SbSb	5	8.64	272.3	269.8	269.8
	BiBi	6	8.0 <sup>a</sup>	165.3	157.4	172.7
VI	OO	2	13.615	1412	1580.4	1580.4
	SS	3	10.357	739.3	799.8	725.7
	SeSe	4	9.75	398.3	380.2	391.8
	TeTe	5	9.007	256.3	251	251
	PoPo	6	$8.4 \pm .3^b$	200.2 $\pm 8.5$	156.3	
VII	FF	2	17.422	1049	1080	(892)
	ClCl	3	12.959	565	604.5	564.9
	BrBr	4	11.844	316.3	312.9	323.2
	II	5	10.44	214.6	214.6	214.6
	AtAt	6	$9.5 \pm .2^b$	172.9 $\pm 4.3$	139.4	

*a*—Richtmyer and Kennard (1947)

*b*—Finkelberg and Stern (1950). Kohlrausch's (1949) estimates for Fr, Po and At are 4.11, 8.3 and 9.4 respectively. Richter (1950) estimates 3.6 for francium.

## DISCUSSION

It will be observed that the discrepancies in the L.L. period have been much reduced. While the calculated results for NaNa, SS, ClCl are satisfactory, there are still large errors in case of SiSi and PP. However, it must be remembered that the observed value of SiSi is uncertain, inasmuch as the identification of the bands as due to SiSi is tentative (Downie

and Barrow, 1947). It is also not certain that the lower state is the ground state. It is significant to note that there are strong vibrational and rotational perturbations in case of PP (Herzberg, 1932 ; Marais, 1946). The calculated value of  $\omega_e$  is also much in error. The points for the VIth and VIIth groups are seen to lie on the same straight line. No determination of the  $\omega_e$  for FrFr, GeGe, SnSn, PoPo and AtAt has been made. The predicted values are given in the table. The predicted value for FrFr is close to Clark's predicted value, but there is much difference for PoPo and AtAt.

#### ACKNOWLEDGMENT

The authors are thankful to the Council of Scientific and Industrial Research for the financial assistance and the permission to publish the results.

#### REFERENCES

- Allen, H. S. and Longair, A. K., 1935, *Phil. Mag.*, **19**, 1052.  
 Badger, R. M., 1934, *J. Chem. Phys.*, **2**, 128.  
 Badger, R. M., 1935, *J. Chem. Phys.*, **3**, 710.  
 Badger, R. M., 1935, *Phys. Rev.*, **48**, 284.  
 Birge, R. T., 1925, *Phys. Rev.*, **25**, 240.  
 Clark, C. H. D., 1935 a, *Phys. Rev.*, **47**, 238.  
 Clark, C. H. D., 1935b, *Phil. Mag.*, **19**, 476.  
 Clark, C. H. D., 1937, *Trans. Faraday Soc.*, **198**, 1308.  
 Clark, C. H. D. and Webb, K. R., 1941, *Trans. Faraday Soc.*, **37**, 293.  
 Coulson, C. A., 1952, *Valence*, (Oxford University Press) p. 88.  
 Downie, A. R. and Barrow, R. P., 1947, *Nature*, **160**, 108.  
 Finkelburg, W. and Stern, F., 1950, *Phys. Rev.*, **77**, 303.  
 Gordy, W., 1946, *J. Chem. Phys.*, **14**, 305.  
 Guggenheimer, K. M., 1946, *Proc. Phys. Soc.*, **58**, 456.  
 Heitler, W. and London, F., 1927, *Z. Phys.*, **44**, 445.  
 Herzberg, G., 1932, *Ann. Physik*, **15**, 677.  
 Huggins, M. L., 1935, *J. Chem. Phys.*, **3**, 473.  
 Huggins, M. L., 1936, *J. Chem. Phys.*, **4**, 308.  
 Kohlrausch, K. W. F., 1949, *Acta Phys. Austriaca*, **3**, 29.  
 Linnett, J. W., 1940, *Trans. Faraday Soc.*, **36**, 1123.  
 Linnett, J. W., 1942, *Trans. Faraday Soc.*, **38**, 1.  
 Marais, E. J., 1946, *Phys. Rev.*, **70**, 499.  
 Matuyama, R., 1934, *Nature*, **133**, 567.  
 Mecke, R., 1925, *Z. Phys.*, **31**, 709.  
 Morse, P. M., 1929, *Phys. Rev.*, **34**, 57.  
 Richter, A. F., 1950, *Casopisu Ceskeho Lekarnictva*, **63**, 280.  
 Richtmyer, F. K. and Kennard, E. H., 1947, *Introduction of Modern Physics*, (McGraw Hill Book Co. Inc.).  
 Sutherland, G. B. B. M., 1938, *Proc. Ind. Acad. Sci.*, **9**, 34.  
 Sutherland, G. B. B. M., 1940, *J. Chem. Phys.*, **8**, 161.  
 Walsh, A. D., 1951, *Proc. Roy. Soc.*, **207**, A, 13.  
 Wu, C. K. and Chao, S. C., 1947, *Phys. Rev.*, **71**, 118.



# IONOSPHERE AND NATURE OF FADING PATTERNS OF RECEIVED RADIO SIGNALS

BY R. N. SINGH

DEPARTMENT OF PHYSICS, B. R. COLLEGE, AGRA

*(Received for publication, January 1, 1953; received after revision, January 4, 1954)*

**ABSTRACT.** Fading of received radio signals on short wave lengths have been studied in great details. Fading patterns on various wave bands for different distances of transmission from Indian as well as foreign transmitting stations have been recorded at different hours and months of the year. The observed fading patterns have been analysed in the light of Rayleigh's formula. The amplitude-distribution curves have been drawn from the fading patterns and compared with the theoretical curves obtained from Rayleigh's probability formula. From these curves, (a) variation of the nature of fading at different hours of the day for the same frequency and distance of transmitter and (b) variation of nature of fading of received radio signals at different hours for different distances but for the same frequency of transmission, have been studied. The discussion of the former, (a), leads to the conclusion that the nature of fading at least partially depends on the electronic densities which vary with the hour of observation in the ionosphere. Discussion on the latter, (b), also shows that the nature of fading may depend on the ionospheric conditions at the hours of observation and not the distance of transmission. Thus this communication intends to indicate that the nature of fading patterns of received radio signals is at least partially determined by the ionospheric conditions regarding the electronic density existing at the hours of observations, in the region of the ionosphere from which the reflections of the radio-waves are arriving at the receiver.

## INTRODUCTION

Potter (1930) made a detailed study of the transmission characteristics of short wave radio signals in America in 1930. One of the conclusions based on his observation was that there might be some relation between the frequencies of transmission and the fading patterns of radio signals. After a lapse of about two years, one of the most important researches on the intensity variations of received radio signals was carried out by Ratchliffe and Pawsey (1933) in England. The observations were made on medium waves between 200 and 500 metres and the distance between the transmitter and the receiver was less than 200 km. According to them the fading of signals may occur due to the effects of absorption in the atmosphere and also due to interference of waves travelling in different paths. They arrived at the conclusion that the rapid variations of signal intensity are mainly due to the interference phenomenon. They finally held the view that most of the fading is due to the interference caused by scattered waves from a series of diffracting centres in the ionosphere. Pursuing the

problem for about two years Pawsey (1935) gave an account of further experiments on fading of radio signals. Working on medium wave lengths between 200 and 500 metres, he found that the time variation of amplitude of a reflected wave was consistent with random scattering at the ionosphere. In 1940, Khastgir and Ray (1940) intended to test whether observed variations (using the wave length 370.4 m) or intensity of received radio signals could be attributed to similar random scattering at the ionosphere as suggested by the earlier workers. They concluded that the time variations of amplitude of down-coming waves agree with Rayleigh's formula for random scattering. At about the same time, Sengupta and Dutt (1941) made some observations on fading of signals on medium waves received at Patna and transmitted from Calcutta and Dacca which are at distances of about 480 and 610 km respectively. They concluded from their observations over a period of two years that while a random scattering is a major factor in accounting for the variation of signal strength of the down-coming waves, the observed data cannot be fully explained by this theory alone for long distance transmission. It may be pointed that the sizes and velocities of the irregularities are also liable to change with local hours and they may also cause changes in the fading patterns. The present communication is intended to show that the ionospheric condition, particularly with regard to the electronic concentration existing in the ionosphere at the hours of observations, is one of the factors responsible for shaping the nature of the fading patterns of short wave radio-signals.

#### DISTANCES AND FREQUENCIES OF TRANSMISSION FOR THE PRESENT INVESTIGATION

It may be noted from the previous section that most of the investigators engaged in the study of fading pattern of radio signals employed medium waves for their observations, and investigations were generally made for short distances between transmitting and receiving stations. Comparatively much less work appears to have been done on short wave length and for long range transmissions. This led to the present investigations by the author, on the phenomenon of fading of radio-signals under the guidance of Dr. S. S. Banerji, Banaras, on various short wave lengths. The observations were recorded for transmission from All India Radio, Delhi and other Indian as well as foreign stations including B. B. C. London, Australia and Ceylon. The observations of Banerji and Singh [1948, 1949(a) 1949(b)], were generally made for 13 to 16 metre bands and some observations for medium waves for transmission from Indian stations were also recorded. The automatic and visual records of Banerji and Singh [1948 and 1949(a)] of fading patterns obtained at different hours of the day and for all the months of the year were studied in detail; the analysis and results of which are given in the following sections.

# RAYLEIGH'S FORMULA AND THE ANALYSIS OF THE NATURE OF FADING PATTERNS

In order to test the true nature of fading patterns of received radio signals on various wave length, it is considered necessary, at the outset, to plot the amplitude-distribution curves for the most commonly occurring random fading patterns and compare them with the theoretical amplitude or intensity distribution curves obtained from Rayleigh's probability formula represented

by  $P = \frac{2X}{R^2} e^{-\frac{X^2}{R^2}}$  where  $R$  is the sum of squares of components of random phases, and  $Pdx$  is the probability of resultant amplitude lying between  $X$  and  $X+dx$ .

With this object in view a number of apparently random looking patterns have been selected from a large number of records of fading patterns and for each of them intensity-distribution curve was drawn. A few of these are shown in the present communication. The procedure adopted for the intensity distribution curves from the experimental records of fading patterns is too well known to need any description.

## VARIATION OF THE NATURE OF FADING AT DIFFERENT HOURS OF THE DAY FOR THE SAME FREQUENCY AND DISTANCE OF TRANSMISSION

In order to show that for the same wave length, the theoretical and practical curves of intensity-distribution sometimes agree and at other occasions they do depart from each other, a set of two intensity-distribution curves for the same wave length has been drawn comparison. The corresponding patterns of fading have also been shown in the diagrams following the intensity distribution curves.

The practical and theoretical intensity-distribution curves shown by continuous and dotted lines respectively on 19m band for transmission between Delhi and Banaras have been shown. The corresponding fading patterns have been shown in figures 3 and 4. It will be seen in figure 1 that the practical curve for intensity-distribution agrees fairly well with the theoretical one but figure 2 shows that for the same frequency of transmission, the practical and theoretical curves completely disagree. In other words, it may be said that although the frequency and distance of transmission are the same in the two cases of fading patterns, the nature of fading is different as indicated by figures 1-4. It may be remembered that the hours of observations for these fading patterns are different. Figures 5 and 6 each show the practical and theoretical curves for intensity distribution on 25 metre band for the same distance of transmission between Banaras and Delhi (678.4 km.). The corresponding fading patterns are shown in figures 7 and 8. In figure 5, we observe almost a complete agreement and in figure 6, disagreement between the practical and theoretical

intensity distribution curves, although the frequency and distance of transmission are the same, only the hours of observations for these patterns shown in figures 7 and 8, are different.

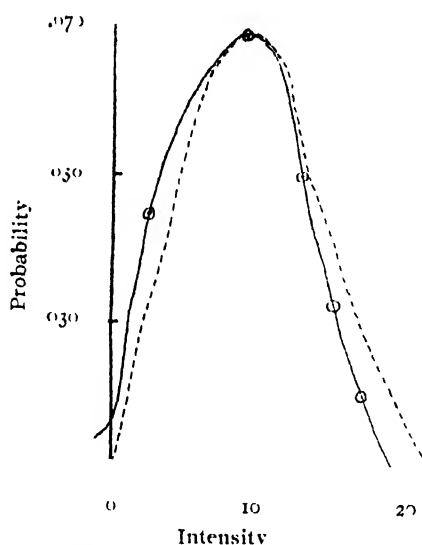


Fig. 1. Delhi, 10m, 18.5.1946, 1054 hours (I.S.T.)

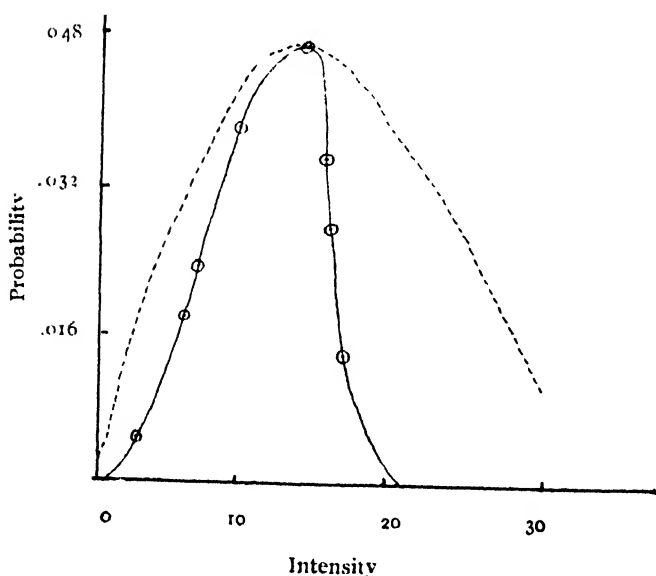


Fig. 2. Delhi, 19m, 1.8.1948, 1830 hours (I.S.T.)

Similarly on 41 metre and 49 metre bands for the same distance of transmission 678.4 km between Delhi and Banaras, sometimes close agreement have been observed. In all these cases, it is only the hours of observation for the fading patterns, that are different.

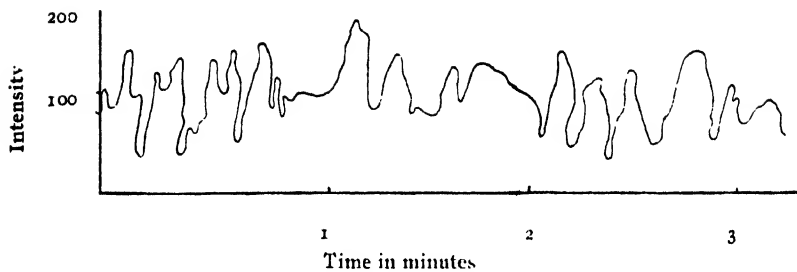


Fig. 3 Delhi, 19m, 18.5.1946, 1054 hours (I.S.T.)

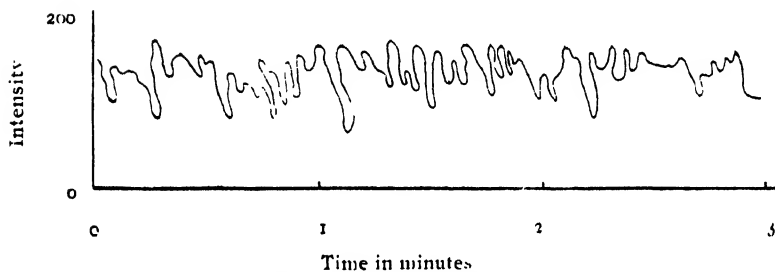


Fig. 4 Delhi, 19m, 18.10.48, 1839 hours (I.S.T.)

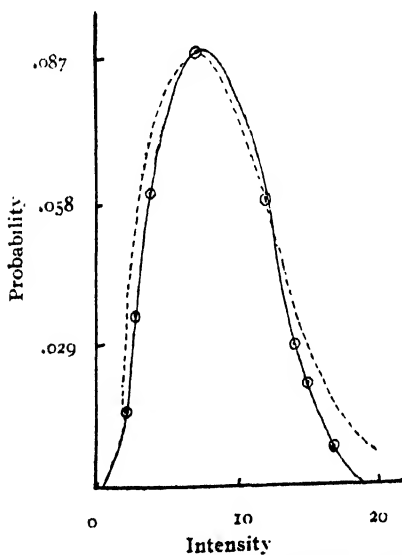


Fig. 5. Delhi, 23m, 21.5.1946, 0723 hours (I.S.T.)

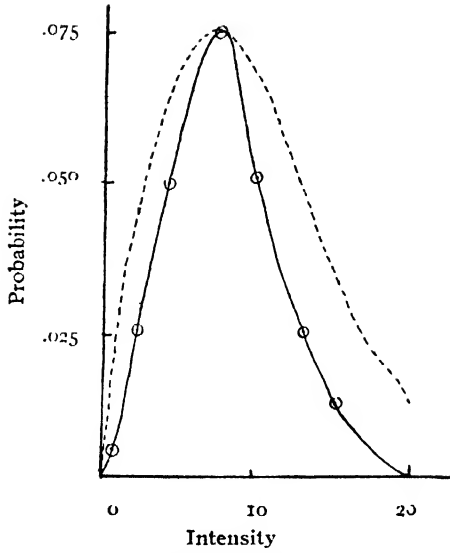


Fig. 6 Delhi, 25m, 2.5.1946, 0900 hours (I S.T.)

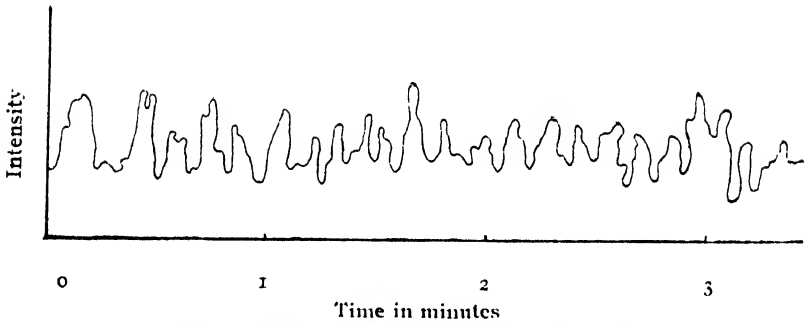


Fig. 7. Delhi, 25m, 21.5.1946, 0723 hours (I S.T.)

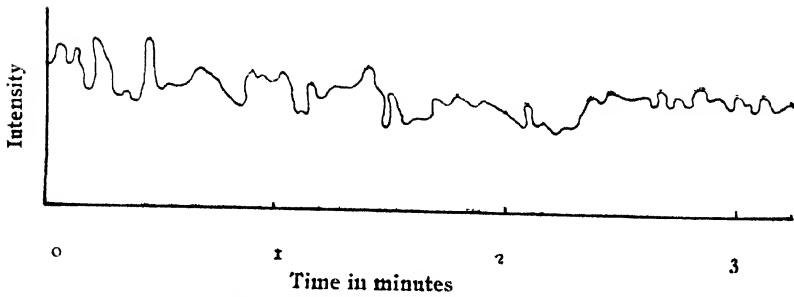


Fig. 8. Delhi, 25m, 2.5.1946, 0900 hours (I.S.T.)

From this detailed analysis, it may be concluded that the nature of fading depends on the hours of their observations. Since the electronic concentrations in the ionosphere, sizes and velocities of the irregularities are liable to vary with the hours of observation, it may be said that the nature of fading depends mainly on the ionospheric conditions, with respect to sizes and velocities of the irregularities and the electronic density, in the ionospheric region, from which the radio waves are being reflected and reaching the receiver. That is, for the same frequency of transmission between two stations, one may obtain different kinds of fading patterns for different hours of observations.

VARIATION OF NATURE OF FADING OF RAD  
SIGNALS AT DIFFERENT HOURS FOR DIFFERENT  
DISTANCES BUT FOR THE SAME FREQUENCY OF  
TRANSMISSION

Intensity-distribution curves on 19 metre band for the distance of transmission between Banaras and Australia are depicted in figures 9 and 10. Figure 9 shows a complete agreement between the practical and the theoretical intensity-distribution curves, while a wide disagreement is shown in figure 10. Their respective fading patterns are shown in figures 11 and 12.

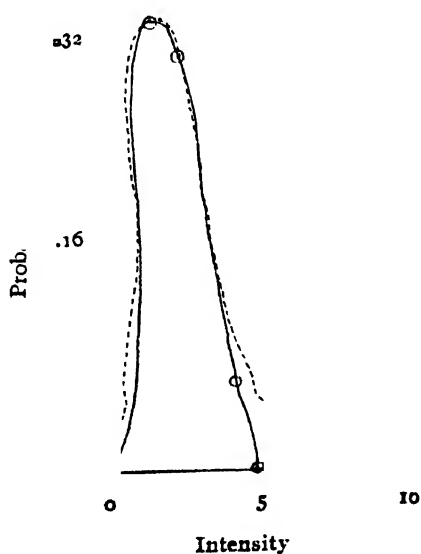


Fig. 9. Australia, 19m, 6.4 1947, 1629 hours (I.S.T.)

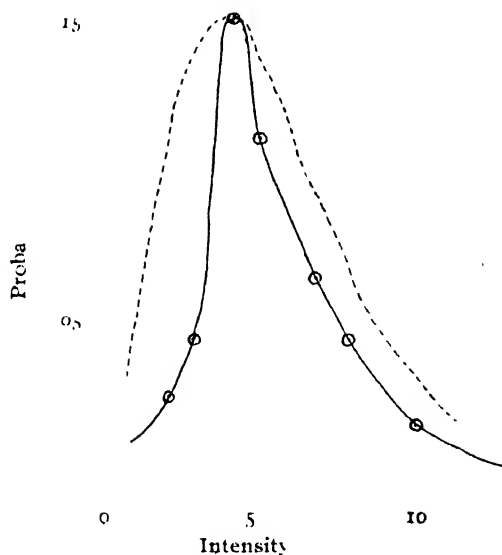


Fig. 10 Australia, 19m, 22.2.1946, 1750 hours (I.S.T.)

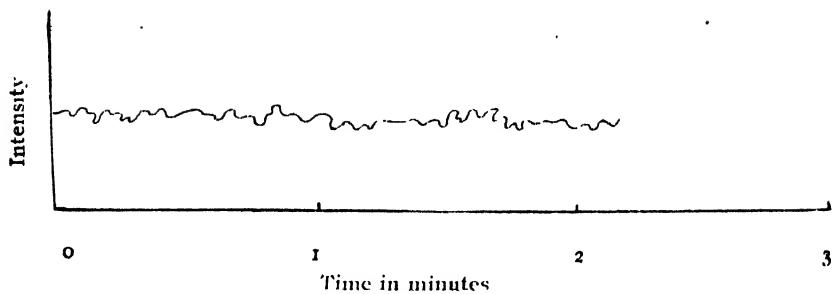


Fig. 11. Australia, 19m, 6.4 1947, hours (I.S.T.)

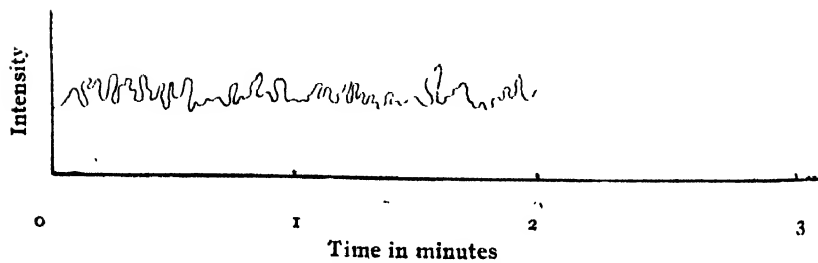


Fig. 12. Australia, 19m, 22.2.1946, 1750 hours (I.S.T.)



Another set of intensity-distribution curves on 19 metre band and for distance of transmission between Banaras (India) and Ceylon was found to show agreement as well as disagreement between theoretical and practical curves at different hours of observation.

From these sets of observations it will be seen that for the distance between Australia and Banaras there is both agreement as well as disagreement between the practical and theoretical intensity distribution curves. For another distance, between Ceylon and Banaras, also there is both agreement as well as disagreement between the said curves for the same frequency of transmission. That is, the same nature of fading pattern of received radio signals can be obtained for various distances of transmission, on a particular frequency, of course, at different hours of observation. This again leads us to conclude that the nature of fading is presumably determined at least partially by the electronic concentration in the ionospheric region from where the reflections are occurring.

#### CONCLUSION

In the discussion above, we have seen that for each of the frequencies of transmission on 19, 25, 41, and 49 metre bands and for the distance of transmission between Delhi and Banaras (678.4 km.) we get different types of fading patterns at different hours of observations, leading us to conclude that the nature of fading may partially depend on the electronic densities which vary with the hour of observation in the ionosphere. Discussion in the previous section on 19 metre band for distances of transmission between Ceylon-Banaras and Australia-Banaras also show that the nature of fading may depend on the ionospheric conditions at the hours of observation and not the distance of transmission. Thus, this communication has attempted to indicate that the nature of fading patterns of received radio signals is at least partially determined by the ionospheric conditions regarding the electronic density, existing at the hours of observations, in the region of the ionosphere from which the reflections of the radio waves are arriving at the receiver.

#### ACKNOWLEDGMENTS

The author is extremely indebted to Dr. S. S. Banerji, D.Sc., who has been guiding the present investigation. He is very grateful to Prof. G. C. Mukerji who has always been a source of help during this period of work. The author feels extremely grateful to Prof. S. K. Mitra whose work and reports have enriched him substantially with information. Lastly, the author wishes to record his grateful thanks to Dr. R. K. Singh, D. Ed. Principal, B. R. College, Agra for his encouragement for research.

## REFERENCES

- Banerji, S. S. and Singh, R. N , 1948, *Ind. J. Phys.*, **22**, 109.  
Banerji, S. S. and Singh, R. N., 1949a, *Science and Culture*, **14**, 293.  
Banerji, S. S. and Singh, R. N., 1949b, *Nature* **164**, 925.  
Khastgir, S. R. and Ray, A K., 1940, *Ind. Jour. Phys.*, **14**, 283.  
Pawsey, J. L., 1935, *Proc Camb Phil. Soc* , **31**, 125.  
Potter, R. K., 1930, *Proc. Inst. Rad. Eng.* , **18**, 581.  
Ratcliffe, J. A. and Pawsey, J L , 1933. *Proc. Camb Phil. Soc.*, **29**, 301  
Sengupta, M. M. and Dutt, S. K., 1941, *Ind. J. Phys* , **15**, 447.

# ON BORN'S APPROXIMATION AND ITS CONNECTION WITH COVARIANT PERTURBATION THEORY

By S. N. BISWAS

DEPARTMENT OF THEORETICAL PHYSICS, INDIAN ASSOCIATION FOR THE CULTIVATION OF SCIENCE, CALCUTTA 34

(Received for publication, January 25, 1954)

**ABSTRACT.** In this paper a connection between the usual perturbation method and the covariant perturbation theory of Feynman and Dyson has been established by considering the scattering of fast electron in a static field. It has been shown that by the usual perturbation method, the second Born approximation for the scattering of Dirac electron by the Coulomb potential gives the same result as obtained by Dalitz using the covariant  $S$ -matrix of Feynman and Dyson. It also agrees with the expression given by McKinley and Feshbach from the complete solution of Mott.

## INTRODUCTION

It is well known that the contributions of higher approximations in the Born's series for the potential scattering of fast electrons become infinite during the transition from Yukawa to Coulomb potential due to the long-range character of Coulomb forces. The non relativistic case was discussed in detail by Distel (1932) and Möller (1933). The calculation was further carried out for the relativistic scattering of Dirac particle by Sexl (1933) Sauter (1936) and Urban (1942). The same divergence difficulties remained in the relativistic case. The error in their development has been pointed out by Dalitz (1952) who, with the aid of covariant formalism of Feynman and Dyson, has obtained the correct second order result which is just the expression given by McKinley and Feshbach (1948). The result McKinley and Feshbach derived from the expansion of Mott's complete solution (1929) of the 2nd order Dirac equation.

In this paper we have shown that the same results as obtained by Dalitz (1952) for the potential scattering of electrons can be obtained from the usual Born's series. Born's approximation in the configuration space contains iterated integrals which come from the solution of an integral equation. [This integral equation can be solved by iteration, as an expansion in powers of the coupling constant, however, the higher order terms are difficult to evaluate. The analytical difficulty lies in the non-separable character of the Green's function  $\exp(ip|\mathbf{r}-\mathbf{r}'|)(4\pi)^{-1}(|\mathbf{r}-\mathbf{r}'|)^{-1}$  of the integral equation of the scattering process. This difficulty in this case is removed by first transforming the whole series by the following Fourier transforms namely,

$$\begin{aligned} & \lim_{\epsilon \rightarrow 0} (2\pi)^{-3} \int \frac{dk}{k^2 - (p^2 + i\epsilon)} \exp(ik(\mathbf{r} - \mathbf{r}')) \\ & \rightarrow (4\pi)^{-1} \exp(ip|\mathbf{r} - \mathbf{r}'|) \cdot (|\mathbf{r} - \mathbf{r}'|)^{-1} \end{aligned}$$

The introduction of this ensures the separability of Green's function.

For the 2nd Born approximation we have first converted the differential equation for the Dirac particle to an integral equation. This is then iterated twice to obtain the 2nd approximation. This may be considered as the direct extension of the method which Sauter (1933a) used to obtain the first approximation.

In another section we have established the connection of the usual perturbation method with the covariant perturbation formalism of Feynman and Dyson. It may be concluded that direct relativistic generalisation of the usual perturbation method corresponds to the covariant  $S$ -matrix of Feynman and Dyson, in the case of scattering of a particle in a static field. For, if we first perform the time integration occurring in the covariant total transition amplitude,  $\langle p|s|q \rangle$ , then we get the same expression as can be obtained for the scattering amplitude in the conventional perturbation formalism.

#### 1. BRON'S APPROXIMATION (2ND ORDER)

The relativistic equation of a Dirac particle is given by

$$\sum_{\nu=1}^3 \gamma_{\nu} \frac{\partial}{\partial x_{\nu}} - \gamma_4(E - V) + m \Bigg] \psi = 0 \quad \dots (1)$$

where  $E$  is the energy and  $V$  is the potential function ( $\hbar = c = 1$  is used)

Multiplying the equation (1) from the left by the operator,

$$\sum_{\nu} \gamma_{\nu} \frac{\partial}{\partial x_{\nu}} - \gamma_4 E - m$$

$$\text{we get} \quad (\nabla^2 + p^2)\psi = - \left( \sum_{\nu} \gamma_{\nu} \frac{\partial}{\partial x_{\nu}} - \gamma_4 E - m \right) \gamma_4 V(r) \psi \quad \dots (2)$$

On converting the differential equation (2) to an integral equation it can be easily shown that  $\psi$  obeys the following integral equation :

$$\psi(r) = \psi_0(r) + \int G(r, r') \left( \sum_{\nu} \gamma_{\nu} \frac{\partial}{\partial x_{\nu}} - \gamma_4 E - m \right) \gamma_4 V(r') \psi(r') d^3 r' \quad \dots (3)$$

where  $\psi_0(r) = e^{ip \cdot r} u(p)$  ;  $u(p)$  is the usual Dirac Spinor and  $\psi_0(r)$  satisfies

$$(\nabla^2 + p^2)\psi_0(r) = 0$$

$G(r, r')$  corresponds to the Green's function of the associated differential equation (2) and it is constructed from the solution of

$$(\nabla^2 + p^2)G(r, r') = \delta(r, r')$$

The value of  $G(r, r')$  may be found to be

$$\frac{e^{ip|\mathbf{r}-\mathbf{r}'|}}{4\pi|\mathbf{r}-\mathbf{r}'|}$$

On integrating by parts (3) reduces to

$$\psi(r) = \psi_0(r) + \left( \Sigma \gamma_v \frac{\partial}{\partial x_v} - \gamma_4 E - m \right) \gamma_4 \int \frac{e^{ip|\mathbf{r}-\mathbf{r}'|}}{4\pi|\mathbf{r}-\mathbf{r}'|} V(r') \psi(r') d^3 r' \quad \dots (4)$$

Asymptotically (4) must be of the form

$$\psi(r) \simeq \psi_0(r) + \frac{e^{ipr}}{r} \cdot f(\theta)$$

i.e. an incident wave plus a radially outgoing wave at infinity, where  $f(\theta)$  is the scattering amplitude and is connected to the differential scattering cross section by

$$\frac{d\sigma}{d\Omega} = |f(\theta)|^2$$

On iterating the equation (4) twice we get the usual 2nd order Born's approximation,

$$\begin{aligned} \psi(r) = & \psi_0(r) + \left( \Sigma \gamma_v \frac{\partial}{\partial x_v} - \gamma_4 E - m \right) \gamma_4 \int \frac{e^{ip|\mathbf{r}-\mathbf{r}'|}}{4\pi|\mathbf{r}-\mathbf{r}'|} V(r') \psi_0(r') d^3 r' \\ & + \left( \Sigma \gamma_v \frac{\partial}{\partial x_v} - \gamma_4 E - m \right) \gamma_4 \int \frac{e^{ip|\mathbf{r}-\mathbf{r}'|}}{4\pi|\mathbf{r}-\mathbf{r}'|} V(r') \left( \Sigma \gamma_v \frac{\partial}{\partial x'_v} - \gamma_4 E - m \right) \gamma_4 \\ & \times \int \frac{e^{ip|\mathbf{r}'-\mathbf{r}''|}}{4\pi|\mathbf{r}'-\mathbf{r}''|} V(r'') \psi_0(r'') d^3 r' d^3 r'' \quad \dots (6) \end{aligned}$$

Now we confine ourselves to evaluating the 3rd term of the above series.

We replace the Green's function  $\frac{e^{ip|\mathbf{r}'-\mathbf{r}''|}}{4\pi|\mathbf{r}'-\mathbf{r}''|}$  occurring in the above term by

$$L_{\epsilon} \frac{t}{\epsilon} (2\pi)^{-3} \int \frac{d\mathbf{k}}{k^2 - (\mathbf{p}^2 + i\epsilon)} \cdot \exp [i\mathbf{k} \cdot (\mathbf{r}' + \mathbf{r}'')] \quad \dots (7)$$

Now changing the sequence of integration in the final result we get in the asymptotic form the following result for the 2nd approximation

$$\begin{aligned} \psi(r) \simeq & \psi_0(r) + \frac{e^{ipr}}{r} \cdot (4\pi)^{-1} \left[ \{i(\gamma \cdot \mathbf{p}) - \gamma_4 E - m\} \gamma_4 \int e^{-i\mathbf{p} \cdot \mathbf{r}'} V(r') e^{i\mathbf{p} \cdot \mathbf{r}'} d^3 r' \right. \\ & + (i\gamma \cdot \mathbf{p} - \gamma_4 E - m) \gamma_4 L_{\epsilon} \frac{t}{\epsilon} (2\pi)^{-3} \int \frac{d\mathbf{k}}{k^2 - (\mathbf{p}^2 + i\epsilon)} \int e^{-i\mathbf{p} \cdot \mathbf{r}'} V(r') e^{i\mathbf{k} \cdot \mathbf{r}'} d^3 r' \\ & \left. (i(\gamma \cdot \mathbf{k}) - \gamma_4 E - m) \gamma_4 \int -i\mathbf{k} \cdot \mathbf{r}'' V(r'') e^{i\mathbf{p} \cdot \mathbf{r}''} d^3 r'' \right] u(\mathbf{p}') \quad \dots (8) \end{aligned}$$

where the function  $\frac{e^{ip|\mathbf{r}-\mathbf{r}'|}}{4\pi|\mathbf{r}-\mathbf{r}'|}$  occurring in both the 2nd and 3rd terms has been written in its asymptotic form, namely,  $\frac{e^{ipr}}{4\pi r} \cdot \exp(-\mathbf{p} \cdot \mathbf{r}')$  assuming  $r$  is large in comparison with  $r'$ . This asymptotic form cannot be used for the function  $\frac{e^{ip|\mathbf{r}'-\mathbf{r}''|}}{4\pi|\mathbf{r}'-\mathbf{r}''|}$  in the 2nd integral of the 3rd term because both  $|\mathbf{r}'|$  and  $r''$  vary from zero to infinity: hence none can be neglected with respect to other.

The integral  $\int e^{-i\mathbf{p} \cdot \mathbf{r}'} V(r') e^{i\mathbf{k} \cdot \mathbf{r}'} d^3r'$  can be easily performed when we consider  $V(r')$  as the Yukawa potential,  $-Ze^2 e^{-\lambda r'}$ . The integral reduces to

$$V(\mathbf{p}-\mathbf{k}) = - \int e^{-i(\mathbf{p}-\mathbf{k}) \cdot \mathbf{r}'} r' (Ze^2) \frac{e^{-\lambda r'}}{r'} d^3r'$$

whence

$$V(\mathbf{p}-\mathbf{k}) = \frac{-4\pi Ze^2}{(\lambda^2 + |\mathbf{p}-\mathbf{k}|^2)}$$

The transition to Coulomb potential can be performed through the limiting process  $\lambda \rightarrow 0$  in the final result.

Hence equation (8) reduces to

$$\begin{aligned} \psi(r) \simeq \psi_0(r) + \frac{1}{4\pi} e^{imr} & \left[ (i(\gamma \cdot \mathbf{p}) - \gamma_4 E - m) \gamma_4 \frac{-4\pi Ze^2}{(\lambda^2 + |\mathbf{p}-\mathbf{p}'|^2)} \right. \\ & + (i(\gamma \cdot \mathbf{p}) - \gamma_4 E - m) \gamma_4 \frac{Lt}{\lambda \rightarrow 0} \frac{(4\pi Ze^2)^2}{(2\pi)^3} \\ & \times \left. \int \frac{d\mathbf{k} (i\gamma \cdot \mathbf{k} - \gamma_4 E - m) \gamma_4}{(k^2 - p^2 - i\epsilon)(\lambda^2 + |\mathbf{p}-\mathbf{k}|^2)(\lambda^2 + |\mathbf{k}-\mathbf{p}'|^2)} \right] u(\mathbf{p}') \end{aligned}$$

Now on comparison with (5) we can write for the relativistic scattering amplitude

$$\begin{aligned} f(\theta) = (Ze^2)(4\pi)^{-1} (i(\gamma \cdot \mathbf{p}) - \gamma_4 E - m) & \left[ \gamma_4 I_0 - \frac{2Ze^2}{\pi} \left( -i(\gamma \cdot (\mathbf{p} + \mathbf{p}')) \right) J/2 \right. \\ & \left. + (\gamma_4 E + m) I \right] u(\mathbf{p}') \end{aligned}$$

where

$$I_0 = V(\mathbf{p}-\mathbf{p}')$$

$$\frac{Lt}{\lambda \rightarrow 0} \int \frac{d\mathbf{k}}{(k^2 - p^2 - i\epsilon)(\lambda^2 + |\mathbf{p}-\mathbf{k}|^2)(\lambda^2 + |\mathbf{k}-\mathbf{p}'|^2)} = I$$

$$\text{and } \frac{Lt}{\lambda \rightarrow 0} \int \frac{-i(\gamma \cdot \mathbf{k}) d\mathbf{k}}{(k^2 - p^2 - i\epsilon)(\lambda^2 + |\mathbf{p}-\mathbf{k}|^2)(\lambda^2 + |\mathbf{k}-\mathbf{p}'|^2)} = -i(\gamma \cdot (\mathbf{p} + \mathbf{p}')) J/2$$

The explicit expressions for  $I$  and  $J$  may be given as

$$I = \frac{-\pi^2}{(p \sin \theta/2) \sqrt{[\lambda^4 + 4p^2(\lambda^2 + p^2 \sin^2 \theta/2)]}} \left\{ \tan^{-1} \frac{\lambda p \sin \theta/2}{\sqrt{[\lambda^4 + 4p^2(\lambda^2 + p^2 \sin^2 \theta/2)]}} \right. \\ \left. + i \ln \frac{\sqrt{[\lambda^4 + 4p^2(\lambda^2 + p^2 \sin^2 \theta/2)]} + 2p^2 \sin \theta/2}{\sqrt{[\lambda^4 + 4p^2(\lambda^2 + p^2 \sin^2 \theta/2)]} - 2p^2 \sin \theta/2} \right\} \\ J = I \left( \frac{\lambda^2 + 2p^2}{2p^2 \cos^2 \theta/2} \right) - \frac{i\pi^2}{2p^4 \cos^2 \theta/2} \left[ \ln \frac{i\lambda}{2p^2 + i\lambda} - \frac{i}{\sin \theta/2} \tan^{-1} \frac{p \sin \theta/2}{\lambda} \right]$$

The scattering cross section is obtained from the above result for the case of Coulombian potential by squaring  $f(\theta)$  and performing the limiting process  $\lambda \rightarrow 0$  in the final result. Thus the scattering cross section up to 2nd Born's approximation is given by

$$\frac{d\sigma}{d\Omega} = |f(\theta)|^2 = \frac{(Ze^2)^2(1-v^2)}{4m^2v^4} [\operatorname{cosec}^2 \theta/2 - v^2 \operatorname{cosec}^2 \theta/2 \\ + \pi Ze^2 v (\operatorname{cosec}^2 \theta/2 - \operatorname{cosec} \theta/2) + \dots]$$

This is the same result as obtained by Dalitz (1952) using the covariant S-matrix formalism of Feynman and Dyson. It may be mentioned that the above result comes through the real parts of  $J$  and  $I$ , however, when the limiting process  $\lambda \rightarrow 0$  is taken,  $I$  gives no contribution to the cross section.

## 2. CONNECTION OF COVARIANT FORMALISM AND NON-COVARIANT FORMALISM

The Dirac equation for a particle under static potential  $V(r)$  is

$$(i\nabla - m)\psi = \mathbf{Y}\psi \quad \dots (1) \\ \mathbf{Y} = \gamma_4 Y(r)$$

(The notations used here are the same as those of Feynman (1949).

The Green's function for (1) is  $K_+(2,1)$  which should satisfy the following

$$(i\nabla - m)_2 K_+(2,1) = i\delta(2,1) \quad \dots (2)$$

(The differential operator operates on the variable  $2$ ,  $x_2(x_{02} \ x_{12} \ x_{22} \ x_{32})$ ). Hence the solution of (1) may be shown to obey the integral equation

$$\psi(1) = \psi_0(1) - ie \int K_+(2,1) \mathbf{Y}(2) \psi(2) d\tau_2$$

where  $d\tau_2$  is the four dimensional volume element.

The function  $K_+(2,1)$  which is the solution of (2) is called the amplitude when there is no external field. A similar function  $K_+^\nabla(2,1)$  has been defined by Feynman given below to denote the amplitude where there is external field  $V(r)$ .

$$K_+^\nabla(2,1) = K_+(2,1) + K_+^{(1)}(2,1) + K_+^{(2)}(2,1) + \dots$$

The first order correction term  $K_+^{(1)}(2, 1)$  is given by

$$K_+^{(1)}(2, 1) = -ie \int K_+(2, 3) \mathbf{Y}(3) K_+(3, 1) d\tau_3$$

Similarly the 2nd order correction term is given by

$$K_+^{(2)}(2, 1) = -e^2 \int K_+(2, 4) \mathbf{Y}(4) K_+(4, 3) \mathbf{Y}(3) K_+(3, 1) d\tau_3 d\tau_4$$

As an analogue of equation (2),  $K_+^{\mathbf{v}}(2, 1)$  satisfies the diff. eq.,

$$(i\nabla - \mathbf{Y}(2) - m)_2 K_+^{\mathbf{v}}(2, 1) = i\delta(2, 1)$$

and, therefore, obeys the integral equation

$$K_+^{\mathbf{v}}(2, 1) = K_+(2, 1) - i \int K_+(2, 3) \mathbf{Y}(3) K_+^{\mathbf{v}}(3, 1) d\tau_3$$

The correction terms are evidently the successive terms of the iterated solution of the above integral equation.

Hence utilising the above facts we may write the wave function  $\psi(1)$  as

$$\psi(1) = \psi_0(1) - ie \int K_+^{\mathbf{v}}(1, 2) \mathbf{Y}(2) \psi_0(2) d\tau_2$$

with

$$K_+^{\mathbf{v}}(1, 2) = K_+(1, 2) - ie \int K_+(1, 3) \mathbf{Y}(3) K_+(3, 2) d\tau_3 + \dots \text{etc.}$$

Now the covariant transition probability that a particle initially at time  $t=0$  and position defined by the co-ordinates  $(1)$  and characterised by momentum  $\mathbf{p}$  should be in a position of co-ordinates  $(2)$  after a time  $t$  being characterised by the momentum  $\mathbf{q}$  is given by the  $S$ -matrix,  $(p | s | q)$  which, according to Feynman and Dyson,

$$(p | s | q) = (0 | s | 0) (p | R | q)$$

where  $(0 | s | 0)$  is the vacuum expectation value of the  $S$ -matrix and  $(p | R | q)$  is called by Feynman as the relative transition probability and is given by

$$\begin{aligned} (p | R | q) &= e \int \psi_{0,p}^* \mathbf{Y}(\tau) \psi_{0,q} d\tau \\ &\quad - ie^2 \int \int \psi_{0,p}^*(1) \mathbf{Y}(1) K_+(1, 2) \mathbf{Y}(2) \psi_{0,q}(2) d\tau_1 d\tau_2 \\ &\quad \dots \text{etc.} \end{aligned}$$

Now writing  $\bar{u}(p)M(p, q)u(q)$  for  $(p | R | q)$  and putting

$$\psi_{0,p}(1) = u(p)e^{-ip_\mu x_1^\mu}; \quad \psi_{0,q}(2) = u(q)e^{-iq_\mu x_2^\mu}$$

$$\text{and} \quad K_+(1, 2) = \lim_{t \rightarrow 0} \int \frac{i(k_\mu \gamma_\mu + m)}{(2\pi)^4} \exp(i k_\mu x_2^\mu - \lambda_1) d^4 k$$

Substituting these values in the above we get for  $M(p, q)$ , the following

$$M(p, q) = \lambda V(p - q) - \frac{i}{(2\pi)^4} \int \lambda V(p - k) \frac{(k_\mu \gamma_\mu + m)}{k_0^2 - k^2 - m^2 - i\epsilon} \lambda V(k - q) d^4 k +$$

$$\text{with} \quad \lambda = -2\pi e \gamma_4; \quad V(p - q) = 2\pi \delta(p_0 - q_0) \int e^{-i\mathbf{p} \cdot \mathbf{x}} d^3 \mathbf{x}$$



Separating the time integration from the space part and defining  $M'(\mathbf{p}, \mathbf{q})$  by

$$M(p, q) = 2\pi\delta(p_0 - q_0)M'(\mathbf{p}, \mathbf{q})$$

we get for  $M'(\mathbf{p}, \mathbf{q})$  after cancelling the  $\delta$ -functions from both sides, the following :

$$M'(\mathbf{p}, \mathbf{q}) = \gamma_4 \mathbf{V}(\mathbf{p} - \mathbf{q}) - (2\pi)^{-3} \int \mathbf{V}(\mathbf{p} - \mathbf{k}) \gamma_4 \frac{(\gamma_4 E - \gamma_i \mathbf{k} + m)}{k^2 - (\mathbf{p}^2 + i\epsilon)} \gamma_i \mathbf{V}(\mathbf{k} - \mathbf{q}) d^3 \mathbf{k} + \dots$$

$$\text{with} \quad \mathbf{V}(\mathbf{p} - \mathbf{q}) = \frac{-4\pi Z e^2}{(\lambda^2 + |\mathbf{p} - \mathbf{q}|^2)}$$

$$\text{and} \quad k_0 = E.$$

The right hand side is a series which evidently becomes the solution by iteration of the following integral equation :

$$M'(\mathbf{p}, \mathbf{q}) = \gamma_i \mathbf{V}(\mathbf{p} - \mathbf{q}) - (2\pi)^{-3} \int \mathbf{V}(\mathbf{p} - \mathbf{k}) \gamma_4 \frac{(\gamma_4 E - \gamma_i \mathbf{k} + m)}{k^2 - (\mathbf{p}^2 + i\epsilon)} M'(\mathbf{k}, \mathbf{q}) d^3 \mathbf{k}$$

Since we are considering here the scattering in a static field, the vacuum expectation value of the  $S$ -matrix,  $|\langle 0 | S | 0 \rangle|^2$  is taken to be unity since the energy is conserved in any real process (it cannot supply the threshold energy for pair creation in the virtual process).

Thus the  $S$ -matrix gives

$$(p | S | q) = (p | R | q)$$

where the right hand side is characterised by  $M'(\mathbf{p}, \mathbf{q})$  which is given by the above integral equation.

Now it remains to show that the same integral equation as above can also be obtained from the usual conventional perturbation theory and then the connection between the covariant and non-invariant formulations is made clear.

From the integral equation (4) of Sec (1) we may write the value of the wave-function.

$$\psi(r) = \psi_0(r) + \left( \Sigma \gamma_v \frac{\partial}{\partial x_v} - \gamma_4 E - m \right) \gamma_4 \int \frac{e^{i\mathbf{p} \cdot \mathbf{r} - \mathbf{r}'}}{4\pi |\mathbf{r} - \mathbf{r}'|} \cdot I(r') \psi(r') d^3 r'$$

Now the conventional method of writing the matrix element for the transition of a particle from a state  $u(\mathbf{p})$  to another state  $u(\mathbf{q})$  is (Schiff, Quantum mechanics)

$$\begin{aligned} \langle \mathbf{p} | H | \mathbf{q} \rangle &= \int \psi_0^*(\mathbf{p}) \gamma_4 V(r) \psi(\mathbf{q}) d^3 r ; \quad V(r) = \frac{-Ze^2}{r} e^{-\lambda r} \\ &= \int \psi_0^*(\mathbf{p}) \gamma_4 V(r) \psi_0(\mathbf{q}) d^3 r + \int \psi_0^*(\mathbf{p}) \gamma_4 V(r) \left( \Sigma \gamma_v \frac{\partial}{\partial x_v} - \gamma_4 E - m \right) \gamma_4 \int \frac{e^{i\mathbf{p} \cdot \mathbf{r} - \mathbf{r}'}}{4\pi |\mathbf{r} - \mathbf{r}'|} \cdot \\ &\quad \times I(r') \psi_0(\mathbf{q}, r') d^3 r d^3 r' \quad \dots \quad (3) \end{aligned}$$

Now putting

$$\psi_0(\mathbf{q}) = u(\mathbf{q})e^{i\mathbf{q}\cdot\mathbf{x}}; \quad \psi_0(\mathbf{p}) = u(\mathbf{p})e^{i\mathbf{p}\cdot\mathbf{x}}$$

and replacing

$$\frac{e^{i\mathbf{p}\cdot(\mathbf{x}-\mathbf{x}')}}{4\pi^3|\mathbf{r}-\mathbf{r}'|} \text{ by } \int_0^\infty \frac{L_1}{s} (2\pi)^{-3} \int \frac{e^{i\mathbf{k}\cdot(\mathbf{x}-\mathbf{x}')}}{R^2 - (p^2 + i\epsilon)} d^3\mathbf{k}$$

the right hand side of the above equation, we proceed to simplify.

Also we write

$$(\mathbf{p} \cdot \mathbf{H} \cdot \mathbf{q}) = \bar{u}(\mathbf{p})f(\mathbf{p}, \mathbf{q})u(\mathbf{q})$$

Through these substitutions we may note that the first term of the above series reduces to

$$\int e^{i(\mathbf{p}-\mathbf{q})\cdot\mathbf{x}} \gamma_1 I'(\tau) d^3\tau = \gamma_1 \frac{4\pi Z e^2}{(\lambda^2 + |\mathbf{p}-\mathbf{q}|^2)} = \gamma_1 I'(\mathbf{p}-\mathbf{q})$$

This  $I'(\mathbf{p}-\mathbf{q})$  is the same as in the covariant case.

The second integral in (3) can be treated similarly. Thus we get the following integral equation for  $f(\mathbf{p}, \mathbf{q})$

$$f(\mathbf{p}, \mathbf{q}) = \gamma_4 I'(\mathbf{p}-\mathbf{q}) - \frac{1}{(2\pi)^3} \int I'(\mathbf{p}-\mathbf{k}) \gamma_4 \frac{(\gamma_1 E - i\gamma_3 \mathbf{k} \cdot \mathbf{m})}{k^2 - (p^2 + i\epsilon)} f(\mathbf{k}, \mathbf{q}) d^3\mathbf{k}$$

Now changing the  $i\gamma$  by  $\gamma$  (since Pauli's  $\gamma$ -matrices, excepting  $\gamma_1$ , differ from those of Feynman by a factor  $i$ ) we get the same integral equation for  $f(\mathbf{p}, \mathbf{q})$  as was obtained from the covariant formulation of Feynman and Dyson.

## CONCLUSION

From the above consideration it appears that both the usual conventional perturbation and covariant perturbation methods are identical. The only difference between these two methods is in the invariance property of the new formulation. Both use an expansion in power of  $e^2/(\hbar c)$ . In the old method the perturbation matrix elements are the transition probability and energy difference while in the new method they are made out of several invariant functions. We have seen how it is possible to obtain the old formula by separating the time part from the space time integrations occurring in the covariant formulation. Evidently, we can obtain the new covariant formulae by means of the old perturbation theory, if it be carried to one step further by introducing the time part in a relativistically invariant way. But apart from this the new formulation brings in one important idea (the mass and charge renormalization) which we have not discussed.

## ACKNOWLEDGMENT

The author's sincerest thanks are due to Dr. D. Basu for suggesting the problem and for his valuable counsel in the preparation of the paper.

## APPENDIX

Evaluation of the integrals in Sec. I.

$$\lim_{\epsilon \rightarrow 0} (2\pi)^{-3} \int \frac{d\mathbf{k}}{k^2 - p^2 - i\epsilon} \exp(i\mathbf{k} \cdot (\mathbf{r} - \mathbf{r}')) = \frac{e^{ip|\mathbf{r} - \mathbf{r}'|}}{5\pi |\mathbf{r} - \mathbf{r}'|}$$

On performing the angular  $k$ -integration we get for the radial part,

$$\begin{aligned} & \lim_{\epsilon \rightarrow 0} \int_0^\infty \frac{k dk}{k^2 - p^2 - i\epsilon} \cdot \sin k |\mathbf{r} - \mathbf{r}'| \\ &= \lim_{\epsilon \rightarrow 0} \frac{1}{2i} \int_{-\infty}^\infty \frac{k dk}{k^2 - p^2 - i\epsilon} e^{ik|\mathbf{r} - \mathbf{r}'|} - \lim_{\epsilon \rightarrow 0} \frac{1}{2i} \int_{-\infty}^\infty \frac{k dk}{k^2 - p^2 - i\epsilon} e^{-ik|\mathbf{r} - \mathbf{r}'|} \\ &= \lim_{\epsilon \rightarrow 0} \frac{1}{2i} \int_{-\infty}^\infty \frac{k dk}{k^2 - p^2 - i\epsilon} e^{ik|\mathbf{r} - \mathbf{r}'|} \end{aligned}$$

(By a change of  $k$  by  $-k$  in the 2nd integral)

This may be evaluated by usual contour integration. The contour is semi-circle in the upper half-plane.

Using Jordan's inequality and considering the only pole at  $k = +(p^2 + i\epsilon)^{1/2}$  we get the value of the integral in the limit  $\epsilon \rightarrow 0$ ,

$$\frac{1}{2} e^{ip|\mathbf{r} - \mathbf{r}'|}$$

The contribution from angular  $k$ -integration,

$$\left( \frac{1}{2\pi^2} \right) \cdot \frac{1}{|\mathbf{r} - \mathbf{r}'|}$$

The value is then  $(4\pi)^{-1} \exp(ip|\mathbf{r} - \mathbf{r}'|) \cdot (|\mathbf{r} - \mathbf{r}'|)^{-1}$

For the integrals  $I$  and  $J$  standard methods of S-matrix calculation (J. R. Chisholm (1952) Dalitz (1951)) may be consulted.

## REFERENCES

- Chisholm, J. R., 1952, *Proc. Camb. Phil. Soc.*, **48**, 300.  
 Dalitz, R. H., 1951, *Proc. Roy. Soc. A.*, **206**, 509.  
 Distel, F., 1932, *Z. f. Phys.*, **75**, 785.  
 Dyson, F. J., 1949, *Phys. Rev.*, **75**, 436.  
 4-1852P-3

- Feynman, R. P., 1949, *Phys. Rev.*, **76**, 769.  
Mott, N. F., 1939, *Proc. Roy. Soc. A.*, **124**, 425.  
McKinley & Feshbach, 1948, *Phys. Rev.*, **74**, 1759.  
Sauter, F., 1933a. *Z. f. Phys.*, **36**, 118.  
Sauter., F., 1933b. *Ann. der. Phys.*, 51<sup>2</sup>, **18**, 61.  
Sextl, T., 1933, *Z. f. Phys.*, **81**, 178.  
Urban., P., 1942, *Z. f. Phys.*, **119**, 67.

## AN X-RAY STUDY OF O-PHTHALIC ACID

By D. M. CHAKRABURTTY

DEPT. OF GENERAL PHYSICS, X-RAYS AND MAGNETISM, INDIAN ASSOCIATION FOR THE  
CULTIVATION OF SCIENCE, JADAVPUR, CALCUTTA 32

(Received for publication, February 2, 1954)

## Plates IIA-C

**ABSTRACT.** From morphological and X-ray study the correct unit cell dimensions for ortho phthalic acid crystal was found to be  $a=5.05\text{\AA}$ ,  $b=14.03\text{\AA}$ ,  $c=9.325\text{\AA}$  and  $\beta=93^\circ 30'$ , number of molecules per unit cell being 4. The extinction conditions of spots from the Weissenberg pictures suggested two space groups  $C_{2h}^2$  and  $C_2$  for the crystal. X-ray analysis, together with chemical consideration and pyro-electric test, suggest the correct space-group for o-phthalic acid to be  $C_2$  or  $Cc$ .

The simple aromatic compound o-phthalic acid, a colourless crystalline substance, prepared usually from naphthalene by oxidation, has a molecular formula  $C_8H_6O_4$ . Morphological and optical studies on this crystal were done earlier, but no attempt has yet been made to determine its complete structure. Becker and Janke (1921) showed that the axial parameters of the single crystals of the substance were  $a=9.33\text{\AA}$ ,  $b=7.13\text{\AA}$ ,  $c=5.1\text{\AA}$  and  $\beta=94^\circ 36'$ , the number of molecules per unit cell being 2 in that case. Later on, some objections were raised about the crystal class and the value of the angle  $\beta$  by Wyckoff (1931). The present work furnishes, beyond all doubt, the correct unit cell dimensions, the number of molecules in the unit cell and also the space group to which the crystal belongs.

Single crystals of requisite size were obtained from alcoholic solution of the substance. The prominent faces developed were  $m(210)$ ,  $q(011)$  and sometimes  $c(001)$ . Morphological studies made by the present author with the help of a two-circle goniometer, gave the following interfacial angles :

$$\begin{aligned} m : \bar{m} &= 210 : 2\bar{1}0 = 39^\circ 4' \\ q : \bar{q} &= 011 : 0\bar{1}1 = 107^\circ 23' \end{aligned}$$

Rotation photographs as well as X-ray Weissenberg photographs taken about the three crystallographic axes (Plates IIA, B, C), gave the axial lengths as,  $a=5.05\text{\AA}$ ,  $b=14.03\text{\AA}$ ,  $c=9.325\text{\AA}$  and the monoclinic angle  $\beta=93^\circ 30'$ . Comparing the values of the unit cell parameters with those found by Becker and Janke (1921) it is seen in the present case that (1) the value of  $b$  is doubled and (2) the values of  $a$  and  $c$  are interchanged. It is obvious that Becker and Janke's values for the parameters are inconsistent with the morphological data. The angle  $\beta$  in the present case is practically the same as Groth's (1917) value obtained by optical methods and is also appreciably different from Becker and Janke's value. The density of the substance was determined by the floatation method and it came out as  $1.594 \pm .001 \text{ gm/cm}^3$  whence the number of molecules per unit cell was found to be 4.

Over-exposed zero layer normal beam Weissenberg pictures about all three axes and equi-inclination pictures for the first and second layer of *a* and *b* were taken in the usual way. The spots were indexed by drawing requisite charts as suggested originally by Schneider (1928). The indices of the spots and their relative intensities are given in Tables I, II and III.

TABLE I

Indexing of spots and their estimated intensities (*c* axis zero-layer)

Plane	Intensity	Plane	Intensity	Plane	Intensity
200	vs	2(10)0	w	510	vw
400	m	2(12)0	w	530	w
040	vs	2(11)0	w	550	ms
060	ms	310	s	570	m
080	m	330	m		
0(10)0	w	350	m		
0(12)0	m				
0(14)0	ms	370	s		
0(16)0	ms	390	m		
110	vs	420	m		
150	ms	440	s		
170	vs	4(10)0	m		
190	ms	4(12)0	m		
220	vs				
260	ms				
280	m				

TABLE II

Indexing of spots and their estimated intensities (*a*-axis zero-layer)

Plane	Intensity	Plane	Intensity	Plane	Intensity	Plane	Intensity
002	s	025	m	04(10)	w	0(10)1	m
004	vs	026	ms	061	s	0(10)2	w
006	m			062	vs	0(10)2	ms
008	vw	027	m	063	s	0(10)4	m
00(10)	m	028	w	064	vs	0(10)5	w
020	vw	029	vw			0(10)7	w
040	vs	02(10)	w	065	w	0(12)1	s
060	ms	041	s	066	vw	1(12)2	vw
080	m	042	w	067	vw	0(12)3	m
0(10)0	w			068	w	0(12)4	vw
0(12)0	m	043	vs	069	m	0(12)5	w
0(14)0	ms	044	m			0(12)6	w
0(16)0	ms	045	w	06(10)	ms	0(14)1	m
021	s	046	m	081	w	0(14)2	m
022	vs	047	ms	082	m	0(14)3	w
023	vs	048	w	083	w	0(14)4	ms
024	ms	049	vw	084	m		
				085	m		

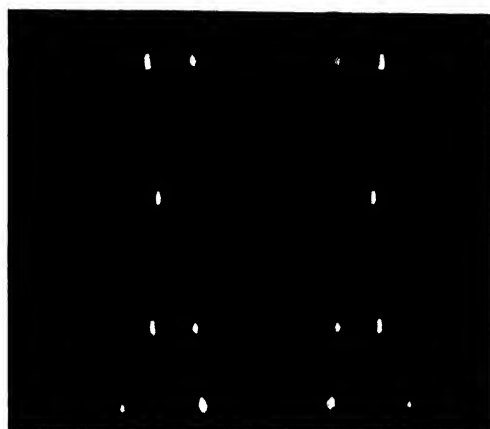


Fig. 1  
Rotation picture with  $c$ -axis vertical ( $l = 5.0$  cm)

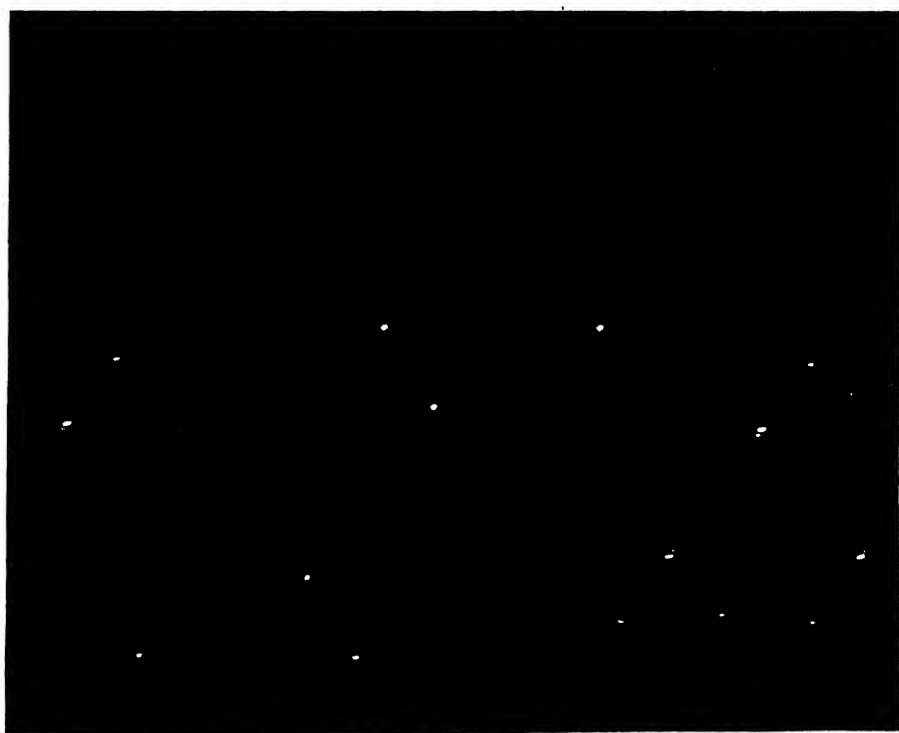


Fig. 2  
Normal-beam Weissenberg picture for zero-layer of  $c$ -axis

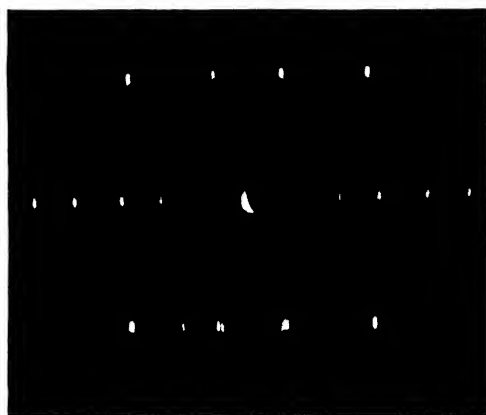


Fig. 3  
Rotation picture with  $a$ -axis vertical ( $\lambda = 5.0$  cm)



Fig. 4  
Normal-beam Weissenberg picture for the zero-layer of  $a$ -axis



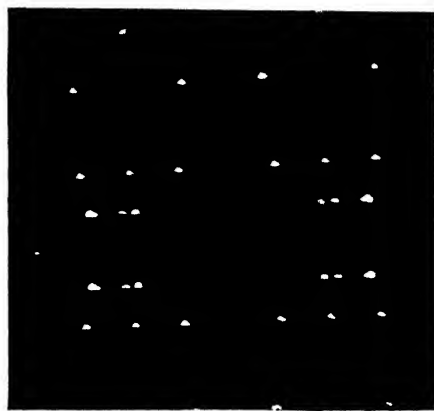


Fig. 5  
Rotation picture with  $b$ -axis vertical ( $\lambda = 4.5$  cm)

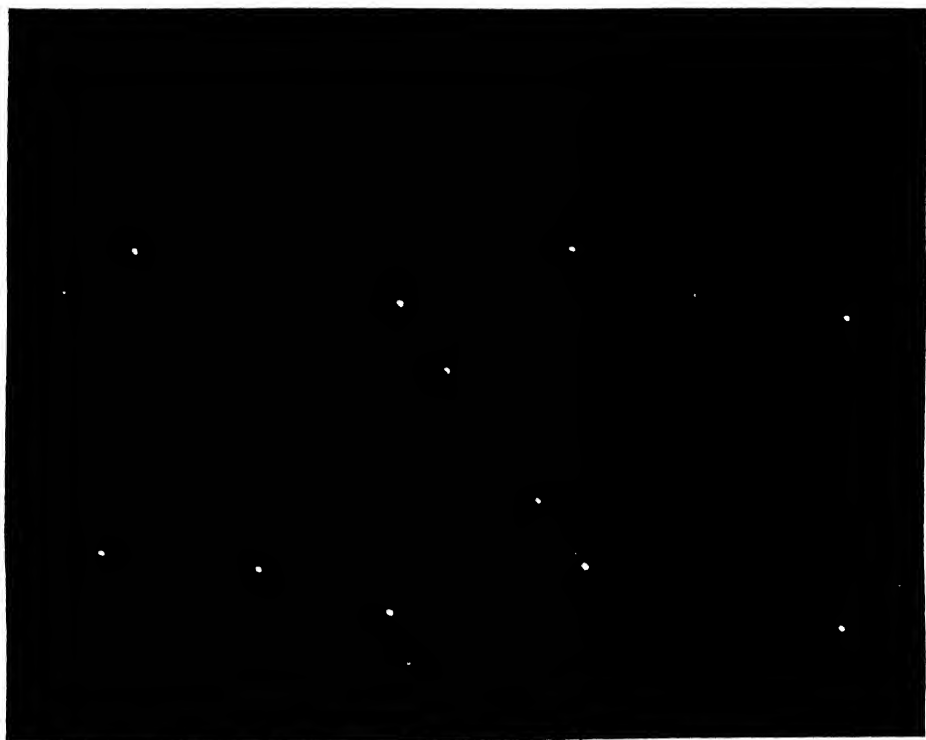


Fig. 6  
Normal-beam Weissenberg picture for the zero-layer of  $b$ -axis



TABLE III

Indexing of spots and their estimated intensities (*b*-axis zero-layer)

Plane	Intensity	Plane	Intensity
200	vs	204	vs
400	m	206	s
002	s	208	m
004	vs	20(10)	s
006	m	402	w
008	w	404	m
00(10)	m	406	w
202	vs		

From the Weissenberg pictures the following conditions for reflections were observed :

- (1) *hkl* planes present when  $h + k = 2n$
- (2) *hol* planes present when  $l = 2n$ ,  $h = 2n$
- (3) *oko* planes present when  $k = 2n$ .

These conditions suggest a *c* face-centered lattice for the crystal with a glide plane *c*. These conditions suggest two space groups namely  $C_{2h}^6$  and  $C_4^2$  for this crystal. The former space groups requires a centre of symmetry while in the latter there is no centre of symmetry. From chemical consideration it is apparent that due to the ortho positions of the two COOH groups in the benzene ring there can be no centre of symmetry for the molecule.

However, definite absence of a centre of symmetry for the crystal was proved by pyro-electric tests, with an improved type of apparatus developed in our laboratory by Basak (1950), based on Lonsdale's (1928 and 1934) work. A crystal of *o*-phthalic acid, approximately 4 mm, was placed between plates of a miniature condenser insulated with mica sheet connected with two insulated copper leads and inserted into a copper tube with one end closed. The wires were taken out through ebonite plug at the mouth of the copper tube, one of the wires being connected to earth and the other to a sensitive tilted gold-leaf electroscope. The plate of the electroscope was given a potential of 1000 volts and the gold leaf was adjusted for the position of maximum sensitivity. The copper tube was immersed suddenly into liquid air. The temperature of the crystal being thus lowered quickly and due to the strain thus set up in the crystal, a small difference of potential was developed on the opposite faces of the crystal which was clearly

indicated by the movement of the gold leaf through about of 3 divisions in the eyepiece scale of the observing telescope. When the copper tube was taken out from the liquid air a similar deflection was observed in opposite direction. This proves beyond doubt the non-existence of a centre of symmetry for the crystal. So we can discard the space group  $C_{2h}^6$  and take  $C_4^1$  or  $C_c$  to be the correct space group for the crystal.

A complete structure analysis of the *o*-phthalic crystal by Fourier analysis is under progress.

#### ACKNOWLEDGMENTS

Thanks are due to Prof. K. Banerjee, D. Sc., for his kind interest in the problem, to Dr. A. Bose, D. Sc., for guidance, to Dr. B. K. Banerjee and Sri D. R. Dasgupta for valuable suggestions and to Sri A. Roy for his help during the progress of the work.

#### REFERENCES

- Basak, B., 1950, Thesis for D. Phil Degree of the Cal. Univ.  
 Becker, K. and Janke, W., 1921, *Z. Physik Chem.*, **99**, p. 242 and 267.  
 Groth, P., 1917, *Chemische Kristallographie*, p. 723.  
 Lonsdale, K., 1928, *Phil. Mag.*, **6**, p. 437.  
 Lonsdale, K., 1934, *Proc. Roy. Soc.*, **144**, p. 63.  
 Schneider W., 1928, *Z. Krist.* (1) **69**, p. 41.  
 Wyckoff, R., 1931, *The Structure of Crystals.*, p. 386

# A RIGID CURVILINEAR POLYGONAL CORE IN AN INFINITE PLATE UNDER TENSIONS AT INFINITY AND SHEAR

By B. KARUNES

DEPARTMENT OF APPLIED PHYSICS  
UNIVERSITY COLLEGE OF SCIENCE AND TECHNOLOGY, CALCUTTA.

(Received for publication, December 19, 1953)

**ABSTRACT.** The function theoretic method of Muschelisvili for solving two dimensional problems in elasticity is employed to obtain solutions to the problems of a rigid curvilinear polygonal core in an infinite plate under (i) an all-round tension at infinity, (ii) a uniform tension at infinity at an inclination to the  $x$ -axis and (iii) a uniform shear in the plane of the plate.

## INTRODUCTION

Muschelisvili (1933) has developed a method of solving plane problems in elasticity by discarding the stress function and introducing two functions of complex variable  $z$  in terms of which all the relevant physical quantities are expressed. He has indicated how, in certain cases, these two functions of  $z$  can be determined easily with the help of the theory of functions of a complex variable. In the present paper this method has been applied to obtain solutions to the problems of a rigid curvilinear polygonal core in an infinite plate acted upon by (i) a uniform all-round tension at infinity, (ii) a uniform tension at infinity in a direction making an angle  $\alpha$  with the  $x$ -axis and (iii) a uniform shear in the plane of the plate.

It has been shown by Muschelisvili that in the state of generalised plane stress the stress combinations

$$\begin{aligned} \widehat{xx} + \widehat{yy} &= 1 \times \text{real part of } \phi_1'(z) \quad \dots (1) \\ &= 2 \times [\phi_1'(z) + \bar{\phi}_1'(\bar{z})] \end{aligned}$$

and

$$\widehat{yy} - \widehat{xx} + 2i\widehat{xy} = 2 \times [z\phi_1''(z) + \psi_1'(z)] \quad \dots (2)$$

where  $\phi_1(z)$  and  $\psi_1(z)$  are two analytic functions of  $z(=x+iy)$  and a bar over a function represents the complex conjugate of the function.

In terms of the above two functions the displacements are obtained from the relation

$$2\mu(u+iv) = K\phi_1(z) - z\bar{\phi}_1'(\bar{z}) - \bar{\psi}_1(\bar{z}) \quad \dots (3)$$

where

$$K = \frac{\lambda' + 3\mu}{\lambda' + \mu}$$

To find the parts of  $\phi_1(z)$  and  $\psi_1(z)$  which give the stresses  $\widehat{xx}=T_1$ ,  $\widehat{yy}=T_2$ ,  $\widehat{xy}=S$  at infinity, we get from (1) and (2)

$$\left. \begin{aligned} T_1 + T_2 &= 4 \times \text{real part of } \phi_1'(z) \\ T_2 - T_1 + 2iS &= 2 \times [z\phi_1''(z) + \psi_1'(z)] \end{aligned} \right\} \quad \dots (4)$$

These give

$$\left. \begin{aligned} \phi_1(z) &= \frac{1}{4}(T_1 + T_2)z \\ \psi_1(z) &= \frac{1}{2}(T_2 - T_1 + 2iS)z \end{aligned} \right\} \quad \dots (5)$$

The imaginary part of the coefficient of  $z$  in  $\phi_1(z)$  is omitted as it gives only a rigid body displacement.

Hence in an infinite plate with a core which exerts no force on the rest of the plate, we can write

$$\left. \begin{aligned} \phi_1(z) &= Bz + \phi_1^0(z) \\ \psi_1(z) &= (B' + iC')z + \psi_1^0(z) \end{aligned} \right\} \quad \dots (6)$$

where  $\phi_1^0(z)$  and  $\psi_1^0(z)$  are analytic outside the boundary of the core.

#### THE SOLUTION

Let an infinite plate containing a rigid core, whose boundary is a curvilinear polygon, be subjected to the prescribed stresses at infinity and let the displacement of the core be a translation  $u$  and a rotation through a small angle  $\epsilon$ . By superposing on the plate an equal and opposite translation we do not alter either the magnitude or the directions of the stresses at infinity. The displacement of any point on the boundary of the core is, therefore, given by  $u = -\epsilon y$ ,  $v = \epsilon x$ , so that  $u + iv = i\epsilon z$  at a point on the boundary of the core. As the resultant traction exerted by the core on the remainder of the plate is zero, the values of  $B$ ,  $B'$ ,  $C'$  in (6) depend only on the stresses at infinity.

We have on the boundary of the core (3)

$$K\phi_1(z) - z\phi_1'(z) - \psi_1(z) = 2\mu i\epsilon z \quad \dots (7)$$

Taking complex conjugate of both sides we get

$$K\phi_1(z) - z\phi_1'(z) - \psi_1(z) = -2\mu i\epsilon z \quad \dots (8)$$

on the boundary of the core.

Let the region outside the boundary of the core in the  $z$ -plane be represented on the region outside the unit circle on the  $\zeta$ -plane by the conformal transformation  $z = \omega(\zeta)$ . Then we get on the unit circle  $\gamma$

$$K\phi(\sigma) - \frac{\omega(\sigma)}{\omega'(\sigma)} \bar{\phi}'(\sigma) - \psi(\sigma) = 2\mu i\epsilon \omega(\sigma) \quad \dots (9)$$

$$K\phi(\sigma) - \frac{\omega(\sigma)}{\omega'(\sigma)} \phi'(\sigma) - \psi(\sigma) = -2\mu i\epsilon \bar{\omega}(\bar{\sigma})$$

where

$$\phi(\zeta) = \phi_1\{\omega(\zeta)\}, \quad \psi(\rho) = \psi_1\{\omega(\zeta)\}$$

If

$$\omega(\zeta) = b(\zeta + a\zeta^{-n})$$

where  $n$  is a positive integer and  $0 \leq na \leq 1$ , the boundary of the core is a curvilinear polygon.

Substituting for  $z$  in (6), we get

$$\left. \begin{aligned} \phi(\zeta) &= Bb\zeta + \phi^0(\zeta) \\ \psi(\zeta) &= (B' + iC')b\zeta + \psi^0(\zeta) \end{aligned} \right\} \quad \dots (10)$$

where  $\phi^0(\rho)$  and  $\psi^0(\rho)$  are analytic outside the unit circle  $\gamma$ , and can be written as

$$\left. \begin{aligned} \phi^0(\zeta) &= \frac{z_1 + i\beta_1}{\zeta} + \frac{z_2 + i\beta_2}{\zeta^2} + \dots \\ \psi^0(\zeta) &= \frac{z_1' + i\beta_1'}{\zeta} + \frac{z_2' + i\beta_2'}{\zeta^2} + \dots \end{aligned} \right\} \quad \dots (11)$$

From equations (9) we have on the boundary of the core, where  $\sigma\bar{\sigma} = 1$ ,

$$\left. \begin{aligned} K\phi^0(\sigma) - \frac{\sigma^{n+1} + a}{\sigma^n(1 - an\sigma^{n+1})} \bar{\phi}^{0'}\left(\frac{1}{\sigma}\right) - \bar{\psi}^0\left(\frac{1}{\sigma}\right) \\ = 2\mu i \epsilon b(\sigma + a\sigma^{-n}) - KBb\sigma + (B' - iC')b/\sigma \\ + Bb \frac{\sigma^{n+1} + a}{\sigma^n(1 - an\sigma^{n+1})} \end{aligned} \right\} \quad \dots (12)$$

and

$$\left. \begin{aligned} K\bar{\phi}^0\left(\frac{1}{\sigma}\right) - \frac{\sigma^n(1 + a\sigma^{n+1})}{\sigma^{n+1} - an} \phi^{0'}(\sigma) - \psi^0(\sigma) \\ = -2\mu i \epsilon b\left(\frac{1}{\sigma} + a\sigma^n\right) - \frac{KBb}{\sigma} + (B' + iC')b\sigma + Bb \frac{1 + a\sigma^{n+1}}{\sigma - an\sigma^{n+1}} \end{aligned} \right\} \quad \dots (13)$$

Multiplying (12) and (13) by  $\frac{1}{2\pi i} \frac{d\sigma}{\sigma - \zeta}$  and integrating along  $\gamma$ , we get

$$\left. \begin{aligned} -\frac{1}{2\pi i} \int_{\gamma} \frac{\sigma + a\sigma^{-n}}{1 - an\sigma^{n+1}} \bar{\phi}^{0'}\left(\frac{1}{\sigma}\right) \frac{d\sigma}{\sigma - \zeta} - K\phi^0(\zeta) \\ = -2\mu i \epsilon b \frac{a}{\zeta^n} - Bb \frac{a}{\zeta^n} - (B' - iC') \frac{b}{\zeta} \end{aligned} \right\} \quad \dots (14)$$

$$\left. \begin{aligned} \phi(\zeta) &= \frac{1}{2} b T \left( \zeta + \frac{a}{K\zeta} \right) \\ \psi(\zeta) &= \frac{1}{2} b T \left\{ \frac{K}{\zeta} + \frac{a(1+a\zeta^2)}{K\zeta(\zeta^2-a)} - \frac{\zeta(1+\zeta^4)}{\zeta^2-a} \right\} \end{aligned} \right\} \quad \dots \quad (28)$$

For  $n=2$ ,

$$\left. \begin{aligned} \phi(\zeta) &= \frac{1}{2} b T \left( \zeta + \frac{a}{K\zeta^2} \right) \\ \psi(\zeta) &= \frac{1}{2} b T \left\{ \frac{K}{\zeta} + \frac{2a(1+a\zeta^3)}{K\zeta(\zeta^3-2a)} - \frac{\zeta^2(1+2a^2)}{\zeta^3-2a} \right\} \end{aligned} \right\} \quad \dots \quad (29)$$

For  $n=3$ ,

$$\left. \begin{aligned} \phi(\zeta) &= \frac{1}{2} b T \left( \zeta + \frac{a}{K\zeta^3} \right) \\ \psi(\zeta) &= \frac{1}{2} b T \left\{ \frac{K}{\zeta} + \frac{3a(1+a\zeta^4)}{K\zeta(\zeta^4-3a)} - \frac{\zeta^3(1+3a^2)}{\zeta^4+3a} \right\} \end{aligned} \right\} \quad \dots \quad (30)$$

For  $n \geq 4$ ,

$$\left. \begin{aligned} \phi(\zeta) &= \frac{1}{2} b T \left( \zeta + \frac{a}{K\zeta^n} \right) \\ \psi(\zeta) &= \frac{1}{2} b T \left\{ \frac{K}{\zeta} + \frac{na(1+a\zeta^{n+1})}{K\zeta(\zeta^{n+1}-na)} - \frac{\zeta^n(1+na^2)}{\zeta^{n+1}-na} \right\} \end{aligned} \right\} \quad \dots \quad (31)$$

Case 2. Uniform tension  $T$  at infinity in a direction making an angle  $\alpha$  with the  $x$ -axis.

Here

$$B = \frac{1}{2} T$$

$$B' + iC' = -\frac{1}{2} T e^{-2i\alpha}$$

and

$$\epsilon = \frac{1}{2} T \frac{a(1+K) \sin 2\alpha}{2\mu(a^2+K)}, \quad \text{for } n=1$$

$$\epsilon = 0 \quad \text{for } n \geq 2$$

We get when  $n=1$

$$\left. \begin{aligned} \phi(\zeta) &= \frac{1}{2} b T \left\{ \zeta + \left( 1 + \frac{2ia(1+K) \sin 2\alpha}{a^2+K} - \frac{2e^{2i\alpha}}{a} \right) \frac{a}{K\zeta} \right\} \\ \psi(\zeta) &= \frac{1}{2} b T \left\{ \left( K + \frac{2ia(1+K) \sin 2\alpha}{a^2+K} \right) \frac{1}{\zeta} - \frac{\zeta(1+a^2)}{\zeta^2-a} 2e^{-2i\alpha}\zeta \right. \\ &\quad \left. + \left( 1 + \frac{2ia(1+K) \sin 2\alpha}{a^2+K} - \frac{2e^{2i\alpha}}{a} \right) \frac{a(1+a\zeta^3)}{K\zeta(\zeta^3-a)} \right\} \end{aligned} \right\} \quad \dots \quad (32)$$



hen  $n=2$ ,

$$\left. \begin{aligned} \phi(\zeta) &= \frac{1}{2} b T \left\{ \zeta + \frac{a}{K \zeta^2} - \frac{2 e^{2 i a}}{K \zeta} \right\} \\ \psi(\zeta) &= \frac{1}{2} b T \left\{ \frac{K}{\zeta} - \frac{\zeta^2 (1 + 2 a^2)}{\zeta^3 - 2 a} - \frac{2 e^{2 i a} (1 + a \zeta^3)}{K (\zeta^3 - 2 a)} \right. \\ &\quad \left. + \frac{2 a (1 + a \zeta^4)}{K \zeta (\zeta^3 - 2 a)} - 2 e^{-2 i a} \zeta \right\} \end{aligned} \right\} \quad \dots \quad (33)$$

When  $n=3$ ,

$$\left. \begin{aligned} \phi(\zeta) &= \frac{1}{2} b T \left\{ \zeta + \frac{a}{K \zeta^3} - \frac{2 i K e^{2 i a} - a e^{-2 i a}}{(K^2 - a^2) \zeta} \right\} \\ \psi(\zeta) &= \frac{1}{2} b T \left\{ \frac{K}{\zeta} + \frac{\zeta^3 (1 + 3 a^2)}{\zeta^4 - 3 a} - \frac{2 (K e^{2 i a} - a e^{-2 i a}) \zeta (1 + 3 a^2)}{(K^2 - a^2) (\zeta^4 - 3 a)} \right. \\ &\quad \left. + \frac{3 a (1 + a \zeta^4)}{K \zeta (\zeta^4 - 3 a)} - 2 e^{-2 i a} \zeta \right\} \end{aligned} \right\} \quad \dots \quad (34)$$

When  $n \geq 4$ ,

$$\left. \begin{aligned} \phi(\zeta) &= \frac{1}{2} b T \left\{ \rho + \frac{a}{K \zeta^n} - \frac{2 K e^{2 i a}}{\{K^2 - (n-2)a^2\} \zeta} + \frac{2 a e^{-2 i a}}{\{K^2 - (n-2)a^2\} \zeta^{n-2}} \right\} \\ \psi(\zeta) &= \frac{1}{2} b T \left\{ \frac{K}{\zeta} - \frac{\zeta^n (1 + n a^2)}{\zeta^{n+1} - n a} - \frac{2 K e^{2 i a} (1 + n a^2) \zeta^{n-2}}{\{K^2 - (n-2)a^2\} \{\zeta^{n+1} - n a\}} \right. \\ &\quad \left. + \frac{2 (n-2) a e^{-2 i a} \zeta^{n-1} (1 + n a^2)}{\{K^2 - (n-2)a^2\} \{\zeta^{n+1} - n a\}} + \frac{n a (1 + a \zeta^{n+1})}{K \zeta (\zeta^{n+1} - n a)} - 2 e^{-2 i a} \zeta \right\} \end{aligned} \right\} \quad \dots \quad (35)$$

*Case 3. Uniform shear S in the plane of the plate.*

Here

$$B=0, B'=0, C'=S$$

Therefore

$$\epsilon = \frac{a(1+K)S}{2\mu(a^2+K)} \quad \text{for } n=1$$

$$\epsilon = 0 \quad \text{for } n \geq 2$$

We get for  $n=1$ ,

$$\left. \begin{aligned} \phi(\zeta) &= \frac{i b S}{\zeta} \cdot \frac{a^2 - 1}{a^2 + K} \\ \psi(\zeta) &= i b S \left\{ \frac{a(1+K)}{(a^2+K)\zeta} + \frac{(a^2-1)(1+a\zeta^2)}{(a^2+K)\zeta(\zeta^2-a)} + \zeta \right\} \end{aligned} \right\} \quad \dots \quad (36)$$

For  $n = 2$ ,

$$\left. \begin{aligned} \phi(\xi) &= -\frac{ibS}{K\xi} \\ \psi(\xi) &= ibS \left\{ \xi - \frac{1+a\xi^3}{K(\xi^3-2a)} \right\} \end{aligned} \right\} \quad \dots (27)$$

For  $n = 3$ ,

$$\left. \begin{aligned} \phi(\xi) &= -ibS \frac{1}{(K-a)\xi} \\ \psi(\xi) &= ibS \left\{ \rho - \frac{(1+3a^2)\xi}{(K-a)(\xi^4-3a)} \right\} \end{aligned} \right\} \quad \dots (38)$$

And for  $n \geq 4$ ,

$$\left. \begin{aligned} \phi(\xi) &= -ibS \frac{1}{K^2-(n-2)a^2} \left( \frac{K}{\xi} + \frac{a}{\xi^{n-2}} \right) \\ \psi(\xi) &= ibS \left\{ \xi - \frac{(1+na^2)\{(n-2)a\xi + K\xi^{n-2}\}}{\{K^2-(n-2)a^2\}(\xi^{n+1}-na)} \right\} \end{aligned} \right\} \quad \dots (39)$$

#### ACKNOWLEDGMENT

The author is grateful to Dr. S. Ghosh under whose constant guidance this paper has been prepared.

#### REFERENCE

Muschelisvili, N. I., 1933, *Zeits. Angew. Math. u. Mech.*, **13**, 264

## EFFECT OF BACKGROUND INTENSITY ON RESOLUTION

By MAHENDRA SINGH SODHA\*

DEPARTMENT OF PHYSICS, ALLAHABAD UNIVERSITY, ALLAHABAD 2

*(Received for publication, November 13, 1953)*

**ABSTRACT** The paper discusses the effect of background intensity on the resolving power. Tables, illustrated by graphs, have been given for the variation of resolving power with background intensity in case of Fabry-Perot etalon, prism, grating and reflecting echelon, and when the instrumental width is negligible.

## INTRODUCTION

This paper discusses the effect of background intensity on the resolving power of spectroscopic instruments, on the Rayleigh's criterion of resolution of spectral lines. The two cases, viz., when the instrumental width is negligible as compared to the Doppler line-width and vice versa have been distinguished.

## RESOLVING POWER WHEN INSTRUMENTAL WIDTH IS NEGLIGIBLE

The intensity distribution of a spectral line of wave number  $\nu_0$  due to Doppler effect is given by

$$I' = I_0 e^{-\beta(\nu - \nu_0)^2}$$

where  $\beta = \frac{\mu c^2}{2RT\nu_0^2}$ ,  $\mu$  being the mass of radiant atoms.

The intensity distribution of another spectral line of wave number  $\nu_0 + \Delta\nu$  and same intensity is

$$I'' = I_0 e^{-\beta(\nu - \nu_0 - \Delta\nu)^2}$$

if  $\Delta\nu$  is small. ( $\beta$  same for both lines).

Putting  $\sqrt{\beta}(\nu - \nu_0) = x$  and  $\sqrt{\beta}\Delta\nu = a$ , the resultant intensity pattern, in the presence of a background intensity  $kI_0$  is given by

$$I = kI_0 + I_0 e^{-x^2} + I_0 e^{-(x-a)^2} \quad \dots (1)$$

Oldenburg (1922) gives the position of maximum as

$$x_{\max} = \frac{a}{e^{a^2} + 1 - 2a^2}$$

In this section we will discuss cases with  $a^2 > 3.524$  and we may assume, as a good approximation,  $x_{\max} \approx 0$ .

\* Now at Defence Science Laboratory, New Delhi.

Hence the intensity maxima and minimum ( $x=a/2$ ) are given by

$$I_{\max}/I_0 = 1 + k + e^{-a^2} \quad \dots (2)$$

and

$$I_{\min}/I_0 = k + 2e^{-a^2/4} \quad \dots (3)$$

Rayleigh's criterion for resolution states

$$I_{\min}/I_{\max} = 0.8$$

Hence we get

$$k = 4(1 + e^{-a^2}) - 10e^{-a^2/4} \quad \dots (4)$$

We find that  $k=0$  when  $a^2=3.524$ . If the resolving power be denoted by  $R$  and its value, when  $k=0$  by  $R_0$  we have

$$R/R_0 = \sqrt{(3.524/a^2)} \quad \dots (5)$$

Table I gives  $R/R_0$  for a few values of  $k$ .

TABLE I

Variation of  $R/R_0$  with  $k$  when instrumental width is negligible.

$a^2$	3.524	4.000	4.400	4.800	5.600	6.400	7.600	9.200	12.000	$\infty$
$R/R_0$	1.00	0.939	0.895	0.857	0.793	0.742	0.671	0.619	0.532	0.00
$k$	0.00	0.39	0.72	1.02	1.55	1.99	2.50	3.00	3.50	4.00

#### RESOLVING POWER OF GRATING, REFLECTING ECHELON AND PRISM

The intensity of a spectral line diffracted by a grating or reflecting echelon is given by

$$I' = B \frac{\sin^2 N\beta}{\sin^2 \beta}$$

where  $N$  is the number of lines of the grating or the number of steps in the reflecting echelon and  $2\beta$  the phase difference between two adjacent beams. If the intensity maximum be denoted by  $I_0$  we have

$$I'/I_0 = \frac{B}{BN^2} \frac{\sin^2 N\beta}{\sin^2 \beta} = \frac{\sin^2 x}{x^2} \quad \dots (6)$$

where  $x = N\beta$ , and  $\beta$  is small.

The above expression also represents the intensity distribution in a prism if  $x = \pi l \sin \theta / \lambda$ .

The intensity distribution of another line of the same intensity and an angular separation corresponding to  $\Delta x = a$  is represented by

$$I''/I_0 = \frac{\sin^2 (x-a)}{(x-a)^2} \quad \dots (7)$$

The resultant intensity distribution of the two lines when the background intensity is  $kI_0$  is given by

$$I/I_0 = k + \frac{\sin^2 x}{x^2} + \frac{\sin^2 (x-a)}{(x-a)^2} \quad \dots (8)$$

The intensity maxima ( $x \approx 0$  or  $a$ ) and central minimum ( $x = a/2$ ) are given by

$$I_{\max} = 1 + k + \frac{\sin^2 a}{a^2} \quad \dots (9)$$

and

$$I_{\min} = k + 2 \frac{\sin^2 a/2}{(a/2)^2} \quad \dots (10)$$

Applying Rayleigh's criterion for resolution we get

$$k = 4'1 + \frac{\sin^2 a}{a^2} - 10 \frac{\sin^2 (a/2)}{(a/2)^2} \quad \dots (11)$$

when  $a = 1.006\pi$ ,  $k = 0$ . Hence if  $R_0$  denotes the resolving power for  $k = 0$  we have

$$R/R_0 = 1.006\pi/a \quad \dots (12)$$

Table II gives  $R/R_0$  for various values of  $k$ .

TABLE II

Variation of  $R/R_0$  with  $k$  for grating, reflecting echelon and prism.

$a$	$1.006 \pi$	$1.10 \pi$	$1.20 \pi$	$1.30 \pi$	$1.40 \pi$	$1.50 \pi$	$1.60 \pi$	$2.00 \pi$
$k$	0.00	0.77	1.55	2.25	2.83	3.28	3.60	4.00
$R/R_0$	1.00	0.91	0.84	0.77	0.72	0.66	0.63	0.50

For  $k > 4$  we get imaginary values for  $a$  showing thereby that no resolution is possible. Physically it means that even single lines are not visible because  $I_{\min}/I_{\max} > 0.8$ .

#### RESOLVING POWER OF FABRY-PEROT ETALON

The intensity of a spectral line in the order  $n_0 + n$ , where  $n$  is small and  $n_0$  an integer, is given in the case of Fabry-Perot etalon by

$$I' = I_0 / \{1 + F \sin^2 \pi(n_0 + n)\} = I_0 / (1 + x^2)$$

where  $x = \pi n F^{1/2}$ ,  $F$  being the coefficient of fineness.

The intensity of another spectral line of equal intensity separated by an order  $\Delta n$  is given by

$$I'' = I_0 / \{1 + F \sin^2 \pi(n_0 + n - \Delta n)\} = I_0 / \{1 + (x-a)^2\}$$

where  $a = \pi F^{1/2} \Delta n$ .

The resultant intensity pattern is

$$I/I_0 = k + [1/(1 + x^2)] + [1/\{1 + (x - a)^2\}] \quad \dots (13)$$

The maximum ( $x \approx 0$  or  $a$ ) and minimum ( $x = a/2$ ) of the resultant intensity pattern, when the background intensity is  $kI_0$ , are given by

$$I_{\min}/I_0 = k + 2/\{1 + a^2/4\} \quad \dots (14)$$

$$\text{and} \quad I_{\max}/I_0 = k + 1 + 1/(1 + a^2) \quad \dots (15)$$

Rayleigh's criterion for resolution requires

$$I_{\min} = 0.8I_{\max}$$

$$\text{or} \quad (4 - k)a^4 - (5k + 16)a^2 - (4k + 8) = 0$$

$$\text{or} \quad a^2 = \frac{(5k + 16) + \sqrt{(5k + 16)^2 + 16(4 - k)(k + 2)}}{2(4 - k)}$$

since  $a$  is real,

The resolving power of the etalon is given by

$$R = \lambda/d\lambda = n_0/\Delta n = \frac{\pi n_0 L^{1/2} \{2(4 - k)\}^{1/2}}{[(5k + 16) + \sqrt{(5k + 16)^2 + 16(4 - k)(k + 2)}]^{1/2}} \quad \dots (16)$$

The resolving power with  $k = 0$  (Meissner, 1941) is

$$R_0 = 1.49n_0 F^{1/2}$$

$$\text{Hence } R/R_0 = 2.109 \left[ 2(4 - k) / \{ (5k + 16) + \sqrt{(5k + 16)^2 + 16(4 - k)(k + 2)} \} \right]^{1/2} \quad \dots (17)$$

Table III gives  $R/R_0$  for some values of  $k$ .

TABLE III  
Variation of  $R/R_0$  with  $k$  for Fabry-Perot etalon.

$k$	0.0	0.5	1.0	1.5	2.0	2.5	3.0	3.5
$R/R_0$	1.00	0.88	0.77	0.67	0.57	0.47	0.38	0.26

For higher values of  $k$  which give high values for  $a$ , eqn. (13) does not hold because  $\sin a$  differs appreciably from  $a$  for large values of  $a$ .

#### DISCUSSION

The variation of  $R/R_0$  with  $k$ , in the three cases discussed earlier is represented graphically in figure 1. It can be seen that the background intensity has an important bearing on the choice of an instrument for a particular investigation. For example, a reflecting echelon, having half the resolving power as a Fabry Perot etalon for  $k = 0$  is superior to it for  $k = 3.5$ .

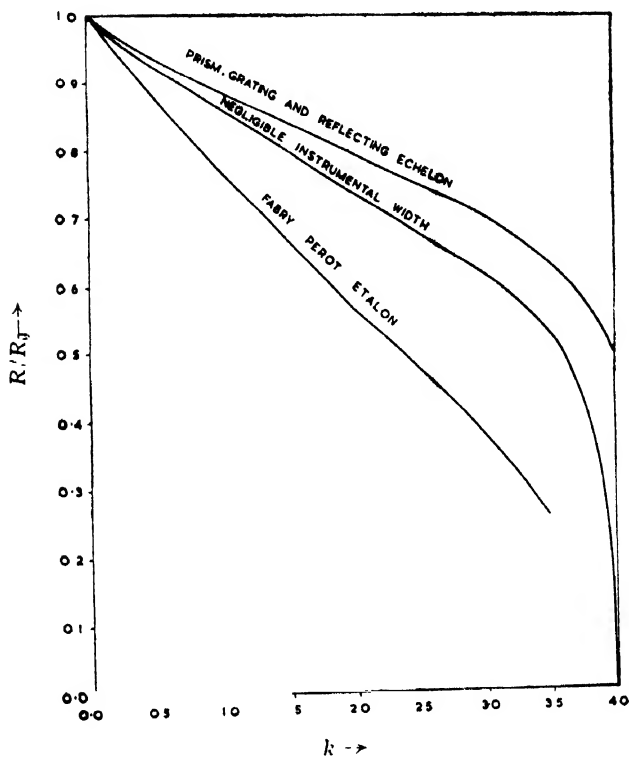


FIG. 1

Variation of  $R/R_0$  with  $k$

#### ACKNOWLEDGMENTS

The author is grateful to Dr. K. Majumdar and Dr. M. L. N. Sastri for their kind interest in the investigation.

#### REFERENCES

- Meissner, 1941, *Jour. Opt. Soc. Amer.*, **31**, 405.  
 Oldenburg, 1922, *Ann. der. Physik.*, **67**, 253





PROCEEDINGS  
OF THE  
INDIAN ASSOCIATION FOR THE  
CULTIVATION OF SCIENCE



# THE EFFECT OF CHAIN TRANSFER ON THE DISTRIBUTION OF MOLECULAR WEIGHTS IN HIGH POLYMERS. PART I—COMBINATION

BY SANTI R. PALIT AND KESAB CHANDRA MAJUMDAR

INDIAN ASSOCIATION FOR THE CULTIVATION OF SCIENCE, CALCUTTA 32

(Received for publication, December 19 1953)

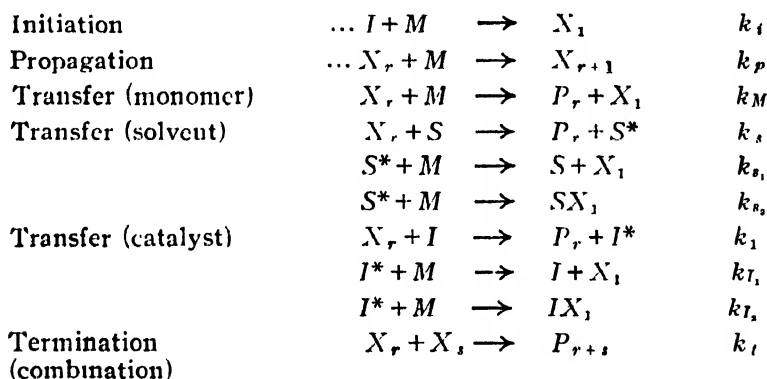
**ABSTRACT** An equation for the distribution of molecular weight taking into consideration all types of chain transfer viz., by monomer, by solvent and by initiator has been theoretically deduced. Besides giving a quantitative measure of the effect of a change in any of the factors involved in polymerization, which has also been graphically described in the paper, this equation leads to a number of interesting conclusions which are amenable to a direct experimental test. They are : (i) If a monomer is polymerized in presence of gradually increasing quantities of a solvent or a catalyst, and if  $\tau_0$ ,  $\bar{P}_n$  and  $\bar{P}_w$  are the most probable D. P., number average D. P. and weight average D. P. respectively, all the above quantities diminish continuously but they satisfy the relation  $P_w > \tau_0 \geq \bar{P}_n$ . (ii) The value of  $\bar{P}_w/P_n$  goes on increasing under similar circumstances from the lowest possible value of 1.5 to its upper limiting value of 2. (iii) The variation of  $\tau_0/P_n$  as well as of  $\bar{P}_w/P_n$  with respect to any of the factors viz., nature of monomer, nature and quantity of solvent and temperature can be represented by a universal equation and hence by the same graph, provided we represent the variations in terms of  $P_n^0/P_n$ , where  $P_n^0$  is the D. P. of the hypothetical bulk polymerization without monomer transfer. (iv) The reciprocal of the interquartile distance of the distribution curve,  $1/\Delta r$  (where  $\Delta r = r_2 - r_1$ ,  $r_2$  and  $r_1$  being the maximum D. P. which cover three-fourths and a quarter of the total weight of the polymer respectively) is a linear function of  $Cs(S/M)$  or  $C_I(I/M)$  with a slope approximately equal to 0.5

The distribution of molecular weights in high polymers is known not to belong to any of the standard types. Many theoretical attempts, notably by Schulz (1939), Flory (1936), Hulbert *et al* (1943), Herrington and Robertson (1942), Melville and Gee (1944), Evans and co-workers (1947), and lately by Tompa and Bamford (1953), and by Jordan and Mathieson (1952), (for polar polymerization), have been made to derive the distribution equation, but quite a few of these equations involve the assumption of some steps which in the light of later knowledge is known to be far removed from reality and so is of academic interest only. The results of these authors, however, are not of much direct concern to us as our main interest lies in the phenomenon of transfer (Basu *et al*, 1950, 1952) and its effect on distribution, which have not been thoroughly considered by these authors. In the present paper, we propose to deduce the theoretical distribution for polymerization in solution taking into account the concurrent transfer by the monomer, the solvent, and the catalyst, and examine some of its implications.

## DERIVATION OF THE DISTRIBUTION EQUATION

To avoid writing asterisk for free radicals we use the notation of Tompa and Bamford (1953) of writing  $X$  for free radicals and  $P$  for 'dead' polymer molecules. We shall indicate by suffix the degree of polymerization. We shall write  $S$ , for solvent, and  $I$  (in italicised capital) for initiator (catalyst). Let  $k_i$ ,  $k_p$  and  $k_t$  stand for initiation, propagation and termination rates respectively and let  $k_M$  stand for the rate of monomer transfer,  $k_I$  for catalyst transfer, and  $k_s$  for solvent transfer. The meaning of the other constants is clear from the scheme below. We shall indicate by  $C_x$  the ratio of any type of rate to  $k_p$  i.e.  $C_x = k_x/k_p$  and therefore,  $C_M$  is the usual monomer transfer,  $C_I$  the catalyst transfer and  $C_s$  the solvent transfer co-efficients and  $C_t = k_t/k_p$ . In the present paper, we have considered termination by coupling only as recent evidences (Mayo, *et al*, 1951) have thrown doubt on the occurrence of termination by disproportionation.

*Kinetic Scheme* (Initiation by catalyst)



*Notations and Abbreviations :*

$$C_M = \frac{k_M}{k_p}; C_s = \frac{k_s}{k_p}; C_I = \frac{k_I}{k_p}; C_t = \frac{k_t}{k_p}; t = \frac{\sqrt{k_i k_t}}{k_p}$$

$$\bar{I} = C_M + C_s \frac{S}{M} + C_I \frac{I}{M} + t \sqrt{\frac{I}{M}}$$

$$a = \frac{1}{2} t q \sqrt{\frac{I}{M}}$$

$$b = C_M + C_s \frac{S}{M} + C_I \frac{I}{M} - a \approx C_M + C_s \frac{S}{M} + C_I \frac{I}{M}$$

$$e = t \sqrt{\frac{I}{M}} + \left( C_M + C_s \frac{S}{M} + C_I \frac{I}{M} \right) \frac{1}{1+q} \approx t \sqrt{\frac{I}{M}} + b = q$$

From the above scheme with the usual steady state assumption and following a method which is essentially due to Melville and Gee (1944) and elaborated by Bawn (1948), we can easily derive the following equation

without any additional assumption whatsoever. The derivation is given in Appendix I, but it may be pointed out that we have introduced  $S/M$  and  $I/M$  as the variable without which simplification seems to be impossible.

$$\frac{dP_r}{dM} = \frac{q(ar+b)}{(1+\epsilon)(1+q)^r} \quad \dots (1)$$

Putting  $W_r$  for the weight fraction of the  $r$ -mers, which is evidently equal to  $r.dP_r/dM$ , we obtain

$$W_r = \frac{q^r(ar+b)}{(1+\epsilon)(1+q)^r} \quad \dots (2)$$

It can be easily shown that  $\epsilon$  is about equal to  $q$  which latter under usual conditions is about  $10^{-4}$  or less and so we can neglect it in comparison with unity. The equation then takes the simple form

$$W_r = \frac{qr(ar+b)}{(1+q)^r} \cong q^r(ar+b)e^{-qr} \quad \dots (3)$$

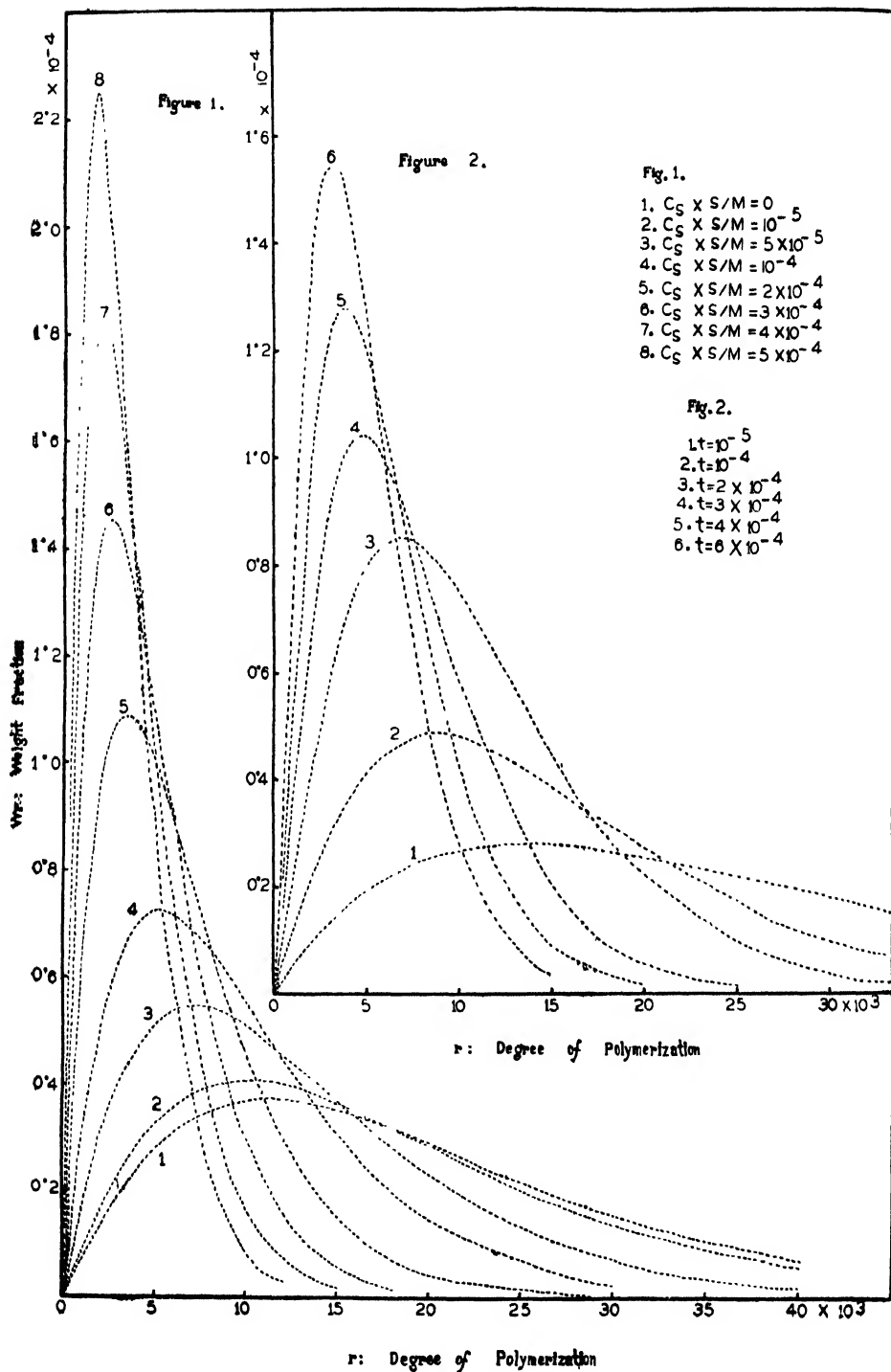
which is our final equation. This is a differential equation and so gives the instantaneous distribution at a given value of  $S/M$  and  $I/M$ . Hence we should apply it at small yields just like the other polymer equations of the differential type, as for example, the solvent transfer equation, and the co-polymerization equation.

#### THE SHAPE OF THE THEORETICAL DISTRIBUTION CURVE

For styrene the absolute values of the rate constants are known with a fair degree of accuracy. We have taken the following values of the constants at  $60^\circ\text{C}$  viz.  $k_p = 176$  and  $k_t = 7.2 \times 10^7$ , and have drawn a set of curves which are shown graphically in figures 1 and 2. The value of  $k_t$ , the thermal initiation rate is discordant among different workers and we have taken the value given by Mathieson and co-workers (Johnson, *et al*, 1942; Walling, 1949) and we have taken  $C_M = 6 \times 10^{-5}$ , being the best available value in literature (Baysal and Toboloky, 1952). The shapes of the distribution curves are very similar to those of the distribution curves obtained by previous workers for bulk polymerization, all curves being as expected a little skew to the right.

*Effect of dilution and solvent transfer.* It would be seen from the form of the equation that since  $C_S$  and  $S/M$  always go together as their product, their effect is exactly the same. In other words the effect of using different solvents can always be duplicated by a change of the ratio, solvent : monomer of one solvent.

In figure 1 we have given eight theoretical curves for styrene at  $60^\circ\text{C}$  for different values of  $C_S(S/M)$  ranging from zero to  $5 \times 10^{-4}$  which cover the usual range of variation in these values. The most striking feature



FIGS. 1 and 2

of these curves is the sudden change of steepness within the  $C_s(S/M)$  range considered. The distribution is fairly flat at  $C_s(S/M)=0$  and  $10^{-5}$  and even a 5 times change in this value makes the curve only slightly steep but from then on a small change makes the curve increasingly steeper. This is easily realised by comparing the enormous change of steepness by changing  $C_s(S/M)$  from  $10^{-4}$  to  $3 \times 10^{-4}$  with the change effected by a ten times variation in  $C_s S/M$  viz. from  $10^{-5}$  to  $10^{-4}$ . Thus we come to the important result that the steepness of the curve is highly sensitive to a change of  $C_s(S/M)$  from near about  $5 \times 10^{-5}$  onwards—a conclusion which is of great practical importance because it is just in this range where most experiments are carried out.

*Effect of catalyst concentration.* A part of the effect of the initiator,  $I$  is very similar to that of the solvent  $S$  as  $I$  always occurs in the expression  $C_s(S/M) + C_I(I/M)$ , and hence needs no further elaboration. The initiator is generally used at a concentration near about one-thousandth mol ratio of the monomer and  $C_I$ , the catalyst transfer coefficient is usually of the order of one thousand times higher than  $C_s$ , the solvent transfer coefficient, and so under such circumstances this initiator term is as important as the solvent term as long as  $C_I$  does not become very small.

The other term involving the initiator is  $t\sqrt{I/M}$  and so its effect can be easily judged from the effect of  $t = \frac{\sqrt{k_t k_i}}{k_p}$  to be shortly discussed. It

would be also seen that wherever  $t$  occurs in thermal initiation,  $t\sqrt{I/M}$  occurs in catalyst initiation and hence we have limited our later discussions to thermal initiation only, remembering that the conclusions arrived at are valid also for catalysed initiation after substituting  $t\sqrt{I/M}$  for  $t$ . Of course,  $C_I(I/M)$  should be added to  $C_s(S/M)$ , which is equivalent to increasing the value of  $C_s(S/M)$ .

*Change of  $C_M$ .* From the form of the equation it is easily seen that  $C_M$  affects the distribution in exactly the same way as a change of  $C_s(S/M)$ . This is, however, of no practical interest as we cannot change  $C_M$  without changing the other constants.

*Change of  $k_t$ ,  $k_p$  and  $k_i$ .* In the distribution equation  $k_t$ ,  $k_p$  and  $k_i$  always occur together as  $t = \frac{\sqrt{k_t k_i}}{k_p}$ . It is evident that a proportionate change of either  $k_t$  or  $k_i$  acts in exactly the same way. Also, the influence of  $k_p$  is stronger than, and is in opposite direction to that of  $k_t$  and  $k_i$ , the effect of a given per cent change in the former being equivalent to a same per cent change in the square root of any of the latter two.

The combined effect has been illustrated in figure 2 where we have drawn a number of theoretical distribution curves for thermal polymerization corresponding to various values of  $t$  for styrene taking  $C_s(S/M)=10^{-5}$ . A feature similar to that observed in the case of a change of solvent transfer

co-efficient is also observed here. The distribution curve remains fairly flat up to  $t = 10^{-4}$  but from then on the curve becomes more and more peaked and in fact an increase in  $t$  gives continuously increasing peakedness. The usual experimental conditions are more concerned with this sensitive portion of the curve and hence this behaviour is of great experimental interest. Since  $t$  increases with temperature it follows that the distribution is expected to be more and more peaked with increase of temperature. This is further helped by a concurrent increase of  $C_M$  and  $C_S$ . This point can be easily tested experimentally.

*Interquartile distance and steepness of distribution.* A fair measure of the steepness of distribution is the interquartile range *i.e.* the range of  $r$  which excludes the lightest and heaviest fractions contributing a quarter each of the total weight. It can be shown (*vide* Appendix II) that the interquartile range,  $\Delta r = r_2 - r_1$ , is given by the following simple equation.

$$\text{Interquartile range, } \Delta r = r_2 - r_1 = x/q \quad \dots (4)$$

where  $x$  is a function of  $\frac{1}{2} t \sqrt{\frac{I}{M}}/q$  but its value always lies between 1.7 and 2.2 and so it may be roughly taken to be equal to 2.

It is evident that the interquartile range decreases with an increase in  $q$  and therefore, with an increase of  $C_S$  or  $S/M$  or  $t$ . It is actually found from an examination of the expression for  $x$  that an increase of  $C_S$  or  $S/M$  decreases the interquartile range not only by an increase of  $q$  but by decrease of  $x$ , of course, within the bounds shown in equation (4). An increase of  $q$  owing to an increase in  $t$ , however, is partly compensated by a simultaneous increase of  $x$ . Hence, we conclude that the distribution becomes steeper with an increase of any of the factors,  $C_M$ ,  $C_S$ ,  $S/M$ ,  $I/M$  or  $t$  but the effect due to the last factor is somewhat less than the other factors which all have equal effect for an equal change—a conclusion which we have already arrived at graphically.

The most interesting part of equation (4), however, is that it predicts a linear relationship between the reciprocal of interquartile range and  $C_S(S/M)$  at constant temperature (*i.e.* constant  $t$ ) with a slope near about half.

$$\frac{1}{\Delta r} = \frac{q}{x} = \frac{C_M}{x} + \frac{1}{x} C_S \frac{S}{M} + \frac{1}{x} C_I \frac{I}{M} + \frac{t}{x} \sqrt{I/M} \quad \dots (5)$$

$$= \frac{C_M}{x} + \frac{1}{x} C_S \frac{S}{M} + \frac{1}{x} C_I \frac{I}{M} + \frac{R_p \delta^2}{M^2} \frac{\sqrt{I/M}}{x} \quad (6)$$

$$\text{or} \quad \left[ \frac{1}{\Delta r} - R_p \frac{\delta^2}{M^2} \frac{\sqrt{I/M}}{x} \right] = \frac{C_M}{x} + C_S \frac{S}{M} + C_I \frac{I}{M} \quad (7)$$

where as already pointed out  $x$  has ordinarily a value near about two. This is a remarkable relation in the field of distribution of high polymers and



## Effect of Chain Transfer on Distribution of Mol. Wts., etc. 7

admits of direct experimental test, particularly so as  $\Delta r$  can be experimentally determined with a fair degree of accuracy. On comparing this with the similar equation involving  $1/P_n$  used in determining chain transfer, it is observed that the latter curve has a slope approximately twice that obtained by using  $1/\Delta r$  in place of  $1/\bar{P}_n$ .

### MOST PROBABLE DISTRIBUTION

*Calculation of  $r_0$  and its relationship with  $\bar{P}_n$* —Calling  $r_0$  the D.P. whose proportion is maximum in a given example, we find that its value is easily obtained by maximising  $W_r$  with respect to  $r$  (vide Appendix III). We thus obtain the following equations.

$$r_0 = \frac{2}{q} - \frac{1}{t} \pm \left( \frac{2}{q^2} - \frac{2}{q} \cdot \frac{1}{t} + \frac{1}{t^2} \right)^{\frac{1}{2}} \quad \dots (8)$$

$$r_0 = \left( \frac{2}{C_M + C_S \frac{S}{M} + t} \right)^{-\frac{1}{t}} \pm \left[ \left( \frac{2}{C_M + C_S \frac{S}{M} + t} \right)^2 - \frac{1}{t} \left( \frac{2}{C_M + C_S \frac{S}{M} + t} \right) + \frac{1}{t^2} \right]^{\frac{1}{2}} \quad \dots (9)$$

But, since for termination by coupling we should have  $\frac{1}{P_n} = C_M + C_S \frac{S}{M} + \frac{1}{2}t$ ,

we have the following relationship between  $\bar{P}_n$  and  $r_0$

$$r_0 = \left( \frac{1}{\bar{P}_n} + \frac{t}{2} \right)^{-\frac{1}{t}} \pm \left( \left( \frac{1}{\bar{P}_n} + \frac{1}{2}t \right)^2 - \frac{1}{t} \left( \frac{1}{\bar{P}_n} + \frac{1}{2}t \right) + \frac{1}{t^2} \right)^{\frac{1}{2}} \quad \dots (10)$$

These equations, though they look complicated, are very simple for calculation. Equation (8) describes the remarkable result that the correlation of  $r_0$  and  $\bar{P}_n$  depends only on the constants of polymerization,  $t = \sqrt{k_t k_i / k_p}$  and not on the nature or proportion of solvent. In other words, a given value of  $\bar{P}_n$  will have the same value of  $r_0$  provided the polymerization of the given monomer has been conducted at the same temperature. Equation (8) gives the variation of  $r_0$  with change of solvent or change in the latter's proportion. A graphical plot of  $r_0$  against  $C_S$  or  $S/M$  with known values of  $C_M$  and  $t$  shows that the  $r_0$  versus  $C_S$  (or  $S/M$ ) curve is concave upwards which is known to be experimentally true.

It can be easily shown from the above equation as also from equation (16) [vide infra] that as the proportion of solvent is increased,  $\bar{P}_n$  no doubt decreases but the ratio  $r_0/\bar{P}_n$  goes on increasing from its initial value of unity to reach a maximum at 1.08 when the average D. P. falls to half the hypothetical bulk value without any monomer transfer and then decreases continuously to reach a value near about unity and then remains

very close to unity. Thus we can say that  $r_0$  is very nearly equal to  $P_n$  under all conditions within a maximum positive deviation of 8%. Since  $1/\bar{P}_n$  is a linear function of  $C_S$  or  $(S/M)$  we shall expect  $r_0$  to be also a linear function either of  $C_S$  at constant  $S/M$ , or of  $S/M$  for the same solvent—a remarkable relation which is subject to direct experimental test.

#### WEIGHT AVERAGE AND NUMBER AVERAGE D. P.

*Weight average D. P.* By employing standard methods (vide Appendix III) we obtain the following equation for the weight average D. P.,  $\bar{P}_w$

$$P_w = \frac{2}{q^2} \left( \frac{3a}{q} + b \right) \quad \dots (11)$$

*Number average D. P.* This is also obtainable by standard methods (vide Appendix III) and we obtain

$$\bar{P}_n = \frac{1}{q - \frac{1}{2}t(1+q)} \simeq \frac{1}{q - \frac{1}{2}t} \quad (\text{since } 1 \gg q) \quad \dots (12)$$

That our distribution equation is correct is shown by the fact that this value of  $\bar{P}_n$  obtained by integration of the distribution function is exactly the same as obtainable from the usual kinetic considerations.

From kinetic considerations, we know

$$\frac{1}{\bar{P}_n} = \frac{\text{rate of cessation of chain}}{\text{rate of propagation}} = C_M + C_S \frac{S}{M} + \frac{1}{2}t \quad \dots (13)$$

$$= q - \frac{1}{2}t \quad \dots (14)$$

where all chain terminations are by coupling and no disproportionation takes place. So the identity of our distribution equation with the kinetic chain length equation is completely established.

*Relation between  $\bar{P}_w$  and  $P_n$ .* By simplification of the above two expressions for  $\bar{P}_w$  and  $P_n$  it is easy to show (vide Appendix III) that

$$\frac{P_w}{\bar{P}_n} = \frac{2(1 + t\bar{P}_n)}{(1 + \frac{1}{2}tP_n)^2} \geq 1.5 \text{ and } \leq 2 \quad \dots (15)$$

This equation gives the remarkable result that by using gradually increasing solvent : monomer ratio at constant temperature, the ratio of the weight average to the number average molecular weight will continuously increase from about 1.5 and tend to attain a limiting value of 2 at infinite dilution of the monomer. So we have set an upper and a lower limit of this ratio which can be tested experimentally.

#### A UNIVERSAL EQUATION

An interesting transformation can be obtained if we express  $1/\bar{P}_n$  in terms of  $\frac{1}{2}t$  in equations (10) and (15). That is, if we put  $1/\bar{P}_n = t(x + \frac{1}{2})$  where  $x$  can take any value from zero to infinity, these two equations respectively become

$$\frac{\bar{P}_w}{\tau_0} = \frac{2(x+1)}{(2x+1)\{1-x+\sqrt{1+x^2}\}} \quad \dots \quad (16)$$

and 
$$\frac{\bar{P}_w}{\bar{P}_n} = \frac{(2x+3)(2x+1)}{2(x+1)^2} = 2 - 1/[2(x+1)^2] \geq 1.5 \leq 2 \quad \dots \quad (17)$$

where 
$$\tau = \left\{ \left( \frac{1}{t} / \bar{P}_n \right) - \frac{1}{2} \right\} = \left\{ (2P_n^0 / \bar{P}_n) - \frac{1}{2} \right\}$$
$$= \frac{C_M + C_{S..}S/M}{t}$$

It is immediately evident that these two equations do not involve  $t$  explicitly, and do not contain any characteristic constant of the monomer, the solvent or the temperature. Hence, the variation of  $\bar{P}_w / \bar{P}_n$  (also  $\tau_0 / P_n$ ) with  $x$  (or  $\bar{P}_n^0 / \bar{P}_n$  where  $\bar{P}_n^0$  is the hypothetical bulk D.P. without any monomer transfer and is equal to  $\frac{1}{2} t$ , will be represented by the same equation and the same curve for all monomers, polymerized at any temperature with any proportion of any solvent.

If we put  $x = \frac{C_M + C_{S..}S/M}{t}$  in the above equations we immediately

obtain equations showing the variations of  $\bar{P}_w / \bar{P}_n$  or  $\tau_0 / P_n$  with  $C_{S..}$  or  $S/M$ . Thus from equation (17) we obtain

$$\frac{\bar{P}_w}{\bar{P}_n} = 2 - \frac{t^2}{2(C_M + C_{S..}S/M + t)^2} \quad \dots \quad (18)$$

If we could have a sensitive method of determining the ratio  $\bar{P}_w / \bar{P}_n$  this equation could have been put to test provided we could have a monomer whose  $C_M$  is very much less than  $t$ . For styrene at 60°C,  $C_M$  is of the order of  $t$  and so the maximum possible variation of  $\bar{P}_w / \bar{P}_n$  would be over a very narrow range close to the value of 2 and so would be hardly detectable experimentally with our present methods.

## EXPERIMENTAL TEST

All the equations deduced so far are subject to a rigid experimental test. The only uncertainty arises from the fact that  $k_t$  being an ordinary rate constant sometimes changes considerably on dilution or change of solvent. In all cases we can eliminate this uncertainty by using  $R_p \delta^2 / M^2$  for  $t$  where  $R_p$  is the observed polymerization rate and  $\delta$  is  $\sqrt{k_t / k_p}$ . Work is in progress to test experimentally the equations developed in the present paper.

## Appendix I

### DERIVATION OF THE DISTRIBUTION FUNCTION

From the given kinetic scheme and assuming that in steady state  $\frac{dX_r}{dt}$ ,  $\frac{dX_1}{dt}$ ,  $\frac{dS^*}{dt}$  and  $\frac{dI^*}{dt}$  are each equal to zero, we obtain,

$$\frac{dX_r}{dt} = k_p X_{r-1} M - k_p X_r M - k_M X_r M - k_S X_r S - k_I X_r I - k_t X_r C^* = 0 \quad \dots (1)$$

$$\begin{aligned} \frac{dX_1}{dt} = k_t I M - k_p X_1 M + k_M C^* M - k_M X_1 M - k_S X_1 S + (k_{S_1} + k_{S_2}) S^* M \\ - k_t X_1 I + (k_{I_1} + k_{I_2}) I^* M - k_t X_1 C^* = 0 \quad \dots (2) \end{aligned}$$

$$\frac{dS^*}{dt} = k_I C^* S - (k_{S_1} + k_{S_2}) S^* M = 0 \quad \dots (3)$$

$$\text{and } \frac{dI^*}{dt} = k_S C^* I - (k_{I_1} + k_{I_2}) I^* M = 0 \quad \dots (4)$$

$$\text{where } C^* = \text{total concentration of radicals} = \sum_{r=1}^{\infty} X_r \quad \dots (5)$$

From (1) we easily get

$$\frac{X_r}{X_{r-1}} = \frac{I + C_M + C_S \frac{S}{M} + C_I \frac{I}{M} + C_t \frac{C^*}{M}}{1 + q} = \frac{1}{1+q} \text{ (say)} \quad \dots (6)$$

where

$$C_X = \frac{k_x}{k_p}$$

and

$$q = C_M + C_S \frac{S}{M} + C_I \frac{I}{M} + C_t \frac{C^*}{M} \quad \dots (7)$$

Thus

$$X_r = \frac{1}{1+q} X_{r-1} = \left( \frac{1}{1+q} \right)^2 X_{r-2} = \left( \frac{1}{1+q} \right)^{r-1} X_1 \quad \dots (8)$$

Hence by (5) and (8)

$$\begin{aligned} C^* = X_1 + X_2 + \dots + X_{\infty} = X_1 + \left( \frac{1}{1+q} \right) X_1 + \left( \frac{1}{1+q} \right)^2 X_1 + \dots \\ = X_1 \left[ 1 + \frac{1}{1+q} + \frac{1}{(1+q)^2} + \dots \right] = \frac{(1+q)}{q} X_1 \quad \dots (9) \end{aligned}$$

Also from (2) we obtain

$$\begin{aligned} X_1 = \frac{\frac{k_t}{k_p} I + C_M C^* + \frac{(k_{S_1} + k_{S_2}) S^* M}{k_p M} + \frac{(k_{I_1} + k_{I_2}) I^* M}{k_p M}}{I + C_M + C_S \frac{S}{M} + C_I \frac{I}{M} + C_t \frac{C^*}{M}} \\ = \frac{\frac{k_t}{k_p} I + C_M C^* + \frac{k_S C^* S}{k_p M} + \frac{k_I C^* I}{k_p M}}{(1+q)} \text{ by (3), (4) and (7)} \end{aligned}$$

or

$$X_1 = \frac{\frac{k_t}{k_p} I + \left( C_M + C_S \frac{S}{M} + C_I \frac{I}{M} \right) C^*}{(1+q)} \quad \dots (10)$$

From this and (9) we get after simplification

$$\frac{k_t}{k_p} I + \left( C_M + C_S \frac{S}{M} + C_I \frac{I}{M} \right) C^* = q C^* = \left( C_M + C_S \frac{S}{M} + C_I \frac{I}{M} + C_t \frac{C^*}{M} \right) C^*,$$

whence we have  $C_t \frac{C^{*2}}{M} = \frac{k_t}{k_p} I$ , giving

$$C^* = \left( \frac{k_t}{C_t k_p} I M \right)^{\frac{1}{2}} = \left( \frac{k_t}{k_t} I M \right)^{\frac{1}{2}} \quad \dots (11)$$

So writing  $t = C_t \left( \frac{k_t}{k_t} \right)^{\frac{1}{2}} = \sqrt{\frac{k_t k_t}{k_p}}$  we have from (7)

$$q = C_M + C_S \frac{S}{M} + C_I \frac{I}{M} + t(I/M)^{\frac{1}{2}} \quad \dots (12)$$

Also substituting the value of  $C^*$  in (10) we get

$$X_1 = \frac{C^* \left( \frac{k_t}{k_p} \frac{I}{C^*} + C_M + C_S \frac{S}{M} + C_I \frac{I}{M} \right)}{(1+q)}$$

and since  $\frac{k_t}{k_p} \frac{I}{C^*} = \frac{k_t}{k_p} \left( \frac{k_t}{k_t} \frac{I}{M} \right)^{\frac{1}{2}} = \sqrt{\frac{k_t k_t}{k_p}} (I/M)^{\frac{1}{2}} = t(I/M)^{\frac{1}{2}}$

this reduces to

$$X_1 = \frac{q \sqrt{\frac{k_t}{k_t} I M}}{(1+q)} \quad \dots (13)$$

So from (8) we have

$$X_r = \frac{q \sqrt{\frac{k_t}{k_t} I M}}{(1+q)^r} \quad \dots (14)$$

Now from the kinetic scheme we also have

$$\frac{dP_r}{dt} = k_M X_r M + k_S X_r S + k_I X_r I + \frac{1}{2} k_t \sum_{j=1}^{r-1} X_j X_{r-j}, \text{ which after substitution}$$

of the value of  $X_r$  from (14) reduces to

$$\begin{aligned} \frac{dP_r}{dt} &= (k_M M + k_S S + k_I I) \frac{q \sqrt{\frac{k_t}{k_t} I M}}{(1+q)^r} + \frac{1}{2} k_t \sum_{j=1}^{r-1} \frac{q^2 \left( \frac{k_t}{k_t} I M \right)}{(1+q)^{j+r-j}} \\ &= \frac{q \left( \frac{k_t}{k_t} I M \right)^{\frac{1}{2}} (k_M M + k_S S + k_I I)}{(1+q)^r} + \frac{\frac{1}{2} k_t (r-1) q^2 \left( \frac{k_t}{k_t} I M \right)}{(1+q)^r} \\ &= \frac{k_p M q \sqrt{\frac{k_t}{k_t} I M}}{(1+q)^r} \left\{ C_M + C_S \frac{S}{M} + C_I \frac{I}{M} + \frac{1}{2} C_t (r-1) q \sqrt{\frac{k_t}{k_t} \frac{I}{M}} \right\} \end{aligned}$$

or

$$\frac{dP_r}{dt} = \frac{k_p M q \sqrt{\frac{k_t}{k_t} \frac{I}{M}}}{(1+q)^r} (ar+b) \quad \dots (15)$$

$$\text{where } a = \frac{1}{2} C_t q \sqrt{\frac{k_t}{k_t} \frac{I}{M}} = \frac{1}{2} q t \sqrt{\frac{I}{M}} \quad \dots (16)$$

$$\begin{aligned} \text{and } b &= C_M + C_S \frac{S}{M} + C_I \frac{I}{M} - \frac{1}{2} C_t q \sqrt{\frac{k_t}{k_t} \frac{I}{M}} \\ &= q - t \sqrt{\frac{I}{M}} - \frac{1}{2} q t \sqrt{\frac{I}{M}} \quad \left. \vphantom{\begin{aligned} &= q - t \sqrt{\frac{I}{M}} - \frac{1}{2} q t \sqrt{\frac{I}{M}} \\ &= q - t \sqrt{\frac{I}{M}} - a \end{aligned}} \right\} \quad \dots (17) \\ &= q - t \sqrt{\frac{I}{M}} - a \end{aligned}$$

Also

$$\begin{aligned} -\frac{dM}{dt} &= k_p C^* M + k_M C^* M - k_M X_1 M + k_t I M + (k_S + k_{S_1}) S^* M - k_S X_1 S \\ &\quad + (k_{I_1} + k_{S_1}) I^* M - k_I X_1 I \\ &= k_p C^* M + k_M C^* M - k_M X_1 M + k_t I M + k_S C^* S - k_S X_1 S + k_I C^* I \\ &\quad - k_I X_1 I, \text{ by (3) and (4)} \end{aligned}$$

Substituting the values of  $C^*$  and  $X_1$  from (11) and (13) we get

$$\begin{aligned} -\frac{dM}{dt} &= (k_p M + k_M M + k_S S + k_I I) \sqrt{\frac{k_t}{k_t} \frac{I}{M}} + k_t I M \\ &\quad - \frac{(k_M M + k_S S + k_I I) q \sqrt{\frac{k_t}{k_t} \frac{I}{M}}}{(1+q)} \\ &= k_p M \sqrt{\frac{k_t}{k_t} \frac{I}{M}} \left\{ \left( 1 + C_M + C_S \frac{S}{M} + C_I \frac{I}{M} + t \sqrt{\frac{I}{M}} \right) \right. \\ &\quad \left. - \frac{\left( C_M + C_S \frac{S}{M} + C_I \frac{I}{M} \right) q}{(1+q)} \right\} \\ &= k_p M \sqrt{\frac{k_t}{k_t} \frac{I}{M}} \left\{ 1 + q - \frac{\left( q - t \sqrt{\frac{I}{M}} \right) q}{(1+q)} \right\} \end{aligned}$$

Or

$$-\frac{dM}{dt} = k_p M \sqrt{\frac{k_t}{k_t} \frac{I}{M}} (1+\epsilon) \quad \dots (18)$$

$$\text{where } \epsilon = q - \frac{\left( q - t \sqrt{\frac{I}{M}} \right) q}{(1+q)} = \frac{q \left( 1 + t \sqrt{\frac{I}{M}} \right)}{(1+q)} = o(q) \quad \dots (19)$$

Hence by (15) and (18) we obtain

$$-\frac{dP_r}{dM} = \frac{dP_r}{dt} \left/ -\frac{dM}{dt} = -\frac{k_p M q \sqrt[k_t]{k_t} IM}{(1+q)^r} (ar+b) \right/ k_p M \sqrt[k_t]{k_t} IM(1+\epsilon)$$

or

$$-\frac{dP_r}{dM} = \frac{q(ar+b)}{(1+\epsilon)(1+q)^r} \quad \dots (20)$$

The instantaneous distribution function of the molecular weights in high polymers will be, then, given by

$$W_r = r \times \left( -\frac{dP_r}{dM} \right) = \frac{qr(ar+b)}{(1+\epsilon)(1+q)^r} \quad \dots (21)$$

where  $r$  varies from 2 to  $\infty$ .

Or neglecting  $\epsilon$ , which is very small in comparison to unity

$$W_r = \frac{qr(ar+b)}{(1+q)^r}, \quad \dots 2 \leq r \leq \infty \quad \dots (22)$$

$$= qr(ar+b)e^{-qr} \quad \dots (23)$$

by putting  $(1+q)^r = e^x$ , as shown under eq. (1) in Appendix II.

## Appendix II

### CALCULATION OF INTERQUARTILE DISTANCE OF THE MOLECULAR WEIGHT DISTRIBUTION

The distribution of the molecular weight fraction is, as obtained in Appendix I,

$$W_r = \frac{qr(ar+b)}{(1+q)^r}, \quad 2 \leq r \leq \infty$$

The lower quartile  $r_1$ , say, of this distribution is obtained by solving the equation

$$\frac{1}{4} = \sum_{r=2}^{r=r_1} W_r = 1 - \sum_{r=r_1}^{r=\infty} W_r; \text{ since } \sum_{r=2}^{r=\infty} W_r = 1$$

$$\text{Or, } \frac{3}{4} = \sum_{r=r_1}^{r=\infty} W_r \approx \int_{r_1}^{\infty} W_r dr = \int_{r_1}^{\infty} \frac{qr(ar+b)}{(1+q)^r} dr \quad \dots (1)$$

If we put  $e^x = (1+q)^r$ , then since  $q$  is very small compared to unity we shall have

$$x = r \ln(1+q) = rq \text{ or } r = \frac{x}{q}$$

With this transformation equation (1) reduces to

$$\begin{aligned} \frac{3}{4} &= \int_{x_1}^{\infty} \frac{q \left( a \frac{x^2}{q^2} + b \frac{x}{q} \right)}{e^x} \frac{dx}{q} \\ &= \frac{a}{q^2} \int_{x_1}^{\infty} x^2 e^{-x} dx + \frac{b}{q} \int_{x_1}^{\infty} x e^{-x} dx \\ &= \frac{a}{q^2} I_1 + \frac{b}{q} I_2 \end{aligned} \quad \dots (2)$$

where  $I_2 = \int_{x_1}^{\infty} x e^{-x} dx = x_1 e^{-x_1} + e^{-x_1}$ , after integrating by parts ;

and

$$\begin{aligned} I_1 &= \int_{x_1}^{\infty} x^2 e^{-x} dx = x_1^2 e^{-x_1} + 2 \int_{x_1}^{\infty} x e^{-x} dx \\ &= x_1^2 e^{-x_1} + 2 I_2 \\ &= x_1^2 e^{-x_1} + 2(x_1 e^{-x_1} + e^{-x_1}) \end{aligned}$$

So equation (2) now simplifies to

$$\frac{3}{4} = \frac{a}{q^2} \{x_1^2 + 2(x_1 + 1)\} e^{-x_1} + \frac{b}{q} (x_1 + 1) e^{-x_1}$$

or

$$\frac{3}{4} e^{x_1} = \frac{a}{q^2} x_1^2 + (x_1 + 1) \left( \frac{2a}{q^2} + \frac{b}{q} \right) \quad \dots (3)$$

Putting the values of  $a$ ,  $b$ ,  $q$  from Appendix I we find

$$\frac{a}{q^2} = \frac{t \sqrt{\frac{I}{M}}}{2q} = \frac{1}{2} \frac{t \sqrt{\frac{I}{M}}}{C_M + C_S \frac{S}{M} + C_I \frac{I}{M} + t \sqrt{\frac{I}{M}}} = p \text{ (say)} \quad \dots (4)$$

$$\begin{aligned} \text{and } \frac{2a}{q^2} + \frac{b}{q} &= \frac{t \sqrt{\frac{I}{M}}}{q} + \frac{q - t \sqrt{\frac{I}{M}} - \frac{1}{2} t q \sqrt{\frac{I}{M}}}{q} = 1 - \frac{1}{2} t \sqrt{\frac{I}{M}} \\ &\approx 1, \text{ as } \frac{1}{2} t \sqrt{\frac{I}{M}} \text{ is very small compared to unity.} \end{aligned}$$

So equation (3) reduces to

$$\frac{3}{4} e^{x_1} = 1 + x_1 + p x_1^2 ; \quad \dots (5)$$

from which by solving for  $x_1$ , we get  $x_1 (= x_1/q)$

The upper quartile  $x_2$ , say, can be obtained by solving

$$\frac{1}{4} = \sum_{r=r_1}^{\infty} W_r \approx \int_{r_1}^{\infty} \frac{q r (ar + b)}{(1 + q)^r} dr, \text{ which in a similar way as above reduces to}$$

$$\frac{1}{4} e^{x_2} = 1 + x_2 + p x_2^2, \quad \dots (6)$$

where

$$x_2 = r_2 q$$



Equations (5) and (6) can be easily solved graphically by plotting the two curves  $y_1 = \frac{3}{4}e^x$  and  $y_2 = \frac{1}{4}e^x$  once for all and on the same graph the plot of  $y = 1 + x + px^2$  may be made for various values of  $p$ , cutting the first two curves for  $y_1$  and  $y_2$  at  $x_1$  and  $x_2$  respectively. Then the interquartile distance is given by

$$\Delta r = r_2 - r_1 = \frac{x_2 - x_1}{q} \quad \dots (7)$$

which will, of course, differ for different values of  $p$ .

From (4) it is easily seen that  $p$  must lie between 0 and 0.5 which thus provides us two limiting values for  $\Delta r$  for any fixed value of  $q$ . From the graphical plot it has been found that for  $p=0$ ,  $x_2 - x_1$  is about 1.7, while for  $p=0.5$ ,  $x_2 - x_1$  is 2.2, so that in general the interquartile distance,  $\Delta r$  lies between  $\frac{1.7}{q}$  and  $\frac{2.2}{q}$ .

### Appendix III

#### (a) DETERMINATION OF AVERAGE D. P.

Weight average D.P. ( $\bar{P}_w$ ):

From definition it follows

$$\left. \begin{aligned} \bar{P}_w &= \frac{\sum r W_r}{\sum W_r} = \sum_{r=2}^{\infty} r W_r, \text{ because } \sum_{r=2}^{\infty} W_r = 1 \\ &\simeq \int_0^{\infty} r W_r dr \end{aligned} \right\} \quad \dots (1)$$

In this integral the range of variation of  $r$  is taken as 0 to  $\infty$ ; but its contribution over the interval  $r=0$  to 2 is so small that the difference between the sum and the integral in (1) is perfectly negligible.

Substituting the value of  $W_r$  and applying the transformation  $e^x = (1+q)^r$  as in Appendix II, we have

$$\begin{aligned} \bar{P}_w &= \int_0^{\infty} \frac{q r^2 (a r + b)}{(1+q)^r} dr = \int_0^{\infty} \left( \frac{a q x^3}{e^x} + \frac{b q x^2}{e^x} \right) \frac{dx}{q} \\ &= \frac{a}{q^3} \int_0^{\infty} x^3 e^{-x} dx + \frac{b}{q^2} \int_0^{\infty} x^2 e^{-x} dx = \frac{a \Gamma(4)}{q^3} + \frac{b \Gamma(3)}{q^2} \\ &= \frac{6a}{q^3} + \frac{2b}{q^2} = \frac{2}{q^2} \left( \frac{3a}{q} + b \right) \\ &= \frac{2}{q^2} \left\{ q + \frac{1}{2} t \sqrt{\frac{I}{M}} (1-q) \right\}, \text{ on substituting the values of } a \text{ and } b. \end{aligned}$$

Or

$$\bar{P}_w \simeq \frac{2}{q^2} \left( q + \frac{1}{2} t \sqrt{\frac{I}{M}} \right) \text{ as } q \ll 1 \quad \dots (2)$$

or 
$$= \frac{2}{-2} (q + \frac{1}{2}t), \text{ for thermal initiation as} \quad (2a)$$

then 
$$\frac{1}{\bar{M}} = \frac{M}{M} = 1$$

Number average D.P. ( $\bar{P}_n$ ) :

The number average D. P. is given by

$$P_n = \frac{\sum r P_r}{\sum P_r} = \frac{\sum W_r}{\sum P_r} = \frac{1}{\sum P_r}, \quad 2 \leq r \leq \infty$$

where  $P_r$  represents the instantaneous distribution of the number of high polymers, that is  $P_r$  is actually used for the differential distribution function

$$\frac{q(ar+b)}{(1+q)^r}.$$

Hence

$$\frac{1}{\bar{P}_n} = \sum_{r=2}^{\infty} P_r \approx \int_0^{\infty} \frac{q(ar+b)}{(1+q)^r} dr = \int_0^{\infty} \frac{(aq)^x q + bq}{e^x} \frac{dx}{q},$$

where  $e^x = (1+q)^r$  as before.

$$\begin{aligned} \text{Or } \frac{1}{\bar{P}_n} &= \frac{a}{q} \int_0^{\infty} x e^{-x} dx + b \int_0^{\infty} e^{-x} dx = \frac{a}{q} \Gamma(2) + b \Gamma(1) \\ &= \frac{a}{q} + b \end{aligned}$$

This, on substituting the values of  $a$  and  $b$  reduces to

$$\frac{1}{\bar{P}_n} = q - \frac{1}{2}t \sqrt{\frac{I}{M}} (1+q) \approx q - \frac{1}{2}t \sqrt{\frac{I}{M}}, \text{ as } q \ll 1 \quad \dots (3)$$

$$\text{or } \quad \quad \quad = q - \frac{1}{2}t, \text{ for thermal initiation} \quad \dots (3a)$$

From (2) and (3) we easily obtain,

$$\bar{P}_w = \frac{2 \left( \frac{1}{\bar{P}_n} + t \sqrt{\frac{I}{M}} \right)}{\left( \frac{1}{\bar{P}_n} + \frac{1}{2}t \left( \frac{I}{M} \right)^{\frac{1}{2}} \right)^2} = \frac{2 \left( 1 + \bar{P}_n t \left( \frac{I}{M} \right)^{\frac{1}{2}} \right) \bar{P}_n}{\left( 1 + \frac{1}{2} \bar{P}_n t \left( \frac{I}{M} \right)^{\frac{1}{2}} \right)^2},$$

so that

$$\frac{\bar{P}_w}{\bar{P}_n} = \frac{2(1 + \bar{P}_n t (I/M)^{\frac{1}{2}})}{(1 + \frac{1}{2} \bar{P}_n t (I/M)^{\frac{1}{2}})^2} \quad \dots (4a)$$

$$\text{or } \quad \quad \quad = \frac{2(1 + \bar{P}_n t)}{(1 + \frac{1}{2} \bar{P}_n t)^2} \text{ for thermal initiation} \quad \dots (4b)$$

$$\text{Let us now apply the transformation} \quad \dots (5)$$

$\frac{\bar{I}}{\bar{P}_n} = t(I/M)^{\frac{1}{2}}(x + \frac{1}{2})$  or  $\frac{\bar{I}}{\bar{P}_n} = t(x + \frac{1}{2})$  in case of thermal initiation ; where  $x$  varies from 0 to  $\infty$

$$\text{as } x = \frac{\bar{I}}{\bar{P}_n t(I/M)^{\frac{1}{2}}} - \frac{1}{2} = \frac{C_M + C_S S/M + C_I I/M}{t(I/M)^{\frac{1}{2}}}$$

$$\text{or } = \frac{C_M + C_S S/M}{t} \text{ for thermal initiation.}$$

Equation (4) then reduces to

$$\frac{\bar{P}_w}{\bar{P}_n} = \frac{2 \left( 1 + \frac{2}{2x+1} \right)}{\left( 1 + \frac{1}{2x+1} \right)^2} = \frac{(2x+1)(2x+3)}{2(x+1)^2} = 2 - \frac{1}{2(x+1)^2} \quad \dots (6)$$

which is a universal equation showing that the variation of  $\bar{P}_w/\bar{P}_n$  with  $x$  is independent of any rate constant or temperature. It may be easily seen from (6) that  $\bar{P}_w/\bar{P}_n$  lies between 1.5 and 2.0

(b) EXPRESSION FOR THE MOST PROBABLE D.P., ( $r_0$ ) :

The D.P. corresponding to the maximum proportion of the distribution can be obtained by maximising  $W_r$  with respect to  $r$ .

$$\frac{\partial W_r}{\partial r} = \frac{\partial}{\partial r} \left\{ \frac{qr(ar+b)}{(1+q)^r} \right\} = 0$$

$$\text{or } \frac{2aqr_0 + bq}{(1+q)^{r_0}} - gr_0 \frac{(ar_0+b) \ln(1+q)}{(1+q)^{r_0}} = 0$$

Since  $\ln(1+q) \simeq q$ , this reduces to

$$aqr_0^2 + (bq - 2a)r_0 - b = 0,$$

$$\text{whence } r_0 = \left( \frac{1}{q} - \frac{b}{2a} \right) \pm \left( \frac{1}{q^2} + \frac{b^2}{4a^2} \right)^{\frac{1}{2}}$$

$$\text{Now } \frac{b}{2a} = \frac{q - t(I/M)^{\frac{1}{2}} - \frac{1}{2}qt(I/M)^{\frac{1}{2}}}{qt(I/M)^{\frac{1}{2}}} = \frac{1}{t(I/M)^{\frac{1}{2}}} - \frac{1}{q} - \frac{1}{2}$$

$$\simeq \frac{1}{t(I/M)^{\frac{1}{2}}} - \frac{1}{q}, \text{ because } \frac{1}{2} \text{ is very small compared to other terms.}$$

$$\text{Hence } r_0 = \frac{1}{q} - \left( \frac{1}{t(I/M)^{\frac{1}{2}}} - \frac{1}{q} \right) \pm \left( \frac{1}{q^2} + \left( \frac{1}{t(I/M)^{\frac{1}{2}}} - \frac{1}{q} \right)^2 \right)^{\frac{1}{2}},$$

$$\text{that is } r_0 = \frac{2}{q} - \frac{1}{t(I/M)^{\frac{1}{2}}} \pm \left( \frac{2}{q^2} - \frac{2}{q} \cdot \frac{1}{t(I/M)^{\frac{1}{2}}} + \frac{1}{t^2 I/M} \right)^{\frac{1}{2}} \quad (7)$$

$$\text{or } = \frac{2}{q} - \frac{1}{t} \pm \left( \frac{2}{q^2} - \frac{2}{q} \cdot \frac{1}{t} + \frac{1}{t^2} \right)^{\frac{1}{2}}, \text{ for thermal initiation } \quad \dots (7a)$$

By (3) and (7) we also have

$$\tau_0 = \frac{2}{\left(\frac{1}{\bar{P}_n} + \frac{1}{2}t(I/M)^{\frac{1}{2}}\right)^2} - \frac{I}{t(I/M)^{\frac{1}{2}}} \pm \left( \frac{2}{\left(\frac{1}{\bar{P}_n} + \frac{1}{2}t(I/M)^{\frac{1}{2}}\right)^2} - \frac{2}{\left(\frac{1}{\bar{P}_n} + \frac{1}{2}t(I/M)^{\frac{1}{2}}\right)t(I/M)^{\frac{1}{2}}} + \frac{I}{t^2 \frac{I}{M}} \right) \dots (8)$$

or for thermal initiation,

$$\tau_0 = \frac{2}{\left(\frac{1}{\bar{P}_n} + \frac{1}{2}t\right)^2} - \frac{I}{t} \pm \left( \frac{2}{\left(\frac{1}{\bar{P}_n} + \frac{1}{2}t\right)^2} - \frac{2}{\left(\frac{1}{\bar{P}_n} + \frac{1}{2}t\right)t} + \frac{I}{t^2} \right)^{\frac{1}{2}} \dots (8a)$$

Applying the same transformation as in (5) we have

$$\tau_0 = \frac{2}{t(I/M)^{\frac{1}{2}}(x+1)} - \frac{I}{t(I/M)^{\frac{1}{2}}} \pm \left( \frac{2}{t^2 \frac{I}{M}(x+1)^2} - \frac{2}{t^2 \frac{I}{M}(x+1)} + \frac{I}{t^2 \frac{I}{M}} \right)^{\frac{1}{2}}$$

$$= \frac{1-x}{t(I/M)^{\frac{1}{2}}(x+1)} \pm \frac{(1+x^2)^{\frac{1}{2}}}{t(I/M)^{\frac{1}{2}}(x+1)} = \frac{\bar{P}_n(x+\frac{1}{2})}{(x+1)} (1-x \pm \sqrt{1+x^2})$$

$$\text{or} \quad \frac{\tau_0}{\bar{P}_n} = \frac{(2x+1)}{2(x+1)} (1-x \pm \sqrt{1+x^2}) \dots (9)$$

Since  $\tau_0/\bar{P}_n$  is a positive quantity,  $x \geq 0$  and  $\sqrt{1+x^2} \geq (1-x)$ , the term  $\sqrt{1+x^2}$  with negative sign in (9) is inadmissible. So we have

$$\frac{\tau_0}{\bar{P}_n} = \frac{(2x+1)(1-x+\sqrt{1+x^2})}{2(x+1)} \dots (10)$$

This gives a universal relation between  $\tau_0/\bar{P}_n$  and  $x$ , which is true for all monomers, polymerized at any temperature with any proportion of any solvent. From this it can be easily seen that  $\tau_0/\bar{P}_n$  is slightly  $\geq 1$  for all values of  $x$  from 0 to  $\infty$  with a maximum of 1.08.

## REFERENCES

- Basu, S., Sen, J. N. and Palit, S. R., 1950, *Proc. Roy. Soc.*, **202A**, 485.  
 Basu, S., Sen, J. N. and Palit, S. R., 1952, *Proc. Roy. Soc.*, **214A**, 247.  
 Bawn, C. R. H., 1948, *The Chemistry of High Polymers*, page 75, (Butterworth's Scientific Publications, Ltd., London).  
 Baysal, B. and Tobolsky, A. V., 1952, *J. Poly. Sci.*, **8**, 529.  
 Evans, M. G., 1947, *J. Chem. Soc.*, 266.  
 Flory, P. J., 1936, *J. Amer. Chem. Soc.*, **58**, 1877.  
 Herrington, E. F. G. and Robertson, A., 1942, *Trans. Faraday Soc.*, **38**, 490.  
 Hulbert, H. M., Harman, R. A., Tobolsky, A. V. and Eyring, H., 1943, *New York Acad. Sci.*, **34**, 371.  
 Johnson, D. H. and Tobolsky, A. V., 1952, *J. Amer. Chem. Soc.*, **74**, 938.  
 Jordan, D. O. and Mathieson, A. R., 1952, *J. C. S.*, Part II, 2358.  
 Mayo, F. R., Gregg, R. A. and Mathieson, M. S., 1951, *J. Amer. Chem. Soc.*, **73**, 1691.  
 Melville, H. W. and Gee, G., 1944, *Trans. Faraday Soc.*, **40**, 240.  
 Schulz, G. V., 1939, *Z. Physik. Chem. B*, **43**, 25.  
 Tompa, H. and Bamford, C. H., 1953, *J. Pol. Sci.*, **10**, 345.  
 Walling, C., *J. Amer. Chem. Soc.*, **51**, 1930.

# OBSERVATION OF SCATTER ECHOES ON HIGH POWER PULSED TRANSMISSIONS

BY S. N. MITRA AND V. C. IYENGAR\*

ALL INDIA RADIO, NEW DELHI

(Received for publication, February 27, 1951)

Plates IIIA-C

**ABSTRACT.** Strong scatter signals are found to occur near the transmitter on high power pulsed transmissions using directive antenna arrays. Two series of observations have been described in the paper, one during November 1950, and the other during May-June, 1951. Various types of scatter are possible depending upon the location of the scatter sources in the ionospheric layers and on the ground. The observations indicate that the most probable mode of scatter is the "Ground E" where the transmitted beam is scattered at the ground, the propagation being through the E layer. From a knowledge of the aerial polar diagram and the ranges of the scatter echoes, it has been possible to locate the ground scattering sources. It is found that one of the important sources of ground scatter is the Himalayan range in the North West Frontier Province. Various aspects of the scattering process have been described and their importance on broadcasting service discussed.

## INTRODUCTION

On long distance transmission, specular reflection from the ionosphere is thought to be the only mode of propagation. Nevertheless, signals have been received for a long time in the past within the skip zone of a transmitter. These have been attributed to irregular scattering from the inhomogenieties known to exist in ionospheric layers. Sometimes, the scatter-signals are so strong that they constitute a good service area around the transmitter within its skip zone. The investigation of scatter signals so far as broadcasting service is concerned necessarily involves a knowledge of the irregular structure of the ionospheric layers and their temporal variation. The object of the present communication is to deal with one such investigation where high power pulsed transmissions were used for observing scatter-echoes.

Eckersley (1940) has observed the scatter-echoes on various wave-frequencies and with various transmitter power using directive antennas. He found that weak signals were coming from the region where the beam penetrated the E-layer followed by stronger groups of signals at a range roughly equal to the equivalent path for a single hop F-layer transmission. He concludes that both these effects are due to back-scatter from ionic clouds in the E-layer. Booker and Wells (1938) have observed diffuse

\* V. C. Iyengar was formerly in the All India Radio

scattering from the F-layer on their  $P'-f$  records regularly in almost all winter nights during 1937-38. They interpreted their results by assuming the existence of spatial irregularities in the F-layer above a certain level so that day-time reflections from the layer are below the level of inhomogeneities. They have further shown that in order to explain the scattering at night enormous irregularities are not required; electronic clouds having densities about two to three times the average maximum electron density in the F-layer are sufficient for the purpose. CRPL observations by Hartsfield and others (1950) of high power pulsed transmissions indicate that contrary to Rickersley's findings, the predominant source of scatter was from the ground, the mode of propagation being through the E-layer. Similar conclusion was also arrived at earlier by Edwards and Jansky (1941). Dieminger (1951) has made a fairly thorough investigation of the problem by using fixed-frequency pulsed transmissions as well as automatic records from  $P'-f$  recorder. He has found that a scatter from the F-layer was a rare phenomenon, the most predominant mode of scatter was, what he calls as  $2 \times F$  scatter, i.e. transmitter to F, to ground, back to F and then back to receiver. Here again, the major source of scatter was considered to be the ground. He found that out of 1053 observations, 98.5% of the scatter-echoes might be considered as  $2 \times F$  type. Benner (1949) has made similar observations using high power pulses. He has evolved a method of computing maximum usable frequencies from the scatter-observations. The method essentially depends upon the assumption that the scatter-echoes originate from the ground. Villard and Peterson (1952) have carried out an experiment in which they have used rotating antenna and a p.p.i. for studying the scatter-echoes. They have found that ground scatter via F-layer and sporadic E are quite common and such information could be utilised for instantaneous prediction of frequencies for long distance radio propagation. Villard, Peterson and Manning (1952) in a later communication have shown that the same experiment could be utilised for studying sporadic E from consistent scatter-echoes returned from them.

In the present paper we shall describe some observations taken with high power pulsed transmission. Since we have used a broadcast transmitter suitably modified for the purpose, our observations were rather limited; the transmitter could only be used during the hours when it was carrying no programme. Two series of observations were taken; one during November 1950 and the other during May-June 1951.

## 2. NOMENCLATURE OF DIFFERENT TYPES OF SCATTER

Since we shall be dealing with many different types of scatter-echoes, it is of advantage to define them in relation to the ionospheric layers and

their mode of propagation from the transmitter to the receiver. Figure 1 shows the modes of propagation and the nomenclature is given below :

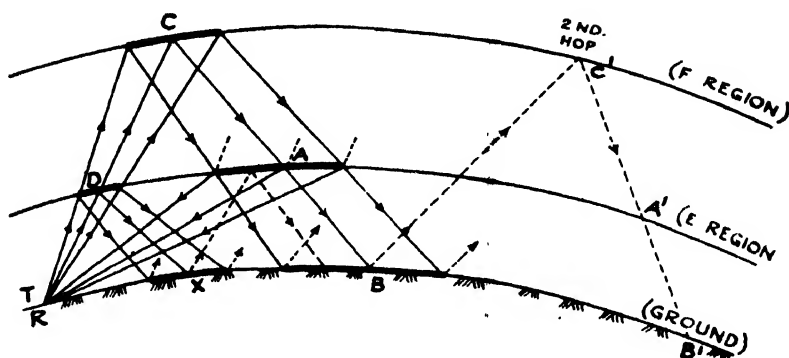


Figure 1 | Possible types of scatter

$T$  represents the location of both the transmitter and the receiver.  $X$  and  $B$  are the ground-reflection points. The various possible paths for the wave to be propagated from the transmitter to the receiver are shown in the diagram.

Type of scatter	Mode of travel	Total path
Short E	$TDT$	$2TD$
Short F	$TCT$	$2TC$
Ground E	$TDXDT$	$4TD$
Ground F	$TCBCT$	$4TC$
FE	$TCAT$	$TC + CA + AT$
FRF	$TCACT$	$2(TC + CA)$

Thus, we find that excluding multiple-hop and M-type propagations, there are six types of scatter. Our ground F scatter is the same as  $2 \times F$  scatter of Dieminger (1951). The scatter-sources may be located at any of the points  $D, C, A, B, X$  and knowing the ranges of the scatter-echoes from the scatter-pattern and the characteristics of the aerials involved, one can locate the source of scatter.

### 3. EXPERIMENTAL TECHNIQUE

In the present series of experiments a 100 kw broadcast transmitter was pulsed in the following way. The screen grid of an early exciter stage was held at a high negative potential through a diode which was normally kept conducting by applying a suitable negative voltage at its cathode. The exciter, under these conditions, was blocked and the carrier was suppressed. Positive pulses from a suitable pulsing source were applied to the cathode of the diode so as to neutralise the standing negative bias for the duration of the pulses. The diode was, therefore, cut-off and the blocking bias on the exciter-screen was removed. The carrier would be on for this small duration. The pulse repetition frequency was kept at 50 c/s and 100 c/s to investigate the long-distance and the short-distance types of scatter.

The high power transmitter was located towards north about 11 km away from the receiving centre. The receivers used in the experiments were commercial Hammarlund Super Pro Communication receivers suitably modified for pulse reception (Mitra and Roy, 1951). In the November series of experiments, the intermediate frequency-output from a similar receiver was used for 21,700 kc/s transmissions since the wave-frequency was beyond the range of the modified receiver. In the May-June series, however, we employed a modified receiver having an amplified output after the second detector from the receiver. The pulse-pattern was displayed on an oscilloscope-screen in the usual way and photographs of the pulse pattern were taken at frequent intervals. A system of height-marks at an interval of 80 km (total path) was incorporated. A typical scatter-pattern is shown in figure 2 (Plate III A). The transmitting aerial used in the experiment was an  $11/4/4/1$  array with a primary lobe maximum at  $7.8^\circ$  vertical and oriented  $316^\circ$  east of north. The width of the lobe was  $\pm 4^\circ$  down to about 60%. This aerial is mainly used to serve Middle East and European countries. Diamond types of receiving aerials and sometimes dipoles were employed to receive the pulses.

Measurements of ionospheric characteristics at vertical incidence were also carried out during the course of the experiment. During the November series, a manually operated ionospheric recorder was employed. During May-June series, however, a panoramic type of ionospheric recorder which was constructed at the Research Department of All India Radio was made available. In this recorder, the frequency range swept through was from 0.5 to 20 Mc/s; the time taken to sweep through this range being 7 seconds. A peak power of about 10 kw was radiated. A typical  $P'-f$  curve taken with this recorder during the period of observation is shown in figure 3 (Plate III A).

#### 4. PROGRAMME OF OBSERVATION

The first series of transmissions was made in November 1950. The transmission-time was from 1100 to 1230 hours IST and from 1500 to 1630 hours IST ( $5\frac{1}{2}$  hours ahead of GMT). The wave frequencies were 21,700 kc/s and 17,740 kc/s. It may, however, be incidentally mentioned that Gherzi's observation (1951) on unidentified pulsed transmission was probably the 21,700 kc/s transmission from Delhi.

In the second series of observations, only 21,700 kc/s was employed. The period of observation was throughout the month of May and 1st June 1951. The time of observation was from 1500 to 1630 hours IST and from 0130 to 0300 hours IST on every alternate day. Panoramic  $P'-f$  records were taken during this series once every half an hour.

#### 5. NATURE OF OBSERVATION

We have mentioned above that in the present paper we shall describe only the scatter-echoes observed at Delhi. The scatter-signals have been



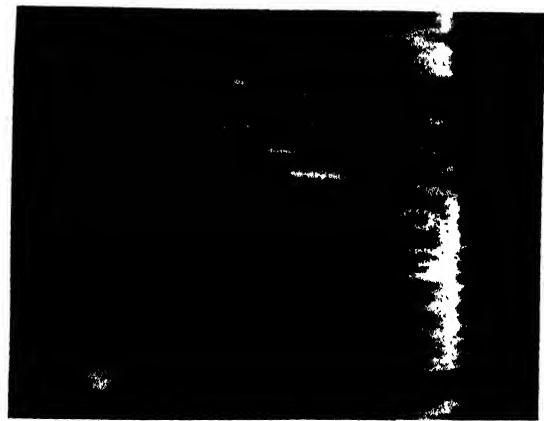


Fig. 2

A typical scatter-pattern  
 Date : 1.6.51, time : 1530 hrs, ISF :  
 frequency : 21.7 Mc/sec

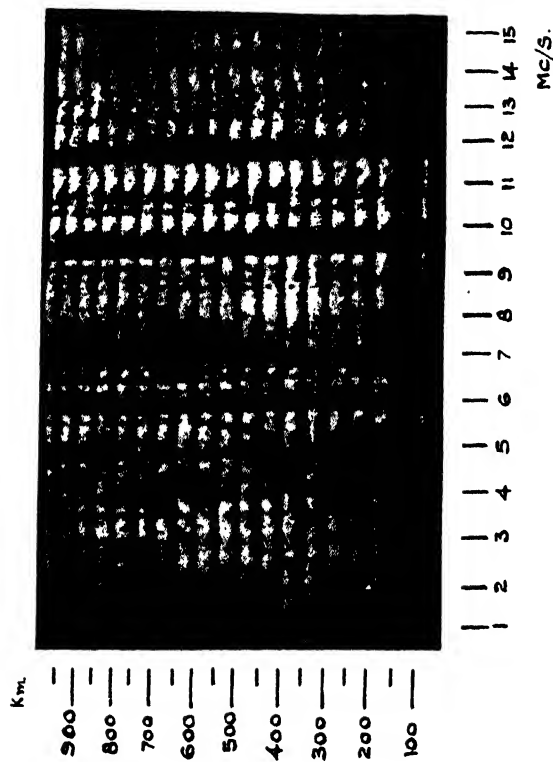


Fig. 3

A typical  $P_z$  record.  
 Date : 31.5.51, time : 0258 hrs, ISF :

## Different types of scatter-patterns

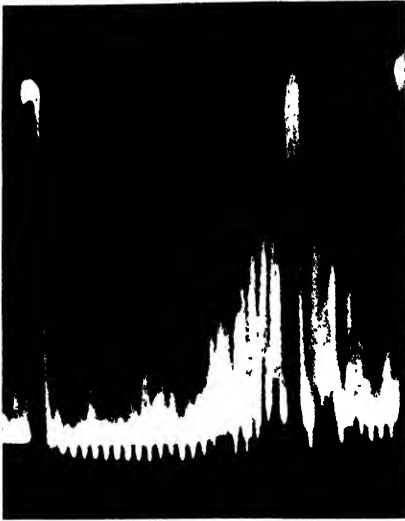


Fig. 4

Date : 1. 6. 51 ; time : 1602 hrs, IST ;  
 leading edge : 1280 km ; max. ampl : 2000  
 km ; trailing edge : 2560 km ; width : 1280  
 km ; aerial : B. B. C. diamond



Fig. 5

Date : 1. 6. 51 ; time : 1528 hrs, IST ;  
 leading edge : 1200 km ; max. ampl : 1280  
 km ; 1840 km ; trailing edge : 2400 km ;  
 width : 1200 km ; aerial : vertical diamond

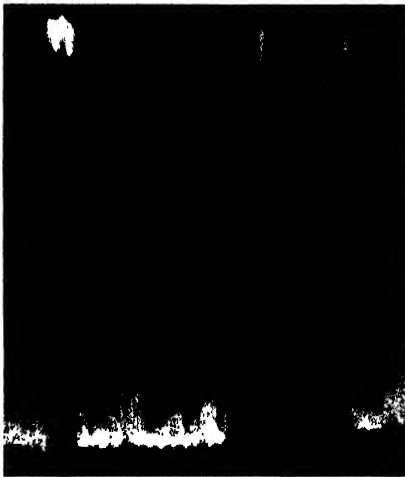


Fig. 6

Date : 1. 6. 51 ; time : 1525 hrs, IST ;  
 leading edge : 1200 km ; max. ampl : four  
 peaks ; trailing edge 2080 km ; width : 880  
 km ; aerial : vertical diamond

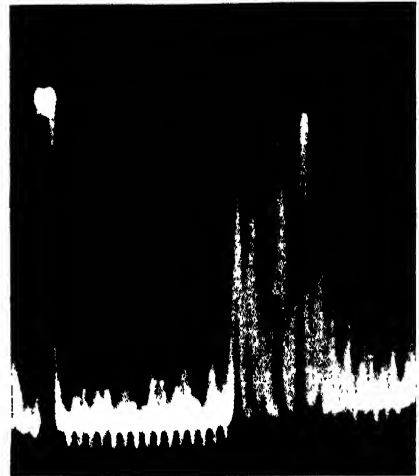


Fig. 7

Date : 1. 6. 51 ; time : 1600 hrs, IST ;  
 leading edge : 1360 km ; max. ampl : 1680  
 km ; trailing edge : 2160 km ; width : 800  
 km ; aerial : B. B. C. diamond

attributed to be due to the existence of irregularities in the ionosphere in the form of ionic clouds. For efficient scattering, the ionic density of the scatter-clouds should be higher than that of the surrounding medium. The motion of the scatter clouds distributed in a random manner will produce an irregular fluctuation of the received signal. In the experiment, a cone of waves having a finite width is incident on the ionosphere; the scatter-pattern, therefore, spreads itself on the screen of the oscilloscope having a well-defined leading edge, a maximum amplitude and a trailing edge, (figure 2) The scattering centres may also be located outside the incident cone and the laterally deviated scattered waves may contribute to the received signal. We shall, however, concentrate mainly on the primary lobe of our transmitting antenna since a  $4^\circ$  deviation from the maximum of the lobe brings a 60% decrease in the emitted power. The directivity of the receiving aerial is also an important factor and has been taken into consideration.

There is yet another phenomenon that has been frequently observed during the course of observation. Transient echoes coming from a low range and lasting only a fraction of a second have been observed during these experiments. These are presumably due to the reflection of the incident beam from ionised trails left by meteors. During the November series of observations, these transient echoes were very frequent and their rate was high. This was probably due to the period of observation coinciding with the Leonids and Andromedid meteoric showers which are known to occur in November. The transient echoes have been photographed and their duration and ranges noted. An analysis of their vertical heights has revealed that the reflection was occurring at the E-layer--thus conforming with many contemporary observations of meteor trails by radio waves.

The two series of observations will be dealt with separately. We shall not make any assumption regarding the nature of irregularities producing the scatter-echoes. The various types of scatter as enumerated in Section 2 and as observed in the experiment will be discussed. The most probable mode of scatter will be obtained from a statistical analysis of the ranges. The probable sources of scatter and their location will be obtained from a knowledge of the aerial polar-diagrams and the most frequent mode of scatter. All the data have been collected from the several hundred photographs that were taken, the necessary information being the ranges of the leading edge, maximum amplitude and the trailing edge of the scatter-groups. Observations during November 1950 were rather less numerous. We shall first describe the observations made in May-June 1951.

#### 6. DIFFERENT TYPES OF SCATTER-PATTERN AND THE EFFECT OF THE TRANSMITTING AERIAL

Our observations indicate that the ranges of the scatter-groups were variable. Before proceeding to describe the effect of the transmitting aerial, we present a few typical photographs of the scatter-pattern from

which the variation in the nature and the ranges of the scatter-groups could be seen see Plate III.

Figure 4 shows a scatter-pattern whose maximum amplitude is clearly defined. The width of the group is about 1280 km. Sometimes, more than two peaks are observed in the same group. Figure 5 gives an example where both the leading and the trailing edges are sharp but there are as many as four peaks within the same group. There is also an indication of a weaker scatter-group at a very close range, the range of the leading edge of the faint group is only 560 km and its width 320 km. On the other hand, the remote major group shows a leading edge at 1200 km with a width of nearly 1200 km. Two minutes later the faint weaker group becomes still weaker, almost submerged into 'noise'; whereas, the remote and the stronger group remains more or less the same (figure 6). This suggests that some dense ionic clouds were probably present in the D-layer which were scattering the incident wave. Figure 7 shows a scatter-pattern where the leading edge is at 1360 km but the total width is only 800 kmA.

Since the scatter-patterns are variable in nature and in their ranges, a statistical analysis of a series of observations would be necessary to arrive at some conclusion regarding the probable mode of scatter and its location.

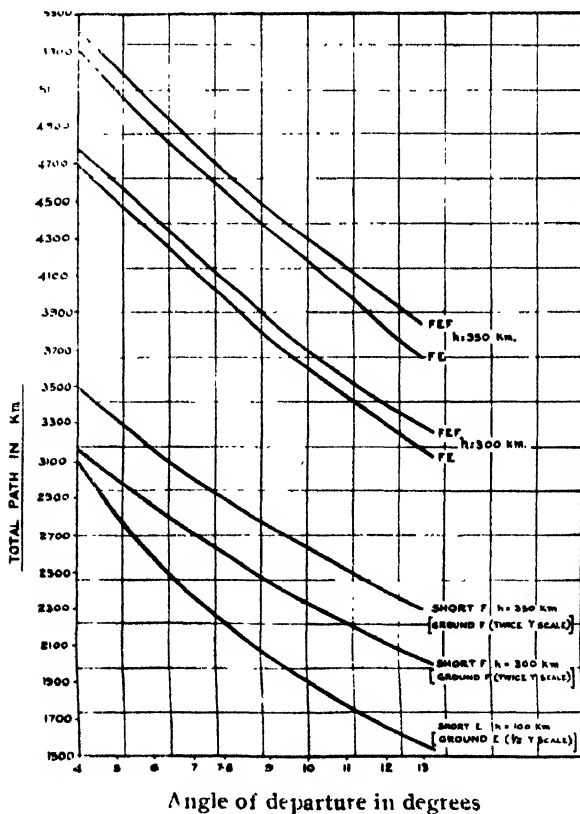


Fig. 8.

Assuming ray propagation in the ionosphere, it is possible to work out the total path for any type of scatter as mentioned in Section 2 provided the vertical height of the ionospheric layer is known. The paths will, however, depend upon the angle of departure of the radiation from the transmitting antenna. The total path for various angles of departure have been calculated for each type of scatter from the geometry of the path by taking into consideration the curvature of the earth. The results are plotted in figure 8. The height of the E-layer has been assumed to be 100 km and the height of the F-layer to be 300 km by day and 350 km by night. Panoramic  $I'f$  records show that the heights of the E- and F-layers as assumed above are in agreement with the observed values.

The paths have been calculated for angles varying between  $4^\circ$  and  $13^\circ$ , the angle for maximum radiation in the primary lobe being  $7.8^\circ$ . Since the total paths for the Ground F and Ground E types of scatter are twice the paths for Short F and Short E types respectively, they have been combined together in the figure. Thus, the curve representing Short F scatter can be used to read Ground F with twice the values in the y-scale and similarly the curve representing Ground E scatter can be utilised to read Short E with half the scale along the y axis. We have taken a cone of rays in the primary lobe from  $4^\circ$  to  $13^\circ$  since the polar diagram of the transmitting antenna shows that outside this cone the energy incident on the ionosphere will be small and scatter-radiations, if any, will be of much lower intensity.

## 7. SCATTER-OBSERVATION DURING MAY-JUNE 195 -

### (a) *Introductory Remarks.*

One of the important objects of the experiment is to determine the probable type of scatter. The scatter-pattern on the screen of the oscilloscope has always got a finite width having well-defined leading and trailing edges. Consequently, the type of scatter into which the two edges will fit might not be the same even though they constitute the same pattern. One can determine the type of scatter from the curves shown in figure 8, provided the range is known. Even then, different modes are possible for the same range depending upon the angle of departure of the transmitted radiation. In order to take into account so many variable factors, we have analysed all the observations on a statistical basis. We have first plotted the distributions of the ranges for the leading edge, maximum amplitude and the trailing edge separately both for day-time and night-time conditions and thus their most frequent ranges are determined. The probable modes of scatter for the leading edge, maximum amplitude and the trailing edges are next determined with reference to figure 8. Effort has, however, been made to concentrate as near to maximum of the primary lobe as possible. The origin of the different probable types of scatter is then discussed and the location of the scattering sources is examined.

The total number of scatter observations during this series is 751 distributed between one and a half hour during day and one and a half hour during night. The wave-frequency was kept at 21.7 Mc/s and the pulse-repetition-frequency 100 c/s. Scatter-echoes having ranges within 3000 km around the transmitter could, therefore, be investigated. The effect of different receiving aerial-systems on the nature of scatter-echoes was also studied. For this purpose, 'diamond' aerials directed towards England, Bombay, Calcutta, Madras and horizontal dipoles were freely employed. Vertical 'diamonds' were also used. We shall have occasion to refer to the effect of different receiving aerials later in the paper.

(b) *Distribution of the Ranges:*

The ranges of the leading edge, maximum amplitude, and the trailing edge from each photograph of the scatter-pattern were first plotted on a time scale. Observations on different dates were plotted independently. Figure 9 shows an example where the observations of 1st June 1951 are

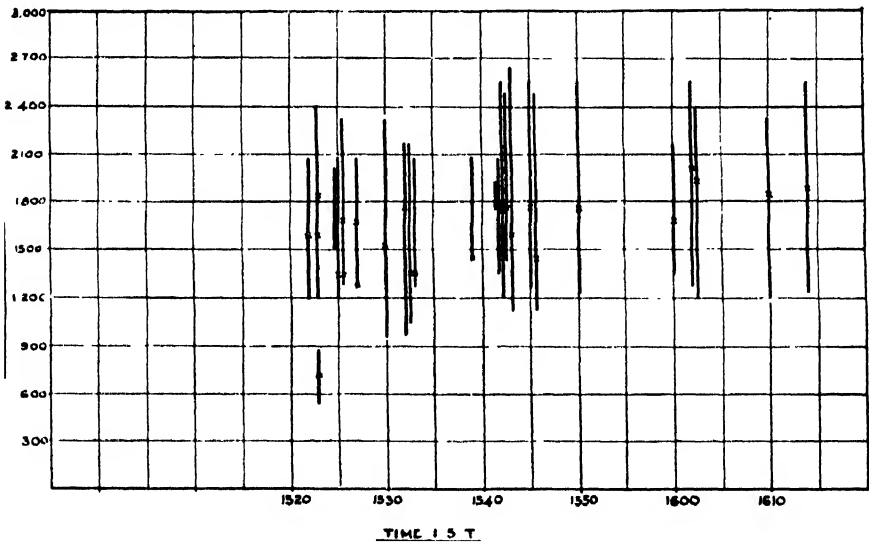


Fig 9. Scatter observation on 21700 kc/sec at Delhi, 1500 to 1615 hrs I S T., June 1, 1951

indicated. The crosses within the solid line indicate the ranges of the maximum amplitude and the length of the line indicates the width of the scatter-pattern. We next group together all such observations and plot the distributions of the ranges for the leading edge, maximum amplitude and trailing edge both for day-time and night-time conditions. Figures 10 to 14 show the distribution diagrams. The most frequent ranges are then determined from these figures and are shown in Table I below :

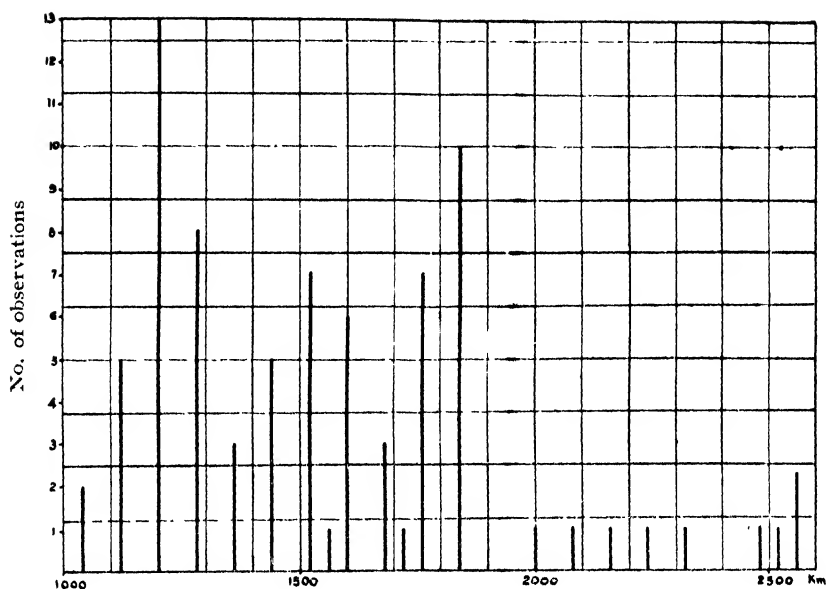


Fig. 10. Distribution of ranges (leading edge - day time)

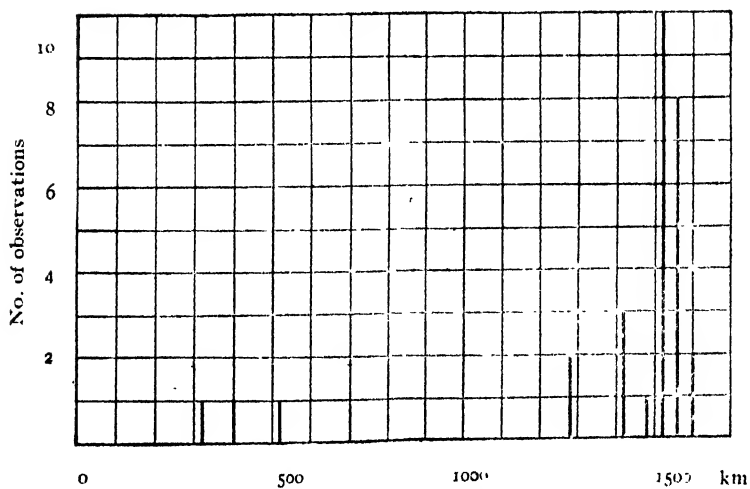


Fig. 11. Distribution of ranges (leading edge - night time)

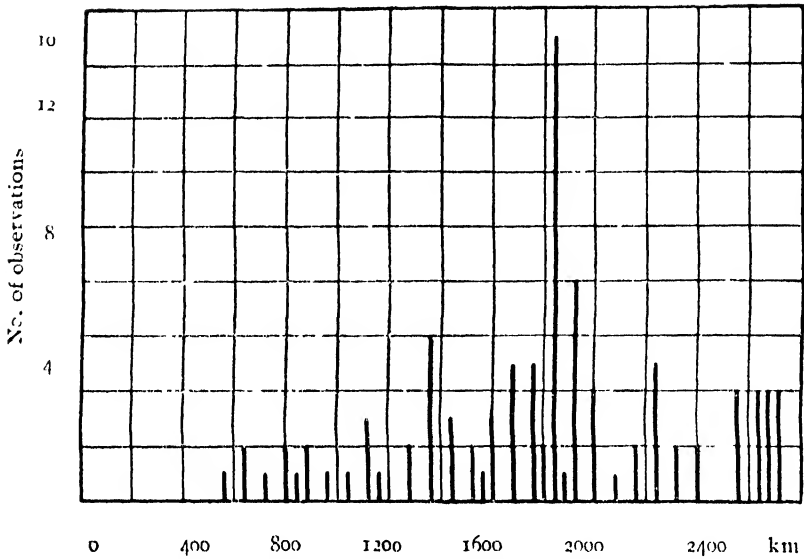


Fig. 12. Distribution of ranges (max. ampl.—day time)



Fig. 13a. Distribution of ranges (max. ampl.—night time)

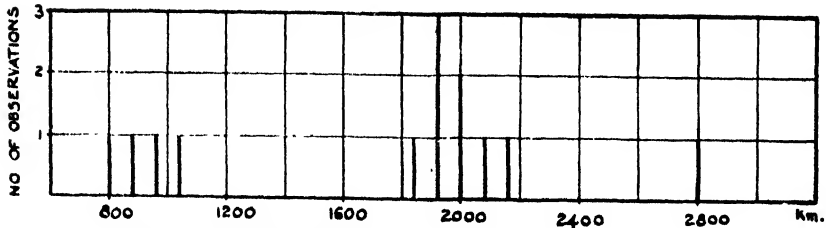


Fig. 13 b. Distribution of ranges (trailing edge—night time)



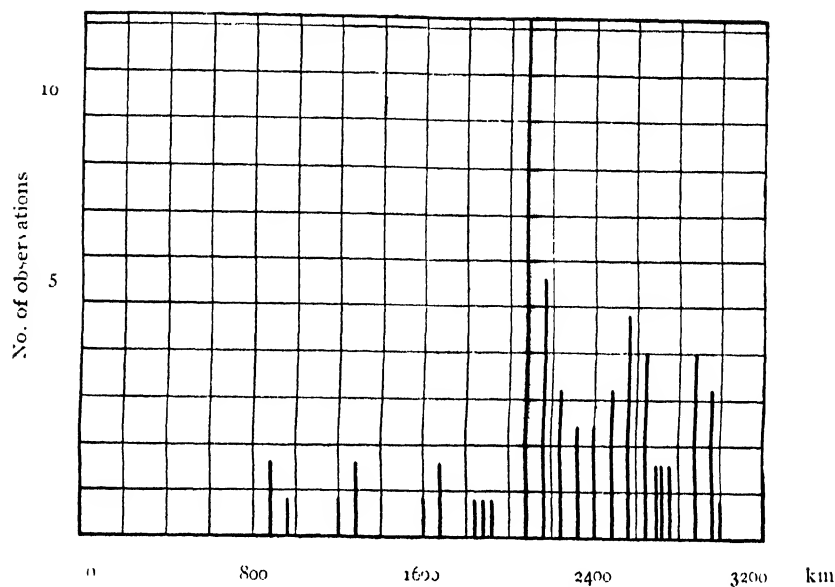


Fig. 11 Distribution of ranges (trailing edge—day time)

TABLE I  
Ranges in km

Most frequent range for	Day	Night	Difference between day and night
Leading edge	1200 km (secondary peak at 1840 km).	1520 km	320 km
Maximum amplitude	1840 km	1680 km	160 km
Trailing edge	2680 km	1920 km	160 km

The most frequent average width of the scatter-group is, therefore, 880 km during day and 400 km during night. The significance of this variation between day and night-time conditions is not clearly understood. One would, however, expect that at night due to less ionospheric absorption scattered radiation from a wider area in the ionosphere would be incident. Smaller width of the scatter-groups at night may indicate the existence of a smaller number of scattering centres and thereby suggesting some sort of a solar control on the occurrence of ionospheric irregularities during day.

(c) Probable mode of scatter :

Knowing the most frequent ranges of the leading edge, maximum amplitude and the trailing edge of scatter-groups, we evaluate the probable mode of scatter for them with reference to curves shown in figure 8.

The leading edge (1200 km) during day corresponds to the Short E type of scatter, the corresponding angle of departure for the transmitted radiation is  $7^\circ$ . The leading edge during night (1520 km) also corresponds to the Short E type at angle of about  $4^\circ$ . The maximum amplitude, however, corresponds to Ground E at angles of departure of about  $10.5^\circ$  during day and  $12^\circ$  during night. The trailing edge during day could be explained either by Ground E for a firing angle of  $9^\circ$  or by Short F for a firing angle of about  $13^\circ$ . But the trailing edge during night could only be explained by Ground E at an angle of about  $10^\circ$ . The Short F does not seem to be a very likely type since we have to assume a high angle of radiation ( $13^\circ$ ) in the primary lobe at which not much energy will be radiated and consequently the back-scattered radiation will be small.

We may, therefore, conclude that except for the leading edge which could be explained by the Short E type, the rest of the scatter-echoes within the scatter-group are due to scattering from the ground, the propagation being through the E-layer.

(d) *Explanation of the mode of scatter:*

In this section we shall try to justify the above mentioned types of scatter which are found to explain the scatter-echoes observed in the experiment.

(i) *Leading edge.* The leading edge of the scatter-group is found to correspond to the Short E type of scatter. It means that some amount of energy in the incident beam was directly scattered back to the receiver from the E-region to constitute the leading edge. It presupposes the existence of a considerable number of irregularities in the E-layer. This is quite possible since the E-region often contains irregularities in the form of ionic clouds constituting the Sporadic E and back-scatter from them would constitute a detectable signal at a sensitive receiver. But the intensity of the back-scatter is usually small and in the experiment we have also observed that the amplitude of the leading edge is generally smaller than the subsequent echoes in the scatter-pattern. Our November series of observations did not show any Short E type for the leading edge mainly because the gain of the receiving equipment (using intermediate frequency output) was not sufficient for the purpose.

The panoramic  $P''$ - $f$  records show incidence of strong Es (almost 'blanketting' type) on the first two days' observations. On subsequent days, however, Es was not so strong although it was present on almost all the days. These facts lend further support to the hypothesis that the back-scatter was originating from ionic irregularities in the E-layer.

(ii) *Maximum amplitude and Trailing edge.* We have seen that the most frequent maximum amplitude and trailing edge of the scatter-groups, both during day and during night, correspond to the Ground E type of scatter within a variation in the angle of departure of the transmitted beam

lying between  $9^{\circ}$  and  $12^{\circ}$ . The angle of departure points rather towards a high value. However, assuming that most of the scatter-echoes are coming from within the primary lobe, considerable amount of energy was being scattered from the ground to reach the receiver via the E-layer. Since the wave-frequency was much above the m. u. f. of the normal E-layer, the mode of propagation for the Ground E type of scatter was presumably through the Es. The incidence of Es both during day and during night has been observed in our  $P'-f$  records. The ground should, therefore, possess considerable irregularities to produce a good scatter-signal. We shall see in the next section that the location of the ground upon which the scattered radiation from the E-layer was incident, lies in a mountainous region, and as such, good scattering of the incident beam is quite probable there.

We, therefore, conclude that both Short E and Ground E types of scatter were the predominant modes to constitute the scatter-echoes observed in this series of experiments. Other modes of scatter may occur but due to very high angle of radiation needed to explain them, we consider them rather unlikely.

(c) Location of the source of scatter :

In the previous section we have seen that the most frequent modes of scatter were Short E and Ground E. In this section we shall examine these two types in more detail and also try to localise the source of scatter for the Ground E type. In arriving at the probable mode of scatter, we analysed all the values for the leading edge, maximum amplitude and the trailing edge. We shall now group together all the values for the different types of scatter and find out the most frequent range for any particular type of scatter.

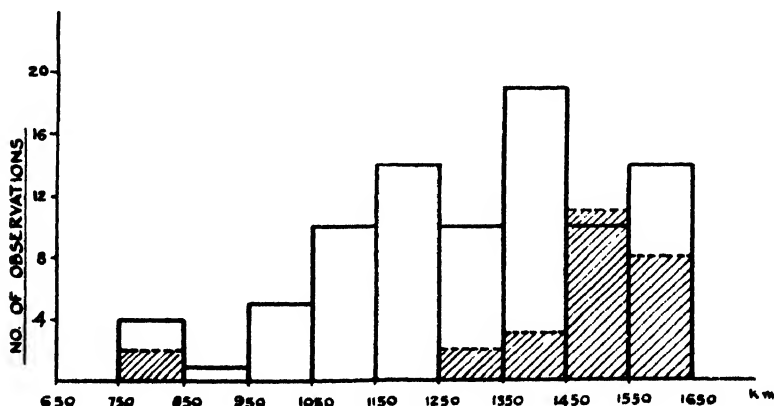


Fig. 15. Short E-scatter range in km (Hatched portions indicate night-time observations)

Figure 15 shows a histogram of all the ranges for Short E type of scatter observed during the experiment. This histogram is drawn by re-grouping the observed individual ranges so as to come under range-groups of convenient width. The hatched portion in the figure indicates the number of observations at night. It will be observed that the most frequent range for the Short E scatter is 1400 km. Night-time observations which are less numerous indicate that 1500 km is the most frequent range.

Figure 16 shows the histogram of day-time Short F type of scatter. The most frequent range is about 2100 km. At night no observation corresponded to the Short F type. In other words, if genuine ionic clouds in the F-layer scatter the incident wave during day, those irregularities are either absent during night or their dimensions and densities are such as to produce no effective scattering on 21.7 Mc/s. This is in contradiction to the findings of Booker and Wells (1938) who found large amount of scattering from the F-layer in the night.

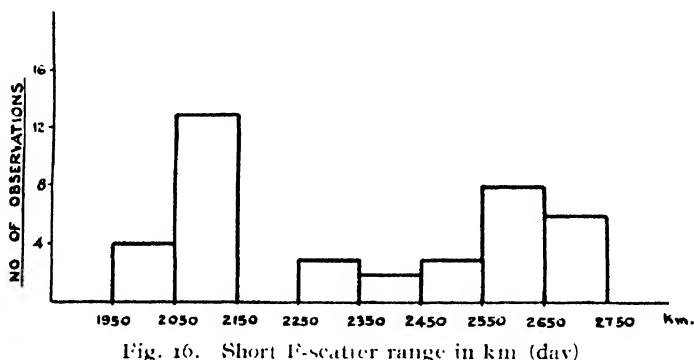


Fig. 16. Short F-scatter range in km (day)

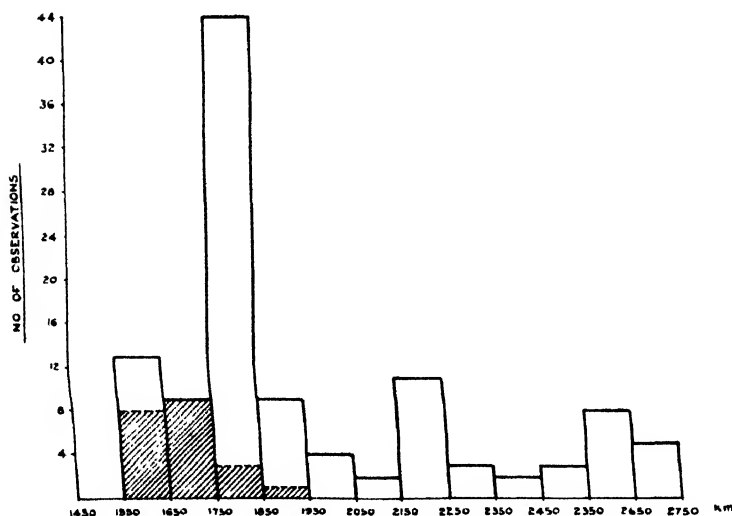


Fig. 17. Ground E-scatter range in km (Hatched portions indicate night-time observations).

Figure 17 shows the histogram of all the ranges for Ground E type of scatter. The hatched portions indicate night-time observations as in the previous case. The figure shows that the most frequent range for the Ground E type is 1800 km during day while during night it is 1700 km. This difference of 100 km between the day-time and night-time values in the most frequent ranges is observed both for Short E and Ground E types of scatter.

We shall now deal with the problem of locating the sources of Ground E scatter. The Short E and the Short F types are due to back-scatter from ionic irregularities in the E and F layers respectively. But for Ground E, the portion of the ground 'illuminated' by the scattered radiation from the E-layer should possess considerable irregularities for an effective re-scattering process. The most frequent range for the Ground E scatter is already known from figure 17. This range is the total path travelled by the signal between the transmitter and the receiver. The great circle path corresponding to this range could be calculated and knowing the polar diagrams of the transmitting and the receiving aerials, the area on the ground 'illuminated' by the incident beam can be located. An estimate of this scattering zone has also been made. In the calculation we have considered only the primary lobe of the transmitting aerial. The hatched portions MNOP and M'N'O'P' in the map (figure 18) indicate the scattering zones on the ground on either side of the transmitter since the beam was a bi-directional one. The distance over the ground of these zones from the trans-

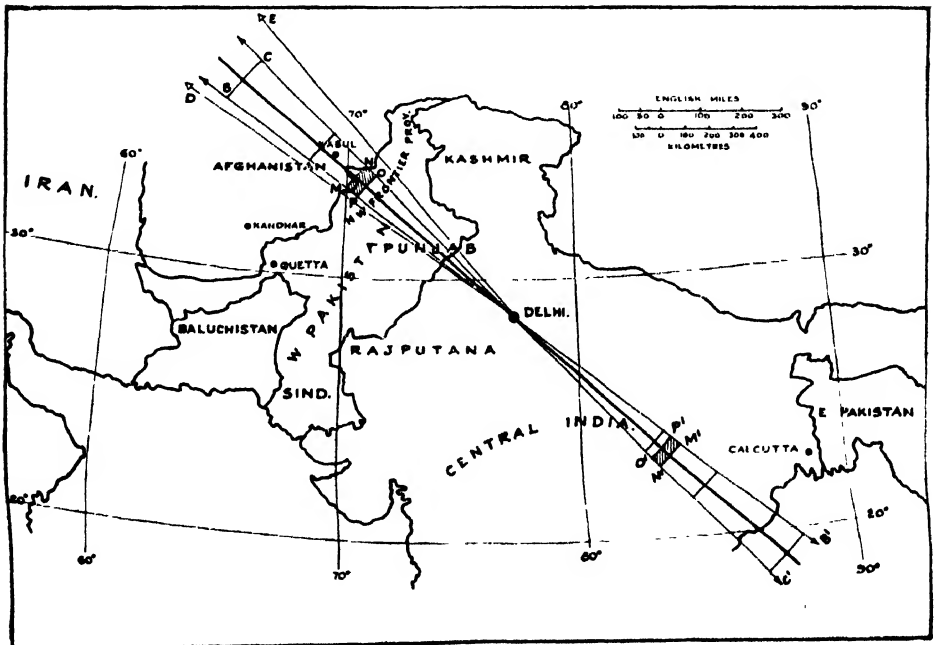


Fig 18 Location of scatter sources

mitter is about 833—890 km. It is, therefore, found that for Ground E type of scatter, contributions from two zones on the ground on either side of the transmitter may jointly or separately occur. It may be mentioned that many workers have found ground-scatter from all directions around the transmitter. We have also searched for similar instances by using highly selective "diamond" aerials directed to different directions. Since we employed directional transmissions, scatter radiation from other directions, although observed, were not so prominent. Some special tests were carried out with the BBC and Calcutta diamonds. Although the angle of elevation for the Calcutta diamond was different from the BBC one, the test gave us some indication regarding the directional properties of the ground-scatter. The BBC diamond whose acceptance cone is marked by *DE* (figure 18) would receive signals only from the north-west direction; in other words, scatter signals from *MNOP* could be received by this aerial (*BC* and *B'C'* show the transmission cone of the  $H/4/4/1$  array). A Calcutta diamond would, however, receive signals from roughly the south-west, i.e. from the zone *M'N'O'P'*. It was found during scatter-observations that when the receiving aerial was quickly switched over from a BBC to a Calcutta diamond, the scatter pattern almost vanished. Figures 19 and 20 show such an example. Calcutta diamond was used for figure 19 where the scatter-pattern could not be seen. Figure 20 shows the pattern where the aerial was switched over to a BBC diamond when a clear scatter-pattern could be observed. Similarly, the effect of diamond aerials directed towards Bombay and Madras was also studied. Experimentally, it was found that most of the scatter-patterns were obtained with the BBC diamond.

It may, therefore, be concluded that the ground-scatter observed in this experiment was due to scattering from the ground in the region *MNOP* (figure 18). The area of this zone is about 8,000 sq. km. This area falls in the mountainous portion of the North West Frontier Province covered by the Himalayan ranges. It is, however, very likely that such a region consisting of highly irregular surfaces may provide efficient scattering of the incident beam. Dieminger (1951) has also observed similar scattering from Alpine ranges.

A general examination of the scatter-photographs shows that the amplitude of the scatter-group is quite large and its width quite considerable. In the absence of regular measurements of the energy in the scattered beam, it is not possible to determine how much energy is being scattered. But there is no doubt that a considerable amount of energy is being scattered at the ground and consequently a smaller field will be produced at the intended service area.

Location of source of scatter

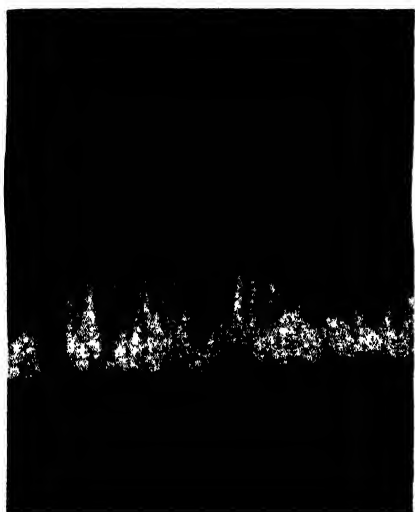


Fig. 19

Date : 1. 6. 51  
Time : 1539 hrs, IST  
Aerial : Calcutta diamond

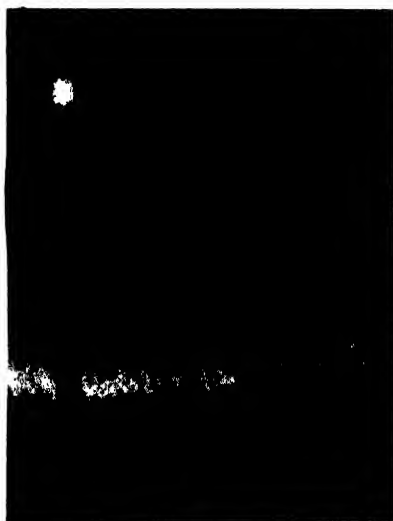


Fig. 20

Date : 1. 6. 51.  
Time : 1541 hrs, IST  
Aerial : B. B. C. diamond





8. SCATTER OBSERVATIONS DURING  
NOVEMBER 1950

(a) Analysis of observation :

In this series, observations were rather less numerous than the previous one. The pulse repetition frequency was 50 c/s. The schedule of observation has been given in Section 4. Since the period of observation was one and half hours around midday and afternoon on any of the two operating frequencies (21.7 Mc/s and 17.74 Mc/s), the general nature of the scatter-pattern might not be greatly affected due to any changes in the ionosphere. We have averaged the values of the ranges for the leading and the trailing edges during each period of observation at different times and the analysis is presented in Table II.

TABLE II

Observed ranges of the leading and the trailing edges of the scatter-groups

No.	Frequency	Date	Time IST	Range of lead- ing edge in km	Range of trailing edge in km
I	21.7 Mc/s	13.11.50	1200— 1230.	2400	3600
II.	21.7 „	15.11.50	do	2300	3320
III	21.7 „	17.11.50	do	2320	3520
IV.	21.7 „	17.11.50	1500— 1630.	2560	4000
V.	17.74 „	19.11.50	do	2000	2960
VI.	17.74 „	21.11.50	1200— 1230.	2160	3040
VII.	17.74 „	21.11.50	1500— 1630.	2000	2800
VIII.	17.74 „	23.11.50	1100— 1230	1920	2960
IX.	17.74 „	23.11.50	1500— 1630.	2000	2960

It will be noted from the table that the average values for the ranges of the leading and the trailing edges are approximately 2000 and 3000 km respectively, the scatter-group having a finite width of the order of 1000 km. The observations during May-June 1951 have indicated that these values were somewhat lower. It is also found that the scatter-patterns on both the frequencies were more or less of the same nature.

Next we determine the most probable mode of scatter corresponding to the ranges of the leading and the trailing edges concentrating, however, near the maximum of primary radiation. For this purpose we make use of figure 8. We find that the Ground E is the most probable mode of scatter to explain all the observations of the leading edge. The average

angle of departure for the observations is  $7.4^\circ$ . Short F may be a possibility but the angle of departure corresponding to this mode is much higher, about  $11^\circ$ . We, therefore, prefer to explain the leading edge by the Ground E type of scatter. The 'equivalent vertical incidence frequencies' for 21.7 Mc/s and 17.74 Mc/s are higher than the normal penetration frequency of the E-layer during the period of observation. In the absence of any measurements of  $P'$ - $f$  curves over Delhi, it was not possible to ascertain the incidence of Es during the period of observation. But since the period coincided with two prominent meteoric showers, it is quite likely that extra ionisation would be present in the E-layer either in the form of an overall increase in the ionisation density of the layer or in the form of localised ionic clouds constituting the Sporadic E or both. We may, however, assume that specially during the month of November, the E-layer had a good share in being responsible for the propagation of a large amount of transmitted energy on either of the two frequencies. (This has further been substantiated by down-coming angle measurements on these pulses conducted by the Radio Research Board, England, where a considerable variation in the angle was observed. This was probably due to the fact that the propagation was through the Es and not through the F-layer). It is, therefore, seen that the ground acts as a major source of scatter in the present experiment.

Regarding the trailing edge and portions in between the two edges, the analysis reveals that Ground E is again a likely possibility. The angle of departure of the beam corresponding to Ground E points rather towards a low value. Short F and FE types of scatter are also possible, but then one will have to assume the existence of irregularities in the F-layer. Since the total number of observations is few in this series, a definite conclusion regarding the most predominant mode of scatter to explain the trailing edge is not possible.

#### 9. SUMMARY AND CONCLUSION

In this section we shall summarise our results outlined in the body of the paper.

The investigation of scatter signals carried out in the present experiment clearly indicates that Ground E is an important mode of scatter. Short E and FE types are also possible. The Himalayan ranges have been found to act as an efficient source of ground-scatter. For the Ground E type of scatter, it is assumed that the propagation is through the E-layer. Since the wave-frequencies used in our experiment are much above the m. u. f. of the normal E-layer, the propagation for the Ground E is presumably through the Sporadic E. The incidence of Sporadic E has been observed in our  $P'$ - $f$  records both during day and night, the day-time Es being much stronger. The occurrence of night-time Ground E scatter is consequently

not so frequent as during the day-time. In the absence of any measurement of reflection coefficient of Es, it has not been possible to determine whether the Sporadic E observed in our experiment was of a "thin layer type" or of the "cloud type". It appears likely that the Ground E type of scatter would not have been so frequently observed during the day had there been no Sporadic E present and one would have expected Ground F type to be more prominent instead.

An interesting object of study in the scatter experiments would be the evaluation of the energy in the scattered radiation in relation to that in the transmitted beam. This would give the amount of energy that is "lost" by the scattering process and which would have otherwise been useful in producing greater field strength in the intended service area for these transmissions. This is rather important for a broadcasting service since the planning of short wave transmissions over long distances demands a good signal to be produced at the intended service area. It has, however, been observed that our service to Europe on 17 and 21 Mc/s bands using the H/4/4/1 array has not always been satisfactory; the field strength of the received signal as reported by BBC sometimes drops to very low values. Even if one includes the unavoidable limitations in the prediction of maximum usable frequencies resulting in a reduction of the received field-strength, such low figures are rather unexpected. This may be explained by the loss of transmitted energy in the form of scattered radiations. It would be interesting to observe back-scatter from the BBC end by employing identical arrangement. The experiment would tell us whether the Alpine ranges produce effects similar to those observed from the Himalayan mountains on transmissions from India. Our Ground E range is the Himalayas, whereas on low angle transmissions from BBC the the Alpine mountains may not produce such appreciable effect since their distances from the transmitter will not be so far as to account for a similar Ground E. Moreover, the incidence of Sporadic E is likely to be stronger at low latitudes. Both these causes will probably produce stronger scattering on transmissions from India towards Europe than from the reverse direction.

It has also been found from our scatter observations that a large amount of signal reaches North West Frontier Province and Afghanistan. The beam should normally skip over these provinces provided the propagation is through the F-layer by the primary lobe of the aerial system as originally intended in the planning of the service. It is, therefore, likely that the scatter-signals could provide a service-area within the skip zone. But it is rather difficult to predict how much satisfactory a service would be when it is based solely on scatter-signals. A systematic study of the incidence of Sporadic E is, therefore, desirable for the purpose. Similarly, an interesting investigation would be the study of the fading of the received

scatter-signals within the skip zone and how much it affects satisfactory listening.

#### ACKNOWLEDGMENTS

The paper forms a part of programme of ionospheric research in All India Radio. The authors gratefully acknowledge helpful cooperation from the Engineer in-Charge, High Power Transmitters, Delhi and his staff for kindly arranging the pulsed transmissions and contributions on the reception of the pulsed transmission from the Station Engineers, Bombay, Madras and Tiruchirapalli stations of all India Radio and also from Prof. S. K. Mitra, University of Calcutta, Dr. S. S. Banerjee, University of Banaras and from Mr. Y. V. Somayajulu, Andhra University. The authors are also indebted to Dr R. L. Smith Rose, Director of Radio Research Board, England for co-operating during the observation and sending his results on the measurement of angle of elevation on these pulsed transmissions. Finally, the authors are grateful to Mr. B. V. Baliga, late Chief Engineer, All India Radio, for his kind interest during the progress of the work and to Mr. A. C. Ramchandani, Chief Engineer, All India Radio, for permission to publish this paper. This paper was read at the Indian Telegraphs Centenary Convention held at New Delhi in November, 1953.

#### REFERENCES

- Benner, A. N., 1939, *Proc Inst. Rad. Engrs.*, **37**, 14.  
 Booker, H. G. and Wells, H. W., 1938, *Proc Inst. Rad. Engrs.*, **43**, 240.  
 Dieminger, W., 1951, *Proc. Phys. Soc., B*, **64**, 159.  
 Eckersley, T. L., 1940, *J. Inst. Elect. Engrs.*, **86**, 548.  
 Edwards, C. F. and Jansky, K. G., 1941, *Proc Inst. Rad. Engrs.*, **29**, 322.  
 Gherzi, E., 1951, *Nature*, **167**, 412.  
 Hartsfield, W. L., Ostrow, S. M. and Silberstein, R., 1950, *J. Res. Nat. Bur. Stds.*, **44**, 199.  
 Mitra, S. N. and Roy, J. M., 1951, *Electrotechnics*, **23**, 56.  
 Villard, O. G. and Peterson, A. M., 1952, *Q. S. T.*, **36**, 11.  
 Villard, O. G., Peterson, A. M. and Manning, L. A., 1952, *Proc Inst. Rad. Engrs.*, **40**, 902.

# ON THE PRODUCTION OF CHARGED MESON PAIRS BY NEUTRAL PARTICLES IN COSMIC RAYS\*

BY S. B. ROY AND R. CHAKRAVARTI†

OPTICS DEPARTMENT, INDIAN ASSOCIATION FOR THE CULTIVATION OF SCIENCE, CALCUTTA 32

(Received for publication, March 23, 1951)

## Plate IV

**ABSTRACT.** The investigation reported by Janossy and Rochester (1951) has been repeated in Calcutta using a modified arrangement so that instead of shielding the whole threefold coincidence counter telescope with anticounters, only the topmost coincidence counter has been shielded almost completely with anticounters. It has been observed that the number of anticoincidences increases slightly even when a lead absorber placed between the two upper coincidence counters is moved from its position just above the lower counter to one just below the upper counter as observed by Rusk and Rosenbaum (1949), but the number increases further when this absorber is shifted from the latter position to one just above the topmost coincidence counter. This increase is again found to be the same as that observed with the diminution of the thickness of a lead absorber placed above the anticounters from 21 cm to 2.5 cm. This increase is found to be statistically significant and about 4% of the total number of charged mesons recorded with the same arrangement.

It is pointed out that the low value, .035%, reported by Janossy and Rochester is due to the failure of the arrangement to record events in which the neutral particles produced at least two charged mesons moving in widely different directions.

## INTRODUCTION

It was first pointed out by Rossi, Janossy, Rochester and Bound (1940) that the results of previous workers regarding the difference between the number of counts in a threefold counter telescope with a lead absorber above the topmost counter and that with the absorber below the topmost counter was mostly due to side showers. Rossi and Regener (1941) combined a set of anticoincidence counters,  $A$ , above a fourfold coincidence counter telescope,  $BCDE$  and observed that when a lead absorber 5 cm thick was shifted from its position below  $B$  to that above it, the number of anticoincidence counts  $BCDE-A$  increased by about 1% of the number of fourfold coincidences. When a lead absorber 2.5 cm thick was placed above the anticoincidence counters this increase was about .75% of the fourfold coincidences. They interpreted the results by assuming that the increase in the number of anticoincidences with the shift of the absorber from its position below the counter  $B$  to that above  $B$  was due to production of mesons in the absorber in its position above  $B$  by neutral particles, which were probably high-

\* Communicated by Prof. S. C. Sirkar.

† Now in the Physics Department, Presidency College, Calcutta.

energy neutrons. These investigations were carried out by them at an altitude of 4300 m from sea level.

Similar investigations were carried out at Calcutta by Sirkar and Ghosh (1942) who used a set of anticounters above a threefold coincidence telescope and recorded the number of anticoincidences with a lead absorber, first below the topmost coincidence counter and next above it. These observations were repeated with lead absorbers of different thicknesses placed above the anticoincidence counters. It was observed by them that the number of neutral particles producing charged mesons in the lead absorber placed above the topmost coincidence counter was 2.1% of the number of threefold coincidences.

Janossy and Rochester (1943) carried out an investigation of similar nature but with some different arrangements of the anticoincidence counters and absorbers. They surrounded the whole coincidence counter telescope first with a large number of anticoincidence counters and then with lead plates so that no charged particle coming from any direction except from the bottom could reach the threefold counter telescope without striking the anticounters. They placed lead absorbers of different thicknesses upto 25 cm on the top of the anticounters placed above the threefold coincidence counter telescope and observed that the number of anticoincidences produced with a lead absorber placed above the topmost coincidence counter increased by about .035% of the total threefold coincidences with the decrease in the thickness of the topmost lead absorber from 25 cm to 5 cm. This effect was interpreted to be due to production of charged mesons in the lead absorber by neutral particles which were probably neutrons.

Sirkar and Bhattacharyya (1942, 1944) repeated the investigation reported by Sirkar and Ghosh (1942) for two directions of the axis of the anticoincidence counter telescope, one vertical and another inclined at an angle of  $30^\circ$  to the vertical. They observed that the increase in the number of anticoincidences with the shift of the lead absorber from its position below the topmost counter to that above it was about 1.4% of the threefold coincidences due to charged mesons for both the directions of the axis of the counter telescope. As the number of threefold coincidences is smaller for the inclined position of the counter telescope than that for the vertical direction owing to the instability of the charged mesons, they concluded that the neutral particles producing charged mesons in the absorber are also unstable and have a life of the same order as that of the charged meson.

The cloud chamber photographs of events in each of which at least two charged particles were produced by a neutral particle was first reproduced by Rochester and Butler (1947). This observation was next confirmed by Seriff *et al* (1950) who observed a large number of such events. Since then Fretter (1951), Bridge and Annis (1951), Leighton *et al* (1951), Thomson *et al* (1951) and many others have observed such V-particles. In the investigations in which cloud chambers are used it is difficult to get exact information

regarding the percentage of neutral particles which produce fork-shaped tracks of two charged particles, because such forks may be hidden in the large number of ionisation tracks which are also produced in the chamber by other charged particles. So, only a counter technique used with suitable arrangement and necessary precautions may give us information regarding the percentage of the neutral particles.

If we examine the counter technique used by previous workers for the investigation of this problem it will be found that the arrangement used by Rossi and Regener (1941) is suitable for detecting events in which a neutral particle produces only a single charged particle or more than one such charged particle. The investigation was, however, carried out at an altitude of 4300 m. Of similar investigations carried out at sea level those of Janossy and Rochester (1941) were made with great precaution to avoid spurious results. It can be seen, however, from the diagram of the arrangement of counters used by them that as there were anticounters on all sides of the counter telescope any event in which a neutral particle produced two charged particles moving along two paths making an angle with each other was not recorded by them, because one of the particles was sure to hit one of the vertical anticounters. They, therefore, recorded only those events in which only one charged particle was produced by the neutral particle in the absorber and also those events in which two such charged particles produced by the neutral particle moved along tracks making only a small angle with each other. In the arrangement used by Sirkar and Ghosh (1942) and Sirkar and Bhattacharyya (1942, 1944) the coincidence counters were not shielded by anticounters and therefore all events in which a neutral particle produced two charged particles could be detected, but the background counts were too high and the number of counts was so small that the statistical error was also too high. It was, therefore, thought worth-while to repeat the investigation after taking precautions to avoid these defects and at the same time to record all events in each of which a neutral particle produces one or two charged mesons in a lead absorber. The results reported in the present paper have been obtained with a threefold coincidence counter telescope, with its topmost counter shielded completely with anticounters. It will be seen from the following sections that with such an arrangement it has been possible to record the percentage of events in which a neutral particle produces in the absorber one or more charged mesons and to avoid spurious increase in the anticoincidences due to side showers and change in the position of the absorber.

#### EXPERIMENTAL

It has been mentioned above that the main source of error, namely, that due to side showers cannot be avoided in this type of investigation simply by shielding completely the whole anticoincidence counter telescope with anticounters, because such a complete shielding prevents the detection

of two charged particles produced by the  $V^0$  particle. Attempt was, therefore, made to find out the effect of shielding only the topmost counter of threefold coincidence counter telescope almost completely as shown in figure 1 in which each hollow circle indicates section of a coincidence

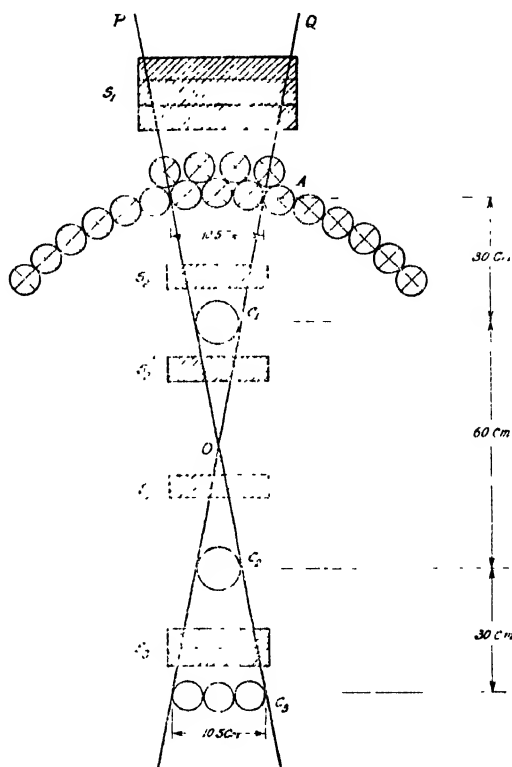


FIG. 1

counter and that filled with a cross an anticoincidence counter. It is evident that in such an arrangement of the counters the probability of side showers striking all the three coincidence counters  $C_1$ ,  $C_2$  and  $C_3$  simultaneously without striking any of the anticounters A is negligible. It was found that when the absorber  $S_2$  was just beneath  $C_1$  the number of anticoincidences per hour recorded with the anticounters only covering the solid angle  $POQ$  above  $C_1$  was almost twice the number of anticoincidences per hour recorded with the arrangement in which  $C_1$  was almost completely shielded. Hence the investigation reported by Sirkar and Ghosh (1942) was repeated with this modified arrangement of counters with the topmost coincidence counter  $C_1$  almost completely shielded with anticounters A.

The counters  $C_1$  and  $C_2$  were each of diameter about 6 cm and length 11.5 cm. System  $C_3$  consisted of three counters, each 3.5 cm in diameter and





Fig. 2  
Photograph of the experimental arrangement



23 cm long. The anticounters  $A$  were of similar dimensions and they were nineteen in number. The distances between  $A$  and  $C_1$  and  $C_2$  and  $C_3$  were each 30 cm and the distance between  $C_1$  and  $C_2$  was 60 cm. The absorbers  $S_2$  and  $S_3$  were lead plates of thicknesses 5 cm and 10 cm respectively.  $S_3$  was placed permanently between  $C_2$  and  $C_1$ . Thickness of lead plates  $S_1$  was changed from 2.5 cm to 13.5 cm and finally iron plates 10 cm thick were placed on 13.5 cm of lead.

All the counters were filled with a mixture of argon and petroleum ether (B.P. 45-60°C) in the ratio 5 : 1. The efficiency of all the anticoincidence counters was tested and found to be 99%. The circuits for the stabilised high voltage and amplifier were the same as those used by Sirkar and Bhattacharyya (1944).

It was observed by Rusk and Resenbaum (1949) that in an arrangement of four horizontal counters placed in a vertical array with the second counter from top acting as an anticounter the number of anticoincidences increases when an absorber placed between the anticounter and the coincidence counter below it is raised from its position just above the latter counter to one just below the anticounter. This increase was explained to be due to shielding of the coincidence counter by the absorber in its lower position against side showers and absence of such a shielding in the higher position. In order to find out and eliminate spurious anticoincidence counts due to such an effect in the present investigation the number of anticoincidence counts with  $S_2$  below  $C_1$  was recorded for two positions of  $S_2$ , one just above  $C_2$  and the other ( $S_2'$ ) just below  $C_1$ , which was about 25 cm above the former position. It was observed that the number of anticoincidences increased with such a shift of  $S_2$ , but when  $S_2$  was placed just above  $C_1$  the number of anticoincidences increased further. These observations were repeated to obtain three sets of readings of anticoincidences for each of the three positions  $S_2$ ,  $S_2'$  and  $S_2''$  of the absorber.

In order to find out whether the difference in the anticoincidences for the two positions  $S_2'$  and  $S_2$  of the absorber was due to production of charged mesons by neutral particles in the absorber, the anticoincidences were recorded with different thicknesses of the absorber  $S_1$  placed above the anticounters filling up the solid angle  $POQ$  subtended by the threefold coincidence counter system.

In order to find out accurately the values of the counts per hour as well as the standard deviation readings for five runs each lasting for 96 hours were taken for each disposition of the absorber  $S_2$  and standard deviation  $S$  was calculated from the formula

$$S = \frac{1}{n-1} \sum (x - \bar{x})^2$$

where  $n$  is the number of runs,  $x - \bar{x}$  is the deviation from arithmetic mean.

A photograph of the experimental arrangement is shown in figure 2

## RESULTS AND DISCUSSION

The number of anticoincidences recorded with three positions  $S_2''$ ,  $S_2'$  and  $S_2$  of the absorber  $S_2$  and 2.5 cm thick lead plate as  $S_1$  are given in Tables I, II and III. The number of anticoincidences recorded with 5 cm thick lead plate used as  $S_2$  and different thicknesses of lead and iron as  $S_1$  are given in Table IV.

TABLE I

Serial no. of runs	Disposition of absorbers	Time in hrs.	Number of anti-coincidences $N$	$x - \bar{x}$	$S = \frac{1}{n-1} \sum (x - \bar{x})^2$
	$S_1$ $S_2$ $S_2'$ $S_2''$ $S_3$				
1	2.5 cm 5 cm 0 0 10 cm	96	28	-.02	$\pm .018$
2	" " " " "	"	30	0	
3	" " " " "	"	29	-.01	
4	" " " " "	"	30	0	
5	" " " " "	"	33	+.03	

Anticoincidence counts per hour =  $3121 \pm .018$

TABLE II

Serial no. of runs	Disposition of absorbers	Time in hours	Number of anti-coincidences	$x - \bar{x}$	$S = \frac{1}{n-1} \sum (x - \bar{x})^2$
	$S_1$ $S_2$ $S_2'$ $S_2''$ $S_3$				
1	2.5 cm 0 5 cm 0 10 cm	96	23	-.0105	$\pm .01$
2	" " " " "	"	25	+.010	
3	" " " " "	"	25	+.010	
4	" " " " "	"	25	+.010	
5	" " " " "	"	24	-.004	

Anticoincidence counts per hour =  $254 \pm .01$

TABLE III

Serial no. of runs	Disposition of absorbers	Time in hrs	Number of anti-coincidences	$x - \bar{x}$	$S = \frac{1}{n-1} \sum (x - \bar{x})^2$
	$S_1$ $S_2$ $S_2'$ $S_2''$ $S_3$				
1	2.5 cm 0 0 5 cm 10 cm	96	18	-.139	$\pm .016$
2	" " " " "	96	19	-.0035	
3	" " " " "	96	21	+.0173	

Anticoincidence counts per hour =  $2014 \pm .016$

TABLE IV

Serial no of runs	Disposition of absorbers	Time in hrs	Number of anti-coincidence	$x - \bar{x}$	$S = \frac{1}{n-1} \sum (\lambda - \bar{x})^2$
	$S_1$ $S_2$ $S_2'$ $S_2''$ $S_3$				
1	13.5 cm 5 cm 0 0 10 cm Pb+10 cm Fe	96	25	+ .01	$\pm .01$
2	" " " " "	96	24	0	
3	" " " " "	96	23	- .01	

Anticoincidence counts per hour = .25 + .01

The number of threefold coincidence counts observed with  $S_1$ ,  $S_2$  and  $S_3$  respectively equal to 2.5 cm, 5 cm and 10 cm of lead was  $14.5 \pm .5$

It can be seen from Tables II and III that as the absorber  $S_2''$  is raised to the position  $S_2'$  still remaining between the counters  $C_1$  and  $C_2$  the number of anticoincidence counts increases from .201 to .254 per hour, and this increase is significant. It can be pointed out here that even if the total number of anticoincidence counts  $N$  in 480 hours of observation is taken into consideration and the standard error is taken as  $\pm .68 \sqrt{N}/480$ , its value is found to be  $\pm .016$ . If again  $S_2'$  is raised to the position  $S_2$  above  $C_1$  the number of anticoincidences increases still further to the value  $.312 \pm .018$  and this increase of  $.058 \pm .02$  counts per hour is again significant. The former increase observed with the shift of the absorber from  $S_2''$  to  $S_2'$  supports the conclusion arrived at by Rusk and Rosenbaum (1949) that at  $S_2''$  the absorber shields the counter  $C_2$  against side showers, but it does not do so when it is raised to the position  $S_2'$  just below  $C_1$ . When, however, the absorber is raised above  $C_1$  to the position  $S_2$  no removal of shielding of any of the coincidence counters can take place. On the contrary, the counter  $C_1$  may be shielded against electrons in side showers moving in inclined directions. However, neglecting such shielding of  $C_1$  in view of the fact that the anticoincidence counters already shield it effectively it can be concluded that the increase in the number of anticoincidence counts which takes place with the shift of the absorber from  $S_2'$  to  $S_2$  is due to production of charged mesons in  $S_2$  by some neutral particles. The data given in Table IV support this view. It is observed that when the topmost absorber  $S_1$  consists of lead plates 13.5 cm thick covered with iron plates 10 cm thick the number of anticoincidence counts is only  $.25 \pm .01$  per hour while this number increases to  $.312 \pm .018$  when  $S_1$  consists of a lead plate only 2.5 cm thick. Thus this diminution in the thickness of  $S_1$  produces the same effect as the shift of the absorber  $S_2'$  to the position  $S_2$ . There may be uncertainty regarding the cause of the increase in the number of anticoincidences produced by the shift of  $S_2'$  to  $S_2$ , but the only reason for the diminution

of the number of anticoincidences with the increase in the thickness of  $S_1$  is the absorption in  $S_1$  of the neutral particles which produced the charged mesons in  $S_2$ . This diminution cannot be explained by any alternative hypothesis. This was pointed out also by Rossi and Regener (1940) who concluded from the results of such investigations carried out by them on Mount Evans (4300 m) that the absorption of the neutral particles producing charged mesons was shown clearly by the diminution of the number of anticoincidences with increase in the thickness of the topmost absorber.

The increase in anticoincidence counts with the diminution of the thickness of the absorber  $S_1$  from 21 cm to 2.5 cm is 0.4% of the threefold coincidence counts. These results do not agree with those reported by Janossy and Rochester (1942) who observed an increase of 0.035% of the total threefold coincidence counts with similar diminution of the thickness of the absorber placed above the topmost anticoincidence counters. This discrepancy is due to the fact that in the arrangement used by Janossy and Rochester (1942) the threefold coincidence counter telescope was surrounded on all sides except at the bottom by anticoincidence counters and any event in which the neutral particle produced two charged mesons moving in directions making large angles with each other was not recorded in their arrangement. As revealed by cloud chamber photographs (Rochester and Butler, 1947) events occur in which a neutral particle produces two charged particles moving in widely different directions. The discrepancy between results reported in the present investigation and those reported by Janossy and Rochester (1942) shows that whenever a neutral particle produces charged mesons, at least two charged mesons are produced in most of these events. Only those events in which the charged mesons produced by the neutral particle moved almost vertically downwards were recorded by Janossy and Rochester (1942).

If we compare the results of the present investigation with those obtained by Rossi and Regener (1940) on Mount Evans it is found that at an altitude of 4300 m they found the number of the neutral particles to be only .31% of the total number of charged mesons at that altitude. In the present investigation this number is .4% of the total number of charged mesons at sea level. If the number of charged mesons on Mount Evans is assumed to be 2.3 times that at sea level as done by Janossy and Rochester, the ratio of the total number of neutral mesons at sea level and that on Mount Evans = 0.56.

The value of this ratio calculated by Janossy and Rochester (1941) from the results obtained by them is 1:40. As pointed out above such a low value of the ratio was obtained by them only because they did not record most of the events in which a neutral particle produced two charged mesons moving in widely different directions. It is, however, surprising that although the absorption of the neutral particles in lead is much larger than that of charged mesons as found by Rossi and Regener (1940) and all other

previous workers who investigated this problem the number of the neutral particles is reduced at sea level to only about half its value at Mount Evans. This fact indicates that probably such neutral particles are being produced in the atmosphere by some unknown process and the diminution in their number in traversing the atmosphere is compensated for by increase due to production of such particles by a different process.

It may be pointed out here that if the results reported by Sirkar and Bhattacharyya (1944) be examined it is found that the difference between the numbers of anticoincidences observed respectively with 5 cm and 30 cm of lead above the anticounters ( $C$ ), is  $.17 \pm .087$  and this difference is just significant. If this difference is assumed to be due to total absorption of the neutral particles in the lead absorber, 30 cm thick, the number of neutral particles is found to be about .8% of the total number of mesons observed with the same arrangement. As shown by Rossi and Regener (1940) a fraction of these anticoincidence counts is due to side showers which could be detected by them by putting two anticounters  $FF$  on both sides of the counter  $D$  in their arrangement. This fraction due to side showers will be larger for larger number of the background counts. In the case of Rossi and Regener's arrangement the fraction was about .3. In the arrangement used by Sirkar and Bhattacharyya it might have a little larger value, but this fraction does not affect seriously the diminution of the number of anticounts which take place with the increase of thickness of the absorber placed above the anticounters. So the corrected value of the percentage of neutral particles observed by Sirkar and Bhattacharyya comes out to be almost the same as that observed in the present investigation. The results of all these investigations show, however, that the increase in the number of anticoincidences observed with the shift of the absorber  $S_2$  from a position much below the topmost coincidence counter to a position above it is not wholly due to production of charged mesons by neutral particles in the absorber in its latter position. But the results of the present investigation show that if the absorber is shifted from a position just below the topmost coincidence counter to a position above it the spurious results can be avoided.

#### ACKNOWLEDGMENT

The authors wish to record their grateful thanks to Professor S. C. Sirkar, D. Sc., F. N. I., for kindly suggesting the problem and his constant guidance throughout the progress of the work.

#### REFERENCES

- Bridge, H. S. and Annis, M., 1951, *Phys. Rev.*, **82**, 445.  
Fretter, W. B., 1951, *Phys. Rev.*, **83**, 1053.  
Janossy, L. and Rochester, G., 1941, *Nature*, **148**, 531.  
Janossy, L. and Rochester, G., 1943, *Proc. Roy. Soc.*, **A**, **181**, 401.

- Leighton, R. B., Wanless, S. D. and Alford, W. L., 1951, *Phys. Rev.*, **83**, 843.  
Rochester, G. and Butler, C. C., 1947, *Nature.*, **160**, 855.  
Rossi, B., Janossy, I., Rochester, G. and Bound, M., 1940, *Phys. Rev.*, **58**, 761.  
Rossi, B. and Regener, V., 1941, *Phys. Rev.*, **59**, 113.  
Rusk, R. D. and Rosenbaum, A., 1949, *Phys. Rev.*, **76**, 1166.  
Seriff *et al.*, 1950, *Phys. Rev.*, **78**, 290.  
Sirkar, S. C., and Bhattacharyya, P. K., 1942, *Science & Culture.*, **8**, 89.  
Sirkar, S. C., and Bhattacharyya P. K., 1944, *Proc. Nat. Inst. Sci.*, **10**, 175.  
Sirkar, S. C., and Ghosh, S., 1942, *Proc. Nat. Inst. Sci.*, **8**, 233.  
Thomson, R. W., Cohn, H. Q., and Flum, R. S., 1951, *Phys. Rev.*, **83**, 175.



# ON THE VALIDITY OF SEMI-EMPIRICAL ATOMIC MASS-FORMULA IN THE REGION OF RARE-EARTH NUCLIDES

By G. P. DUBE AND LAL SAHEB SINGH

DEPARTMENT OF PHYSICS, PATNA UNIVERSITY, PATNA-5

(Received for publication, February 3, 1954.)

**ABSTRACT.**— It has been shown in the present paper that the Fermi's semi-empirical atomic mass-formula is quite inadequate for the calculation of alpha-decay energy in the region of rare-earths. The calculated alpha decay energy is much lower and even negative in several cases while the observed one ranges from 2 Mev to 4 Mev nearly. A suitable correction term has been added to the Fermi's mass-formula in the rare-earth region on the basis of Duckworth's new atomic mass-data. With the introduction of the correction-term the calculated alpha-disintegration energy is in agreement with the observed results.

## INTRODUCTION

The reliable determination of alpha-decay energy has gained much importance since the discovery of a number of short-lived alpha-emitters in the rare-earth region with half-lives ranging from a few minutes to a few days and alpha-disintegration energy in the range 2 Mev to 4.2 Mev (Thompson, Ghiorso et. al, 1949; Weaver, 1950; Rasmussen, 1950; Rasmussen and Thompson and Ghiorso, 1953). The problem of alpha-activity in these lighter elements has been considered at various times. But the alpha-decay isotopes of elements below  $Z=83$  has not been reported prior to 1949 (Thomson, Ghiorso, 1949) excepting the natural alpha-emitter samarium ( $Z=62$ ) discovered by Havesy and Pahl (1932). Methods of studying and predicting the properties of radioactive nuclei in the heavy nuclide-region have been discussed by Perlman, Ghiorso and Seaberg (1950) in their paper on systematics of alpha-activity.

The exact knowledge of atomic masses has been extremely useful for a clear understanding of many nuclear problems. Unfortunately, atomic masses are not known to a sufficient degree of accuracy, the error in mass spectroscopic measurements being of the order of 5 in  $10^5$  or about .01 M. U., i. e., 10 Mev. As such these data are not of much help in understanding the decay properties of radioactive nuclei.

Several attempts have been made during the last few years to establish a suitable semi-empirical mass-formula for the estimation of atomic masses when the experimental data are not available. The semi-empirical formula developed by Feenberg (1947) and Bohr and Wheeler (1939) has been extremely useful. But for the estimation of alpha-decay energy the Fermi-Weizsäcker formula with the empirical correction-term added by Stern (1949) has been

helpful in the region of heavy elements. It has been shown by Jha and Dube (1950) that in rare-earths the agreement between the observed and calculated alpha-decay energy ( $E_\alpha$ ) from Fermi-Weizsäcker formula is far from being satisfactory. The failure of the formula in this region, like the region of heavy elements is to be attributed to the absence of a suitable correction-term similar to the one proposed by Stern for heavy elements.

It has been shown here that the Fermi's semi-empirical mass-formula (Fermi, 1951) with a suitable correction-term which is a function of both  $A$  and  $Z$  gives reliable estimates of alpha-decay energy in the rare-earth region. The correction-term has been determined with the help of Duckworth's new atomic masses in the rare-earths.

#### CALCULATION OF ALPHA-DISINTEGRATION ENERGY: $E_\alpha$ :

Considering an alpha-emitter of atomic mass  $M(Z, A)$  and the daughter atom of mass  $M(Z-2, A-4)$ , the alpha-decay energy  $E_\alpha$  is given by

$$E_\alpha = M(Z, A) - M(Z-2, A-4) - M(^4_2\text{He}) \quad \dots (1)$$

where  $M(^4_2\text{He}) = 4.00391$ .

According to Fermi's mass-formula

$$M(Z, A) = 0.99391A - 0.00085Z + 0.014A^{2/3} + 0.083 \frac{(A/2 - Z)^2}{A} + 0.000627Z^2/A^{1/3} + \delta(A, Z) \quad \dots (2)$$

where  $\delta(A, Z) = 0$  for  $A$  odd,  $Z$  anything.

$$= \mp 0.036A^{-3/4} \text{ for } A \text{ even, } Z \begin{cases} \text{even} \\ \text{odd} \end{cases}$$

substituting (2) in (1)  $E_\alpha$  in Mev. is given by

$$E_\alpha = -27.90728 + 13.03610 \{A^{2/3} - (A-4)^{2/3}\} - 77.28545 \frac{(A-2Z)^2}{A(A-4)} + 0.58383 \left\{ \frac{Z^2}{A^{1/3}} - \frac{(Z-2)^2}{(A-4)^{1/3}} \right\} + 931.15 \{ \delta(A, Z) - \delta(A-4, Z-2) \} \quad \dots (3)$$

The last term in (3) is zero for  $A$  odd,  $Z$  anything and

$$= \pm 33.52140 \times \{ (A-4)^{-3/4} - A^{-3/4} \} \text{ for } A \text{ even, } Z \begin{cases} \text{even} \\ \text{odd} \end{cases}$$

A number of alpha-emitters are known in the rare-earth region and they are identified to be the nuclides of  $\text{Gd}^{148,149}$ ,  $\text{Tb}^{149}$ ,  $\text{Dy}^{150}$ ,  $\text{Sm}^{147}$ ,  $\text{Eu}^{147}$ , and  $\text{Ho}^{151}$  and possibly  $\text{Ho}^{153}$ ,  $\text{Dy}^{151}$ ,  $\text{Tb}^{148,150}$  (Thompson, 1949; Rasmussen, 1950; Hoff, 1950; Rasmussen, Thomson & Ghiorso, 1953). The formula (3) has been used for the calculation of  $E_\alpha$  in the isotopes of rare-earths from  $Z=60$  to  $Z=67$  and the results are given in Table I.

TABLE I

Alpha-activity in the rare-earth region.

Nuclides	Half-life	Observed $E_\alpha \times \frac{A}{A-4}$	Calculated $E_\alpha$	Difference $E_\alpha \text{ obs.} - E_\alpha \text{ cal.}$	$E_\alpha$ Calculated with the correction- term.
$^{60}\text{Nd}^{144}$	... ..	... < 2 Mev.*	-0.67 Mev.	< 2.67	1.02 Mev.
$^{61}\text{Pm}^{145}$	... ..	... ..	-0.212	... ..	1.638
$\text{Pm}^{147}$	... ..	1.57 <sup>†</sup>	-0.601	2.171	1.320
$^{62}\text{Sm}^{146}$	$10^4$ to $10^6$ yrs.	< 2.4 <sup>†</sup>	+0.271	< 2.13	2.104
$\text{Sm}^{147}$	... ..	2.18	+0.077	2.103	1.988
$\text{Sm}^{148}$	... ..	< 2.1 <sup>†</sup>	-0.140	< 2.24	1.760
$\text{Sm}^{152}$	... ..	... ..	-0.751	... ..	1.090
$^{63}\text{Eu}^{146}$	... ..	... ..	+0.754	... ..	2.734
$\text{Eu}^{147}$	$\approx 6 \times 10^{13}$ yrs.	2.87	+0.730	2.14	2.670
$\text{Eu}^{148}$	... ..	... ..	+0.717	... ..	2.637
$\text{Eu}^{149}$	... ..	... ..	+0.693	... ..	2.593
$^{64}\text{Gd}^{147}$	735 yrs.	3.181	1.043	2.137	3.101
$\text{Gd}^{148}$	735 yrs.	3.181	1.071	2.109	3.068
$\text{Gd}^{149}$	$4 \times 10^3$ yrs.	3.08	0.997	2.083	3.034
$\text{Gd}^{160}$	$\approx 10^8$ yrs.	2.771	0.975	1.795	3.001
$^{65}\text{Tb}^{148}$	7m	4.311	1.687	2.623	3.807
$\text{Tb}^{149}$	4.1 hrs	4.05	1.598	2.452	3.707
$\text{Tb}^{160}$	19.0 hrs	3.531	1.419	2.111	3.519
$\text{Tb}^{151}$	19.0 hrs	3.531	1.250	2.28	3.280
$149 \leq A \leq 155$					
$^{66}\text{Dy}^{149}$	7m	4.311	2.190	2.12	4.355
$^{66}\text{Dy}^{150}$	19m	4.111	2.033	2.277	4.205
$\text{Dy}^{151}$	2.3 hrs	3.691	1.863	2.247	4.023
$\text{Dy}^{152}$	2.3 hrs	3.691 ...	1.70	1.99	3.888
$\text{Dy}^{153}$	... ..	... ..	1.531	... ..	3.729
$^{67}\text{Ho}^{150}$	... ..	... ..	2.55	... ..	4.79
$\text{Ho}^{151}$	4m	4.31	2.425	1.885	4.660
$\text{Ho}^{153}$	... ..	... ..	2.179	... ..	4.394

Note : \* Values are estimates ; for † values masses have been tentatively assigned.

It is clear from the table that the agreement between the observed and calculated values is far from being satisfactory although the general trend of increase in  $E_{\alpha}$  with the decrease in mass-number is reproduced here also like the heavy nuclide-region (Dube and Singh, 1954). The calculated values are very low and even negative in several cases which definitely establishes the inadequacy of the semi-empirical formula. The empirical correction-term added by Stern (1949) to Fermi-Weizsäcker formula which was applicable to  $A \geq 208$  is of no help in rare-earth region. The failure of Fermi's formula may be attributed to the absence of a suitable correction-term in this region.

Recent mass-measurements by Duckworth et al (1951) and their comparison with the estimated masses have helped to determine a correction-term which fits in well with the experimental results. The calculated masses have been compared with the observed ones in Table II for  $Z=74, 72, 60, 58, 56$  and  $52$ . The difference  $\Delta m$  between the calculated and observed masses ranges from .0116 to .0173 mass units in the region  $126 \leq A \leq 184$ .

TABLE II

Calculated atomic masses compared with Duckworth's experimental data.

Nuclides	Mass calculated	Atomic mass observed	Difference	Mass calculated with correction-term
$^{184}\text{W}$	184.0185	$184.0052 \pm .0011$	.0133	184.0010
$^{183}\text{W}$	183.0175	$183.0059 \pm .0013$	.0116	183.0030
$^{182}\text{W}$	182.0153	$182.0033 \pm .0011$	.0120	182.0020
$^{178}\text{Hf}$	178.0006	$177.9936 \pm .0013$	.0160	177.9942
$^{176}\text{Hf}$	176.0066	$175.9923 \pm .0011$	.0143	175.9945
$^{144}\text{Nd}$	143.9604	$143.9560 \pm .0008$	.0134	143.9591
$^{142}\text{Ce}$	141.0602	$141.0537 \pm .0009$	.0155	141.9544
$^{138}\text{Ba}$	137.9671	$137.9498 \pm .0009$	.0173	137.9502
$^{137}\text{Ba}$	136.9653	$136.9502 \pm .0010$	.0151	136.9505
$^{136}\text{Ba}$	135.9637	$135.9488 \pm .0010$	.0149	135.9507
$^{130}\text{Te}$	129.9626	$129.9467 \pm .0009$	.0159	129.9436
$^{128}\text{Te}$	127.9607	$127.9471 \pm .0010$	.0136	127.9450
$^{126}\text{Te}$	125.9573	$125.9427 \pm .0010$	.0146	125.9449

From the isotopes of W, Hf, Ba and Te it is observed that  $\Delta m$  decreases with the decrease of  $A$  but increases with the decrease of  $Z$ . The dependence of correction-term on  $A$  only like the Stern's one cannot be regarded as

satisfactory. The empirical correction-term which is a function of both  $A$  and  $Z$  is given by,

$$\Delta m = 0.0185 - 2\{KA^{1.2} - K'Z^{1.5}\} \text{ M. U. } \dots (4)$$

where  $K = 0.0002$  and  $K' = 0.00014$ . The masses calculated with this correction-term have been shown in Table II, the difference from the observed ones ranges from  $-0.0021$  to  $+0.0033$  M. U. for  $126 \leq A \leq 181$ .

*Calculation of  $E_\alpha$  with the correction-term.*

With the application of the above correction-term in the Fermi's mass-formula, the calculated values of  $E_\alpha$  are changed considerably. The correction-term to  $E_\alpha$  is given by

$$\Delta E_\alpha = K_1\{Z^{1.5} - (Z-2)^{1.5}\} - K_2\{A^{1.2} - (A-4)^{1.2}\} \text{ Mev. } \dots (5)$$

where  $K_1 = 0.26072$  and  $K_2 = 0.37246$ . The last column of Table I contains the estimated values of alpha-decay energy with this correction-term i. e.  $E_\alpha + \Delta E_\alpha$ .

#### DISCUSSION OF THE RESULTS

In the region of rare-earth nuclides the estimated  $E_\alpha$  with the correction-term is in good agreement with the observed data. For  $\text{Sm}^{147}$  the estimated value is 1.988 Mev while the observed one is 2.18 Mev. For other isotopes of samarium such as  $\text{Sm}^{148}$  and  $\text{Sm}^{149}$  the estimated values are 1.76 and 1.09 Mev respectively and thus they will have half-lives of the order of  $10^{11}$  or  $10^{15}$  years and hence will behave as stable nuclei. Thus the inevitable conclusion is that the natural alpha-activity of samarium should be definitely assigned to  $\text{Sm}^{147}$  as has been shown experimentally by Weaver and others (1950). The estimated value for  $\text{Sm}^{146}$  is 2.19 Mev and, therefore, a part of the natural alpha-activity of samarium may as well be assigned to  $\text{Sm}^{146}$ . The prevailing notion that it does not occur in nature may be due to the fact that the quantity in which it is present is such that it has not been possible to detect it by the present experimental technique.

The estimated values in the case of  $\text{Tb}^{148,149}$ ,  $\text{Dy}^{151}$ ,  $\text{Ho}^{153}$ , lie between 3.5 to 4.4 Mev. This fully supports the view that they should be short-lived alpha-emitters. The 3.44 Mev alpha-activity has been tentatively assigned to  $\text{Tb}^{151}$ , though the possibility of  $\text{Tb}^{150}$  has not been ruled out (Rasmussen Thomson and Ghiorso, 1953). The estimated values for  $\text{Tb}^{151}$  and  $\text{Tb}^{150}$  respectively are 3.28 Mev and 3.52 Mev which are in agreement with the observed data. In case of dysprosium isotopes the three alpha-emitters with decay-energies 4.21 Mev, 4.06 Mev and 3.61 Mev have been found out and the masses lie within the limits 149 to 153 (Rasmussen Thomson and Ghiorso, 1953). These results are in numerical agreement with the calculated values of  $E_\alpha$  due to  $\text{Dy}^{150}$ ,  $\text{Dy}^{151}$  and  $\text{Dy}^{153}$  respectively ( $E_\alpha$  cal. being 4.20 Mev, 4.02 Mev and 3.73 Mev respectively).

The probable mass-assignment of 3.1 Mev alpha-activity (half-life greater than 35 yrs) has been indicated to  $Gd^{148}$  although the possibility of an assignment to  $Gd^{147}$  is not too improbable (Rasmussen Thomson and Ghiorso, 1953).  $E_\alpha$  calculated in the two cases are 3.068 Mev and 3.101 Mev respectively. Similarly 3.0 Mev alpha-activity which has been definitely attributed to  $Gd^{149}$  fully tallies with our calculated one which comes to 3.034 Mev. For  $Ho^{141}$  which is definitely known to be alpha-emitter with 4.2 Mev energy, the alpha-disintegration energy is estimated to be 4.66 Mev.

$Eu^{147}$  has been shown to be an alpha-emitter with a reported alpha-decay energy of 2.8 Mev (Rasmussen, Thomson and Ghiorso, 1953) which is in fair agreement with  $E_\alpha$  cal (2.67 Mev). No detectable alpha-activity has been found out with the present experimental technique in cases of  $Eu^{145}$ ,  $Eu^{148}$ ,  $Eu^{149}$ . Our calculations show that if they are alpha-emitters, their alpha-disintegration energy should be 2.734, 2.637 Mev and 2.593 Mev respectively.

Thus it is definitely established that Fermi's semi-empirical atomic mass-formula is completely inadequate in the study of decay-properties of radioactive nuclei in the rare earths. The importance of our correction-term has been shown by the agreement of our calculated alpha-decay energies with the experimental data.

#### REFERENCES

- Bohr and Wheeler, 1939, *Phys. Rev.*, **56**, 426.  
 Dube, G. P. and Singh, L. S. 1954, *Proc. Ind. Acad. Sci.*, in course of Publication  
 Duckworth, H. E., Keglev, C. L., Olsan, J. M. Strasford, G. S., 1951  
*Phys. Rev.*, **83** 1114  
 Duckworth, H. E. and Preston, R. S., 1951 *Phys. Rev.*, **82**, 468  
 Feenberg, 1947, *Rev. Mod. Phys.*, **19**, 239.  
 Fermi, E. 1951, Nuclear Physics (Chicago University Press, page 7.  
 Havesy, G. and Pahl, M., 1932, *Nature*, **130**, 846.  
 Hoff et al, 1951, *Phys. Rev.* **83**, 1058.  
 Jha, S. and Dube, G. P., 1952, *Ind. J. Phys.* **26**, 15  
 Perlman, I., Ghiorso, A. and Seaberg, G. T., 1950, *Phys. Rev.* **77**, 26.  
 Rasmussen et. al, 1950, *Phys. Rev.* **80**, 475.  
 Rasmussen, J. O., Thompson, S. G. and Ghiorso, A., 1953, *Phys. Rev.*, **89**, 33.  
 Stern, O., 1949 *Rev. Mod. Phys.*, **21**, 316.  
 Thompson, S. G. and Ghiorso, A. et. al., 1949 *Phys. Rev.*, **79**, 1406.  
 Weaver, Boyd, 1950, *Phys. Rev.*, **80**, 301.

# A NEW ELECTRODYNAMIC METHOD OF MEASURING MAGNETIC FIELDS

By S. K. DUTTA ROY

DEPARTMENT OF GENERAL PHYSICS, X-RAYS AND MAGNETISM, INDIAN ASSOCIATION FOR THE CULTIVATION OF SCIENCE, CALCUTTA-32.

(Received for publication, March 3, 1954)

## Plate V

**ABSTRACT.** A new electrodynamic method has been developed for the measurement of magnetic fields. The new method is based upon the measurement of the maximum couple exerted upon a small current-bearing coil suitably suspended with a fine torsion fibre in the magnetic field. The method is very simple, quick and with reasonable precautions gives an absolute field accuracy of the same order as standard ballistic or electrodynamic methods. In this paper the details of the method are described and results of several field values are compared with those from search coil and crystal methods.

## INTRODUCTION

In a few recent papers Bose and Mitra (unpublished) have found that the anisotropies of the paramagnetic ions  $\text{Cu}^{++}$  and  $\text{Ni}^{++}$  change from salt to salt in the isomorphous Tutton series approximately in accordance with alkali cation radius. These observations have been attributed mainly to the variation of the long range asymmetric crystalline electric fields (direct and indirect) from salt to salt. Since the observed changes in the anisotropies are small and their accuracy depends to a large extent on the room temperature values measured by Krishnan et al (1933-38) it is necessary at this stage to check and improve upon these earlier values. The method of measurement of magnetic anisotropy of single crystals, of which details need not be given, depends upon the measurement of the maximum couple exerted upon a crystal suspended vertically in a homogeneous horizontal magnetic field  $H$ , with a fine quartz fibre from a torsion head. The anisotropy  $\Delta\chi$  in the horizontal plane is given by the general equation

$$c(\theta - \phi) = \frac{2m}{M} \Delta\chi H^2 \sin 2\varphi \quad (1)$$

where  $m$  is the mass of the crystal,  $M$  its molecular weight,  $H$  the field strength,  $c$  the torsion constant of the fibre,  $\theta$  the torsion angle of the fibre and  $\phi$  the angle which the direction of the maximum susceptibility of the crystal in the horizontal plane makes with the field direction.

In pursuance of our present programme of improving the accuracy of anisotropy measurements to 0.1% or better, the accurate determination of

the torsion constant  $c$  was undertaken by Datta (1953). Since the square of the magnetic field comes in the equation, it is also necessary to determine this with a high degree of accuracy. The values of the field by the earlier workers in this laboratory were obtained by the usual search coil method of which the accuracy was not probably more than about 1 to  $\frac{1}{2}$ %. A crystal itself may be used for simple and quick field measurement provided its anisotropy has been measured in a well standardised field. Later on, it has been the practice in this laboratory to use for this purpose a crystal standardised by the ballistic method and checked by the Gouy method using  $\text{NiCl}_2$  solution. A crystal gaussmeter has been devised by Dupony (1951) following the same principle. But evidently, the accuracy of the crystal method depends ultimately on that of the primary method used. The bismuth spiral method (Bates, 1951), though sometimes convenient is also a secondary method of only moderate accuracy. Methods dependent on the rotating search coil, Zeeman effect,  $\beta$ -ray spectrometry, proton resonance, etc. (Bates, *loc. cit.*), though of great accuracy, are not available to every laboratory and are suitable only for specialised purposes. Absolute electrodynamic methods, depending upon the measurement of translational force upon a current-bearing conductor placed in the magnetic field, have been developed by Cotton, Piccard and Devaud (1932) and by Briggs and Harper (1936) and though the accuracy claimed are as high as .02 to .1 per cent, the arrangements are rather cumbersome and cannot be used for exploration of fields. Klopsteg (1913) has utilised the damping of a galvanometer coil suspended in a magnetic field to measure it. But the method though ingenious cannot claim an accuracy of more than 1 or 2%.

It occurred to us to use Klopsteg's experimental system in a manner exactly analogous to our crystal anisotropy method for measuring the magnetic field. The method is simple, quick and with reasonable precautions capable of giving an absolute field accuracy of the same order as standard ballistic (1939) or electrodynamic methods.

#### THEORY

For a coil of  $n$  turns and mean effective area  $A$ , carrying a current  $i$  suspended in a homogeneous magnetic field  $H$  with a fibre of small torsion constant  $c$ , the equilibrium condition at the angle  $\phi$  which the normal to the plane of the coil makes with the direction of the field, is given by

$$c(\theta - \phi) = niAH \sin \phi \quad \dots (2)$$

where  $\theta$  is the torsion angle of the fibre.

Starting with the plane of the coil at right angles to the field and no torque on the fibre, *i.e.*,  $\phi = 0^\circ$  and  $\theta = 0^\circ$ , if the fibre is gradually twisted the plane of the coil will follow but through a smaller angle until the position of maximum couple due to field ( $\phi = 30^\circ$ ) is reached, For  $\theta$  very



large compared to  $\phi$  this is also an unstable equilibrium position of the coil, which will now sharply spin round with the slightest increase of the torsion angle or with little disturbance. In this critical position which can be accurately marked

$$H = \frac{c(\theta_c - \pi/2)}{nAi} \quad \dots (3)$$

from which the field can be accurately measured. This is an exact electrodynamic analogue of the crystal method so long used by us. For small values of  $\theta_c$ , a correction might be made as obtained from the condition of instability in eqn (2), thus

$$H = \frac{c}{nAi} \frac{(\theta_c - \pi/2 - \sigma)}{\cos \sigma} \quad \dots (4)$$

$$\text{where } \sin \sigma = \frac{c}{iN\bar{A}H}$$

But the procedure is then not capable of high accuracy. As we could not procure very fine phosphor-bronze strips or metal-coated quartz fibre for suspension of the coil, we had to use fine silver strips, which did not stand large torsions without slight yielding, and so our critical angles of torsion could not be made large. Hence in practice the above method could not be used profitably.

A slightly different procedure, avoiding the correction factor, was to find the maximum couple in the field by adopting a null method which though somewhat more elaborate is particularly suitable for small angles of torsion and has one obvious practical advantage over the previous method, that the final observation here is for a static position. The coil is placed in the maximum torque position in the field, with no torsion on the fibre in the absence of the field (*i.e.*  $\phi = 90^\circ$ ,  $\theta = 0^\circ$ ). The field is put on and the coil is deflected, when it is brought back to the original position by twisting the fibre. The simpler equation

$$H = \frac{c\theta_{\max}}{nAi} \quad \dots (5)$$

then holds for any value of the maximum angle of torsion.

#### PREPARATION OF THE COIL

The preparation of the coil is the most important part in the construction of the apparatus. Very great care is necessary in selecting the material of the former, on which the coil is wound. Libonite samples had to be rejected as most of them showed a stray tendency of setting in the magnetic field possibly owing to ferromagnetic impurities. Several kinds of insulating paper samples also were rejected for the same reason. Very thin-walled (about 0.1 mm) pyrex tube of about 1.5 to 1 cm. diameter and of the same length was found to be very suitable for the purpose and in a field of about

5000 gauss showed no setting tendency. The former was thoroughly cleaned and then coated with specially prepared shellac varnish. One layer of fine double silk-covered copper wire was closely and accurately wound on the former mounted on a small jeweller's lathe, keeping a constant tension on the wire. The coil was soaked with thin shellac varnish and dried several times and finally baked for several hours in an air-oven below  $100^{\circ}\text{C}$ . The first and last windings were fixed firmly with Durofix cement. Precautions were taken to avoid dust as far as possible during these procedures. The two free ends of the copper wire passed through short lengths of fine pyrex capillary tubes, attached diametrically at the opposite sides of the spool with pure shellac or Durofix cement. After this it was again checked for any setting tendency due to possible impurities in the wire and shellac varnish. Several coils were prepared some of about 1 cm. diameter and some 1.5 cms. The smaller ones were wound with 60 s.w.g. and the larger ones with 44 s.w.g. wire. Two very light small triangular mirrors prepared from microscope cover slips were attached at right angles to each other on the top of the coil, axially to the suspension fibre.

#### SUSPENSION SYSTEM

The entire suspended rotating coil system is shown in Plate V. The suspension fibre was a fine silver wire .001 mm. diameter and about 40 cms. long. With fine phosphor bronze or metal-coated quartz fibre the results can be easily improved. The silver wire was carefully selected to avoid kinks or non-uniformities, and allowed to hang under a sufficient load and heated by an electric current to dull red heat to make it straight otherwise serious uncertainties in the results might occur. One end of the fibre is soldered, using a microjet and specially prepared tin solder and diamagnetic resin flux, axially to the adjustable brass pin of a torsion head, with a vernier reading to  $1/10$  of a degree and an insulating ebonite knob for turning. The free end of the torsion fibre was soldered to the upper terminal of the coil and a silver helical spring of very small torsion constant to the lower terminal. To prevent draughts disturbing the system, it was enclosed in a glass tube, with plane front and back windows for viewing the reflecting mirror. The free spring end was soldered to the adjustable brass pin of another small torsion head, with an ebonite turning knob, fitted to the lower end of the enclosing glass tube. The two torsion heads and the entire suspension system were made coaxial with the greatest precaution. Special care was taken to see that the plane of the coil was vertical and the suspension fibre along the central vertical diameter of the coil.

#### MODE OF MEASUREMENT

##### (i) *Measurement of Radius:*

The coil radius was ascertained very accurately with the help of a comparator reading to  $1/1000$  mm. At a particular point on the axis of the

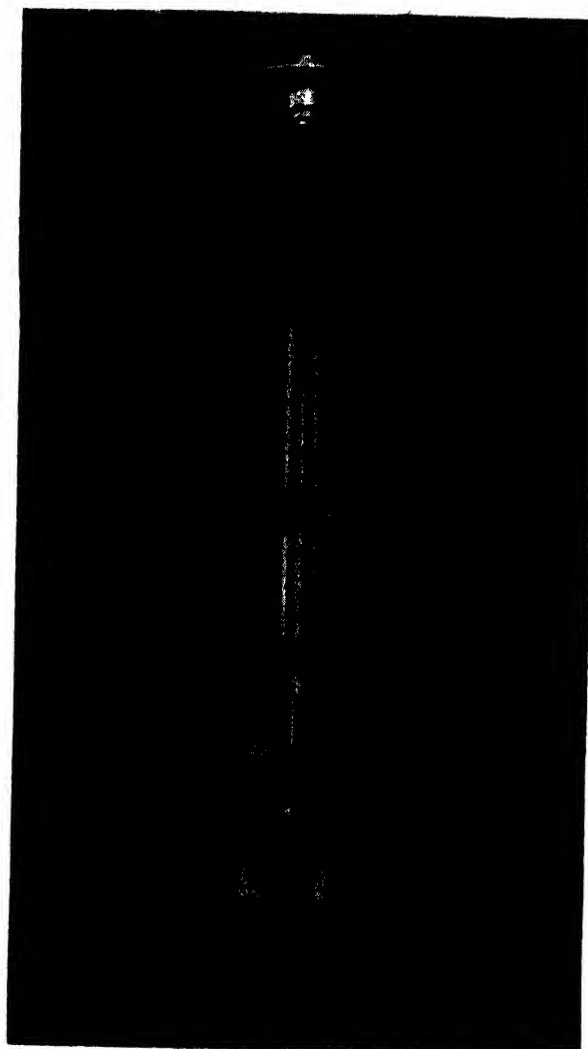


Fig. 1.

Photograph of the experimental arrangement

- |                                |                              |
|--------------------------------|------------------------------|
| <i>a.</i> Torsion head         | <i>f.</i> Spring             |
| <i>b.</i> Ebonite turning knob | <i>g.</i> Clamp              |
| <i>c.</i> Torsion fibre        | <i>h.</i> Lower torsion head |
| <i>d.</i> Coil                 | <i>m.</i> Glass case         |
| <i>e.</i> Mirror               | <i>l.</i> Window             |
|                                | <i>n.</i> Magnet             |



glass tube the two diameters before and after winding were measured at a large number of positions along the circumference and the mean taken from which, allowing for the insulation thickness, the effective area was calculated. A small difference in the area not more than  $\frac{1}{2}\%$  and changing linearly to within .0001 cm. was found to occur along the entire axis of the glass tube. So, taking the mean of as many readings along the axis as there were number of turns we were able to find the mean effective area of the entire coil with a high degree of accuracy.

(ii) *Measurement of Torsion Constant:*

Before attaching to the coil, the torsion constant of the fibre was measured very accurately following the procedures described by Datta (*l. c.*) using one of his standard glass discs, suspended from the fibre with its plane vertical and noting the time period of the system with a stop watch reading to  $1/10$  sec. and checked periodically against a standard clock.

(iii) *Measurement of Current in the Coil:*

The current in the coil was of the order of microamperes and was taken from a single lead storage cell of large capacity through a megohm range rheostat. The actual values of the current could be measured for ordinary use with a Weston microammeter carefully calibrated potentiometrically against a L & N standard 100 ohm resistance, kindly lent to us by Dr. P. C. Mahanti of the Applied Physics Laboratory, Calcutta University. But for standardization work the currents were directly measured from the fall of potential across the standard 100 ohm resistance with a L & N Dial type potentiometer reading 5 microvolts per small division. With the very feeble currents used in the coil, about 25 to 70 microamperes, the heating effect was negligible.

(iv) *Measurement of Maximum Angles of Torsion in Magnetic Fields:*

The apparatus was arranged so that the coil was placed centrally between the parallel square pole pieces ( $4'' \times 4'' \times$  pole gap  $1\frac{1}{2}''$ ) of an electromagnet which we usually use for magnetic anisotropy measurements of crystals at room temperature. On exciting the coil and the magnet simultaneously the plane of the coil tended to set at right angles to the field and by releasing the torsion on the fibre and the spring by rotating both the upper and the lower torsion heads, the coil set perfectly and showed no movement when the current in the coil was switched on or off. This condition could be accurately brought about by observing through a telescope the image of an illuminated scale upon one or the other of the two mirrors attached to the coil. Currents

were then switched off and both the torsion heads were rotated through  $90^\circ$  in the same direction to bring the plane of the coil along the direction of the field, corresponding to the position of maximum magnetic couple on the coil which was noted carefully in the eye piece scale of the telescope. Any residual inaccuracy in this position of initial setting could be easily eliminated by reversing the magnetic field, but not the coil current, obtaining the corresponding setting position beginning from the opposite side and taking the mean of the two observations if a slight difference was observed, which was rare.

When this had been accurately achieved the magnetic field was reversed several times to obtain a steady magnetic state, taking care to switch off the current in the suspended coil. At this juncture, before switching on finally the magnet-current the residual field could be measured and its constancy for different experiments checked by balancing the deflection of the coil, when a known current was sent through it, by turning the torsion head. A current between 25 to 70 microamperes was then allowed to flow through the coil. The coil was deflected and the torsion head was rotated to bring the coil accurately back to its initial setting as observed by the telescope and scale arrangement. We have not used any special device for automatically stabilizing the magnet current except that we have taken the current from a 10 kilowatt compound wound D.C. generator instead of directly from our 6 phase rectified D.C. mains which fluctuates rather badly and also relied upon the high inductance of the magnet to stabilise the current further. At any rate the accurate balance position of the coil (a static position) for a given current could always be adjusted with a rheostat and an accurate Weston ammeter viewed through a low power microscope. For four values of magnet current between 2 to 5 amperes passed for short intervals only, the heating of the magnet core was inappreciable. The torsion angle measured to 0.1 of a degree is proportional to the magnetic field  $H$ , which can then be calculated. The experiment was repeated with current in the coil reversed and also with magnetic field reversed and the mean of all four sets taken. This eliminates to a large extent any slight accidental asymmetries in the construction of the coil, in suspension, the initial and final balancing positions any any distortions of the magnetic fields. The experiment was further repeated with three different values of coil current for each of the four values of the magnetic field to observe any systematic error in the current measurement, in the torsion measurement or due to heating effect in the coil. After every reading the initial position of the coil was checked which remained perfectly steady with moderate torsions used by us. The values of the fields were compared with those obtained by the ballistic method using a search coil of approximately the same size as the suspended coil and also by the crystal anisotropy method, already mentioned using  $\text{CuSO}_4 \cdot 5\text{H}_2\text{O}$  crystal suspended with the  $c$ -axis vertical (Krishnan and Mukherjee, 1938).

## EXPERIMENTAL RESULTS

*Torsion Constant of the Fibre.*

For standard glass vibrator :

$$\text{mass, } M = .8280 \text{ gms. } \pm .0001$$

$$\text{radius } r = .9986 \text{ cms. } \pm .0001$$

$$\text{thickness} = .1067 \text{ cms } \pm .0001$$

$$\text{Moment of inertia} = I = M/4 \left( r^2 + \frac{l^2}{5} \right)$$

$$= .2088 \text{ c g.s. } \pm .0001$$

Mean time period

$$T = 5.384 \pm .002$$

$$T_0 = T \left( 1 - \frac{\lambda^2}{2\pi^2} \right)$$

$$= 5.384 \pm .002$$

$$\text{Torsion constant } c = 4\pi^2 \frac{I}{T_0^2}$$

$$= .2815 \pm .0002$$

*For the coil :*No. of complete turns of wire,  $n = 48$ 

$$\text{mean } R^2 = .5258 \pm .0004$$

where  $R$  = effective radius of the coil.TABLE I  
Values of  $H$ 

Current in the magnet in amps	Current in the coil in micro amps	$\theta$ in degrees (Mean values)	$H$ in Oersteds	Mean for two latter values	$H$ , Search coil values	$H$ , Crystal values
2.2	25.47 $\pm$ .01	70.3 $\pm$ .1	1728	1726 $\pm$ 1.5	1727 $\pm$ 5	1727
	49.05 "	135.2 "	1726 }			
	70.49 "	194.2 "	1725 }			
3.0	25.47 "	86.4 "	2123	2119 $\pm$ 1.5	2124 $\pm$ 5	2122
	49.05 "	166.1 "	2120 }			
	70.49 "	238.4 "	2118 }			
4.0	25.47 "	99.7 "	2450	2447 $\pm$ 1.5	2450 $\pm$ 5	2448
	49.05 "	191.6 "	2447 }			
	70.49 "	275.2 "	2446 }			
5.0	25.47 "	111.6 "	2743	2741 $\pm$ 1.5	2748 $\pm$ 5	2748
	49.05 "	214.6 "	2740 }			
	70.49 "	308.7 "	2742 }			

The values for the residual fields have been measured after steady magnetic state has been obtained in the usual manner for different coil currents given in the table and come out as  $74 \pm 2.5$ ,  $87 \pm 0.9$  respectively. We may then take the mean of the last two values as most probable and  $86 \pm 1.1$  Oersteds. The corresponding search coil value is 55 Oersteds. The present method is thus much superior to the latter method for small fields.

It is evident from Table I that the first value of the magnetic field corresponding to the lowest coil current is not very accurate since the angle of torsion is rather low. The latter two values are individually more reliable and compare well with each other. So the mean of these two have been taken as the most representative of the values of the fields. Use of higher coil currents leads to difficulties in measurement due to heating effect, distortions in the field, yielding of the silver fibre, etc. The values of the fields obtained are estimated to be accurate to within about 8 to 10 parts in 10,000. Agreement with other methods are good though these are less accurate. The error in the crystal method is not exactly known for the anisotropy value is taken from Krishnan and Mukherjee's paper in which field was measured by a search coil and fluxmeter but the accuracy of measurement was not mentioned.

#### ACKNOWLEDGMENTS

The author expresses his sincerest thanks to Dr. A. Bose, D.Sc. for suggesting the problem and for his keen interest throughout the progress of the work. Thanks are also due to Sri A. K. Dutta and Sri S. Datta for their kind help.

#### REFERENCES

- Bates, L. F., 1951, *Modern Magnetism*, Cambridge.  
 Briggs, G. H. & Harper, A. F. A., 1936, *Jour. Sci. Inst.*, **13**, 119.  
 Cotton, A. and Dupouy, G., 1952, *Congr. Int. Elect.*, **3**, 207  
 Datta, S., 1953, *Ind. Jour. Phys.* **27**, 155  
 Klogsleg, P. E., 1913, *Phys. Rev.*, **2**, 390  
 Krishnan, K. S. and Mukherji, A., 1938, *Phys. Rev.* **54**, 533 & 841  
 Nettleton, H. R. and Sugdan, S., 1939, *Proc. Roy-Soc.*, **173**, 313



# ON THE TIME OF RELAXATION OF SOME ORGANIC MOLECULES IN PURE LIQUID STATE \*

By DILIP KUMAR GHOSH

OPTICS DEPARTMENT, INDIAN ASSOCIATION FOR THE CULTIVATION OF SCIENCE, CALCUTTA 32.

(Received for publication, March 10, 1954).

**ABSTRACT**—The absorption of U.H.F. radio waves in the range 250-920 Mc/sec and 3.18 cm microwaves in benzyl alcohol, benzyl chloride and benzyl amine has been studied by the direct optical method by avoiding formation of stationary waves. Maximum absorption of 3.18 cm microwaves has been exhibited by benzyl alcohol, benzyl chloride and benzyl amine at temperatures 55°C, -15°C and -20°C respectively and these are assumed to be due to rotation of the substituent groups about a diameter of the benzene ring passing through the point of substitution.

In the U.H.F. region in the case of benzyl chloride peaks have been observed at 400 Mc/sec at 28°C and at 790 Mc/sec at 25°C which are due to dimers and monomers respectively. Similarly, in the case of benzyl amine a peak due to dimer at 275 Mc/sec at 25°C and a peak due to monomer at 700 Mc/sec at 0°C have been observed. In the case of benzyl alcohol absorption maxima have not been observed in this region, but indication of the existence of a maximum beyond 850 Mc/sec has been observed. The radius of the rotor in this case comes out too low to be that of the molecule. In all the cases the absorption peaks in the U.H.F. region shift with change of temperature according to Debye's theory.

The results obtained in the present investigation show that in these substituted benzenes the time of relaxation has different discrete values in each case and the occurrence of 'effective time of relaxation' postulated by Fisher is corroborated by these results.

## INTRODUCTION

It was reported previously by Sen (1950), Kastha (1952) and by the present author (Ghosh, 1953a) that some substituted benzenes exhibit absorption maxima in the frequency range 250-900 Mc/sec at suitable temperatures and that the diameters of the rotors calculated from Debye's theory correspond to those of the single molecules in some cases and to those of the dimers in other cases. It was also pointed out by the present author that with lowering of temperature of the liquid associated groups of molecules are formed in the liquid state and they exhibit new absorption maxima corresponding to their times of relaxation. It was further observed by the present author (Ghosh, 1953b) that some organic liquids, such as chloroform ethylene chloride etc., absorb microwaves of wavelength 3.18 cm at suitable temperatures and the absorption becomes maximum for certain values of the temperatures of the liquids. The radius of the rotor calculated from Debye's theory in the case of ethylene chloride was found to be smaller than that of the single molecule and it was pointed out that the rotor may be one half

\* Communicated by Prof. S. C. Sirkar



was tested by noting the variation of the input voltage with the corresponding change in the output voltage. It was observed that the output voltage remained constant when the input voltage was changed from 220 to 240 volts. The output voltage was also observed to remain constant over a wide range of loads. A GR 857-A and a GR 1209-A with its shield removed was used as the source of radio waves of frequencies ranging from 250 Mc/sec to 920 Mc/sec. The liquids studied were of chemically pure quality. They were all distilled in vacuum after proper dehydration. In order to study the absorption at different temperatures the cell filled with the liquid was placed in baths at different temperatures and when the liquid attained the temperature of the bath, the cell was taken out and its outer surfaces were cleaned before being placed in the path of the waves between the oscillator and the receiver. The reading of the microammeter in the receiving circuit with the cell filled with benzene placed in a suitable position in the path of the waves was taken as the incident intensity, in all the cases. In the case of microwaves the position of the cell was adjusted till the transmission was maximum and the formation of stationary waves was avoided in this way.

## RESULTS

The values of apparent absorption coefficient,  $\mu$  were calculated from the relation

$$\mu = \frac{2.34}{x} \log_{10} \left( \frac{I_0}{I} \right) \quad \dots (1)$$

where  $x$  is the thickness of the liquid absorber.

The values of  $\mu$  have been plotted against the temperatures in figures 2, 4 and 8 for the microwave region and the values of  $\mu$  have been plotted

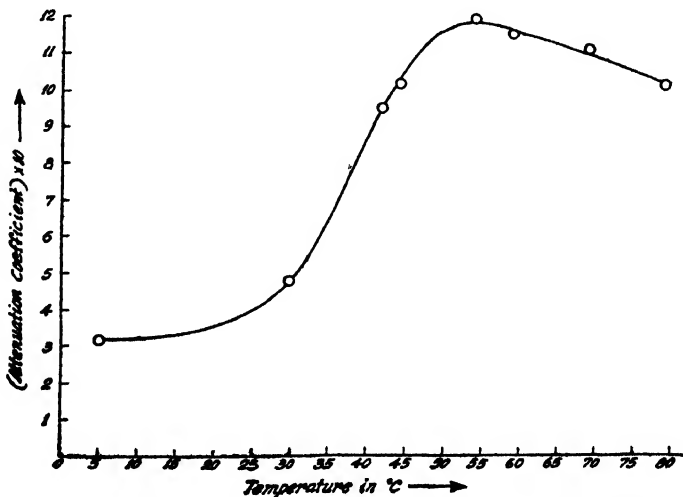


Fig. 2 Benzyl alcohol at 9413 cm. Thickness of the liquid 1 cm.

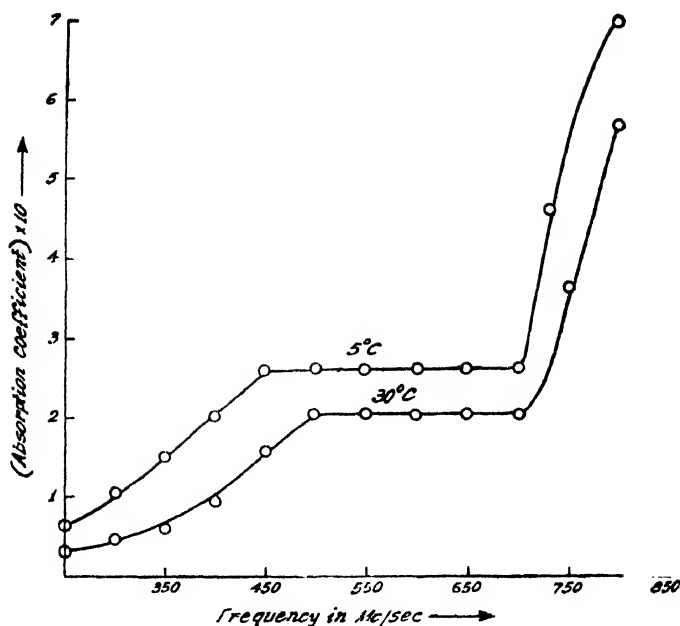


Fig. 3 Benzyl alcohol. Thickness of the liquid, 3.5 cm.

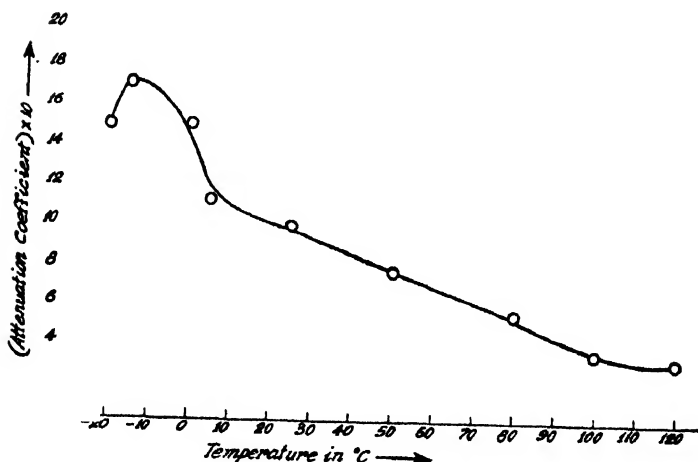


Fig. 4 Benzyl chloride at 9415 Mc/sec. Thickness of the liquid, 1 cm

against frequencies in the figures 3, 5, 6 and 7 for the U.H.F. region. Times of relaxation have been calculated from Debye's equation

$$\omega\tau = \frac{\epsilon_0 + 2}{\epsilon_1 + 2} \sqrt{\frac{\epsilon_1}{\epsilon_0}} \quad \dots (2)$$

and the values of  $a^3$ , the cube of the radius of the rotor, have been obtained again from Debye's equation

$$a^3 = \frac{\tau kT}{4\pi\eta} \quad \dots (3)$$

The values of different constants involved in the calculation of  $\tau$  and  $a^3$  are given in Table I.

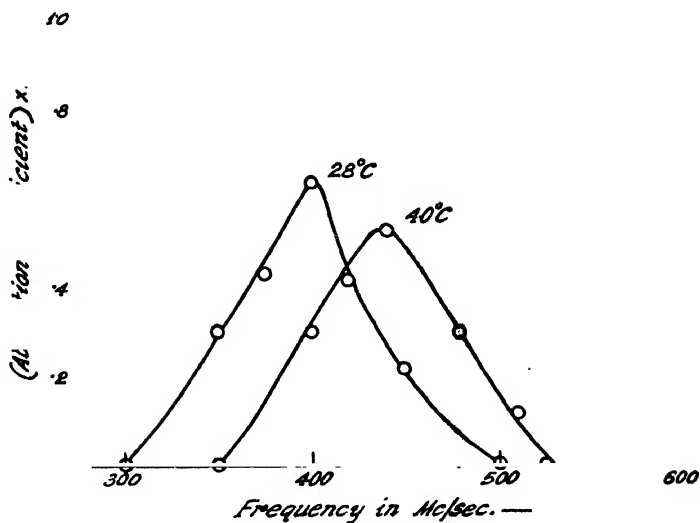


Fig. 5 Benzyl chloride. Thickness of the liquid, 3.5 cm.

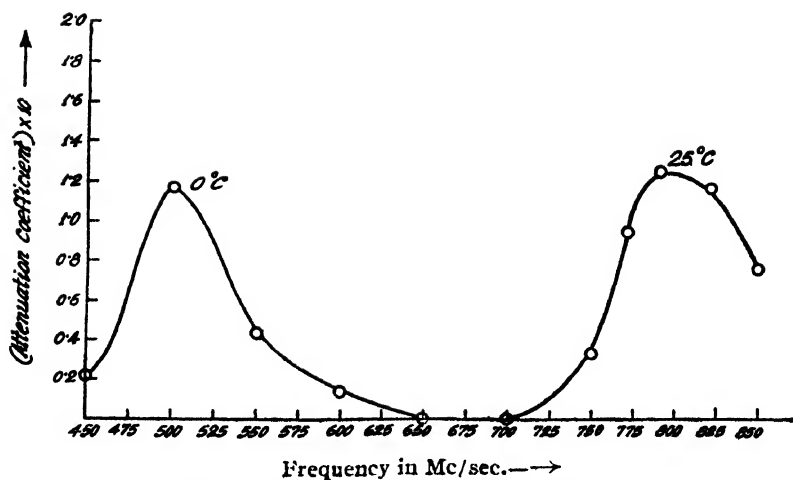


Fig. 6 Benzyl chloride. Thickness of the liquid, 3.5 cm.

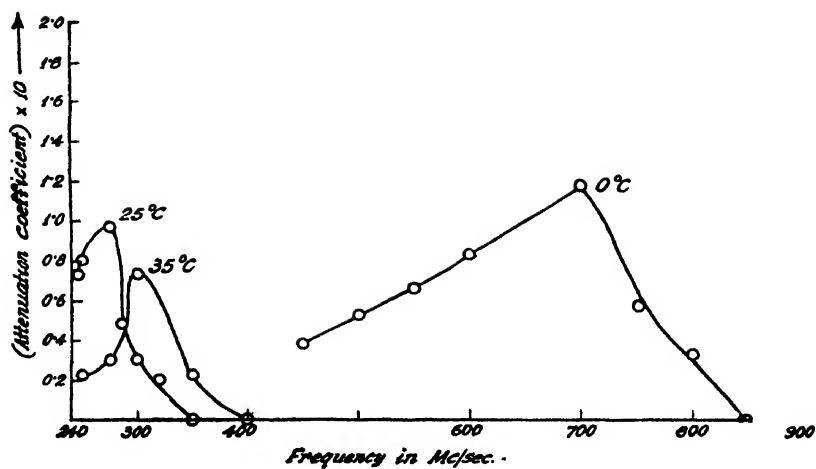


Fig. 7 Benzyl amine at 9451 Mc/sec. Thickness of the liquid 3 cm.

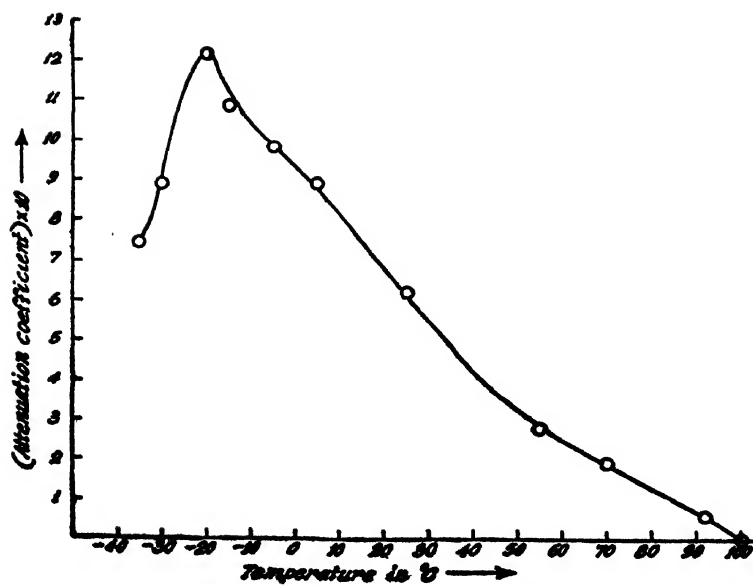


Fig. 8 Benzyl amine. Thickness of the liquid 1.5 cm.

TABLE I

Liquid	$\frac{\omega}{2\pi}$ in Mc/sec	$T^\circ\text{K}$ for max. absorption	$\epsilon_0$	$\epsilon_1$	$\eta \times 100$	$\tau \times 10^{11}$	$a^3 \times 10^{24} \text{ c.c.}$
Benzyl alcohol	900 (aprox)	303	2.37	12.4	4.3	12.24	9.354
	9415	328		10.3	2.8	1.249	1.095
Benzyl chloride	400	301	2.371	5.75	1.2	34.76	95.04
	440	313		4.5	1	33.53	114.3
	500	273		8.1	1.76	25.34	42.85
	750	208		6	1.28	17.5	44.1
	9415	258		9.3	1.97	1.303	1.843
Benzyl amine	275	208	2.381	4.5	1.50	53.47	100.2
	300	308		4.45	1.18	49.15	116.6
	700	273		5.55	1.81	20.13	32.56
	9415	253		7	2.06	1.409	1.88

The values of  $\eta$  are obtained by extrapolation from the results reported in Handbook of Chemistry and Physics published by Chemical Rubber Publishing Co., the International Critical Tables and from Physico-chemical constants of pure organic compounds published by J. Timmermans (1950). The values of  $\epsilon_1$  have been obtained from the table of dielectric constants of pure liquids published by National Bureau of Standards, United States, Department of Commerce, and also from the International Critical Tables. The results at very low temperatures have been obtained by extrapolation. The values of  $\epsilon_0$  have been assumed to be equal to square of  $n$ , the refractive index at  $20^\circ\text{C}$  for sodium D line, because the values of  $n$  at lower temperatures were not available.

#### DISCUSSIONS

It can be seen from Table I that all the three liquids exhibit maximum absorption of 3.18 cm microwaves at suitable temperatures and cubes of the radii of the rotors are 1.595, 1.83 and  $1.88 \times 10^{-24}$  cc. in the case of benzyl alcohol, benzyl chloride and benzyl amine respectively. As the cubes of radii of the molecules are many times larger than these values, the rotors cannot be the whole molecules. The radii, however, agree to some extent with those of the circles along which the substituent groups would move if they had rotational freedom. Thus probably, these absorption maxima are due to rotation of the substituent groups about a diameter of the benzene ring passing through the carbon atom of the ring with which the substituent group is attached.

As regards the absorption in the U.H.F. region, the behaviour of benzyl alcohol is different from that of either benzyl chloride or benzyl amine.

Each of the latter two liquids shows two absorption maxima in the region between 250 Mc/sec and 900 Mc/sec. The radius of the rotor corresponding to one of the two absorption maxima lies between 3 Å and 4 Å in both these cases and that corresponding to the other maximum is about 4.8 Å. The lower value may correspond to that for a monomer and the higher value may correspond to the radius of the dimer. The agreement is fairly satisfactory in view of the fact that the values of the macroscopic viscosities have been taken in the calculation and these values have again been obtained by extrapolation. The fact that the absorption peaks both at lower and higher frequencies shift with change of temperature of the liquid as shown in figures 3, 5, 6 and 7 shows that the absorption is genuine. The change of dielectric constant which takes place with the change of temperature cannot explain the shift of the peaks if it is assumed that the apparent absorption is due to formation of stationary waves in the cell.

The results obtained in the present investigation show that in these substituent benzenes the time of relaxation has different values in each case and the occurrence of 'effective time of relaxation' postulated by Fischer (1949) is corroborated by these results. The influence of constitution of the substituents on the value of the radius of the rotor is quite evident from a comparison of the results for benzyl alcohol with those for the other two liquids. In the former case no absorption peak is observed in the range 250-900 Mc/sec and there is indication of the occurrence of a peak at a frequency higher than 850 Mc/sec. Even if the frequency is taken as 900 Mc/sec the cube of the rotor calculated from Debye's theory becomes  $0.35 \times 10^{-24}$  cc. This is much smaller than the corresponding values for the other two molecules. This discrepancy may be due to the fact that the macroscopic viscosity is much larger in the case of benzyl alcohol than that in the case of the other two liquids and that the viscous forces actually acting on the molecule during its orientation in the liquid are much weaker than the macroscopic viscosity as pointed out by Sirkar (1953). Probably the presence of OH groups facilitates hydrogen-bonding among neighbouring molecules increasing thereby the macroscopic viscosity, but a small percentage of single molecules still exists in the liquid and when these molecules try to orient, the forces acting on them are just ordinary viscous forces and not the forces increased in strength by hydrogen-bonding.

Investigations with other molecules of similar structure are in progress.

#### ACKNOWLEDGMENT

The author wishes to express his grateful thanks to Prof. S. C. Sirkar, D.Sc., F.N.I., for kindly suggesting the problem and for his constant guidance during the progress of the work.



REFERENCES

- Cole, K, S. and Cole, R. H., 1941, *J. Chem Phys* , **9**, 341.  
Fischer, Von. E., 1949, *Z. Naturforsch*, **4a**, 707.  
Ghosh, D. K , 1953*a*, *Ind. J. Phys.* **27**, 285  
Ghosh, D. K., 1953*b*, *Ind. J. Phys.*, **27**, 511.  
Hamilton, Knip and Kuper, 1948, *Klystrons and Microwave Triodes*.  
Kastha, G. S., 1952, *Ind. J. Phys.*, **26**, 103.  
Sen, S. N., 1950, *Ind J Phys* **24**, 163.  
Sirkar, S. C., 1953, *Ind. J. Phys.*, **27**, 475.



# PSEUDOSCALAR INTERACTION AND PROTON-PROTON SCATTERING

By D. BASU

DEPARTMENT OF THEORETICAL PHYSICS, INDIAN ASSOCIATION  
FOR THE CULTIVATION OF SCIENCE, CALCUTTA-32

(Received for publication, March 30, 1954)

**ABSTRACT.** It is shown here that in the nuclear interaction the presence of contact potentials of the form of  $\delta$ -function helps to make the scattering isotropic as required to explain the p-p scattering at high energies. The  $\delta$ -function potential which occurs naturally in the field theoretical interaction may be regarded as the analogue of the 'hard core' potential which Jastrow assumed ad-hoc in the singlet state only.

## INTRODUCTION

The nuclear experiments involving meson indicate that the meson responsible for the nuclear interaction is to be described by the pseudoscalar field theory. The pseudoscalar interaction consists of two parts : the central force term and the tensor force term ; the two terms have different influences on nuclear scattering cross sections. The scattering by the central force term gives large values of cross sections for small angles, as such the scattering depends considerably on angle, further the value of the total scattering cross section decreases with increasing energy ; whereas the scattering by the tensor force term does not depend strongly on the angle and the total cross section either tends to increase (for relativistically high energies) or remains constant (for not very high energies) with increasing energy.

The high energy experiments on proton-proton scattering show that the differential cross section is very nearly independent of the angle and the value of the total cross section does not appreciably vary with energy of the incident particle. It has been possible to explain the above two features of the p-p scattering on the basis of a nuclear interaction which can be derived from field theoretical consideration. Various phenomenological potentials between two nucleons have been proposed, of them the 'hard core' model of Jastrow (1951) gives better agreement with experimental observations than any other. However, on theoretical grounds it has not been possible to justify the existence of a 'hard core' in case of singlet state as suggested by Jastrow. Though it is understandable why it is necessary to assume a 'hard core' for the singlet state, in the singlet state the tensor force term vanishes, only the central force term remains, so the central force term alone gives highly anisotropic scattering which will be contrary to experimental observations. To obviate this contradiction, Jastrow

for the cross section show that the scattering is very nearly isotropic with angle when  $k^2 > 1$  and further as long as the energy of the incident particle is much less than the rest energy of the nucleon which is about 1000 Mev., the cross section is independent of the energy also. However, the nearly isotropic scattering obtained here is mainly due to the tensor force term which is common to both the interactions, the advantage of the presence of the  $\delta$ -function term will be apparent when we consider the singlet state in which the tensor force does not contribute to the scattering. For the singlet state the scattering cross sections calculated with the interactions (1) and (2) are as follows :

$$d\sigma^s = \frac{g^4 M^4}{E_0^2} \frac{k^4}{3(1+k^2)^2} \quad (11)$$

$$d\sigma^s = \frac{g^4 M^4}{E_0^2} \frac{1}{3(1+k^2)^2} \quad (12)$$

We notice that the expression (11) gives nearly isotropic scattering, but the scattering cross section given by (12) is highly anisotropic. So the presence of the  $\delta$ -function, as it occurs in interaction (1), helps to make the scattering isotropic.

The calculations for the cross sections have been made in Born approximation, they are valid for energies greater than 100 Mev. The condition that  $k^2 > 1$ , would hold for energies of the order of 340 Mev.

#### REFERENCES

Jastrow, 1951, *Phys. Rev.*, **81**, 165.

# ON THE RAMAN SPECTRA OF ETHYLENE DICHLORIDE IN SOLUTIONS OF DIFFERENT STRENGTHS\*

BY SUKHIENDU BIKASH BANERJEE

OPTICS DEPARTMENT, INDIAN ASSOCIATION FOR THE CULTIVATION OF SCIENCE, CALCUTTA—32

(Received for publication, March 20, 1954)

Plates VI A, B

**ABSTRACT**—The Raman spectra of solutions of ethylene dichloride of concentrations 25% and 50% by volume in heptane and cyclohexane have been studied and the relative intensities of the lines  $754\text{ cm}^{-1}$  and  $654\text{ cm}^{-1}$  have been measured in each case and compared with the values observed in the case of pure liquid. It has been observed that the ratio  $I_{754}/I_{654}$  increases when the liquid is dissolved in either of the two solvents to make 50% solutions and the ratio increases further when the concentration is diminished. It is pointed out that these results support the conclusion arrived at by Bishui (1948) that one of these two lines is due to associated molecules and are contradictory to the conclusions drawn by Kuratani (1952) that association of molecules has nothing to do with origin of these lines.

## INTRODUCTION

It was first pointed out by Sirkar and Bishui (1945) that in the liquid state some of the molecules of ethylene dibromide might exist as associated pairs. Bishui and Sanyal (1947) studied the relative intensities of the lines  $660$  and  $551\text{ cm}^{-1}$  in the Raman spectra of ethylene dibromide dissolved in various solvents and came to the conclusion that the line  $551\text{ cm}^{-1}$  is due to associated group of molecules while the line  $660\text{ cm}^{-1}$  is due to single molecules. Bishui (1948) also studied the Raman spectra of ethylene dichloride (1,2-dichloroethane) and 1,1-dichloroethane in the liquid and solid states and came to the conclusion that the line  $654\text{ cm}^{-1}$  of the former liquid is due to associated molecules while the line  $754\text{ cm}^{-1}$  is due to single molecules. Recently, Kuratani (1952) has studied the infra-red absorption bands of ethylene dichloride (1,2-dichloroethane) in solution in various solvents and has studied the intensity-ratio of the bands  $1284$  and  $1230\text{ cm}^{-1}$  assumed to be due to gauche and trans forms respectively. He has observed that the intensity-ratio of the two absorption bands does not change with the change of concentration of solution of ethylene dichloride in carbon tetrachloride and carbon disulphide, and assuming the two bands to be due respectively to the gauche and trans forms of the molecule, he has concluded that the association theory put forward by Bishui (1948) is contradicted by these results.

\* Communicated by Prof. S. C. Sirkar

On going through the results reported by Bishui and Sanyal (1947), however, it is found that the relative intensities of the lines  $660$  and  $551\text{ cm}^{-1}$  of ethylene dibromide do not change appreciably when the liquid is dissolved in carbon tetrachloride, and therefore, it cannot be expected that the intensity ratio will change with change in the concentration of the solution. On the other hand, Bishui and Sanyal (1947) observed that the intensity-ratio changes considerably when the liquid is dissolved in hexane and such a change might be expected also in the case of solution of ethylene dichloride in hexane or similar solvents, and the influence of concentration on the intensity-ratio could be expected only in the case of these solutions in which the intensity of the line  $654\text{ cm}^{-1}$  of ethylene dichloride is less than that for the pure liquid. It was, therefore, thought worthwhile to study the influence of concentration on the relative intensities of the lines  $754$  and  $654\text{ cm}^{-1}$  of ethylene dichloride dissolved in suitable solvents in different proportions. The results for solutions of ethylene dichloride in heptane and cyclohexane have been discussed in present paper.

#### EXPERIMENTAL

The liquid ethylene dichloride and the two solvents, cyclo-hexane and the heptane used in the present investigation were of chemically pure quality and were supplied by B. D. H. and May Baker. The liquids were distilled in vacuum in large quantities before use. The Raman spectrum of the pure liquid was first photographed, using a Fuess glass spectrograph giving a dispersion of about  $12\text{ A.U. per mm}$  in the  $4046\text{ \AA}$  region and Ilford Zenith plates. Two solutions of known strengths were prepared first with heptane as the solvent, the strengths being about  $65\%$  and  $38\%$  by weight. The Raman spectra of these two solutions were recorded using plates from the same packet and developing them exactly in the same way as the plate for the pure liquid mentioned above. The process was repeated for the solutions of the liquid in cyclohexane of strengths  $62\%$  and  $35\%$  by weight. The Wood's tube containing either the pure liquid or the solutions was provided with a jacket filled with a dilute solution of sodium nitrite which cut off the  $3650\text{ \AA}$  group of mercury lines and prevented production of continuous fluorescence by the solution or the pure liquid. The strength of this filtering solution was the same in all the cases. Intensity marks were next taken on another Zenith plate taken from the same packet by varying the width of the slit of the spectrograph and using a glowing tungsten filament bulb as the source of continuous radiation. Microphotometric records were taken with a Kipp and Zonen type self-recording microphotometer. Blackening-log intensity curves were drawn for the wavelengths corresponding to the lines  $654\text{ cm}^{-1}$  and  $754\text{ cm}^{-1}$  excited by both the  $4077\text{ \AA}$  and  $4358\text{ \AA}$  lines of mercury. The values of  $I_{754}/I_{654}$ , the ratio of intensities of the lines  $754$  and  $654\text{ cm}^{-1}$  were then calculated for the pure liquid and for the solutions using these blackening-log intensity curves.

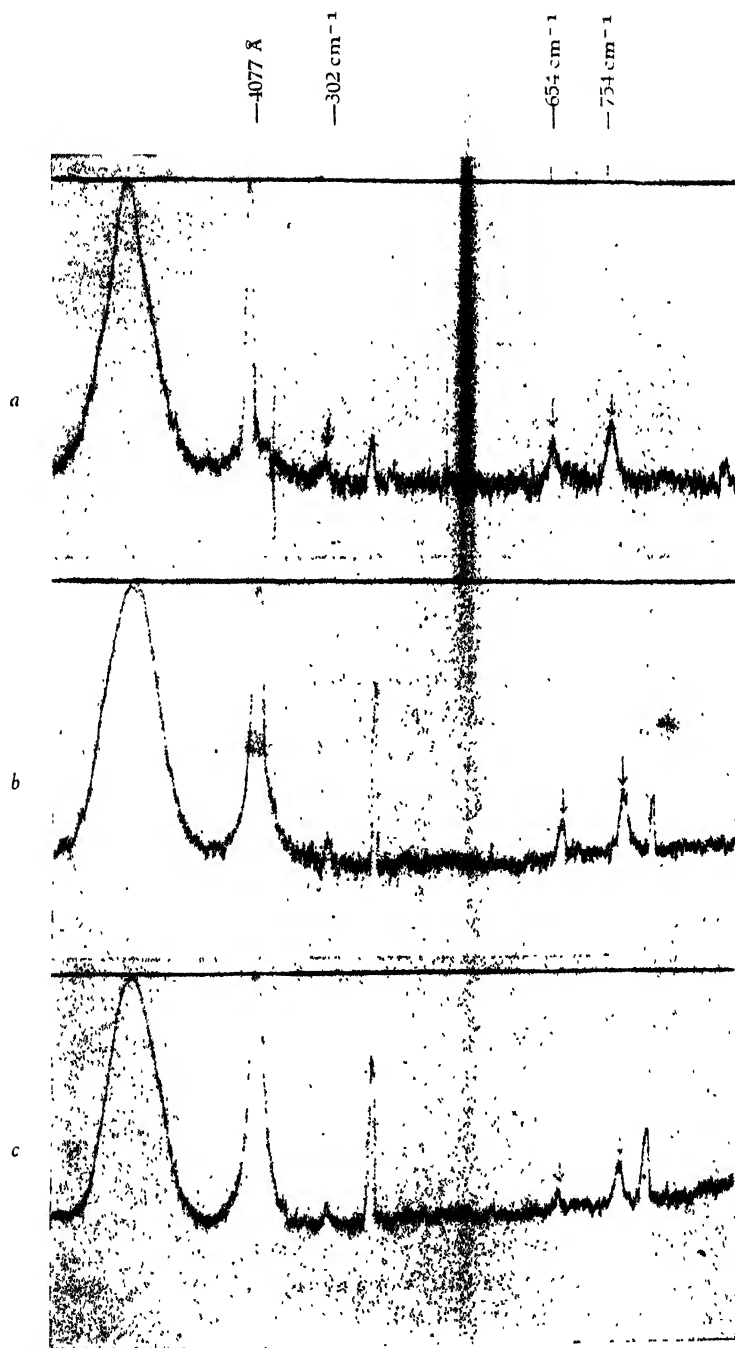


Fig. 1

Microphotometric records of Raman spectra.

- (a). Ethylene dichloride, liquid at 28°C  
 (b). 50% Solution ( by volume ) of ethylene dichloride in cyclohexane  
 (c). 25% " " " " " " " " "

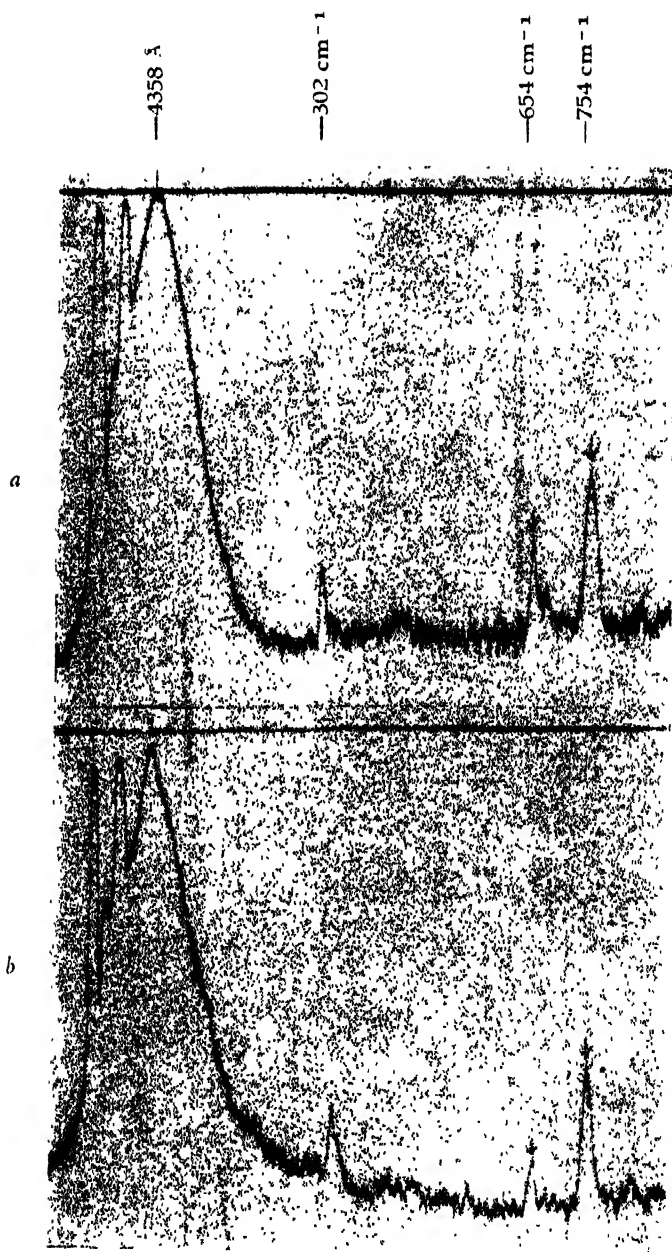


Fig. 2

Microphotometric records of Raman spectra

(a) 50% solution ( by volume ) of ethylene dichloride in heptane

(b) 25%    "    "    "    "    "    "    "    "



## RESULTS AND DISCUSSION

The microphotometric records of the spectrograms for the pure liquid and solutions in cyclohexane are reproduced in Plate VIA and those for the solution in heptane are reproduced in Plate VIB. The values of  $I_{754} : I_{654}$  calculated with the help of these records and the blackening-log intensity curves are given in Table I. In calculating these values the relative widths of the two lines were taken into account, and therefore, the values given in Table I are those of integrated intensities. The temperature was about 28°C in all the cases.

TABLE I

Solvent used	Concentration of $C_2H_4Cl_2$ by weight	$I_{754} / I_{654}$
Heptane	100%	2.0
	65%	3.1
	38%	4.3
Cyclohexane	100%	2.0
	62%	2.8
	35%	3.1

It can be seen from Table I that the ratio of the integrated intensities of the lines 754 and 654  $\text{cm}^{-1}$  for the pure liquid at 23°C is 2.0 which is the same as the value reported by Mazumder (1953) for the liquid at 135°C. This ratio therefore does not change appreciably with the rise of temperature. The value of the ratio, however, increases considerably as the liquid is dissolved either in cyclohexane or in heptane even for a concentration just above 60%. This change is larger in the case of solution in heptane than for the solution in cyclohexane. The ratio increases in the case of solution in heptane from 3.1 to 4.3 when the concentration is diminished from 65% to 38%. In the case of the solution in cyclohexane also the ratio increases with dilution of the solution, but this increase is smaller than that in the former case. These results can be clearly seen from a comparison of the relative intensities of the lines 302  $\text{cm}^{-1}$  and 654  $\text{cm}^{-1}$  in the spectrograms due to the pure liquid and the solution in cyclohexane reproduced in Plate VIA.

The results thus demonstrate the dependence of the intensity-ratio on the concentration of the solution. Such an influence can be expected if the line 654  $\text{cm}^{-1}$  is assumed to be due to associated molecules and the line 754  $\text{cm}^{-1}$  is attributed to the single molecule. The hypothesis that the liquid consists of molecules of two forms the relative populations, of which are determined by the temperature cannot explain these results. Hence the conclusion arrived at by Kuratani (1952) is not supported by the results of the present investigations. On the other hand, these results support the

view expressed by Bishui and Sanyal (1947) that association of some of the molecules in the liquid state to form pairs gives rise to the line  $654\text{ cm}^{-1}$ . The formation of virtual bond between neighbouring molecules may either alter the orientation of one half of the molecule about the other half or it may alter the strength of the C-Cl bond. The results reported by Mazumder (1953) also show that there is a catastrophic change in the relative intensities of the lines  $654$  and  $754\text{ cm}^{-1}$  with the vaporization of the liquid without change of temperature. Those results also support the view that some strong intermolecular field is responsible for producing the change in relative intensities of the two lines mentioned above.

The fact that different solvents have different types of influence on the relative intensities of the two lines shows that the relative numbers of the molecules of two forms which are assumed to be present in the liquid by previous workers (Mizushima and Morino, 1938) depend on intermolecular field. As it is observed in the present investigation that saturated hydrocarbon molecules as solvents have greatest influence on the relative numbers of the two forms it is quite probable that the number changes in this case owing to breaking up of the associated molecules in the solution.

#### ACKNOWLEDGMENT

The author's thanks are due to Prof. S. C. Sirkar, D.Sc., F.N.I., for kindly suggesting the problem and for his guidance throughout the progress of the work.

#### REFERENCES

- Bishui, B. M., 1948, *Ind. J. Phys.*, **22**, 319  
Bishui B. M. and Sanyal, S. B., 1947, *Ind. J. Phys.*, **21**, 234.  
Kuratani, K., 1952, *Rept. Inst. Sci. and Technol. Univ. Tokyo*, **6**, 221  
Mazumder, M., 1953, *Ind. J. Phys.*, **27**, 496.  
Mizushima, S. and Morino, Y., 1938, *Proc. Ind. Acad. Sci.*, **1**, **8**, 315

# SPECTROSCOPIC CONSTANTS OF MOLECULES—II. ON THE VIBRATION FREQUENCIES OF DIATOMS OF THE TYPE XY

BY K. MAJUMDAR AND Y. P. VARSHNI  
DEPARTMENT OF PHYSICS, ALLAHABAD UNIVERSITY, ALLAHABAD

(Received for publication, March 27, 1954)

**ABSTRACT** Relation of the vibration frequency of diatom XY with the vibration frequencies of diatoms XX and YY has been studied, X and Y belonging to the same group of the periodic table. If  $\omega_e'^{65}$  for XY be represented by  $\phi(XY)$ , then it is found that

$$\phi(XY) = \frac{\phi(XX) + \phi(YY)}{2}$$

The calculated values are in good agreement with the observed values. Many undetermined frequencies have been predicted.

## INTRODUCTION AND FORMULA

Several attempts have been made to find a relation between  $a = \omega_e(XY)$ ,  $b = \omega_e(XX)$  and  $c = \omega_e(YY)$ , where  $a$ ,  $b$  and  $c$  are the ground state vibration frequencies of the diatoms XY, XX and YY respectively. X and Y belong to the same group in the periodic table.

Clark (1935 b, 1937 a) and Howell (1936) independently suggested :

$$a = .5(b + c) \quad \dots (1)$$

The errors in  $a$  were found to be always positive, and hence it was modified (Clark, 1937 b) to

$$a = .491(b + c) \quad \dots (2)$$

However, both equations (1) and (2) are not very satisfactory.

Clark (1935 b, 1937 c) later proposed : (when  $c > b$ )

$$a^3 = .815 bc^2 \quad \dots (3)$$

The formula gives satisfactory results.

It is found that for such molecules the function  $\omega_e'^{65}$  is additive. The function will be denoted by  $\phi$ . Thus

$$\omega_e'^{65}(XX) = \phi(XX)$$

The 'atomic' values may be denoted by  $\phi(X) = \frac{1}{2} \phi(XX)$ .<sup>1</sup>

Then

$$\phi(XY) = \frac{\phi(XX) + \phi(YY)}{2}$$

$$= \phi(X) + \phi(Y)$$

44

The results obtained by the formula (4) will be compared with those by Clark's formula (3).

It will be observed that while Clark's formula (3) is unsymmetrical, formula (4) is not. If  $b = c = a$ , then the formula should yield the value  $a$ . Formula (3) does not, while formula (4) does.

Table I gives the calculations of the atomic values (obviously these atomic values cannot be expected to have any physical significance with regard to the atom). Table II records the calculated values of the vibration frequencies of the diatoms XY by the formula (4). Clark's calculated values are shown in column 5.

There is no uniform practice of denoting the molecule XY (X being heavier than Y) regarding which atom should be placed first. Herzberg (1950) and Rosen (1951) have placed the heavier atom first in most of the cases, but instead of BiSb they give SbBi. Herzberg has tabulated both CsRb and RbCs. In Table II, the heavier atom is placed first.

#### EXPERIMENTAL DATA

Data for molecules whose vibration frequencies have been determined with certainty, has been taken from Herzberg and Rosen (see authors, 1954 a), and is tabulated in Table I. In some cases experimental and estimated values used by Clark (1937b, 1937c) are much different. As the calculated values by the two formulae will be compared, the values used by Clark are also included in Table I, column 3. Sources for other molecules are as follows:

FrFr, PoPo, AtAt—No experimental data are available. The authors (1954 a) and Clark (1937 c) have estimated values for these. The first line against these diatoms gives the calculations by the authors' values (the uncertainties which are about 3% have been neglected), the second line by Clark's values. It will be observed that the values given in second line are slightly different from those given in column 'Clark'. The reason being that Clark used rounded values of his estimates.

GeGe and SnSn—Estimated values by authors (1954 a) have been used.

SiSi—The reported value is 750. But it is uncertain, in as much as the identification of the bands as due to SiSi is tentative (Downie and Barrow 1947). It is also not certain that lower state is the ground state. The estimated value (authors, 1954 a) is 987. It is noticed that vibration frequency in a group falls with increasing atomic number. This criteria is satisfied by both 750 and 987, as both lie between the values for CC and GeGe. Another evidence is the behaviour of the force constants. Their behaviour for other groups is similar to that of the vibration frequencies. The force constants for CC, GeGe, SnSn and PbPb are 9.522, 6.425, 5.048 and 4.016 (Des.) respectively. The force constant values of GeGe and SnSn are empirical values. Now the observed value for SiSi is 4.649, while the empirical value is 8.04. Though the values for GeGe and SnSn are empirical, and it cannot be said with

TABLE I

Group	Molecule	$\omega_e$ Clark	$\omega_e$	$\phi$ (XX)	$\phi$ (X)
I	LiLi	351.4	351.4	45.16	22.58
	NaNa	150.2	150.2	26.90	13.495
	KK	92.6	92.64	18.98	9.49
	RbRb	57.8	57.3	13.80	6.945
	CsCs	42	42	11.35	5.67
	FrFr	29	30.7	9.26	4.63
IV			30.1	9.14	4.57
	CC	1641.6	1641.3	123	61.5
	SiSi	...	987	88.372	44.186
		...	(750)	73.94	36.97
	GeGe	...	543	59.93	29.96
	SnSn	...	380	47.52	23.76
V	PbPb	420	256.5	36.83	18.42
	NN	2300	2359.6	155.7	77.86
	PP	780.4	780.4	75.86	37.93
	AsAs	432.1	429.4	51.44	25.72
	SbSb	268	269.8	38.03	19.014
	BiBi	172.7	172.7	28.46	14.23
VI	OO	1580.3	1580.4	120.66	60.93
	SS	727.4	725.7	72.355	36.177
	SeSe	387.8	391.8	48.47	24.234
	TeTe	250.9	251	36.29	18.145
	PoPo	156	200.2	36.33	15.665
		...	156.3	26.67	13.335
VII	FF	1080	1049	91.916	45.958
	ClCl	564.9	564.9	61.49	30.745
	BrBr	323.9	323.2	42.78	21.39
	II	214.3	214.6	32.78	16.39
	AtAt	139	172.9	28.482	14.241
		..	139.4	24.76	12.38

TABLE II

Group	Molecule	$\phi(X) + \phi(Y)$	$\omega$ , calc Authors	$\omega$ , calc. Clark	$\omega$ , Observed
I	NaLi	36.075	248.7	252.1	...
	KLi	32.07	207.4	210.5	(207)
	RbLi	29.525	182.7	179.8	(185)
	CsLi	28.25	170.8	161.7	(167)
	FrLi	27.21	161.2	143	...
	"	27.15	160.6	...	..
	KNa	22.985	124.3	124.2	123.20
	RbNa	20.44	103.8	106.1	106.6
	CsNa	19.165	93.55	95.4	(98)
	FrNa	18.125	86.25	84.5	..
	"	18.065	85.8	..	..
	RbK	16.435	74.22	73.9	.
	CsK	15.16	65.55	66.4	..
	FrK	14.12	58.74	58.5	..
	"	14.06	58.34	..	...
	CsRb	12.615	49.4	48.5	49.41
	FrRb	11.575	43.27	43	...
	"	11.515	42.93	..	.
	FrCs	10.30	36.16	34.5	...
	"	10.24	35.83	..	...
IV	SiC	105.686	1300	..	...
	"	98.47	1165.5	...	...
	GeC	91.46	1039.7	...	...
	SnC	85.26	934	..	..
	PbC	79.92	845.4	972.4	...
	GeSi	74.146	753.3	...	...
	"	66.93	643.6	...	...
	SnSi	67.946	658.7	..	...
	"	60.73	554.3	...	...
	PbSi	62.606	580.8	...	...
	"	55.39	481	...	...
	SnGe	53.72	459	..	...

TABLE II—*contd.*

Group	Molecule	$\phi$ (X) + $\phi$ (Y)	$\omega$ , calc Authors	$\omega$ , calc Clark	$\omega$ , Observed
V	PbGe	48.38	390.5	.	...
	PbSn	42.18	316.3	..	..
	PN	115.79	1495.7	1524.7	1337.2
	AsN	103.58	1260	1252.0	1068
	SbN	96.874	1137	1068	912
	BiN	62.00	1051	922	.
	AsP	63.65	505.8	598.5	..
	SbP	56.941	501.9	510	.
	BiP	52.16	438.5	141	.
	SbAs	44.734	346.2	344	.
	BiAs	39.95	291	297.3	..
	BiSb	33.244	219.3	216.2	220
VI	SO	96.207	1125	1139.8	1123.7
	SeO	84.204	917.2	924.2	907.1
	TeO	78.175	817.6	799.4	796
	PoO	75.695	777.9	683.5	...
	"	73.365	741.4	...	..
	SeS	60.411	540.7	550.9	..
	TeS	54.322	466.9	476.1	.
	PoS	51.842	434.4	197.5	..
	"	49.512	405	.	..
	TeSe	42.379	318.6	313.3	322 <sup>A</sup>
	PoSe	39.899	290.4	268	..
	"	37.569	264.7	.	.
	PoTe	33.81	225.1	200.5	..
	"	31.48	201.7	...	...
VII	ClF	76.703	794	812.7	793.2
	BrF	67.348	640.9	675.2	671
	IF	62.348	577.1	588.4	6108
	AtF	60.199	546.7	509.5	...

TABLE II—*contd.*

Group	Molecule	$\phi(X) + \phi(Y)$	$\omega$ , calc. Authors	$\omega$ , calc. Clark	$\omega$ , Observed
	AtI <sup>a</sup>	58.338	523	..	...
	BrCl	51.135	438.2	138.4	(430)
	ICl	47.135	375.4		384.1
	AtCl	44.986	349.3	330.5	..
	..	13.125	327.3	.	
	IBr	37.78	267	.	268.4
	AtBr	35.631	244	228	...
	..	33.77	224.6	.	..
	AtI	30.631	193.3	173.5	...
	..	28.77	175.7		

<sup>a</sup>—D. Sharma (private communication)<sup>b</sup>—Durie (added in proof)

certainty that SiSi value should lie between 9.522 and 6.425, yet one expects that it should be sufficiently greater than 4.016 (PbPb) and nearer to 9.522 (CC). These considerations support the empirical value. However, calculations for both values have been done. The first line gives the values for the estimated vibration frequency and the second for the observed one.

FF—The observed value is 892 which is uncertain. Clark (1935 *a*, 1937 *b*, 1937 *c*) estimates 1080. The authors' (1954 *a*) value is 1049, and it has been used (see discussion below).

#### DISCUSSION

It will be observed that in most cases the agreement between the observed and the calculated values is quite satisfactory. However, there are three notable exceptions—PN, AsN and SbN. Howell (1936) suggests that the experimental values of PN and AsN molecules might not refer to their ground states. Clark (1937 *b*) adduces other reasons also in support of this suggestion. Further experimental work would decide whether such molecules are to be treated as 'anomalous' or whether these errors are due to uncertainty in the assignment of the ground state frequencies of PN, AsN and SbN. It may be noted that another molecule of the same group *viz.*, BiSb obeys the formula very well. The difference between the observed and the calculated values for PN, AsN and SbN is nearly 180.

In such cases where the experimental values used of XX and YY are same, the calculated values for XY by authors' formula (4) and Clark's formula (3) are close to each other.



## Vibration frequency of FF

The experimental value for the vibration frequency of FF is uncertain. It will be noticed that the calculated values for ClF and BrF are quite close to experimental values, both by authors' and Clark's formulae though they have been calculated by assuming a vibration frequency for FF which is much different from the experimental value. By assuming the values for ClF and BrF we can obtain a near approximation to the value for FF by back calculation. This has been done in Table III.

TABLE III.

Starting Molecule	Formula	$\omega$ for FF	Mean
ClF	Clark	1041	1064
BrF	Clark	1071	
ClF	Authors	1048	
BrF	Authors	1097	

These calculations show that the vibration frequency of FF should be close to 1064.

## ACKNOWLEDGMENTS

The authors are thankful to the Council of Scientific and Industrial Research for the financial assistance and the permission to publish the results. Thanks are also due to Dr. D. Sharma for making available his results on TeSe prior to publication.

## REFERENCES

- Clark, C. H. D., 1935 a, *Trans. Faraday Soc.*, **31**, 585.  
 Clark, C. H. D., 1935 b, *Trans. Faraday Soc.*, **31**, 5917.  
 Clark, C. H. D., 1937 a, *Nature*, **139**, 508.  
 Clark, C. H. D., 1937 b, *Trans. Faraday Soc.*, **33**, 1390.  
 Clark, C. H. D., 1937 c, *Trans. Faraday Soc.*, **33**, 1398.  
 Downie, A. R., and Barrow, R. F., 1947, *Nature*, **160**, 198.  
 Durie, R. A., 1951, *Proc. Roy. Soc.*, **A207**, 388.  
 Howell, H. G., 1936, *Nature*, **138**, 36, 290.  
 Majumdar, K., and Varshni, Y. P., 1954 a, *Ind. J. Phys.*, **23**, 103.

# FORCE CONSTANTS AND THERMODYNAMIC PROPERTIES OF $\text{TiCl}_4$

BY D. TIRUMALIESA AND V. RAMAKRISHNA RAO\*

DEPT. OF PHYSICS, ANDHRA UNIVERSITY, WALT AIR

(Received for publication, February 9, 1954)

**ABSTRACT.** Sets of force constants are calculated for the  $\text{TiCl}_4$  molecule by using the known fundamental frequencies and Wilson's normal coordinate treatment. By comparing the results with data from other sources, one particular set of constants is recommended. The heat content, free energy, entropy and heat capacity of this molecule are calculated for a harmonic oscillator, rigid rotator approximation for temperature varying from 100°K to 1000°K.

## INTRODUCTION

Considerable progress has been made in the evaluation of force constants in organic molecules by the Wilson's normal coordinate treatment using a most general potential energy function. In the case of inorganic molecules, however, our knowledge of the force constants is very meagre. What little is known, is obtained by the use of very approximate methods based upon assumptions like central field forces and pure valence forces. In view of this, we have undertaken a systematic investigation of the force constants of these inorganic polyatomic molecules with particular reference to those belonging to the point group  $T_d$ , (A regular tetrahedral structure). An additional point of interest in these molecules is that most of them give rise to diatomic molecular emission and absorption spectra. We can compare with profit the information derived from this with that obtained from the study of the vibrations of the corresponding polyatomic molecules by Raman effect and/or infra-red absorption. To start with, we have chosen the  $\text{TiCl}_4$  molecule as the emission band spectrum of the diatomic molecule  $\text{TiCl}$  has been thoroughly investigated by one of us (V. R. Rao, 1949).

## FORCE CONSTANTS

The Raman frequencies for the  $\text{TiCl}_4$  molecule are obtained by various authors. (Ta-You-Wu, 1946). They lie in the low frequency region ( $< 500 \text{ cm}^{-1}$ ), as can be expected for a heavy inorganic molecule. Of the four observed frequencies, one is strongly polarized and the other three depolarized. Assuming a tetrahedral structure as in  $\text{CH}_4$ ,  $\text{SiF}_4$ ,  $\text{CCl}_4$  etc. the four frequencies are assigned as one totally symmetric vibration ( $A_1$ , polarized) and one doubly degenerate vibration ( $E$ ) and two triply degenerate vibrations ( $T_2$ ), (see Table II). The infrared absorption of this molecule does not appear to have been studied.

\* Life Fellow, Indian Physical Society

The force constants for this molecule have been calculated by earlier authors by using central force and valence force treatments. (Herzberg, 1949). No attempts have yet been recorded to obtain the force constants by Wilson's normal coordinate treatment using the most general second degree potential energy function. As there are only four fundamentals and no data on the isotopic molecule is available, the following potential function is used :

$$\begin{aligned}
 V = & f_d \left( \sum_{i=1}^4 \Delta d_i^2 \right) + f_{dd} \left( \sum_{i \neq j, i=1}^4 \Delta d_i \Delta d_j \right) \\
 & + f_{da} \left( \sum_{i \neq j, i=1}^4 \Delta d_i \Delta \alpha_{j,i} \right) + f'_{da} \left( \sum_{i \neq j \neq k, i=1}^4 \Delta d_i \Delta \alpha_{j,i} \right) \\
 & + f_a \left( \sum_{i \neq j, i=1}^4 \Delta \alpha_{i,j}^2 \right) + f_{aa} \left( \sum_{i \neq j \neq k, i=1}^4 \Delta \alpha_{i,j} \Delta \alpha_{j,k} \right) \\
 & + f_{aa'} \left( \sum_{i \neq j \neq k \neq l, i=1}^4 \Delta \alpha_{i,j} \Delta \alpha_{k,l} \right)
 \end{aligned}$$

Where :

$f_d$  represents Ti-Cl bond stretching force constant

$f_{dd}$  represents that of interaction between two TiCl bonds

$f_a$  represents Cl-Ti-Cl angle bending force constant

$f_{aa}$  represents that of interaction between two Cl-Ti-Cl angles with a common Ti-Cl bond

$f_{za}$  represents that of interaction between two Cl Ti-Cl angles without a common Ti-Cl bond

$f_{da}$  represents that of interaction between a Cl-Ti-Cl angle and a Ti-Cl bond with two common atoms

$f_{da'}$  represents that of interaction between a Cl-Ti-Cl angle and a Ti-Cl bond with only one common atom.

In view of the inadequacy of the number of fundamentals a unique determination of  $f_d$  and  $f_{da}$  and hence the other constants was not possible. So various reasonable values of the ratio  $f_{da}/f_d$  were assumed (0 to 0.5) and sets of force constants were determined. Such sets are given in Table I. Tetrahedral angles are assumed and the following constants are used in the calculations :

Reciprocals of masses of atoms :

$$\begin{aligned}
 \mu_{\text{Cl}} &= 1.6986 \times 10^{22} \text{ gm}^{-1} \\
 \mu_{\text{Ti}} &= 1.2574 \times 10^{23} \text{ gm}^{-1}
 \end{aligned}$$

and for equilibrium bond distance

$$\begin{aligned}
 \text{Cl-Cl} &= 3.61 \text{ \AA} \text{ (Wierl, 1931)} \\
 \text{Ti-Cl} &= 2.21 \text{ \AA} \text{ (derived value).}
 \end{aligned}$$

Real values could be obtained for the force constants involved in the triply degenerate vibrations without any further approximation. All sets of force constants given in Table I reproduce the frequencies to the nearest  $\text{cm}^{-1}$ .

Table I shows that  $f_d$  depends considerably on  $f_{dd}$ , so that when this is made arbitrarily zero, too high a value for  $f_d$  results. Also we have two sets of constants (A & B) for  $(f_{da}-f_{da}')$ ,  $(f_a-f_{aa})$ ,  $(f_a-f_{aa}')$ , since we will have to solve a quadratic equation. If  $f_{aa}'$  is assumed to be zero (as this should be much smaller than  $f_{aa}$  which in itself is very small), then it is possible to give individual values for  $f_a$  and  $f$  as in columns 8 and 9 in Table I. However,  $f_{da}$  and  $f_{da}'$  cannot be separated like this. As the A sets have much larger bending constants than the B sets, it is reasonable to prefer the latter. Hence the individual values of  $f_a$  and  $f_{aa}$  are given for B sets only.

It will be noted that the force constants in Table I are given to four significant figures. This is found adequate and necessary to reproduce the frequencies to the nearest  $\text{cm}^{-1}$  (as can be seen from the last column of Table I).

Off hand, it is not easy to choose the best set of force constants for this molecule from Table I. But we could set limits to some of them, as was done in  $\text{SiF}_4$  (Voelz, Meister and Cleveland, 1951). As  $f_{dd}$  is reasonably expected to be less than half a unit our, calculations are limited to the ratio  $f_{dd}/f_d = 0.5$ . Consequently, we have,  $f_d = 3.114 \dots 1.246$ ,  $f_{dd} = 0 \dots 0.623$ ,  $f_{da} - f_{da}' = 0.273 \dots (-0.218)$ ,  $f_a = 0.13 \dots 0.528$ ,  $f_{aa} = 0.016 \dots 0.215$ ,  $f_a - f_{aa} = \dots 0.114 \dots 0.313$ ,  $f_a - f_{aa}' = 0.13 \dots 0.528$ .

An attempt is made to compare this data with that from other sources like central field forces, (C.F.) valence forces, (V.F.), etc. and diatomic data. The value of  $f_d$  was calculated from  $\omega_e = 455 \text{ cm}^{-1}$  in the emission spectrum of the diatomic molecule  $\text{TlCl}$  (V. R. Rao, *loc. cit.*) from the formulae

$$\omega_e \times r_e^3 = 3 \times 10^{-21} \text{ cm}^2$$

and

$$K = 2.490 \times 10^5 \times (z_1 z_2) \times r_e^{-1.81}$$

where  $z_1$  and  $z_2$  are the number of outer electrons and  $r_e$  is the equilibrium bond distance and  $K$  is the force constant

TABLE I  
Force constants in millidynes/Ångstrom

$f_{da}/f_d$	Set	$f_d$	$f_{dd}$	$f_{da}-f_{da}'$	$f_a-f_{aa}$	$f_d-f_{aa}'$	$f_a$	$f_{aa}$	$f_{aa}'$	Frequency in $\text{cm}^{-1}$ (calculated)
0	A	3.114	0	1.188	.544	.989	...	...	...	386,119,139,491
	B	3.114	0	.273	.114	.130	.130	.016	0	
0.05	A	2.708	.135	1.158	.620	1.141	...	...	...	386,119,139,491
	B	2.708	.135	.059	.100	.102	.102	.002	0	
0.10	A	2.396	.240	1.086	.656	1.214	...	...	...	386,119,139,491
	B	2.396	.240	-.075	.111	.124	.124	.013	0	
0.15	A	2.148	.322	1.006	.673	1.248	...	...	...	386,119,139,491
	B	2.148	.322	-.149	.132	.165	.165	.033	0	
0.20	A	1.947	.389	.924	.680	1.261	...	...	...	386,119,139,491
	B	1.947	.389	-.193	.155	.213	.213	.058	0	
0.25	A	1.780	.445	.845	.680	1.261	...	...	...	386,119,139,491
	B	1.780	.445	-.218	.184	.26	.264	.083	0	
0.50	A	1.246	.623	.482	.529	1.159	...	...	...	386,119,139,491
	B	1.246	.623	-.190	.313	.528	.528	.215	0	

TABLE II  
Fundamental frequencies of  $\text{TiCl}_4$  molecule

Designation	Wave No	Degeneracy	Type
$\nu_1$	385	Nil	$A_1$
$\nu_2$	119	2	$E_g$
$\nu_3$	139	3	$T_2$
$\nu_4$	491	3	$T_2$

TABLE III

	C.F.	V.F.	G. (Guggenheimer, 1950)	Diatomic data
$f_a$	2.190	3.113	3.06	2.806
$f_a^d$	...	0.100	...	...

TABLE IV

Heat content, free energy, entropy, heat capacity of  $\text{TiCl}_4$  in gaseous state at 1 atmos pressure ( $\text{cal mole}^{-1} \text{degree}^{-1}$ )

$T(^{\circ}\text{K})$	$H^{\circ} - H_0^{\circ}$ $T^{\circ}$	$-F^{\circ} - H_0^{\circ}$ $T^{\circ}$	$S^{\circ}$	$C_p^{\circ}$
100	11.39	51.61	63.00	15.89
200	14.93	60.68	75.61	20.57
300	17.24	67.30	84.63	22.89
400	18.81	72.37	91.18	24.01
500	19.92	76.74	96.66	24.61
600	20.73	80.43	101.16	24.96
700	21.36	83.65	105.01	25.17
800	21.85	86.52	108.37	25.33
900	22.24	89.14	111.38	25.43
1000	22.56	91.51	111.07	25.51

The relevant results are tabulated in Table III. Considering the fact that the molecules could be represented by all these methods to various degrees of approximation, it is felt that the set nearest to the values in this table may represent a reliable set of force constants. So within the

limits cited above we are inclined to choose the set  $f_d = 2.708$ ,  $f_{dd} = 0.135$ ,  $f_{da} - f_{da'} = 0.05$ ,  $f_a = 0.102$ ,  $f_{aa} = 0.002$ ,  $f_{aa'} = 0$  as most probably representing the values of the force constants in  $\text{TiCl}_4$  molecule.

#### THERMODYNAMIC PROPERTIES

The heat content, free energy, entropy and heat capacity of  $\text{TiCl}_4$  molecule were calculated for temperatures ranging from  $100^\circ\text{K}$  to  $1000^\circ\text{K}$  to a rigid rotator, harmonic oscillator approximation. The values are for the ideal gaseous state at one atmosphere pressure. Using a Cl-Cl bond distance of  $3.61\text{\AA}$  and assuming tetrahedral angles, one obtains the moments of inertia as  $I_{xx} = I_{yy} = I_{zz} = 462$  at. wt. Angstrom units. The symmetry number for a pentatomic  $T_d$  type molecule is 12. Birge's (1941) values of the physical constants are used. Table II contains the degeneracies of fundamental frequencies. The calculated thermodynamic properties are given in Table IV.

#### ACKNOWLEDGMENT

The authors wish to thank Prof. K. R. Rao for his kind interest in the work.

#### REFERENCES

- Birge, R. T., 1941, *Rev. Mod. Phys.*, **13**, 233.  
 Guggenheimer, 1950, *Discussions of the Faraday Society*, **9**, 221.  
 Herzberg, G., 1940, *Infra-red and Raman Spectra of Polyatomic Molecules*, pps. 167, 182.  
 Ramakrishna Rao, V., 1949, *Ind. J. Phys.*, **23**, 535.  
 Ta-You-Wu, 1946, *Vibrational spectra and Structure of Polyatomic Molecules*, pp 233.  
 Voelz, F. L., Meister A. G., Cleveland F. F., 1951, *J. Chem. Phys.*, **19**, 1084.

# PROTON - PROTON SCATTERING AT 340 MEV

By C. C. BANERJEE

DEPARTMENT OF THEORETICAL PHYSICS, INDIAN ASSOCIATION FOR THE CULTIVATION  
OF SCIENCE, CALCUTTA-32

(Received for publication, March, 30, 1954)

**ABSTRACT.** The proton-proton scattering has been considered in this paper with an interaction which involves only the tensor part of the pseudoscalar interaction. The theoretical results have been compared with experimental data at 340 Mev. It is found that the tensor force alone can fairly explain the experimentally observed isotropy of scattering. It also explains qualitatively the independence of differential cross sections with energies of the incident particles.

## INTRODUCTION

The experiments on proton-proton scattering at high energies (105—390 Mev) show that the differential cross section is isotropic and is also independent of the energy of the incident protons. For low energy particles some anisotropy is noticeable particularly at small angles, this is due to the fact that at small energies the coulomb scattering which is anisotropic has a magnitude quite comparable with that of nuclear scattering.

The phenomenological studies of p-p scattering by Christian and Noyce (1950), Case and Pais (1950) and Jastrow (1951) are different attempts to explain the experimental observations, of the above, the 'hard core' model of Jastrow agrees most with the observed results. Jastrow assumes a hard-core for the singlet state only. At high energies (340 Mev) this repulsive core makes  $^1S$  phase shift negative and  $^1D$  phase shift positive and in consequence there is a rise in the differential cross section at  $90^\circ$  and a dip at  $40^\circ$ , whereas the contribution to the scattering by the triplet interaction is just the opposite, as such the two together give a flat curve. But no justification for the assumption of a hard-core for the singlet state only has been advanced by him though the idea of a repulsive core has been recommended by Kramers and Bethe (1935) from the viewpoint of saturation of nuclear forces. There is also much doubt as to how far such a model would meet relativistic requirements.

This paper attempts to show that only the tensor part of the pseudoscalar interaction can explain fairly the isotropy observed in p-p scattering experiments. The calculations have been carried out by Born approximation which is valid at the energy considered here.

## THE INTERACTION

The static potential obtained from symmetrical pseudoscalar meson theory based on weak coupling between nucleon and meson fields is given by

$$V_{ps} = -\frac{1}{3}(\tau_1\tau_2) \left[ (\sigma_1\sigma_2) + \left\{ \frac{3(\sigma_1r)(\sigma_2r)}{r^2} - (\sigma_1\sigma_2) \right\} \left\{ 1 + \frac{3}{\chi r} + \frac{3}{\chi^2 r^2} \right\} \right] \frac{e^{-\chi r}}{r} \cdot \frac{f^2}{4\pi} \quad \dots (1)$$

We consider in this paper the tensor part of the above interaction

$$V = -\frac{1}{3}(\tau_1\tau_2) S_{12} \left( 1 + \frac{3}{\chi r} + \frac{3}{\chi^2 r^2} \right) \frac{e^{-\chi r}}{r} \cdot \frac{f^2}{4\pi} \quad \dots (2)$$

$$\text{where } S_{12} \equiv \frac{3(\sigma_1r)(\sigma_2r)}{r^2} - (\sigma_1\sigma_2)$$

The amplitude of the scattered wave in Born approximation is,

$$C(\theta) = -\frac{M}{4\pi\hbar^2} \cdot \frac{f^2}{4\pi} \int e^{ikr \cos \theta'} \cdot \chi_{m_{S'}} \cdot S_{12} \cdot \chi_{m_S} \left( 1 + \frac{3}{\chi r} + \frac{3}{\chi^2 r^2} \right) \frac{e^{-\chi r}}{r} \cdot d\tau \quad \dots (3)$$

where

$$K = 2k \sin \theta/2$$

#### TENSOR FORCE OPERATOR $S_{12}$

To consider the effect of the tensor force operator  $S_{12}$  on the spin-dependent parts of the wave functions in case of p-p scattering let us consider a frame of reference as in figure 1. Let  $k\hbar n_0$  be the momentum of the incident proton in the centre of mass system and  $k\hbar n$  its momentum after scattering. The vectors  $n_0$  and  $n$  represent the unit vectors in the directions of initial relative motion and scattering respectively. We would consider  $n_0$  also as the axis of quantisation of the spin functions.

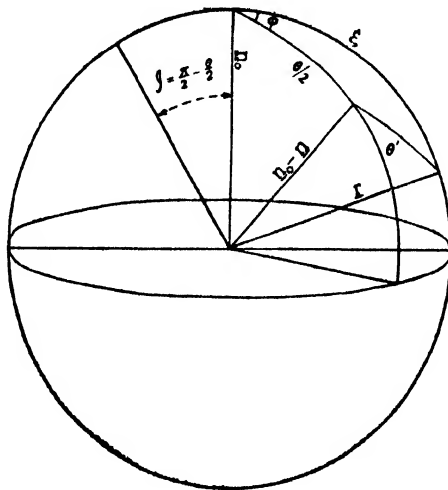


FIG. 1



The tensor force operator on triplet spin functions for various values of the magnetic quantum numbers yields the following matrix and on singlet spin function it gives zero.

$\begin{array}{c} ms' \\ \backslash \\ m \end{array}$	1	0	-1
1	$3 \cos^2 \xi - 1$	$3 \sqrt{2} \cos \xi \sin \xi e^{-i\phi}$	$3 e^{-2i\phi} \sin^2 \xi$
$(Amsms') = 0$	$3 \sqrt{2} \sin \xi \cos \xi e^{i\phi}$	$-2(3 \cos^2 \xi - 1)$	$-3 \sqrt{2} \sin \xi \cos \xi e^{-i\phi} \dots$
-1	$3 e^{2i\phi} \sin^2 \xi$	$-3 \sqrt{2} \cos \xi \sin \xi e^{i\phi}$	$3 \cos^2 \xi - 1$

The elements of the above matrix when considered in the direction of the scattered wave become

$\begin{array}{c} ms' \\ \backslash \\ ms \end{array}$	1	0	-1
1	$3 \sin^2 \theta/2 - 1$	$3 \sqrt{2} \sin \theta/2 \cos \theta/2 e^{-i\phi}$	$3 e^{-2i\phi} \cos^2 \theta/2$
$(Bmsms') = 0$	$3 \sqrt{2} \sin \theta/2 \cos \theta/2 e^{i\phi}$	$-2(3 \sin^2 \theta/2 - 1)$	$-3 \sqrt{2} \sin \theta/2 \cos \theta/2 e^{-i\phi}$
-1	$3 e^{2i\phi} \cos^2 \theta/2$	$-3 \sqrt{2} \sin \theta/2 \cos \theta/2 e^{i\phi}$	$3 \sin^2 \theta/2 - 1$

... (5)

Substituting the elements of the matrix (A) in equation (3) and performing the integration in each case and considering the effect in the direction of the scattered wave, we get, the scattered amplitude as,

$$C(\theta) = -\frac{M}{4\pi^2 \hbar^2} \cdot \frac{f^2}{4\pi} \int_0^\infty e^{iKr \cos \theta'} \cdot \frac{(3 \cos^2 \theta' - 1)}{2} \cdot (3 \sin^2 \theta'/2 - 1) \cdot \left( 1 + \frac{3}{\chi r} + \frac{3}{\chi^2 r^2} \right) e^{-\chi r} dr$$

$$= -\frac{M}{4\pi^2 \hbar^2} \cdot \frac{f^2}{4\pi} \int_0^\infty e^{iKr \cos \theta'} \cdot \frac{(3 \cos^2 \theta' - 1)}{2} \cdot (Bmsms) \cdot \left( 1 + \frac{3}{\chi r} + \frac{3}{\chi^2 r^2} \right) \frac{e^{-\chi r}}{r} \cdot r^2 dr d(\cos \theta') \dots (6)$$

The amplitude and hence the intensity in scattering in the triplet state does not depend on  $\phi$  as during integration and averaging such terms vanish. Since the diagonal elements of the above matrix vanish, Askin and Wu (1948) have considered the average of their squares while Rosenfield in discussing the saturation properties of nuclear forces considers the average value of  $S_{12}$  as  $(3 \cos^2 \xi - 1)$ . We would follow the former in our discussion.

$$C(\theta) = -\frac{M}{4\pi^2 \hbar^2} \cdot \frac{f^2}{4\pi} \cdot \frac{2\pi}{2} \cdot (Bmsms) \int_0^\infty e^{iKr \cos \theta'} \cdot (3 \cos^2 \theta' - 1) \cdot \left( 1 + \frac{3}{\chi r} + \frac{3}{\chi^2 r^2} \right) \frac{e^{-\chi r}}{r} \cdot r^2 dr d(\cos \theta')$$

$$\begin{aligned}
 &= -\frac{M}{4\pi\hbar^2} \cdot \frac{f^2}{4\pi} \cdot \frac{2\pi}{2} \cdot (B_{msms}) \int_0^\infty (-4) \left\{ \frac{3(\sin Kr - Kr \cos Kr)}{(Kr)^3} - \frac{\sin Kr}{Kr} \right\} \\
 &\quad \times \left\{ 1 + \frac{3}{\chi r} + \frac{3}{\chi^2 r^2} \left\{ \frac{e^{-\chi r}}{r} \cdot r^2 \cdot dr \right. \right. \\
 &= \frac{Mf^2}{4\pi\hbar^2} \cdot (B_{msms}) \cdot \frac{K^2}{\chi^2} \cdot \frac{1}{K^2 + \chi^2} \quad \dots (7)
 \end{aligned}$$

Since we have considered a potential which involves a tensor force operator without any central force term there is evidently no contribution to the singlet scattering. In case of triplet p-p scattering the charge is symmetric and the spin functions are symmetric and hence the spatial functions involved in the expression for scattered amplitude must be antisymmetric and since we do not know anything about the nature of polarisation of the interacting particles, the differential cross section is given by

$$\begin{aligned}
 \sigma(\theta) &= \frac{1}{9} \cdot \frac{3}{4} \cdot S [C^2(\theta) + C^2(\pi - \theta) + C(\theta)C(\pi - \theta)] \left( \frac{Mf^2}{4\pi\hbar^2} \right)^2 \\
 &= \frac{1}{2} \cdot \frac{3}{4} \cdot S \cdot \left( \frac{Mf^2}{4\pi\hbar^2} \right)^2 \cdot \frac{1}{\lambda^4} \left[ \left( \frac{4k^2 \sin^2 \theta/2}{4k^2 \sin^2 \theta/2 + \lambda^2} \right)^2 + \left( \frac{4k^2 \cos^2 \theta/2}{4k^2 \cos^2 \theta/2 + \lambda^2} \right)^2 \right. \\
 &\quad \left. + \left( \frac{4k^2 \sin^2 \theta/2}{4k^2 \sin^2 \theta/2 + \lambda^2} - \frac{4k^2 \cos^2 \theta/2}{4k^2 \cos^2 \theta/2 + \lambda^2} \right)^2 \right] \quad \dots (8)
 \end{aligned}$$

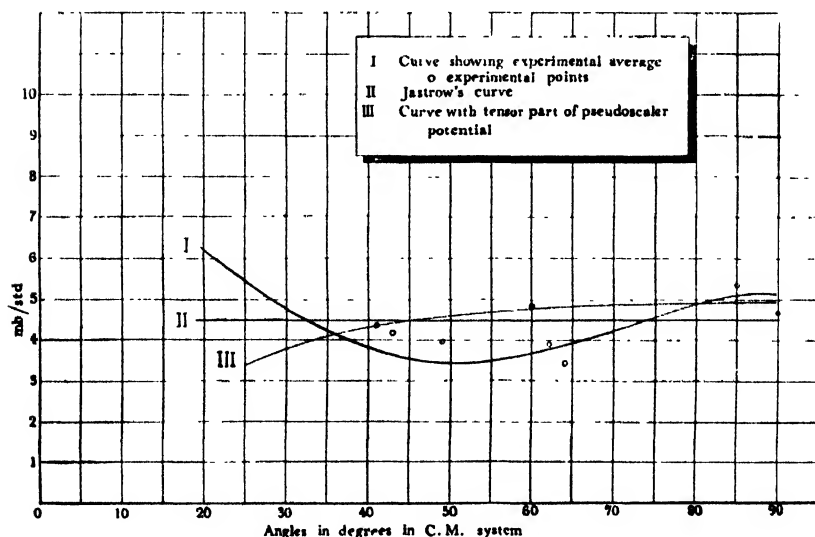


FIG. 2

Curve I is the experimental curve for 340 Mev. o, Experimental points.

Curve II is Jastrow's curve for 340 Mev.

Curve III is theoretical curve for 340 Mev computed from (8).

The computed magnitudes of the differential cross sections from equation (8) for 340 Mev are given in Table I and a curve has been drawn to represent them along with the experimental curve at this energy. We have given here also Jastrow's curve for comparison.

TABLE I

Angles in degrees in the centre of wave system	25°	30°	40°	50°	60°	70°	80°	90°
$\sigma(\theta)$ in mb/std for 340 Mev. as computed from (8)	3.51	3.83	4.31	4.50	4.75	5.87	4.90	4.92

## DISCUSSION

A study of the computed values of differential cross sections and of the corresponding curve shows that the differential cross sections exhibit isotropy well within the variation admissible by the experimental errors. Agreement is fairly quantitative for the energy considered with an average value of 4.46 mb/std as against the experimental average 4.5 mb/std (Chamberlain and Wiegand, 1950). As the energy of the incident particles becomes smaller and smaller the magnitude of the differential cross sections given by (8) diminishes due to the decreasing contributions of the nuclear scattering and the experimental high value is primarily due to coulomb scattering.

At high energy where  $X^2/K^2$  can be neglected in comparison with unity the theoretical average value of the differential cross sections from (8)

is  $2 \left( \frac{Mf^2}{4\pi h^2} \right)^2 \cdot \frac{1}{X^4}$ . This is independent of the energy of the incident particles as required by experiments. The computed magnitude of this expression comes to 5.55 mb/std which is about 20% higher than the experimental average.

The author (1953) has studied previously the p-p scattering at high energies for the complete pseudoscalar potential and found that the differential cross sections show a tendency towards qualitative isotropy at large angles (60° and above) due to the predominance of the tensor force contributions over those of the central force. At small angles, however, the cross sections were found to be strongly dependent on angles due to relative importance of the central force term and as a result the differential cross sections exhibited anisotropy even at high energies. Banerjee (1953)

has also considered the p-p scattering with  $S_{12} \frac{e^{-\pi r}}{x r^2}$  and  $S_{12} \frac{e^{-\pi r}}{x^2 r^3}$  as poten-

tials of the interacting particles. He has found that the latter potential which contains  $1/r^3$  singularity shows a better tendency towards qualitative isotropy at higher energies. We, however, observe in this paper that the sum of the potentials involving  $1/r$ ,  $1/r^2$  and  $1/r^3$  singularities, which occur in the tensor part of the pseudoscalar interaction, gives better results and the agreement with the experimental results at 340 Mev is not only qualitative but also fairly quantitative.

In our calculations we have taken the value of  $\frac{f^2}{hc} = .7$  which has been obtained after normalising the value of total n-p scattering cross section at 90 Mev determined experimentally by Fox, Leith and others (1950). The experimental data which we have considered in this paper belong to Chamberlain and Wiegand (1950).

### CONCLUSION

The p-p scattering cross section, as calculated from the simple Yukawa interaction, depends too strongly on the scattering angle, as such this potential alone or in combination with the tensor force term cannot explain isotropy of p-p scattering as experimentally observed. The tensor force term  $S_{12} \frac{e^{-\mu r}}{r}$

multiplied by the factor  $\left(1 + \frac{3}{\chi r} + \frac{3}{\chi^2 r^2}\right)$  gives better isotropy of scattering than any of the interaction  $S_{12} \frac{e^{-\chi r}}{r}$ ,  $S_{12} \frac{e^{-\chi r}}{\chi^2 r^2}$  and  $S_{12} \frac{e^{-\chi r}}{\chi^2 r^3}$  individually.

### ACKNOWLEDGMENT

The author expresses his sincere thanks to Dr. D. Basu, Ph.D., for his kind suggestion of the problem and helpful guidance throughout the progress of the work

### REFERENCES

- Askin J. and Wu, T., 1948, *Phys. Rev.*, **73**, 973.  
 Banerjee, C. C., 1953, *Ind. J. Phys.*, **27**, 173.  
 Banerjee, P., 1953, *Ind. J. Phys.*, **27**, 557.  
 Bethe, H. A. and Kramers, H. A., 1935, Ann. Arbor Summer Physics Symposium.  
 Case, K. M. and Pais, A., 1950, *Phys. Rev.*, **80**, 263.  
 Chamberlain and Wiegand, 1950, *Phys. Rev.*, **79**, 81.  
 Christian, R. S. and Novce, H. P., 1950, *Phys. Rev.*, **79**, 85.  
 Fox, Leith, Wouters and Mackenzie, 1950 *Phys. Rev.*, **80**, 23; 1951, *Phys. Rev.*, **81**, 165.  
 Jastrow, R., 1951, *Phys. Rev.*, **81**, 165; 1950, **79**, 389.

# ON THE KINETIC ENERGY OF FISSION-FRAGMENTS FROM $U^{235}$ .

By G. P. DUBE AND LAL SAHEB SINGH

UNIVERSITY DEPARTMENT OF PHYSICS, PATNA UNIVERSITY, PATNA

(Received for publication March, 29, 1954)

**ABSTRACT.** In the present paper it has been shown that Fermi's semi-empirical mass-formula used for the estimation of kinetic energy of fission-fragments gives values less than the observed ones by about 30 Mev. Applying a suitable correction-term based on Duckworth's recent mass-spectrographic measurements the kinetic energy of fission fragments has been estimated to be 171.2 Mev which agrees with the recent measurement of 167.1 Mev.

## INTRODUCTION

Several attempts have been made to measure the total energy released in the fission of uranium nucleus (Turner, 1940). The value of the total kinetic energy of the recoiling nuclei calculated from total ionization has been reported to be 175 Mev per fission (Henderson, 1939) while the American Physical Society at its Pittsburgh meeting gave a result of 180 Mev per fission (Henderson, 1940a). Application of various corrections has changed the value to  $177 \text{ Mev} \pm 1 \%$  per fission.

Calorimetric method was employed to measure the heat produced in fission and this has given the weighted average of  $177 \pm 5 \text{ Mev}$  per fission, for the kinetic energy of fission-fragments (Henderson, 1940b). The result has the probable error of about 1 %. All the delayed beta particles produced by numerous radioactive substances created in the fission-process also contributed to total heating and this amounted to nearly 12 Mev. Thus the true recoil energy of fission-fragments from calorimetric method is 165 Mev. This calculation cannot be an accurate one. Kanner and Barschall (1940) have found the value 160 Mev by measuring the energy of individual members of the pairs of fission-fragments. This has been revised to 165 Mev.

Kinetic energies of paired fission-fragments have also been measured recently (Brunton and Hanna, 1949). Through the analysis of ionization data obtained from careful measurements of fission-fragments by Brunton et al (1949, 1950) and by Deutsch and Ramsay (1946) with double ionization chamber, the value reported on the average kinetic energy of the fragments is 154.7 Mev. The large variations in measured kinetic energy have been shown to be due to variation in number of neutrons emitted per fission (Way and Wigner, 1948) and due to variation in nuclear charges of primary fragments (Brunton, 1949). It has also been shown that fission-fragments, stopped in a

gas, spend large averages of energy per ion-pair than alpha particles stopped in the same gas and as such ionization experiments based on the alpha particles of known energy give low energy-values for the fission-fragments.

Leachman (1952) has measured the velocity distribution of fragments from slow neutron-induced fission by a time-of-flight method. His velocity data indicate that the kinetic energies of the fragments exceed those reported by ionization chamber measurements by 5.7 Mev for the most probable light and by 6.7 Mev for the most probable heavy fragments. His corrected value is 167.1 Mev.

Since mass-spectrographic data in the region of heavy and medium heavy elements are not very precise, it is worthwhile examining the validity of semi-empirical atomic mass-formula in the estimation of kinetic energy of fission-fragments.

The Fermi's semi-empirical mass-formula (1950) has been utilised here for the computation of kinetic energy of fission-fragments from  $U^{235}$ . This gives results which are lower than the observed ones by about 30 Mev. This Fermi's formula gives error in masses of the order of 5 Mev for  $A=50$  to 19 Mev for  $A=200$  (Raymond, 1952). By a careful examination of the mass data (Duckworth, 1950) it has been possible to find a correction term to Fermi's mass-formula which fits in well with the experimental data (Dube and Singh, 1953). The semi-empirical mass-formula with the new correction-term has been utilised here to calculate the kinetic energy of fission-fragments with a view to judging its reliability.

#### CORRECTION TO FERMI'S SEMI-EMPIRICAL MASS-FORMULA

Fermi's semi-empirical mass-formula is

$$M(A, Z) = 0.99391A - 0.00055Z + 0.014A^{2/3} + 0.083 \frac{(A/2 - Z)^2}{A} \\ + \frac{0.00627Z^2}{A^{1/3}} + \delta(A, Z) \quad (1)$$

where

$\delta(A, Z) = 0$  for  $A$  odd

$$= \mp \frac{0.036}{A^{3/4}} \text{ for } A \text{ even } \begin{cases} Z \text{ even} \\ Z \text{ odd} \end{cases}$$

$M(A, Z)$  is the mass of an atom of mass-number  $A$  and atomic-number  $Z$ .

The correction-term in the region of medium heavy mass number based on Duckworth's recent mass measurements (Duckworth, 1950) has been found to be (Dube and Singh, 1953).

$$\Delta m = -(0.0006A^{1.2} - 0.00042Z^{1.5} - 0.0290) \quad (2)$$

where  $\Delta m$  is the correction to atomic masses in M. U.

The mass of  $U^{235}$  is known from the spectrographic mass of  $Pb^{206}$  and  $U^{235} - Pb^{206}$  mass difference (Duckworth, 1951, 1952)

$$M(235,92) = 235.1156 \pm .0010.$$

This value calculated by Stern (1949) by the radioactive data differs from the recent one by about 1.5 Mev and as such is not taken for present calculation.

#### KINETIC ENERGY OF FISSION-FRAGMENTS

The total energy-release in fission is made up of the following :

- (a)  $E_k$ , the kinetic energy of the two fission-fragments
- (b)  $E_p$ , the kinetic energies of prompt neutrons and gamma rays.
- (c) Binding energy of prompt neutrons.

That is, 
$$E_p = E_k + E_x \quad \dots (3)$$

where  $E_p$  = prompt fission-energy associated with all possible pairs of charges ; and  $E_x$  is the excitation-energy of primary fragments =  $E_p$  + binding energy of prompt neutrons.

whence  $E_k$  is equal to  $E_p - E_x \quad \dots (3a)$

For fission in  $U^{235}$ , the prompt fission-energy  $E_p$  is given by Brunton (1949)

$$E_p = M(235,92) + M_n - [M(A_L, Z_L) + M(A_H, Z_H)] \text{ M. U.} \quad \dots (3b)$$

where  $M(A_L, Z_L)$  = mass of light fragments of mass-number  $A_L$  and charge  $Z_L$ .

$M(A_H, Z_H)$  = mass of heavy fragments of mass-number  $A_H$  and atomic-number  $Z_H$ .

Equation (3b) gives the value of  $E_k$  if the neutron binding-energy is known. We can readily calculate the neutron binding-energy  $B_n$  for the nucleus  $(A+1, Z)$  from Fermi's mass-formula.

$$B_n(A+1, Z) \text{ in Mev.} = 931 [M(A, Z) + M_n - M(A+1, Z)] \quad \dots (4)$$

where  $M_n$  = mass of the neutron = 1.00898 M. U.

$$B_n(A+1, Z) \text{ Mev} = 0.931 [15.04 + 14 \{A^{2/3} - (A+1)^{2/3}\} + 83 \left\{ -\frac{(A/2 - Z)^2}{A} - \frac{\{(A+1)/2 - Z\}^2}{A+1} \right\} + 0.627 Z^2 \{A^{-1/3} - (A+1)^{-1/3}\} + \delta] \quad \dots (4a)$$

where 
$$\delta = \mp \frac{36}{A^{3/4}} \text{ for } A \text{ even} \begin{cases} Z \text{ even} \\ Z \text{ odd} \end{cases}$$

$$= \pm \frac{36}{A^{3/4}} \text{ for } A \text{ odd} \begin{cases} Z \text{ even} \\ Z \text{ odd} \end{cases}$$

The mean value of  $E_x$  is about 20 Mev (Brunton) and is estimated as follows :

the average value of neutron kinetic energy per fission	= 5 Mev.
(Glendemin, 1949)	
The average value of prompt gamma-rays per fission	= 4.6 Mev.
the mean value of neutron binding energy per fission calculated from (4a)	≈ 12.4 Mev.
<b>Total.</b>	<b>... ≈ 22 Mev.</b>

# ELECTRON CAPTURE BY IONS PASSING THROUGH GASES

By N. C. SIL

DEPARTMENT OF THEORETICAL PHYSICS, INDIAN ASSOCIATION FOR THE CULTIVATION OF SCIENCE, JADAVPUR, CALCUTTA-32.

*(Received for publication, March 30, 1954)*

**ABSTRACT**--The cross section for the capture in different excited  $s$ -states of an electron by an ion passing through gaseous matter has been evaluated ; the method followed is an extension to that of Brinkman and Kramers. It is found that the first term of the series obtained here for the  $1s$ - $ns$  capture agrees with Brinkman and Kramers' approximate result.

## INTRODUCTION

The importance of the problem of the capture of an electron by an ion passing through gaseous matter has, of late, increased in view of its application to the explanation of some of the lines emitted by solar corona (Saha, 1942) and aurora borealis (Fan and Meinel, 1953). The theoretical study in this line has been mainly done by Oppenheimer (1928), Brinkman and Kramers (1930), Massey and Smith (1933), Saha and Basu (1945), Jackson and Schiff (1953) and others. Brinkman and Kramers have considered in detail the case in which an ion captures in its  $1s$  orbit an electron which was originally in the  $1s$  orbit of the atom constituting the gaseous matter. The present work is an extension of the theoretical investigation of Brinkman and Kramers for the more general case of capture of the electron in excited orbits. The necessity of considering the cross section of capture of electrons to excited orbits arises from the suggestion of Saha (1942) to explain the origin of He-lines in the spectrum of the chromosphere. In it we notice, in addition to the extremely strong neutral helium lines, the well-known line of ionised helium  $\lambda$  4686Å whose appearance is unexpected in view of the fact that this line has an excitation potential of nearly 75.25 volts while the ordinary excitation of the chromosphere is 9 to 14 volts. The occurrence of this latter line has been explained by assuming that high velocity  $\alpha$ -particles generated in the solar body due to some nuclear process get slowed down by losing energy through ionisation. After being considerably slowed down they begin to capture electrons in excited orbits which jump back to lower orbits emitting the well-known lines of ionised helium. The capture problem is expected to play an important role in explaining the spectrum of aurora borealis. The aurora borealis is most likely to be excited by high-speed ions penetrating into the upper atmosphere. Meinel (1951) detected a violet Doppler wing on



H $\alpha$  line extending to an energy greater than 57 Kev thus proving the existence of protons as one of those causing the excitation. A preliminary experiment by Meinel and Fan (1952) using accelerated protons with rarefied air sample, showed a striking similarity between the laboratory spectrum and that of the aurora.

## DERIVATION OF THE RESULT

The type of collision considered in this paper comes under the general head of rearrangement collisions because here the electron initially attached to one hydrogen-like atom of charge  $Ze$  forms finally another hydrogen-like atom of charge  $Z'e$  by simple rearrangement. The differential cross section of a general binary collision, in which a system  $A$  in state  $m$  collides with a system  $B$  in state  $n$  to form systems  $C$  in state  $s$  and  $D$  in state  $t$ , has been derived (Schiff, 1949) using the first Born approximation. In our problem, of the two initial systems, one is a hydrogen-like atom with charge  $Ze$  and mass  $AM$  of the nucleus to which an electron of charge  $-e$  and mass  $m$  is bound in the  $n, l, m$  orbit and the other is a free particle with charge  $Z'e$  and mass  $A'M$  moving with the velocity  $\mathbf{v}$  with respect to the atom; the final systems are respectively a hydrogen-like atom with charge  $Z'e$  and mass  $A'M$  of the nucleus, the electron being in the  $n', l', m'$  orbit, and a free particle with charge  $Ze$  and mass  $AM$  relative to which the atom moves with a velocity  $\mathbf{v}'$ . Figure 1 gives us the co-ordinate system for our collision process.

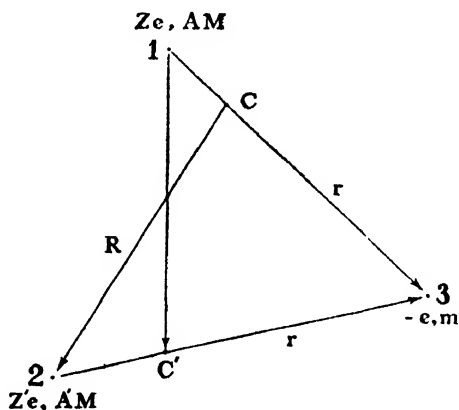


Figure 1. Co-ordinate system. The points marked  $C$  and  $C'$  are centres of mass of the initial and final atoms.

Following the calculations given in L. I. Schiff's 'Quantum Mechanics', we get the differential cross section for capture of the electron in the final  $n, l', m'$  state from the initial  $n, l, m$  state as in Jackson and, Schiff's paper (1953) viz,

$$\frac{dQ}{d\Omega} = \left( \frac{\mu f}{2\pi\hbar^2} \right) \left( \frac{v'}{v} \right) |I|^2, \quad (1)$$

$$\text{with } I = \int \exp(-i\mathbf{K}' \cdot \mathbf{R}') \psi_{n',l',m'}^*(\mathbf{r}') V \exp(i\mathbf{K} \cdot \mathbf{R}) \psi_{n,l,m}(\mathbf{r}) d\tau_r d\tau_{R'}, \quad (2)$$

where  $\psi_{n,l,m}(\mathbf{r})$  is the normalised initial state wave-function for the electron in atom  $Z$  and  $\psi_{n',l',m'}^*(\mathbf{r}')$  is the normalised final state wave function for the electron in the atom  $Z'$ ,

$$\left. \begin{aligned} (h/2\pi)\mathbf{K} &= \mu_i \mathbf{v} \\ (h/2\pi)\mathbf{K}' &= \mu_f \mathbf{v}' \end{aligned} \right\}, \quad (3) \quad \left. \begin{aligned} \mu_i &= A'M(A'M+m)/(A+A')M+m \\ \mu_f &= AM(A'M+m)/(A+A')M+m \end{aligned} \right\}, \quad (4)$$

and  $V$  is the perturbation Hamiltonian.

Using as the independent coordinates  $\mathbf{r}, \mathbf{r}'$  instead of  $\mathbf{r}, \mathbf{R}$  we may write

$$I = \int \exp(-i\mathbf{C} \cdot \mathbf{r}') \psi_{n',l',m'}^*(\mathbf{r}') V(\mathbf{r}, \mathbf{r}') \exp(i\mathbf{B} \cdot \mathbf{r}) \psi_{n,l,m}(\mathbf{r}) d\tau_r d\tau_{r'}, \quad (5)$$

$$\text{where } \mathbf{C} = \mathbf{K} - \frac{A'M}{A'M+m} \mathbf{K}' \text{ and } \mathbf{B} = \frac{AM}{A'M+m} \mathbf{K} - \mathbf{K}'. \quad (6)$$

The perturbation Hamiltonian consists of two parts ; (1) the Coulomb interaction between the electron and the incident particle and (2) the Coulomb interaction between the nucleus and the incident particle. Brinkman and Kramers (1930) considered only the first term neglecting the second one in their calculation of capture cross section for electrons from initial  $1s$  orbit to final  $1s$  orbit. Saha and Basu (1945) extended the method of Brinkman and Kramers to calculate the capture of electron from  $1s$  to  $2p$  orbit. It has been mentioned by Jackson and Schiff (1953) that in an exact calculation, the second term in the perturbation Hamiltonian would have actually a negligible contribution ; however, they claim that better results are obtained by taking into consideration the contribution of the second term which is no longer negligible when the calculations are based on the approximate method of Born. Here we shall follow Brinkman and Kramers, and shall carry out the calculation for the capture of electron in the final  $ns$  state from initial  $1s$  state by the first of the two alternative methods given by them.

As the perturbation potential we may take either the initial perturbation

$$V_i = -\frac{Z'e^2}{r'} \text{ or the final perturbation } V_f = -\frac{Ze^2}{r}. \text{ However, it has been proved}$$

by Jackson and Schiff (1953) that in the first Born approximation the ambiguity in the choice of the perturbation potential does not lead to any ambiguity in the result for the transition probability. They show that when  $V = V_i$

$$I = - \left( \frac{(h/2\pi)^2 C^2}{2m_f} + \epsilon_f \right) \phi_{n,l,m}(\mathbf{B}) \phi_{n',l',m'}^*(\mathbf{C}), \quad (7a)$$

and for  $V = V_f$

$$I = - \left( \frac{(h/2\pi)^2 B^2}{2m_i} + \epsilon \right) \phi_{n,l,m}(\mathbf{B}) \phi_{n',l',m'}^*(\mathbf{C}), \quad (7b)$$

where  $m_i$  and  $m_f$  are the reduced masses of the electron when attached to the atoms  $Z$  and  $Z'$  respectively

$$m_i = \frac{AMm}{AM+m} \text{ and } m_f = \frac{A'Mm}{A'M+m}, \quad (8)$$

$$\phi_{n,l,m}(\mathbf{B}) = \int \exp(i\mathbf{B} \cdot \mathbf{r}) \psi_{n,l,m}(\mathbf{r}) d\tau_r \quad (9)$$

$$\phi'_{n',l',m'}(\mathbf{C}) = \int \exp(i\mathbf{C} \cdot \mathbf{r}') \psi'_{n',l',m'}(\mathbf{r}') d\tau_{r'}$$

and  $\epsilon$ ,  $\epsilon'$  are the binding energies of the electron in atoms  $Z$  and  $Z'$  respectively.

Now from the conservation of energy requirement *viz.*,

$$\frac{1}{2} \mu_i v^2 - \epsilon - \frac{1}{2} \mu_f v'^2 - \epsilon',$$

we get with the help of equations (4), (6) and (8)

$$\frac{(h/2\pi)^2 C^2}{2m_f} + \epsilon' = \frac{h^2 B^2}{2m_i} + \epsilon \quad (10)$$

Hence  $l = l'$ .

The evaluation of  $\phi_{n,l,m}(\mathbf{K})$  for a hydrogen-like atom with charge  $Ze$  of the nucleus has been done by Podolsky and Pauling (1929):

$$\begin{aligned} \phi_{n,l,m}(\mathbf{K}) = & \left\{ \frac{1}{(2\pi)^{1/2}} e^{im\beta} \left\{ \left( \frac{(2l+1)(l-m)!}{2(l+m)!} \right)^{1/2} P_l^m(\cos\alpha) \right\} \right. \\ & \left. - (i)^l \pi^{1/2} 2^{2l+4} l! \left( \frac{n(n-l-1)!}{(n+l)!} \right)^{-1} \frac{\zeta^{l+1}}{(\zeta^2+1)^{l+3/2}} C_{n-l-1}^{l+1} \left( \frac{\zeta^2-1}{\zeta^2+1} \right) \right\}, \quad (11) \end{aligned}$$

where  $K$ ,  $\alpha$ ,  $\beta$  are the polar co-ordinates of  $\mathbf{K}$ ,

$\zeta = \frac{K}{\gamma_n}$  with  $\gamma_n = \frac{Z}{na} = \frac{Ze^2 m^*}{n\hbar^2}$ ,  $m^*$  being the reduced mass of the electron in

the atom, and  $C_q^p$  is the Gegenbaur function which may be defined by the generating function

$$Q \equiv (1-2ut+u^2)^{-p} = \sum C_q^p(t) u^q, \quad (12)$$

$$u < 1$$

Hence from (1), (7) and (11), the differential cross section is known in general for capture of the electron in any final state from any initial state.

From (11) we have in particular

$$\begin{aligned} \phi_{1,0}(\mathbf{B}) &= -8\pi^{1/2} \gamma_1^{5/2} (B^2 + \gamma_1^2)^{-2} \\ \phi_{n,0}(\mathbf{C}) &= -8\pi^{1/2} \gamma_n^{5/2} (C^2 + \gamma_n^2)^{-2} C_{n-1}^1 \left( \frac{C^2 - \gamma_n^2}{C^2 + \gamma_n^2} \right), \quad (13) \end{aligned}$$

$$\text{where } \gamma_1 = \frac{Z}{a_o} \quad \text{with} \quad a_o = \frac{\hbar^2}{m_i e^2} \quad (14)$$

$$\text{and } \gamma_n = \frac{Z'}{na'_o} \quad \text{with} \quad a'_o = \frac{\hbar^2}{m_f e^2} \quad \Bigg\}$$

With the help of (7) and (10) we get

$$I = 2^{\frac{1}{2}} \pi \hbar^2 \frac{m_f}{m_i^{\frac{1}{2}}} \gamma_1^{5/2} \gamma_n^{5/2} (C^2 + \gamma_n'^2)^{-3} C_{n-1}^1 \left( \frac{C^2 - \gamma_n'^2}{C^2 + \gamma_n'^2} \right) \quad (15)$$

To get the total cross section we require the integral of  $|I|^2$  over all directions of orientation of the solid angle  $\Omega$ . Now  $C_{n-1}^1(\cos \Theta)$  is the coefficient of  $u^{n-1}$  in the expansion of  $(1 - 2u \cos \Theta + u^2)^{-1}$  when  $u < 1$ . (cf. eqn. (12)).

Hence

$$\{C_{n-1}^1(\cos \Theta)\}^2 = \left\{ \frac{\sin n\Theta}{\sin \Theta} \right\}^2 = 2 \sum_{r=0}^{n-1} (-)^r \frac{n^2(n^2-1^2)\dots(n^2-r^2)}{\{2(r+1)\}!} (2 \sin \Theta)^2 \quad (16)$$

Putting

$$\frac{C^2 - \gamma_n'^2}{C^2 + \gamma_n'^2} = \cos \Theta = 1 - 2x, \quad (17)$$

we have

$$\lambda = \frac{\gamma_n'^2}{C^2 + \gamma_n'^2} = \frac{1 - \cos \Theta}{2} \quad (18)$$

$$x(1-x) = \frac{(C^2 - \gamma_n'^2)^2}{(C^2 + \gamma_n'^2)^2} = \frac{1}{4} \sin^2 \Theta, \quad (19)$$

and from (6)

$$d\lambda = -2\lambda K K' \frac{\gamma_n'}{(C^2 + \gamma_n'^2)^2} \sin \theta d\theta, \quad (20)$$

where  $\lambda = A'M/(A'M + m)$  and  $\theta$  is the angle between  $\mathbf{K}$  and  $\mathbf{K}'$ . Thus utilising the above results we get from (15),

$$2\pi \int_0^\pi |I|^2 \sin \theta d\theta = \frac{2^{10} \pi^3 \hbar^4 m^2 r \gamma_1^{5/2}}{\lambda K K' m_i^4 \gamma_n'^{5/2}} \sum_{r=0}^{n-1} \int_{x(\theta=\pi)}^{x(\theta=0)} S_r(O, n) x^{1+r} (1-x)^r d\lambda, \quad (21)$$

$$\text{with} \quad S_r(O, n) = (-)^r 2^r \frac{n^2(n^2-1^2)\dots(n^2-r^2)}{\{2(r+1)\}!} 4^{2r}. \quad (22)$$

Under the usual condition

$$\begin{aligned} K &\simeq \lambda K' \gg \gamma_n' \\ &\gg |K - \lambda K'| \end{aligned} \quad (23)$$

Then from (18) and (6) we have

$$x(\theta=\pi) = \frac{\gamma' n^2}{(K + \lambda K')^2 + \gamma' n^2} \approx 0$$

and

$$x(\theta=0) = x_0 = \frac{\gamma' n^2}{(K - \lambda K')^2 + \gamma' n^2} \approx \gamma' n^2 / \left\{ \frac{1}{2} (\gamma_1^2 + \gamma'^2) + \pi^2 \sigma^2 + \frac{(\gamma_1^2 - \gamma' n^2)^2}{16\pi^2 \sigma^2} \right\}, \quad (\text{vide appendix}) \quad (24)$$

with

$$\sigma = \frac{mv}{h}.$$

For the evaluation of the integral in the right hand side of the eqn. (21), we may note that  $\int_0^{x_0} x^{4+r} (1-x)^r dx$  is the incomplete beta-function  $B_{x_0}^1(5+r, 1+r)$  the numerical value of which can be obtained easily.

Now since  $m \ll M$  we may write  $\mu_f \approx \mu_1$ ,  $m_f \approx m_1 \approx m$ ,  $\lambda \approx 1$ , and  $a'_0 \approx a_0$ . Hence from (1) & (21) the total capture cross section from 1s orbit to ns orbit is given by

$$Q = 2^8 \pi \frac{e^4}{(h/2\pi)^2 v^2 a_0^2} \left( \frac{nZ}{Z'} \right)^5 \sum_{r=1}^{n-1} S_r(O, n) B_{x_0}(5+r, 1+r). \quad \dots \quad (25)$$

### DISCUSSION

The expression given by B. K. for the 1s-ns capture cross section is approximate being only the first term of our series in eqn. (25). In fact the contribution of the other terms of the series is not at all negligible for low energy of the incident particle. However, for very high energy of the incident particle the result on the basis of our expression differs very little from that of B. K., the main contribution being due to the first term. Thus at high energies of the incident particle we have an inverse  $n^3$  law for the capture cross section as given also by Oppenheimer.

### APPENDIX

To prove

$$\gamma' n^2 + (K - \lambda K')^2 \approx \frac{1}{2} (\gamma_1^2 + \gamma' n^2) + \pi^2 \sigma^2 + \frac{(\gamma_1^2 - \gamma' n^2)^2}{16\pi^2 \sigma^2},$$

we have from (3) and (4)

$$(K - \lambda K')^2 = \frac{4\pi^2}{S^2} \left\{ \frac{AM \cdot A'M}{h} (v - v') + A'M\sigma \right\}^2$$

where

$$S = (A + A')M + m$$

and

$$-- \quad mv$$

From (10) we may write with the help of (3), (4), (6) and (14),

$$\begin{aligned} \gamma'^2 + \frac{4\pi^2}{S^2} \left\{ \frac{AM.A'M}{h} (v-v') + A'M\sigma \right\}^2 \\ = \gamma_1^2 + \frac{4\pi^2}{S^2} \left\{ \frac{AM.A'M}{h} (v-v') - AM \cdot \frac{mv}{h} \right\}^2 \\ \approx \gamma_1^2 + \frac{4\pi^2}{S^2} \left[ \left\{ \frac{AM.A'M}{h} (v-v') + A'M\sigma \right\} - S\sigma \right]^2 \end{aligned}$$

upto the first order of approximation. We take  $(v-v')/v$  and  $m/M$  as small quantities of the first order.

Then

$$\frac{2\pi}{S} \left\{ \frac{AM.A'M}{h} (v-v') + A'M\sigma \right\} = \frac{\gamma_1^2 - \gamma'^2}{4\pi\sigma} + \pi\sigma.$$

Hence follows the result.

#### ACKNOWLEDGMENT

The author is thankful to Dr. D. Basu for suggesting the problem and for his kind help and guidance during the progress of the work.

#### REFERENCES

- Brinkman, H. C. and Kramers, H. A., 1930, *Proc. Amst.*, **33**, 973.  
 Fan, C. Y. and Meinel, A. B., 1953, *Astrophys. Jour.*, **118**, 205.  
 Jackson, J. D. and Schiff, H., 1953, *Phy. Rev.*, **89**, 359.  
 Massey, H. S. W. and Smith, R. A., 1933, *Proc. Roy. Soc. (London)*, **A 142**, 142  
 Meinel, A. B., 1951, *Astrophys. Jour.*, **113**, 50  
 Meinel, A. B., and Fan, C. Y., 1952, *Astrophys. Jour.*, **115**, 330.  
 Oppenheimer, J. R., 1928, *Phys. Rev.*, **31**, 349.  
 Podolsky, B. and Pauling, L., 1929, *Phys. Rev.*, **34**, 109.  
 Saha, M. N., 1942, *Proc. Nat. Inst. Sc.*, **8**, 99.  
 Saha, M. N. and Basu, D., 1945, *Ind. J. Phys.*, **19**, 121.  
 Schiff, L. I., 1949, *Quantum Mechanics*, McGraw-Hill Book Co. P. 230.

# ACCURATE DETERMINATION OF THE MAGNETIC ANISOTROPIES OF THE HYDRATED SALTS OF SOME ELEMENTS OF THE IRON GROUP

BY SUNILKUMAR DATTA

DEPARTMENT OF GENERAL PHYSICS, X-RAYS AND MAGNETISM, INDIAN ASSOCIATION FOR THE CULTIVATION OF SCIENCE, CALCUTTA—32

(Received for publication, April 24, 1954)

**ABSTRACT.** Van Vleck's recent theory of magnetic anisotropy of paramagnetic crystals indicate the importance of the effects of long range crystalline electric fields which were previously assumed to be small in comparison with short range ones. Experimental verification of this theory necessitates very accurate determination of the magnetic anisotropy of such crystals. This has been undertaken in the present work in which attempts have been made to improve the existing methods in order to eliminate or minimise errors that arise in its measurement, especially in the control and measurement of the magnetic field. The results obtained on a large number of crystals show considerable differences from those obtained by the previous workers. The use of single crystals as secondary standards in the measurement of magnetic fields has been discussed.

## 1. INTRODUCTION

The most extensive measurement of the magnetic anisotropies of the single crystals of paramagnetic salts has been done by Krishnan and his co-workers in this laboratory (1933, *et seq.*) with the intention of verifying and elucidating many important aspects of the crystalline electric field theory of Van Vleck (1932) and Penney and Schlapp (1932). Some of their earlier works were, however, found to be largely in error; for example, the principal gram molecular anisotropy of  $\text{NiSO}_4 \cdot 6\text{H}_2\text{O}$  was found to be  $83.0 \times 10^{-6}$  at  $303^\circ\text{K}$  by Mookerjee (1946) and  $81.6 \times 10^{-6}$  at  $303^\circ\text{K}$  by Stout and Grieffel (1950), as against  $109 \times 10^{-6}$  by Krishnan *et al* (1933). Joglekar (1938) also found for some of the ammonium Tutton salts a difference of even 8% from the anisotropies given by the earlier workers. The 'oscillation method' used by the earlier workers was not evidently very reliable. Even in the later works following the 'critical couple method' the over-all experimental accuracy perhaps never exceeded 1 to 3%, the main uncertainty lying in the field stabilization and measurement, crystal purity and perfection and accurate torsion determinations.

According to Van Vleck's later theory (1939) the direct and the indirect effects,—particularly the latter,—of the long range asymmetric crystalline electric fields on the paramagnetic ions are not negligible in comparison with the short range ones. In fact, the indirect effect may be sometimes

comparable with and even predominant to that of the latter, and in general these two effects are superimposed to give the total asymmetry of the Jahn Teller clusters (1937) about the paramagnetic ions. For a given paramagnetic ion the effect of the asymmetric long range fields should vary from salt to salt and to detect such an effect accurate values of the magnetic anisotropies and their temperature variations would be most useful. In view of this the present redeterminations have been undertaken to improve the accuracy to 0.1% or better of the anisotropies of a large number of salts. A number of new salts, interesting from magnetic and structural view point, not previously measured are also included. Temperature variation measurements over a wide range are nearing completion and theoretical discussions of the present results are left over till then.

## 2. IMPROVEMENTS IN THE EXPERIMENTAL METHODS

The principle of the method for anisotropy measurement is the same as in the later works of Krishnan *et al* and need not be described in detail. It depends on the measurement of the critical torsion angle of a fine quartz fibre, attached at the upper end to a torsion head and with the crystal at the lower end placed in a homogeneous horizontal magnetic field  $H$ . In the position of unstable equilibrium of the crystal under the opposing couples due to the fibre and the field the condition is given by

$$\Delta\chi = \frac{\alpha_c - \pi/4 - \sigma_c}{\cos 2\sigma_c} \times \frac{2MC}{mH^2}$$

where  $\sin 2\sigma_c = MC/mH^2\Delta\chi$ ,  $\Delta\chi$  the magnetic anisotropy of the crystal in the horizontal plane,  $M$  is the gm molecular weight of the crystal of mass  $m$  and  $C$  is the torsion constant of the quartz fibre.

The values of  $M$  are obtained from the International Critical Tables on the basis of the molecular formula of the salts, which might differ appreciably from the stoichiometric proportions of the containing elements only in the case of imperfect crystals containing sufficient occlusions of mother liquor or other impurities. Such cases were summarily rejected. The salts taken were always of the analytical qualities of Kahlbaum, E. Merck (of these two we had some pre-war stock in our laboratory) or Malinckrodt or B. D. H., or else prepared by ourselves from such analytical quality starting materials (e.g., the fluo-salts). The salts were recrystallized twice or thrice using double distilled water and were always tested for the final purity. The final crystallization was done in a quiet, dust free and vibration-proof chamber, by moderately slow evaporation of a nearly saturated aqueous solution. It was unfortunate that our resources did not allow us to have an air-conditioned room. The best of the crystals were chosen first with a magnifying glass and then under a petrographic microscope. Finally, goniometric measurement was done as test cases which agreed very well with the standard data for these salts.



The mass of the crystal varied between 0.1 and 0.05 gm and was determined accurately to 0.1% or better with a calibrated Bungé balance giving a direct rider reading to 0.1 mgm and by oscillation to 0.03 mgm. The weights were corrected for buoyancy of air. The method of accurately determining  $C$ , the torsion constant of the quartz fibre has been discussed in a previous paper by the author (1953), the accuracy of which is 0.1% or better.

### 3. CONTROL AND MEASUREMENT OF THE MAGNETIC FIELD

As equation (1) involves the square of the field  $H$ , much improvement upon the usual method is called for to arrive at an accuracy of about 0.05% in its measurement. The value of the residual field and the initial state of magnetization of the magnet core and the pole pieces decide to a large extent the final total field when the magnetizing current is established. To arrive at a steady initial condition of the magnet for a given final magnetizing current a reversing switch with a rheostat is arranged in the magnet circuit and the core and pole pieces are subjected to several hysteresis cycles before the final current is established. The current for the magnet was taken from a special 10 kW 220 V d.c. compound wound generator on which no other load was allowed during these measurements. The huge self-inductance of the magnet was by itself a stabilizing factor. The current was read on a calibrated 5" mirror-dial Weston ammeter of 5 ampere range, the fine needle of which touching a desired scale-division was observed against the cross-wires of a low power microscope. Fluctuations of the current could thus be easily detected to 0.5 milliamperes, *i.e.*, 0.01% in 5 amperes. No low frequency fluctuations were observed by us. But very slow drifts by about 10 milliamperes occurred over 8 to 10 minutes, perhaps due to heating of the circuit and other causes. More troublesome were sudden kicks by about 0.1 ampere, probably due to fluctuations in the 440 a.c. mains. If such a kick occurred at the moment when the crystal to be measured has been rotated nearly to the unstable position in the field, very often the result was to make the crystal spin round prematurely. The result of such an observation was forthwith rejected. Otherwise all variations in the current were controlled to a nicety with the help of a fine-wire screw motion sliding contact rheostat placed in the circuit. Particular check on the exact value of the current was kept near the unstable position.

Before the actual measurement of the field was carried out the uniformity of the field over the central region of the pole-gap was checked. The pole-gap was 4 cm between 10 cm  $\times$  10 cm flat non-tapered pole pieces made parallel accurately to 1/1000 mm. The exciting current was 4 amperes. The method was to measure the critical couple on a very well-developed crystal of  $\text{CuSO}_4 \cdot 5\text{H}_2\text{O}$ , about 4 mm  $\times$  3 mm  $\times$  2 mm (the anisotropy  $\Delta\chi$  with the  $c$  axis vertical, as measured by Krishnan and Mookerjee (1938) to be

observing the crystal through a telescope arrangement described later. But small additional uncertainties may arise in both the initial and final positions due to residual field, anisotropy of shape of the crystal, eccentricities of mounting of the crystal and the torsion head, etc. Elimination of the anisotropy of shape is discussed in a later section whilst the others are eliminated completely by taking the mean of the clockwise and anticlockwise rotations of the torsion head. The final position is also very much dependent upon the fluctuations in the magnet field (also discussed later), quick and yet smooth operation of the torsion head during measurement, etc. A moderate rotation of the torsion head by two revolutions, say, could be smoothly given in about a minute without making the crystal oscillate much near the critical position. Actually, several readings never differed by more than 0.1% and their mean was taken.  $\sigma_c$  is a small correction term for large angles of torsion and is less than 0.1% above  $680^\circ$ . For smaller angles it becomes appreciable and can be readily calculated with a sufficient degree of accuracy for our purpose.

#### 6. ANISOTROPY OF SHAPE AND ITS ELIMINATION

The anisotropy of shape in crystals of representative members of the Tutton salts was estimated by grinding out thin plates measuring about  $10\text{mm} \times 6\text{mm} \times 1\text{mm}$  and determining their anisotropy in air and again in a balancing bath of the same mean susceptibility, following the method of Krishnan, *et al* (1933) for determining the anisotropy of  $\text{Mn}^{++}$  and  $\text{Fe}^{+++}$  salts. For cobalt, iron and copper salts the anisotropy of shape even with such high asymmetry of shape was found to be less than 0.1%, whereas for nickel salts it amounted to a few parts in a thousand, of the true magnetic anisotropy of the crystal. For example, a  $\text{NiSO}_4 \cdot 6\text{H}_2\text{O}$  crystal, about  $(12\text{mm} \times 12\text{mm}) \times 1\text{mm}$  thick had an anisotropy of  $81.3 \times 10^{-6}$  in air and  $80.8 \times 10^{-6}$  in the balancing bath. Our actual crystals were chosen to have developments to comparable extent on all sides as far as possible to minimise this effect. However, in such cases as above balancing baths were always used in subsequent measurements. To use crystals in the form of discs would be a good procedure for many purposes, but for the present we avoided it in order to minimise (a) errors in locating the axes of the crystal and hence measuring the orientation of the crystal in the field directly and (b) chances of contamination, both of which may be considerable.

#### 7. MEASUREMENT OF $\theta$ AND $\psi$

For monoclinic crystals in addition to the principal anisotropies the angles between the crystallographic  $a$  axis and the magnetic  $\chi_2$  axis and that between  $c$  and  $\chi_1$  axis denoted by  $\theta$  and  $\psi$  respectively which are connected by

the relation  $\theta + \psi + \pi/2 = \beta$  according to the notations adopted by Krishnan, was also measured in an improved manner than the earlier workers, as follows. A  $\text{NiSO}_4 \cdot 6\text{H}_2\text{O}$  crystal belonging to the tetragonal system with large well-developed  $c$  (001) face was mounted with the tetrad axis horizontal, and the torsion head adjusted till the crystal was under no torsion in the field. This position can be obtained without much difficulty to within  $0.1^\circ$  taking into consideration the slight uncertainty due to the residual field and the limitations of the reading of the vernier torsion head. The lamp and telescope, previously arranged to view the crystal horizontally approximately normal to the direction of the field, was then adjusted so as to get the image of the filament of the lamp over the cross wire, being reflected by the  $c$  face of the crystal which set itself along the field. The orientation of any vertical face with respect to the field, of any other crystal also, could then be determined quite easily. For example, in a monoclinic crystal suspended with the  $b$  axis vertical the angle between the  $\chi_1$  and  $a$  axis (that is  $90 - \theta$ ) was directly determined in magnitude with an accuracy of  $0.1^\circ$ . The sign of  $\theta$  was determined by noting the position of any other (hol) plane with respect to the  $\chi_1$  direction, since according to conventions  $\theta$  (or  $\psi$ ) is taken as positive when it lies within the monoclinic angle  $\beta$ , otherwise negative.  $\psi$  was then calculated from the previous relation or measured directly if the crystal had suitably developed faces.

For monoclinic crystals the three usual modes of suspension were used :

(i)  $b$  axis vertical, giving

$$\Delta\chi = \chi_1 - \chi_2 \quad (2)$$

(ii)  $a$  axis vertical, giving

$$\Delta\chi = \pm \{ (\chi_1 - \chi_2) \sin^2 \theta - (\chi_1 - \chi_3) \} \quad (3)$$

and (iii) (001) plane horizontal, giving

$$\Delta\chi = \pm \{ (\chi_1 - \chi_2) \cos^2 \theta - (\chi_1 - \chi_3) \} \quad (4)$$

the +ve or -ve sign being chosen according as the ( $b$ ) axis lies normal or along the field.

For orthorhombic crystals suspensions along the principal diad axes  $a$ ,  $b$ ,  $c$  were used whilst for tetragonal or trigonal crystals the tetrad or the triad axes were suspended horizontally.

The data recorded below represent in all cases the mean value for at least five crystals agreeing with each other to within 0.3 to 0.1% or better. The temperature of measurement varied from about  $25^\circ$  to  $30^\circ\text{C}$  but they have been converted to  $300^\circ\text{K}$  from the slopes at this point of the temperature-anisotropy curves of Bose (1945), Guha (1951) or from author's own measurements to be published elsewhere.

TABLE I

Magnetic anisotropy ( $\times 10^{-6}$ ) of crystals at 300°K. Figures within parentheses denote the values obtained by the previous workers referred to against them.

Crystal	Crystal class	$\chi_1 - \chi_2$	$\chi_1 - \chi_3$	$\theta^\circ$	$\psi^\circ$	Reference
1. $K_2Fe(SO_4)_2, 6H_2O$	Mono-clinic	1696 (1841)	-279.0 (-314)	-43.4 (-43.8)	+57.9 (+58.3)	1
2. $(NH_4)_2Fe(SO_4)_2, 6H_2O$	"	2179 (2582)	180.1 (213)	-37.4 (-37)	+53.4 (+54)	1
3. $FeSO_4, 7H_2O$	"	1166 (1289)	1143 (1270)	-8.1 (-7.5)	+22.4 (+22)	1
4. $K_2Co(SO_4)_2, 6H_2O$	"	2432 (2532)	1772 (1832)	+30.5 (+30.5)	-15.6 (-15.5)	1
5. $(NH_4)_2Co(SO_4)_2, 6H_2O$	"	3042 (3023)	1543 (1541)	+60.2 (+60)	-43.3 (-43)	1
6. $CoSO_4, 7H_2O$	"	1823 (1928)	956 (1094)	+68.6 (+69.1)	-54.6 (-54.4)	1
7. $K_2Ni(SO_4)_2, 6H_2O$	"	131.2 (158)	130.5 (165)	+26.7 (+27)	-11.4 (-12)	1
8. $(NH_4)_2Ni(SO_4)_2, 6H_2O$	"	93.8 (110)	91.5 (106)	+31.0 (+31)	-13.4 (-14)	1
9. $Rb_2Ni(SO_4)_2, 6H_2O$	"	143.3 (144)	136.8 (137)	+27.5 (+27.0)	-11.4 (-11.0)	2
10. $Tl_2Ni(SO_4)_2, 6H_2O$	"	113.7 (114)	107.4 (108)	+26.5 (+27.3)	-10.1 (-20.9)	2
11. $Cs_2Ni(SO_4)_2, 6H_2O$	"	132.2 (134)	126.1 (127)	+27.1 (+27.7)	-10.1 (-10.7)	2
12. $NiSO_4, 7H_2O$	Orthorhombic	$\chi_a - \chi_b = 159.6$ (169) (163)		$\chi_a - \chi_c = 31.9$ (49) (35)		1 4
13. $NiSO_4, 6H_2O$	Tetragonal	$\chi_1 - \chi_2 = 80.8$ (109) (83) (81.6)				1 4 6
14. $K_2Ni(SeO_4)_2, 6H_2O$	Mono-clinic	127.3 (146)	107.2 (146)	+31.0 (+27.5)	-16.5 (-13.0)	2
15. $(NH_4)_2Ni(SeO_4)_2, 6H_2O$	"	92.6 (116)	79.6 (96)	+38.1 (+44.2)	-22.1 (-27.9)	2
16. $Rb_2Ni(SeO_4)_2, 6H_2O$	"	136.5 (157)	117.0 (147)	+28.0 (+28.2)	-12.7 (-12.9)	2
17. $Tl_2Ni(SeO_4)_2, 6H_2O$	"	122.5 (123)	116.5 (118)	+32.7 (+32.7)	-17.1 (-17.1)	2
18. $Cs_2Ni(SeO_4)_2, 6H_2O$	"	131.5 (164)	110.7 (135)	+28.5 (+33.8)	-11.3 (-17.6)	2
19. $NiSeO_4, 6H_2O$	Tetragonal	$\chi_1 - \chi_2 = 86.6$ (90)				2

TABLE I—contd

Crystal	Crystal class	$\chi_1 - \chi_2$	$\chi_1 - \chi_3$	$\theta^\circ$	$\psi^\circ$	Reference
20. $K_2Ni(BeF_4)_2 \cdot 6H_2O$	Monoclinic	132.1	128.5	+28.5	-13.4	
21. $(NH_4)_2Ni(BeF_4)_2 \cdot 6H_2O$	"	105.8 (107)	101.1 (106)	+29.2 (+31.0)	-12.5 (-14.3)	2
22. $Rb_2Ni(BeF_4)_2 \cdot 6H_2O$	"	122.3	118.4	+27.1	-10.8	
23. $Tl_2Ni(BeF_4)_2 \cdot 6H_2O$	"	121.0	117.9	+26.9	-11.1	
24. $Cs_2Ni(BeF_4)_2 \cdot 6H_2O$	"	117.3	115.2	+26.2	-9.1	
25. $NiSiF_6 \cdot 6H_2O$	Trigonal	$\chi_1 - \chi_2 = 18.18$				
26. $K_2Cu(SO_4)_2 \cdot 6H_2O$	Monoclinic	322.3 (367)	72.4 (74)	-88.1 (-88)	-77.4 (-77.5)	1
27. $(NH_4)_2Cu(SO_4)_2 \cdot 6H_2O$	"	285.7 (300)	67.6 (62)	-60.1 (-61)	+75.0 (+77)	1
28. $Rb_2Cu(SO_4)_2 \cdot 6H_2O$	"	329.7 (351)	94.2 (100)	+84.7 (+86.1)	-59. (-704.0)	2
29. $Tl_2Cu(SO_4)_2 \cdot 6H_2O$	"	302.5 (283)	84.9 (71)	+88.5 (+88.2)	-72.1 (-72.6)	2
30. $Cs_2Cu(SO_4)_2 \cdot 6H_2O$	"	320.7 (339)	111.2 (114)	+87.9 (+88.1)	-71.8 (-71.9)	2
31. $K_2Cu(SeO_4)_2 \cdot 6H_2O$	"	310.3 (367)	111.8 (95)	-61.5 (+66.9)	+74.0 (-53.5)	2
32. $(NH_4)_2Cu(SeO_4)_2 \cdot 6H_2O$	"	322.6 (353)	111.6 (118)	-52.1 (-51.2)	+68.0 (+66.7)	2
33. $Rb_2Cu(SeO_4)_2 \cdot 6H_2O$	"	326.3 (354)	77.1 (78)	-86.5 (+88.0)	-78.8 (-73.3)	2
34. $Tl_2Cu(SeO_4)_2 \cdot 6H_2O$	"	305.1 (328)	71.3 (22)	-87.5 (+87.3)	-77.6 (-72.3)	2
35. $K_2CuCl_4 \cdot 2H_2O$	Tetragonal	$\chi_1 - \chi_2 = 260.1$ (268) (263)				3 5
36. $(NH_4)_2CuCl_4 \cdot 2H_2O$	"	"	255.3 (265) (258)			3 5
37. $Rb_2CuCl_4 \cdot 2H_2O$	"	"	254.6 (265) (262)			3 5
38. $(NH_4)_2CuBr_4 \cdot 2H_2O$	"	"	235.5			

References: 1. Krishnan, Chakravorty and Banerjee (1933), 2. Krishnan and Mookerjee (1938), 3. Krishnan, Mookerjee and Bose (1939), 4. Mookerjee (1946), 5. Mookerjee (1945), 6. Stout and Griefel (1950).

## 8 DISCUSSIONS

Without going into theoretical interpretation of the above data at present, several points of interest relating to them may be mentioned. A glance at the table will show that the values of anisotropy obtained by the present author are considerably at variance with those of Krishnan, Chakravorty and Banerjee (1933) whose values for iron, nickel and copper salts are upto 20% higher in some cases. This may possibly be due to the "oscillation" method being not sufficiently accurate. The values given by Krishnan and Mookerjee (1938) are more near to the present values, though almost systematically high by a few per cent. This might arise due to their value of magnetic field being slightly in error (about 1.5 to 2%) on the negative side. The values of  $\theta$  and  $\psi$ , however, in all cases agree quite closely with the previous values, except in the case of  $\text{K}_2\text{Cu}(\text{SeO}_4)_2 \cdot 6\text{H}_2\text{O}$  for which the previous workers gave:  $\theta = +66.9^\circ$  and  $\psi = -54.5^\circ$ , as against those of the present author:  $\theta = -61.5^\circ$  and  $\psi = +74.9^\circ$ . Obviously, the difference in sign in the two values of  $\theta$  is of significance and explains the discrepancy pointed out by Bleaney *et al* (1949) between the value of  $\psi$  obtained by Krishnan and that from their own paramagnetic resonance experiments, namely  $+73^\circ$ . The present author's value is in agreement with that of Bleaney.

It has been one of the objects of our researches in this laboratory to use the present method for the determination of field strength using a suitable crystal of accurately known anisotropy. The great advantage of this method (which is, of course, restricted to homogeneous horizontal fields) lies in its extreme simplicity and accuracy. On account of the smallness of the size of the crystal in comparison with the search coil it may conveniently be used even in very narrow spaces within the pole-gap; different parts of the field may also be explored, as has been done in the present measurements. Crystals of  $\text{CuSO}_4 \cdot 5\text{H}_2\text{O}$  have hitherto been used in this laboratory and elsewhere (*c.f.* Selwood, 1950) for this purpose; these crystals sometimes contain occlusions in the form of bluish white patches, possibly of a basic composition. Moreover, they do not give reproducible values of anisotropy after storage for a few months. On the other hand,  $\text{NiSO}_4 \cdot \text{K}_2\text{SO}_4 \cdot 6\text{H}_2\text{O}$  crystallizes very well and is practically free from occlusions, flaw or strain, as revealed from their optical examination, and gives reproducible values even after long storage. These crystals are also magnetically quite stable, that is, the change in  $\theta$  and  $\psi$  are quite small over a wide range of temperatures. These properties make the substance very suitable for measuring magnetic fields.

## ACKNOWLEDGMENTS

The author wishes to express his gratitude to Dr. A. Bose, D.Sc., for kind help and keen interest in connection with this work.

# REFERENCES

- Bleaney, B., Penrose, P., and Plumptre, B. P., 1949, *Proc. Roy. Soc.* **A198**, 406.
- Bose, A., 1947, *Ind. J. Phys.* **21**, 275 ;
- "    1948, " " " **22**, 73, 195, 275, 483.
- Bose, A. and Mitra, S. C., 1952, *Ind. J. Phys.*, **26**, 393, 543.
- "    "    1953, " " " **27**, 95.
- "    "    1954, *Proc. Roy. Soc.*, (In course of publication).
- Datta, S., 1953, *Ind. J. Phys.* **27**, 155.
- Dutta Roy, S., 1954, *Ind. J. Phys.* **28**, (In course of publication).
- Guha, B. C., 1951, *Proc. Roy. Soc.*, **206**, 355.
- Hahn, H. and Teller, E., 1937, *Proc. Roy. Soc.* **A161**, 220.
- Joglekar, M. S., 1938, *Z. Krist.* **98**, 411.
- Krishnan, K. S., Chakravorty, N. C., and Banerjee, S., 1933, *Phil. Trans. Roy. Soc.*,  
    **A232**, 99.
- "    and Mookerjee, A., 1938, *Phil. Trans. Roy. Soc.*, **A237**, 99.
- "    "    1938, *Phys. Rev.*, **54**, 533, 841.
- Mookerjee, A., 1945, *Ind. J. Phys.*, **19**, 63.
- Mookerjee, A., 1946, *Ind. J. Phys.*, **20**, 9.
- Penney, W. G., and Schlapp, R., 1932, *Phys. Rev.*, **42**, 666.
- Selwood, P. W., 1952, *J. Amer. Chem. Soc.*, **74**, 2364.
- Stout, J. W., and Grieffel, M., 1950, *J. Chem. Phys.*, **18**, 1449.
- Van Vleck, J. H., 1932, *Theory of Electric and Magnetic Susceptibilities*, (Oxford)
- "    1932, *Phys. Rev.*, **41**, 208.
- "    1939, *J. Chem. Phys.*, **7**, 61.





# PEAK AMPLITUDE RECORDER FOR INVESTIGATION ON FADING

BY S. C. MAZUMDER AND S. N. MITRA  
RESEARCH DEPARTMENT, ALL INDIA RADIO, NEW DELHI

(Received for publication, May 3, 1954)

## Plate VII

**ABSTRACT.** On pulsed transmissions, the different order ionospheric returns are received at distinct time intervals and they are represented as separate echoes. This paper describes an experimental arrangement which can select any one of these 'echoes' and record its amplitude variation.

## INTRODUCTION

Fading of a down-coming wireless wave has opened an important field of study on the irregular structure of ionospheric layers. Ionosphere is known to contain irregularities in the form of ion-clouds and an incident radio wave is returned to the earth as a cone of waves after diffractive scattering from them. Their motion either with a steady wind velocity (Mitra, 1949a) or in a random manner (Mitra, 1949b) has been suggested to be the cause of amplitude fluctuation of down-coming waves. In order to investigate the problem, it is very necessary to design suitable experimental arrangement to eliminate the possible errors. On continuous wave transmissions, it is impossible to isolate the effect of motion of the ionospheric irregularities since the interference between the ground wave and several sky waves will always introduce some degree of uncertainty. On pulsed transmissions, however, this difficulty is easily obviated since the different sky waves are represented as separate echoes corresponding to their different paths. Thus, an experimental arrangement which can select any echo and record the variation of its amplitude is ideal for the purpose. Still there is another source of error. Very frequently, a single wave comes back from the ionosphere as two split echoes due to magnetoionic double refraction. The interference between these two echoes, when the resolution in the receiver is not sufficient, is liable to show fading which is not due to the motion of the irregularities (Mitra, 1950). A polarised aerial in the receiving system may be used when only one of the components will be received. Alternatively, a suitable wave-frequency may be chosen which gives two components distinctly separated when the fading of one of them could be studied. The present paper deals with the design of an experimental arrangement which could be utilised to investigate the fading on pulsed transmissions.

## EXPERIMENTAL PROCEDURE

In this section, we shall briefly discuss the main principle of the experimental design. It has been mentioned in the introduction that in order to

investigate the fading of a single echo, it is necessary to have suitable experimental arrangement which can record fading of only one echo in the presence of the ground pulse and the other returns.

An electronic gate of variable width and variable delay is first generated employing conventional flip-flop circuit and phasing arrangements. The gate is then applied to the suppressor grid of a pentode mixer stage. The suppressor grid is normally biased to cut-off and no current flows through the valve. The positive gate pulse makes the valve conducting during its duration and the mixer behaves as an ordinary amplifier. Ionospheric signal received by a receiver on vertical incidence pulse sounding is then applied to the control grid of the mixer valve. The signal consists of the ground pulse and the successive ionospheric echoes and is viewed on a monitor oscilloscope. The gate pulse is also passed on to the oscilloscope for monitoring facilities. Now, the gate can be made to select any echo and the output of the mixer will contain the amplified echo-signal. Since the duration of the gate is adjusted to be very nearly equal to the duration of the echo, the mixer amplifies only the selected signal while the other portion of the received echo-pattern, including the ground pulse and noise, is left out. We, therefore, have gated signal and the output of the mixer at any instant will represent the amplitude of the echo whose fading is desired to be studied.

For recording purposes, the gated pulse is made to charge a condenser which leaks through a high resistance (time-constant = 0.25 sec). The voltage to which the condenser charges up depends upon the amplitude of the echo at any instant. Since the time constant of the circuit is quite small, it can follow rapid fluctuation of the echo-amplitude. A recording valve is employed which acts as a cathode-follower stage. The control grid of this valve receives the voltage fluctuation from the condenser and an Easterline Angus Recorder connected in series with the cathode resistance records the current changes in the valve, thereby representing the fading of the gated echo. A typical fading record taken in the experiment is shown in figure 1.

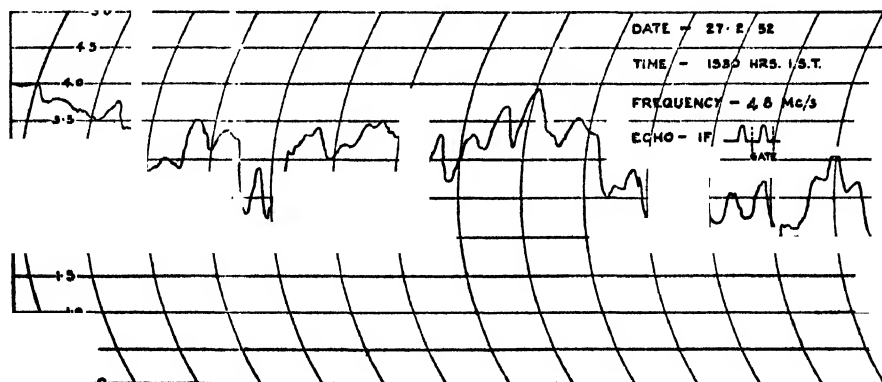


Fig 1 A typical fading record

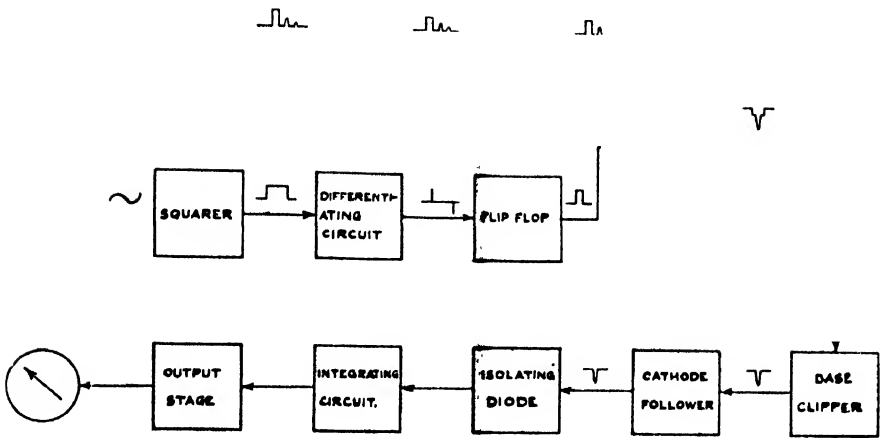


Fig. 2 Block diagram—peak amplitude recorder

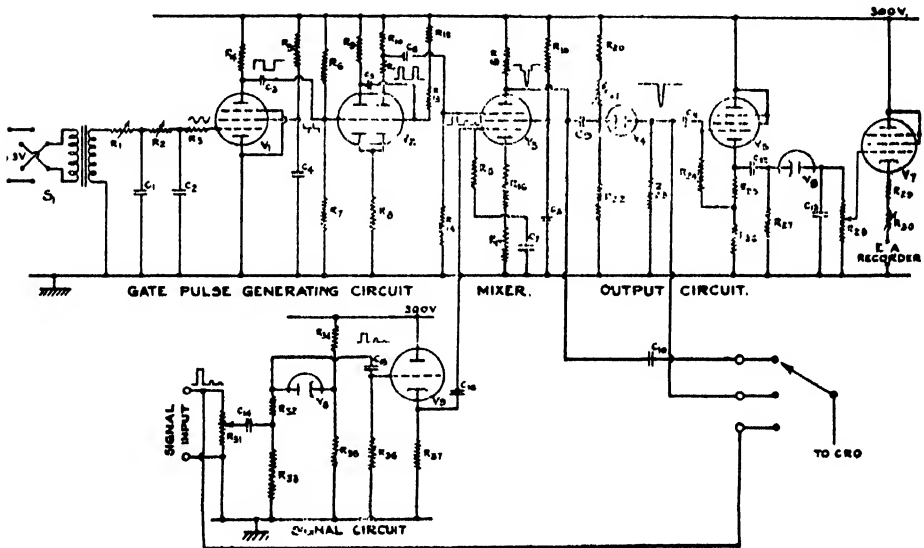


Fig. 3 Circuit diagram—peak amplitude recorder

### EXPERIMENTAL DESIGN

In this section, we shall describe the various component parts in the peak amplitude recorder. A block schematic is shown in figure 2 from which the sequence of operation of the recorder as a whole could be seen.

The peak amplitude recorder could be conveniently divided into the following parts :—

**Signal Circuit** (figure 3)—It consists of a voltage dividing input potentiometer ( $R_{31}$ ), one diode clipper ( $V_8$ ) and one cathode follower ( $V_9$ ). The diode clipper is found necessary in order to limit the amplitude of the ground pulse when the recorder is placed near the pulse transmitter. If ground

pulse is absent or if it is weak when the pulse transmitter is situated at a distance, the diode clipper stage may not be necessary. In actual operation, however, the voltage divider  $R_{s1}$  is so adjusted that the amplitude of the selected echo never goes higher than the clipping level (4.5 volts)

*Gate Pulse Generating Circuit* (figure 3).—It consists of a phase-shifting network ( $R_1, R_2, C_1, C_2$ ) for providing variable delay in the gate pulse, a squarer ( $V_1$ ), a differentiator ( $C_3, R_7$ ) and a flip-flop stage ( $V_2$ ) for generating the gate pulse. The various wave-forms at different places in the circuit are shown in figure 3.

The phase-shifting network is capable of providing a shift of about  $180^\circ$ . Moreover, a phase-reversal switch ( $S_1$ ) has been incorporated at the input of the squarer so that the total delay in the gate pulse could cover nearly the whole of the cycle and therefore an echo occurring at any place in the cycle could be gated.

The gate is generated in the following way: First a square wave of steep sides is generated by the squarer ( $V_1$ ) from the input sine wave. The square wave is then differentiated by  $C_3$  and  $R_7$  and sharp positive and negative pulses for triggering the flip-flop are obtained. The positive pulses are utilised for triggering the flip-flop ( $V_2$ ) which works as a cathode-coupled multivibrator. When the positive pulse is of sufficient amplitude usual switching action takes place due to capacity-coupling between the plate of the left triode section and the grid of the right triode section of  $V_2$ . Thus, the left portion becomes conducting while the right portion is cut off. But the position is normalised due to discharge of condenser  $C_5$  through resistances  $R_{12}$  and  $R_{13}$  and the right portion becomes conducting, the left portion being cut-off till the arrival of the next positive pulse. Thus during each cycle, we get a positive gate-pulse at the plate of the right triode portion of  $V_2$ . Other values being fixed, the duration of the gate pulse depends upon the values of  $C_5$  and  $R_{12} + R_{13}$  as these components determine the discharge time of  $C_5$  (figure 3).

*The Mixer* (figure 3).—The mixer is a pentode where the received signal is applied to its control grid whereas the gate pulse is applied to the suppressor. The circuit proportions are such that due to current flowing through the screen grid, the voltage drop in the cathode resistor is sufficient to bias the suppressor to cut off. Now, the amplitude of the positive gate-pulse is about the same as the bias voltage and during the gate-interval, the valve behaves as a normal amplifier. When none of the echoes is made to coincide with the gate, the output contains the gate-pulse with its sign reversed. But when the gate-pulse is made to select an echo, we get a pedestal at the output of the mixer where the echo 'sits' upon the gate.

*The Output Circuit* (figure 3).—The output circuit consists of a base clipper ( $V_4$ ) for removing the gate from the output of the mixer, one cathode follower ( $V_5$ ) for charging the condenser ( $C_{13}$ ), one isolating diode stage ( $V_6$ ) for preventing the condenser from discharging through the cathode resistor

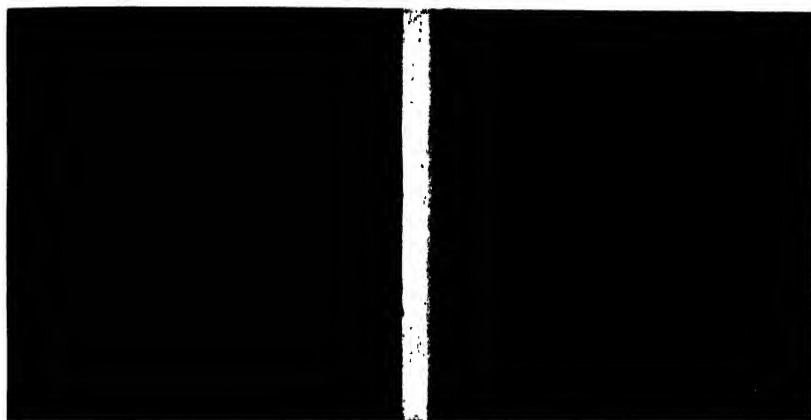


Fig. 4  
Gate

Fig. 5  
Echo pattern

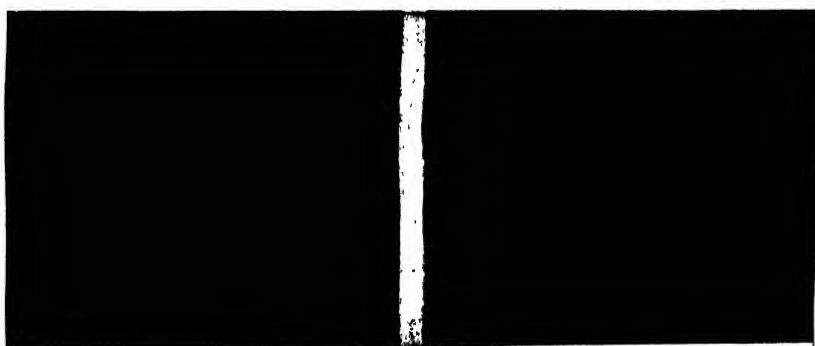


Fig. 6  
First echo selected

Fig. 7  
Second echo selected

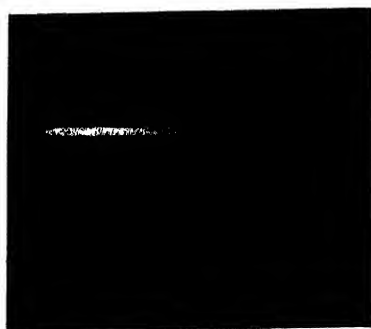


Fig. 8  
Selected echo after clipping off the pedestal



( $R_{25}$ ,  $R_{26}$ ), integrating R. C. circuit ( $C_{13}$ ,  $R_{28}$ ) for developing the control voltage and the last cathode follower ( $V_7$ ) for recording the cathode current. The 'no signal' current of the last cathode follower ( $V_7$ ) is adjusted by  $R_{30}$  so that nearly full-scale deflection (5 ma) is obtained in the recorder. Input to the grid of  $V_7$  is tapped from  $R_{28}$  and the tapping point is kept fixed for a whole set of observations so that the current variation in this valve may be proportional to the echo-amplitude at any instant.

A few photographs (Plate VII) are shown to indicate the performance of the recorder. Figure 4 shows the gate generated at the output of  $V_2$  the width of which could be varied by  $R_{12}$ . Figure 5 shows an echo pattern where the first and the second reflections are seen. Figure 6 shows the 'pedestal' where the first echo has been 'gated'. Figure 7 shows the second echo selected by the gate by adjusting the 'phase-delay' at the input of the 'squarer'. The base-clipper ( $V_4$ ) removes the gate as shown in figure 8 and the amplitude of the echo thus selected is then recorded in the Easterline Angus Recorder.

## CONCLUSION

The peak amplitude recorder has been designed and built to study fading on pulsed transmissions. The equipment was extensively used during observations of solar eclipse on 25th February, 1952 (Mitra, 1953). A large number of fading records on different frequencies and at different times have already been taken.

## ACKNOWLEDGMENTS

The work described in this paper forms part of a programme of ionospheric research of All India Radio. The authors are grateful to Sri B. V. Baliga, former Chief Engineer, All India Radio, for his kind interest during the progress of the work and to Sri A. C. Ramchandani, Chief Engineer, All India Radio, for permission to publish this paper.

## REFERENCES

- Mitra, S. N., 1949, *Proc. Inst. Elect. Eng.*, **96**, Pt. III, 441.
- Mitra, S. N. 1949, *Proc. Inst. Elect. Eng.*, **96**, Pt. III, 505.
- Mitra, S. N., 1950, *Ind. Jour. Phys.*, **24**, 197.
- Mitra, S. N., 1953, *Jour. Sci. Indust. Res.*, **12A**, 319.

# CALCULATION OF PERTURBATIONS IN CERTAIN MOLECULAR ELECTRONIC TERMS. PART I. ${}^2\Sigma - {}^4\Pi$

By D. PRÉMASWARUP

PHYSICS DEPARTMENT, ANDHRA UNIVERSITY, WALT AIR

(Received for publication, April 21 1954)

**ABSTRACT.** In this paper expressions are derived for the course of energy levels at the point of intersection of two mutually perturbing molecular electronic states. The method of treatment is given in detail and applied to the perturbation  ${}^2\Sigma - {}^4\Pi$ .

## INTRODUCTION

Calculation of perturbations has been carried out by a number of investigators previously for the cases of perturbations between singlet-singlet, singlet-triplet, triplet-triplet and doublet-doublet terms. The method employed by these investigators, chief of whom are Ittmann (1931), Budö and Kovács (1938, 1939) is invariably the wave mechanical treatment given by Krönig (1928) and Van Vleck (1929). Budö and Kovács (1939) have extended this work for higher multiplicity terms in their calculation for the perturbation of a  ${}^4\Sigma$  term by a second  ${}^4\Sigma$  term.

In this series of papers the writer proposes to present the results of perturbation calculations for certain electronic terms such as  ${}^2\Sigma - {}^4\Pi$ ,  ${}^2\Pi - {}^4\Sigma$ ,  ${}^2\Pi - {}^4\Pi$ ,  ${}^4\Sigma - {}^4\Pi$ ,  ${}^4\Pi - {}^4\Pi$  and between those of higher multiplicity like quintets, sextets etc. The importance of these calculations arises on account of the possibility of detecting such terms in the band spectra of the halides and oxides of the heavier elements, Yt, Ta, Cr, Mn, etc. which are under investigation by the author and others in this laboratory.

## THEORY

The wave mechanical treatment of the diatomic molecule was given simultaneously by Van Vleck and Krönig. The wave-function  $\psi$  of a diatomic molecule with moving nuclei is given by the equation

$$H_0 - \frac{h^2}{8\pi^2 M r^2} \left\{ \frac{\partial}{\partial r} \left( r^2 \frac{\partial}{\partial r} \right) + \cot \theta \frac{\partial}{\partial \theta} + \frac{\partial^2}{\partial \theta^2} + \operatorname{cosec}^2 \theta \frac{\partial^2}{\partial \omega^2} \right\} - W | \psi = 0 \quad \dots (1)$$

where  $H_0$  is the Hamiltonian of a stationary molecule and the other symbols have their usual significance. This equation cannot be readily solved as it is, but if certain small terms are neglected it can be split up into the product of three functions  $\phi$ ,  $R$  and  $u$ , of which  $\phi$  is the solution of the wave equation for a stationary diatomic molecule,  $R$  is the wave-function satisfying



the equation of vibration of the nuclei while  $u$  is the wave-function satisfying the equation of a symmetric top. The neglected terms are

$$\frac{\hbar^2 i}{8\pi^2 M r^2} \left[ \cot \theta (P_x - iP_y P_z - iP_z P_y) + 2 \operatorname{cosec} \theta P_y \frac{\partial}{\partial \omega} + 2 P_x \frac{\partial}{\partial \theta} \right] \psi \quad (2)$$

and the high frequency part of the expression

$$\frac{\hbar^2}{8\pi^2 M r^2} \left[ (P_x^2 + P_y^2) \phi' - 2r \frac{\partial \phi'}{\partial r} - r^2 \frac{\partial^2 \phi'}{\partial r^2} - \frac{2r^2}{R} \frac{\partial R'}{\partial r} \cdot \frac{\partial \phi'}{\partial r} \right] Ru \quad (3)$$

The neglected parts can now be taken into consideration by means of a perturbation calculation, treating the electronic wave-functions  $\phi$  as the unperturbed functions. The different types of the finer interaction terms when taken as the perturbing terms give rise to the different correction terms like  $\Lambda$ -doubling, spin-splitting in  $\Sigma$  states etc. The same procedure can also be applied for the case of the irregular perturbations occasioned by the accidental crossing or the very near approach of two unperturbed wave-functions.

Van Vleck, in his work referred to above, has given expressions for the matrix elements of the total Hamiltonian formed with the unperturbed eigenfunctions  $\phi$ . They are

$$\left. \begin{aligned} H^0(n, v, \Lambda, \Sigma; n, v, \Lambda, \Sigma \pm 1) &= B[J(J+1) - \Omega(\Omega \pm 1)]^{1/2} \\ &\quad [S(S+1) - \Sigma(\Sigma \pm 1)]^{1/2} \\ H^0(n, v, \Lambda, \Sigma; n, v, \Lambda \pm 1, \Sigma) &= 2(BL_y)(n, v, \Lambda; n, v, \Lambda \pm 1) \\ &\quad [J(J+1) - \Omega(\Omega \pm 1)]^{1/2} \\ H^0(n, v, \Lambda, \Sigma; n, v, \Lambda \pm 1, \Sigma \mp 1) &= (AL_y + 2BL_y)(n, v, \Lambda; n, v, \Lambda \\ &\quad \pm 1)[S(S+1) - \Sigma(\Sigma \mp 1)]^{1/2} \\ H^0(n, v, \Lambda, \Sigma; n', v', \Lambda, \Sigma) &= C(n, v, \Lambda; n', v', \Lambda) \end{aligned} \right\} \dots \quad (4)$$

Here  $n \neq n'$ , while the diagonal terms  $W^0$  are given, by

$$C(n, v, \Lambda; n, v, \Lambda) + A(n, v, \Lambda; n, v, \Lambda) \Lambda \Sigma + B[J(J+1) - \Omega^2 + S(S+1) - \Sigma^2] \dots \quad (5)$$

where in case of  $\Sigma$  states the factor (Kramer's spin-spin interaction term)  $\epsilon[3\Sigma^2 - S(S+1)]$  is also to be added. The rest of the matrix elements vanish. In all these matrix elements the phase factors are omitted as, for the purpose of the calculations presented in this paper, only the squares of the absolute values of these matrix elements (*i.e.*,  $H_{ik}H_{ik}^* = |H_{ik}|^2$ ) are necessary. However, it is to be remembered that

$$\left. \begin{aligned} L_y(\Pi, \Sigma) &= (-1)^\Sigma L_y(-\Pi, \Sigma) \text{ and} \\ L_y(\Lambda, \Lambda') &= L_y(-\Lambda, -\Lambda') \text{ for } \Lambda, \Lambda' \neq 0 \end{aligned} \right\} \quad (6)$$

where the  $\Sigma$  in the exponent is even or odd according as the  $\Sigma$  state under consideration is positive or negative.

It can be seen from the above matrix elements that they connect terms with  $\Delta\Omega = 0, \pm 1$  and  $\Delta\Lambda = 0, \pm 1$  and there are no matrix elements between

terms of different multiplicities. Hence the observed perturbations between terms of different multiplicities cannot be explained by this means. This is because in the above calculations the interaction between the orbital and spin moments of the individual electrons [which is given by  $\sum a_i(l_i s_i)$ ] is neglected. If this interaction is taken into consideration, it will not only alter the energies (*i.e.* the diagonal terms) by the small amount  $\Delta \wedge \Sigma$ , but also change the unperturbed wave-functions slightly so that the new wave-functions are linear combinations of the old unperturbed wave-functions.

Since the matrix elements of  $\sum a_i(l_i s_i)$  connect terms with  $\Delta \wedge = 0, \pm 1$ ,  $\Delta S = 0, \pm 1$  and  $\Delta \Omega = 0$ , all such terms have to be considered in taking the linear combinations. Thus, for example, for  $\phi(^4\Pi_1)$  can be written

$$\phi(^4\Pi_1) = C\phi^{\circ}(^4\Pi_1) + r_1\phi^{\circ}(^4\Sigma_1^+) + r_2\phi^{\circ}(^4\Sigma_1^-) + r_3\phi^{\circ}(^4\Sigma_1') + r_4\phi^{\circ}(^4\Delta_1) \\ + r_5\phi^{\circ}(^2\Sigma_1^+) + r_6\phi^{\circ}(^2\Sigma_1^-) + r_7\phi^{\circ}(^2\Pi_1) + \dots \quad (7)$$

where the unperturbed functions are denoted by  $\phi^{\circ}$  and the perturbed ones by  $\phi$ , and the dots denote the other terms. The constants  $r$  are given by equations of the type

$$r_i = \frac{\int \phi^{\circ*}(^4\Sigma_1^+) \sum a_i(l_i s_i) \phi^{\circ}(^4\Pi_1) d\tau}{\int \phi^{\circ*}(^4\Pi_1) \phi^{\circ}(^4\Sigma_1^+) d\tau} \dots \quad (8)$$

It can also be noted that for the first order of approximation  $C$  can be put equal to zero while second power terms in  $r$  can always be neglected wherever they occur. Using these perturbed wave-functions the matrix elements of  $H$  are given as linear combinations of the above unperturbed matrix elements  $H^{\circ}$ . Thus, for example, the following matrix elements can be written down from equation (7) and similar equations for  $\phi(^2\Sigma_1)$  and  $\phi(^2\Pi_1)$ .

$$H(^2\Sigma_1, ^4\Pi_1) = \bar{r}_1 H^{\circ}(^2\Sigma_1, ^2\Pi_1) + \bar{r} H^{\circ}(^4\Sigma_1, ^4\Pi_1) + \bar{r}_3 \bar{r}_4 H^{\circ}(^4\Pi_1, ^4\Delta_1) + \dots \quad (9a)$$

$$H(^2\Sigma_1, ^2\Pi_1) = H^{\circ}(^2\Sigma_1, ^2\Pi_1) + \bar{r}_1 H^{\circ}(^2\Pi_1, ^2\Delta_1) + \dots \quad (9b)$$

Here  $\bar{r}_i$  are the approximate mean values of  $r_i$ . In equations of the type (9a) second order terms in  $r$  can be neglected while in equations of the type (9b) even first order terms in  $r$  can be neglected.

Once the matrix elements connecting the different states under consideration have been determined, the secular equation can be easily formed and the perturbed energies obtained by solving the same. The method of solving the secular equation is explained in detail for the perturbation case  $^2\Sigma - ^4\Pi$  discussed in this paper; for the others the main results alone are reported.

#### CALCULATIONS AND RESULTS

The different states that have to be taken into consideration for the  $^2\Sigma - ^4\Pi$  perturbation are  $^2\Sigma_1, ^2\Sigma_{-1}, ^4\Pi_{5/2}, ^4\Pi_{3/2}, ^4\Pi_{1/2}, ^4\Pi_{-1/2}, ^4\Pi'_{-5/2}, \Pi'_{-3/2}, \Pi'_{-1/2}, \Pi'_{1/2}$  where by  $\Pi$  and  $\Pi'$  are represented the states with  $\wedge$  positive and negative

respectively. In this as well as in all other cases of perturbations the secular equation formed with wave-functions of this type can always be split up into two lower order equations under the transformation of these wave-functions into new functions  $\phi_1'$  and  $\phi_2'$  such that

$$\begin{aligned}\phi_1'(\Lambda, \Sigma) &= 2^{-\frac{1}{2}}[\phi(\Lambda, \Sigma) + \phi(-\Lambda, -\Sigma)] \\ \phi_2'(\Lambda, \Sigma) &= 2^{-\frac{1}{2}}[\phi(\Lambda, \Sigma) - \phi(-\Lambda, -\Sigma)]\end{aligned}\quad \dots \quad (10)$$

The new wave-functions  $\phi_1'$  and  $\phi_2'$  are identical with the Krönig symmetric and antisymmetric functions and possess the property that they go over into themselves (either with or without a change of sign) under reflection at the origin of all the coordinates concerned. In all the calculations below all the matrix elements will be given only after such a transformation has been effected. Numbering the new eigenfunctions from 1 to 10 with the first two representing the  $\Sigma$  states, the various matrix elements are obtained as follows :

$$\begin{aligned}W_1^0 &= B_{\Sigma}(J + \frac{3}{2})(J + \frac{1}{2}) & W_2^0 &= B(J + \frac{1}{2})(J - \frac{1}{2}) \\ W_3^0 &= W_7^0 = h\nu(\Sigma, \Pi) + B_{\Pi}[J(J+1) - \frac{1}{4}] + \frac{3}{2}A & W_4^0 &= W_8^0 = h\nu(\Sigma, \Pi) \\ & & & + B_{\Pi}[J(J+1) + \frac{5}{4}] + \frac{1}{2}A \\ W_5^0 &= W_9^0 = h\nu(\Sigma, \Pi) + B_{\Pi}[J(J+1) + \frac{1}{4}] - \frac{1}{2}A & W_6^0 &= W_{10}^0 = h\nu(\Sigma, \Pi) \\ & & & + B_{\Pi}[J(J+1) + \frac{5}{4}] - \frac{3}{2}A \\ H_{34}^0 &= H_{78}^0 = B_{\Pi}\sqrt{(J + \frac{5}{2})(J - \frac{3}{2})} & H_{45}^0 &= H_{89}^0 = 2B_{\Pi}\sqrt{(J + \frac{3}{2})(J - \frac{1}{2})} \\ H_{56}^0 &= H_{910}^0 = \sqrt{\frac{2}{3}}B_{\Pi}(J + \frac{1}{2}) \\ H_{14}^0 &= H_{28}^0 = [\pm 1 \pm (-1)^{\Sigma}]\phi_1\sqrt{(J + \frac{3}{2})(J - \frac{1}{2})} & -H_{16}^0 &= H_{210}^0 = [\pm 1 \pm (-1)^{\Sigma}]\mu_2 \\ H_{18}^0 &= H_{24}^0 & -H_{110}^0 &= H_{26}^0 \\ H_{15}^0 & & H_{29}^0 & \\ &= [\pm 1 \pm (-1)^{\Sigma}]\{\mu_1 + \phi_2(J + \frac{1}{2})\} & &= [\pm 1 \pm (-1)^{\Sigma}]\{\mu_1 - \phi_2(J + \frac{1}{2})\} \\ H_{25}^0 & & H_{19}^0 & \\ H_{12}^0 &= 0 \quad \text{and} & H_{1k}^0 &= H_{k1}^{0*} = H_{k1}^{0*}.\end{aligned}$$

here  $\phi_1$ ,  $\phi_2$ ,  $\mu_1$  and  $\mu_2$  are constants independent of  $J$  and depending only on the electronic structure of the molecule.

With these matrix elements the 10th order secular determinant breaks up into two fifth order determinants, each of which can be separately equated to zero. These determinants are identical in all respects except that one of these contains only positive terms while the other contains only the negative terms for each  $J$ . Hence only one of these is solved here since exactly similar equations apply to the other case also.

The form of this secular determinant is

$${}^4\Sigma \left( \begin{array}{ccccc} W_1^0 - W & 0 & H_{14}^0 & H_{15}^0 & H_{16}^0 \\ 0 & W_3^0 - W & H_{34}^0 & 0 & 0 \\ {}^4\Pi \left\{ \begin{array}{l} H_{41}^0 \\ H_{51}^0 \\ H_{61}^0 \end{array} \right. & \vdots & \begin{array}{l} H_{43}^0 \\ 0 \\ 0 \end{array} & \begin{array}{l} W_4^0 - W \\ H_{54}^0 \\ 0 \end{array} & \begin{array}{l} H_{45}^0 \\ W_5^0 - W \\ H_{65}^0 \end{array} & \begin{array}{l} 0 \\ H_{56}^0 \\ W_6^0 - W \end{array} \end{array} \right) \quad (12)$$

Now we transform this matrix with a unitary matrix  $S$  so that in the transformed matrix ( $H = S^{-1}H^0S$ ) the  ${}^4\Pi$  portion becomes diagonal. The eigenvalues of the  ${}^4\Pi$  state in the general intermediate case of coupling are given by Brandt (1936). If these are denoted by  $W'_3$ ,  $W'_1$ ,  $W'_5$ , and  $W'_6$  then the elements of  $S$  are given by

$$\left. \begin{aligned} S_{ik} &= [s_3^2 k + s_4^2 k + s_5^2 k + \frac{2}{6} k]^{-1/2} s_{ik} \quad (i, k = 3, 4, 5, 6) \\ s_{3k} &= [3(J - \frac{3}{2})(J + \frac{5}{2})]^{1/2} [(W'_5 - W_k)(W'_6 - W_k) - 3(J + \frac{1}{2})^2] \\ s_{4k} &= -(W'_3 - W_k) [(W'_5 - W_k)(W'_6 - W_k) - 3(J + \frac{1}{2})^2] \\ s_{5k} &= 2[(J - \frac{1}{2})(J + \frac{3}{2})]^{1/2} (W'_3 - W_k)(W'_1 - W_k) \\ s_{6k} &= -2[3(J - \frac{1}{2})(J + \frac{3}{2})]^{1/2} (J + \frac{1}{2})(W'_3 - W_k) \end{aligned} \right\} \quad (13)$$

Further  $S_{11} = 1$  and the remaining elements of  $S$  are zero. If the  ${}^4\Pi$  state belongs to case (a) the  $S$  matrix becomes a unit matrix, while if it belongs completely to case (b) coupling the  $S$  matrix is given by

$$\begin{pmatrix} \left(\frac{2J-3}{16J}\right)^{\frac{1}{2}} & \left(\frac{3(2J-3)}{16J}\right)^{\frac{1}{2}} & \left(\frac{3(2J+3)(2J-3)}{16J(2J-1)}\right)^{\frac{1}{2}} & \left(\frac{(2J+5)(2J+3)}{16J(2J-1)}\right)^{\frac{1}{2}} \\ \left(\frac{3(J+1)}{16J}\right)^{\frac{1}{2}} & \left(\frac{(2J+5)^2}{16(J+1)(2J+1)}\right)^{\frac{1}{2}} & \left(\frac{(2J+3)(2J-7)^2}{16(J+1)(2J+1)(2J-1)}\right)^{\frac{1}{2}} & \left(\frac{3(2J+5)(2J+3)(2J-3)}{16(J+1)(2J+1)(2J-1)}\right)^{\frac{1}{2}} \\ \left(\frac{3(2J+1)}{16J}\right)^{\frac{1}{2}} & \left(\frac{(2J-3)^2}{16(2J+1)J}\right)^{\frac{1}{2}} & \left(\frac{(2J+9)^2(2J-1)}{16(2J+3)(2J+1)J}\right)^{\frac{1}{2}} & \left(\frac{3(2J+5)(2J-1)(2J-3)}{16(2J+3)(2J+1)J}\right)^{\frac{1}{2}} \\ \left(\frac{2J+5}{16(J+1)}\right)^{\frac{1}{2}} & \left(\frac{3(2J+5)}{16(J+1)}\right)^{\frac{1}{2}} & \left(\frac{3(2J+5)(2J-1)}{16(2J+3)(J+1)}\right)^{\frac{1}{2}} & \left(\frac{(2J-1)(2J-3)}{16(2J+3)(J+1)}\right)^{\frac{1}{2}} \end{pmatrix} \quad (14)$$

After the transformation the secular equation can be represented by

$$\begin{array}{ccccc} W_1 - W & H_{13} & H_{14} & H_{15} & H_{16} \\ H_{21} & W_3 - W & 0 & 0 & 0 \\ H_{41} & 0 & W_4 - W & 0 & 0 \\ H_{51} & 0 & 0 & W_5 - W & 0 \\ H_{61} & 0 & 0 & 0 & W_6 - W \end{array} = 0 \quad (15)$$

where  $H_{1k} = S^*_{k4}H^0_{14} + S^*_{k5}H^0_{15} + S^*_{k6}H^0_{16}$ , and  $H_{kl} = H^*_{lk}$

Now it can be shown that at the crossing point of two levels (say, the levels  $i$  and  $k$ ) the effect of all matrix elements except those directly connecting these levels ( $H_{ik}$  and  $H_{ki}$ ) is negligible. Hence for the calculation of the perturbed energy values in the immediate neighbourhood of the crossing point of two levels it will be sufficient to diagonalise just this part of the secular determinant. Thus we have for the perturbed energy  $W'_i$  and  $W'_k$

$$\begin{aligned} W'_{i,k} = W_i + W_k \pm \sqrt{\left(\frac{W_i - W_k}{2}\right)^2 + |H_{ik}|^2} \end{aligned} \quad (16)$$

For the present purpose  $i=1$  and  $k=3, 4, 5, 6$ .

On solving the second determinantal equation the same final equation will be obtained except that here  $i=2$  and  $k=7, 8, 9, 10$ . Thus we see that one set of the  $\Lambda$  components of the  $^4\Pi$  state are perturbed only by one component of the  $^2\Sigma$  state, while the other set of the  $^4\Pi$  components are perturbed by the remaining component of the  $^2\Sigma$  state.

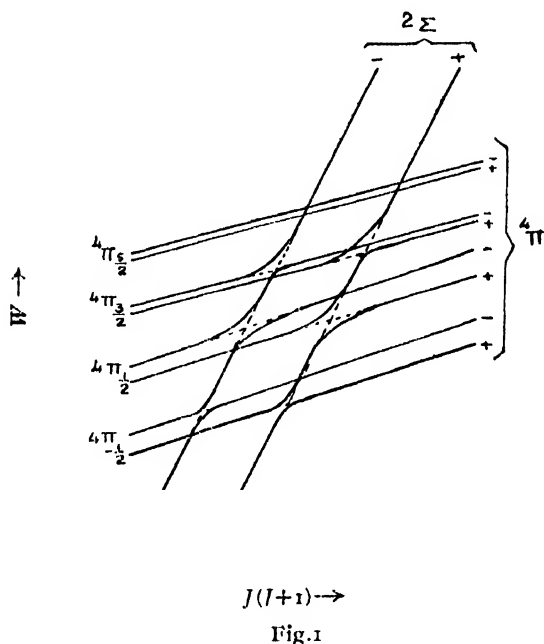


Fig.1

A diagrammatic representation of this case is given in figure 1, where the energy levels  $W$  are plotted against  $J(J+1)$ . The figure is not drawn to scale but the relative magnitudes of the various perturbations are qualitatively correct. The thin lines represent the unperturbed levels while the thick lines represent the perturbed levels.

## ACKNOWLEDGMENTS

The author wishes to acknowledge his deep indebtedness to Prof. K. R. Rao for his invaluable guidance in carrying out this work. The author wishes to express his thanks to the Government of India for the award of a senior research scholarship.

## REFERENCES

- Brandt, W. H., 1936, *Phys. Rev.*, **50**, 778.  
 Budö, A. and Kovács, I., 1938, *Zetts. f. Phys.*, **109**, 393.  
 „ 1939, *ibid.*, **111**, 633.  
 „ 1951, *Acta Physica.*, **1**, 84.  
 Ittmann, G. P., 1931, *Zetts. f. Phys*, **71**, 616.  
 Kovács, I. 1938, *ibid.*, **109**, 387.  
 „ 1939, *ibid.*, **111**, 640.  
 Kovács, I. and Lagerqvist, A. 1950 *Ark. f. Fysik.*, **2**, 111  
 Krönig, R. De. 1928, *Zetts. f. Phys*, **80**, 347.  
 Van Vleck, J. H. 1929. *Phys. Rev.*, **33**, 467

# DISTORTION IN ELECTRON LENS

By M. L. DE AND D. K. SAHA

INSTITUTE OF NUCLEAR PHYSICS, CALCUTTA AND INSTITUTE OF JUTE TECHNOLOGY, CALCUTTA

(Received for publication, May 11, 1954)

## Plate VIII

**ABSTRACT.** The distortion produced by an electromagnetic lens of an electron microscope has been measured in different parts of the image field. From the data obtained, the distortion coefficient of the lens has been evaluated, and compared with similar values obtained by other workers.

### 1. INTRODUCTION

It is a familiar experience to all workers in electron microscopy, that at low settings of the projector lens, the final image is seen to suffer from pincushion type of distortion. A set of electron micrographs of a 200 mesh metal grid is reproduced in figure 1. Here the projector lens power and hence the magnification increases from left to right. Pincushion distortion is seen to be very prominent in frames of lower magnifications where the peripheral

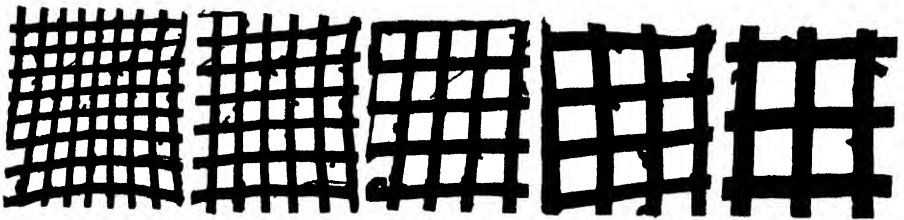


FIG. 1

meshes are found to have elongated shapes. At low magnifications, therefore, the distorted image gives an erroneous representation of the shape and size of the object being imaged.

Occasions, however, often arise, e.g. for working with fairly large specimens, when one is constrained to work at low projector magnifications in order that the whole of the magnified image may remain within the final field of view. Under such conditions a knowledge of the amount of distortion in different zones of the image field is of essential importance in order to get a correct appraisal of the true size and shape of the specimen under examination.

An estimation of distortion is also of importance in lens designing in that by experimenting on pole-pieces of various designs, one can find out from the

experimental data the values of the distortion coefficient of different pole-pieces. By correlation of values of distortion coefficient with the lens parameters one can ascertain the optimum design parameters for pole-pieces of minimum distortion.

## 2 THEORETICAL CONSIDERATIONS

In electron microscopes using only one projector lens besides the objective, the distortion is contributed solely by the projector lens (Zworykin *et al*, 1948). The aberration, resulting in a lateral shift of an image point from its true geometric position, can be expressed thus (Zworykin *et al*, 1948) :

$$dr = S_p(M_o r_o)^3 \quad (1)$$

where  $dr$  is the displacement on the final field of view of the image point whose conjugate distance from the optic axis referred to the object plane is  $r_o$ ,  $S_p$  is the coefficient of distortion and  $M_o$  is the magnification due to the objective lens. Since the lens field has rotational symmetry, the displacement is mostly in the radial direction.

The magnitude of distortion can be found out by following the method of Hillier (1946) with a little modification. The method is briefly as follows: The specimen chosen is a replica of a grating whose constant is accurately known. Let  $O$  be the point of intersection of the optic axis of the projector lens on the final field of view (figure 2). The co-ordinates  $XOX'$  and  $YOY'$  are

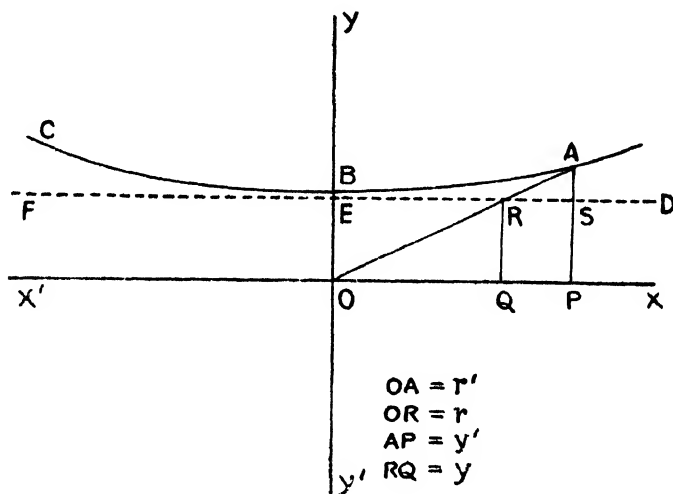


FIG. 2

drawn such that the  $X$ -axis lies along the direction of the grating lines on the final field of view. The specimen is moved about and locked so that one grating line lies on and along the  $X$ -axis. Let  $ABC$  be another grating line which has suffered distortion, and let  $DEF$  be the line which would have been



the geometric position of  $ABC$  had there been no distortion. An arbitrary point  $A$  on  $ABC$  is joined with  $O$ . Since the distortion is mostly radial, the point  $R$  is the true geometric position of point  $A$ . Calling the distances  $RQ$ ,  $AP$ ,  $OR$  and  $OA$  as respectively  $y$ ,  $y'$ ,  $r$  and  $r'$ , it follows from the geometry of the figure that

$$r = r', y/y' \quad (2)$$

If  $ABC$ , the line chosen is the  $n^{\text{th}}$  line from the centre, and if the grating constant  $G_c$  and overall magnification  $M$  of the microscope be known, then evidently,

$$y = n, G_c M \quad (3)$$

$r'$  and  $y'$  in expression (2) are directly measureable on the final field of view or can be measured conveniently on a micrograph. Hence  $r$  in expression (2) i.e. the true undistorted distance corresponding to  $r'$  is found out. The difference  $r' - r = dr$  is the amount of distortion corresponding to the observed image point  $A$  situated at  $r'$  as seen in the final image. By choosing systematically several image points, their true geometric positions and their corresponding amounts of distortion can therefore, be easily found out. By plotting  $r$  and  $dr$  against  $r'$ , curves are drawn to give immediately the distortion in the various zones of the final image field.

From the results thus obtained the coefficient of distortion is ascertained as follows : Since  $dr = S_p(M_o r_o)^3$  and  $r = M_o M_p r_o$  we have,

$$dr = S_p(r/M_p)^3 \quad (4)$$

where  $M_o$  and  $M_p$  are the objective and projector magnifications respectively. Since  $dr$  corresponding to  $r$  is already ascertained,  $S_p$  can be calculated if  $M_p$  is known. An accurate knowledge of  $M_p$  is therefore required to be known. Then, by plotting  $dr$  against  $(r/M_p)$  a straight line can be drawn, whose slope gives the value of  $S_p$ .

### 3. EXPERIMENTAL METHOD AND RESULTS

#### (i) Magnitude of distortion :

A collodion replica of a grating of constant  $1.85\mu$  was mounted on a microscope grid. By proper manipulation of the object stage movement, a grating line was made to lie such that a straight grating line was obtained at the centre on the final field of view. Micrographs were then made and the beam voltage and the objective and projector currents were noted. A typical micrograph is reproduced in Plate VIII.

The microscope was then calibrated with polystyrene latex for overall magnification with these voltage and currents. This magnification multiplied by the grating constant, gave the magnitude of the spacings for a distortion-free geometric image, from which the value of  $y$  in expression (3) was found out. The values of  $r'$  and  $y'$  were determined from the grating micrograph.



determined. The value of  $r/M_p$  was then calculated, from which, by substituting in expression (4),  $S_p$  was found out.  $d\tau$  was next plotted against  $(r/M_p)^3$  and a mean straight line was drawn (figure 4). The slope of the line gave the coefficient of distortion  $S_p$ , which was found to have the value of  $6.42 \times 10^3$ .

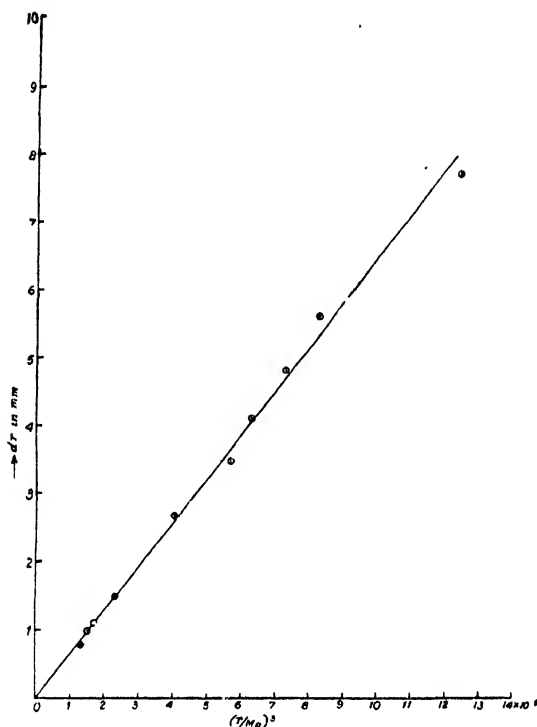


FIG. 4

## DISCUSSION

From figure 3 which gives both  $r$  and  $d\tau$  as a function of  $r'$  one can ascertain at a glance the true geometric position of an image point whose apparent position is known on a micrograph or on the fluorescent screen, and also the amount of distortion. These two curves therefore are of immediate practical importance. From curve II in figure 3 which gives the distortion as a percentage, it is found that the distortion remains to within 10% upto a distance of 2.5 cm. from the centre.

If, after Zworykin *et al* (1948) it is assumed that  $S_p$  can be expressed by a formula of the following type viz.,

$$S_p = M_p \cdot C/D^2 \quad \dots (5)$$

where  $C$  is a lens constant, we can determine the value of  $C$  of our lens from the knowledge of  $D$ , the clear diameter of the pole-piece, and  $M_p$ , the lens

magnification. For our case,  $S_p = 6.42 \times 10^3$ ,  $D = 0.195$  cm.,  $M_p = 65$ , so that  $C = 3.75$ . This value is to be compared with the value of 2.2 estimated by Zworykin *et al* (1948) for a cylindrical lens.

#### ACKNOWLEDGMENTS

The authors wish to express their sincere thank to Professor M. N. Saha, F. R. S., for his kind interest and to Prof. N. N. Dasgupta for his helpful guidance. Thanks are also due to the Ministry of Education, Government of India for financial aid.

#### REFERENCES

- Hillier, J. 1946, *J. App. Phys*, **17**, 411.  
Zworykin, V. K. and others, 1948, *Electron Optics and the Electron Microscope*, 1st. Ed., p. 639, p. 640.

# ATOMIC NITROGEN AS A CONSTITUENT FOR REGION F<sub>1</sub>\*

By A. P. MITRA

IONOSPHERE RESEARCH LABORATORY, THE PENNSYLVANIA STATE UNIVERSITY,  
STATE COLLEGE, PENNSYLVANIA

(Received for publication, May 4, 1954)

**ABSTRACT**—The case of atomic nitrogen as one of the possible constituents for Region F<sub>1</sub> is studied by examining simultaneously the problem of dissociation of molecular nitrogen and that of the ionization of the resulting nitrogen atoms. The dynamic condition of the atmosphere is taken into account. It is shown that the maximum of ionization produced as a result of photoionization of atomic nitrogen lies between 150 to 200 km, for overhead sun, the best value being somewhere around 170 km. Further to give adequate ionization for the F<sub>1</sub>-layer, the concentration of atomic nitrogen at the height where diffusive separation takes place need not be larger than  $\frac{1}{10}n(\text{N}_2)$ .

Possible contribution from the ionization of atomic oxygen at third ionization potential is also discussed.

## 1. INTRODUCTION

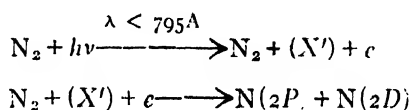
An attempt has been made in the present paper to examine in some detail the case of atomic nitrogen as an active constituent for Region F<sub>1</sub>. This has been considered necessary because of the fact that, although some half a dozen theories have been advanced so far, none has been found entirely satisfactory. The atmospheric constituents present in sufficient number at the level of the F<sub>1</sub>-region are atomic oxygen, molecular nitrogen and possibly atomic nitrogen. Of these, the evidence of twilight spectra precludes the possibility of N<sub>2</sub><sup>+</sup> (Bates, 1949), while atomic oxygen (at the first ionization potential) gives an ionization maximum at the wrong location somewhere between the E and F<sub>1</sub>-regions (Bates and Seaton, 1950).

In the past, there has been a tendency to overlook possible ionization through atomic nitrogen. This was no doubt due to the general belief that the dissociation efficiency of N<sub>2</sub> is very low outside the auroral zone. This belief was fostered partly by the absence of a simple photodissociation process for N<sub>2</sub> analogous to that of O<sub>2</sub>, and partly by the presence of molecular nitrogen spectra at the very high levels seen in sunlit aurora. The latter, particularly, made it difficult to believe that atomic nitrogen can be a constituent of the upper atmosphere at normal times to any degree of importance.

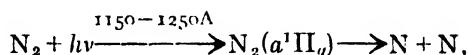
\* The research reported in this note has been sponsored by the Geophysical Research Division of the Air Force, Cambridge Research Center, Air Research and Development Command under Contract AF19(122)—44.

† Communicated by Prof. S. K. Mitra.

Such objections have, however, been removed in recent years by the discovery of atomic nitrogen lines in airglow, (Courtes, 1950 ; Dufay, 1951) by the realization that atomic nitrogen may be produced appreciably by the dissociation recombination process (Bates, 1951 ; S. K. Mitra, 1951)



and, at low heights, by the Herzberg-Herzberg process (1948) :



and the suggestion that  $\text{N}_2^+$  may also be formed by  $\text{N} + \text{N}^+ \longrightarrow \text{N}_2^+$  (Nicolet, Pastiels, 1952 ; Nicolet 1950).

The case of atomic nitrogen as a possible source of the  $F_1$ -region has not been completely ignored in the past. Bates and Seaton (1950) have considered the possibility, but they arrived at the discouraging conclusion that, in order to produce the  $F_1$ -region, the concentration of atomic nitrogen at the level of the maximum should be as large as  $3 \times 10^{16}/\text{cm}^3$ \*—a value difficult to accept. Whether the same result is obtained with recently deduced upper atmospheric characteristics (which are appreciably different from Bates and Seaton's) remains to be seen. Further, the problem of the distribution of atomic nitrogen at  $F_1$ -region heights has to be investigated. This involves a critical examination of the dissociation of  $\text{N}_2$  at  $F_1$ -region heights, of the various processes of recombination of atomic nitrogen and consideration of a dynamical atmosphere.

The present paper attempts a simultaneous examination of the problem of  $\text{N}_2$ -dissociation and the problem of ionization of the resulting nitrogen atoms. The two problems are examined together with a view to obtaining a consistent overall picture. It is shown that atomic nitrogen appears to contribute at least partly to the ionization of Region  $F_1$ .

## 2. GENERAL CONSIDERATIONS

According to the theory of Chapman, the rate of electron production,  $q$ , due to the ionization of an atmospheric constituent by solar ultraviolet radiation is given by

$$q = AnQ_a \exp(-AnH \sec\chi) \quad \dots (1)$$

where

$A$  is the absorption coefficient for the constituent concerned.

$n$  is the density of the constituent at any height  $h$ .

\* In obtaining this value no account was taken of the attenuation of the incoming radiation through absorption by O and  $\text{N}_2$  which is larger than that by N. Consideration of such absorption improves the situation appreciably.

$Q_a$  is the number of solar photons at the relevant wave length reaching the terrestrial atmosphere.

$\chi$  is the solar zenith angle.

$H$  is the scale height.

For an isothermal atmosphere, where the density is given by

$$n = n_0 e^{-z/H}$$

where  $z$  is the "reduced" height, Eq (1) gives, for the density at the height of the maximum ionization, :

$$n_m = \frac{\cos \chi}{AH} \quad (2)$$

For a non-isothermal atmosphere where the scale height  $H$  varies linearly with height :

$$H = H_0 + \beta z,$$

Eq (3) becomes

$$n_m = \frac{\cos \chi (1 + \beta)}{AH} \quad (4)$$

Eq (4) gives the expression almost invariably used in discussing an ionization mechanism.

It is possible, however, to improve Eq (4).

The radiation responsible for the photoionization of the active constituent,  $i$ , is not absorbed by  $i$  alone, but frequently by other atmospheric constituents as well. Although such absorption is usually ignored, it is not always proper to do so, especially when, as in the case of atomic nitrogen, the active constituent is not the main absorbing constituent. This means that one has to replace Eq (1) by

$$q = A_i n_i Q_a \exp \left[ - (A_i n_i H_i + \sum_k A_k n_k H_k) \sec \chi \right] \quad \dots \quad (5)$$

where the subscript  $k$  refers to any atmospheric constituent, other than the one ionized, which absorbs the relevant radiation.

In the expressions (3) and (4) the recombination coefficient  $\alpha$  is assumed constant. In Region F<sub>1</sub>,  $\alpha$  is very nearly so, but there are indications that  $\alpha$  in this region probably depends on temperature and may be approximately represented by (A. P. Mitra, 1952)

$$\frac{H}{H_0} \quad (6)$$

where  $\tau$  is of order of unity.

In a study of Region F<sub>1</sub> we are concerned with the atmosphere at levels 150 km to 250 km, most of which is in diffusive equilibrium although the lower levels around 150 km are probably in a transitional state between mixing and diffusion. This means that, for most of the height levels of interest for the present work,  $H_k$  is different for the different constituents. The new expression replacing (4) now becomes :

$$A_{inim} + \sum_k A_{knkm} = \frac{\cos \chi (1 + \beta_i - r\beta_i)}{H_{im}} \quad \dots (7)$$

The above expression is to be used in discussing the adequacy of any constituent whose distribution is determined only by the atmospheric temperature distribution.

Complications, however, appear when the distribution of the active constituent is determined by photochemical reactions rather than by the atmospheric temperature distribution. In the case of atomic nitrogen such complications exist. Consider that the distribution of atomic nitrogen in the upper atmosphere is given by

$$n(N) = n_0(N) \xi^l h \quad \dots (8)$$

The absorption of the incoming radiation is mainly controlled by atomic oxygen and molecular nitrogen and, hence, to a first approximation, we may neglect the term  $A_{inim} H_i \sec \chi$  in the exponent of Eq(5). We may, then, write :

$$N_i^2 = \frac{A(N)n_0(N)Q_h}{\sim} \xi(h) \frac{H}{H_0} \exp - \sum A_{knkm} H_{k0} \sec \chi \left( \frac{H}{H_0} \right)^{-\beta_k} \quad (9)$$

This gives, at the height of the maximum ionization,

$$\sum_k A_{knkm} \sec \chi + \frac{r\beta_i}{H_i} + \frac{\xi'}{\xi} = 0 \quad \dots (10)$$

where  $\xi'$  is the first derivative of  $\xi$  with respect to height.

Equation (10) is general and applies to any kind of distribution.

### 3. UPPER ATMOSPHERE CHARACTERISTICS

The region of interest in the present study is the height range 150-250 km. Rocket results regarding pressure are available up to 220 km; but estimation of temperature and density from these results are made difficult by lack of proper information regarding the amount of dissociation of the constituents  $N_2$  and  $O_2$ . There are several accounts of the probable distributions of the main constituents in this region based on rocket results (Gerson, 1952; Nicolet and Mange, 1954; Kallman, 1953; The Rocket Panel, 1952). These results differ somewhat because of the different temperature distributions and different dissociation rates assumed.

In calculating the concentrations, it is perhaps best to start with the temperature distribution as known. Of the various published distributions, the one given by Nicolet and Mange seems to us the most reasonable, but temperatures higher by as much as 25 percent are also possible.

In the present work three different models of temperature have been used (figure 1). Model 1 is the Nicolet-Mange model; Model 2 is a possible upper limit of the temperatures and Model 3 is a likely compromise



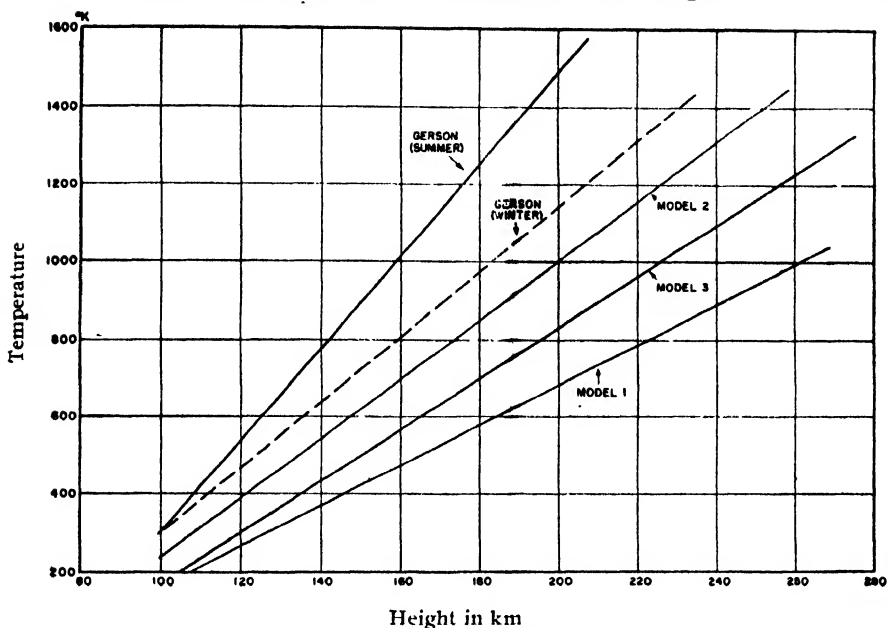


Fig. 1. Variation of atmospheric temperature with height for different models

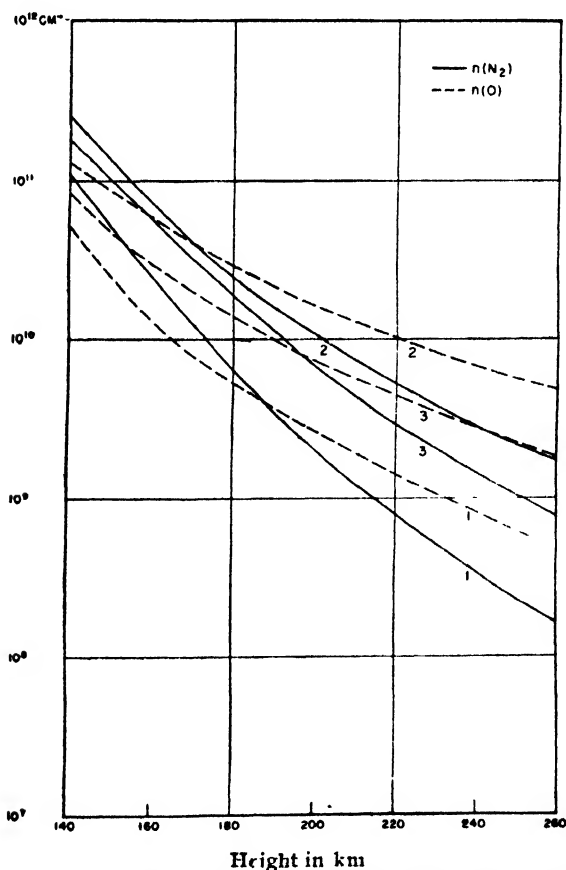


Fig. 2 Distribution of  $\text{N}_2$  and  $\text{O}$  with height for different temperature models

between Models 1 and 2. The models used by Gerson are also shown ; but they are considered too high, in that they are based on the preliminary rocket data, and have not been used. The particle concentrations for  $N_2$  and O for these different models are shown in figure 2. In each case the atmosphere is supposed to fall into diffusive separation above 160 km.

#### 4. PHYSICAL DATA

##### 4.1 Absorption Coefficients

We are interested in the absorption coefficients of the various constituents in three distinct wave length regions: one at  $\lambda \leq 795 \text{ \AA}$  where photoionization of  $N_2$  occurs, and another at  $\lambda \leq 855 \text{ \AA}$  where ionization of N occurs, and the third at  $\lambda \leq 910$  where the first ionization of atomic oxygen takes place. Values of the absorption coefficients for the different atmospheric constituents (Bates and Seaton, 1950 ; Clark, 1950 ; Chapman and Price, 1936 ; Weissler and Lee, 1952 ; Weissler, Lee and Mohr, 1952) for these wave lengths are given in Table I.

TABLE I  
Absorption coefficient  $A$  in  $\text{cm}^{-1}$

$\lambda 795$				$\lambda 855$				$\lambda 910$		
$N_2$	$O_2$	O	N	$N_2$	$O_2$	O	N	$N_2$	$O_2$	O
$10^{-17}$	$18 \times 10^{-17}$	$5 \times 10^{-18}$	$10^{-14}$	$3 \times 10^{-18}$	$1.4 \times 10^{-17}$	$3 \times 10^{-18}$	$9 \times 10^{-18}$	$1 \times 10^{-18}$	$1 \times 10^{-17}$	$2.5 \times 10^{-18}$

##### 4.2 Intensity of Solar Radiation

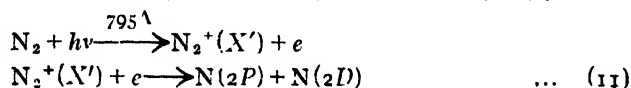
The rocket results of Tousey et al (1951) between the wave lengths 1050A and 795A showed that the solar intensity between these wave lengths correspond to a flux density of  $5 \times 10^{11}$  to  $3 \times 10^{12}/\text{cm}^2/\text{sec}$ . On the assumption that the equivalent solar temperature is constant in this range, the corresponding temperature is  $7200^\circ K$ . Also, with  $Q_a = 10^{12}/\text{cm}^2/\text{sec}$  at  $\lambda 1050$ ,

$$\begin{aligned} Q_a(\leq 855) &= 2 \times 10^{10} \text{ cm}^{-2} \text{ sec}^{-1} \\ Q_a(\leq 790) &= 3.6 \times 10^9 \text{ cm}^{-2} \text{ sec}^{-1} \\ Q_a(\leq 910) &= 8 \times 10^{10} \text{ cm}^{-2} \text{ sec}^{-1} \end{aligned}$$

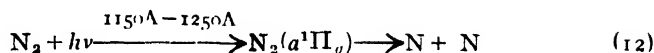
#### 5. THE CASE OF ATOMIC NITROGEN

##### 5.1 Distribution of Atomic Nitrogen

Atomic nitrogen is formed, mainly, by the dissociative recombination process (Bates, 1950 ; S. K. Mitra, 1951 ; Herzberg and Herzberg, 1948) :

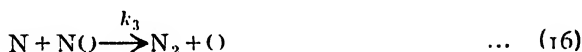


and by the Herzberg-Herzberg process :



However, as Deb (1952) has shown, at heights of 150 km or above, the levels of interest in the present study, we need only consider the former process.

Nitrogen atoms so formed may disappear through a number of processes, such as :



Deb (1952) has discussed the relative importances of the reactions (13), (14) and (15) for the atmospheric model given by Gerson and has shown that processes (14) and (15) are much slower than process (13). With the atmospheric models 1, 2 and 3 used in the present work, it can be easily shown that the three-body recombination process given by (15) is never very important, while process (14) may be important if

$\frac{n(\text{O})}{n(\text{N})}$  is  $10^3$  or more. At 200 km and above, the ratio is certainly not large

enough to make process (14) important. Presumably, the process may be ignored for the lower levels of the F<sub>1</sub>-region too, since, as will be pointed

out later,  $\frac{n(\text{O})}{n(\text{N})}$  is not expected to be much larger than 100 above 150 km.

Now consider the two-body process given by Eq (16). The rate is given by  $k_3 n(\text{N})n(\text{NO})$ . Hence

$$\frac{\text{Rate of process (16)}}{\text{Rate of process (13)}} = \frac{k_3}{K} \frac{n(\text{NO})}{n(\text{N})} \quad (17)$$

The coefficient  $k_3$  is temperature-dependent with values about  $8 \times 10^{-15} \text{ cm}^3/\text{s}$  and  $5 \times 10^{-14} \text{ cm}^3/\text{s}$  at 150 and 200 km where the temperatures are of the order of 450°K and 700°K. Hence, the ratio (17) is about  $2 \times 10^4 [n(\text{NO})/n(\text{N})]$  at 150 km and about  $[10^5 n(\text{NO})/n(\text{N})]$  at 200 km. Now, for a fixed atmosphere, NO has a concentration of about  $10^8/\text{cm}^3$  at

80 km (Nicolet, 1953 ; A. P. Mitra, 1953), so that  $\frac{n(\text{NO})}{n(\text{N}_2)} \approx 2 \times 10^{-7}$  This

ratio will remain constant upto 150 km because of mixing and will be approximately the same even above 150 km, under conditions of diffusive separation, because the respective scale heights of NO and N<sub>2</sub> are not

appreciably different. A consequence of this is that the NO-concentration is about  $2 \times 10^4/\text{cm}^3$  at 150 km and  $10^3/\text{cm}^3$  at 200 km. Now as will be shown later,  $n(\text{N}) \approx \frac{1}{100} n(\text{N}_2)$  at 150 km and perhaps about  $\frac{1}{10} n(\text{N}_2)$  at 200 km. Hence, the ratio (17) becomes 0.3 at 150 km and about 0.2 at 200 km. One may, therefore, also ignore this process.

The height variation of the dissociation rate is of particular interest. Table II shows the variation of  $J$ , the rate coefficient of reaction (11) with height (for  $\lambda = 0^\circ$ ) for the three models chosen :

TABLE II

 $J$  (per sec.)

Height (km)	Model		
	1	2	3
160	$5.2 \times 10^{-9}$	$1.3 \times 10^{-13}$	$1.1 \times 10^{-10}$
180	$1.5 \times 10^{-8}$	$3.2 \times 10^{-11}$	$1.3 \times 10^{-9}$
200	$2.3 \times 10^{-8}$	$3.3 \times 10^{-10}$	$6.4 \times 10^{-9}$
220	$2.9 \times 10^{-8}$	$1.1 \times 10^{-9}$	$1.1 \times 10^{-8}$
240	$3.2 \times 10^{-8}$	$2.9 \times 10^{-9}$	$1.6 \times 10^{-8}$
260	$3.4 \times 10^{-8}$	$5.4 \times 10^{-9}$	$2.2 \times 10^{-8}$

The coefficient  $J$ , therefore, varies from a value of about  $2 \times 10^{-8}$  to the very small value of  $10^{-13}$  in the height range of interest (160–260 km) and depending on the type of the atmosphere model used. These values lead us to the following conclusions :

(i) If equilibrium is allowed, then the concentration of atomic nitrogen around 200 km would be about  $10^9/\text{cm}^3$ , and the total number of nitrogen atoms in a column of unit cross-section would be about  $4 \times 10^{16}/\text{cm}^2$ ,  $2 \times 10^{16}/\text{cm}^2$  and  $3 \times 10^{16}/\text{cm}^2$  for models 1, 2 and 3, respectively. The corresponding values for molecular nitrogen are about  $2 \times 10^{17}/\text{cm}^2$ ,  $4 \times 10^{17}/\text{cm}^2$  and  $3 \times 10^{17}/\text{cm}^2$ .

(ii) Since the time,  $T_{eq}$ , required for  $n_t(\text{N})$  to grow to a value  $e^{-1}$  times the equilibrium value is given by

$$T_{eq} = \frac{1}{2\sqrt{[JKn(\text{N}_2)]}}$$

a period of several years is necessary in order that photochemical equilibrium may be established.

Now the time of mixing at these heights is probably of the order of a week, while the time of diffusion is of the order of several hours at 160 km and several minutes at 250 km (Nicolet and Mange, 1954). Somewhere between 150 and 200 km, therefore, the diffusive separation will begin to be effective. It is difficult to locate at present the height where it begins, but there seems to be no doubt that the process will be effective at least above 200 km. Thus, above 200 km, one may safely write :

$$n(N) = n_{200}(N) \left( \frac{H}{H_0} \right)^{\left[ 1 + \frac{1}{\beta(N)} \right]}$$

where  $\beta(N)$  is the scale height gradient relevant to atomic nitrogen.

Below 150 km, where the mixing effect still predominates, the concentration of atomic nitrogen will follow the main atmosphere. It is difficult to give an exact figure of the ratio  $[n(N)/n(N_2)]$  for these levels, but from examination of Table II and of the possible values of  $K$ , Nicolet's (1952) value of 1/100 seems reasonable.

The region between 150 to 200 km is probably a transition region. It is possible that diffusive separation begins to predominate even at 160 km in which case the transition region may be confined between 150 to 160 km.

For purposes of calculation, two different non-equilibrium distributions have been used. In the first (case I) mixing predominates up to about 150 km with the ratio  $n(N)/n(N_2) = 1/100$ ; transition from mixing to diffusive separation occurs between 150 to 200 km, the ratio  $n(N)/n(N_2)$  increasing to a value of 1/10 at 200 km; above 200 km atomic nitrogen is distributed according to its own scale height. In the second case (case II) transition is supposed to occur between a narrow strip at 140-150 km with the concentration falling according to its own scale height above 150 km. The real situation is probably somewhere between these two.

The value  $\frac{n(N)}{n(N_2)} = \frac{1}{10}$  is a conservative value, and has been chosen on

the basis of the values mentioned before, of the total number of nitrogen atoms\* and molecules in a column of unit cross-section. These values are such that they allow for an average ratio of about 1/10 over the entire region even when mixing transfers the nitrogen atoms from one place to another.

### 5.2. Atomic Nitrogen as a Constituent for Region F<sub>1</sub>

The experimental results regarding F<sub>1</sub> are that the equivalent height of maximum ionization is about 190 km at summer noon and about 210 km at winter noon for a medium latitude. The actual heights are not known, but they may be appreciably lower than the above values. The electron density at the height of the maximum ionization is about  $2.5 \times 10^5/\text{cm}^3$  for sunspot minimum, and  $4 \times 10^5/\text{cm}^3$  for sunspot maximum.

Consider now the photoionization of atomic nitrogen for the distributions

\* Estimated under equilibrium conditions.

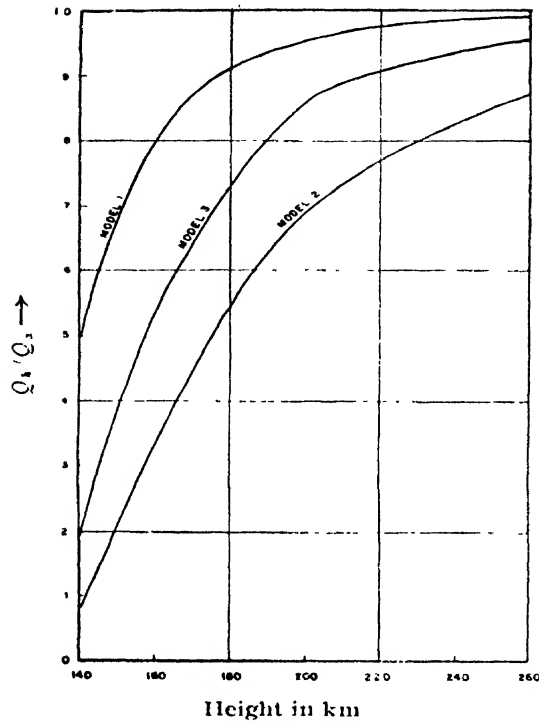


Fig. 3  $Q_h/Q_a$  as a function of height

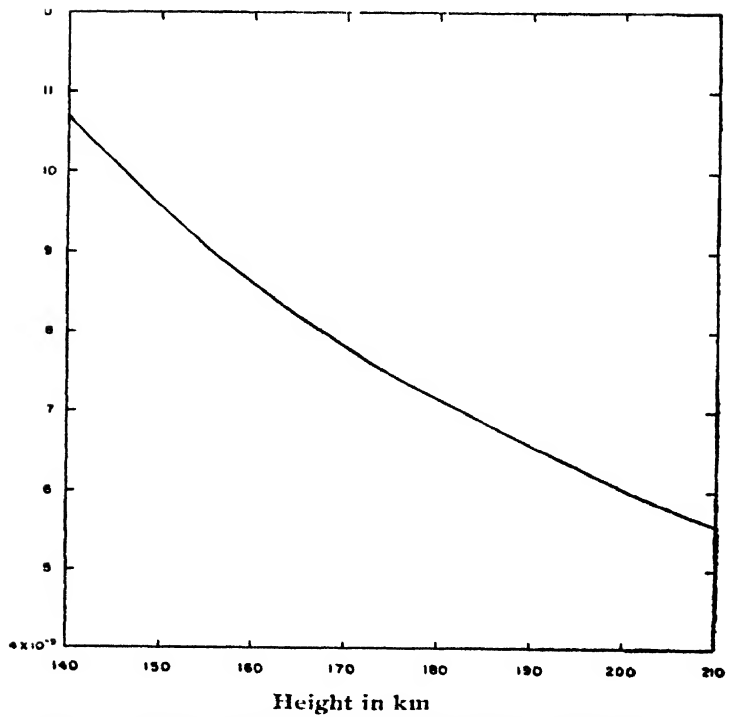


Fig. 4. Probable variation of recombination coefficient.

(cases I and II) indicated in the previous section for an atmosphere in which photochemical equilibrium cannot be reached. Now, absorption of the incoming solar radiation by atomic nitrogen is negligible compared to that by oxygen and molecular nitrogen for this case. Under these conditions the intensity of the ionizing radiation at any height will be independent of whichever distribution of atomic nitrogen we select. In figure 3 the intensity of this radiation at various heights is plotted as a ratio of the unattenuated intensity for the three atmospheric models. The height of maximum ionization and the maximum ionization densities calculated with the help of these figures (and for the recombination coefficient distribution given in figure 4) are shown in Table III. For comparison purposes, the results for the idealised case of photochemical equilibrium are also shown.

TABLE III

Height and concentration of maximum ionization for different cases

Model	Non-equilibrium				Equilibrium	
	Case I		Case II			
	$h_{\max}$ (km)	$N_e$ (cm <sup>-3</sup> )	$h_{\max}$ (km)	$N_e$ (cm <sup>-3</sup> )	$h_{\max}$ (km)	$N_e$ (cm <sup>-3</sup> )
1	160	$9 \times 10^4$	150	$2.5 \times 10^5$	164	$2.9 \times 10^5$
2	218	$1.5 \times 10^5$	175	$2.6 \times 10^5$	222	$1.8 \times 10^5$
3	182	$1.4 \times 10^5$	160	$2.9 \times 10^5$	192	$2.4 \times 10^5$

It may be remarked here that for such cases as in II (non-equilibrium case), the only assumption needed for determination of the location of maximum ionization is the assumption of diffusive separation. If it is accepted that such a separation takes place somewhere below the maximum of the F<sub>1</sub>-layer, then one is permitted to use, for the regions of interest, the expression :

$$n(\text{N}) = n_0(\text{N}) \left( \frac{H}{H_0} \right)^{-\left[ 1 + \frac{1}{2(N_2)} \right]}$$

which yields, for  $h_m$ ,

$$2Hn(\text{N}_2) \sum_k A_k n_{mk} \sec \chi = 1 + 2\beta(\text{N}_2) - 2r\beta(\text{N}_2)$$

The results for such a case for overhead sun have already been given (case II, Table III). They are also indicated in figure 5 where the results for other values of  $\chi$  have been included.

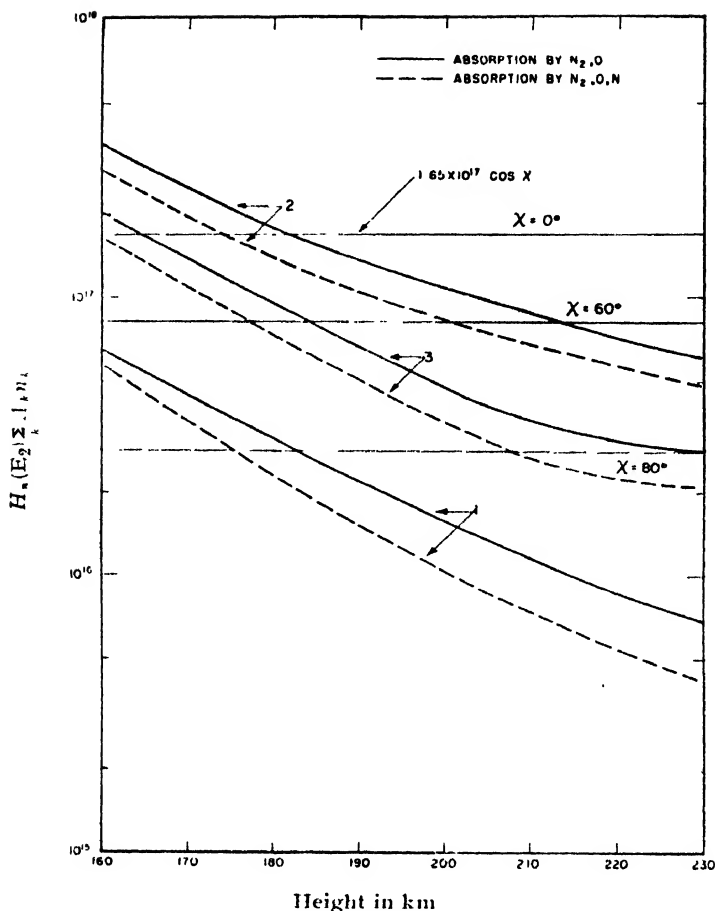


Fig. 5. Location of maximum ionization for the second non-equilibrium case

## 6. DISCUSSION

It seems probable that, for a dynamic atmosphere, the maximum of ionization produced as a result of the photoionization of atomic nitrogen lies between 150 to 200 km (for  $\chi=0^\circ$ ) depending on the atmospheric model assumed; the best value being somewhere around 170 km. There is still a discrepancy of the order of a scale height between the theoretical value and the observed equivalent height. But, as Nicolet (1952) has pointed out, the measured equivalent heights may differ from the actual heights by such an amount.

In order that atomic nitrogen should give adequate ionization for the  $F_1$ -layer, the concentration of atomic nitrogen at the height where diffusive separation takes place need not be larger than  $\gamma_0^1 n(N_2)$ . Such a ratio is not impossible. It seems likely, therefore, that atomic nitrogen will contribute at least partly to the ionization of the  $F_1$ -region.

The case of atomic oxygen has not been discussed so far. Ionization of atomic oxygen at the first ionization potential is not suitable. With



$A(O) = 2.5 \times 10^{-18} \text{ cm}^2$ ,  $A(O_2) = 1.1 \times 10^{-17} \text{ cm}^2$  and  $A(N_2) = 3 \times 10^{-18} \text{ cm}^2$  for  $\lambda \leq 910 \text{ \AA}$ , it is easily shown that the ionization maximum is around 140 km for  $\chi = 0^\circ$  for all the three models chosen. But although ionization of atomic oxygen at the first ionization potential does not seem adequate, ionization of O at the third ionization potential (13.5 eV) may be of importance.\*  $A(O)$  at this wave length is about  $10^{-17} \text{ cm}^2$ , of the same order as  $A(N)$  at 855, so that the ratio of ionization yield through atomic oxygen at  $\lambda \leq 665$  and that through atomic nitrogen at  $\lambda \leq 885$  is given by

$$\frac{q(O)}{q(N)} \simeq \frac{n(O)Q(O)}{n(N)Q(N)}$$

$Q(O)/Q(N)$  is probably of the order of  $10^{-2}$  so that  $n(O)/n(N)$  should be about  $10^2$  or larger in order that ionization through atomic oxygen should be important. At lower F<sub>1</sub> heights such a ratio presumably does exist, but at higher levels (i.e. at the level of the maximum ionization and above  $n(O)/n(N)$  may not be large enough. Another interesting point about ionization of O at  $\lambda \leq 655$  is that the ionization maximum occurs at a height around 200 km i.e. at the correct height.

It has been pointed out that the F<sub>1</sub> and the F<sub>2</sub>-regions may both arise from a single ionization mechanism by a process of bifurcation (Bradbury, 1938; Bates, 1949; Mitra, 1952; Ghosh, 1955; Chatterjee, 1953). On this hypothesis the theory of F<sub>1</sub> formation will have bearing on the F<sub>2</sub>-region as well. Although the theoretical arguments for such a hypothesis seems well-grounded, to date no experimental confirmation has been available. Some confirmation was sought during the present work by studying the departures of the hourly values of the ordinary wave critical frequencies from the hourly means for both the F<sub>1</sub> and F<sub>2</sub>-layers using the following parameters:

$$P(F_1) = \frac{(foF_1)^2 - (\overline{foF_1})^2}{(\overline{foF_1})^2} \times 100\%$$

$$P(F_2) = \frac{(foF_2)^2 - (\overline{foF_2})^2}{(\overline{foF_2})^2} \times 100\%$$

$P(F_1)$  and  $P(F_2)$  have been plotted against each other as a scatter diagram. The correlation is high—a typical case is shown in figure 6.

Now, the ionization of F<sub>2</sub> increases by a factor of 3 from sunspot minimum to sunspot maximum and that for F<sub>1</sub> by about 1.6. The resulting

value  $\frac{\Delta N(F_2)}{\Delta N(F_1)} \simeq 3.4$  may be considered as an amplification factor and must

depend, primarily, on changes in solar intensity; since local dynamical effects

\* The author is grateful to Dr. Nicolet for pointing out this possibility and for interesting discussion on this point.

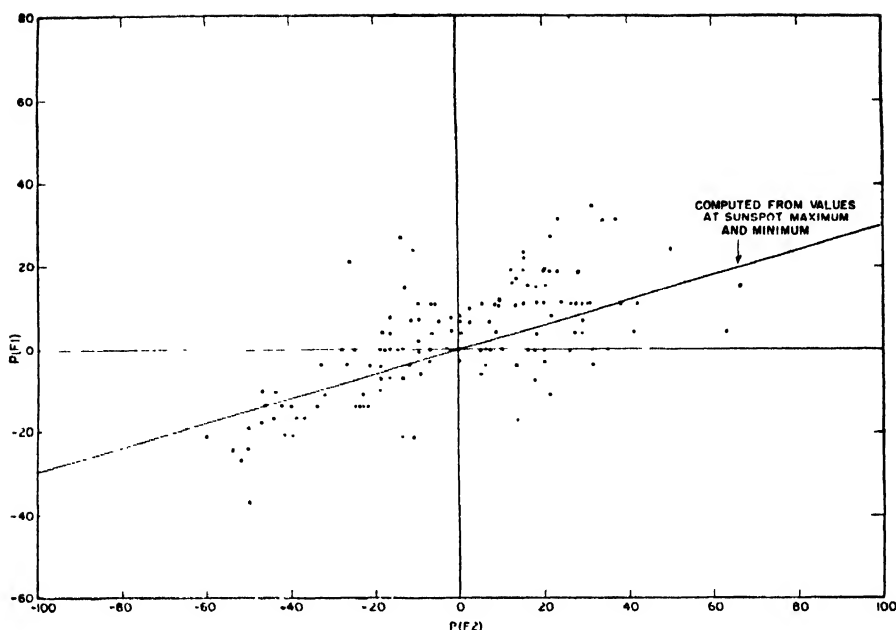


Fig. 6. Correlation between the fluctuations of  $f_0F_1$  and  $f_0F_2$  for May 1948, Washington

will be averaged out. It is a remarkable fact that the points in figure 6 do scatter around the straight line giving  $\frac{\Delta N(F_2)}{\Delta N(F_1)} \simeq 3.4$ . If this is interpreted

as indicating that fluctuations in  $F_1$  and  $F_2$ -ionizations are due mostly to fluctuations in the relevant solar intensity, then it seems likely (though not certain) that the same radiation is involved in the ionizations of  $F_1$  and  $F_2$ . If this is accepted, then the theory of bifurcation requires that: (1) the  $F_1$ -ionization should also supply the ionization of  $F_2$  and that (2) the scale heights and recombination coefficient of the active constituent should be consistent with our ideas of these parameters not only at  $F_1$ -region but at  $F_2$ -region as well.

There is little doubt that at  $F_1$  and  $F_2$  heights, recombination occurs through a dissociation process of the type (Bates and Massey, 1947):  $XY^+ + e \longrightarrow X' + Y'$ , where  $XY^+$  may be formed through



For the charge transfer process to be possible, the ionization potential of  $XY$  must be less than that of  $Z$ . This means that the molecule  $XY$  cannot be  $N_2$ . The only atmospheric molecules which have sufficiently low ionization potentials are  $O_2$  and  $NO$  of which the concentration of  $NO$  at  $F$ -region heights is negligible. If, therefore, we identify  $XY$  as  $O_2$ , then  $Z'$  would be either  $O^+$  or  $N^+$ . Since the rates for these processes are not known, it is not possible to choose between them at present. However, this point has

to be remembered in evaluating the contributions of O<sup>+</sup> and N<sup>+</sup> to the F<sub>1</sub>-layer.

The typical values of scale heights associated with F<sub>1</sub> and F<sub>2</sub>-ionizations are about 30 km and 70 km respectively (S. K. Mitra, 1952). Although these values are by no means exact, particularly the values for F<sub>2</sub>-region (Gerson, 1951), we may consider that they are of the right order. Now, with diffusion starting at 160 km, the values of scale heights associated with individual atmospheric constituents, are given in Table IV.

TABLE IV

200 km (F <sub>1</sub> )				300 km (F <sub>2</sub> )			
H(O)	H(N)	H(N <sub>2</sub> )	H'	H(O)	H(N)	H(N <sub>2</sub> )	H'
39.0	44.6	22.3	30	69.0	78.8	39.4	70

H' = scale height obtained from ionospheric measurements

Even allowing for the uncertainties in the ionospheric measurements, H(N<sub>2</sub>) appears to be too low for both F<sub>1</sub> and F<sub>2</sub>-regions and suggests, once again, that N<sub>2</sub> is probably not the active constituent. On the other hand, both H(O) and H(N) are of the right order.

It appears, therefore, that ionizations from both atomic nitrogen and oxygen ( $\lambda \leq 655$ ) are likely to contribute to the F<sub>1</sub> and F<sub>2</sub>-layers; though nothing can be said at present about their respective proportions.

## REFERENCES

- Bates, D. R., 1949, *Proc. Roy. Soc. A*, **196**, 562.  
 Bates, D. R., 1950, *Phys. Rev.*, **78**, 492.  
 Bates, D. R. and Massey, H. S. W., 1947, *Proc. Roy. Soc.*, **192**, 1.  
 Bates, D. R. and Seaton, M. J., 1950, *Proc. Phys. Soc., B.*, **63**, 129.  
 Bradbury, N. E., 1938, *Terr. Mag. Atmos. Elect.*, **43**, 55.  
 Chapman, S and Price, W. C., 1936, *Rep. Prog. Phys.*, **3**, 60.  
 Chatterjee, B, 1953, *J. Geophys. Res.*, **58**, 353.  
 Clark, K. C., 1948, *Phys. Rev.*, **73**, 1250.  
 Courtes, G., 1950, *Comptes Rendus*, **231**, 62.  
 Deb, S., 1952, *J. Atmosph. Terr. Phys.*, **2**, 309.  
 Dufay, G., 1951, *Comptes Rendus*, **233**, 419.  
 Gerson, N. C., 1951, *Rep. Prog. Phys.*, **14**, 316.  
 Gerson, N. C., 1952, *Advance in Geophysics* Edited by H. R. Landsburg, Vol. 1, 155-242, Published by Academic Press, Inc. Publishers, New York.  
 Ghosh, M., 1953, *J. Geophys. Res.*, **58**, 41.  
 Herzberg, G. and Herzberg, L., 1948, *Nature*, **161**, 283.  
 Kallman, H. K. 1953, *J. Geophys. Res.*, **58**, 209.

- Mitra, A. P. 1953, Scientific Report No. 46, Pennsylvania State College, May 15; also  
*J. Atmosph. Terri. Phys.* (In Press).
- Mitra, A. P., 1952, *Ind. J. Phys.*, **26**, 79.
- Mitra, S. K., 1951, *Nature*, **167**, 897.
- Mitra, S. K., 1952, Upper Atmosphere, published by the Asiatic Society, Ed. 11, pp.  
 290-291.
- Nicolet, M., 1945, *Inst. R. Meteor. Belgium, Memoires*, **19**, 1.
- Nicolet, M., 1950, *Proc. Conf. Ion. Res.*, Pennsylvania State College, p. 11BB.
- Nicolet, M., 1953, *Scientific Report No. 52*, Pennsylvania State College, October 25.
- Nicolet, M. and Pastiel, R., 1952, *Mem. Soc. R. Sci. Liege*, **12**, 147.
- Nicolet, M. and Mange, P., 1954, *J. Geophys. Res.*, **59**, 15.
- The Rocket Panel, 1952, *Phys. Rev.*, **88**, 1027.
- Ta-You Wu, 1944, *Phys. Rev.*, **66**, 65.
- Tousey, R., Watanabe, K. and Purcell, J. D., 1951, *Phys. Rev.*, **83**, 792.
- Weissler, G. L. and Lee Po, 1952, *J. Opt. Soc. Amer.*, **42**, 200.
- Weissler, G. L., Lee and Mohr, E. L., 1952, *J. Opt. Soc. Amer.*, **42**, 84.

# MULTIPLY SEPARATION FACTORS IN THE SPECTRUM OF CHROMIUM II

By V. SURYANARAYANA AND V. RAMAKRISHNA RAO

DEPARTMENT OF PHYSICS, ANDHRA UNIVERSITY, WALT AIR

(Received for publication, April 10, 1954)

**ABSTRACT.** Formulae for the multiplet separation factors in the configurations  $3d^4.4s$  and  $3d^4.4p$  are derived and used for the calculation of the multiplet separations. The values are compared with the experimental data.

## INTRODUCTION

In continuation of our earlier work on the term values of Cr II, the multiplet separation factors in the configurations  $3d^4.4s$  and  $3d^4.4p$  were calculated. The theory of multiplet separation factors was given for equivalent electron configuration by Goudsmit (1928) and for the addition of an  $s$  or  $p$  electron by Goudsmit and Humphreys (1928). The working details may again be found in two papers by V. R. Rao (1918). The formulae for  $3d^4.4s$  and  $3d^4.4p$  were not available in literature as far as we were aware and so were derived by us. The results are described below.

## CONFIGURATION $3d^4$

Table I gives the results for  $3d^4$  configuration. The theoretical values for  $A$ , the multiplet separation factor, is zero, in every term. The experimental values, as given in the last column, are all very nearly equal to zero for all sextet and quartet terms. In the term scheme we find a partial inversion of the multiplet levels as in a  $a^4G_{7/2}$  to  $a^4G_{5/2}$ . This means that in the actual spectrum, the lines are very close together and occur in no definite order. For the assignments of such lines the method of constant differences is not of much help and evidence from Zeeman effect and hyperfine structure studies would be essential.

## CONFIGURATIONS $3d^4.4s$ AND $3d^4.4p$

The formulae for the multiplet separations in these configurations were derived by us and given in column 3 in Tables II and III. They are obtained by considering the value of  $(A')$  in the configuration  $3d^4$  of Cr III and given in terms of  $a$ . In the case of  $3d^4.4p$  the individual formulae contain terms in  $a_2$  also, which is the contribution by a  $p$  electron to the value in  $3d^4$ . These  $a_2$  values are not capable of evaluation and so they have to be eliminated by taking  $\Sigma A'$  for (1) all terms of same multiplicity or (2) all terms of same  $L$  value and so on.

TABLE I  
Multiplet separations in the observed terms of Cr II  $3d^5$  configuration

Term	$\Delta\nu$	Separation factor (%)
$a^6S_{2\frac{1}{2}}$	0.0	0.0
$a^4G_{2\frac{1}{2}}$	5.7	
$G_{8\frac{1}{2}}$	1.5	.08
$G_{4\frac{1}{2}}$	-7.1	
$G_{5\frac{1}{2}}$		
$a^4P_{\frac{1}{2}}$		
$P_{1\frac{1}{2}}$	0.6	-0.33
$P_{2\frac{1}{2}}$	-1.9	
$b^4D_{\frac{1}{2}}$	7.5	
$D_{1\frac{1}{2}}$	3.9	-0.23
$D_{2\frac{1}{2}}$	-13.1	
$D_{3\frac{1}{2}}$		
$a^2I_{5\frac{1}{2}}$	6.4	+0.98
$I_{6\frac{1}{2}}$		
$a^2D_{2\frac{1}{2}}$	-180.5	-72.2
$D_{1\frac{1}{2}}$		
$a^2F_{3\frac{1}{2}}$	-247.8	-70.8
$F_{2\frac{1}{2}}/2$		
$b^4F_{1\frac{1}{2}}$	10.7	
$F_{2\frac{1}{2}}$	-18.3	0.95
$F_{3\frac{1}{2}}$	17.6	
$F_{4\frac{1}{2}}$		
$b^2H_{4\frac{1}{2}}$	97.2	17.7
$H_{5\frac{1}{2}}$		
$a^2G_{3\frac{1}{2}}$	170.8	38.0
$G_{4\frac{1}{2}}$		
$c^2F_{2\frac{1}{2}}$	134.9	38.5
$F_{3\frac{1}{2}}$		
$b^2S_{\frac{1}{2}}$	0.0	0.0
$d^2D_{2\frac{1}{2}}$	-18.1	-7.2
$D_{\frac{1}{2}}$		
$1$		
$d^2G_{3\frac{1}{2}}$	23.2	5.15
$G_{4\frac{1}{2}}$		

The observed data given in this table are due to Keiss (1951)

Table II contains the data on  $3d^4.4s$  configuration. The experimental values of  $A$  are calculated both from adjacent levels and total separation and average values are given in column 7. These are to be compared with the calculated values given in column 8. We find in  $3d^4.4s$  configuration there is a good agreement. The inverted nature of  $c^4D$  and  $b^2D$  was also observed experimentally.

In the configuration  $3d^4.4p$ , the value of  $A'$  (Cr III) is calculated from that of  $A$  (Cr II) by the formulae and given in column (7) in Table III.

TABLE II

Multiplet separation factor calculation in the terms of  
Cr II  $3d^4.4s$  configuration.

Configuration and base term	Term	(1) Formula for $A$ in terms of $A'$	(2) Separation factor ( $A$ ) in terms of ( $a$ )	Separation factor (1) calculated from			(4) calculated from formula (2)
				adjacent levels	Total separation	Average value	
$3d^4(a^6D)4s$	$*a^6D$ $*a^4I$	$A = 4A'/5$ $A = 6A'/5$	$A = a/5$ $A = 3a/10$	47 1, 46 1 44.6, 42 8 68.6, 66 7 64.6	44 6 66.1	41 6 66.5	43 9 65 9
$3d^4(a^3P_-)4s$ $3d^4(^3P_+)4s$	$b^4P_-$ $^4P_+$	$A = 2A'/3$ $A = 2A'/3$	$A = a/3$	237, 222.8	228 1	229 3	73 2
$3d^4(a^3P_-)4s$ $3d^4(^3F_+)4s$	$a^4F_-$ $^4F_+$	$A = 2A'/3$ $A = 2A'/3$	$A = a/18$	13 8, 14 7 11.3	13 0	13 2	12.2
$3d^4(a^3P_-)4s$ $3d^4(^3P_+)4s$	$a^2P_-$ $^2P_+$	$A = 4A'/3$ $A = 4A'/3$	$A = 2a/3$	464 4	464.4	464.4	146.5
$3d^4(a^3F_-)4s$ $3d^4(^3F_+)4s$	$b^2F_-$ $^2F_+$	$A = 4A'/3$ $A = 4A'/3$	$A = a/9$	11.0	11 0	11.0	24 4
$3d^4(a^3D)4s$	$c^4D$ $b^2D$	$A = 2A'/3$ $A = 4A'/3$	$A = -a/18$ $A = -a/9$	-22.5 19.1 -13.0	-16 9 -35.4	-17 9 -35.4	-12.2 -24 4
$3d^4(a^3G)4s$ $3d^4(a^3G)4s$	$b^4G$ $c^2G$	$A = 2A'/3$ $A = 4A'/3$	$A = a/10$ $A = a/5$	-35 4 29 5, 21.9 13.7 31 2	20 4 31.2	21.4 31.2	22.0 43.9
$3d^4(a^3H)4s$ $3d^4(a^3H)4s$	$*a^4H$ $a^2H$	$A = 2A'/3$ $A = 4A'/3$	$A = a/15$ $A = 2a/15$	13.8, 14 5 14.3 33.1	14.3 33.1	14.2 33.1	14.7 29.3
$3d^4(a^1S)4s$	$a^2S$	$A = 0$	$A = 0$	0.0	0.0	0.0	0.0
$3d^4(a^1G)4s$	$b^2G$	$A = 0$	$A = 0$	12.0	12.0	12.0	0.0
$3d^4(a^1D)4s$	$c^2D$	$A = 0$	$A = 0$	24 5	24.5	24.5	0 0
$3d^4(^1S)4s$	$^2S$	$A = 0$	$A = 0$				0.0
$3d^4(^1D)4s$	$^2D$	$A = 0$	$A = 0$				0.0
$3d^4(a^1F)4s$	$d^2F$	$A = 0$	$A = 0$	-5.9	-5.8	-5.8	0 0
$3d^4(^1G)4s$	$^2G$	$A = 0$	$A = 0$	—	—	—	0.0
$3d^4(a^1I)4s$	$b^2I$	$A = 0$	$A = 0$	-4.1	-4.1	-4.1	0.0

$a = 219.7$

The base terms with no suffix before them are only theoretically possible terms and are not experimentally identified.

The values of the terms with asterisks are employed in the calculation of the value of  $a$ . The mean value of  $A'$  obtained from various sources (like all 'P' terms, or all sextets etc. arising out of the same base term) is given at the end of the same column. This is to be compared with the value given in the last

TABLE III

Electron configuration	Term	Equation	Separation factor $A$ calculated from			$A'$ calculated from (4)	Separation factor $A'$ calculated from the ion data	
			Adjacent levels	Total separation	Mean value		Adjacent levels	Mean value
$3d^4(d^5D)4p$ $l' = 2, s' = 2$ $l_2 = 1, s = 1/2$	$2^4P$	$A = 6.1'/5 - a_2/10$	36.9, 40.3	36.9	38.7			
	$2^6D$	$A = 2.1'/3 + a_2/30$		28.7	28.7			
	$2^4F$	$A = 8.1'/15 + a_2/15$	54.6, 54.0 55.4, 52.8 52.2	51.6	53.1			
	$2^4P$	$A = 9.1'/5 + a_2/10$	171.1, 138.3	150.6	153.3			
$2^4D$	$2^4D$	$A = 1' - a_2/30$	54.4, 50.4 45.4	48.9	49.8			
	$2^4F$	$A = 4.1'/5 - a_2/15$	34.1, 34.1, 34.1	34.1	34.1		60.0, 60.0, 57.3, 55.0,	57.2 57.9
	$P$ terms	$\Sigma A = 3.1'$				64.0		
	$D$ terms	$\Sigma A = 5.1'/3$				47.1		
All sextets	$F$ terms	$\Sigma A = 4.1'/3$				65.5		
	All sextets	$\Sigma A = 12.1'/5$				50.2		
	All quartets	$\Sigma A = 18.1'/5$				65.9		
	Total	$\Sigma A = 6.1'$				59.6		
							Mean value of $A'$ 58.6	



TABLE III (contd.)

Electron configuration	Term	Equation	Separation factor $A'$ calculated from			$A'$ calculated from (A)	Separation factor $A'$ calculated from the ion data		
			Adjacent levels	Total separation	Mean value		Adjacent levels	Total separation	Mean value
$3d^4(a^3H)4p$ $l'=5, s'=1$ $l_3=1, s_3=1/2$	$^2G$	$A = 12A'_{15} - a_2/15$	28.5, 29.2, 59.2	40.9	39.5				
	$^2H$	$A = 58A'_{90} + a_2/90$	23.4, 25.9, 28.0	26.0	25.8				
	$^2I$	$A = 5'A'_{19} + a_2/18$	36.8, 30.5, 25.9	30.5	30.9				
	$^2G$	$A = 8A'_{15} + a_2/15$	30.5	30.5	30.5				
	$^2H$	$A = 58A'_{90} - a_2/90$	47.4	47.4	47.4				
	$^2I$	$A = 10A'_{19} - a_2/18$	12.7	12.7	12.7				
	G terms	$\Sigma A = 12A'_{15}$				29.2	24.8, 22.7	23.6	23.7
	H terms	$\Sigma A = 29A'_{15}$				37.9			
	I terms	$\Sigma A = 5A'_{13}$				26.2			
	All quartets	$\Sigma A = 2A'$				48.2			
	All doublets	$\Sigma A = 4A'$				22.5			
	Total	$\Sigma A = 6A'$				25.6			

Mean value of  $A'$  31.6

TABLE III (contd.)

Electron configuration	Term	Equation	Separation factor $A$ calculated from			$A'$ calculated from $A$	Separation factor $A'$ calculated from the ion data		
			Adjacent levels	Total separation	Mean levels		Adjacent levels	Total separation	Mean value
$3^1d(a^3G)4P$ $l' = 4, s' = 1$ $s = 1, s_2 = 1/2$	$^3F$	$A = 5A'/6 - a_2/12$		14.3	14.3				
	$^3G$	$A = 19A'/30 + a_2/60$	31.5, 56.0, 36.5	41.7	41.4				
	$^3H$	$A = 8A'/15 + a_2/15$	32.0, 32.4, 33.5	33.0	33.0				
	$^3F$	$A = 5A'/3 + a_2/12$		76.5	76.5				
	$^3G$	$A = 19A'/15 - a_2/60$		15.1	15.1				
	$^3H$	$A = 16A'/15 - a_2/15$		0.83	0.83				
	$F$ terms	$\Sigma A = 5A'/2$				36.3	37.5, 28.4	32.4	32.4
	$G$ terms	$\Sigma A = 19A'/10$				29.8			
	$H$ terms	$\Sigma A = 8A'/5$				21.1			
	All quartets	$\Sigma A = 2A'$				44.3			
	All doublets	$\Sigma A = 4A'$				23.1			
		Total $\Sigma A = 6A'$				30.2			

Mean value of  $A' = 30.8$

TABLE III (contd.)

Electron configuration	Term	Equation	Separation factor $A$ calculated from			$A'$ calculated from ( $A$ )	Separation factor $A'$ calculated from the ion data	
			Adjacent levels	Total separation	Mean value		Adjacent levels	Mean value
$3d^4(b^2F)4p$ $l' = 3, s' = 1$ $l_3 = 1, s_3 = 1/2$	$^2D$	$A = 8A'/9 - a_2/9$		1.1	1.1			
	$^4F$	$A = 11A'/18 + a_2/36$	3.0, 1.9, 12.2	3.3	5.1			
	$^4G$	$A = .A'/2 + a_2/12$		1.8	1.8			
	$^2D$	$A = 16A'/9 + a_2/9$		126.2	126.2			
	$^2F$	$A = 11A'/9 - a_2/36$		50.4	30.4			
	$^2G$	$A = .A' - a_2/12$		45.4	45.4			
	$D$ terms	$\Sigma A = 8A'/3$				47.7		
	$F$ terms	$\Sigma A = 11A'/6$				30.3		
	$G$ terms	$\Sigma A = 3A'/2$				31.2		
	All quartets	$\Sigma A = 36A'/18$				4.0		
$3d^4(b^2F)4p$ $l' = 3, s' = 1$ $l_3 = 1, s_3 = 1/2$	All doublets	$\Sigma A = 4A'$				55.2		
		Total $\Sigma A = 6A'$				38.1		
	$^2G$	$A = .A' - a_2/12$		26.0	26.0			
	$^2D$	$A = 16A'/9 + a_2/9$		-25.1	-25.1	* - 5.6		

 Mean value of  $A'$  ... 34.4

TABLE III (contd.)

Electron configuration	Term	Equation	Separation factor $A$ calculated from			Separation factor $A'$ calculated from the ion data	
			Adjacent levels	Total separation	Mean value	Adjacent levels	Total separation
$3d^4(d^3D)4p$ $l'=2, s'=1$	$x^1P$	$A = A' - a_1/6$	-93.5, 135.2	-109.1	-112.6		
	$w^4D$	$A = 5A'/9 + a_1/18$	3.5, 9.7, 14.1	10.5	9.5		
	$w^4F$	$A = 4A'/9 + a_1/9$	18.2, 30.0, 18.0	22.0	22.0		
$l_2=1, s_2=1/2$	$y^3P$	$A = 2A' + a_2/6$	87.2	87.2	87.2		
	$x^3D$	$A = 10A'/9 - a_2/18$	-69.8	-69.8	-69.8		
	$x^3F$	$A = 8A'/9 - a_2/9$	91.9	91.9	91.9		
All quartets All doublets	$P$ terms	$\Sigma A = 3A'$					-19
	$D$ terms	$\Sigma A = 5A'/3$					
	$F$ terms	$\Sigma A = 4A'/3$					
	All quartets	$\Sigma A = 2A'$					
	All doublets	$\Sigma A = 4A'$					
Total		$\Sigma A = 6A'$					

Mean value of  $A' \dots 33.8$ 

The underlined value of  $A'$  given in the last column of the table is not experimentally observed but is calculated from the observed data for Cr III itself.

TABLE III (contd.)

Electron configuration	Term	Equation	Separation factor $A$ calculated from			$A'$ calculated from ( $A$ )	Separation factor $A'$ calculated from the ion data	
			Adjacent levels	Total separation	Mean value		Adjacent levels	Total separation
$3d^4(4p)4p$ $l' = 1, s' = 1$ $l_2 = 1, s_2 = 1/2$	$^4D$	$A = A'/3 + a_1/6$	172.9, 154.8, 135.8	149.6	153.3			
	$^4P$	$A = A'/3 + a_2/6$	65.9, 148.8	117.6	110.8			
	$^2S$	$A = 0$	0.66	0.66	0.66			
	$^2D$	$A = 2A'/3 - a_2/6$	145.0	145.9	145.0			
	$^2P$	$A = 2A'/3 - a_2/6$	132.2	132.2	132.2			
	$^2S$	$A = 0$	0	0	0			
	$D$ terms	$\Sigma A = A'$				298.3		
	$P$ terms	$\Sigma A = A'$				243.0		
	$S$ terms	$\Sigma A = 0$					342.0	342.0
	All quartets	$\Sigma A = 2/3 A' + a_2/3$						
	All doublets	$\Sigma A = 4A'/3 - a_2/3$						
		Total $\Sigma A = 2A'$						

Mean value of  $A' \dots 270.5$

TABLE III (contd.)

Electron configuration	Term	Equation	Separation factor $A$ calculated from			$A'$ calculated from ( $A$ )	Separation factor $A'$ calculated from the ion data	
			Adjacent levels	Total separation	Mean value		Adjacent levels	Mean value
$3d^4(a^1)4p$	$2^3K$	$A = a_3/7$	28.7	28.7	28.7			
	$3^2I$	$A = a_2/42$	0.4	0.4	0.4			
	$2^3H$	$A = -a_3/6$	45.7	45.7	45.7			
		total $\Sigma A = 0$	-1.5	-1.5	-1.5			
$3d^4(a^1F)4p$	$2^3D$	$A = -a_3/3$	20.7	20.7	20.7			
	$2^3F$	$A = a_3/12$	81.4	81.4	81.4			
	$2^3G$	$A = a_3/4$						
		total $\Sigma A = 0$	44.0	44.0	44.0			
$3d^4(a^1D)4p$	$2^3P$	$A = -a_3/2$	52.9	52.9	52.9			
	$2^3D$	$A = a_3/6$	57.0	57.0	57.0			
	$2^3F$	$A = a_3/3$						
		total $\Sigma A = 0$						

TABLE III (contd)

Electron configuration	Term	Equation	Separation factor $A$ calculated from			$A'$ calculated from (A)	Separation factor $A'$ calculated from the ion data		
			Adjacent levels	Total separation	Mean value		Adjacent levels	Total separation	Mean value
$3d^4(a^1G)4p$	$w^3F$	$A = -a_2/4$	-31.1	-31.1	-31.1				
	$w^3G$	$A = a_2/20$	20.8	20.8	20.8				
	$w^3H$	$A = 12a_2/60$	-34.8	-34.8	-34.8				
$3d^4(a^1S)4p$	$^1S$	total $\Sigma A = 0$							
	$^3P$	$A = a_2/6$	-42.6	-42.6	-42.6				
		Total $\Sigma A =$							

The values of  $(A')$  marked with asterisk for the term  $b^3F$  in  $3d^44p$  configuration are obtained by solving the two equations for the terms  $a^3G$  and  $a^3D$ .

column for  $A'$  as calculated from the ion data (Cr III). The agreement is quite good in the case of  $^5D$ ,  $^3H$  and  $^3G$ . In the case of  $^3P$  and  $^3F$  terms both of which occur twice in the configuration  $3d^4$ , the agreement is not satisfactory. In case of such terms only an average value of the separation factor for the two similar terms is given by the formula. In general both the terms are rarely observed and unless we have the data of both the terms, it is not possible to take the average value from the experimental data. In case of  $^3D$  the value given in column 10 is obtained by calculation from Cr III data itself. It was not observed experimentally. This might possibly account for the considerable discrepancy between this value and the one shown in column 7. The case of doublets of Cr II arising out of singlets of Cr III is interesting. The  $A'$  factors are zero. So the  $A$  factor is obtained in terms of  $a_2$ . The values of  $A$  for all terms arising out of the same base term are zeroes as can be seen from Table III. From the nature of the formula it appears as if we can calculate the value of  $a_2$  from the experimental value of the separation factor  $A$  for a few doublets. However, on comparison with a few such calculated values, the values of  $a_2$  is found to be very erratic. Evidently no useful information could be obtained from these data. The separation factor for the added  $p$  electron  $a_2$  is not capable of direct calculation.

#### ACKNOWLEDGMENT

The authors wish to take this opportunity to express their thanks to Prof. K. R. Rao for his kind interest in the work.

#### REFERENCES

- Bowen, 1937, *Phys. Rev.*, **52**, 1153.  
 Goudsmit, 1928 *Phys. Rev.*, **31**, 946.  
 Goudsmith and Humphreys, 1928, *Phys. Rev*, **31**, 960.  
 C. C. Kiess, 1951, *J. Res. Nat. Bur. Stand.*, **47**, 423.  
 V. R. Rao and K. R. Rao, 1948, *Ind. J Phys.*, **22**, 175  
 V. R. Rao and K. R. Rao 1948, *Ind. J Phys.*, **22**, 180



# ON THE RAMAN SPECTRA OF ACETYL CHLORIDE AND CHLOROACETYL CHLORIDE IN THE VAPOUR STATE\*

BY MONOMOHAN MAZUMDER

OPTICS DEPARTMENT, INDIAN ASSOCIATION FOR THE CULTIVATION OF SCIENCE, CALCUTTA—32

(Received for publication, May 18, 1954)

## Plates IXA B

**ABSTRACT.** The Raman spectra of acetyl chloride and chloroacetyl chloride in the vapour state at 100°C and 150°C respectively have been studied and compared with those of the substances in the liquid state at room temperatures nearly equal to those of the vapour. It is observed that the relative intensities of some of the prominent lines undergo changes in both the cases when the change from liquid to vapour state takes place. The intensity of the line  $590\text{ cm}^{-1}$  in the case of acetyl chloride and  $560\text{ cm}^{-1}$  in the case of chloroacetyl chloride increases appreciably with vaporization. The frequency-shifts of some of the prominent lines in both the cases increase with vaporization of the liquids. It is pointed out that the influence of strong intermolecular field between the neighbouring molecules in the liquid state owing to the presence of chlorine atom in the molecule is responsible for all these changes.

## INTRODUCTION

It was reported in a previous paper (Mazumder, 1953) that in the case of ethylene dichloride in the vapour state the ratio of intensities of the lines  $654\text{ cm}^{-1}$  and  $755\text{ cm}^{-1}$  remains almost unaltered when the temperature of the vapour changes from 135°C to 170°C. It was concluded from these results that if the two lines are attributed to two forms of the molecule the energy-difference of the two forms is as small in the vapour state as in the liquid state. The ratio of the intensity of the two lines, however, diminishes abruptly with change from liquid state at 135°C to vapour state at 135°C. This indicates that the intermolecular field in the liquid state is responsible for the increase in the relative population of molecules of the particular form which gives the line  $654\text{ cm}^{-1}$ . The influence of intermolecular field on asymmetric molecules formed by substitution in the ethane molecule has not been studied systematically. It would be interesting to compare this influence observed in the case of substituted ethanes containing one complete  $\text{CH}_3$  group with that observed in the case of similar molecules which are asymmetric and in which the hydrogen atom has

\* Communicated by Prof. S. C. Sirkar.

been substituted in both the  $\text{CH}_3$  groups. It is necessary for this purpose to study the Raman spectra of the substances in the liquid state at high temperatures and to compare it with the spectra of the substances in the vapour state at corresponding temperatures. A programme has been undertaken to study the problem systematically in the case of substituted paraffins and the results obtained with acetyl chloride and chloroacetyl chloride have been discussed in the present paper.

#### EXPERIMENTAL

The experimental arrangement was similar to that used by the author in his previous investigation (Mazumder, 1953). The liquids, acetyl chloride and chloroacetyl chloride were distilled several times before being introduced in the long and stout Wood's tube described before. The window of the Wood's tube was improved this time by fusing a plane disc of Pyrex glass at one end of a Pyrex tube which was sealed inside the stouter tube at the broad end of the latter. A narrow tube of porcelain blackened thoroughly was placed between the window and condensing lens to cut off all the extraneous light coming out from the side of the Wood's tube. With this arrangement it was possible to run the exposure for seven to ten days without over-exposure of the prominent mercury lines. The temperature of the vapour was raised to about  $100^\circ\text{C}$  in the case of acetyl chloride (B.P.  $52^\circ\text{C}$ ) and  $150^\circ\text{C}$  in the case of chloroacetyl chloride (B.P.  $105^\circ\text{C}$ ), and the pressure developed inside the Wood's tube at those temperatures by the vapours of the corresponding liquids was about four atmospheres in each case. Two mercury arcs of length about 16 inches made in the laboratory were used to illuminate the vapour inside the tube. Elliptical reflectors of highly polished aluminium sheets were used to focus the incident light on the tube containing the vapour.

The Adam Hilger two-prism spectrograph used in the previous investigation was used in the present case also. Ilford Zenith plates taken from a fresh packet were used to photograph the spectra.

Microphotometric records of the Raman lines were taken with a Kipp and Zonen type self-recording microphotometer. The approximate relative intensities of any particular pair of Raman lines were found out from the densities of the lines with the help of blackening—log intensity curves for the two wavelengths corresponding to those two lines drawn with the help of the intensity marks. In both the cases Raman spectra of the liquids at room temperature and at temperatures nearly equal to the temperature of the vapour were also photographed for comparison.

#### RESULTS AND DISCUSSION

The Raman spectra of acetyl chloride in the liquid state at  $32^\circ\text{C}$  and  $90^\circ\text{C}$  and in the vapour state at  $100^\circ\text{C}$  are reproduced in the Plate IXA, figures 1(a), 1(b) and 1(c). The spectra of chloroacetyl chloride in the

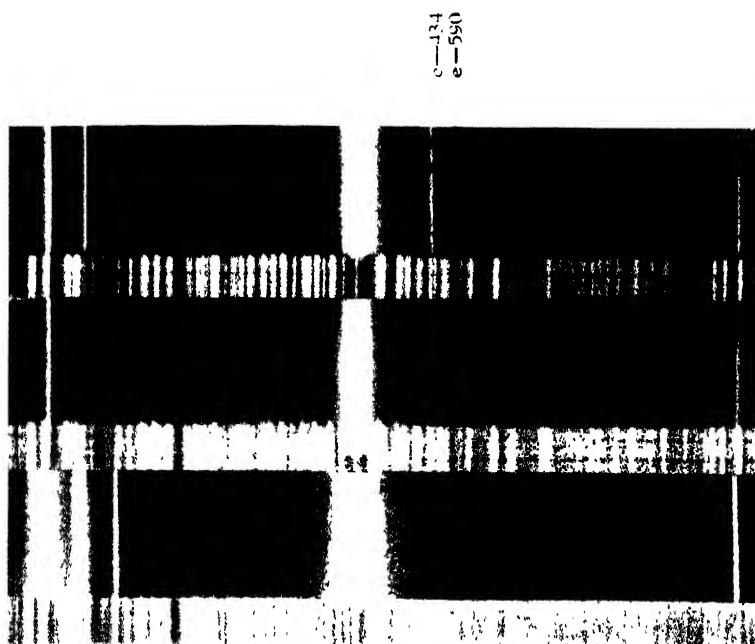


Fig. 1

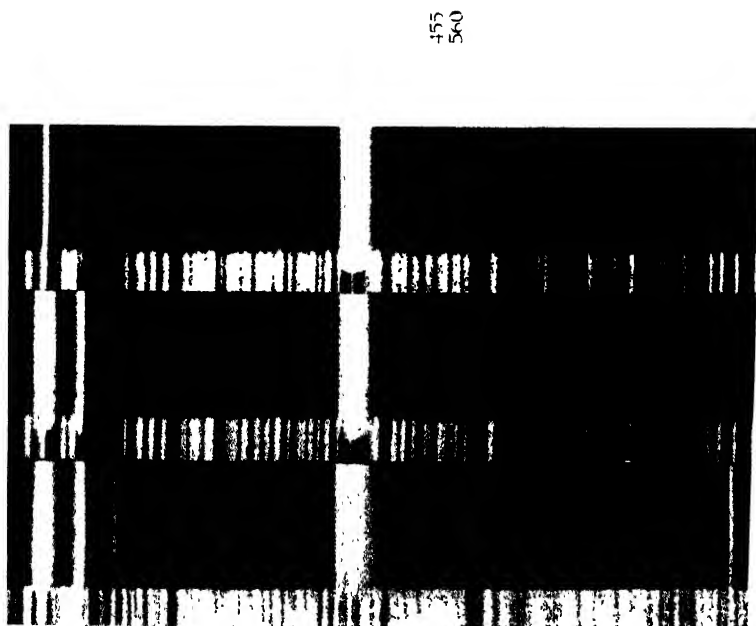


Fig. 2  
Raman spectra

Fig. 1 Acetyl chloride  
 (a) Liquid at 32°C  
 (b) " " 90°C  
 (c) Vapour " 100°C

Fig. 2 Chloroacetyl chloride  
 (a) Liquid at 34°C  
 (b) " " 150°C  
 (c) Vapour " 150°C

## Microphotometric records of Raman spectra.

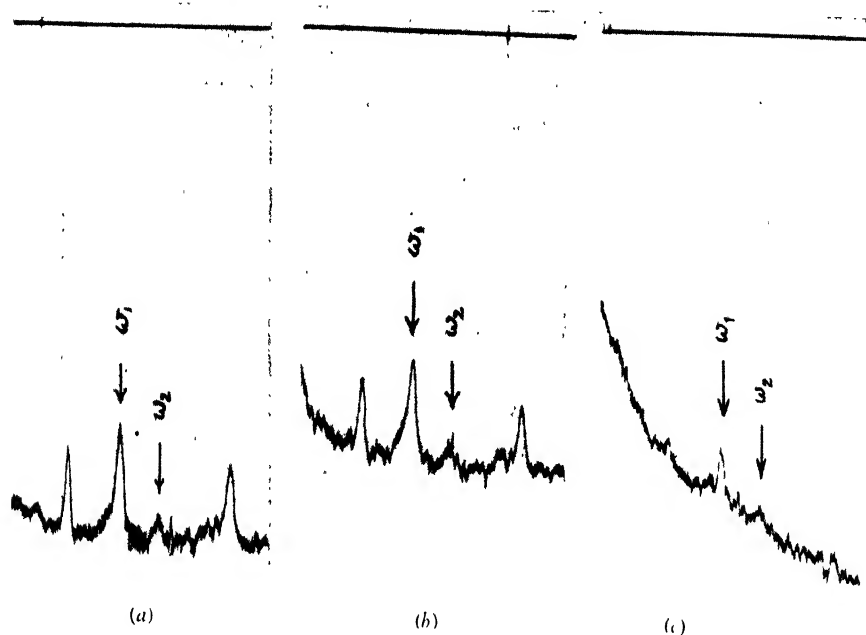


Fig 3

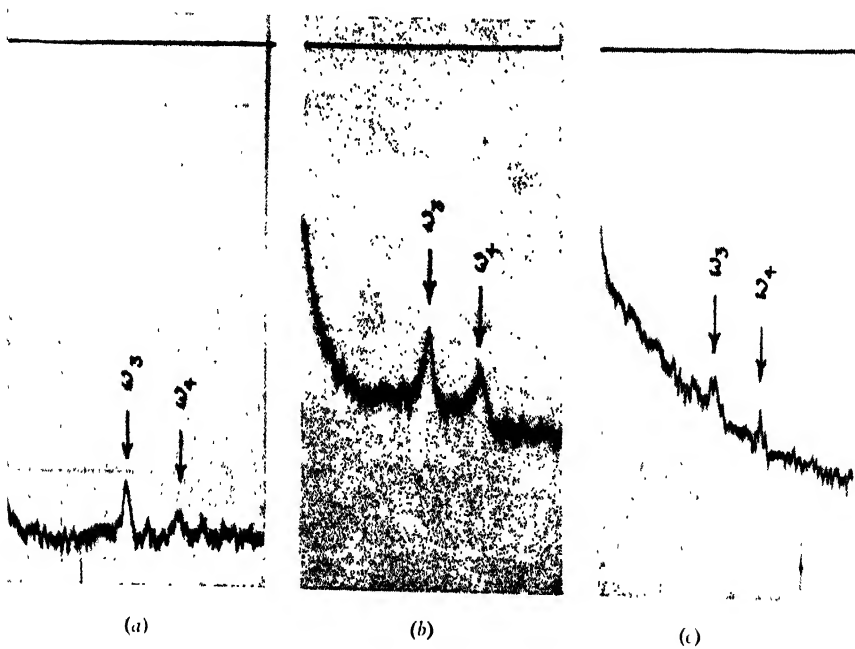


Fig 4

Fig 3 Chloroacetyl chloride

(a) Liquid at 34°C

(b) " " 150°C

(c) Vapour " 150°C

(  $\omega_1 = e - 455$ ,  $\omega_2 = e - 560$ ,  $\omega_3 = e - 434$ 

Fig 4 Acetyl chloride

(a) Liquid at 32°C

(b) " " 90°C

(c) Vapour " 100°C

(  $\omega_4 = e - 590$  )

liquid state at 34°C and 150°C and in the vapour state at 150°C are also reproduced in the same plate in figures 2(a), 2(b) and 2(c). The frequency shifts are given in Tables I and II respectively. Microphotometric records of the lines 434 and 590  $\text{cm}^{-1}$  in the case of acetyl chloride and of the lines 300, 453 and 560  $\text{cm}^{-1}$  in the case of chloroacetyl chloride are reproduced in figures 3(a), 3(b), 3(c) and 4(a), 4(b), 4(c). The spectrograms due to the vapours being weak, feeble lines were not recorded.

It is found on examining the spectrograms that the relative intensities of some of the prominent lines undergo changes when the change from liquid to vapour state takes place. This can be seen from the microphotometric records reproduced in figures 3 and 4. It would be seen from these records that as the liquid is vaporized the intensity of the line 590  $\text{cm}^{-1}$  relative to that of the line 434  $\text{cm}^{-1}$  increases in the case of acetyl chloride. Again in the case of chloroacetyl chloride in the liquid state the intensity of the line 560  $\text{cm}^{-1}$  is only about one fifth of that of the line 445  $\text{cm}^{-1}$ , and the line becomes a little stronger when the liquid is heated to 150°C. But when the liquid is vaporized at 150°C the intensity of the line 560  $\text{cm}^{-1}$  increases so much that it is almost two thirds as intense as the line 445  $\text{cm}^{-1}$ .

TABLE I  
Acetyl chloride,  $\text{CH}_3\text{COCl}$   
 $\Delta\nu$  in  $\text{cm}^{-1}$ .

Liquid state		Vapour state
at 32°C	at 90°C	at 100°C
238 (0b) e,k;P	238 (0) e,k	
348 (1) e,k;P	348 (1) e,k	
434 (16) e,k;P	434 (10) e,k	434 (5) e,k
590 (5) e,k;P	590 (4) e,k	603 (3) e,k
956 (2) e,k;D	956 (1) e,k	
1101 (2) e,k;P	1101 (1) e,k	
1360 (1) e,k;D	1360 (0) e,k	
1425 (3) e,k;D	1425 (1) e,k	
1800 (2) e,P	1810 (2) e	
2935 (5) e,k,P	2935 (3) e,k	2944 (3) e,k
2991 (2) e,k;D	2991 (0) e,k	
3020 (3) e,k;D	3020 (1) e,k	

TABLE II  
Chloroacetyl chloride,  $\text{ClCH}_2\text{COCl}$   
 $\Delta\nu$  in  $\text{cm}^{-1}$

Liquid state		Vapour state
at $34^\circ\text{C}$	at $155^\circ\text{C}$	at $150^\circ\text{C}$
300 ( 8 ) e, k ; P	300 ( 4 ) e, k	300 ( 2 ) e, k
455 ( 10 ) e, k ; P	455 ( 5 ) e, k	455 ( 3 ) e, k
560 ( 2 ) e, k ; P	560 ( 1 ) e, k	560 ( 2 ) e, k
712 ( 1 ) e, k ; P	712 ( 1 ) e, k	
780 ( 8 ) e, k ; P	780 ( 5 ) e, k	801 ( 3 ) e, k
970 ( 1b ) e, k ; P	970 ( 0 ) e, k	
1402 ( 1 ) e, k ; P	1402 ( 0 ) e, k	
1806 ( 1b ) e, k ; P	1806 ( 0b ) e, k	
2950 ( 2 ) e, k ; P	2950 ( 5 ) e, k	2972 ( 2 ) e, k
2972 ( 0 ) e, k ; P	2992 ( 0 ) e, k	

Tables I and II further show that the frequency-shifts of some of the lines increase with change from liquid to vapour state. Thus in the case of acetyl chloride the lines  $590$  and  $2935\text{ cm}^{-1}$  shift respectively to  $603$  and  $2944\text{ cm}^{-1}$  with vaporisation of the liquid. Similarly in the case of chloroacetyl chloride the lines  $780$  and  $2950\text{ cm}^{-1}$  shift respectively to  $801$  and  $2972\text{ cm}^{-1}$ . Such an increase in the frequency-shifts may be due to one of the two causes, namely (1) there may be an increase in the strength of the bonds with vaporisation, and (2) there may be change in the angles between different bonds in the molecule. These lines in both the cases may be assumed to be due respectively to C—Cl and C—H stretching vibration. Since these lines are affected simultaneously by the change of state mentioned above, the affinity of hydrogen atom of one molecule with chlorine atom of its nearest neighbour in the liquid state may be responsible for the weakening of these bonds in the liquid state. The increase in the intensity of the lines due to C—Cl stretching oscillation in the molecules with change from liquid to vapour state may be due to the fact that the C—Cl groups are linked with the neighbouring molecules in the liquid state and they are set free in the vapour state and that the change of polarisability during the oscillation is reduced appreciably when the C—Cl group is linked to a neighbouring molecule.

These results for the vapours of these substances thus furnish direct evidences of the existence of such affinity of chlorine atoms with hydrogen atoms of the neighbouring molecule. It is thus quite evident that the study

of Raman spectra of such organic compounds in the vapour state throw much light on the nature of interaction between molecules in the liquid state.

It would be interesting to compare these results with the changes observed with the change from liquid to solid state in the case of acetyl chloride by Bishui (1948) and in the case of chloroacetyl chloride by Sanyal and Mazumder (1949). In the former case the frequency-shifts of the lines 590 and  $1800\text{ cm}^{-1}$  decrease slightly with solidification and lowering of temperature to  $-180^{\circ}\text{C}$ . So, the change of intermolecular field with solidification is very small in this case. It is significant that in this case no new line in the low frequency region appears when the liquid is solidified. The main change in the intermolecular field therefore takes place in this case with the vaporisation of the liquid. In the case of chloroacetyl chloride the lines 455, 560 and  $712\text{ cm}^{-1}$  shift respectively to 459, 565 and  $724\text{ cm}^{-1}$  with solidification (Sanyal and Mazumder, 1949). The line  $712\text{ cm}^{-1}$  which is broad in the liquid state becomes sharper in the solid state but it is not observed in the case of the vapour, probably due to increase in the width of the line. So there is a prominent change in the nature of the line  $712\text{ cm}^{-1}$  with solidification and it is significant that a new line at  $48\text{ cm}^{-1}$  appears in the solid state. But in this case also the main change in the relative intensities of the prominent lines 455 and  $560\text{ cm}^{-1}$  takes place with vaporisation of the liquid, and this indicates a great influence of the intermolecular field in the liquid state.

#### ACKNOWLEDGMENT

The author is indebted to Prof. S. C. Sirkar, D. Sc., F. N. I., for his kind interest and helpful guidance throughout the progress of the work and to the Government of India for the award of a scholarship.

#### REFERENCES

- Bishui, B. M., 1948, *Ind. J. Phys.*, **22**, 447.  
Mazumder, M. M., 1953, *Ind. J. Phys.* **27**, 406.  
Sanyal, S. B., and Mazumder, M. M., 1949, *Ind. J. Phys.* **23**, 1.





# THE RAMAN SPECTRA OF *m*- AND *p*-XYLENE IN THE SOLID STATE AT DIFFERENT LOW TEMPERATURES\*

BY D. C. BISWAS

OPTICS DEPARTMENT, INDIAN ASSOCIATION FOR THE CULTIVATION OF SCIENCE, CALCUTTA 32

(Received for publication, May 6, 1954)

Plates X A—C

**ABSTRACT.** The Raman spectra of meta and para xylenes in the liquid state and in the solid state at different low temperatures were recorded. Both the substances in the liquid state yield a few feeble extra Raman lines not reported in earlier publications. Some of the prominent Raman lines of both these compounds shift slightly with solidification of the compounds, but the number of lines undergoing such changes in their frequency-shifts is much greater in the case of meta xylene than in the case of the para compound.

Three new lines appear in the low-frequency region when the meta compound is solidified while two such lines in the low frequency region appear in the case of the para compound. With lowering of temperature of the solidified mass to  $-180^{\circ}\text{C}$  the low-frequency lines of the former substance show little change except that the band at  $81\text{ cm}^{-1}$  shifts to  $90\text{ cm}^{-1}$  while in the case of the other compound the number of low-frequency lines increases from two to five with the lowering temperature to  $-180^{\circ}\text{C}$ . The probable origin of these low frequency lines is discussed. The difference in the Raman spectra of these two isomers in the solid state is explained by assuming that the influence of the intermolecular field on the molecules of the substance depends on the relative positions of the substituent groups in the benzene ring.

## INTRODUCTION

It was pointed out earlier (Biswas, 1954) that the study of the influence of temperature on the intensities and positions of the low-frequency Raman lines which appear when some organic liquids are solidified may lead to the proper understanding of the origin of such lines. The results obtained by Swamy (1951, 1952 and 1953) and Deb (1952, 1953, 1954) in their investigations on the ultraviolet absorption spectra of substituted benzenes and naphthalene compounds show that the influence of intermolecular field on the electronic energy level in the solid state depends on the relative positions of the substituent groups. A comparison of the Raman spectra of ortho and meta compounds in the solid state at different temperatures may indicate to what extent the intensities and positions of the lines can be correlated with the relative positions of the substituent groups and also with the intermolecular field indicated by the results of investigation of the ultraviolet absorption spectra under similar conditions. With this object in view the Raman spectra of meta and para xylene in the solid state at different low temperatures have been investigated and the results have been discussed in the present paper.

\*Communicated by Professor S. C. Sirkar.

## EXPERIMENTAL

The liquids of the present investigation were secured from Fischer Scientific Co., New York and were of chemically pure quality. They were distilled in vacuum, as usual. The Raman spectra of the substances in the liquid state were photographed and compared with the Raman shifts of these liquids reported by previous workers to test the purity of the samples. The technique for recording the Raman lines of the solidified substances is same as that described earlier (Biswas, 1954). In all the cases the spectra were recorded on Ilford Zenith plates using a Fuess glass spectrograph having a dispersion of about  $11 \text{ \AA}^\circ$  in the  $4047 \text{ \AA}^\circ$  region. Each spectrogram contains an iron arc spectrum for comparison.

## RESULTS AND DISCUSSIONS

The calculated Raman shifts of the substances both in the liquid state and in the solid state at different temperatures are given in Tables I and II.

TABLE I

*m*-Xylene  $\text{C}_6\text{H}_4(\text{CH}_3)_2$ , $\Delta\nu$  in  $\text{cm}^{-1}$ 

Liquid		Solid (present author)	
Magat (1936)	Present author	At about $-80^\circ\text{C}$	At $-180^\circ\text{C}$
		41 (2) e	41 (1) e
		59 (2) e	59 (2) e
		81 (6) e, k	90 (2b) e, k
200 (4)	206 (3) $\pm$ e		
224 (6)	231 (5) $\pm$ e, k	236 (1) e, k	236 (0) e, k
295 (3)	282 (3) $\pm$ e, k	282 (0) e, k	282 (0) e, k
	318 (1b) e, k		
	461 (2) $\pm$ e, k		
514 (4)	517 (4) e, k	513 (1) e, k	513 (0) e, k
538 (6)	540 (7) $\pm$ e, k	536 (2) e, k	534 (1) e, k
	588 (0) e		
	647 (1) e		
	679 (0) e		
725 (10)	727 (10) $\pm$ e, k, i	721 (5) e, k	721 (3) e, k
770 (0.5)	766 (1) e, k		

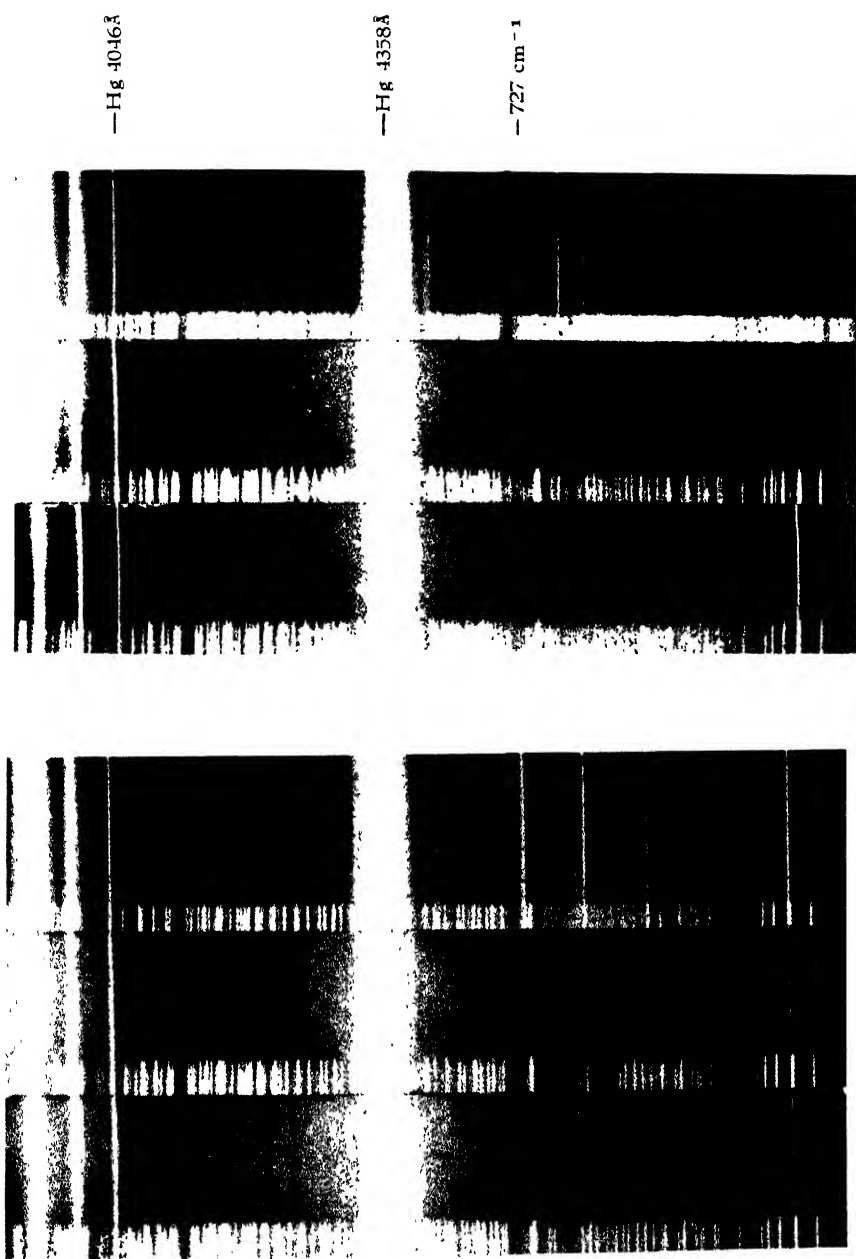
TABLE I—*contd.*

Liquid		Solid (present author)	
Magat (1936)	Present author	At about $-80^{\circ}\text{C}$	At $-180^{\circ}\text{C}$
819 (3b)	812 (o) c 828 (3) e, k 887 (1b) c  913 (1) e 968 (1) c	826 (o) c, k	826 (o) c, k
1000 (12)	1000 (12) e, k, i	1000 (7) e, k	1000 (5) e, k
1032 (1)	1035 (2) e, k	1035 (o) c, k	1035 (o) c, k
1094 (1)	1093 (2) e, k	1093 (o) e, k	1093 (o) c, k
1167 (1)			
	1210 (2) e, k	1210 (o) e, k	1210 (1) e, k
1246 (4)	1250 (4) e, k	1248 (2) e, k	1248 (1) e, k
1268 (0.5)	1265 (2) e, k		
1342 (5)	1349 (1) e		
1375 (5)	1380 (5) e, k	1374 (2) e, k	1374 (1) e, k
1448 (1b)	1446 (2b) e, k		
1592 (1)	1592 (3) e, k	1592 (o) e	1592 (o) e
1613 (3)	1616 (5) e, k	1610 (1) e, k	1610 (1) e, k
2571 (o)			
2731 (0.5)			
2866 (3)	2874 (3b) e, k	2868 (1) k	2868 (o) k
2917 (8b)	2920 (6b) e, k	2911 (4b) e, k 2962 (1) k	2911 (2b) e, k 2962 (1) k
3014 (3)			
3045 (7b)	3058 (4) e, k	3015 (2) k	3045 (1) k
3217 (1b)			

TABLE II

*p*-Xylene, C<sub>6</sub>H<sub>4</sub> (CH<sub>3</sub>)<sub>2</sub> $\Delta\nu$  in cm<sup>-1</sup>

Liquid		Solid (present author)	
Magat (1936)	Present author	At about -30°C	At -180°C
		55 (o) c	50 (1) e, k 68 (1) c, k 87 (2) e k
		91 (2b) c, k	108 (2) c k 148 (1b) c
170 (o 5)			
311 (7)	310 (7) $\pm$ e, k	316 (1) c, k	316 (1) e, k
389 (o)	389 (1) c		
460 (8)	460 (10) $\pm$ e, k	460 (1) c, k	460 (1) e, k
540 (o)			
	593 (1) e		
643 (6)	647 (1) $\pm$ e, k	647 (1) e, k	647 (1) e, k
697 (o)	697 (1) c		
	725 (1) c		
	754 (1) c		
811 (4)	809 (4) $\pm$ e, k	809 (o) c	809 (o) c
827 (12)	820 (12) $\pm$ e, k, i	820 (3) e, k	820 (3) e k
	1000 (1) c k		
1030 (o)			
	1120 (2) e, k		
1182 (2)	1182 (2) e, k	1185 (o) e	1185 (o) e
1212 (8)	1210 (10) e, k i	1210 (5) e, k	1210 (5) e, k
1310 (2)	1319 (1) e		
	1370 (o) c		
1382 (5)	1380 (6) e, k	1371 (o) e, k	1375 (1b) e, k
-1452 (2b)	1450 (2b) e, k	1448 (o) c	1448 (1b) e, k
	1466 (1b) e		



Raman spectra

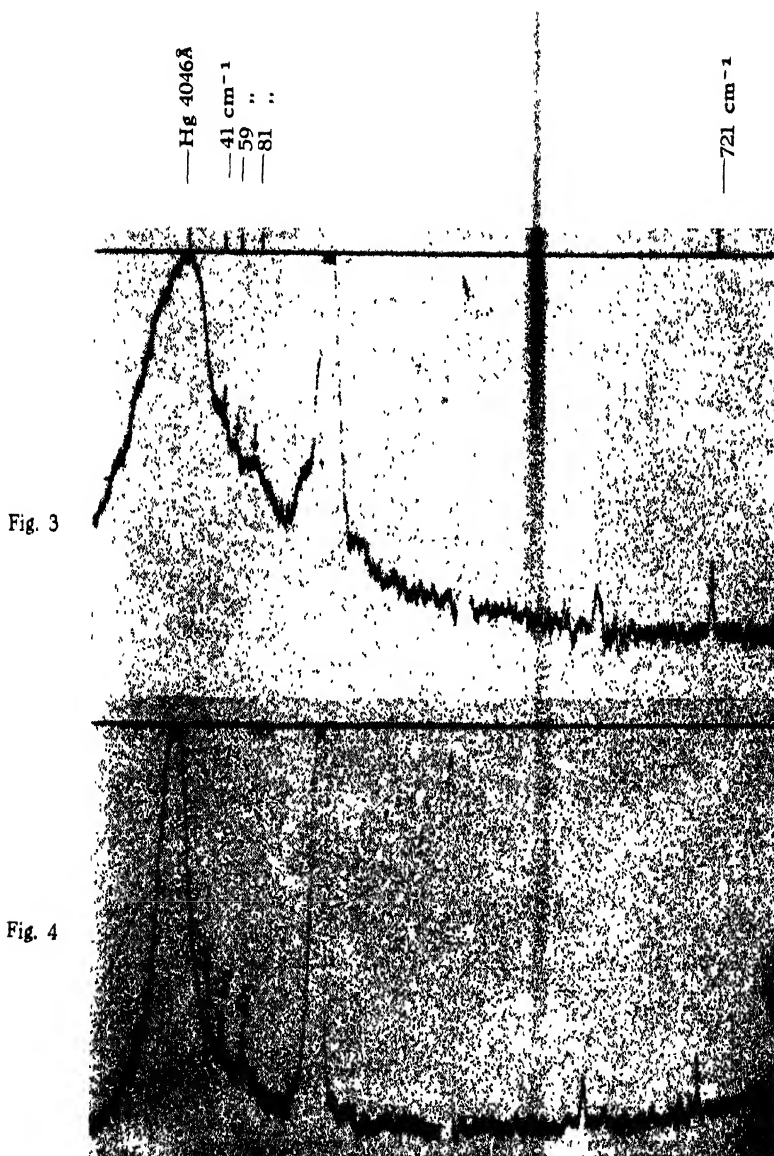
Fig. 1. Meta xylene

- (a) Liquid at 30°C
- (b) Solid at -80°C
- (c) Solid at -180°C

Fig. 2. Para xylene

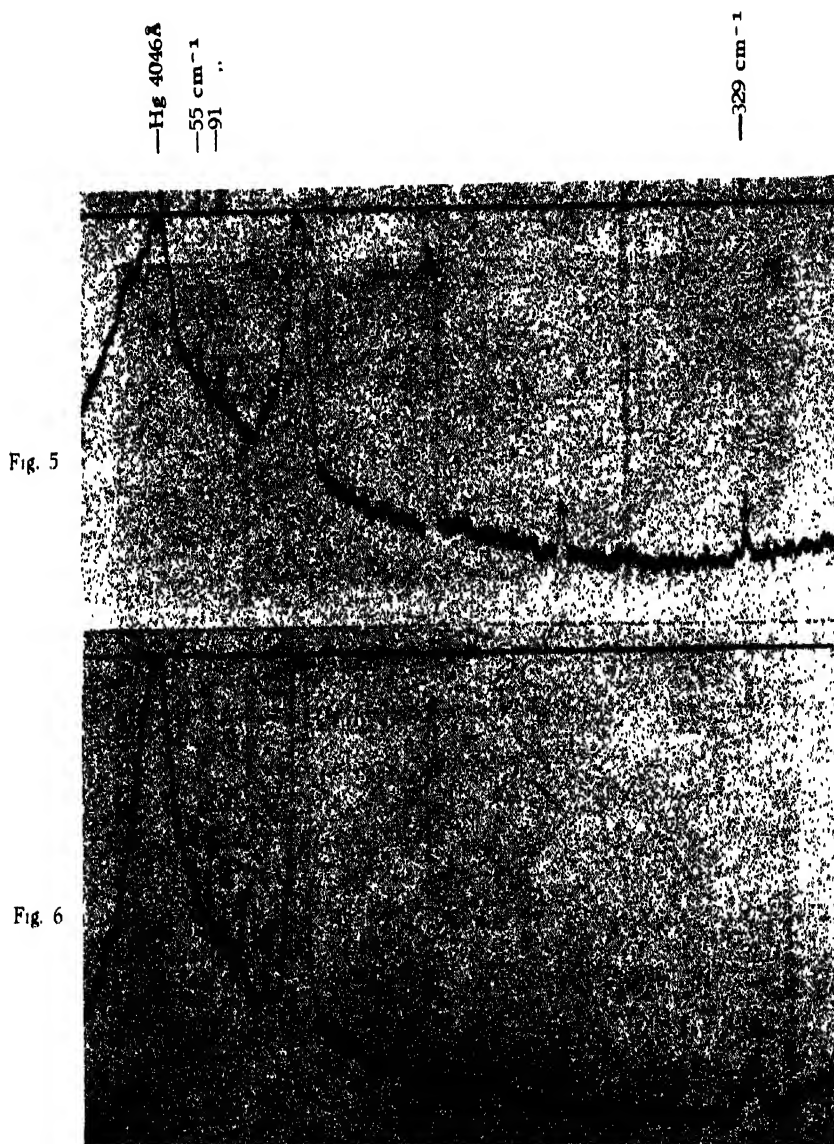
- (a) Liquid at 30°C
- (b) Solid at -30°C
- (c) Solid at -180°C





Microphotometric records of Raman spectra

Fig. 3. Meta xylene at  $-80^{\circ}\text{C}$ Fig 4. " " at  $-180^{\circ}\text{C}$ (  $\omega_1 = 41 \text{ cm}^{-1}$ ,  $\omega_2 = 59 \text{ cm}^{-1}$ ,  $\omega_3 = 90 \text{ cm}^{-1}$  )



Microphotometric records of the Raman spectra

Fig. 5. Para xylene at  $-30^{\circ}\text{C}$ Fig. 6. .. .. at  $-180^{\circ}\text{C}$ 

(  $\omega_1 = 50 \text{ cm}^{-1}$ ,  $\omega_2 = 68 \text{ cm}^{-1}$ ,  $\omega_3 = 87 \text{ cm}^{-1}$ ,  $\omega_4 = 108 \text{ cm}^{-1}$ ,  $\omega_5 = 148 \text{ cm}^{-1}$  )



TABLE II—*contd.*

Liquid		Solid (present author)	
Magat (1936)	Present author	At about $-30^{\circ}\text{C}$	At $-180^{\circ}\text{C}$
	1519 (o) e		
1575 (1)	1580 (2) e, k	1580 (o) e	1580 (o) e, k
1616 (f)	1622 (8) e, k	1620 (o) e	1620 (3) e, k
273 (2)	2740 (2) e, k	2740 (o) k	2740 (o) k
	2865 (1b) e, k		
2867 (5)	2870 (3b) e, k	2868 (1b) k	2868 (1b) k
2920 (9b)	2922 (5b) e, k	2921 (1b) e	2921 (2b) e, k
		2942 (c) e	2942 (2) e, k
3017 (51)	3014 (2) e, k	3014 (2) e	3014 (2) k
	3026 (2) e, k	3026 (2) e	3026 (2) k
3050 (7b)	3063 (4) e, k	3061 (3) e, k	3061 (4) e, k
3214 (1b)			

The tables also include for comparison the Raman shifts of these substances in the liquid state reported by some previous workers. The spectrograms are reproduced in figures 1 and 2, Plate XA. Microphotometric records showing the intensities of the low frequency lines at different temperatures relative to some other lines due to intramolecular oscillations are also reproduced in figures 3—6 (Plates X B—C).

(a) Raman lines of the substances in the liquid state :

Tables I and II show that some of the weak lines observed in the present investigation for these two compounds have not been recorded by previous workers. Such extra lines observed in the case of *m*-xylene are at 318 (1b), 461 (2), 588 (o), 647 (1), 812 (o), 887 (1b), 943 (1), 968 (1) and 1210 (2)  $\text{cm}^{-1}$  and in the case of the other compound the extra lines are at 593 (o), 725 (1), 754 (1), 1000 (1), 1120 (2), 1360 (o), 1466 (1b), 1519 (o) and 2805 (1b)  $\text{cm}^{-1}$ . As the extra lines 461 (2), 647 (1), 812 (o) and 1210 (2)  $\text{cm}^{-1}$  observed in the case of *m*-xylene coincide in positions with the strongest lines of the para compound, it is suspected that a small percentage of para compound is present as impurity in the experimental substance used as meta-xylene in this investigation. Similarly, the presence of the extra lines 725 (1) and 1000 (1)  $\text{cm}^{-1}$  in

the spectrum of the liquid para xylene indicates the contamination of the substance by minute traces of the meta compound. The other extra lines observed in the present investigation seem to be genuine Raman lines of the respective liquids.

Previous authors, on the other hand, have reported the existence of four lines not found in our spectrogram in the case of each of the two xylenes. For meta xylene such extra lines are at 1167 (o), 2571 (o), 2731 (o.5) and 3217 (1b)  $\text{cm}^{-1}$  while for the other compound they are at 170 (o.5), 540 (o)?, 1036 (o) and 3214 (1b)  $\text{cm}^{-1}$ . The lines assigned by previous workers as 2731  $\text{cm}^{-1}$  and 3217  $\text{cm}^{-1}$  in the case of meta xylene and as 3214  $\text{cm}^{-1}$  in the case of the para compound cannot be attributed to the C—H valence oscillation, because although there are traces of the lines at their positions corresponding to 4046 Å excitation, no trace of them is found at the positions corresponding to the much stronger excitation by 4358 Å Hg line. They can be satisfactorily attributed to the C—C valence vibration and the C—H deformation vibration excited by the 4358 Å Hg line. These lines are assigned as the lines 943  $\text{cm}^{-1}$  and 1446  $\text{cm}^{-1}$  of the meta compound and the line 1466  $\text{cm}^{-1}$  of the para compound as given in Tables I and II respectively.

(b) *Raman lines of the substances in the solid state :*

It can be seen from Tables I and II that meta xylene when solidified and cooled to  $-80^{\circ}\text{C}$ , (m. p. of *m*-xylene is  $-52^{\circ}\text{C}$ ) gives rise to three new Raman lines in the low-frequency region while the para compound in the solid state at  $-30^{\circ}\text{C}$  (m. p. of *p*-xylene is  $13^{\circ}\text{C}$ ) gives rise to two new lines in the low-frequency region. When the solidified mass is cooled down to  $-180^{\circ}\text{C}$ , the low-frequency lines of the meta compound show little change in their intensities and positions except the shift of the band at 81  $\text{cm}^{-1}$  to 90  $\text{cm}^{-1}$ . The low-frequency lines of the para compound, on the other hand, show remarkable changes with the lowering of temperature of the polycrystalline mass to  $-180^{\circ}\text{C}$ . Two more low frequency lines at 68  $\text{cm}^{-1}$  and 148  $\text{cm}^{-1}$  respectively appear and the broad line at 91  $\text{cm}^{-1}$  breaks up into two equally intense lines at 87  $\text{cm}^{-1}$  and 108  $\text{cm}^{-1}$  when the solid mass is cooled to  $-180^{\circ}\text{C}$ . Thus, with lowering of temperature of the solid para xylene from  $-30^{\circ}\text{C}$  to  $-180^{\circ}\text{C}$ , the number of low-frequency lines increases from two to five. Moreover, it is evident from the microphotometric records reproduced in figures 3—6 that the intensities of some of the low-frequency lines do not diminish appreciably with the lowering of temperature of the crystals of meta and para xylenes to  $-180^{\circ}\text{C}$ . On the other hand, the intensities of some of the low-frequency lines increase while those of the other lines practically do not show any change with lowering of temperature.

We can now try to understand the above results of our investigation from the points of view of different theories regarding the origin of these low-frequency lines. The ultraviolet absorption spectra of these xylenes were

studied previously by Swamy (1952). It was observed that the absorption bands of these substances become sharper with the solidification of the samples and with the lowering of the temperature to  $-180^{\circ}\text{C}$ . He concluded from these results that with the lowering of temperature angular oscillation of the molecules tends to cease. We can, therefore, see that if the low-frequency lines originate from the angular oscillations of the molecules fixed in the crystal lattice as postulated by some previous workers their intensities should invariably diminish with the lowering of temperature of the solid mass. The evidence being on the contrary, we conclude that at least some of these lines cannot be due to the angular oscillations of the xylene molecules fixed in the crystal lattice. An alternative explanation of the origin of these low-frequency lines was given by Sirkar (1936). According to his theory, the low-frequency lines are due to the intermolecular vibrations in groups of molecules formed by virtual bonds amongst the molecules in each group. In this associated group, the molecules may execute both translational and rotational oscillations giving rise to the new Raman lines in the low-frequency region observed in the case of crystals. The enhancement of the frequency shifts of the low-frequency lines with the lowering of temperature can be easily understood to be the result of the increase in the strength of the virtual bonds which are formed between neighbouring molecules in the solid state with the lowering of temperature. Moreover, at lower temperatures the molecules come closer together and association between next neighbours may take place. These new virtual bonds may be responsible for the increase in the number of low-frequency lines at lower temperature.

This hypothesis of association of the molecules in the solid state in this particular case seems to be unavoidable in view of the fact that the intermolecular field in the liquid state is too weak to make the frequency of angular oscillation as high as  $10^{12}/\text{sec}$ . This can be seen from the results of investigation on the absorption of U. H. F. radio waves in meta xylene reported by Ghosh (1953). He observed an absorption peak of frequency  $8.2 \times 10^9/\text{sec}$  in the case of *m*-xylene at  $-30^{\circ}\text{C}$  and this peak was attributed to dimers. The peak due to monomer was expected to have a frequency of the order of  $10^9/\text{sec}$ . The frequency of the angular oscillation of the single molecule in the solid state, therefore, cannot be greater than  $10^9/\text{sec}$  in this case, unless there is a thousandfold increase in the intermolecular field. As the frequencies of the new lines are of the order of  $10^{12}/\text{sec}$  the intermolecular field is much stronger in the solid state than that in the liquid, as pointed out recently by Sirkar (1951).

A comparison of the number and positions of the low-frequency lines of the two compounds studied in the present investigation show that the relative positions of the substituents in the benzene ring have considerable influence on the low-frequency lines exhibited by these crystals. Also it is clear that the low-frequency lines of the para compound show considerable changes with lowering of temperature to  $-180^{\circ}\text{C}$ , while those of the meta compound

practically do not show such changes under similar condition. This difference in the behaviour of these two compounds with lowering of temperature is certainly related with the relative positions of the substituent groups in the benzene ring. The molecule of the meta compound, due to their unsymmetrical structure, possesses permanent electric moment. Hence the polar molecules of the meta compound get associated more easily even at a temperature just below the freezing point than the symmetrical molecules of the para compound, and with further lowering of temperature only the virtual bond may strengthen a little in the former case. The molecules of the para compound, however, come closer and closer together when the temperature is brought down to  $-180^{\circ}\text{C}$  and the molecules probably disturb the symmetry of their neighbours only when they are sufficiently close to each other. The association of molecules in the case of the para compound is, therefore, complete only at very low temperatures and not at a temperature just below its freezing point.

(c) *Lines of single molecule in the solid state :*

All the prominent Raman lines of both the meta and the para compound in the liquid state are found in the Raman spectra of these substances in the solid state and the relative intensities of these lines remain unaltered with solidification. The frequency-shifts of the intense lines 517, 540, 727, 1380, 1616 and  $2920\text{ cm}^{-1}$  diminish slightly while that of the line  $231\text{ cm}^{-1}$  increases with solidification of the substance. In the case of the para compound also the lines 310 and  $1380\text{ cm}^{-1}$  shift respectively to 316 and  $1375\text{ cm}^{-1}$  while a new line at  $2942\text{ cm}^{-1}$  appears with solidification. This probably indicates that the influence of the intermolecular field on the modes of vibration of the molecules in the solid state depends on the symmetry of the molecule and that meta xylene molecule being more asymmetric than the para xylene molecule greater number of vibrations are affected by intermolecular field in the former case than in the latter case.

The line at  $2874\text{ cm}^{-1}$  of the meta xylene due to C—H valence oscillation shifts to  $2868\text{ cm}^{-1}$  with the solidification of the substance. Another line at  $2920\text{ cm}^{-1}$  of meta xylene due to this C—H valence oscillation splits up into two lines at  $2911\text{ cm}^{-1}$  and  $2962\text{ cm}^{-1}$  with the solidification of the substance. Similarly for the para compound the line at  $2922\text{ cm}^{-1}$  breaks up into two lines at  $2921\text{ cm}^{-1}$  and  $2942\text{ cm}^{-1}$  with the solidification of the substance. Such changes in the lines due to C—H valence oscillation of the xylene molecules, when the other intramolecular oscillations of xylene molecule are little affected with solidification, may lead one to conclude that the association of the neighbouring molecules in the solid state in case of xylenes probably takes place through the hydrogen atom. It may be pointed out here that even when polymerization takes place at the expense of a regular C—C bond in in methylmethacrylate, the other lines of the methylmethacrylate molecule do

not change appreciably (Roy, 1953). Hence in the case of the xylenes also considerable changes in the positions and intensities of other lines are not expected if association takes place through C—H bonds.

#### ACKNOWLEDGMENT

The author is indebted to Prof. S. C. Sirkar, D Sc., F.N.I. for his kind interest and constant guidance throughout this work.

#### REFERENCES

- Biswas, D. C., 1954, *Ind. J. Phys.*, **28**, 85  
Deb, A. R., 1952, *Ind. J. Phys.*, **26**, 201  
„ 1953, *Ind. J. Phys.*, **27**, 183  
„ 1954, *Ind. J. Phys.*, **28**, 21.  
Ghosh, D. K., 1953, *Ind. J. Phys.*, **27**, 285.  
Magat, M., 1936, Annual Table of constants p. 26—77.  
Roy, N. K., 1953, *Ind. J. Phys.*, **27**, 167.  
Sirkar, S. C., 1936, *Ind. J. Phys.*, **10**, 189.  
„ 1951, *J. Chem. Phys.*, **19**, 256.  
Swamy, H. N., 1951, *Ind. J. Phys.*, **25**, 261.  
„ 1952, *Ind. J. Phys.*, **26**, 233.  
„ 1953, *Ind. J. Phys.*, **27**, 55.

# ELECTRICAL CONDUCTIVITY OF SINGLE CRYSTALS OF GRAPHITE ALONG THE BASAL PLANE AND A NEW AND SIMPLE METHOD OF MEASURING ELECTRICAL CONDUCTIVITIES

BY AJIT KUMAR DUTTA AND AMALENDU CHOWDHURY  
INDIAN ASSOCIATION FOR THE CULTIVATION OF SCIENCE, CALCUTTA-32

(Received for publication, June 8, 1954)

**ABSTRACT.** The electrical conductivity of single crystals of graphite for currents along the basal plane, shows a gradual increase with decrease of thickness. This has been shown to be due to the fact that owing to the large electrical anisotropy, the current distribution is not uniform throughout the entire thickness and in consequence all methods involving the question of actual electrical contacts will not give the proper value of the conductivity. The present paper gives the details of a very simple method of measuring the electrical conductivity of specimens in the form of thin plates, in which the question of electrical contacts have altogether been eliminated. The method depends upon the observation of the damping produced due to eddy currents generated in the specimen when oscillating in a uniform magnetic field. Finally, it has been shown that the conductivities obtained from crystals of different thicknesses remain practically the same.

## INTRODUCTION

Graphite is a well known hexagonal layer latticed crystal. It occurs in nature in the form of thin flakes parallel to the basal plane. It exhibits various peculiar electrical and magnetic properties (Ganguli and Krishnan 1936, 1939, 1941). Recent measurements by Dutta (1953) of its principal electrical conductivities over a wide range of temperatures have shown that, the conductivity along the basal plane,  $\sigma_{\parallel}$ , is of the order of  $10^4 \text{ ohm}^{-1} \text{ cm}^{-1}$  while  $\sigma_{\perp}$ , the conductivity perpendicular to the basal plane is about  $1 \text{ ohm}^{-1} \text{ cm}^{-1}$ . Moreover, it has been observed that for currents along the basal plane there is a gradual increase of conductivity, with decreasing thickness and that there is no such effect for currents perpendicular to the basal plane. The reason for this appears to be that owing to the large electrical anisotropy of the crystal, the current density over the area of cross-section normal to the basal plane, is not uniform and hence the effective thickness of the crystal (i.e. the equivalent thickness carrying the mean current through the cross section on the assumption of uniform current density) with the usual methods\* for measuring  $\sigma_{\perp}$  is much smaller than the actual thickness of the

\* The usual method consists in measuring the drop of potential along a rectangular crystal flake through which a known current is passing, the two ends of the crystal specimen being electrolytically coppered to form the potential terminals. For details of measurements one may refer to original paper (Dutta, loc cit.)

crystal. Consequently the values of  $\sigma_1$  calculated on the basis that the entire thickness of the crystal is effective in conducting the current, will naturally give values which are too low—the values being smaller the greater the thickness. Since in all the existing methods of conductivity measurement, the question of electrical contact is involved, none of them will evidently be suitable for electrical measurements with highly anisotropic crystals like graphite. Dutta (*loc. cit.*), however, from a large number of measurements with decreasing thickness of the crystal, tried to extrapolate the value of the conductivity to an infinitely small thickness, giving the true conductivity. But the accuracy of this procedure is limited by the fact that very thin crystals beyond about .01 mm, as will be necessary for a proper extrapolation, is difficult to prepare and take measurements with. In the present paper, following Dutta's suggestions (*loc. cit.*) a new method in which the above difficulties may be overcome, has been developed, suitable for specimens in the form of thin plates, depending upon the observation of the damping produced by eddy currents generated in the specimen oscillating in a uniform magnetic field.

#### THEORY OF THE METHOD

When a rectangular specimen of the single crystal is suspended with its plane vertical from the end of a fine calibrated quartz fibre and executes small oscillations in a uniform magnetic field, the mean position being such that maximum number of lines of force cuts the plane of the specimen normally, the oscillations will be damped due to the following causes: (1) resistance and viscosity of the air, (2) internal friction in the suspensions, (3) eddy currents and (4) magnetic anisotropy of the specimen. The equation of motion can then, evidently be represented by

$$I_0 \frac{d^2\theta}{dt^2} + F \frac{d\theta}{dt} + q^2\theta = 0 \quad \dots (1)$$

where  $I_0$  is the moment of inertia of the specimen about its axis of suspension,  $F$  is the damping coefficient,  $q^2$  is the torsional moment of the suspension fibre per unit angle of displacement, and  $\theta$  is the angular displacement of the specimen at any time  $t$ .

From eq. (1), we obtain the solution

$$\theta = e^{-at} (A \cos bt + B \sin bt)$$

where

$$a = \frac{F}{2I_0}, \quad b = \frac{1}{2} \sqrt{\frac{4q^2}{I_0} - \frac{F^2}{I_0^2}},$$

and  $A$  and  $B$  are constants depending on boundary conditions.

The time period,  $T$ , will, therefore, be given by

$$T = \frac{2\pi}{b} = 4\pi \sqrt{\frac{I_0^2}{4q^2 I_0 - F^2}} \quad \dots (2)$$

The corresponding logarithmic decrement,  $\Lambda$ , is given by

$$\Lambda = \frac{\pi a}{b} = \frac{\pi F}{\sqrt{4q^2 I_0 - F^2}} \quad \dots (3)$$

The coefficient of damping  $F$  is given by

$$F = 4I_0 \frac{\Lambda}{T} \quad \dots (4)$$

This includes dampings due to all the various causes stated above, i. e.

$$F = f_1 + f_2 + f_3 + f_4$$

where  $f_1$  is the coefficient of damping due to eddy currents,

$f_2$ , that due to viscosity and resistance of air,

$f_3$ , that due to internal friction of the suspension system and

$f_4$ , that due to the magnetic anisotropy of the crystal.

Knowing independently  $f_2$ ,  $f_3$  and  $f_4$ , we can at once find out the value of  $f_1$  in which alone we are interested.

Now, if a small rectangular specimen of length  $l$  and breadth  $b$  oscillates in a uniform magnetic field  $H$  in a manner already indicated, then

the e.m.f. induced in it at any instant is given by expression,  $lbH \frac{d\theta}{dt}$ ,

where  $\frac{d\theta}{dt}$  is the angular velocity. The current so generated will be  $\frac{lbH}{R} \frac{d\theta}{dt}$

where  $R$  is the resistance of the specimen in the vertical plane of suspension. The moment of the force due only to this induced current opposing the motion of the specimen, is evidently given by the expression

$$\frac{l^2 b^2 H}{R} \frac{d\theta}{dt} \quad \dots (5)$$

(Obviously, then,

$$f_1 = \frac{l^2 b^2 H^2}{R} \quad \dots (6)$$

Again the resistance,  $R$ , in the path of the eddy currents in the specimen will be given by (Drysdale and Jolley, Vol. I)

$$R = \rho \frac{2(l+b)}{bd}, \text{ where } \rho, \text{ is the specific resistance of the specimen in the}$$

vertical plane of suspension and  $d$  its thickness. Therefore

$$\rho = \frac{l^2 b^2 d H^2}{2f_1(l+b)}$$

i. e., the conductivity

$$\sigma = \frac{2f_1(l+b)}{l^2 b^2 d H^2} \times 10^9 \text{ ohm}^{-1} \text{ cm}^{-1}, \quad \dots (7)$$



EXPERIMENTAL

As it appears from the above considerations, the method of measuring conductivity would be simply to suspend the specimen in a uniform magnetic field with its plane vertical from a calibrated quartz fibre, and to observe the time periods and logarithmic decrements with the magnetic field switched on and off. But the complication due to  $f_L$ , arises in the particular case of the single crystals of graphite. When a crystal of graphite suspended with its basal plane vertical is placed in a uniform magnetic field, owing to its high diamagnetic anisotropy, the crystal immediately sets with its basal plane along the direction of the field after making a few heavily damped oscillations, thereby making it impossible to observe any eddy current damping. This difficulty has been overcome in the present work by attaching another crystal of graphite of mass and size, very much larger in comparison, below the experimental specimen vertically and having their planes at right angles to each other. When this composite system is placed in a uniform magnetic field, the bigger crystal will practically set itself along the field keeping at the same time the plane of the experimental specimen at right angles to the field.

Small rectangular specimens having their planes parallel to the basal

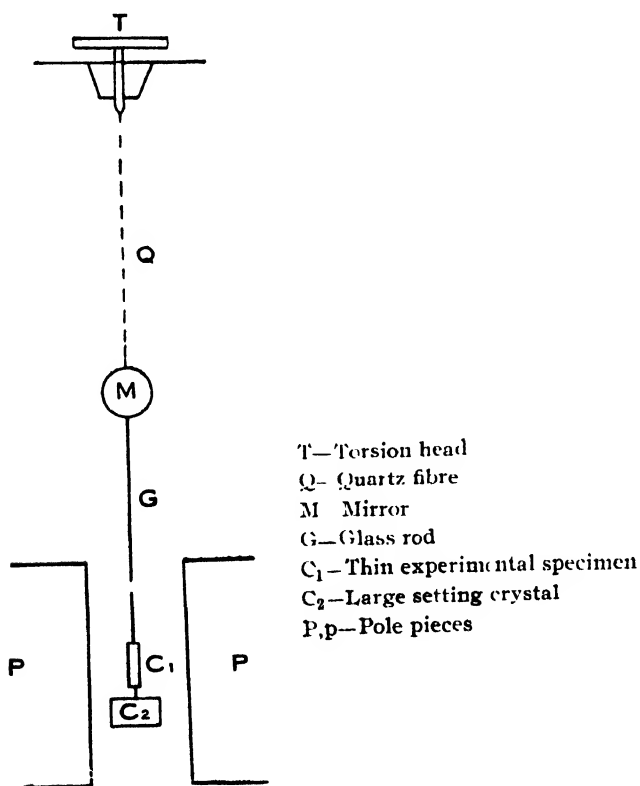


FIG. 1.

plane were cut from different samples of crystals of graphite—their dimensions being accurately measured with the help of a travelling microscope and a micrometer, both reading upto .001 mm. These specimens are attached, having their planes vertical, to the end of a thin and rigid glass rod whose other end is fixed to a calibrated quartz fibre. The bigger crystal is attached below the specimen having its plane vertical and at right angles to that of the upper one. The attachment between the two crystals is effected in such a way that they are electrically insulated from each other. A small circular mirror is attached at the top of the glass rod. The entire system is suspended from the pin of a graduated torsion head and enclosed in a glass tube to prevent the effect of wind and dust. This arrangement is placed in a magnetic field in such a way that the crystal specimen remains always at the centre of the field gap. The arrangement is shown diagrammatically in figure 1. Applying slight twist to the torsion head the crystal system was made to execute small torsional oscillations. The time period and decrements of oscillations were observed by means of a telescope and scale arrangement.

In order to find out the values of the different damping coefficients  $f_2$ ,  $f_3$  and  $f_4$  stated above, the time periods and decrements of oscillations in and outside the magnetic field were determined with each of the crystals (the smaller experimental specimen and the bigger setting crystal) separately, as also with the combination. The different values are represented in Table I. It may be mentioned in this connection that the damping due to the diamagnetic anisotropy has been found to originate from both the crystals, the upper smaller one as well as the lower bigger one.

#### DISCUSSION OF THE RESULTS

Before actually measuring the conductivities of the single crystals of graphite, the accuracy of the method was tested by experimenting with a small rectangular specimen of pure and annealed copper. The value of the specific resistance was obtained to be  $2.654 \times 10^{-6}$  ohm cms. The same specimen when measured with a Kelvin's double bridge yielded a value  $2.665 \times 10^{-6}$  ohms cms.

Measurements on graphite were made with a large number of single crystals obtained from different sources. A typical set of such measurements on crystals of varying thicknesses obtained from a particular sample are represented in Table I. The values of conductivities at different thicknesses obtained by Dutta (l. c.) are also shown in Table II.

On a perusal of the present results we find that due to a variation of thickness by about 7 times, the value of conductivity varies unsystematically and is well within experimental errors. In the measurements by Dutta, for such a change of thickness, the conductivity varied by a factor of about 2.

TABLE I

Sample No	Dimensions in cms l—length b—breadth d—thickness	Magnetic field strength in Gauss	Value of the expression, log decrement/time period for						$\sigma_l \times 10^4$ ohms <sup>-1</sup> cm <sup>-1</sup>	
			Combined system		Bigger crystal		Smaller crystal			
			with out field	with field	without field	with field	without field	with field		
1.	l—.381 b—.188 d—.0838	505	.01671	.01817	.01693	.02013	.01705	.01803	.00076	1.017
2.	l—.184 b—.381 d—.6417	505	.01656	.01833	.01698	.02065	.01710	.01798	.00098	1.018
3.	l—.2946 b—.1955 d—.04965	505	.01576	.01613	.01678	.02102	.01702	.01753	.00051	1.009
4.	l—.2946 b—.1955 d—.02789	505	.01130	.01209	.01750	.01886	.01766	.01804	.00019	1.008
5.	l—.3962 b—.1955 d—.01390	505	.01485	.01663	.01510	.01760	.01797	.01821	.00018	1.011
6	l—.1866 b—.395 d—.01375	505	.01518	.01644	.01616	.01799	.01581	.01618	.0002	1.009

TABLE II

Crystal thickness in cms	$\sigma_1 \times 10^4$ $\text{ohm}^{-1} \text{cms}^{-1}$
.0584	524
.0325	8333
.0294	9901
.0253	1.006
.0114	1.012

Thus it can be argued now that the explanation put forward by Dutta in his paper (loc. cit.) appears to be a plausible one. There may be other reasons also, e. g. the structural difference from layer to layer which as yet could not be correlated by electrical measurements.

## ACKNOWLEDGMENTS

The authors wish to express their best thanks to Dr. A. Bose for his constant helpful discussions and to Prof. M. N. Saha D. Sc., F. R. S. for his kind interest in the work.

## REFERENCES

- Drysdale and Jolly, Electrical Measuring Instruments, Vol. I.  
 Dutta, A. K., 1953, *Phys Rev*, **90**, 187  
 Ganguli, N., 1936, *Phil. Mag.*, **21**, 355  
 „ & Krishnan, K. S., 1941, *Proc. Roy. Soc.*, **A 177**, 168  
 Krishnan, K. S. and Ganguli, N., *Z. Kristallogr*, **A 100**, 530

# MOLECULAR ORBITAL THEORY AND THE REACTIVITY OF POLYPHENYLS

By SADHAN BASU

INDIAN ASSOCIATION FOR THE CULTIVATION OF SCIENCE, CALCUTTA-32.

(Received for publication, April 6, 1954)

**ABSTRACT**—Resonance energies, electronic transitions and  $\pi$ -electron densities have been calculated by LCAO MO method for polyphenyls; The electron densities have been correlated with the chemical reactivities of these compounds at different positions of the ring. Possibility of using frontier electron density instead of  $\pi$ -electron density has also been indicated.

## INTRODUCTION

Many properties of unsaturated organic molecules may be, at least qualitatively correlated with the distribution of electron densities in the isolated molecule. Such properties include the ease of cationoid substitution at different positions of the molecule. Extensive work has already been done in this field by Huckel (1931), Pauling *et al* (1953), Coulson (1947) and others for a large number of aliphatic, aromatic and hetero-cyclic conjugated organic molecules. In the present paper is reported the results of molecular orbital calculations for three polyphenyls, namely, biphenyl, terphenyl and tetraphenyl. The chemistry of biphenyl is fairly well established and a correlation of the reactivity of this compound with  $\pi$ -electron density has been made. The chemistry of two other compounds are not yet fully established. A prediction of their reactivity from theoretical calculation will constitute a test of the validity of such calculation as the chemistry of these compounds are investigated.

Application of molecular orbital theory to these system is expected to be rather unjust. The C—C bond distance between two benzene rings is greater than those in the ring itself ; consequently a complete overlap of the  $\pi$ -electron wave function cannot be freely assumed. However, recent application of electron gas theory to the spectra of these compounds by Nakajima (1953) and its fair agreement with experimental result show that the concept of complete overlap of the wave function is approximately correct. Furthermore such overlapping will be possible if the rings lie on the same plane ; but if they take up a multiplanar configuration the interaction between various rings will be destroyed and the system will behave like a collection of benzene rings. But since in co-planar configuration resonance effect will reduce the energy of the system appreciably, this configuration

will be most favoured in the ground state, although in the excited state multiplaner configuration will be possible.

### THEORETICAL FOUNDATION

The method of calculation is well known. It is assumed that in the conjugated system the greater reactivity may be attributed to  $\pi$ -electrons and not  $\sigma$ -electrons. Attention will therefore be restricted to the former. It is convenient to express the molecular orbitals (MO) of the  $\pi$ -electrons as linear combination of atomic orbitals (LCAO) of the carbon atoms constituting the conjugated system. Each MO is then written in the form

$$\psi = \sum_r C_r \phi_r \quad \dots (1)$$

where  $\phi_1$  to  $\phi_r$  are the  $2p_z$  atomic orbitals of the carbon atoms 1 to  $r$  in the system constituting  $r$  atoms in conjugation. It is further assumed that the atomic orbitals (AO) are orthogonal and normalized, viz.

$$\int \phi_r \phi_s d\tau = 1, \text{ if } r=s \\ = 0, \text{ otherwise} \quad \dots (2)$$

On these assumptions, the energy of an electron ( $E$ ) in  $\psi$  is given by the usual secular equations

$$(E_r - E) C_r + \sum_{s \neq r, (r=1,2,3\dots r)} \beta_{rs} C_s = 0 \quad \dots (3)$$

$$\text{where } \left. \begin{aligned} E_r &= \int \phi_r H \phi_r d\tau = \text{Coulomb integral} \\ \beta_{rs} &= \int \phi_r H \phi_s d\tau = \text{resonance integral} \end{aligned} \right\} \quad \dots (4)$$

In solving these equations for the molecules under consideration we assume that

$$\beta_{rs} = \begin{cases} \beta, & \text{if } r \text{ and } s \text{ are bonded} \\ 0, & \text{otherwise} \end{cases} \quad \dots (5)$$

where  $\beta$  has the same value for all C - C bonds. We assume also that the Coulomb integral  $E_r$  has got the same value for all the carbon atoms and write it as  $E_0$ .

With these assumptions, the secular equation (3) takes the form

$$(E_0 - E) C_r + \sum_{s \text{ bonded to } r} \beta C_s = 0$$

Or more briefly

$$W C_r + \sum \beta C_s = 0 \quad \dots (6)$$

It is evident from equation (6) that for simplest case of biphenyl with 12 carbon atoms in conjugation, we get 12 secular equations from which we can construct a  $12 \times 12$  determinant in  $W$  and  $\beta$ , the solution of which will give us 12 roots for  $W$  and consequently for  $E$  the energy states of the  $\pi$ -electrons. Each of these energy states will be occupied by two electrons of opposite spin; so in the ground state lower 6 of 12 energy states will be occupied. Substituting these roots in the secular equation (6) and applying

the condition that  $C_1^2 + C_2^2 + \dots + C_{12}^2 = 0$ , the coefficients  $C_1, C_2, C_3$ , etc. for various energy states can be calculated. The total density of  $\pi$ -electrons at, say atom 5, is given by  $2\sum C_5^2$  where the summation is taken over all the occupied orbitals.

## APPLICATION OF GROUP THEORY

From what has been said it is clear that in order to get energy states of the  $\pi$ -electrons we are faced with the solution of a 12 order equation in the case of biphenyl, 18 order equation in terphenyl and 24 order equation in tetraphenyl. Difficulties, labour and uncertainties associated with such calculations are well known. However, the symmetric structure of many organic molecules enables us to break up these higher order equations into a number of lower order ones by applying the group theory. We will illustrate the method by taking the case of biphenyl.

The symmetry group in biphenyl is  $D_{2h}$  and  $\pi$ -electron molecular orbitals are of species  $B_{1u}, B_{2g}, B_{3g}$  and  $A_u$ . The numbering of atomic orbitals are shown in figure 1.

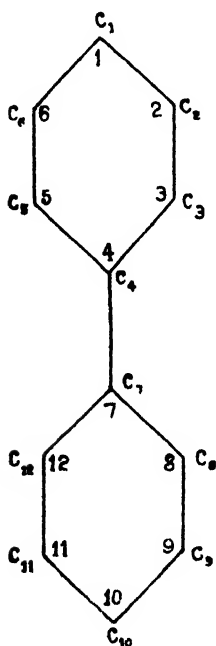


FIG. 1.  
AO forming the MO for biphenyl.

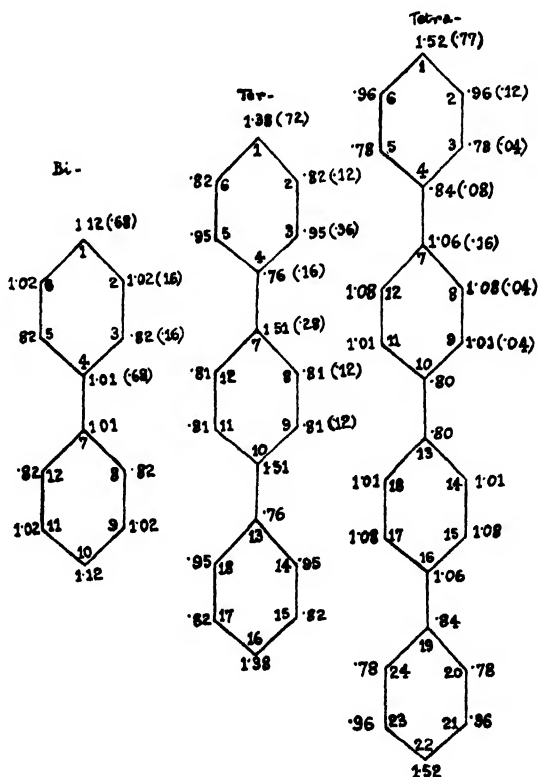


FIG. 2.

Total  $\pi$ -electron density at different carbon atoms (number within parenthesis indicate frontier electron density).

We then have for MO species

$$B_{1u} : C_2 = C_6 = C_9 = C_{11}, C_3 = C_5 = C_8 = C_{12}, C_1 = C_{10} \text{ and } C_4 = C_7.$$

$$B_{2g} : C_2 = C_6 = -C_9 = -C_{11}, C_3 = C_5 = -C_8 = -C_{12}, C_1 = -C_{10} \text{ and } C_4 = -C_7.$$

$$B_{3g} : C_2 = -C_6 = C_9 = -C_{11}, C_3 = -C_5 = C_8 = -C_{12}, \text{ and}$$

$$C_1 = C_4 = C_7 = C_{10} = 0$$

$$\text{and } A_u : C_2 = -C_6 = -C_9 = C_{11}, C_3 = -C_5 = -C_8 = C_{12} \text{ and}$$

$$C_1 = C_4 = C_7 = C_{10} = 0$$

Applying these conditions to equation (6) we can break up the original 12 order determinant into two fourth order and two second order equations, the solution of which gives us the values for twelve energy states out of which lower six will be occupied in the ground state. The equations were solved by 'pinch' method correct up to first decimal place.

The calculated electron densities are shown in the figure 2 for three polyphenyls. Values are necessarily approximate.

**Resonance energies :** Total single electron energy in the occupied states for biphenyl is  $6E_0 + 8.4\beta$  and since each energy state is occupied by 2 electrons the total  $\pi$ -electron energy is  $12E_0 + 16.8\beta$ . For two Kekule structures of the biphenyl with fixed bonds we have the total  $\pi$ -electron energy  $12E_0 + 12\beta$ . So the resonance or delocalisation energy of biphenyl is  $(12E_0 + 16.8\beta) - (12E_0 + 12\beta) = 3.8\beta$ . Similarly for ter- and tetraphenyl the calculated resonance energies are  $6.36\beta$  and  $9.40\beta$  respectively. It is evident therefore that the energies are increasingly lower with increase in the number of phenyl rings.

**Absorption spectra :** The first intense absorption line in the UV region takes place due to a transition of the  $\pi$ -electron from the highest filled level to the lowest vacant level ( $N \rightarrow V$  transition). For biphenyl this transition corresponds to an energy change of  $2\beta$ . If we assume this to be equal to the centre of gravity of the UV line ( $39,2000 \text{ cm}^{-1}$ ) in biphenyl, then the value of  $\beta$  comes out to be  $19,000 \text{ cm}^{-1}$ . (For simple benzene system  $\beta = 23,000 \text{ cm}^{-1}$  (Nakajime, 1953.)) With this value of  $\beta$  we calculate the value of the centre of gravity of the absorption line for ter- and tetraphenyl from the corresponding energy changes ( $1.6\beta$  and  $1.35\beta$  respectively) in  $N \rightarrow V$  transition. The calculated values for ter- and tetraphenyl are respectively  $31,560 \text{ cm}^{-1}$  and  $26,460 \text{ cm}^{-1}$  compared to the experimental values of  $35,000 \text{ cm}^{-1}$  and  $32,700 \text{ cm}^{-1}$ . Although the absolute values do not agree closely enough, the shift in the absorption frequencies are in the right direction, namely, towards red region (the familiar red-shift in resonating molecules). This disagreement, however, is not surprising. The experimental values are for solutions of these compounds in some organic solvent, while the theoretical values are true for crystalline solid where the molecule takes up a coplanar structure as established by X-ray investigation (Dhar, 1932). Measurement of UV spectra will therefore constitute a real test of the theory when applied to crystalline solid.



*$\pi$ -Electron density and chemical reactivity :* The problem of predicting the reactivity of organic molecule at a particular position has been solved to some extent by means of LCAO molecular orbital method. In treating such problems, two methods have been used by several authors: one may be called the 'transition state' method (Wheland, 1942) and the other ' $\pi$ -electron density' method (Pauling, 1935). In the former method the configuration of transition complex is assumed *a priori* on the basis of some other theoretical or empirical arguments, and the method is usually associated with tedious calculations. In the latter method, on the other hand, the density of  $\pi$ -electron at various positions are calculated as has been done in the present case (figure 2). Next, it is assumed that the greater the calculated  $\pi$ -electron density at one position, the greater the ease and rate of substitution at that position by cationoid reagent, while anionoid substitution proceeds most readily at the position where the calculated density is lowest. In biphenyl position of highest electron densities are 1 and 10. So it gives 1 : 10 dinitro, dibromo, dichloro and disulfonated products. Next in order of reactivity are the position 4 and 7. These positions are sterically hindered and an attack at these positions brings about the degradation of the molecule leading to the formation of benzoic acid. With boiling nitric acid, however, biphenyl gives 1 : 3 and 10 : 8 dinitro derivatives. This is similar to ortho-para substitution in benzene. Consequently we may assume that under this condition biphenyl takes up a multiplaner configuration. Similar is the case of oxidation with ozone when a tetraquinone is formed. That the ring system takes up a multiplaner configuration in these compounds has been established by their optical activity (Gilman, 1947).

In the case of terphenyl the electron densities are maximum at 7 and 10 position. Consequently this compound will undergo easy oxidation to benzoic acid, but will never form terephthalic acid. Next in order of reactivity are the positions 1 and 16, which will give derivatives fairly easily. Central ring in this compound will be least reactive and the compound will decompose before any substitution can enter the central ring.

Tetraphenyl will be more stable than terphenyl, electron density being maximum at 1 and 22 position. Further more substitution will enter the terminal rings leaving the central rings unaffected. Degradation of this compound will lead to formation of benzoic acid but not dibenzoic acid.

All these predictions are valid for co planer configuration. With hot nitric acid reaction may take different course due to multiplaner configuration of the molecule.

*Frontier electron density and reactivity :* From what has been said above it is clear that the  $\pi$ -electron density qualitatively predicts the reactivity of different positions of biphenyl towards various reagents. When we try to make a semi-quantitative calculation of the percent yield of a product we are faced with some difficulties. Thus if  $M$  be the sum of  $\pi$ -electron densities at different positions and  $N$  the  $\pi$ -electron

density at the position, say 1, then the percent yield of, say nitrated product with substitution at 1 and 2 for biphenyl should be respectively 30.9 and 13.2. But in actual practice no product with substitution at 2 position is obtained. Such discrepancies have also been noticed in the case of spiro-hydrocarbons. In order to get around these difficulties Fukui *et al* (1953) introduced the concept of frontier electron density method in predicting the reactivity of conjugated compounds. They assumed that in a chemical reaction the electron at the top of the filled energy level enters into reaction, i. e. the electrons at the top has got some kind of valency character. So they assumed that it is the density of frontier electron that will govern the actual extent of reaction. Such calculations have given encouraging result for spiro-hydrocarbons. The results of frontier electron density calculation for polyphenyls are also shown in figure 2 (within paranthesis). It will be evident that the frontier electron density at 2, 3, 5 and 6 positions are all equal and the percent yield of monosubstituted product at 1 and at any other position are respectively 34 and 8. Although frontier electron density method improves the result, still it is far from being quantitative. Further it is not clear why frontier electrons should govern the extent of reaction, because the course of reaction is controlled by the attractive force between the approaching radical or ion and the particular position of the molecule. This evidently will depend on the total  $\pi$ -electron density. It may, however, be argued that although the point of maximum attack will be governed by the total  $\pi$ -electron density, the extent to which the reaction will proceed may be governed by the frontier electron density. How far these assumptions are justified will become clear as more and more frontier electron density calculations are made and compared with experimental results.

#### ACKNOWLEDGEMENT

Thanks are due to Dr. P. C. Dutt. and Mr. P. N. Bagchi for helpful discussions.

#### REFERENCES

- Coulson, C., 1947, *Trans Farad. Soc.*, **43**, 87.  
 Dhar, J., 1932, *Ind J. Phys* **7**, 43.  
 Fukui, K., Tenezawa, T. and Shingu, H. 1952, *J. Chem. Phys.*, **20**, 722.  
 Gilman, H., 1947, *Organic Chemistry, an advanced treatise*, Vol. I,  
 Huckel, E., 1931, *Z. Physik.*, **70**, 204.  
 Nakajima, T., 1953, *Sci. Rep. Res. Inst., Tohoku Univ.*, **8**, 98.  
 Pauling, L. and Wheland, G., 1933, *J. Chem. Phys.*, **1**, 362.  
 Pauling, L. and Wheland, G., 1935, *J. Amer. Chem. Soc.*, **57**, 2586.  
 Wheland, G., 1932 *ibid.*, **31**, 1111

# THEORETICAL CALCULATION OF SHIFTS IN SUBSTITUTED BENZENES

By S. RAMAMURTY

DEPARTMENT OF MATHEMATICAL PHYSICS, ANDHRA UNIVERSITY, WALT AIR

(Received for publication April 12, 1954)

**ABSTRACT.** Using the M. O. method of Herzfeld the effect of  $\text{CH}_3$  and  $\text{NH}_2$  substitutions in benzene in shifting the o,o position of the band system of benzene has been calculated. It is suggested that the inductive effect is also to be taken into account.

## INTRODUCTION

It was pointed out by Herzfeld (1947) that the M. O. method can be applied to the computation of the wavelength shift of the o,o position of the band system consequent on substitution in molecules with conjugated  $\pi$  bonds. Herzfeld performed the calculation for F and OH substitutions in benzene. For the F substitution the calculated value was somewhat agreeing with the observed shift. For OH, however, the difference was large, being only slightly less than 30 % of the experimental value.

There are two principal effects of substitution—"migration of charge into the ring" and "the inductive effect". In Herzfeld's computations, the migration effect alone was considered. This was in accordance with Sklar's (1939) empirical estimate of the importance of the two effects in relation to the intensification of the spectra consequent upon substitution.

## HERZFELD'S METHOD

If  $\phi_j$  be the  $j^{\text{th}}$  M.O. of the ring,  $\zeta$  of the substituent, then neglecting charge distortion in the ring by the substitution, the ring electrons will be in orbitals  $\phi_j$ , and the electrons in the substituent will, in the substituted compound, be in the orbitals  $\sum \Lambda_j \phi_j + b\zeta$ .  $\Lambda_j$ 's define the extent of migration of the substituent electrons into the ring. Normalisation requirement leads to the expression

$$\sum \Lambda_j^2 + 2 \sum \Lambda_j b S_j + b^2 = 1 \text{ where } S_j = \int \phi_j \zeta d\tau \quad \dots (1)$$

The energy of the molecule will be  $\int \psi^* H \psi d\tau$  where  $\psi$  is the wavefunction for the whole molecule, obtained by multiplying the orbitals for the various electrons, antisymmetrising and normalising. This can be shown to be equal to

$$\sum \Lambda_j^2 \omega_j + 2 \sum \Lambda_j b \rho_j + b^2 \omega$$

(summation over unfilled orbitals). Here  $\omega$ ,  $\omega_j$  are the energies of the

orbital in the substituent and the ring respectively as modified by the perturbation of the other, and  $\rho_j$  is the exchange integral. The energy in substituent, however, is  $\omega$ . The energy change is then

$$U = \Sigma \Lambda_j^2 \omega_j + 2 \Sigma \Lambda_j b \rho_j + b^2 \omega - \omega \quad \dots (2)$$

Minimising this, in the light of (1), leads to

$$\Lambda_j = \frac{\rho_j - \omega S_j}{\omega - \omega_j} \quad \dots (3)$$

putting  $b \approx 1$ . Substituting (3) in (2)

$$U = \Sigma (\omega - \omega_j) \Lambda_j^2$$

Now, considering an electronic transition, in the ground state all orbitals upto a certain  $n$  are filled up, only the remaining are available for migration ( $j > n$ ) and

$$U_g = \Sigma_{j > n} (\omega - \omega_j) \Lambda_j^2$$

whereas in the excited state one electron of orbital  $n$  is raised to a higher orbital  $\phi_m$  ( $m > n$ ) (say). The orbital  $\phi_m$  is thus "half closed" for migration and the orbital  $\phi_n$  is "half opened" for it. The same might be thought of as complete closing up of  $\phi_m$  for immigration of electrons and complete opening up of  $\phi_n$  for the same process; and change in the excited energy level consequent upon migration is

$$U_e = \Lambda_n^2 (\omega - \omega_n) + \Sigma_{j > n} (\omega - \omega_j) \Lambda_j^2 - (\omega - \omega_m) \Lambda_m^2$$

The wavenumber shift is then

$$\Delta v = \frac{U_e - U_g}{hc} = \Lambda_n^2 \frac{\omega - \omega_n}{hc} - \Lambda_m^2 \frac{\omega - \omega_m}{hc} \quad \dots (4)$$

To compute the quantities occurring in (4) a number of simplifying assumptions are made, e.g., the distance between the carbon atom and the substituent is unaltered by excitation to a higher level, similarly overlap integrals between non-neighbouring atoms are negligible. It proves possible to write

$$\Lambda_j = c_s^{(j)} \left\{ \frac{1}{\omega - \omega_j} \left[ \rho' - \frac{1}{2} S \int \phi_j H \times \phi_j d\tau \right] - \frac{S}{2} \right\} \quad \dots (5)$$

using (3) above and writing  $S_j = c_s^{(j)} S$ ,  $S = \int p_s \zeta d\tau$ ,  
 $\rho_j = c_s^{(j)} [\rho' + \frac{1}{2} S (\omega + \omega_j)]$ ,  
 $2\rho' = \int p_s (H_R + H_X) \zeta d\tau$

with Herzfeld. Here  $c_s^{(j)}$  is the coefficient of  $p_s$ , the  $2\pi$  A. U. of  $s^{th}$  atom, in  $\phi_j$ ,  $\omega$ ,  $\omega_j$  are the energies of  $\zeta$ ,  $\phi_j$  respectively. The notation is the same as in Herzfeld's paper. In (5) all the quantities can be computed (Herzfeld's formulae 27, 28, 29) using the values of integrals given by Sklar and Lyddane (1939).

APPLICATION TO CH<sub>3</sub> AND NH<sub>2</sub> SUBSTITUTIONS

This method has now been applied for the CH<sub>3</sub> and NH<sub>2</sub> substitutions in benzene. In doing this the fact that the migrating electrons are coming from the hybridised orbitals in the substituent is remembered in the evaluation of the overlap integrals from formulae (23) Sklar's paper (1939).

The ionisation potentials of the radicals in the compounds, and the electron affinity of the methyl radical, are taken from the same paper. The values of the integrals (excepting  $Q_{22}$ ) are obtained by graphical plotting from the values given in Sklar and Lyddane's paper (1939).  $Q_{22}$  has been calculated directly from formula (18). For methyl group the overlap integrals have been taken from Mulliken, Rieke and others (1948-49).

These results together with those of Herzfeld for F and OH are tabulated below. For CH<sub>3</sub> substitution the figure given is the resultant red shift for all the three orbitals in the substituent.

TABLE I

Molecule	Calculated red shift	Observed red shift
C <sub>6</sub> H <sub>5</sub> I	-230	-271
C <sub>6</sub> H <sub>5</sub> OH	-1170	-1730
C <sub>6</sub> H <sub>5</sub> NH	-1964	-4055
C <sub>6</sub> H <sub>5</sub> CH <sub>3</sub>	-44.38	-605

DISCUSSION

In discussing the results it should be kept in view that in CH<sub>3</sub> substitution there are no unbound electrons. In the other molecules the migration of only the unbound electrons is considered. But in C<sub>6</sub>H<sub>5</sub>CH<sub>3</sub> only the migration of bound electrons can be considered. If an orbital in the substituent is  $\zeta$  and the orbitals in the ring be  $\phi_j$ , then, in the substituted compound, neglecting inductive effect, the electron in the substituent will be in the orbitals

$$\sum \Lambda_j \phi_j + b \zeta$$

$\Lambda_j$ 's here define the extent of migration of the substituent electron from orbital  $\zeta$  into orbitals  $\phi_j$ . For bound electrons  $\Lambda_j$ 's will be different from 0 i.e., a certain amount of migration will take place even for bound electrons. (In fact it must be supposed that even the ring electrons migrate to a certain extent into the substituent; but this is negligible compared with the migration in the opposite direction. The additional space made available for the movement of electrons of the ring by the substituent is negligible compared with the space made available for the movement of the electrons

of the substituent by the ring.) But it is reasonable to presume that the migration of  $\text{CH}_3$  electrons into the ring in  $\text{C}_6\text{H}_5\text{CH}_3$  will be very small. For the other molecules considered, there will be greater degree of migration than in  $\text{C}_6\text{H}_5\text{CH}_3$  connected with the fact that there are unbound electrons in these other molecules. This feature may account for the increasing divergence between the calculated and observed shifts in the substituents F, OH,  $\text{NH}_2$ ,  $\text{CH}_3$  whereas in  $\text{CH}_3$  actually the inductive effect predominates.

It appears, therefore, that the inductive effect has also to be considered in accounting for the observed shifts especially in compounds involving migration of only bound electrons.

#### ACKNOWLEDGMENT

The author would like to express his indebtedness to Prof. K. R. Rao for his kind guidance and interest in the work.

#### REFERENCES

- Hertzfeld, K. M., 1947, *Chem. Rev.*, **41**, 223.  
Mulliken, R. S., Rieke, C. A., Orloff, D., and Orloff, H., 1948-49. ONR contract report for period Sept. 1, 1948 to May 31, 1949 Part II  
Sklar, A. L., and Lyddane, R. H., 1939, *J. Chem. Phys.*, **7**, 374.  
Sklar, A. L., 1937, *J. Chem. Phys.*, **7**, 986.

# ON THE INTENSITY-DISTRIBUTION IN THE WING OF THE RAYLEIGH LINE DUE TO LIQUID OXYGEN\*

BY G. S. KASTHA

OPTICS DEPARTMENT, INDIAN ASSOCIATION FOR THE CULTIVATION OF SCIENCE, CALCUTT. 32.

(Received for publication, May 20, 1954)

## Plate XI

**ABSTRACT**—The intensity-distribution in the wing accompanying Rayleigh radiation from liquid oxygen has been studied quantitatively by the method of photographic spectrophotometry, using a suitable spectrograph and Hg 4047Å line as exciting radiation. It has been shown that the intensity distribution in the wing shows a clear maximum at about  $40\text{ cm}^{-1}$  from the centre of the exciting line and the intensity, instead of increasing continuously as the centre of the line is approached, falls off and becomes zero at a distance of  $9\text{ cm}^{-1}$  from the centre of exciting line. The probable causes of the discrepancy between this result and that reported by Crawford *et al* (1952) have been discussed.

## INTRODUCTION

It is well known that the wing which accompanies the Rayleigh line due to molecules in the gaseous state generally consists of discrete lines, while in the case of organic liquids the wing shows a continuous intensity-distribution. The question whether in the case of heavy diatomic molecules in the liquid state, such as  $\text{O}_2$ , the rotational lines are resolved from each other as in the gaseous state was first investigated by Saha (1940). He observed a continuous wing in the neighbourhood of the Rayleigh line due to liquid oxygen and the intensity-distribution showed a maximum at a distance of  $50\text{ cm}^{-1}$  from the Rayleigh line. These results, when compared with those reported by Trumphy (1933) for gaseous oxygen at a pressure of 60 atmospheres, show that the change of state has a marked influence on the width of rotational lines. Trumphy (1933) observed discrete rotational lines with the line of maximum intensity at a distance of  $50\text{ cm}^{-1}$  from the Rayleigh line and the lines were slightly broader than those observed in the case of the gas at ordinary pressures. Recently, Crawford *et al* (1952) have investigated the distribution of intensity in the wing due to  $\text{O}_2$ ,  $\text{N}_2$  and  $\text{CH}_4$  in the liquid state. In the case of liquid oxygen they also have observed a continuous wing, but they have failed to notice any maximum in the intensity-distribution. They attributed this discrepancy to the fact

\* Communicated by Prof. S. C. Sirkar

that Saha did not take into account the blackening produced by the Rayleigh line in its neighbourhood owing to over-exposure. On examining the microphotometric records of the incident and scattered lines reproduced by Saha (1940), however, it was observed by the present author that there was an inflexion in the curve in the record of the scattered line and this hump was absent in the record due to the incident line. It was, therefore, thought worthwhile to reinvestigate the Raman spectrum of liquid oxygen, using an arrangement in which stray light could be reduced as much as possible so as to avoid over-exposure of the Rayleigh line and a spectrograph which would give a suitable dispersion and an image of the slit free from coma. Fortunately, such a spectrograph was available in the laboratory and with this the Raman spectrum of a column of liquid oxygen, about 15 cm long, has been photographed. The results of analysis of the spectrum are discussed in the present paper.

#### EXPERIMENTAL

The experimental arrangement used in the present investigation was a simple one as shown in figure 1. *D* is a Dewar flask made of Pyrex glass, the walls at the bottom of which are blown flat so as to make the central areas plane and almost parallel to each other. The tube *T* containing liquid air is held in a vertical position and aligned centrally with the help

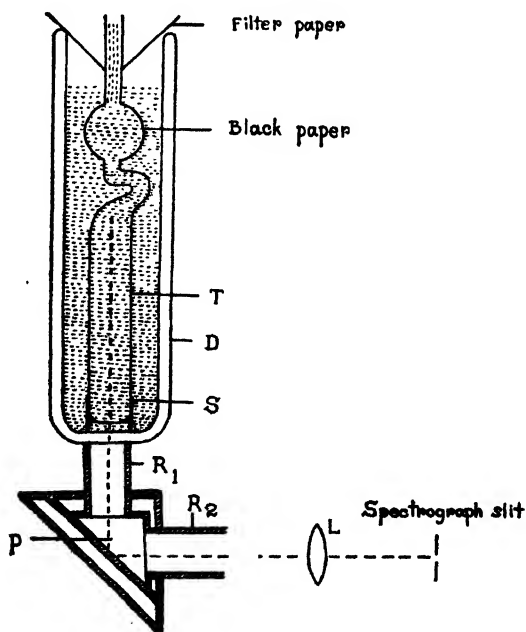


FIG. 1

of a stand and a collar *S* inside the Dewar flask *D* containing liquid air. The outer surface of the Dewar flask *D*, excepting the window



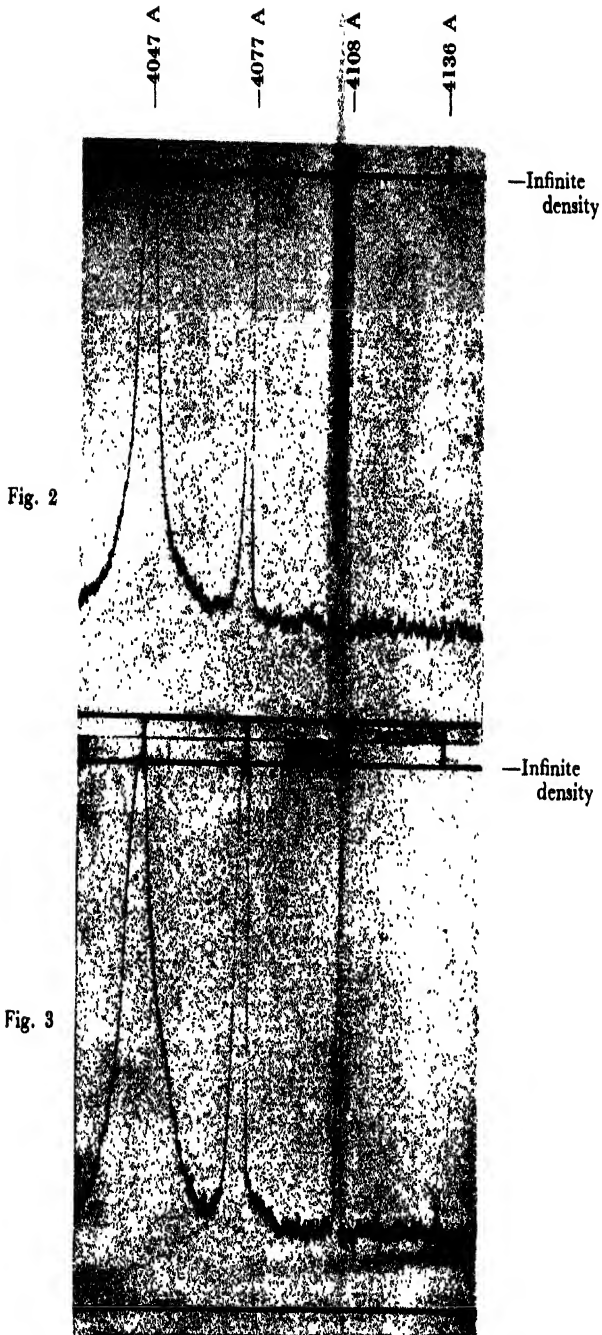


Fig. 2—Microphotometric record of Hg 4047 Å group (incident)

Fig. 3—Microphotometric record of Hg 4047 Å group scattered by liquid O<sub>2</sub>.



at the bottom and two fairly long parallel apertures on either side used for illuminating the liquid is painted dull black. The tube *T* is provided with a flat window at the lower end which reaches almost the bottom of the Dewar flask, and the other end is blown into the shape of a horn, the outer surface of which is covered with black paper. The collar *S* and the black paper tube surrounding the lower end of the tube *T* serve the purpose of preventing direct light from the mercury arcs and the light scattered by the outer liquid oxygen envelope from reaching the window of the tube.

The Dewar flask with the Wood's tube *T* was clamped with suitable clamps and placed vertically on the box *B* containing a totally reflecting prism *P*. Two long tubes *R*<sub>1</sub> and *R*<sub>2</sub> were attached at right angles to the prism box in order to reduce stray light as far as possible. The whole arrangement was then aligned accurately along the optical axis of the spectrograph and the scattered light was focussed on the slit of the spectrograph with the lens *L*. The Dewar flask *D* and the tube *T* were filled simultaneously with liquid oxygen filtered through filter papers, so that no ice was deposited on the window of the tube *T*. Though bubbles were formed in the liquid oxygen contained in the Dewar flask, the liquid oxygen inside tube *T* was free from such bubbles. Liquid oxygen was replenished from time to time in the Dewar flask as well as in the tube so that the level of the liquid oxygen in the tube was always below that of the liquid oxygen in the Dewar flask.

The liquid oxygen in the tube *T* was illuminated with the light from two vertical mercury arcs, through the transparent windows on the outer wall of the Dewar flask. The scattered light from the back end of the Wood's tube *T* was focussed with the condensing lens *L*, on the slit of a Fuess spectrograph. This spectrograph has a dispersion of 11 Å/mm in the region 4047 Å. The aperture of the condensing lens *L* was adjusted so that the scattered beam entering into the spectrograph filled up about  $\frac{1}{4}$ ths of the aperture of the collimating lens. The image of the slit produced by the spectrograph with this arrangement was free from coma on the Stokes side. The width of the slit was .04 mm.

Ilford Special Rapid plates were used to photograph the spectra. These plates were suitably backed to prevent the formation of haloes. An exposure of three and a half hours was sufficient to bring out the wing and the vibrational Raman line of liquid oxygen with moderate intensity. By trial, the spectrum of light from the mercury arc was recorded on a plate from the same packet, using different exposures so that the fourth mercury line of 4047 Å group was of the same density as in the spectrogram due to scattered light. The plates were developed under identical conditions.

For the purpose of calculating intensities from the densities in the neighbourhood of the Hg-line 4047 Å in the spectra due to scattered and

incident light, intensity marks were taken on a plate from the same packet, using tungsten filament lamp as the source of continuous radiation and varying the width of the slit of the spectrograph.

Microphotometric traces of the spectrograms and intensity marks were recorded with a Moll recording Microphotometer taking all sorts of necessary precautions. From the traces of the intensity marks a density *vs.* log intensity curve was drawn for the wavelength 4050 Å.

Care was taken to take the microphotometric records through corresponding points of the 4047 Å line in the scattered and incident spectra so that the distance between the centres of the lines 4108 Å and 4047 Å was exactly the same in both the records.

The values of intensity on the Stokes side of the scattered Hg-line 4047 Å were calculated for different distances from the centre of the 4047 Å line. The centre was located by measuring the distance from the 4108 Å line. On the spectrogram due to incident light the intensities at the corresponding points on the Stokes side of the incident line 4047 Å were also calculated in the same way and these were deducted from the intensity values obtained for the spectrum of the scattered light. Each of these values were corrected for back-ground intensity and the final values for intensity were plotted as ordinates against wavenumber separation from the centre of the line 4047 Å as abscissa.

#### RESULTS AND DISCUSSION

The microphotometric records are reproduced in figures 2 and 3 (Plate XI). The relative intensities at different distances from the centre of the 4047 Å line in the spectra due to the incident and scattered light are plotted in figure 4. It will be seen from figures 2 and 3 that the fourth line of the

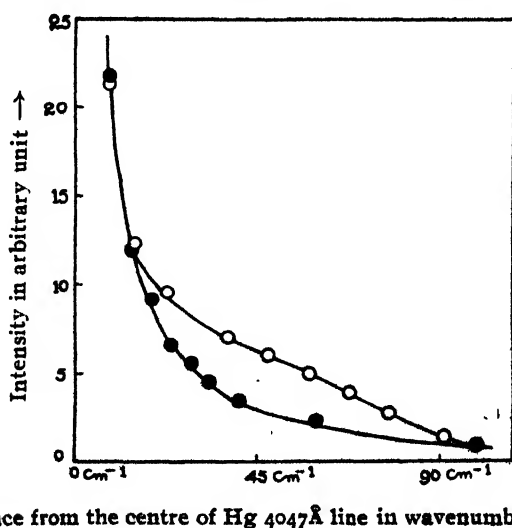
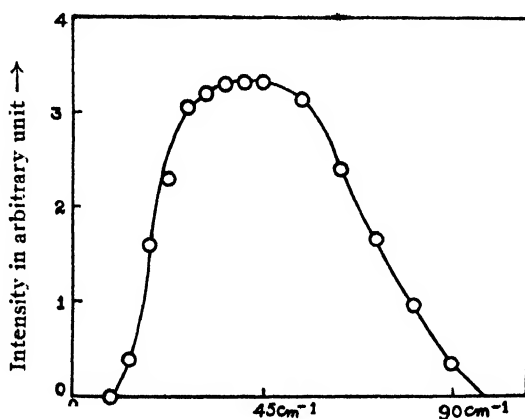


FIG. 4.  
Black circles give intensity of incident radiation and white circles give intensity of scattered radiation.

4047 Å group of mercury lines is of the same intensity in both the spectra due to the incident and scattered light respectively and figure 4 shows that upto a distance of about  $9\text{ cm}^{-1}$  from the centre of the 4047 Å line the intensity distribution in the spectrum of the scattered light is exactly the same as that in the spectrum due to the incident light. As the distance increases further the intensity in the spectrum due to scattered light is larger than that in the incident spectrum and the difference between the two values first increases and then gradually falls off to zero as shown in figure 5. This difference is due to the rotational Raman spectrum and it shows a maximum at a distance  $40\text{ cm}^{-1}$  from the centre of Rayleigh line. It may be mentioned that the  $1550\text{ cm}^{-1}$  line of  $\text{O}_2$  was recorded with almost three times the intensity of Hg line  $4136\text{ Å}$ .



Distance from the centre of Hg 4047 Å line in wavenumbers →

FIG. 5

Difference of intensity between the scattered and incident radiation

The results obtained in the present investigation support the conclusion arrived at by Saha (1940) that in the case of liquid oxygen the intensity distribution in the wing accompanying the Rayleigh line has a maximum not at the centre of the Rayleigh line but at a certain distance from it. This distance was given by him as  $50\text{ cm}^{-1}$ , but in the present investigation the quantitative curve showing the intensity distribution gives the position of the maximum at about  $40\text{ cm}^{-1}$  from the centre of the Rayleigh line. The conclusion drawn by Crawford *et al* (1952) that the maximum lies at the centre of the Rayleigh line is not correct. It is difficult to account for the discrepancy between the results obtained by them and those of the present investigation. It has to be pointed out in this connection, however, that if any coma be present on the Stokes side of the line 4047 Å, its extent will depend on the method of focussing the light on the slit of the spectrograph and the extent of the coma in the line due to the incident light may not be identical with that in the line due to

scattered light and in that case it is difficult to get correct information regarding the distribution of intensity in the wing. It is therefore essentially necessary to use a spectrograph which, besides having sufficient dispersion, should produce no coma even when the wing is over-exposed. It is almost impossible to get such a spectrograph, but fortunately, out of half a dozen Fuess spectrographs of this laboratory one was found to produce absolutely no coma on the Stokes side of the  $4047 \text{ \AA}$  line even when the Hg  $4136 \text{ \AA}$  line was recorded with moderate intensity, and the dispersion was quite sufficient. Secondly, in such an investigation the incident line has to be chosen carefully so that there is no band in the neighbourhood of the line at least on one side. Hg  $2537 \text{ \AA}$  line is not suitable, because it is always accompanied by a band and a wing on the Stokes side. The  $4047 \text{ \AA}$  line appears to be most suitable for the purpose of the present investigation as can be seen from microphotometric records reproduced in figure 2. Probably, Crawford *et al* used the line  $2537 \text{ \AA}$  as the exciting line and in that case it would be difficult to get the intensities due to incident line correctly.

#### ACKNOWLEDGMENT

The author is indebted to Prof. S. C. Sirkar for his keen interest and helpful suggestion and guidance during the progress of the work.

#### REFERENCES

- Crawford, Welsh and Harrold, 1952, *Canadian J. Phys* , **30**, 81  
Saha, B., 1940, *Ind J. Phys* , **14**, 123.  
Trumpy, B , 1933, *Z. f. Phys.*, **84**, 282.

# THE LEAD ABSORPTION OF COSMIC RAYS

By P. S. GILL

DEPARTMENT OF PHYSICS, ALIGARH UNIVERSITY, ALIGARH

(Received for publication, May 13, 1954)

## Plate XII

**ABSTRACT.** Detailed measurements of the absorption of cosmic rays in lead have been made at Gulmarg (8890 ft.), Srinagar (5000 ft.), Aligarh (600 ft.), and Swarthmore (296 ft.) with a view to determining the reported anomalies in the lead absorption curves at low latitudes. The data do not bring out any abnormality in curves other than at Gulmarg, where there is an indication of a dip at  $p/\mu = .557$  Bev/c corresponding to 35 cm lead thickness.

In recent years Aiyar Chandrashekar (1944), Swann and Morris (1947), Fanyves and Haiman (1950), and Gill (1950), have observed anomalies in the absorption of cosmic rays in lead at low altitudes. The abnormalities, however, occur at different thicknesses of lead as reported by different authors. This inconsistency in the various measurements could perhaps be attributed to numerous causes such as, different geometries employed, the placement of lead in the telescopes, the different latitudes and altitudes, where such observations were made.

In the summer of 1950, an experiment was planned to study the above mentioned anomalies in the lead absorption curves in further details at widely different latitudes by employing similar apparatus. The general plan was concerned with measuring cosmic ray intensity through different thicknesses of lead. In comparison of intensity for different thicknesses, it is vitally important that the cosmic ray intensity during the observations shall remain constant, or that the observations shall be taken in such a way as to eliminate the effect of variations in the intensity as far as possible.

It was decided to make observations by straddling the data for different thicknesses in the following manner. A possible schedule appropriate to sea level observations founded upon utilization of 55 cm of lead within the telescope may be given as under :

1. Take observations for 0, 8 and 12 cm. of lead.
2. From 12 cm to 30 cm, take observations for every 2 cm of lead.
3. From 30 cm to 55 cm observations are to be taken for every 5 cm of lead.

The observations for these 17 thicknesses were to be straddled in such a manner that every thickness of lead was covered by all periods of the day.

At higher altitudes, the period of observation could be made shorter in such a manner as to produce the same number of counts for any given thickness of lead.

#### COSMIC RAY TELESCOPES

Cosmic ray telescope consisted of four trays of seventeen counters each (see Plate XII). Each tray of 17 G-M tubes provided a sensitive area of 100 square centimeters. The outer two trays, separated by a distance of 80 cm allowed 55 cm of lead to be interposed between them. Each tray consisted of 17 identical G-M counters, connected in parallel and overlapped to present an uninterrupted horizontal plane of dimensions 10 cm  $\times$  10 cm. These counter trays were connected in quadruple coincidence. Four exactly similar telescopes were made at the Bartol Research Foundation.

One of these instruments was operated at Swarthmore (geomagnetic latitude  $52^{\circ}\text{N}$ , altitude 296 feet) in a thin wooden shelter on roof of the laboratory (data were supplied by the courtesy of Dr. W. F. G. Swann and [Mr. David W. Seymour). Two of the telescopes collected data first at Aligarh (geomagnetic latitude  $18^{\circ}12'\text{N}$ , altitude 600 feet), then at Srinagar (geomagnetic latitude  $23^{\circ}32'\text{N}$ , altitude 5000 feet), and lastly at Gulmarg (geomagnetic latitude  $23^{\circ}32'\text{N}$ , altitude 8890 feet).

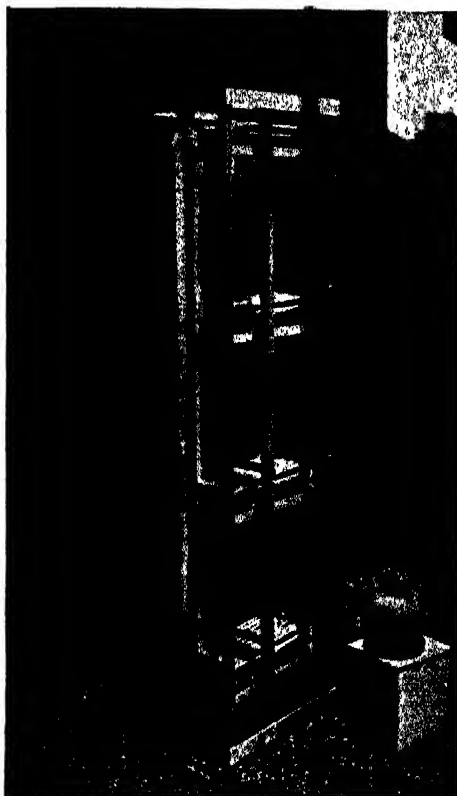
At all the stations except Srinagar the data collected at each thickness of lead was of such an accuracy as to give a standard deviation of about one percent or less. The observations at Gulmarg were made during September-October of 1951 and 1952, while at Aligarh the time of observation was March-April of 1951 and December of 1952. All the points on the curves thus obtained during the two years at Aligarh and Gulmarg did not differ from each other except what would be expected due to statistical fluctuations.

Every day between 9 A.M. and 10 A.M. each G-M counter of all the trays was tested individually. Only rarely a counter was found to have changed its characteristics in which case it was immediately replaced by a new one. At Aligarh, Srinagar and Gulmarg the instruments were continuously run for 24 hours except for approximately an hour in the morning when the counters were being tested.

#### RESULTS

The experimental results are shown in Table I. In figure 1, curves A, B, C and D represent the absorption of cosmic ray particles in lead at Gulmarg, Srinagar, Swarthmore and Aligarh respectively. No marked





A view of the cosmic ray telescope showing the placement of the four counter trays.



abnormality is apparent in other than the Gulmarg curve which indicates a dip in the neighbourhood of 40 cm lead thickness.

The differential curves of figure 2 are obtained from the smooth curves of figure 1. The intensity at 8 cm for each curve is taken as 100 percent. The units are percent of total intensity per hundred million electron volts. These differential curves also do not bring out any striking abnormality.

TABLE I

The location of the stations, the rate of quadruple coincidences for each thickness of lead together with the standard deviation are shown.

Gulmarg (8890 ft.)			Aligarh (650 ft.)		Brinagar (5000 ft)		Swarthmore (295 ft.)	
Thickness of lead in cms	Rate. counts per minute	Error $\pm$	Rate counts per minute	Error $\pm$	Rate. counts per minute	Error $\pm$	Rate counts per minute	Error $\pm$
0	4.224	.033	2.162	.016	2.86	0.053	2.26	0.02
8	2.748	.026	1.747	.014	2.32	0.052	1.90	0.02
12	2.535	.024	1.665	.013	2.25	0.049	1.84	0.02
14	2.430	.024	1.664	.014	2.15	0.048	1.73	0.02
16	2.466	.024	1.605	.013	2.10	0.047	1.77	0.02
18	2.358	.023	1.627	.013	2.05	0.076	1.74	0.02
20	2.363	.024	1.603	.013	1.98	0.065	1.75	0.02
22	2.314	.023	1.587	.013	1.92	0.063	1.68	0.02
24	2.270	.024	1.545	.013	1.88	0.063	1.68	0.02
26	2.228	.022	1.571	.013	1.90	0.063	1.62	0.02
28	2.225	.022	1.497	.013	1.75	0.060	1.65	0.02
30	2.181	.022	1.512	.013	1.85	0.066	1.62	0.02
35	2.069	.023	1.475	.012	1.64	0.058	1.59	0.02
40	2.013	.023	1.420	.012	1.66	0.060	1.55	0.02
45	1.881	.021	1.366	.013	1.63	0.063	1.45	0.02
50	1.862	.021	1.380	.012	1.70	0.061	1.44	0.02
55	1.811	.020	1.324	.012	1.59	0.060	1.38	0.02

In light of the comments of Dr. W. F. G. Swann which he very kindly sent on my request (see Appendix), the Gulmarg (8890 ft.) curve was plotted against momentum (figure 3). To get an empirical expression for the functional relationship which would show a point of inflection, a third degree curve of the form

$$n = a + bp + cp^2 + dp^3$$

does not give a very good fit with the experimental points but it shows a point of inflection at  $p/\mu = .557$  Bev/c. If the dip in the lead absorption curve has any reality, as is indicated by the curve of figure 3, then the range corresponds to 35 cm of Pb thickness.

Near sea-level, however, the data show a smooth absorption curve, in agreement with Swann and Scymour's curve at Swarthmore. Kennedy (1953) measured the absorption of the vertically incident cosmic rays in lead at sea level at geomagnetic latitude of  $43.5^\circ\text{S}$  and got a smooth absorption curve.

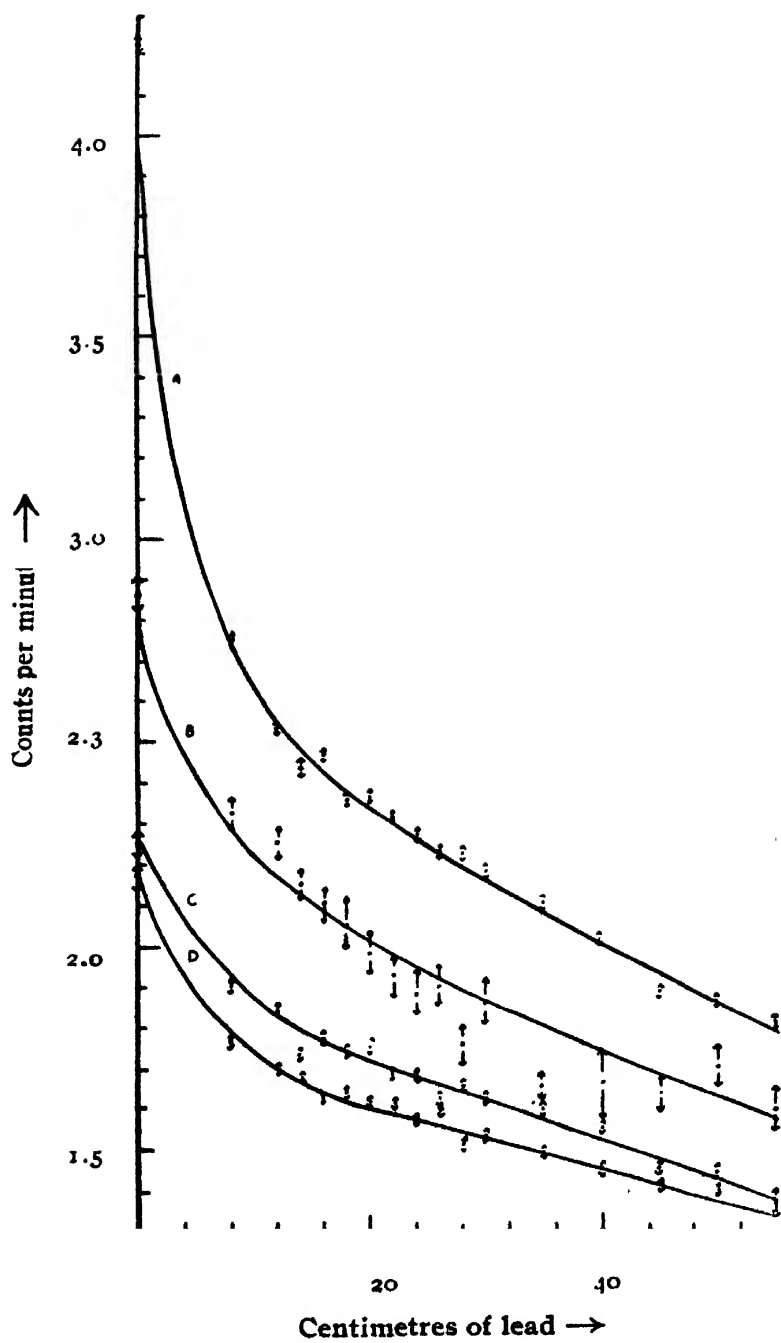


FIG. 1

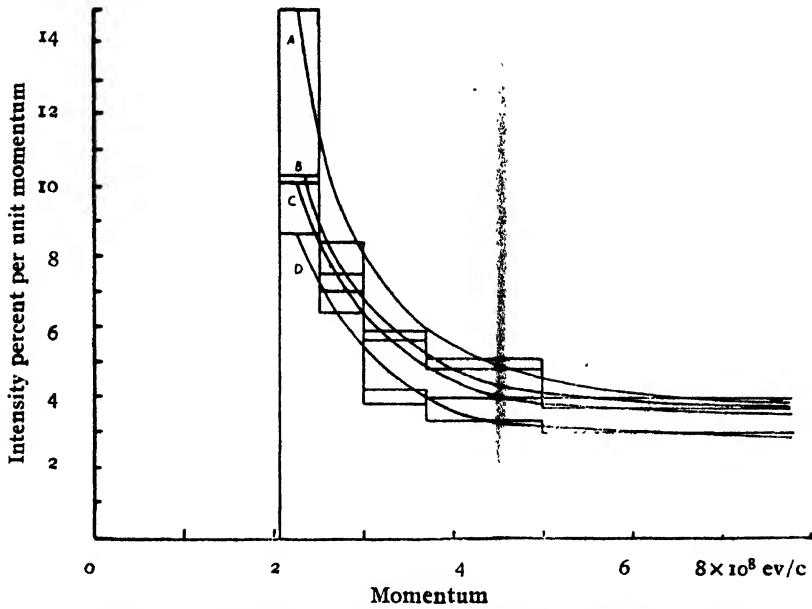


Fig. 2. A—Gulmarg, B—Srinagar, C—Swarthmore D,— Aligarh

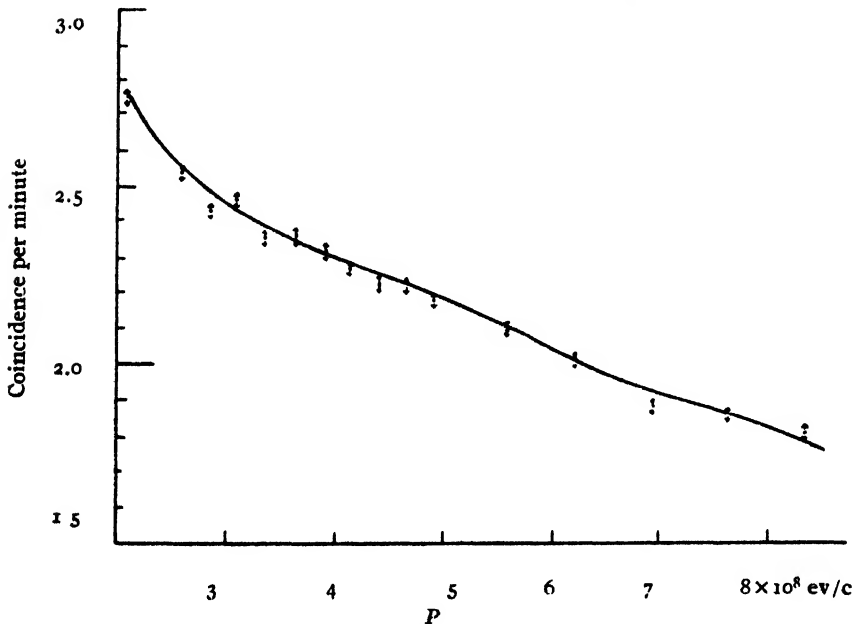


FIG. 3

#### ACKNOWLEDGMENTS

The autor wishes to express his thanks to Dr. W. F. G. Swann for his comments, to Mr. David W. Seymour for his valuable help in the construction of the telescopes, and to the Research Scholars at Aligarh who helped in the collection of data at great personal inconveniences.

The author acknowledges the financial help by the American Philosophical Society, which enabled him to spend two months at the Bartol Research Foundation.

## REFERENCES

- Aiya Chandrashekhar, S. V., 1944, *Nature.*, **153**, 375.  
 Fanyves, B., and Haiman, O., 1950, *Nature.*, **165**, 244  
 Gill, P. S., 1950, *Nature*, **165**, 318.  
 Kennedy, W. L., 1953, *Aust. J. Phys.*, **6**(3), 500.  
 Swann, W. F. G., and Morris, P. A., 1947, *Phys. Rev.*, **72**, 1262.

## APPENDIX

Comments on Professor P. S. Gill's Paper

"THE LEAD ABSORPTION OF COMSIC RAYS"

By W. F. G. Swann

Professor Gill has kindly invited me to comment on the results cited in his paper under the above title.

## GENERAL THEORY

Suppose that the number,  $n$ , of rays observed through a cosmic ray telescope containing a lead absorber is plotted against the momentum,  $p$ , necessary for a mesotron to penetrate the various thickness of lead involved\*. Then, if  $f(p)$  is the spectral distribution function for the radiation

$$-\frac{dn}{dp} = f(p) \quad \dots (1)$$

The maximum of the spectral distribution curve is given by

$$\frac{df(p)}{dp} = 0 \quad \dots (2)$$

so that this maximum corresponds to  $d^2n/dp^2=0$ , and so to a point of inflection in the curve of  $n$  versus  $p$ .

The point of inflection gives the picture of a drop in the  $n$  versus  $p$  curve in the vicinity of the value of  $p$  corresponding to the point of inflection, the drop being more pronounced the shorter the momentum range in which it occurs. To investigate this matter further, let us consider the  $f(p)$  curves for different altitudes, and as an example, let us take the data cited by Schein, Wollan and Groetzinger (1940). Our interest centers in the two curves shown in figure 3 by these authors. The sharp curve, which we shall call A, corresponds to altitude 6.7 km, while the flat curve, which we shall call B, corresponds to sea level. The curves give the spectral distribution in terms

\* For the relation between thickness of penetration and momentum, see B. Ross and K. Greisen, *Rev. Mod. Phys.*, **13**, 240 (1941).

of energy, but in figures 1 and 2 we have plotted them in terms of momentum. By measuring the areas of the curves from the extreme right to different values of  $p$ , we get from these areas the values of  $n$ , corresponding to rays

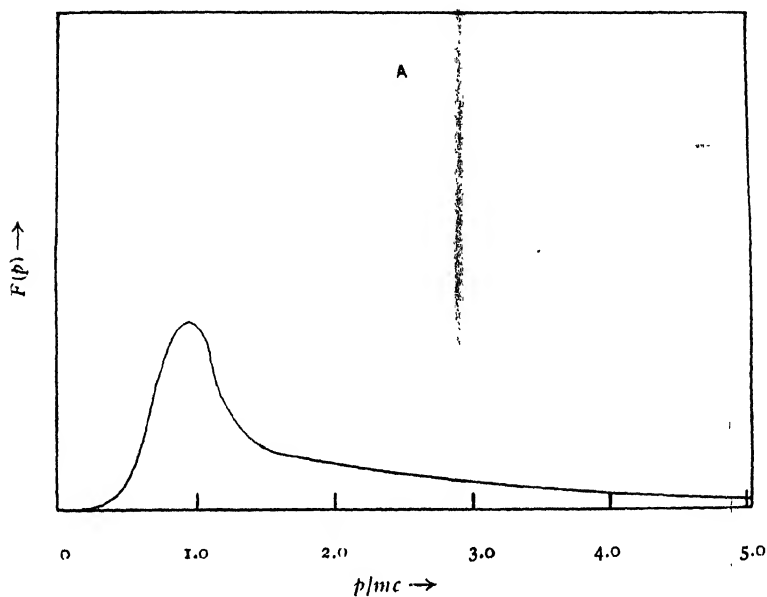


FIG. 1

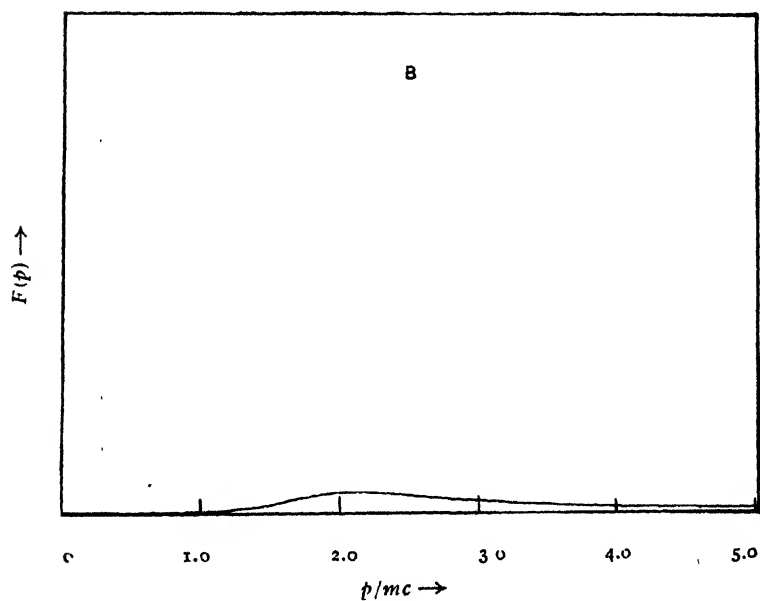


FIG. 2

with momentum less than the largest value. It is then convenient to normalize these curves to the same value of  $n$  for  $p=0$ . The results are shown in figure 3. They exemplify graphically a conclusion, which can, of course, be established analytically, to the effect that the sharpness of the high altitude  $f(p)$  curve is responsible for a more pronounced drop in the  $n$  versus  $p$  curve for the high altitude curve than is found for the sea level curve.

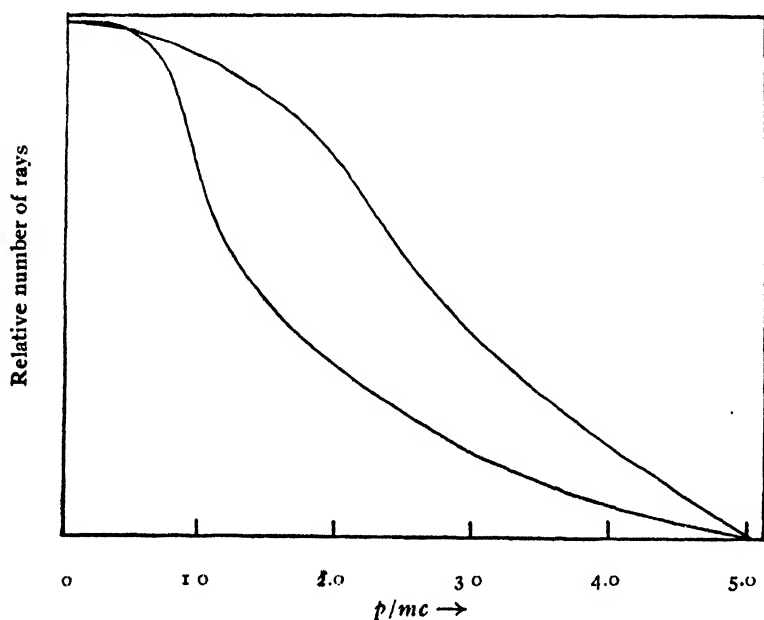


FIG. 3

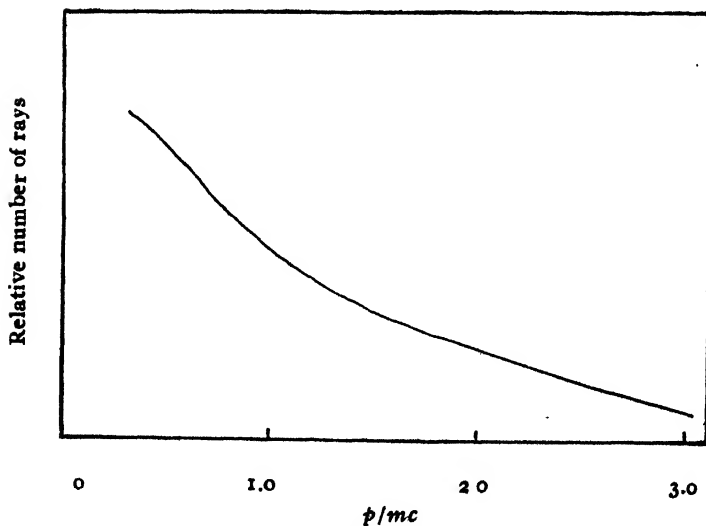


FIG. 4



Several observers have reported sudden dips in the  $n$  versus  $p$  curves, and as a rule these dips have been more pronounced at high altitudes than at sea level. The point of inflection corresponding to the dip occurs, as already stated, at the value of  $p$  for which the  $f(p)$  curve has a maximum.

#### EXPERIMENTAL

A large number of observations taken by different observers (Glasser *et al*, 1950) agree in assigning the maximum for the  $f(p)$  curve at sea level at  $p=1.0$  Bev/c.

Now figure 4 shows the  $n$  versus  $p$  data obtained by W. F. G. Swann and D. Seymour at Swarthmore (sea level)\*. It is estimated that the point of inflection occurs at about  $p=0.9$  Bev/c, in remarkably good agreement with the value 1.0 Bev/c cited above.

*Professor Gill's Experiments.* We need not attend to observations with less than about 12 cms of lead, since these are contaminated with electron component. Our interest centres upon the points of inflection referred to above.

The curves at such altitudes as those of Gulmarg and Aligarh cannot be expected to reveal a point of inflection for lead thicknesses less than 56 cms, since the point of inflection for sea level in the  $f(p)$  versus  $p$  curve corresponds to about 700 gms/cm<sup>2</sup> of lead. The D curve over the range concerned shows no point of inflection. Curve C shows an abnormality at about 40 cms of lead. However, the abnormality is within the experimental error and in view of this fact, combined with the fact that the observations of Swann and Seymour do not show it, indicates that, indeed, the apparent abnormality is accidental.

The statistical errors in curve B do not warrant drawing anything other than a smooth curve. As far as A is concerned, however, we have a point of inflection at 40 cms of lead. There is sense in supposing that this point of inflection may be real†, because a point of inflection may be expected to occur for a smaller thickness of lead at 8890 feet than at sea level.

If we plot the intensity against  $p/mc$  and also against lead thickness, and if a point of inflection in one curve occurs at  $p=p_0$  and in the other curve at a length  $L$ , it does not follow that  $p_0$  is exactly the momentum corresponding

\*. The points to the right of the curve were obtained by extending the range of absorption data, utilizing the Bartol Foundation's 30 ft. water tank.

†. When a phenomenon stands unsupported by additional "reasons", statistical uncertainty may forbid the placing of any reliance upon it. When it stands supported by additional evidence, however, statistical uncertainty, if not too great, plays a less dominant role.

to the range  $L$ ; for if  $x$  refers to thickness of lead,  $d^2n/dp^2=0$  corresponds to

$$0 = \frac{d}{dp} \left( \frac{dn}{dx} \frac{dx}{dp} \right) = \frac{d^2n}{dx^2} \frac{dx}{dp} + \frac{dn}{dx} \frac{d^2x}{dp^2}$$

so that  $d^2n/dp^2=0$  does not quite correspond to  $d^2n/dx^2=0$ . However, the result is approximately true, and to the extent that it is true\*, we may say that the point of inflection at 40 cms of lead corresponds to a point of inflection in the  $n$  versus  $p/mc=0.63$  Bev/c, which is the momentum corresponding to a range of 40 cms in lead. This value of  $p/mc$  is not unreasonable for the altitude 8890 feet since, as may be seen from figures 1 and 2, the value of  $p/mc$  for the point of inflection is, at 6.7 km altitude, less than half that at sea level †

\*. We can, of course, avoid the complexity of discussion in this matter by replotting Professor Gill's curves against  $p/mc$ .

†. The sea level value is unity. This value does not agree with the value deduced from the results yielded by Figs 1 and 2. However, these figures correspond to rather old data and were only used for semi-quantitative illustrations of the effect of altitude on the  $f(p)$  curves, and particularly of the effect of altitude on the value of  $p$  which yields a maximum in such curves.

#### REFERENCES

- Glasser, D. A., Hamermesh, B. and Safonov, G., 1950, *Phys. Rev.*, **80**, 625.  
 Schein, M. Wollan, E. O. and Groetzingcr, G. 1940, *Phys. Rev.*, **58**, 1021.

# A TABLE FOR THE CALCULATION OF SURFACE TENSION FROM MEASUREMENTS OF SESSILE DROPS

By N. R. TAWDE

PHYSICS DEPARTMENT, KARNATAK UNIVERSITY, DHARWAR,

AND

K. G. PARVATIKAR

PHYSICS DEPARTMENT, RAJARAM COLLEGE, KOLHAPUR

*(Received for publication, April 26, 1954)*

**ABSTRACT.** The present paper is an extension of the work of Tawde and Parvatikar on sessile drops. A table is prepared of the values of  $a^2/r^2$  against  $h/r$  in the range from 0.5100 to 0.5708 at interval of 0.0002.

Taylor and Alexander (1944) have fitted up an empirical equation in the case of sessile drops from which the values of  $a^2/r^2$  are obtained for the corresponding values of  $h/r$ , where  $a^2$  is the capillary constant defined by  $2\gamma/g\rho$ ,  $\gamma$  being the surface tension of the liquid,  $\rho$  its effective density,  $r$ , the radius of the sessile drop, and  $h$ , the height of it from the equatorial plane. From the knowledge of the measurable quantity  $h/r$ ,  $a^2/r^2$  could be known from the tables and hence  $\gamma$ , the surface tension could be determined.

Recently, the authors (1951) have shown that this function of  $h/r$  and  $a^2/r^2$  could also be obtained by modifying the standard tables of Bashforth and Adams (1883). The table thus drawn up has been put to test for its usefulness by using the experimental measurements on sessile drops. By a rigorous study it has been shown that this table is also equally dependable for the determination of surface tension from measurements of sessile drops. This table gave values of  $h/r$  and  $a^2/r^2$  for the values of  $\beta$  ( $\beta = 2b^2/a^2$ , where  $b$  is the radius of curvature at the apex of the drop) ranging from 25 to 50 at interval of unity and from 50 to 100 at interval of two. It was suggested therein that a more accurate table could be drawn up by using any other available intermediate values of  $\beta$ . Since it is noticed that the tables of Bashforth and Adams are at intervals of 0.1 in  $\beta$  in the range 0.0 to 46.7, and as our earlier table was only exploratory with a large interval in  $\beta$  of the order of 1.0 and 2.0 as mentioned above, it is thought desirable to calculate here the values of  $h/r$  and  $a^2/r^2$  for all intermediate values corresponding to 0.1 interval in  $\beta$  and prepare a more detailed and comprehensive table. This table is worked out only for the range of  $\beta = 22.0$  to 46.7. The values of  $h/r$  and  $a^2/r^2$  are calculated first in the same way as shown in the

It will be interesting to examine whether observations on the sessile drop in conjunction with this table can serve as one of the standard methods for the measurement of surface tension. This work is now in progress.

#### ACKNOWLEDGMENTS

One of us (K. G. P.) takes this opportunity to offer his grateful thanks to the authorities of Rajaram College, and to Professor B. N. Biswas, for their continued interest and encouragement.

#### REFERENCES

- Bashforth, B. D. and Adams, J. C., 1883, "An Attempt to Test the Theories of Capillary Action". Cambridge University Press.  
Taylor H. J. and Alexander, J., 1944, *Proc. Ind Acad. Sc.*, **19**, A. 149.  
Tawde, N. R. and Parvatikar, K. G., 1951, *Ind J. Phys.*, **28**, 473.

**PROCEEDINGS  
OF THE  
INDIAN ASSOCIATION FOR THE  
CULTIVATION OF SCIENCE**



# THE EFFECT OF CHAIN TRANSFER ON THE DISTRIBUTION OF MOLECULAR WEIGHTS IN HIGH POLYMERS. PART II. TERMINATION BY DISPROPORTIONATION

BY KESAB CHANDRA MAJUMDAR AND SANTI R. PALIT

INDIAN ASSOCIATION FOR THE CULTIVATION OF SCIENCE, CALCUTTA-32, INDIA

(Received for publication, May 22, 1954)

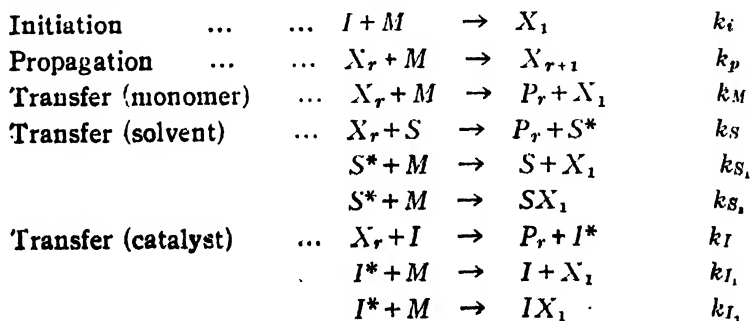
**ABSTRACT.** An equation for distribution of molecular weights taking into account chain transfer with monomer, solvent and catalyst has been derived under the assumption that the chain termination is exclusively by disproportionation. From this equation values of  $P_n$ ,  $\bar{P}_n$ , etc., have been derived and a number of relations deduced. All these equations are compared with similar equations derived previously assuming chain termination by combination of two growing radicals.

## INTRODUCTION

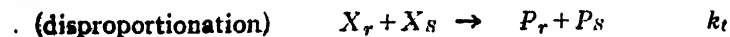
In the previous paper of this series (Palit and Majumdar, 1954) we discussed the case where the termination takes place exclusively by coupling of two free radicals as is generally believed to be the case. However, as the possibility of termination by disproportionation cannot be completely ruled out we have considered in the present paper this latter mode of termination only, and have compared our previous findings with the present results.

## DERIVATION OF THE DISTRIBUTION EQUATION

Let us consider the following kinetic scheme wherein we have used the same notations and abbreviations as in our earlier paper.



### Termination



Also, let  $q = C_M + C_S S/M + C_I I/M + t \sqrt{I/M}$ ; and  $t = \frac{\sqrt{k_i k_t}}{k_p}$

From the above scheme with the usual steady state assumption and using a method exactly similar to that used in our previous paper (vide Appendix) the following distribution equation is obtained.

$$\omega_r = 1 \times \left( -\frac{dP_r}{dM} \right) = \frac{q^2 r}{(1+q)^2 (1+\epsilon)} \approx \frac{q^2 r}{(1+q)^2} \quad \dots (1)$$

where  $\omega_r$  is the weight fraction of the  $r$ -mers. Making reasonable approximations (vide Appendix) we finally obtain

$$\omega_r = q^2 r e^{-qr} \quad \dots (2)$$

This equation is very similar to that obtained by Bawn (1948) without considering any kind of transfer.

Equation (2) is a differential equation and so gives the instantaneous distribution at a given value of  $S/M$  and  $I/M$  and so it should be applied to experimental data at small yields.

It should be noted that the distribution equation is a function of  $q$  only and does not involve any other quantity explicitly and hence the effect of a change of any factor is simply obtained by noting the effect of a change of  $q$  only. Thus, we need not consider individually the effect

of the single factors, viz.,  $S$ ,  $I$ ,  $C_M$ ,  $C_S$ ,  $C_I$  and  $t = \frac{(k_i k_t)^{1/2}}{k_p}$ , but we need

only study the distribution curves within the usual experimental range of variation of  $q = C_M + C_S S/M + C_I I/M + t \sqrt{I/M}$ , which has been done in the next section.

#### THE SHAPE OF THE THEORETICAL DISTRIBUTION CURVE

In figure 1 we have drawn a set of curves with values of  $q$  from  $1 \times 10^{-4}$  to  $5 \times 10^{-4}$ . It may be mentioned that  $q = 1.24 \times 10^{-4}$  would represent polymerization of styrene at  $60^\circ\text{C}$  and so curves with  $q = 2 \times 10^{-4}$  and higher would represent its gradual change either by addition of a solvent or a catalyst, or by raising temperature. The shape is quite similar to the theoretical curves for termination by combination but the present curves are a little steeper. To have a comparative idea we have drawn in figure 2 two curves corresponding to the same polymerization constants, the mechanism of termination being by coupling and disproportionation respectively. It is found that on changing from coupling to disproportionation, the major change in the distribution curve is that the height of the maximum is somewhat raised and the value of the most probable D. P. is somewhat lowered. This is more easily seen from the expressions of these quantities given in a table later.



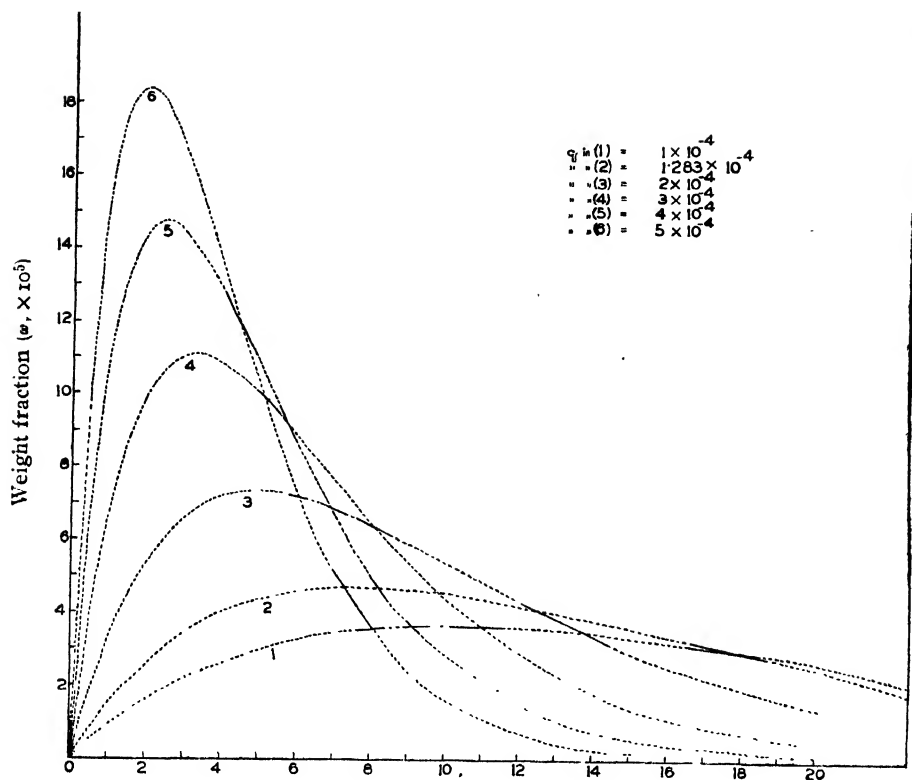


FIG. 1. Degree of polymerization ( $r \times 10^{-3}$ )

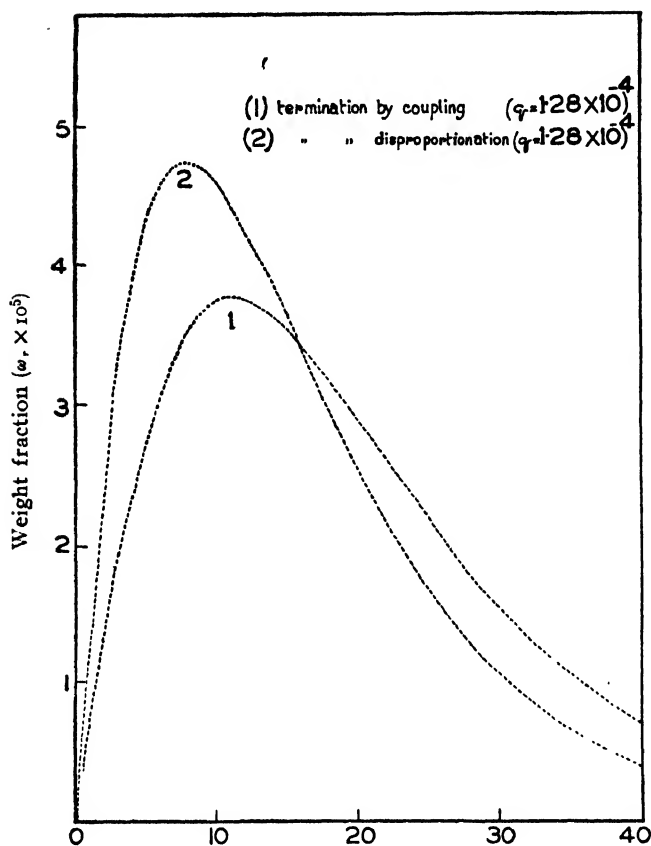
The main difference between the present distribution function for disproportionation and that for combination can be brought forth to a sharp relief by rewriting the latter as shown below.

$$\begin{aligned} \text{Coupling : } \omega_r &= q^2 r e^{-qr} \left( 1 - \frac{1}{q} \sqrt{\frac{\bar{I}}{M}} \left\{ 1 - \frac{q(1-1)}{2} \right\} \right) \\ &\approx q^2 r e^{-qr} \left( 1 - t \sqrt{\frac{\bar{I}}{M}} \left\{ \frac{1}{q} - \frac{r}{2} \right\} \right) \end{aligned}$$

$$\text{Disproportionation : } \omega_r = q^2 r e^{-qr}$$

It can be clearly seen from the above equations that for the same set of values of the constants  $\omega_r$  for combination contains an additional factor to  $\omega_r$  for disproportionation, this factor being

$$1 - t \sqrt{\frac{\bar{I}}{M}} \left\{ \frac{1}{q} - \frac{r}{2} \right\}$$

FIG. 2. Degree of polymerization ( $r \times 10^{-3}$ )

which is equal to, less than or greater than unity according as

$$r = \frac{2}{q}, < \frac{2}{q} \text{ or } > \frac{2}{q}$$

respectively. This is clearly shown graphically in figure 2 where it would be seen that the combination line runs lower than the disproportionation line up to  $2/q$ , from beyond which the reverse is the case.

#### INTERQUARTILE DISTANCE AND STEEPNESS OF DISTRIBUTION

The interquartile range  $\Delta r$  is given by a very simple relation (vide Appendix),

$$\Delta r = r_2 - r_1 = \frac{1.7}{q} = 1.7 \overline{P_n} \quad \dots (3)$$

Thus  $\Delta r$  depends only on  $q$  and is inversely proportional to  $q$ , so that interquartile range decreases with an increase in  $q$  and therefore, with an increase of  $C_S$  or  $S/M$  or  $I/M$  or  $t$ . Therefore,  $1/\Delta r$  bears an exact linear relationship with  $q$  and hence, with  $C_S(S/M)$  at any temperature (i. e. for

any value of  $t$  with a slope of 0.58. In the case of coupling such relation between the reciprocal of interquartile range and  $C_S'(S/M)$  is only approximately linear at constant temperature with a slope varying from 0.48 to 0.58 i. e., near about half.

#### MOST PROBABLE DISTRIBUTION

The D. P.,  $r_0$ , the proportion of which is maximum in a given sample, is calculated in the usual manner (vide Appendix) and is found to be exactly equal to  $1/q$  and hence to  $\bar{P}_n$ , the number average D. P. In other words correlation of  $r_0$  and  $\bar{P}_n$  does not depend upon any rate constant or proportion of solvent and is independent of temperature. This is not the case with distribution for coupling, where the correlation of  $r_0$  and  $\bar{P}_n$  does depend on temperature (i. e.,  $t$ ), although  $r_0$  is very nearly equal to  $\bar{P}_n$  under all conditions (also at any temp.) within a maximum positive deviation of 8% (i. e.  $1 \leq \frac{r_0}{\bar{P}_n} \leq 1.08$ ).

#### WEIGHT AVERAGE AND NUMBER AVERAGE D. P.

By employing standard methods (vide Appendix) we obtain the following relation between the weight average D. P.,  $\bar{P}_w$  and number average D. P.,  $\bar{P}_n$

$$\bar{P}_w = \frac{1}{2} \bar{P}_n = \frac{1}{q} \quad \dots (4)$$

From kinetic considerations, also we get

$$\frac{1}{\bar{P}_n} = \frac{\text{rate of cessation of chain}}{\text{rate of propagation}} = C_M + C_S \frac{S}{M} + C_I \frac{I}{M} + t \sqrt{\frac{I}{M}} = q$$

which is quite in agreement with that obtained by direct integration of the distribution equation and so the identity of our distribution equation with the kinetic chain length equation is also completely established in case of chain termination by disproportionation.

Equation (4) shows that the ratio  $\bar{P}_w/\bar{P}_n$  is uniquely given by  $\bar{P}_w/\bar{P}_n = 2$  and neither depends upon any rate constant nor on temperature nor on the proportion of any solvent, unlike in the case of chain terminations by coupling, in which case we have  $1.5 \leq \bar{P}_w/\bar{P}_n \leq 2$ . From most experimental results the ratio is found to be near about 2, but if some experimental condition is obtained with  $S=0$  and  $t \gg C_M$ ,  $\bar{P}_w/\bar{P}_n$  will be very near to 1.5, in which case one can decisively conclude the absence of termination by disproportionation.

#### MAXIMUM WEIGHT FRACTION

It has been shown in the Appendix that the maximum weight fraction  $w_n$ , corresponding to the most probable D. P. enters into a simple relation with  $q$  in either termination by disproportionation or by coupling.

Thus, in case of disproportionation

$$\omega_r = 0.37q = 0.37/\bar{P}_n = 0.37/r_0$$

or

$$\omega_r = 0.37t\sqrt{I/\bar{M}} = 0.37(C_M + C_S S/M + C_I I/M)$$

and in case of combination  $\omega_r = 0.37q - 0.1t\sqrt{I/\bar{M}} = 0.37/\bar{P}_n + 0.085t\sqrt{I/\bar{M}}$

or

$$\omega_r = 0.27t\sqrt{I/\bar{M}} = 0.37(C_M + C_S S/M + C_I I/M)$$

Thus, the expressions for the maximum weight fraction for both the termination processes are similar with the only difference that  $\omega_r$  in the case of combination is less than that for disproportionation by an amount  $0.1t\sqrt{I/\bar{M}}$  which can be, at the most, 27 per cent when  $t\sqrt{I/\bar{M}}$  is equal of  $q$  that is when  $C_M \rightarrow 0$  and uncatalysed bulk polymerization is considered.

It is also seen that the plot of  $\omega_r$  minus  $0.37t\sqrt{I/\bar{M}}$  in case of disproportionation and minus  $0.27t\sqrt{I/\bar{M}}$  in case of combination against  $C_S S/M$  is exactly linear with a slope of 0.37 for same monomer and catalyst (initiation) and at any temperature. These result may be experimentally tested.

#### COMPARISON OF COMBINATION AND DISPROPORTIONATION

In order to bring into focus the distinction between the two cases the main features are summarised in the table below.

	Disproportionation	Combination
Distribution equation	$\omega_r = q^2 r e^{-qr}$	$\omega_r = qr(a+b)e^{-qr}$ $= q^2 r e^{-qr} \left[ 1 - t\sqrt{I/\bar{M}} \left( \frac{1-r}{q} - \frac{1}{1} \right) \right]$
Maximum weight fraction	$\omega_r = \frac{q}{c} = 0.37q$ $= 0.37/\bar{P}_n$	$\omega_r = t\sqrt{I/\bar{M}}(1 + \sqrt{1+x^2})e^{-(1-x+\sqrt{1+x^2})}$ $\approx 0.37q - 0.1t\sqrt{I/\bar{M}} = 0.37/\bar{P}_n$ $+ 0.085t\sqrt{I/\bar{M}}$
Most probable D. P. $r_0$	$r_0 = 1/q$	$r_0 = 2/q - \frac{1}{t\sqrt{I/\bar{M}}}$ $+ \sqrt{\frac{2}{q^2} - \frac{2}{q} \cdot \frac{1}{t\sqrt{I/\bar{M}}} + \frac{1}{t^2 I/\bar{M}}}$
Number average $\bar{P}_n$	$\bar{P}_n = 1/q$	$\bar{P}_n = 1/(q - \frac{1}{2}t\sqrt{I/\bar{M}})$
Weight average D. P. $\bar{P}_w$	$\bar{P}_w = 2/q$	$\bar{P}_w = \frac{2}{q} + \frac{t\sqrt{I/\bar{M}}}{q^2}$
Relation between $\bar{P}_n$ and $\bar{P}_w$	$\bar{P}_w = 2\bar{P}_n$	$\bar{P}_w \leq r_0 \leq 1.08\bar{P}_w$
Relation between $\bar{P}_n$ and $r_0$	$\bar{P}_w/\bar{P}_n = 2$	$1.5 \leq \frac{\bar{P}_w}{\bar{P}_n} \leq 2.0$
Variation in interquartile distances	$\frac{1}{\Delta r} = \frac{q}{1.7} = \frac{1}{1.7\bar{P}_n}$	$\frac{1}{\Delta r} \approx \frac{q}{2} = \frac{1}{2\bar{P}_n} + \frac{1}{2}t\sqrt{I/\bar{M}}$

## EXPERIMENTAL TEST

All equations deduced so far are subject to experimental test and experimental work is in progress with a view to obtaining data not only to test these equations quantitatively but also to throw light on the nature of the terminating process.

## APPENDIX

*Derivation of the Distribution Function :*

For the given kinetic scheme we have for steady state

$$\frac{dX_r}{dt} = k_p X_{r-1} M - k_p X_r M - k_M X_r M - k_s X_r S - k_I X_r I - k_t X_r C^* = 0 \quad (1)$$

$$\begin{aligned} \frac{dX_1}{dt} = & k_i I M - k_p X_1 M + k_M C^* M - k_M X_1 M - k_S X_1 S + (k_{S_1} + k_{S_2}) S^* M \\ & - k_I X_1 I + (k_{I_1} + k_{I_2}) I^* M - k_t X_1 C^* = 0 \end{aligned} \quad (2)$$

$$\frac{dS^*}{dt} = k_S C^* S - (k_{S_1} + k_{S_2}) S^* M = 0 \quad (3)$$

$$\text{and } \frac{dI^*}{dt} = k_I C^* I - (k_{I_1} + k_{I_2}) I^* M = 0 \quad (4)$$

$$\text{where } C^* = \text{total concentration of radicals} = \sum X_r \quad (5)$$

The above equations and the further steps upto the derivation of the expression for  $X_r$  are exactly similar to those in Appendix I of our previous paper (Palit and Majumdar, 1954). Hence the following results are simply quoted without going again into the details of those steps.

$$C^* = \left( \frac{k_i}{k_t} I M \right)^{\frac{1}{2}} \quad (6)$$

$$X_1 = \frac{q(k_i/k_t I M)^{\frac{1}{2}}}{(1+q)} \quad (7)$$

$$X_r = \frac{q(k_i/k_t I M)^{\frac{1}{2}}}{(1+q)^r} \quad (8)$$

$$\text{where } q = C_M + C_S \frac{S}{M} + C_I \frac{I}{M} + t \sqrt{\frac{I}{M}} \quad (9)$$

$$\text{and } C_X = k_X/k_p$$

Now from the kinetic scheme for the termination by disproportionation we have,

$$\frac{dP_r}{dt} = k_M X_r M + k_S X_r S + k_I X_r I + k_t X_r C^*, \text{ which by (8) and (9) reduces to}$$

$$\frac{dP_r}{dt} = k_p M q X_r = \frac{k_p M q^2 \{ (k_i/k_t) I M \}^{\frac{1}{2}}}{(1+q)^r} \quad \dots \quad (10)$$

Also  $-\frac{dM}{dt} = k_p C^* M + k_M C^* M - k_M X_1 M + k_i I M + (k_s + k_{\bar{s}}) S^* M$   
 $- k_S X_1 S + (k_{I_1} + k_{I_2}) J^* M - k_1 X_1 I - k_t X_1 C^*$   
 $= k_p C^* M + k_M C^* M - k_M X_1 M + k_i I M + k_S C^* S$   
 $- k_S X_1 S + k_I C^* I - k_I X_1 I - k_t X_1 C^*, \text{ by (3) and (4)}$

Substituting the values of  $C^*$  and  $X_1$  from (6) and (7) this reduces after simplification to

$$-\frac{dM}{dt} = k_p M (k_i/k_t I M)^{\frac{1}{2}} \left( 1 + \frac{q}{1+q} \right) = k_p M (k_i/k_t I M)^{\frac{1}{2}} (1+\epsilon) \quad \dots \quad (11)$$

where  $\epsilon = \frac{q}{1+q} \ll 1$

From (10) and (11) we thus have

$$-\frac{dP_r}{dM} = \frac{dP_r/dt}{-dM/dt} = \frac{q^2}{(1+q)^r (1+\epsilon)} \quad \dots \quad (12)$$

as  $\epsilon \ll 1$

This is exactly the same as the expression found by Bawn, but with

$$k_M = k_S = k_{S_1} = k_{\bar{S}_1} = k_e = k_{I_1} = k_{I_2} = k_1 = 0$$

The instantaneous distribution function of the molecular weights is then given by

$$\omega_r = r \times \left( -\frac{dP_r}{dM} \right) = \frac{r q^2}{(1+q)^r (1+\epsilon)}$$

or neglecting  $\epsilon$  as compared to unity

$$\omega_r = \frac{q^r}{(1+q)^r} \quad q^2 r e^{-qr} \quad (13)$$

by putting  $(1+q)^r = e^x$ , whence  $x = r \ln(1+q) \approx rq$  as  $q \ll 1$

#### INTERQUARTILE DISTANCE OF THE DISTRIBUTION FUNCTION

If  $r_1$  and  $r_2$  be the lower and upper quartiles respectively we shall have

$$\frac{1}{4} = \int_0^{r_1} \omega_r dr = \int_{r_2}^{\infty} \omega_r dr$$

Substituting for  $\omega_r$  from (13) we have after integrating by parts

$$\frac{1}{4} = \int_0^{r_1} q^2 r e^{-qr} dr = q^2 \left\{ \left[ -\frac{r e^{-qr}}{q} \right]_0^{r_1} + \frac{1}{q} \left[ -\frac{e^{-qr}}{q} \right]_0^{r_1} \right\} = -q r_1 e^{-q r_1} - e^{-q r_1} + 1$$

or  $\frac{3}{4} e^{x_1} = 1 + x_1 \quad \dots \quad (14)$

where

$$x_1 = q\tau_1$$

Similarly,

$$\frac{1}{4}e^{x_1} = 1 + x_2 \quad \dots (15)$$

where,

$$x_2 = q\tau_2$$

The equations in (14) and (15) can be solved graphically exactly in the same way as the corresponding equations of Appendix II of our previous paper (Palit and Majumdar, 1954), taking as if  $p$  is zero. The solution will yield

$$\Delta x = x_2 - x_1 = 1.7 \text{ so that}$$

$$\Delta \tau = \tau_2 - \tau_1 = \frac{x_2 - x_1}{q} = \frac{1.7}{q} \quad \dots (16)$$

which is the interquartile distance.

#### WEIGHT AVERAGE D. P. ( $\bar{P}_w$ )

From definition it follows

$$\begin{aligned} P_w &= \frac{\sum \tau \omega_r}{\sum \omega_r} = \sum \tau \omega_r, \text{ because } \sum \omega_r = \int_0^\infty \omega_r d\tau = \int_0^\infty q^2 \tau e^{-q\tau} d\tau = 1 \\ &\simeq \int_0^\infty \tau \omega_r d\tau = \int_0^\infty \tau^2 q^2 e^{-q\tau} d\tau = \frac{2}{q} \quad \dots (17) \end{aligned}$$

#### NUMBER AVERAGE D. P. ( $\bar{P}_n$ )

Similarly the number average D. P. is given by

$$P_n = \frac{\sum \tau P_r}{\sum P_r} = \frac{\sum \tau \omega_r}{\sum q^2 \tau^2 e^{-q\tau}} = \frac{1}{q^2 \int_0^\infty \tau^2 e^{-q\tau} d\tau} = \frac{1}{q} \quad \dots (18)$$

Evidently

$$\bar{P}_w / \bar{P}_n = 2$$

#### MOST PROBABLE D. P. ( $\tau_0$ )

The D. P. corresponding to the maximum proportion (weight fraction) of the distribution is obtained by maximising  $\omega_r$  with respect to  $\tau$ . Thus  $\tau_0$  is the solution of

$$\frac{\partial \omega_r}{\partial \tau} = \frac{\partial}{\partial \tau} [q^2 \tau e^{-q\tau}] = 0$$

$$\text{or } -q\tau_0 e^{-q\tau_0} + e^{-q\tau_0} = 0, \text{ giving } \tau_0 = \frac{1}{q} \quad \dots (19)$$

It can be easily seen from (17), (18) and (19) that

$$\tau_0 = \bar{P}_n = \frac{1}{2} \bar{P}_w = \frac{1}{q} \quad \dots (20)$$

MAXIMUM WEIGHT FRACTION ( $w_r$ )

Expression for the maximum weight fraction  $w_r$  will be obtained by putting the value of  $r_0$  in distribution equation. Thus for disproportionation we have by virtue of relation (19)

$$w_r = q^2 r_0 e^{-qr_0} = \frac{q}{e} = 0.37(C_M + C_S S/M + C_I I/M + t\sqrt{I/M}) \quad \dots (21)$$

Similar expression for  $w_r$  for termination by coupling can also be derived in the following way. This was, however, not discussed in our previous paper. For the termination by coupling we get

$$w_r = qr_0(\frac{1}{2}qt\sqrt{I/M}r_0 + q - t\sqrt{I/M})e^{-qr_0} \quad \dots (22)$$

Since  $r_0$  in such case is

$$r_0 = \frac{2}{q} - \frac{1}{t\sqrt{I/M}} + \sqrt{\frac{2}{q^2} - \frac{2}{qt\sqrt{I/M}} + \frac{1}{t^2 I/M}} \quad \dots (23)$$

then on substitution of (23) in (22) and applying the transformation

$$x = \frac{C_M + C_S S/M + C_I I/M}{t\sqrt{I/M}} = \frac{q - t\sqrt{I/M}}{t\sqrt{I/M}} \quad \dots (24)$$

the expression in (22) for the maximum weight fraction for combination reduces to

$$\frac{w_r}{t\sqrt{I/M}} = (1 + \sqrt{1+x^2})e^{-(1-x+\sqrt{1+x^2})} \quad \dots (25)$$

From this it is easily seen that  $\frac{w_r}{t\sqrt{I/M}}$  is represented by an universal

equation independent of temperature, monomer, solvent or any catalyst initiator or their proportion in a particular reaction. Equation (25) although looks complicated represents a straight line upto the range even beyond the value of  $x=400$  a value which we shall never have in practice.

The slope and intercept of the straight line found statistically (by fitting a straight line to a number of points obtained from (25) and then applying usual chi-square test) are respectively 0.37 and 0.27, so that for combination we can write

$$\frac{w_r}{t\sqrt{I/M}} = 0.27 + 0.37x$$

Substituting in this the value of  $x$  from (24) we get

$$= 0.27 + 0.37 \left( \frac{q - t\sqrt{I/M}}{t\sqrt{I/M}} \right)$$

$$\text{or } w_r = 0.37q - 0.1t\sqrt{I/M} = 0.37(C_M + C_S S/M + C_I I/M) + 0.27t\sqrt{I/M} \quad \dots (26)$$

## REFERENCES

- Bawn, C. E. H., 1948, *The Chemistry of High Polymers*, London, p. 78  
 Palit, S. R. and Majumdar, K. C., 1954, *Proc. Ind. Assn. Cult. Sci.* **37**, 1.



# ELECTRON OPTICAL TREATMENT OF CURRENT DIVISION IN RADIO VALVES\*

By S. DEB

INSTITUTE OF RADIO PHYSICS AND ELECTRONICS, CALCUTTA UNIVERSITY

(Received for publication, June 2, 1954)

Plate XIII

**ABSTRACT.** The simple electron optical treatment, which has been developed by the author previously in connection with the problem of current division in a plane triode, has been extended to include the cases of other forms of triodes and also of a pentode. Formulae are given for, (i) the focal length of the aperture as constituted by two consecutive grid wires of a cylindrical triode, (ii) the ratio of grid current to the total current of a triode with electrodes of cylindrical structure, and (iii) the ratio of screen grid current to plate current for a pentode. It is pointed out that the expression for the current division can always be obtained in the same general form involving two dimensionless parameters, namely, the screening constant and the relative aperture of the electron lens consisting of the opening between two consecutive grid wires. This general relationship has been presented in the form of a set of current division curves applicable to any type of grid.

Account is given of experiments made with a rubber membrane model to check the formula for the focal length of the electron optical lens system of a cylindrical triode.

Results obtained from characteristics of commercial pentodes are shown to support the expressions deduced for the screen grid-anode current ratio of such tubes.

## 1. INTRODUCTION

It has recently been shown by the author (Deb, 1952) that the problem of current division in a plane triode may be very simply solved, subject to certain reasonable simplifying assumptions, by the application of this electron optical considerations. The method is much less complicated than those that have been hitherto employed (Spangenberg, 1940, Jonker and Tellegen, 1948). The case first investigated by the author was that of a plane triode only having a grid composed of straight parallel equidistant wires. It was shown that the expression, as obtained for current division in such a valve, involves two dimensionless parameters, viz., the screening constant and the relative aperture of the electron lens composed of the strips between two consecutive grid wires. In the present paper it will be shown that a slightly modified form of the equation derived earlier holds for triodes having other grid geometries and also for multigrid valves like a pentode. An expression for the focal length of the grid aperture for a cylindrical triode will be derived. Results obtained with a

\* Communicated by Prof. S. K. Mitra

rubber membrane model will be shown to support this deduction. A set of current division curves having general validity is also given and discussed.

## 2. GENERAL FORM OF THE EXPRESSION FOR CURRENT DIVISION

Electron optical treatment of the problem of current division in a plane triode having a grid composed of parallel equidistant wires is based on the assumption that the lateral deviation of electrons is primarily due to the grid aperture behaving as a cylindrical lens of focal length

$$f = \frac{2V_{eq}}{E_2 - E_1} = - \frac{2b \left( 1 + \frac{\phi}{\mu} \right)}{(1 - \phi) + \frac{b}{a}}, \quad \dots (1)$$

$$\text{where } V_{eq} = \text{the equivalent grid sheet potential} = \frac{V_g + \frac{V_a}{\mu}}{1 + \frac{1}{\mu} + \frac{1}{\mu} \frac{b}{a}},$$

$b$  = grid to anode distance,

$a$  = grid to cathode distance,

$\mu$  = amplification factor of the valve,

$E_2, E_1$  = gradient of electrostatic potential on the anode and the cathode sides of the grid respectively,

$$\phi = \text{ratio of anode to grid potential} = \frac{V_a}{V_g}.$$

Assuming that the lens action is free from spherical aberration and that the effects due to initial velocities of electrons, space charge and secondary emission are negligible one obtains for the case when reflection of electrons in front of the cathode is neglected

$$\frac{I_g}{I_a} = \frac{1 - \frac{cn}{4f}}{\frac{c}{2\tau_g} - \frac{cn}{4f}}, \quad \dots (2)$$

where  $n$  is the width of the region of lens action expressed in terms of the grid wire radius  $\tau_g$  and  $c$  is the pitch of the grid. For all practical purposes  $n=2$ . A more convenient form of the above equation is obtained by expressing the lens width  $\delta$  in terms of the pitch. Writing  $\delta = mc$ , Eq. (2) becomes

$$\frac{I_g}{I_a} = S \frac{1 - mR/2S}{1 - mR/2}, \quad (3)$$

where  $R$  = relative aperture of the lens,

$S$  = screening constant of the grid.

It will be shown in the following sections that relations of the form of Eq. (3) are valid for triode valves having other geometries. In Sec. 4 this idea will be extended to the case of a pentode valve.

### 3. APPLICATION TO TRIODES

*Plane Triodes.* We shall consider first two special types of plane triodes :

(i) Grid consisting of a plane sheet with regularly spaced circular apertures.

(ii) Grid consisting of a wire gauze of square meshes.

In case (i) all the apertures in the sheet are assumed to be of the same radius  $r_0$ , there being  $n'$  apertures per unit area. The screening constant will then be given by

$$S = 1 - \pi r_0^2 n'. \quad \dots (4)$$

This also gives the ratio  $I_g/I_e$  in the absence of any lateral deviation. In order to investigate the case when lateral deviation exists we consider a section of the valve containing a single aperture and passing through the axis of the latter (figure 1). Let  $O$  be the point of intersection of the axis

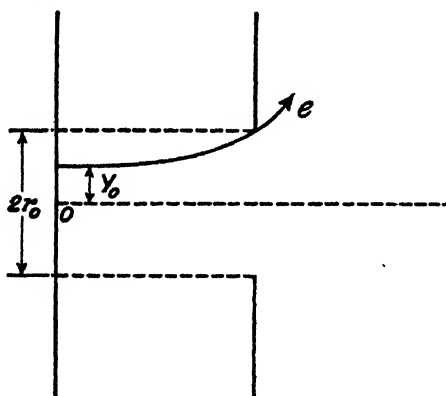


FIG. 1. The limiting trajectory for capture of an electron by the grid of a plane triode grid consisting of circular holes.

with the cathode. Let us suppose that due to the electron optical action of the aperture an electron originating at a point distant  $y_0$  from  $O$  ( $y_0 < r_0$ ) just grazes the aperture periphery. This increases the ratio  $I_g/I_e$  which now becomes

$$I_g/I_e = 1 - \pi y_0^2 n'. \quad \dots (5)$$

To determine the value of  $y_0$  we note that the angular deviation of an electron as it emerges out of the aperture is given by

$$\theta = -y/f, \quad \dots (6)$$

where  $y$  is the radial distance of the point of incidence of the electrons and  $f$  is the focal length. If  $\delta$  is the lens width then the radial displacement

$$r_0 - y_0 = -\frac{\delta y_0}{2f}$$

or,

$$y_0 = \frac{\tau_0}{1 - \frac{\delta}{2f}}$$

Putting

$$\delta = m\tau_0,$$

$$y_0 = \frac{\tau_0}{1 - \frac{m\tau_0}{2f}} \quad \dots (7)$$

From (5) and (7)

$$\begin{aligned} \frac{I_g}{I_c} &= \frac{1 - \frac{m\tau_0}{f} + \left(\frac{m\tau_0}{2f}\right)^2 - \pi\tau_0^2 n'}{1 - \frac{m\tau_0}{f} + \left(\frac{m\tau_0}{2f}\right)^2} \\ &= \frac{1 - \frac{m\tau_0}{f} - \pi\tau_0^2 n'}{1 - \frac{m\tau_0}{f}}, \text{ if } \frac{m\tau_0}{f} \text{ is small.} \end{aligned}$$

Hence from (4)

$$\frac{I_g}{I_c} = S \frac{1 - \frac{mR}{2S}}{1 - \frac{mR}{2}}$$

where  $R = \frac{2\tau_0}{f}$ . This last relation is seen to be of the same form as Eq. (3).

The expression for the focal length of a 'lens' of circular aperture is given by (Davisson and Calbicks, 1932)

$$f = \frac{4V_{cg}}{E_2 - E_1}$$

Comparing with (1) it is found that if  $\mu$  and  $\phi$  are the same and  $c = 2\tau_0$  then the relative aperture of the grid openings of a triode, using parallel equidistant wires as grid, will be twice as large as those of the same triode using a plane sheet with circular apertures as grid at the same position as before. However, for the same value of  $\delta$ , the value of  $m$  in the former case will be half that in the latter. The ratio  $I_g/I_c$  will therefore be the same in both the cases.

We next consider case (ii), the case of a grid consisting of square meshes. We assume that the squares are all of the same size. If  $\tau_g$  be the radius of the grid wires and  $c$  the length of the sides of the squares, then the screening fraction is given by

$$S = \frac{4\tau_g}{c} \left(1 - \frac{\tau_g}{c}\right).$$

The second factor within brackets takes into account the effect due to overlapping and may be neglected if  $r_g$  is small.

It is somewhat difficult to visualise the lens action of a square aperture. The problem, may, however, be simplified by converting the given valve into an equivalent one having the same value of screening fraction and electrode spacing but whose grid is composed of a system of parallel wires of radius  $r_g$  and spacing  $c/2$ . The value of  $\mu$  and  $\delta$  for the latter valve will be sensibly equal to those for the original one. If, therefore,  $\phi$  is kept the same the ratio  $I_g/I_o$  for the two valves will also be identical. One can, therefore, use Eq. (3) in this case as well, provided

$$\frac{4r_g}{c} \left( 1 - \frac{r_g}{c} \right) \approx \frac{r_g}{c/2} = S,$$

and  $f$  is given by Eq. (1).

*Cylindrical Triode:*—We shall now consider two types of cylindrical triode, viz.

(i) Grid consisting of a set of straight wires lying on a cylindrical surface coaxial with the cathode wire.

(ii) Grid consisting of a cylindrical helix coaxial with the cathode wire.

Considering case (i) let  $r_c$ ,  $r_g$  and  $r_p$  represent respectively the radii of the cathode wire, the grid cylinder and the anode cylinder. Consider a symmetrical section containing a single aperture between two consecutive grid wires (figure 2). In the absence of any lateral deviation all the electrons emitted from a strip  $AB$  of the cathode would travel to the anode. Due to lateral electron optical deviation suffered in passing through

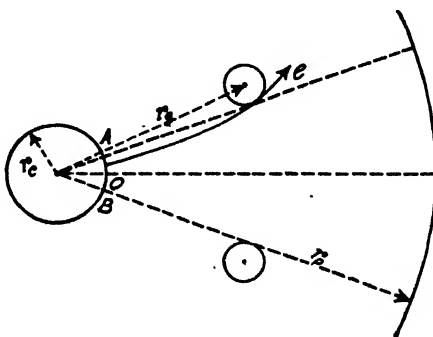


FIG. 2. The limiting trajectory for capture of an electron by the grid of a cylindrical triode-grid consisting of a system of wires parallel to the axis.

the grid the angular width of the strip contributing to the anode current will be less than  $AOB$ . In other words, the grid wire radius will be effectively increased. If  $R_g$  be the radius of the grid wires and  $c$  the pitch of the grid helix then, by the same argument as used in the case of plane triodes, one obtains readily,

$$\frac{I_u}{I_e} = S \frac{1 - mR/2S}{1 - mR/2},$$

where  $S = \frac{2R_g}{c}$  and  $R = \frac{c}{f}$ ,  $f$  being the focal length and  $m$ , a constant.

It remains only to find an expression for  $f$ . This will not be much different from that of the focal length of a longitudinal uniform slit cut over a cylindrical surface and can be derived by well known electron optical methods. A simple method consists in evaluating the lateral component of the field in the plane of the slit by solving the equations (Bedford, 1934)

$$\text{div } E = 0$$

$$\text{curl } E = 0,$$

$E$  being the potential gradient. Expressed in polar co-ordinates

$$\frac{1}{r} \frac{\partial}{\partial r} (rE_r) + \frac{1}{r} \frac{\partial E_\theta}{\partial \theta} = 0$$

$$\frac{\partial}{\partial r} (rE_\theta) - \frac{\partial E_r}{\partial \theta} = 0,$$

where  $E_r$  and  $E_\theta$  are respectively the radial and the lateral component of field. But

$$d(rE_\theta) = \frac{\partial}{\partial r} (rE_\theta) dr + \frac{\partial}{\partial \theta} (rE_\theta) d\theta$$

$$= \frac{\partial E_r}{\partial \theta} dr - r \frac{\partial}{\partial r} (rE_r) d\theta$$

$$= -r \frac{\partial}{\partial r} (rE_r) d\theta,$$

if we imagine the region of the lens to be of such small aperture that  $E_r$  does not vary appreciably with  $\theta$ . Hence, integrating between the limits 0 to  $\theta$ ,

$$E_\theta = -\theta \frac{\partial}{\partial r} (rE_r).$$

If  $v_r$  is the average radial velocity of electrons during transit through the lens, then the change in angular momentum in crossing the lens is given by

$$(mrv_\theta) = -e \int_1^2 r \frac{\partial}{\partial r} (rE_r) \theta \frac{dr}{v_r},$$

where the limits 1 and 2 refer to the two surfaces of the lens. If the lens be assumed to be thin, so that  $r$  can be taken a constant, then writing

$\theta = \frac{x}{r}$  and  $v_r = \sqrt{\frac{2eV_{eg}}{m}}$ , where  $V_{eg}$  is the equivalent grid sheet potential, we get

$$v_\theta/v_r = \text{lateral angular deviation} = -\frac{y}{2V_{cg}}[E_{r2} - E_{r1}] = -\frac{y}{f} \text{ (say).}$$

Hence,

$$f = \frac{2V_{cg}}{E_{r2} - E_{r1}} \quad \dots (8)$$

Now, in a cylindrical triode of the type under consideration

$$\left. \begin{aligned} E_{r1} &= \frac{2V_{cg}}{\tau_g \ln \frac{\tau_g}{\tau_c}} \\ E_{r2} &= \frac{V_a - V_{cg}}{\tau_g \ln \frac{\tau_g}{\tau_g}} \\ V_{cg} &= \frac{V_g + \frac{V_a}{\mu}}{1 + \frac{1}{\mu} \left[ \frac{\ln \tau_p / \tau_c}{\ln \tau_g / \tau_c} \right]} \end{aligned} \right\} \quad \dots (9)$$

From Eqs. (8) and (9)

$$E_{r2} - E_{r1} = \frac{1}{\tau_g \ln \frac{\tau_g}{\tau_g}} \left[ \frac{V_a \ln \frac{\tau_g}{\tau_c} - V_g \ln \frac{\tau_g}{\tau_c}}{\ln \frac{\tau_g}{\tau_c} + \frac{1}{\mu} \ln \frac{\tau_p}{\tau_c}} \right] \quad \dots (10)$$

and

$$f = \frac{2\tau_g \left( 1 + \frac{\phi}{\mu} \right) \ln \frac{\tau_p}{\tau_g}}{\phi - \frac{\ln \tau_p / \tau_c}{\ln \tau_g / \tau_c}} \quad \dots (11)$$

We may check the validity of Eqs. (10) and (11) by considering closely the concept of 'equivalent grid'—a surface of uniform appropriate charge density—which replaces the line charges of the grid wires, in so far as its influence on the motion of electrons is concerned. The advantage of such a consideration is that it avoids the complications raised by the presence of isolated charged grid wires in between the cathode and the anode surface and allows one to regard the field as a purely radial one. The action of the equivalent grid sheet may be conveniently visualised in terms of a lens coincident with the grid plane *AB* and a cylindrical coaxial mirror *DM* placed between the same and the cathode (figure 3). The effect of *DM* is to give rise to an image of the grid charge at the inverse point defined by

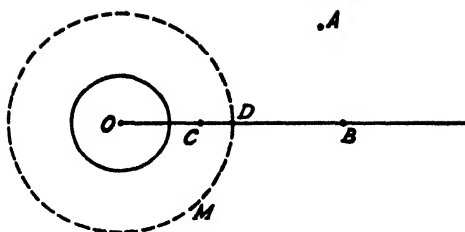


FIG. 3. The electron optical system corresponding to the 'equivalent grid sheet' in the case of a cylindrical triode.

$$OC \cdot r_g = OD^2 \quad \dots (12)$$

or 
$$r_g(r_g - BC) = OD^2$$

If  $OD$  is such that the image of  $C$  due to the grid lens at  $AB$  is formed at  $O$ , then the field will be everywhere radial. Obviously this requires that

$$\frac{1}{BC} - \frac{1}{r_g} = \frac{1}{f},$$

or 
$$BC = \frac{r_g f}{r_g + f}.$$

Substituting in (12) one gets

$$OD = r_g \sqrt{\frac{r_g}{r_g + f}}. \quad \dots (13)$$

The charge  $\tau_g$  per unit length of the grid wire is of course given by

$$- \frac{1}{N} \frac{V_{eg}}{2 \ln \frac{r_g}{OD}},$$

where  $N$  is the total number of grid wires. Using (13) we get

$$- \tau_g = \frac{V_{eg}}{N \ln(1 + f/r_g)} \approx \frac{r_g V_{eg}}{N f}, \text{ if } \frac{f}{r_g} \text{ is small;}$$

or 
$$f = - \frac{r_g V_{eg}}{N \tau_g}. \quad \dots (14)$$

But the value of  $\tau_g$  has been shown to be

$$\tau_g = - \frac{1}{2N \ln \frac{r_p}{r_g}} \frac{V_a \ln \frac{r_g}{r_c} - V_g \ln \frac{r_p}{r_c}}{\ln \frac{r_g}{r_c} + \frac{1}{\mu} \ln \frac{r_p}{r_c}}. \quad \dots (15)$$

Substituting (15) in (14) one readily obtains (11). Thus, it is found that the expression for  $f$  derived here is true as long as  $r_g \gg f$ . This condition is approximately fulfilled in most of the cases encountered in practice.



An experimental verification of Eq. (11) using a rubber membrane model will be described in Sec.6 to follow.

Case (ii) for a cylindrical grid using helical wires may be treated in the same manner as case (i). An expression for the focal length of the grid aperture may be derived by solving the div and the curl equations in  $(r, z)$  co-ordinates. However, the expression derived cannot be subjected to experimental test with a rubber membrane model as the electronic path in this case is not confined to a plane normal to the axis of symmetry. Of course, as in Sec.3 (ii), we can think of equivalent valve using the same screening fraction and electrode spacing by a parallel wire grid and then apply Eqs.(3) and (2) in as straightforward manner.

#### 4. APPLICATION TO PENTODES

The problem of current division in a pentode is complicated because here one must consider actions of three grid-controls, the grid, the screen grid and the suppressor grid. It becomes easier if the effect of the control grid is assumed to be small. For a sharp cut off pentode this assumption is quite reasonable because, such pentodes have always a small control grid pitch. For a super-control pentode, however, the pitch is variable within appreciable range and hence the assumption might introduce error. But such error will always be of secondary importance. Following the procedure adopted by Spangenberg (1948) the effects of the other two grids will now be considered separately remembering that under normal operating conditions, the screen grid acts as a diverging lens and the suppressor as a converging lens.

*Plane Pentode.* The action of the screen grid may be considered by converting the system consisting of the control grid  $G_1$ , the screen grid  $G_2$ , the suppressor grid  $G_3$  and the plate  $P$  into an equivalent triode as indicated in figure 4. The actual control grid and the plate are now replaced by a single equivalent electrostatic plane  $P'$ . Two methods are available for determining the position and the potential of this new plane  $P'$ . These are

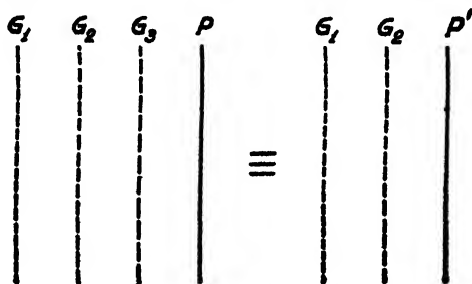


FIG. 4. The manner in which the plate and the grid system of a plane pentode may be converted into an equivalent triode.

the concept of equivalent grid sheet and that of  $q$ -plane (Dow, 1952). Both the methods lead to the same final result, but, for purely electrostatic purposes, the concept of equivalent grid plane is distinctly advantageous,

as the new sheet is made to coincide with the plane of the grid. We shall, therefore, use this concept and assume that the position of  $P'$  is coincident with that formerly occupied by  $g_3$ . It also follows that the potential of this equivalent sheet is approximately given by

$$V_{P'} = \frac{V_s + \frac{V_1}{\mu_{s1}} + \frac{V_2}{\mu_{s2}} + \frac{V_P}{\mu_{sP}}}{1 + \frac{1}{\mu_{s1}} + \frac{1}{\mu_{s2}} + \frac{1}{\mu_{sP}}} \approx \frac{\frac{V_2}{\mu_{s2}} + \frac{V_P}{\mu_{sP}}}{1 + \frac{1}{\mu_{s2}} + \frac{1}{\mu_{sP}}} \quad (16)$$

where  $V_2$  = the screen grid potential.

$V_P$  = the plate potential.

$V_1$  = the control grid potential which is generally small compared to  $V_2$  and  $V_P$ .

$V_s$  = the suppressor grid potential which is normally zero.

$\mu_{s2}$  = the amplification factor of the suppressor grid in relation to the screen grid.

$\mu_{sP}$  = the amplification factor of the suppressor grid in relation to the plate.

$\mu_{s1}$  = the amplification factor of the suppressor grid in relation to the control grid and is always large compared to  $\mu_{s2}$  and  $\mu_{sP}$ .

Now,

$$\mu_{sP} = - \frac{2\pi \frac{d_{sP}}{c_s}}{\ln 2 \sin \frac{\pi r_s}{c_s}} \quad (17)$$

$$\mu_{s2} \mu_{s2}' = - \frac{2\pi \frac{d_{23}}{c_s}}{\ln 2 \sin \frac{\pi r_s}{c_s}}, \quad (18)$$

where  $\mu_{s2}'$  is the amplification constant of  $g_3$  in relation to a plane sheet occupying the position of  $g_2$ ,  $c_s$  is the suppressor grid pitch and  $r_s$  is the suppressor grid wire radius. Substituting (14) and (18) in (16) and noting

that  $\frac{\pi r_s}{c_s}$  is always small, we obtain

$$V_{P'} = \frac{[V_2 d_{sP} + V_P d_{23}] \ln \frac{2\pi r_s}{c_s}}{d_{2P} \ln \frac{2\pi r_s}{c_s} - \frac{2\pi}{c_s} d_{23} d_{sP}} \quad (19)$$

For r.f. pentodes

$$d_{sP} \approx d_{23} \approx \frac{d_{2P}}{2}$$

and

$$V_{P'} = \frac{[V_2 + V_P] \ln \frac{2\pi r_s}{c_s}}{2 \ln \frac{2\pi r_s}{c_s} - \frac{\pi}{c_s} d_{2P}} \quad (20)$$

For many power tubes  $d_p \ll d_{23}$  and  $c_3 > d_{23}$ . In such cases the effective suppressor plane potential has to be calculated by taking into account the effect of image grid due to the plate. However, it can be shown that this affects the final results very little.

If now the equivalent triode system as shown in figure 4, be considered, then from Eq. (1), the focal length of the lens due to the screen grid aperture is found to be

$$f_2 = \frac{2d_2 \left( 1 + \frac{\mu'_{23}}{d_{23}} \right)}{(1 - \phi) + \frac{d_{23}}{d_{32}}} \quad (21)$$

where  $\mu'_{23}$  is the amplification factor of the screen grid in relation to the equivalent suppressor grid sheet, and

$$\phi = \frac{V_p}{V_2}$$

From (3) and (21) one obtains the ratio of the current flowing past the screen grid and the current collected ( $I'_{sg}$ )

$$\frac{I_c - I'_{sg}}{I'_{sg}} = \frac{c_2}{2r_2} \frac{1 - \frac{2r_2}{c_2}}{1 - \frac{m c_2^2}{4r_2 f_2}} = \delta_1 (\text{say}), \quad (22)$$

where  $c_2$  is the screen grid pitch and  $r_2$  the screen grid wire radius.

It now remains to consider the effect of the suppressor grid. In all pentodes the suppressor grid acts as a converging lens of such a focal length that all electrons incident along the axis converge towards the plate. However, some of the electrons suffering large deviation in the preceding grid tend to hit the suppressor grid wire directly and are reflected back by the grid. According to experimental observation (Spangenberg,

1948) such electrons constitute a fraction  $\frac{I_3}{c_3}$  of the total current. Thus, the

ratio of the current flowing past the suppressor grid, to the current sent back to the screen grid ( $I''_{sg}$ ) is given by

$$\frac{I_c - I'_{sg} - I''_{sg}}{I''_{sg}} = \frac{c_3}{r_3} - 1 = \delta_2 (\text{say}) \approx \frac{I_c - I'_{sg}}{I''_{sg}} \quad (23)$$

From Eqs. (22) and (23) one obtains the approximate ratio of plate current ( $I_p$ ) to the screen current

$$\frac{I_p}{I_{sg}} = \frac{I_c - (I'_{sg} + I''_{sg})}{I'_{sg} + I''_{sg}} = \frac{I_c - I'_{sg}}{I'_{sg} + I''_{sg}} = \frac{\delta_1 \delta_2}{\delta_1 + \delta_2} \quad (24)$$

In a power pentode the suppressor may act as a weak converging lens and for these the reflection effect may not be pronounced. For such a case

$$\frac{I_p}{I_{sg}} = \delta_1 \quad (25)$$

**Cylindrical Pentode:**—The current division in a cylindrical pentode may be derived by calculating the appropriate value of the equivalent suppressor grid potential and then using Eqs. (15) and (3).  $V_p'$  can be calculated by making the following substitutions in Eqs. (17) and (18).

$$d_{23} \ln \frac{d_{2p}}{d_{23}} \text{ for } d_{3p}$$

$$d_{3p} \ln \frac{d_{2p}}{d_{3p}} \text{ for } d_{23}.$$

It is to be noted that actually electrodes in a pentode are often neither plane nor cylindrical (excepting perhaps for the plate). In such cases expressions for the plane case may be used with the average values of the various electrode distances. Two examples are given below in this connection.

**Examples:** The usefulness of Eqs. (22) and (23) may be illustrated by considering the cases of two commercial pentodes viz. power valve EL50 and pentode 6J7 which were utilised to test the results of earlier worker on the subject. For EL50 we have the following average dimensions :

$$\begin{aligned} d_{12} &= 1.13 \text{ mm}; & c_2 &= 1.2 \text{ mm}; & 2r_2 &= 0.080 \text{ mm}; \\ d_{23} &= 3.30 \text{ mm}; & c_3 &= 4.5 \text{ mm}; & 2r_3 &= 0.125 \text{ mm}; \\ d_{3p} &= 1.50 \text{ mm}. \end{aligned}$$

From the above data we obtain  $\mu_2' = 10$ , and for  $V_2 = V_p$  one obtains from Eq. (20),  $\phi = 0.57$ ; and from (24),

$$\frac{I_p}{I_{sp}} = 9.3.$$

This agrees well with the average experimental value 9.5. For 6J7 we have the following average values :

$$\begin{aligned} d_{12} &= 1.42 \text{ mm}; & c_2 &= 0.40 \text{ mm} & 2r_2 &= 0.0625 \text{ mm} \\ d_{23} &= 2.74 \text{ mm}; & c_3 &= 1.25 \text{ mm}. & 2r_3 &= 0.113 \text{ mm}. \\ d_{3p} &= 2.75 \text{ mm}. \end{aligned}$$

From the above data we obtain  $\mu_2' = 56$  and from Eqs. (20) and (24),

$$\text{for,} \quad V_2 = V_p, \quad \phi = 0.15, \quad \frac{I_p}{I_{sp}} = 3.96$$

$$\text{for,} \quad V_2 = 0.4 V_p, \quad \phi = 0.27, \quad \frac{I_p}{I_{sp}} = 4.00.$$

These again agree very well with the experimental values of 3.8–4.0 observed within the above range of electrode potentials.

## 5. CURRENT DIVISION CURVES

The wide range of applicability of Eq. (3) as illustrated in the foregoing sections makes it desirable to present the same in the form of a set of

curves useful for practical computations. Such a set of curves giving the ratio  $\frac{I}{S} \frac{I_2}{I_0}$  against  $\frac{c}{f}$ , with  $S$  as a parameter, have been drawn in figure 5.

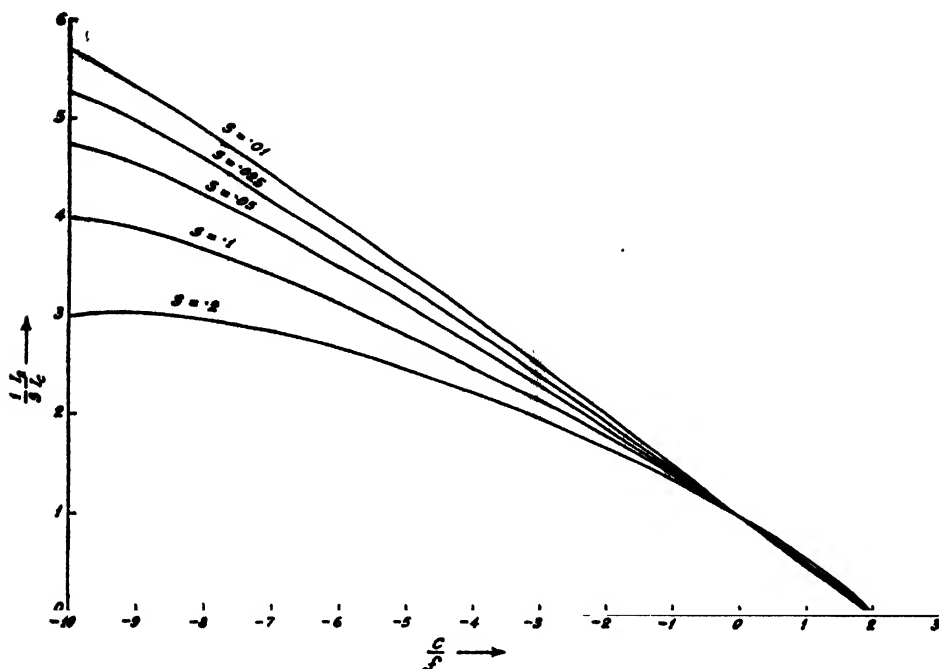


FIG. 5. Current division curves as are valid for any type of grid.  $I_2$  = grid current,  $I_0$  = total current,  $S$  = screening fraction,  $c$  = grid pitch and  $f$  = focal length of the openings in the grid.

It would be noticed from the curves that for  $S < 0.1$ , a condition which is generally fulfilled by many practical valves,  $\frac{I}{S} \frac{I_2}{I_0}$  changes little with  $S$ . With these curves evaluation of current division is reduced simply to calculate the ratio  $\frac{c}{f}$ .

## 6. EXPERIMENTAL STUDIES WITH RUBBER MEMBRANE MODEL

As mentioned in Sec. 3 experiments have been carried out with rubber membrane model of a valve of cylindrical structure (Fig. 2). The object was to check the deduction regarding the focal length as given by Eq. (11). The model was constructed so as to represent a cross section of the valve perpendicular to the axis (cathode). The model grid wires and the cathode consisted of straight cylindrical metal rods and that of the anode a cylindrical metal ring. The model electrode elements were of appropriate sizes and were so arranged and spaced on a plane board that the distances of the various elements were proportional to the potential differences

of the corresponding electrode in the valve. The plane board holding the electrodes was carefully levelled. A circular rubber membrane was spread over a metallic ring and kept stretched by cords passing through a number of regularly spaced eyelets in the periphery. The stretched membrane was then so pressed over the model electrode assembly that its surface made contact with the surfaces of the electrodes. The membrane was thus undulated in a manner characteristic of the heights and disposition of the electrodes. Small steel balls held close to the front of the 'cathode' were now released, a few at a time, by means of an electro-magnetic device. The tracks of the moving balls were intermittently illuminated 50 times per second by flooding the membrane surface with light from a fluorescent lamp connected to a 50 c. p. s. power line. The tracks were found generally to have a tendency to come to a focus, though on account of the presence of a certain amount of spherical aberration and of the electron optical action of interelectrode field the foci were not sharp. Figure 7 (Plate XIII) shows the tracks of steel balls for four models. The relevant data for the models corresponding to cases A, B, C and D in the plate are given respectively in rows 1, 2, 3 and 4 of Table I.

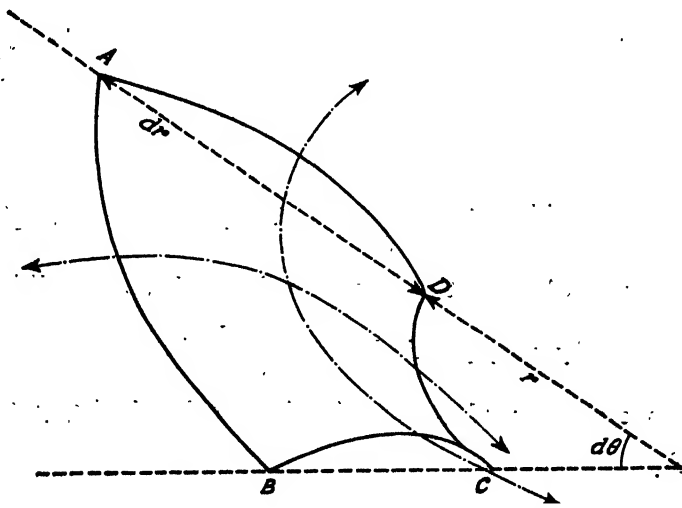


FIG. 6. An element of a distorted circular membrane. Under static condition the net force acting on the element must vanish.

TABLE I

Model No.	$r_c$	$r_g$	$r_p$	$R_0$	$N$	$\phi$	$f$ (experimental)	$f$ (theoretical)
1	.5	6	13	.5	4	-8.8	2.0	1.8
2	.5	6	13	.5	4	-15	2.5	2.3
3	.5	6	13	.5	4	-22	3.2	2.9
4	.5	6	13	.25	4	-8.8	3.1	3.0

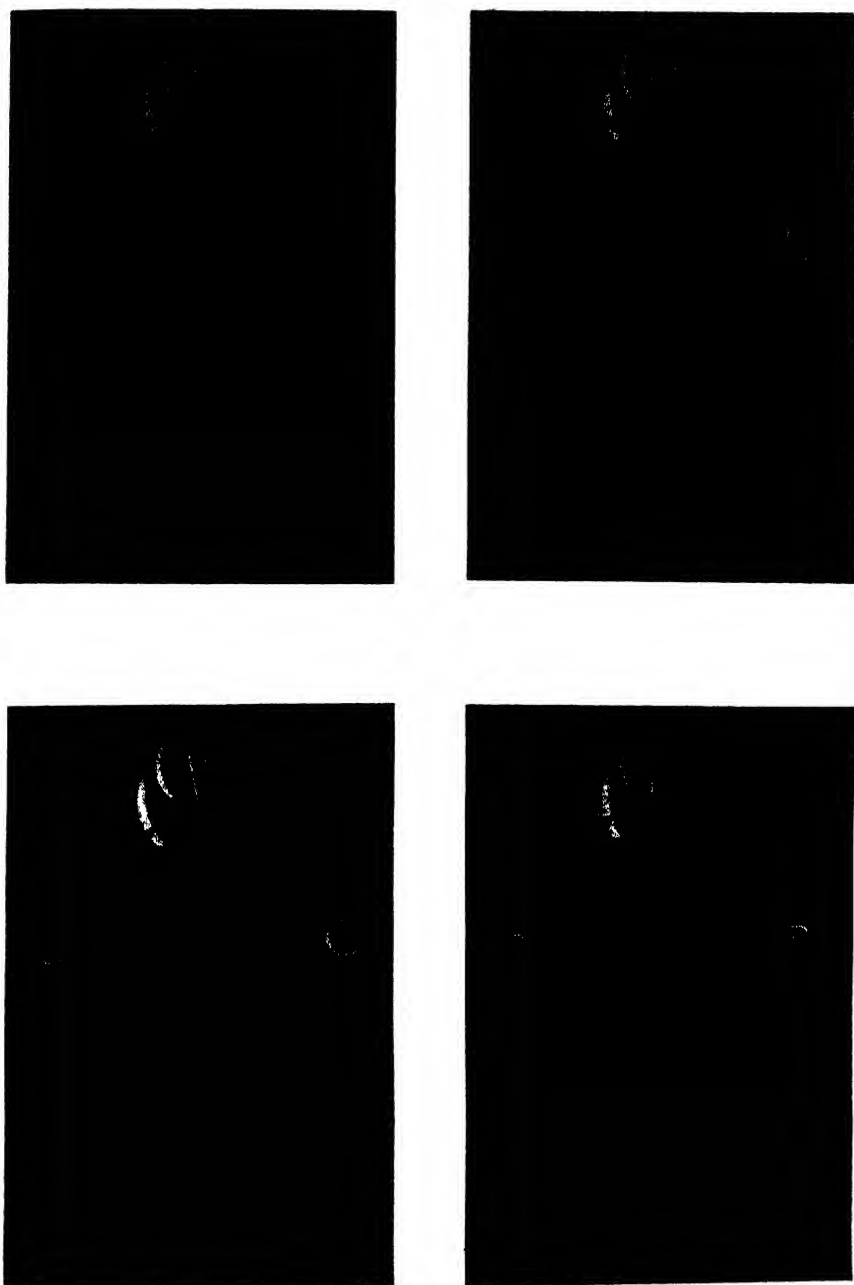


Fig. 7

Photographic records of trajectories of steel balls illustrating focussing effect. A, B, C and D are for models described in rows 1, 2, 3 and 4 respectively of Table I.





For comparing these experimental results with theory it will be convenient first to establish in a simple manner the analogy between the motion of an electron in a valve with that of a small round mass rolling over the surface of a stretched circular membrane distorted as above. It is clear that at every point of the membrane there will be a vertical component of the tension. Under static condition the total force of this tension over any element of area must vanish. If we consider one such element  $A B C D$  (figure 6) subtending an angle  $\delta\theta$  at the origin and bounded by two concentric arcs of radius  $r$  and  $r + dr$ , then for small slopes, the net vertical force acting over its sides is

$$\frac{\delta}{\delta r} \left( T \delta\theta \frac{\delta Z}{\delta r} \right) \delta r + \frac{\delta}{\delta \theta} \left( T \delta r \frac{\delta Z}{\delta \theta} \right) \delta \theta,$$

where  $Z$  is the vertical displacement and  $T$  the tension. Under condition of equilibrium this expression is equal to zero. Rearranging the terms, one thus obtains

$$\frac{1}{r} \frac{\delta}{\delta r} \left( r \frac{\delta Z}{\delta r} \right) + \frac{\delta^2 Z}{\delta \theta^2} = 0,$$

which is identical in form with Laplace's equation for a potential field in polar co-ordinates. The vertical displacement  $Z$  in the former equation is analogous to the potential  $V$  in Laplace's equation. It, therefore, follows that the pattern of vertical elevation produced in the rubber membrane of the valve model stimulates the potential field in the electronic valve.

Now, the motion of a ball on the stretched membrane under the action of gravity (neglecting effects due to rotational inertia) is governed by the principle of least action,

$$\delta \int m v ds = 0.$$

Since the motion is in a conservative field of force, the above integral reduces to

$$\delta \int_1^2 \sqrt{Z} ds = 0. \quad \dots (26a)$$

If the slope is small,

$$ds^2 = \delta r^2 + r^2 \delta \theta^2 + \delta Z^2 \approx \delta r^2 + r^2 \delta \theta^2. \quad \dots (26b)$$

Again, for an electron moving in a potential field in the  $(r, \theta)$  plane we have

$$v^2 = 2eV,$$

or

$$v \propto \sqrt{V}$$

Hence, the principle of least action for this case takes the form

$$\int_1^2 \sqrt{V} ds = 0, \quad (27a)$$

where,

$$ds^2 = \delta r^2 + r^2 \delta \theta^2. \quad \dots (27b)$$

A comparison of Eqs. (26) and (27) shows that the projection of the path of the ball on the  $(r, \theta)$  plane is analogous to the electron trajectories in the valve.

Bearing in mind the above analogy we can compare the values of focal length as obtained from experiments with the model valve, with those calculated from Eq. (11). From Table I it will be found that the two sets of values are in reasonable agreement, although, the experimental values are generally somewhat larger. This discrepancy may be accounted for, at least partly, as due to spherical aberration, to rotational inertia of the rolling ball and due to the lack of validity of some of the assumptions involved in the derivation of Eq. (11).

#### ACKNOWLEDGMENT

I have much pleasure in thanking Professor S. K. Mitra for his constant encouragement and helpful advice in course of preparation of the paper.

#### REFERENCES

- Bedford, L. H., 1934, *Proc Phys. Soc.*, **46**, 882.
- Davisson, C. J. and Calbicks, C. J., 1932, *Phys. Rev.*, **42**, 580.
- Deb S., 1952, *Ind. Jour. Phys*, **28**, 377.
- Dow, W. G. 1952, *Fundamentals of Engineering Electronics*, John Wiley, New York.
- Jonker, J. H. L. and Tellegen, B. D. H., 1948, *Phillips Research Report*, **1**, 13.
- Spangenberg, K. R., 1940, *Proc. I. R. E.*, **28**, 226.
- Spangenberg, K. R., 1948, *Vacuum Tubes*, McGraw Hill Book Co., New York.

# ON THE RAMAN SPECTRA OF STYRENE AND POLYSTYRENE AT $-180^{\circ}\text{C}^*$

By N. K. ROY

OPTICS DEPARTMENT, INDIAN ASSOCIATION FOR THE CULTIVATION OF  
SCIENCE, CALCUTTA-32

(Received for publication June 25, 1954)

Plates XIV A, B

**ABSTRACT**—The Raman spectrum of monomeric styrene solidified and cooled down to  $-180^{\circ}\text{C}$  has been recorded and compared with that obtained for the substance at room temperature. It is observed that in the case of the monomer the intensity of the line  $1630\text{ cm}^{-1}$  diminishes slightly, but that of the line  $772\text{ cm}^{-1}$  diminishes considerably with solidification and lowering of temperature to  $-180^{\circ}\text{C}$ . The C-H valence oscillations also undergo some changes. It is pointed out that the lines  $772\text{ cm}^{-1}$  and  $1630\text{ cm}^{-1}$  disappear completely and the intensities of some other fainter lines diminish considerably with polymerization of the liquid. When the polymer is cooled to  $-180^{\circ}\text{C}$  no further change in the Raman lines takes place, but two fluorescence bands appear at  $4260\text{ \AA}$  and  $4556\text{ \AA}$  respectively.

The monomer at  $-180^{\circ}\text{C}$  yields four sharp new lines in the low-frequency region and a corresponding wing is also observed in the Raman spectrum of the polymer at room temperature. These results have been discussed in detail.

## INTRODUCTION

In a previous investigation (Roy, 1953) it was observed that when monomeric methyl methacrylate is solidified and cooled to  $-180^{\circ}\text{C}$  the intensity of the line  $1640\text{ cm}^{-1}$  diminishes to half its value observed in the case of the liquid phase while that of the line  $1722\text{ cm}^{-1}$  which shifts to  $1700\text{ cm}^{-1}$  with solidification, remains unchanged. When the substance polymerizes the line  $1640\text{ cm}^{-1}$  disappears completely and the intensity of the line  $1722\text{ cm}^{-1}$  also diminishes appreciably. So in the case of monomer in the solid state also association between neighbouring molecules takes place at the expense of C=C bond, but side chains are not formed in this case at the expense of C=O bond although in the case of the polymer the formation of such side chains is indicated by the diminution of the intensity of the C=O line. In the case of styrene, Signer and Weiler (1932) first observed that the line  $1640\text{ cm}^{-1}$  due to C=C group vanishes with polymerization of the substance. Mizushima *et al* (1937) pointed out that although the intensity of the line  $1634\text{ cm}^{-1}$  diminishes greatly with polymerization it does not disappear completely and they concluded from these results that the polymer consists of thread-like

\* Communicated by Prof. S. C. Sirkar,

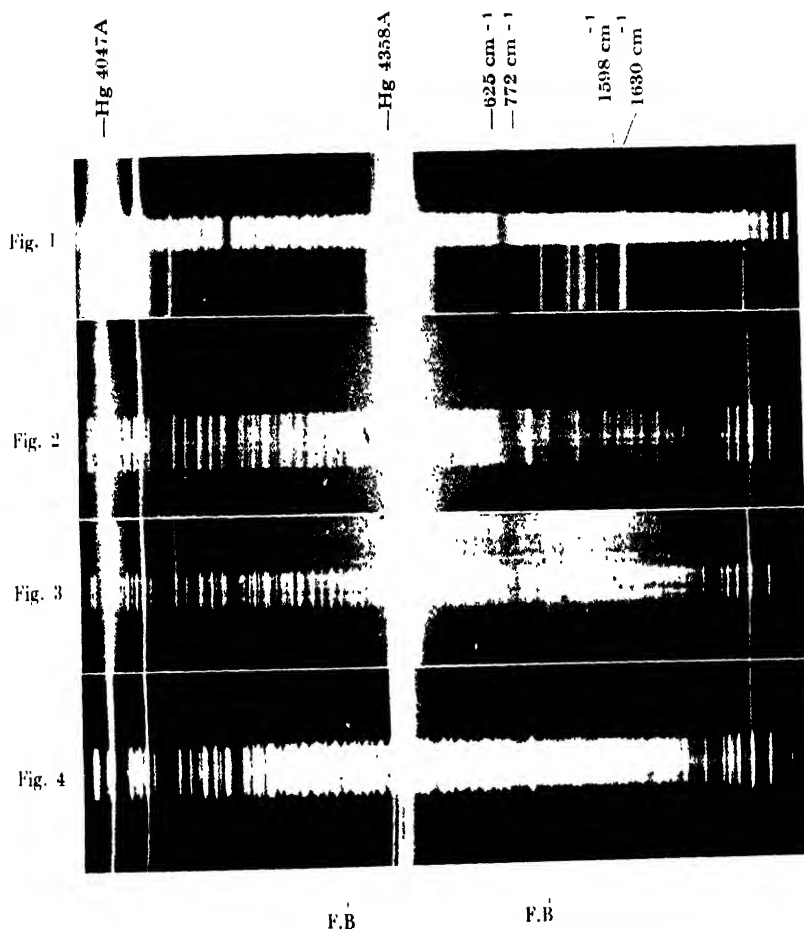
of the monomer also indicates that in some of the molecules the C=C bond of the side chain is changed to C-C bonds due to linkage with neighbouring molecules.

Table I  
Styrene  
 $\Delta\nu$  in  $\text{cm}^{-1}$

Monomer at room temp.		Monomer at $-180^\circ\text{C}$	Polymer at $30^\circ\text{C}$	Polymer at $-180^\circ\text{C}$
Mizushima et al, 1937	Present author			
		46 (2) 69 (2) 90 (2) 110 (2)	A wing upto $90\text{ cm}^{-1}$ from the Rayleigh line	
212 (1)	211 (1)			
241 (3)	242 (3)	230 (2) 242 (2)	230 (ob)	
445 (1b)	438 (1b)	435 (1)		
510 (1)				
558 (1)	556 (1)			
621 (3)	625 (2)	625 (1)	625 (1)	625 (o)
774 (4)	772 (4)	772 (1)		
796 (o)				
835 (o)				
909 (2)	908 (1)	906 (1)		
999 (9)	996 (10)	1000 (5)	1000 (5)	1000 (4)
	1018 (o)		1016 (2)	1016 (1)
1035 (2)	1032 (2)	1032 (o)		
1156 (2)	1156 (2)	1156 (1)	1160 (1b)	1160 (ob)
1183 (3)	1182 (3)	1182 (1)		
1204 (6)	1208 (5)	1208 (2)	1198 (1b)	1198 (ob)
1240 (o)		1220 (1)		
1301 (1)	1298 (o)			
1321 (3)	1320 (2)	1328 (1)		
1414 (6)	1412 (5)	1412 (3)	1420 (o)	
1450 (o)				
1496 (2)	1495 (2)	1495 (ob)		
1555 (o)				
1575 (1)	1572 (1)	1572 (1)		
1601 (10)	1598 (10)	1600 (5)	1605 (3)	1605 (2)
1632 (20)	1630 (15)	1632 (5)		
2909 (3)				
3009 (3)	3010 (2)	3014 (2)		
3059 (7)	3063 (5)	3053 (4) 3083 (2)	3063 (5b)	3063 (2)

The line  $772\text{ cm}^{-1}$  is probably due to a mode of vibration of the benzene nucleus because this line is absent in methyl methacrylate. The disappearance of this line with polymerization is probably due to the formation of net-like structure which restricts the motion of the atoms in the nucleus during this mode of vibration. Since this line becomes weaker when the monomer is solidified it appears that in the solid state also such a restriction occurs.

In the case of partially polymerised sample obtained by heating the monomer to  $35^\circ\text{C}$ – $40^\circ\text{C}$  for 46 days the line  $772\text{ cm}^{-1}$  is weaker than the

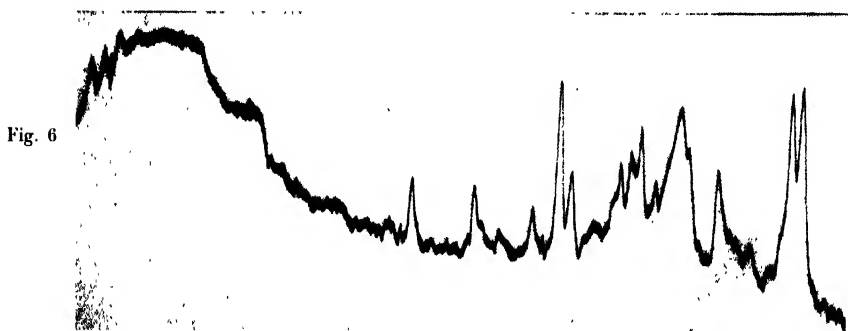
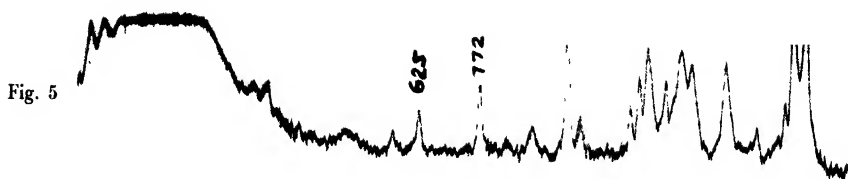


## Raman spectra

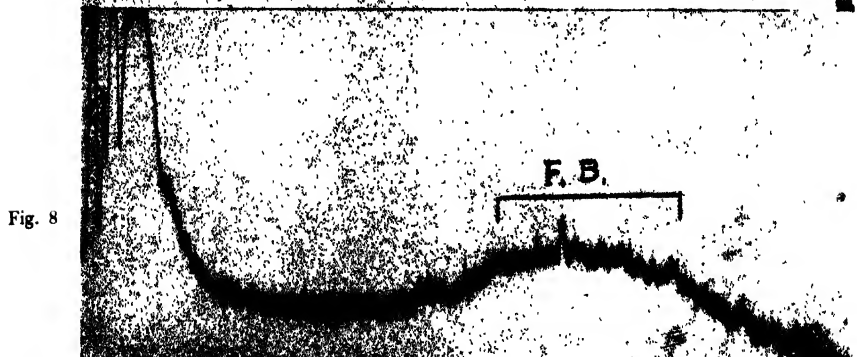
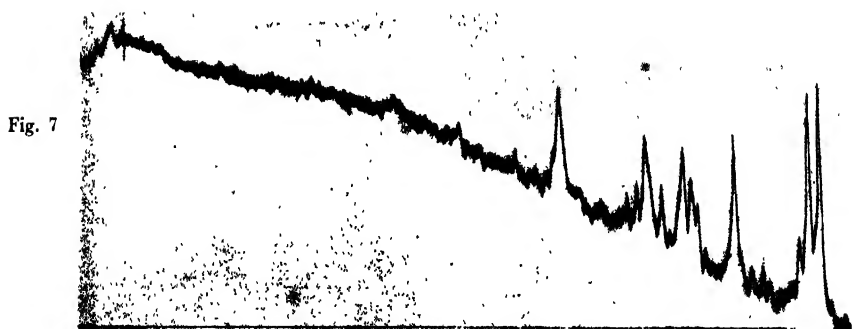
- Fig. 1—Styrene monomer at 30°C  
 Fig. 2—Styrene monomer at -180°C  
 Fig. 3—Polystyrene at 30°C  
 Fig. 4—Polystyrene at -180°C

Hg 4358

1598 1630



Hg 4358A



Microphotometric records of Raman spectra of styrene

Fig. 5—Monomer at 30°C. Fig. 6—Polymerised partially at 35-40°C for 46 days.  
Fig. 7—Monomer at -180°C. Fig. 8—Polymer at -180°C

line  $625\text{ cm}^{-1}$ , but the two lines  $242\text{ cm}^{-1}$  and  $211\text{ cm}^{-1}$  are replaced by a broad line at  $230\text{ cm}^{-1}$ . Also the lines  $1598\text{ cm}^{-1}$  and  $1630\text{ cm}^{-1}$  are of equal intensities although the latter is stronger in the case of the monomer. This can be seen from figure 6. Hence it appears that initially the molecules become attached to each other at points other than the C=C bond, so that the lines  $772\text{ cm}^{-1}$  and  $242\text{ cm}^{-1}$  are affected predominantly and finally the C=C bonds in the molecules disappear rather quickly to complete the polymerization.

In the case of the monomer in the solid state at  $-180^{\circ}\text{C}$  the line  $211\text{ cm}^{-1}$  is absent but the line  $242\text{ cm}^{-1}$  splits up into two lines at  $230$  and  $242\text{ cm}^{-1}$ . The intensity of the line  $1032\text{ cm}^{-1}$  diminishes with solidification of the monomer as with polymerization but not to the same extent. The changes exhibited by the lines due to C-H valence oscillation with polymerization are quite different from those observed with solidification of the monomer and cooling down to  $-180^{\circ}\text{C}$ . In the case of polymerization the line  $3010\text{ cm}^{-1}$  disappears and the line  $3063\text{ cm}^{-1}$  becomes broader. With solidification of the monomer, the line  $3010\text{ cm}^{-1}$  shifts to  $3014\text{ cm}^{-1}$  but persists with undiminished intensity and a new line at  $3083\text{ cm}^{-1}$  is observed. The line  $3014\text{ cm}^{-1}$  may be due to  $\text{CH}_2$  group and disappearance of this line in the case of the polymer probably shows that the hydrogen atoms form virtual bonds with neighbouring molecules so that in place of  $\text{CH}_2$  group a CH group is left and the latter gives the frequency near about  $3063\text{ cm}^{-1}$ . In the case of the solid monomer at  $-180^{\circ}\text{C}$  such a linkage does not take place but in this case the C-H group of the benzene ring is affected by the neighbouring molecules giving rise to the line  $3083\text{ cm}^{-2}$ .

In the case of the monomer in the solid state at  $-180^{\circ}\text{C}$  there are four new lines  $46, 69, 90$  and  $110\text{ cm}^{-1}$ . A close examination of the spectrogram due to the polymer at  $30^{\circ}\text{C}$  also revealed the presence of a wing in the region. Thus these lines become broader in the polymer and are not resolved from each other. The sample of the polymer used in the investigation was a homogeneous solid mass so that the wing cannot be due to liquid state. This shows that the wing is not due to rotation of the molecules. The appearance of the four sharp lines of equal intensities in the case of the monomer at  $-180^{\circ}\text{C}$  probably indicates that the benzene nuclei oscillate against each other in four different modes in the lattice and the low value of the strength of the virtual bond among the molecules gives rise to these lines in the low frequency region. The angular oscillations of the nucleus about its axes would have very small amplitude at such a low temperature and would not produce such intense lines. The frequency of angular oscillations would also be much smaller if the intermolecular field would be of the same order as in the liquid state as observed by Ghosh (1953). So these modes are probably due to translational oscillation of the nuclei

connected to each other through virtual bonds. The regular arrangement of the surrounding molecules gives rise to discrete lines due to these oscillations, but if the arrangement be irregular as in the case of the polymer, the lines are expected to be broader and to merge into one another to form a wing. There is an indication of the persistence of this continuous wing even in the case of the polymer at  $-180^{\circ}\text{C}$ . The polymer at  $-180^{\circ}\text{C}$  yields two fluorescence bands at 4260Å and 4556Å respectively. The difference between the frequencies is  $1524\text{ cm}^{-1}$ . Other disubstituted benzenes such as chlorotoluene (Sanyal, 1953) bromotoluene (Biswas, 1954) etc., also yield such bands. These are disubstituted compounds having a halogen atom as one of the substituents in the nucleus.

It is known from the results obtained by Swamy (1953) that the chlorine atom as the substituent helps the formation of virtual bonds among neighbouring molecules. Since in the styrene molecules the benzene nucleus is monosubstituted and it exhibits fluorescence similar to that observed in chlorotoluene or bromotoluene, the results probably indicate that the benzene nucleus in polystyrene at low temperature ( $-180^{\circ}\text{C}$ ) becomes associated with neighbouring molecules.

#### ACKNOWLEDGMENT

The author is indebted to Prof. S. C. Sirkar for kindly suggesting the problem and for helpful guidance during the progress of the work.

#### REFERENCES

- Biswas, D. C., 1954, *Ind. J. Phys.*, **28**,
- Ghosh, D. K., 1953, *Ind. J. Phys.*, **27**, 285.
- Mizushima, S. I., et al., 1937, *Bull. Chem. Soc., Japan.*, **12**, 136.
- Palm Ann., 1952, *J. Phys. Colloid. Chem.*, **55**, 1320.
- Roy, N. K., 1953, *Ind. J. Phys.*, **27**, 167.
- Sanyal, S. B., 1953, *Ind. J. Phys.*, **27**, 447.
- Signer, R., and Weiler, J., 1932, *Helv. Chem. Acta.*, **15**, 649.
- Swamy, H. N., 1953, *Ind. J. Phys.*, **27**, 55.



# EFFECT OF STEEPNESS OF RISE AND FALL OF THE INPUT PULSE ON THE RESPONSE OF PULSE AMPLIFIERS (PART II) \*

By BIMAL KRISHNA BHATTACHARYYA†

INSTITUTE OF NUCLEAR PHYSICS, 92, UPPER CIRCULAR ROAD, CALCUTTA - 9

(Received for publication, June 20, 1954)

**ABSTRACT.** A study of the response characteristics of shunt-compensated amplifiers has been made for a ramp function input. The magnitude of the decreasing peaks of the highly damped overshoot oscillation has been determined. It has been shown that the amplitude of the peak overshoot may be made insignificant for many applications when the rise time of the incoming wave-front is several times the RC time-constant of the plate circuit of the amplifier. In this case the contribution of the amplifier to the rise and delay times of the output pulse has also been found to be negligible and it has been observed that the output may be sharper compared to the input for values of  $m = (L/CR^2)$  higher than a lower limit which is determined by the rise time of the incoming pulse.

The periods of overshoot oscillations and the reduction factor of the successive overshoot peaks have been given in the form of a table for all the interesting values of  $m$ . In the cases of pulses having sharp rise and fall, expressions for the maximum output voltage obtainable have been derived. The peaks of undershoots have also been determined.

## INTRODUCTION

In a previous communication (Bhattacharyya, 1954) a study of the effect of steepness of rise and fall of the input pulse on the response characteristics of an RC-coupled pulse amplifier was made. It was observed that the two important figures of merit of such an amplifier, e.g. rise and delay times of the transmitted pulse, are markedly dependent on the build-up time of the input waveform.

This paper presents a detailed study of the response characteristics of a shunt-compensated amplifier to pulses of the following types: (i) a ramp function input, (ii) a pulse with linear rise and fall and (iii) a saw-tooth pulse. In this type of amplifier the advantage of decrease in rise and delay times is somewhat offset due to the appearance of over-shoots and overshoot oscillations in the case of a ramp function input. The resistances in series with the coil that is used for high-frequency compensation make

\*Communicated by Prof. M. N. Saha.

† Now at Indian Institute of Technology, Kharagpur, in the Dept. of Geology and Geophysics.

the overshoot oscillations highly damped. The decreasing peaks of such oscillations and the times corresponding to the peaks have been determined.

In the steady state analysis of such amplifiers stress is generally laid on achieving constant gain and linear phase relations over the utilised range of frequency. When the interest is switched over to the determination of transient characteristics, the main object in the design lies in obtaining a monotonically increasing response. But it is not possible to attain such a response with two or four-pole coupling networks consisting of all the three linear circuit elements, e.g. resistances and inductors and capacitors.

The influence of the circuit parameter  $m$ , which is a dimensionless quantity defined as the ratio of inductance  $L$  and  $CR^2$ , on the response has also been studied in order to choose a suitable value of  $m$ . It is known that by an increase in  $m$  we obtain a significant improvement in the rise time of the amplifier with a consequent increase in the magnitude of overshoots and overshoot oscillations. So the value of  $m$  should be chosen with the object of having a reduced figure of both the rise time and the peak of the overshoot oscillation. This paper attempts to furnish all the necessary informations regarding the nature of the response for all the widely used values of  $m$ . In the cases of pulses having sharp rise and fall, expressions for the maximum output voltage obtainable and the peaks of undershoots have been derived.

#### RESPONSE TO A RAMP FUNCTION INPUT PULSE

A typical circuit diagram of a shunt-compensated amplifier is given in figure 1. Only the high frequency equivalent circuit (figure 2) of the amplifier will be considered. With the aid of this figure the expression for the output voltage may be written as :

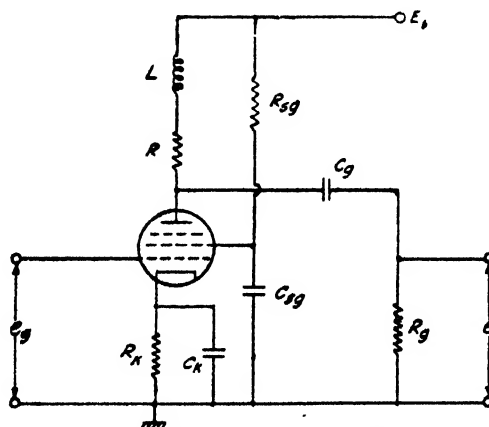


FIG. 1. Circuit diagram of a shunt-compensated amplifier

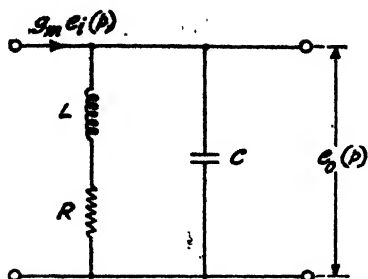


FIG. 2 High frequency equivalent circuit of a shunt-compensated amplifier.

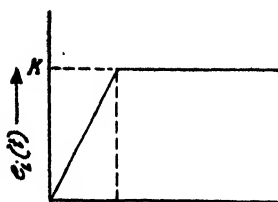


FIG. 3. A ramp function input pulse

$$e_o(p) = g_m e_i(p) \cdot \frac{R + pL}{p^2 LC + pRC + 1} \quad \dots (1)$$

where

$e_i(p)$  = Laplace transform of the input excitation voltage,

$g_m$  = mutual transconductance of the tube,

$R$  = equivalent resistance in series with the coil,

$L$  = inductance of the coil.

and  $C$  = stray and wiring capacitances across the coil.

Since the input pulse is a ramp-function (figure 3) we obtain (Bhattacharyya, 1954) :

$$e_i(p) = \frac{1}{t_1} \cdot \frac{1 - e^{-pt_1}}{p^2} \quad (2)$$

where  $t_1$  is the build-up time of the input.

Substituting (2) in (1), we have

$$e_o(p) = \frac{g_m}{t_1} \cdot \frac{1 - e^{-pt_1}}{p^2} \cdot \frac{R + pL}{p^2 LC + pRC + 1} \quad (3)$$

Now introducing the circuit parameter

$$m = L/CR^2 \quad (4)$$

in (3), we shall obtain,

$$e_o(p) = \frac{g_m R}{t_1} \cdot \frac{1 - e^{-pt_1}}{p^2} \cdot \frac{1 + (pCR) \cdot m}{(pCR)^2 \cdot m + (pCR) + 1} \quad (5)$$

Normalizing (5) by the substitution  $t = t/CR$  and  $e_o(t) = \frac{e_o(p)}{g_m R}$ , we have

$$e_o(p) = \frac{1 - e^{-pt_1}}{t_1} \cdot \frac{1 + mp}{p^2(m p^2 + p + 1)} \quad \dots (6)$$

where  $t_r = t_1/RC$

Equation (6) may be expressed as

$$e_o(p) = \frac{1 - e^{-pt_1}}{t_1} \cdot \frac{(p + a_1)}{p^2(p + a_2)(p + a_3)} \quad \dots (7)$$

where  $a_1 = 1/m$ ,  $a_2 = (1/2m)$ ,  $(1 + \sqrt{1-4m})$  and  $a_3 = (1/2m)$ ,  $(1 - \sqrt{1-4m})$ . Taking the inverse Laplace transform of (7), we have

$$e_0(t) = \frac{1}{t_r} \cdot \left[ \frac{(a_1 - a_2)}{a_2^2(a_3 - a_2)} \cdot e^{-a_1 t} + \frac{(a_1 - a_3)}{a_3^2(a_2 - a_3)} e^{-a_1 t} + \frac{a_1}{a_2 a_3} t \right. \\ \left. + \frac{a_2 a_3 - a_1(a_2 + a_3)}{a_2^2 a_3^2} \right] - \frac{1}{t_r} \cdot \left[ \frac{(a_1 - a_2)}{a_2^2(a_3 - a_2)} \cdot e^{-a_1(t-t_r)} \right. \\ \left. + \frac{(a_1 - a_3)}{a_3^2(a_2 - a_3)} \cdot e^{-a_1(t-t_r)} + \frac{a_1}{a_2 a_3} (t - t_r) + \frac{a_2 a_3 - a_1(a_2 + a_3)}{a_2^2 a_3^2} \cdot u(t - t_r) \right] \dots (8)$$

With the help of equation (8), the equations for the transient response may be written in the following way :

$$e_0(t) = \frac{1}{t_r} \cdot \left[ \frac{(a_1 - a_2)}{a_2^2(a_3 - a_2)} e^{-a_1 t} + \frac{(a_1 - a_3)}{a_3^2(a_2 - a_3)} e^{-a_1 t} + \frac{a_1}{a_2 a_3} t \right. \\ \left. + \frac{a_2 a_3 - a_1(a_2 + a_3)}{a_2^2 a_3^2} \right] \quad (0 \leq t \leq t_r) \dots (9)$$

and

$$e_0(t) = \frac{1}{t_r} \cdot \left[ \frac{(a_1 - a_2)}{a_2^2(a_3 - a_2)} (1 - e^{a_1 t_r}) e^{-a_1 t} + \frac{(a_1 - a_3)}{a_3^2(a_2 - a_3)} (1 - e^{a_1 t_r}) e^{-a_1 t} \right] \\ + \frac{a_1}{a_2 a_3}, \quad (t \geq t_r) \dots (10)$$

Both the equations (9) and (10) lead to an identical result at the time  $t = t_r$ .

We shall now consider three special cases, e.g. (i)  $m < \frac{1}{4}$ , (ii)  $m = \frac{1}{4}$  and (iii)  $m > \frac{1}{4}$ . For the first case we obtain from equations (9) and (10):

$$e_0(t) = \frac{1}{t_r} \cdot \frac{m}{\sqrt{1-4m}} \cdot e^{-t/2m} \cdot \left[ \frac{1 + \sqrt{1-4m}}{1-2m - \sqrt{1-4m}} \cdot e^{\sqrt{1-4m} \cdot t/2m} \right. \\ \left. - \frac{1 - \sqrt{1-4m}}{1-2m + \sqrt{1-4m}} \cdot e^{\sqrt{1-4m} \cdot t/2m} \right] + \frac{1}{t_r} (t + m - 1), \quad (0 \leq t \leq t_r) \quad (11)$$

and

$$e_0(t) = \frac{1}{t_r} \left[ A_1 e^{-(1 - \sqrt{1-4m})t/2m} - A_2 e^{-(1 + \sqrt{1-4m})t/2m} \right] + 1, \quad (t \geq t_r) \quad (12)$$

where

$$A_1 = \frac{m^2(1 + \sqrt{1-4m})}{\sqrt{1-4m}(1-2m - \sqrt{1-4m})}, \quad 1 - e^{(1 - \sqrt{1-4m})t_r/2m}$$

and

$$A_2 = \frac{m^2(1 - \sqrt{1-4m})}{\sqrt{1-4m}(1-2m + \sqrt{1-4m})}, \quad 1 - e^{(1 + \sqrt{1-4m})t_r/2m}$$

## Effect of Steepness of Rise and Fall of Input Pulse, etc. 375

For case (ii) ( $m = \frac{1}{2}$ ), the equations for the transient response may be given in the following form :

$$e_o(t) = \frac{2m}{t_r} [(t+6m)e^{-t/2m} + 2(1-3m)], (0 \leq t \leq t_r) \quad (13)$$

and

$$e_o(t) = \frac{2m}{t_r} \{ (t+6m)e^{-t/2m} (1 - e^{t_r/2m}) \} + 2e^{-(t-t_r)/2m} + 1, (t \geq t_r) \quad \dots \quad (14)$$

We shall now consider the last and the most important case ( $m > \frac{1}{2}$ ) in which the constants  $a_1$ ,  $a_2$  and  $a_3$  are given

$$a_1 = \frac{1}{m}, a_2 = \frac{1}{2m} (1 + j\sqrt{4m-1}) \text{ and } a_3 = \frac{1}{2m} (1 - j\sqrt{4m-1}).$$

Substituting these values in equations (9) and (10) and simplifying, we obtain

$$e_o(t) = \frac{1}{t_r} \frac{e^{-t/2m}}{\sqrt{4m-1}} \left[ (1-m)\sqrt{4m-1} \cos \left( \frac{\sqrt{4m-1}}{2m} t \right) + (1-3m) \sin \left( \frac{\sqrt{4m-1}}{2m} t \right) \right] + \frac{1}{t_r} (t+m-1), (0 \leq t \leq t_r) \quad (15)$$

and

$$e_o(t) = \frac{1}{t_r} \frac{e^{-t/2m}}{\sqrt{4m-1}} \left[ A \cos \left( \frac{\sqrt{4m-1}}{2m} t \right) + B \sin \left( \frac{\sqrt{4m-1}}{2m} t \right) \right] + 1, \quad t \geq t_r \quad (16)$$

where

$$A = (1-m)\sqrt{4m-1} - e^{t_r/2m} \cos \left( \frac{\sqrt{4m-1}}{2m} t_r \right) + (1-3m) e^{t_r/2m} \sin \left( \frac{\sqrt{4m-1}}{2m} t_r \right) \quad (17)$$

and

$$B = (1-3m) \left[ 1 - e^{t_r/2m} \cos \left( \frac{\sqrt{4m-1}}{2m} t_r \right) - e^{t_r/2m} (1-m) \sqrt{4m-1} \sin \left( \frac{\sqrt{4m-1}}{2m} t_r \right) \right] \quad (18)$$

The object of this investigation is to form a correct idea about the reproduction of the sharp leading edges with shunt-compensated amplifiers using practical values of  $m$ . The values of  $m$  chosen are given below :

- (i)  $m=0.1$ , (ii)  $m=0.2$ , (iii)  $m=0.35$ , (iv)  $m=0.41$ ,  
(v)  $m=0.50$ , (vi)  $m=0.60$  and (vii)  $m=1.00$ .

The response characteristics have been plotted in figures 4-8 with the aid of equations (11), (12), (15) and (16) for various values of  $t_r$ . A plot of the step-function response of such an amplifier is given in Fig. 9. The response function is given by the following expression (Goldman, 1949) :

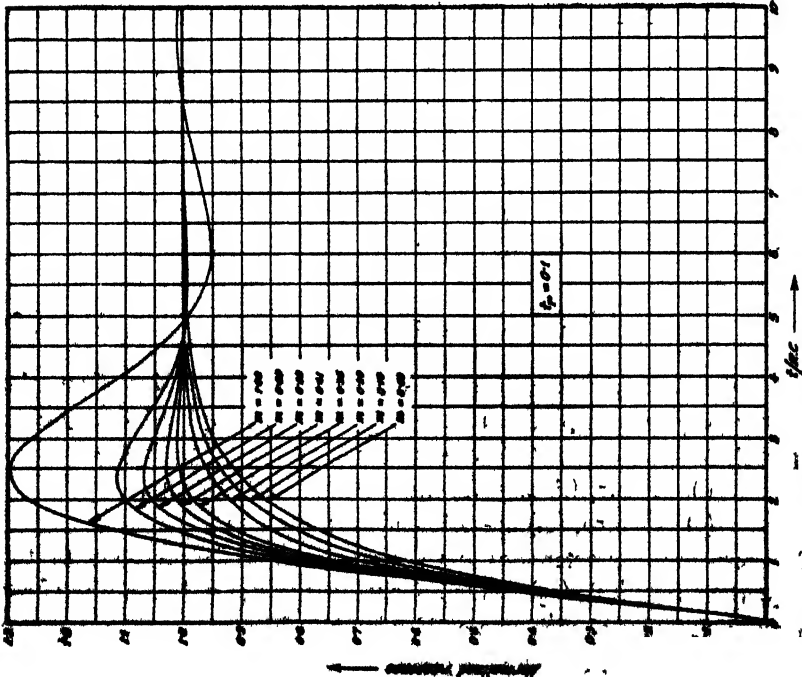


Fig. 4—Response of a shunt-compensated amplifier to a ramp-function input ( $t_r = 0.1$ ).

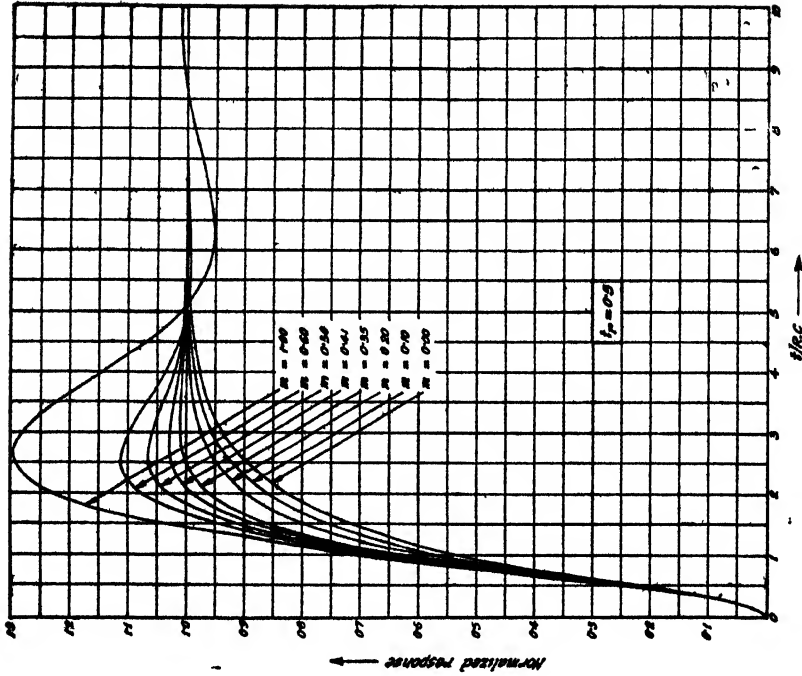


Fig. 5—Response of a shunt-compensated amplifier to a ramp-function input ( $t_r = 0.5$ ).

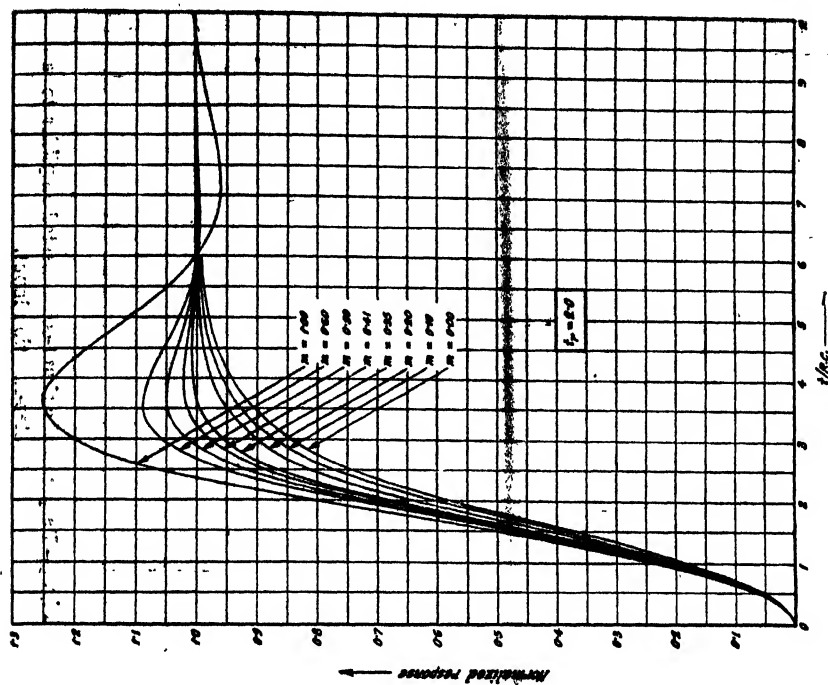


Fig. 7—Response of a shunt-compensated amplifier to ramp-function input ( $t_r = 2.0$ ).

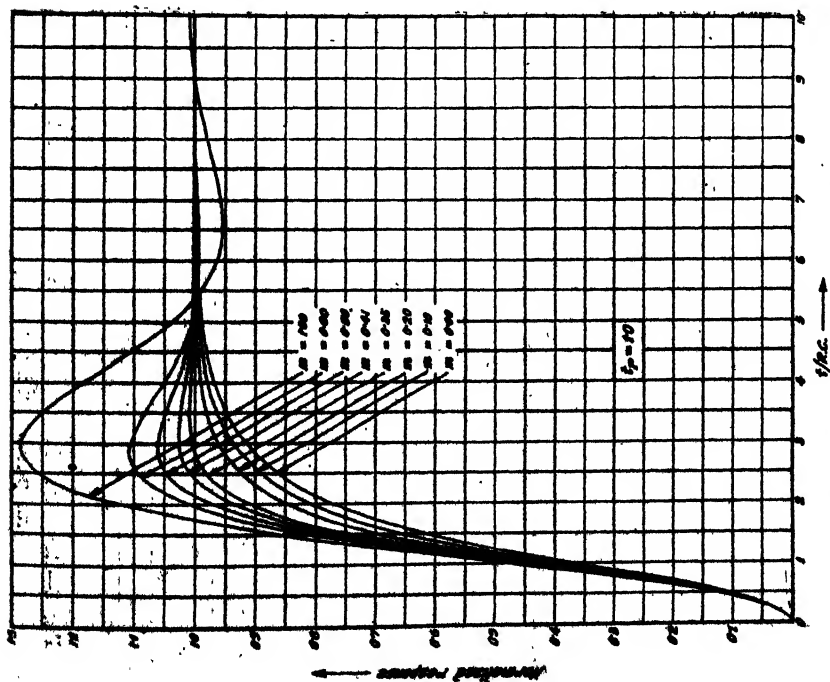


Fig. 6—Response of a shunt-compensated amplifier to a ramp-function input ( $t_r = 1.0$ ).

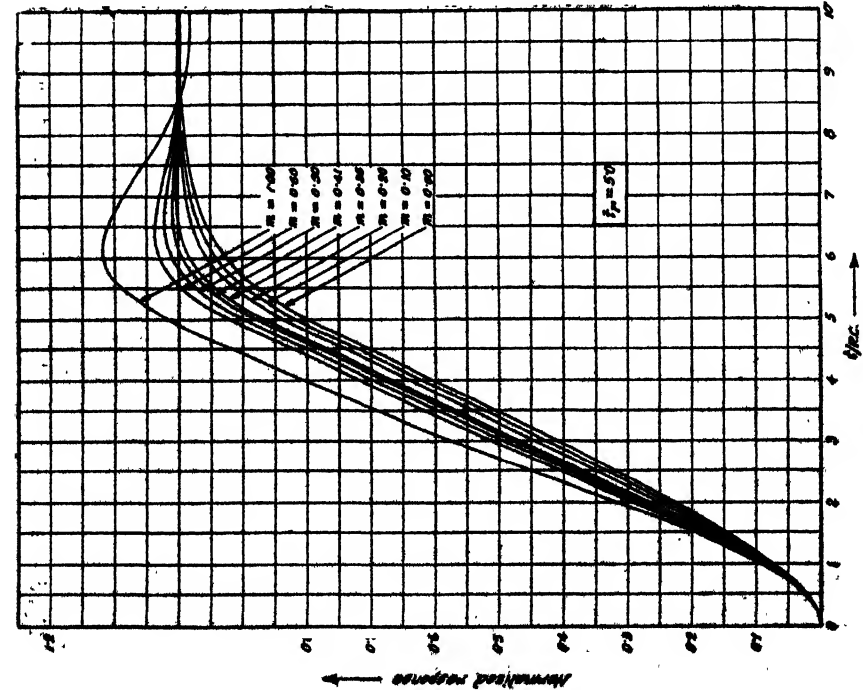


Fig. 8—Response of a shunt-compensated amplifier to a ramp-function input ( $f_p = 50$ .)

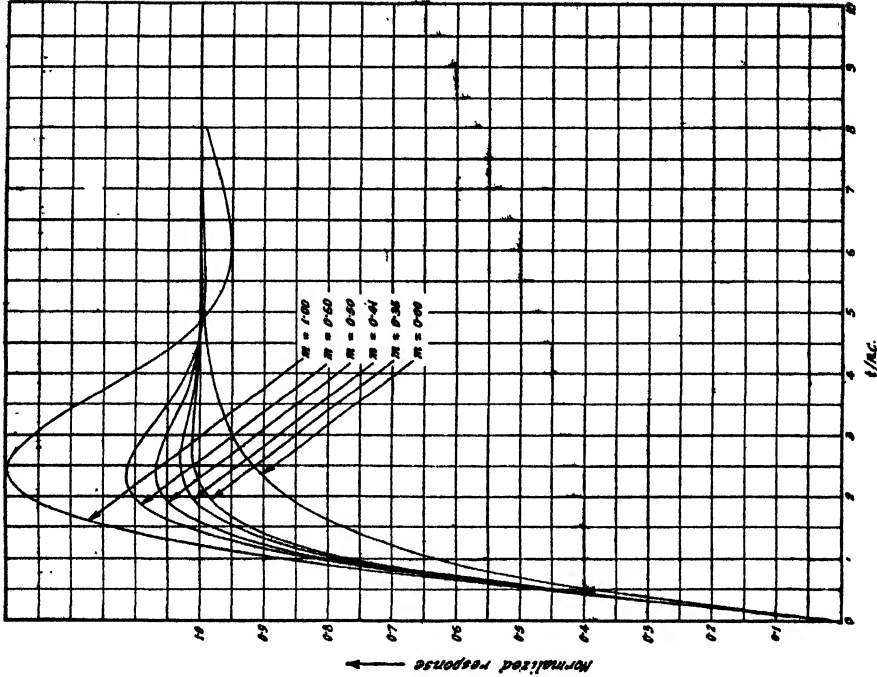


Fig. 9—Response of a shunt-compensated amplifier step-function input.



$$e_o(t) = 1 - e^{-t/2m} \left[ \cos \left( \frac{\sqrt{4m-1}}{2m} t \right) + \frac{(1-2m)}{\sqrt{4m-1}} \sin \left( \frac{\sqrt{4m-1}}{2m} t \right) \right], \quad (m > 0.25)$$

Since the step-function response of a shunt-compensated amplifier has been determined by many authors, we have not here considered the other two cases; e.g. (i)  $m < 0.25$  and (ii)  $m = 0.25$ . For the sake of comparison, the responses of an ordinary RC-coupled amplifier have been given in every figure.

*Characteristics of over-shoot oscillations:*—A judicious choice of the circuit parameter  $m$  to obtain a well-shaped response with full details of the input requires a previous information regarding the nature of overshoot oscillations. With this purpose in view this section presents the formulae for computing the times of occurrences and the magnitudes of overshoots for various values of  $m$ . For  $m \leq 0.25$ , the nature of response is very much akin to that of an RC-coupled amplifier excepting for slight improvement in rise and delay times. This is why we have considered only the values of  $m$  greater than 0.25. The overshoot oscillation generally starts at a time  $t > t_r$ . With the help of (16) we, then, obtain

$$\frac{de_o(t)}{dt} = \frac{e^{-t/2m}}{t_r} \left[ \left\{ \frac{B}{2m} - \frac{A}{2m\sqrt{4m-1}} \right\} \cos \frac{\sqrt{4m-1}}{2m} t - \left\{ \frac{A}{2m} + \frac{B}{2m\sqrt{4m-1}} \right\} \sin \frac{\sqrt{4m-1}}{2m} t \right], \quad (19)$$

At the peaks of overshoot oscillation, either positive or negative, the slope of the response function will be zero. Hence, we have from (19):  
either

$$e^{-t/2m} = 0 \quad (20)$$

or

$$\left\{ \frac{B}{2m} - \frac{A}{2m\sqrt{4m-1}} \cos \frac{\sqrt{4m-1}}{2m} t \right\} - \frac{A}{2m} \frac{B}{2m\sqrt{4m-1}} \sin \frac{\sqrt{4m-1}}{2m} t = 0 \quad (21)$$

By solving (20) or (21) we shall obtain the times corresponding to the maximum or minimum points of oscillation. It is evident that equation (20) cannot give any practicable solution. We can express equation (21) in the following way:

$$A_o \cos (\theta t + \phi) = 0 \quad (22)$$

where

$$A_o \cos \phi = \frac{B}{2m} - \frac{A}{2m\sqrt{4m-1}}$$

$$A_o \sin \phi = \frac{A}{2m} + \frac{B}{2m\sqrt{4m-1}}$$

$$\theta = \frac{\sqrt{4m-1}}{2m} \text{ and } \tan \phi = \frac{B + A\sqrt{4m-1}}{B\sqrt{4m-1} - A}$$

Solving (22), we obtain the times  $t_0$  corresponding to the peaks of overshoot oscillation. The solution is

$$t_0 = \frac{(n + \frac{1}{2})\pi - \phi}{\theta} \quad \dots (23)$$

where  $n$  is an integer having values 0, 1, 2, ...  $n$ . Differentiating (19) again we get

$$\frac{d^2 e_0(t)}{dt^2} = -\frac{e^{-t/2m}}{t_r} \left[ \frac{A_0}{2m} \cos(\theta t + \phi) + A_0 \theta \sin(\theta t + \phi) \right] \quad \dots (24)$$

At the time  $t_0$ , this expression reduces to

$$\frac{d^2 e_0(t)}{dt^2} = -\frac{e^{-t_0/2m}}{t_r} A_0 \theta \sin(\theta t_0 + \phi) \quad \dots (25)$$

An examination of (25) leads us to the conclusion that the peak overshoot points given by (23) correspond to the positive peaks when  $n$  is even and to the negative when  $n$  is odd.

Fig. 10 shows a typical nature of the overshoot oscillation in which

$t_{01}, t_{02}, \dots$  are the times of occurrences of positive peaks,

and  $t_{02}, t_{04}, \dots$ , times of occurrences of negative peaks.

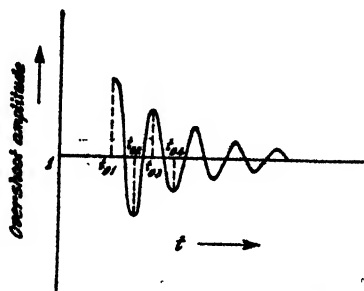


Fig. 10. Nature of the overshoot oscillation.

With the help of (23), we can now set up a relation amongst  $t_{01}, t_{02}, t_{03}, t_{04}$ , etc. We can write

$$\left. \begin{aligned} t_{02} &= t_{01} + \pi/\theta, \\ t_{03} &= t_{02} + \pi/\theta, = t_{01} + 2\pi/\theta \\ t_{04} &= t_{01} + 3\pi/\theta \text{ and so on.} \end{aligned} \right\} \quad \dots (26)$$

So the period of overshoot oscillation is given by  $2\pi/\theta$  which is independent of the rise time of the input pulse.

With the aid of (16), the overshoot amplitude at the time  $t=t_{01}$  may be expressed in the following way :

$$O(t_{01}) = \frac{I}{t_r} \cdot \frac{e^{-t_{01}/2m}}{\sqrt{4m-1}} \left[ A \cos \theta_{t_{01}} + B \sin \theta_{t_{01}} \right] \quad \dots (27)$$

At the time  $t=t_{02}$ , the overshoot amplitude may be written as

$$O(t_{02}) = -\frac{I}{t_r} \cdot \frac{e^{-t_{02}/2m}}{\sqrt{4m-1}} \left[ A \cos \theta_{t_{01}} + B \sin \theta_{t_{01}} \right] \quad \dots (28)$$

since,

$$\theta_{t_{02}} = \pi + \theta_{t_{01}}.$$

Therefore, we have

$$R = \frac{O(t_{02})}{O(t_{01})} = -e^{-\pi/2\theta m} \quad \dots (29)$$

where  $R$  denotes the reduction factor of the successive peaks of overshoot oscillations.

Similarly,

$$\frac{O(t_{03})}{O(t_{01})} = e^{-\pi/\theta m} = R^2 \quad \dots (30)$$

Equations (29) and (30) give the ratios of attenuation between the successive positive and negative peaks. The periods of overshoot oscillations and the reduction factors for all the important values of  $m$  are given in Table I. This table will give an idea about the sharp decrease in successive overshoot amplitudes.

TABLE I

$m$	Period of oscillation	Reduction factor $R$	$R^2$
0.35	6.957008	-0.006948	.000048
0.41	6.442860	-0.019672	.000388
0.50	6.285714	-0.043160	.001863
0.60	6.374878	-0.070215	.004930
1.00	7.258120	-0.162915	.026541

With the help of equations (23), (26), (27), (29) and (30) we have plotted the times reckoning the peaks of overshoot oscillations and the amplitudes of the overshoots in figures 11 and 12.

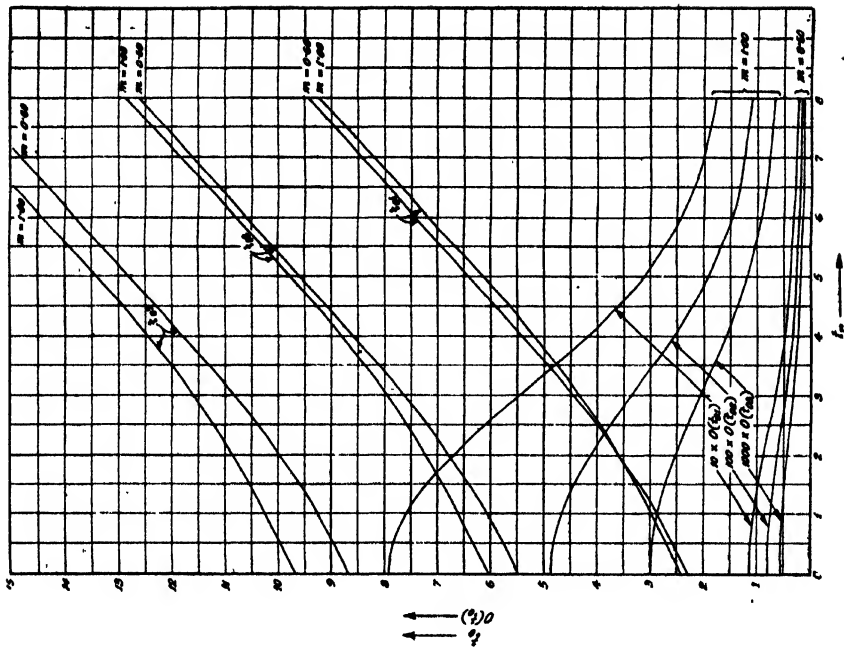


Fig. 12—Plot of the times reckoning the decreasing peaks of overshoot oscillation and amplitudes of the overshoots as a function of  $t$ .

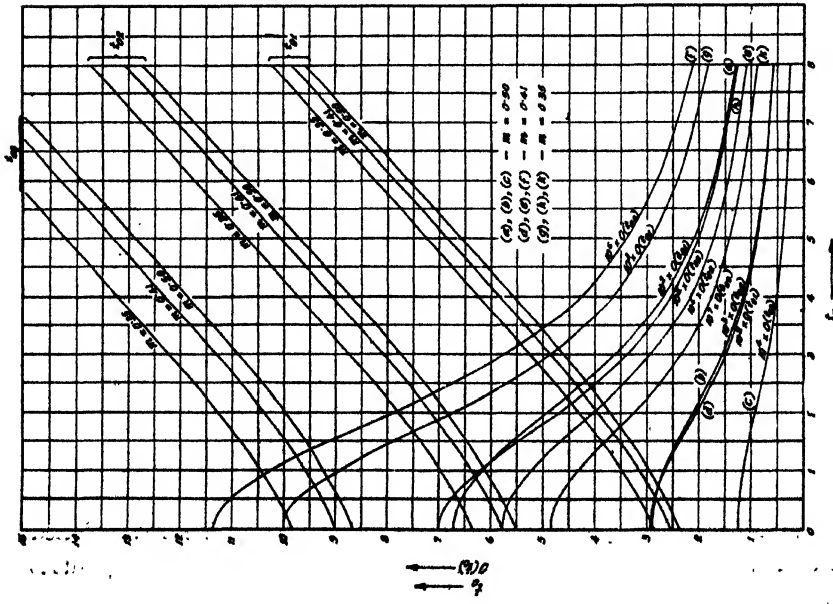


Fig. 11—Plot of the times reckoning the decreasing peaks of overshoot oscillation and amplitudes of the overshoots as a function of  $t$ .

A study of figures 11 and 12 will show that the overshoot of an amplifier using shunt-compensation assumes its maximum at  $t_r=0$  (a step-function input) for all possible values of  $m$ . For small values of  $t_r$  (from  $t_r=0$  to  $t_r=0.3$  approximately) the magnitude of the peak overshoot remains almost constant. As  $t_r$  increases from its value 0, the overshoot amplitude begins to decrease very sharply. The nature of decrease is practically exponential. The overshoot amplitudes  $O(t_{01})$  for  $t_r=0.1$  and  $t_r=8.0$  are given in Table II for a better understanding of their rapid rate of fall. It may be concluded from this theoretical study that for an application where 10 per cent overshoot is not very much objectionable but the contribution of the amplifier to the rise time of leading edge of the output should be very low, the value of  $m=1.0$ , for example, may be used in a specific case,  $t_r=6.0$ , when  $O(t_{01})=0.091325$  and  $t_u-t_l-0.8t_r=-0.6254$ . [See next section].

TABLE II

$t_r$	$m=0.35$ $O(t_{01})$	$m=0.41$ $O(t_{01})$	$m=0.50$ $O(t_{01})$	$m=0.60$ $O(t_{01})$	$m=1.00$ $O(t_{01})$
0.1	0.010034	0.029294	0.066960	0.113398	0.298315
8.0	0.001812	0.005454	0.012988	0.022883	0.066858

#### RISE AND DELAY TIMES OF THE OUTPUT PULSE

In the previous publication (Bhattacharyya, 1954) we have noticed that the actual contribution of the pulse amplifier to the rise and delay times of the reproduced waveforms is determined by the expressions  $(t_u-t_l-0.8t_r)$  and  $(t_d-0.5t_r)$  respectively, where  $t_u$ ,  $t_d$  and  $t_l$  have been defined such that

$$e_0(t_u)=0.9, \quad e_0(t_d)=0.5 \quad \text{and} \quad e_0(t_l)=0.1.$$

In order to study the effect of  $t_r$  on the reproduction of the leading edge of a pulse in a shunt-compensated pulse amplifier it is now necessary to derive analytical expressions for these three parameters  $t_u$ ,  $t_d$  and  $t_l$  as a function of  $t_r$ .

With the aid of (15), we can write the following equation relating  $t_u$  to  $t_r$  (when  $t_u \leq t_r$ ):

$$e_0(t) = \frac{1}{t_r} \left[ \frac{e^{-t/2m}}{\sqrt{4m-1}} \left\{ (1-m)\sqrt{4m-1} \cos \left( \frac{\sqrt{4m-1}}{2m} t \right) + (1-3m) \sin \left( \frac{\sqrt{4m-1}}{2m} t \right) \right\} + \frac{1}{t_r} (t+m-1) \right] = \frac{9}{10} \quad (32)$$

The solution of (32) for various values of  $t_r$  will show the nature of variation of  $t_u$  with the rise time of the input pulse. This transcendental equation (32) may be solved by either graphical or numerical methods. We have used here the Newton-Raphson process (Scarborough, 1919) of finding out the roots of such equations to a sufficient degree of accuracy.

When  $t_h \geq t_r$  equation (16) will have to be utilised to determine correctly the 90% points. We then have,

$$e_o(t) = \frac{1}{t_r} \cdot \frac{e^{-t/2m}}{\sqrt{4m-1}} \left[ A \cos \left( \frac{\sqrt{4m-1}}{2m} t \right) + B \sin \left( \frac{\sqrt{4m-1}}{2m} t \right) \right] + 1 = \frac{9}{10} \quad \dots (33)$$

Following a similar process we can now easily compute the 10% and 50% points of the response. The curves showing the rise and delay times of the output response as a function of  $t_r$  have been plotted in figures 13 and 14. The corresponding diagrams for a RC-amplifier have been included in the above figures for the purpose of visualizing the difference in response characteristics in the two cases.

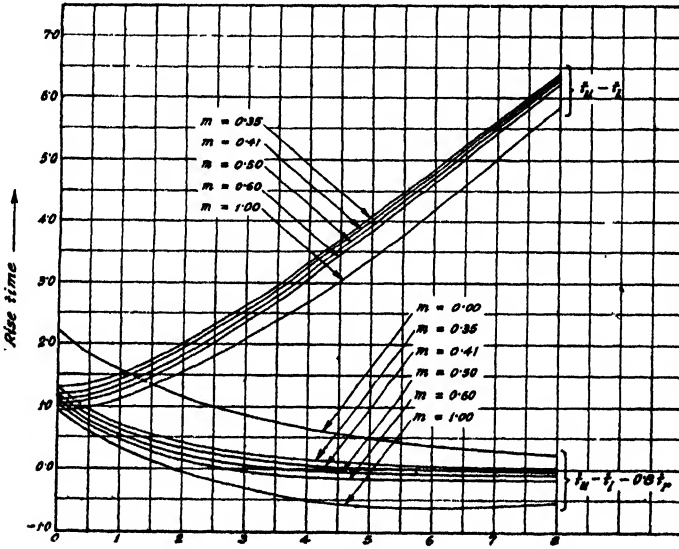


Fig. 13—Plot of time as a function of  $t_r$ .

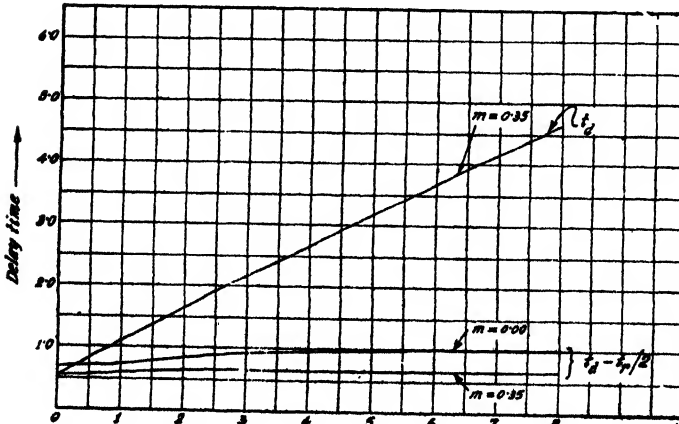


Fig. 14—Plot of delay time as a function of  $t_r$ .

The contribution of the pulse amplifier to the increase of rise time of the output is significant at very small values of  $t_r$ . It reaches the maximum value for a step-function input ( $t_r=0$ ) and then begins to decrease at an appreciable rate with the increase of  $t_r$ . The most interesting point in the response of a shunt-compensated amplifier to such a type of input is the sharpening of the leading edge of the pulse when  $t_r$  is greater than a certain value for a specified  $m$ . Due to this reason, the curve  $(t_u - t_i - 0.8t_r)$  versus  $t_r$  crosses the base line, say at  $t_r = t_{r1}$ . This indicates that the rise time of the reproduced pulse is less than that of the input when the magnitude of  $t_r$  surpasses the lower limit  $t_{r1}$  which is given by

$$(t_u - t_i) = 0.8t_r \quad \dots (34)$$

Table III will give an idea about the actual measure of sharpening of the leading edge of the pulse for a particular value of  $t_r$ , equal to 8.0.

TABLE III

$(t_u - t_i - 0.8t_r)$	$m=0.35$	$m=0.41$	$m=0.50$	$m=0.60$	$m=1.00$
(Rise time of the output) - (rise time of the input)	0.126	-0.0308	-1.1004	-1.821	-5.433

The delay in transmission of the input pulse by the amplifier has been shown in figure 14 as a function of  $t_r$ . Because of the very small change of the delay time  $t_d$  with the variation of  $m$ ,  $t_d$  has been plotted against  $t_r$  only for the case  $m=0.35$ . The values of  $t_d$  for other cases have been given in Table IV.

TABLE IV

$m$	$t_r=0.1$ $t_d$	$t_r=0.5$ $t_d$	$t_r=1.0$ $t_d$	$t_r=2.0$ $t_d$	$t_r=5.0$ $t_d$
0.35	0.603000	0.811970	1.091636	1.652683	3.157100
0.41	0.598130	0.806574	1.082724	1.630984	3.104042
0.50	0.590000	0.797572	1.070715	1.603830	3.026846
0.60	0.583650	0.790345	1.060766	1.579841	2.946921
1.00	0.570630	0.775010	1.038642	1.522298	2.711985

With the help of this Table we may now calculate the delay introduced by the amplifier for all the interesting cases. It is noticed that with the decrease of steepness of pulse fronts the delay caused by the amplifier does not increase appreciably.

# RESPONSE TO A PULSE WITH LINEAR RISE AND FALL

A pulse with linear rise and fall (figure 15) can be expressed as

$$e(t) = K \left[ \frac{t}{t_1} u(t) - \frac{t_2}{t_1} \cdot \frac{(t-t_1)}{(t_2-t_1)} \cdot u(t-t_1) + \frac{(t-t_2)}{(t_2-t_1)} \cdot u(t-t_2) \right] \quad \dots (35)$$

where  $K$  represents the height of the pulse.

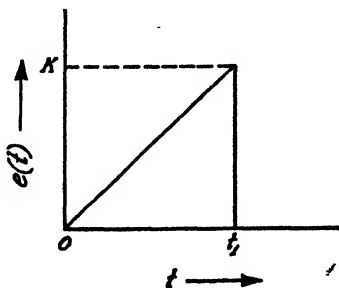


Fig. 15—A pulse with linear rise and fall.

The high-frequency equivalent circuit of the amplifier (figure 2) will only be considered. Then the normalized output voltage may be expressed in the following way :

Case I ( $m < \frac{1}{2}$ ) :

(i)  $0 \leq t \leq t_r$

$$e_o(t) = \frac{1}{t_r} \cdot \frac{m^2}{\sqrt{1-4m}} e^{-t/2m} \left[ \frac{1 + \sqrt{1-4m}}{1-2m - \sqrt{1-4m}} e^{\sqrt{1-4m} t / 2m} - \frac{1 - \sqrt{1-4m}}{1-2m + \sqrt{1-4m}} e^{-\sqrt{1-4m} t / 2m} \right] + \frac{1}{t_r} (t + m - 1), \quad \dots (36)$$

(ii)  $t_r \leq t < t_f$

$$e_o(t) = A_2 e^{-(1-\sqrt{1-4m})t/2m} - A_3 e^{-(1+\sqrt{1-4m})t/2m} - \frac{t - t_f + m - 1}{t_f - t_r}, \quad \dots (37)$$

(iii)  $t \geq t_f$

$$e_o(t) = C_2 e^{-(1-\sqrt{1-4m})t/2m} - D_2 e^{-(1+\sqrt{1-4m})t/2m} \quad \dots (38)$$

where

$$t_r = \frac{t_1}{RC}, \quad t_f = \frac{t_2}{RC},$$

$$A_2 = \frac{m^2}{\sqrt{1-4m}} \cdot \frac{1 + \sqrt{1-4m}}{1-2m - \sqrt{1-4m}} \cdot \frac{1}{t_r} \left[ 1 - \frac{t_f}{(t_f - t_r)} e^{(1-\sqrt{1-4m})t_r/2m} \right],$$



$$A_1 = \frac{m^2}{\sqrt{1-4m}} \cdot \frac{1 - \sqrt{1-4m}}{1-2m + \sqrt{1-4m}} \cdot \frac{1}{t_r} \left[ 1 - \frac{t_f}{(t_f - t_r)} \cdot e^{(1 + \sqrt{1-4m})t_r / 2m} \right]$$

$$C_2 = \frac{m^2}{\sqrt{1-4m}} \cdot \frac{1 + \sqrt{1-4m}}{1-2m - \sqrt{1-4m}} \cdot \frac{1}{t_r} \left[ 1 - \frac{t_f}{(t_f - t_r)} e^{(1 - \sqrt{1-4m})t_r / 2m} \right. \\ \left. + \frac{t_f}{(t_f - t_r)} e^{(1 - \sqrt{1-4m})t_f / 2m} \right]$$

$$D_2 = \frac{m^2}{\sqrt{1-4m}} \cdot \frac{1 - \sqrt{1-4m}}{1-2m + \sqrt{1-4m}} \cdot \frac{1}{t_r} \left[ 1 - \frac{t_f}{(t_f - t_r)} \cdot e^{(1 + \sqrt{1-4m})t_r / 2m} \right. \\ \left. (t_f - t_r) \cdot e^{(1 + \sqrt{1-4m})t_f / 2m} \right]$$

Case II ( $m = \frac{1}{4}$ )

(i)  $0 \leq t \leq t_r$

$$e_0(t) = \frac{2m}{t_r} \left[ (t + 6m)e^{-t/2m} + 2(t - 3m) \right] \quad \dots (39)$$

(ii)  $t_r \leq t \leq t_f$

$$e_0(t) = \frac{2m}{t_r} (t + 6m)e^{-t/2m} \left[ 1 - \frac{t_f}{(t_f - t_r)} e^{t_r/2m} \right] + \frac{2mt_f}{(t_f - t_r)} e^{-(t-t_r)/2m} \\ + \frac{4mt_f}{(t_f - t_r)} - \frac{4m(t-3m)}{(t_f - t_r)} \quad \dots (40)$$

(iii)  $t \geq t_f$

$$e_0(t) = \frac{2m}{t_r} (t + 6m)e^{-t/2m} \left[ 1 - \frac{t_f}{(t_f - t_r)} e^{t_r/2m} + \frac{t_r}{(t_f - t_r)} e^{t_f/2m} \right] \\ - \frac{2mt_f}{(t_f - t_r)} e^{-(t-t_r)/2m} - \frac{2mt_f}{(t_f - t_r)} e^{-(t-t_r)/2m} \quad (41)$$

Case III ( $m > \frac{1}{4}$ )

(i)  $0 \leq t \leq t_r$  ;

$$e_0(t) = \frac{1}{t_r} \cdot \frac{e^{-t/2m}}{\sqrt{4m-1}} \left[ (1-m) \sqrt{4m-1} \cos \left( \frac{\sqrt{4m-1}}{2m} t \right) \right. \\ \left. + (1-3m) \sin \left( \frac{\sqrt{4m-1}}{2m} t \right) \right] + \frac{1}{t_r} (t + m - 1) \quad \dots (42)$$

(ii)  $t_r \leq t \leq t_f$ 

$$e_0(t) = A_1 \cos \left( \frac{\sqrt{4m-1}}{2m} t \right) e^{-t/2m} + B_1 \sin \left( \frac{\sqrt{4m-1}}{2m} t \right) e^{-t/2m} - \frac{(t-t_r) + m-1}{(t_f-t_r)} \dots (43)$$

and

(iii)  $t \geq t_f$ 

$$e_0(t) = C_1 e^{-t/2m} \cos \left( \frac{\sqrt{4m-1}}{2m} t \right) + D_1 e^{-t/2m} \sin \left( \frac{\sqrt{4m-1}}{2m} t \right) \dots (44)$$

where

$$A_1 = \frac{(1-m)}{t_r} - \frac{t_f e^{t_r/2m}}{t_r(t_f-t_r)} \left[ (1-m) \cos \left( \frac{\sqrt{4m-1}}{2m} t_r \right) - \frac{(1-3m)}{\sqrt{4m-1}} \sin \left( \frac{\sqrt{4m-1}}{2m} t_r \right) \right],$$

$$B_1 = \frac{(1-3m)}{t_r \sqrt{4m-1}} - \frac{t_f e^{t_r/2m}}{t_r(t_f-t_r)} \left[ (1-m) \sin \left( \frac{\sqrt{4m-1}}{2m} t_r \right) + \frac{(1-3m)}{\sqrt{4m-1}} \cos \left( \frac{\sqrt{4m-1}}{2m} t_r \right) \right],$$

$$C_1 = A_1 + \frac{e^{t_f/2m}}{(t_f-t_r)} \left[ (1-m) \cos \left( \frac{\sqrt{4m-1}}{2m} t_f \right) - \frac{(1-3m)}{\sqrt{4m-1}} \sin \left( \frac{\sqrt{4m-1}}{2m} t_f \right) \right]$$

and

$$D_1 = B_1 + \frac{e^{t_f/2m}}{(t_f-t_r)} \left[ (1-m) \sin \left( \frac{\sqrt{4m-1}}{2m} t_f \right) + \frac{(1-3m)}{\sqrt{4m-1}} \cos \left( \frac{\sqrt{4m-1}}{2m} t_f \right) \right]$$

We shall consider here only the last case ( $m > \frac{1}{4}$ ). With the help of equations (42-44) the response functions have been plotted in figures 16-20.

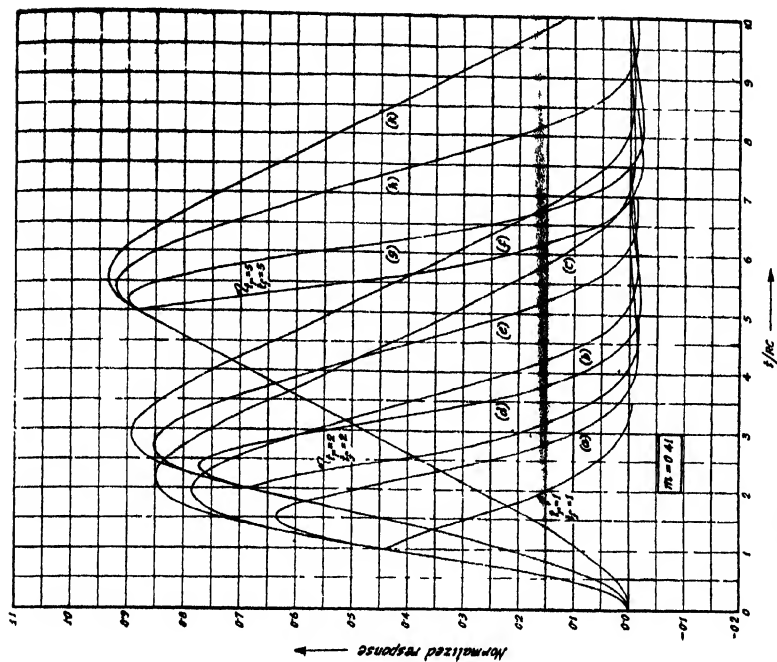


Fig. 17—Response of a shunt-compensated amplifier to a pulse with linear rise and fall ( $m=0.41$ ).

- (a)  $t_r=1, t_f=2$ ; (b)  $t_r=1, t_f=4$ ,  
(c)  $t_r=1, t_f=6$ ; (d)  $t_r=2, t_f=3$ ,  
(e)  $t_r=2, t_f=5$ ; (f)  $t_r=2, t_f=7$ ,  
(g)  $t_r=5, t_f=6$ ; (h)  $t_r=5, t_f=5$ ,  
(i)  $t_r=5, t_f=10$ .

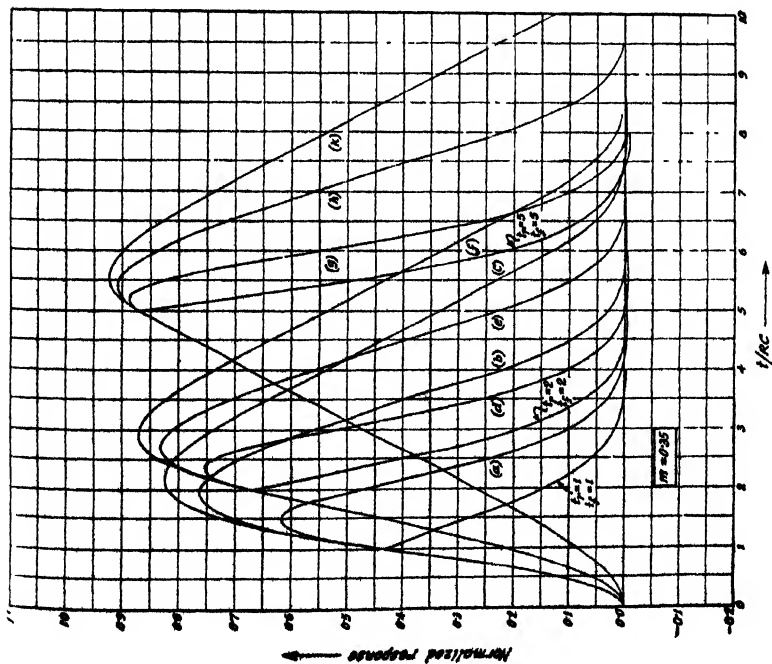


Fig. 16—Response of a shunt-compensated amplifier to a pulse with linear rise and fall ( $m=0.35$ ):

- (a)  $t_r=1, t_f=2$ ; (b)  $t_r=1, t_f=4$ ;  
(c)  $t_r=1, t_f=6$ ; (d)  $t_r=2, t_f=3$ ;  
(e)  $t_r=2, t_f=5$ ; (f)  $t_r=2, t_f=7$ ;  
(g)  $t_r=5, t_f=6$ ; (h)  $t_r=5, t_f=5$ ,  
(i)  $t_r=5, t_f=10$ .

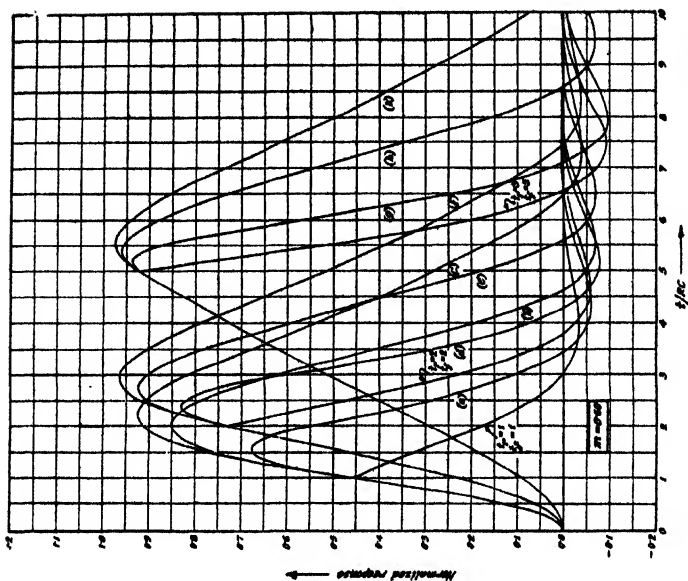


Fig. 19—Response of a shunt compensated amplifier to a pulse with linear rise and fall ( $m = 0.60$ ):

- (a)  $t_r = 1, t_f = 2$ ; (b)  $t_r = 1, t_f = 4$ ;  
 (c)  $t_r = 1, t_f = 6$ ; (d)  $t_r = 2, t_f = 3$ ;  
 (e)  $t_r = 2, t_f = 5$ ; (f)  $t_r = 2, t_f = 7$ ;  
 (g)  $t_r = 5, t_f = 6$ ; (h)  $t_r = 5, t_f = 8$ ;  
 (i)  $t_r = 5, t_f = 10$ .

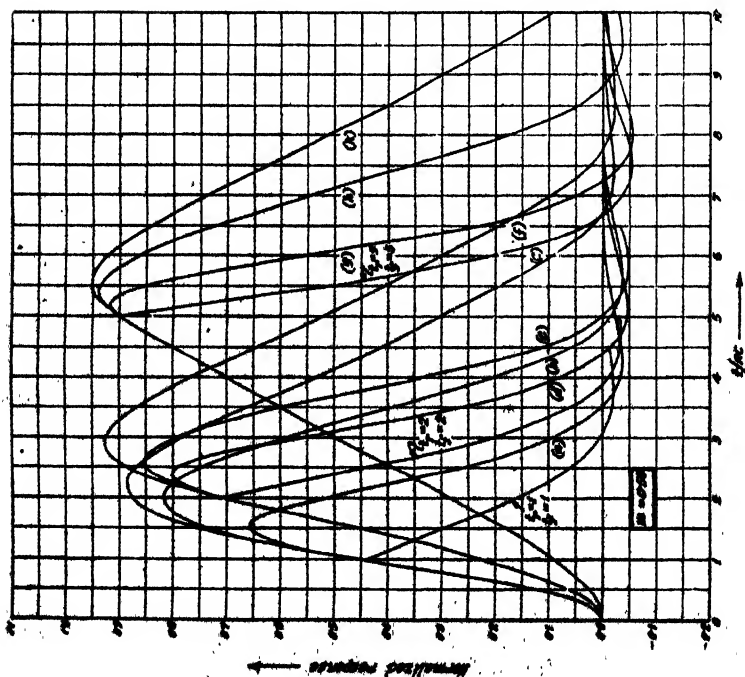


Fig. 18—Response of a shunt compensated amplifier to a pulse with linear rise and fall ( $m = 0.50$ ):

- (a)  $t_r = 1, t_f = 2$ ; (b)  $t_r = 1, t_f = 4$ ;  
 (c)  $t_r = 1, t_f = 6$ ; (d)  $t_r = 2, t_f = 3$ ;  
 (e)  $t_r = 2, t_f = 5$ ; (f)  $t_r = 2, t_f = 7$ ;  
 (g)  $t_r = 5, t_f = 6$ ; (h)  $t_r = 5, t_f = 8$ ;  
 (i)  $t_r = 5, t_f = 10$ .

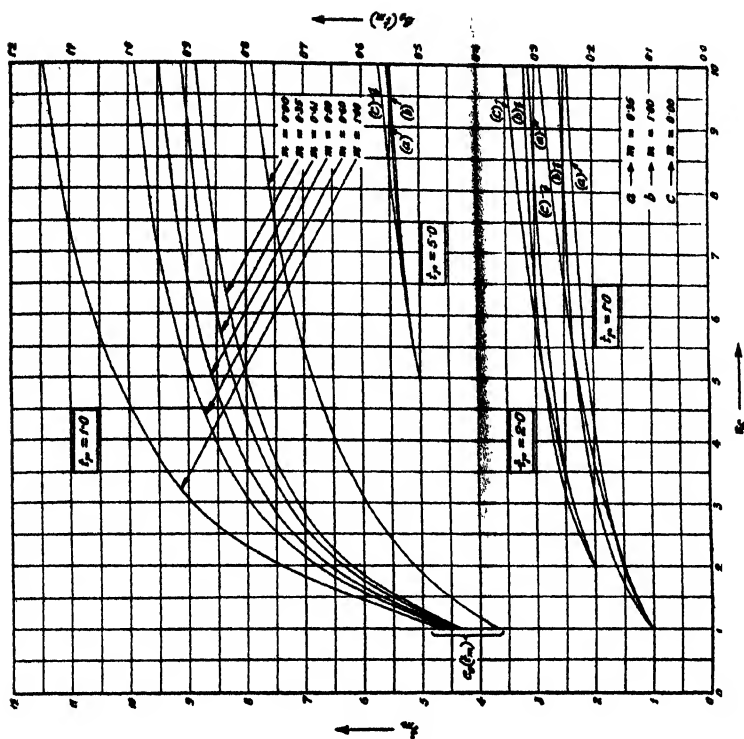


Fig. 21—A plot of  $t_r$  and  $e_r(t_r)$  against  $t_r$  for different values of  $t_f$ .

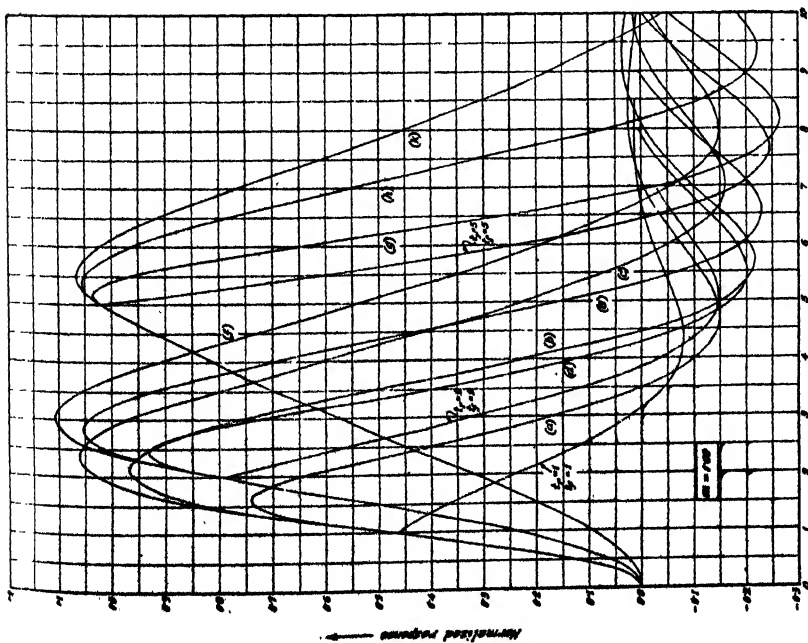


Fig. -Response of a shunt compensated amplifier to pulse with linear rise and fall ( $m=1.0$ ):

- (a)  $t_r = 1, t_f = 2$ ; (b)  $t_r = 1, t_f = 4$ ;
- (c)  $t_r = 1, t_f = 6$ ; (d)  $t_r = 2, t_f = 3$ ;
- (e)  $t_r = 2, t_f = 5$ ; (f)  $t_r = 2, t_f = 7$ ;
- (g)  $t_r = 5, t_f = 6$ ; (h)  $t_r = 5, t_f = 8$ ;
- (i)  $t_r = 5, t_f = 10$

It is noticed from the figures that the maximum amplitude gradually increases as the steepness of fall is reduced for a constant time of rise. The maximum amplitude occurs at a time  $t_m$  which lies within the interval  $t_r \leq t_m \leq t_f$ . So by differentiating the expression for the output voltage  $e_o(t)$  (equation 43) and equating  $de_o(t)/dt$  to zero we can obtain an equation the root of which is equal to  $t_m$ . The equation is given below :

$$\begin{aligned} & e^{-t/2m} \cos \left( \frac{\sqrt{4m-1}}{2m} t \right) \left[ B_1 \frac{\sqrt{4m-1}}{2m} - \frac{A_1}{2m} \right] \\ & - e^{-t/2m} \sin \left( \frac{\sqrt{4m-1}}{2m} t \right) \left[ A_1 \frac{\sqrt{4m-1}}{2m} + \frac{B_1}{2m} \right] = \frac{1}{(t_f - t_r)} \end{aligned} \quad \dots (45)$$

The values of  $t_m$  obtained by solving (45) are substituted in (43) to find out the magnitude of the maximum amplitude for particular values of  $t_r$  and  $t_f$ .

A plot of  $t_m$  against  $t_f$  for different values of  $t_r$  is given in figure 21. Only two values of  $m$ , viz. (i)  $m=0.35$  and (ii)  $m=1.00$  have been considered because of the very small change of  $t_m$  with  $m$ . Curves of the maximum amplitude  $e_o(t_m)$  have been drawn against  $t_f$  in figures 21-23 for three values of  $t_r$  viz. (i)  $t_r=1.0$ , (ii)  $t_r=2.0$  and (iii)  $t_r=5.0$ . For the sake of comparison, the maximum amplitude curves of ordinary RC-coupled amplifiers have also been included in every figure. It is noticed that the peak of the output voltage of a shunt-compensated amplifier is considerably greater than that of an RC-coupled amplifier.

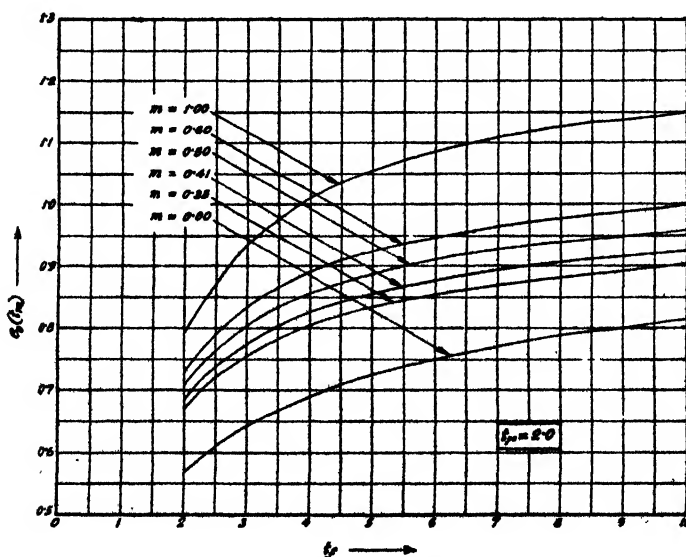
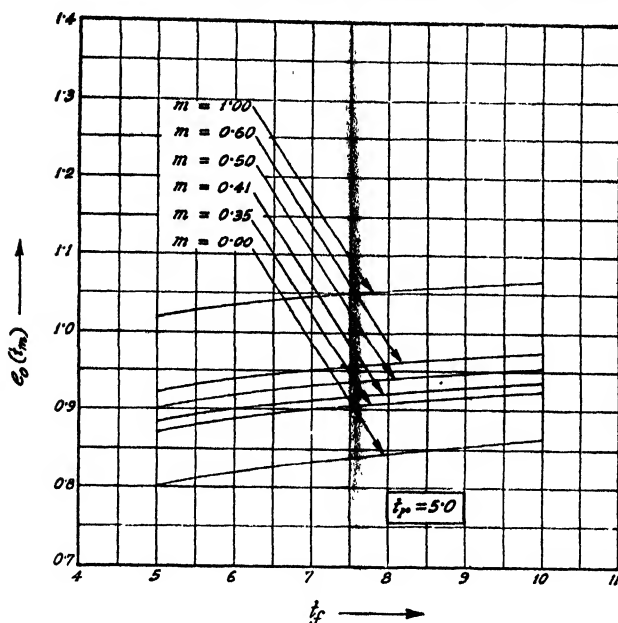


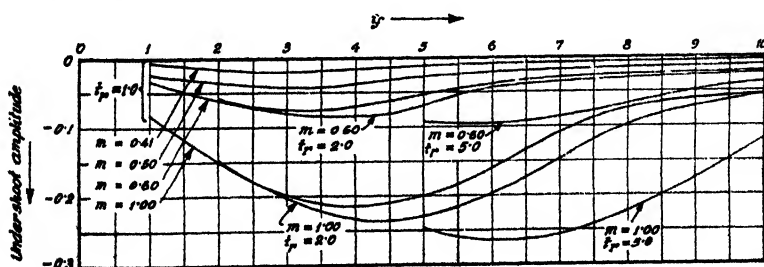
Fig. 22—A plot of  $e_o(t_m)$  against  $t_f$  ( $t_r=2.0$ ).


 Fig. 23—A plot of  $c_o(t_m)$  against  $t_f$  ( $t_r = 5.0$ ).

Figures 16–20 also indicate that the amplitudes of the undershoots are appreciable when  $m > 0.50$ . Undershoots reach the peak value at times  $t_0 > t_f$ . These points may be accurately determined by solving the following equation which is obtained by differentiating (44)

$$\left[ \frac{D_1}{2m} + C_1 \frac{\sqrt{4m-1}}{2m} \sin \frac{\sqrt{4m-1}}{2m} t - \frac{C_1}{2m} + D_1 \frac{\sqrt{4m-1}}{2m} \right] \cos \left( \frac{\sqrt{4m-1}}{2m} t \right) \quad (46)$$

The times  $t_0$  thus determined are then substituted in (44) to obtain the peak magnitude of the undershoot. The nature of variation of these peak values with change in  $t_f$  has been shown in figure 24. The other


 Fig. 24—A plot of undershoot amplitudes against  $t_f$ .

characteristics of the undershoot oscillation are similar to those observed in the case of the overshoots of a shunt-compensated amplifier for a ramp function input and may be determined in the same way as outlined previously.

## RESPONSE TO A SAW-TOOTH PULSE

When  $t_f = t_r$ , the pulse shown in figure 15 takes the shape of a saw-tooth waveform and may be represented by

$$e(t) = K \frac{t}{t_1} [u(t) - u(t - t_1)] \quad \dots (47)$$

In this case the normalized response functions are given by the following expression ( $m > \frac{1}{4}$ ):

$$e_0(t) = \frac{1}{t_r} \cdot \frac{e^{-t/2m}}{\sqrt{4m-1}} \left[ (1-m) \sqrt{4m-1} \cos \left( \frac{\sqrt{4m-1}}{2m} t \right) + (1-3m) \sin \left( \frac{\sqrt{4m-1}}{2m} t \right) \right] + \frac{1}{t_r} (t+m-1), \quad 0 \leq t \leq t_r \quad \dots (48)$$

and

$$e_0(t) = \frac{1}{t_r} \cdot \frac{e^{-(t-t_r)/2m}}{\sqrt{4m-1}} \left[ A_0 \cos \left( \frac{\sqrt{4m-1}}{2m} t \right) + B_0 \sin \left( \frac{\sqrt{4m-1}}{2m} t \right) \right] + e^{-(t-t_r)/2m} \left[ \cos \left\{ \frac{\sqrt{4m-1}}{2m} (t-t_r) \right\} - \frac{(1-2m)}{\sqrt{4m-1}} \sin \left\{ \frac{\sqrt{4m-1}}{2m} (t-t_r) \right\} \right], \quad t \geq t_r \quad \dots (49)$$

where

$$A_0 = (1-m) \sqrt{4m-1} \left[ e^{-t_r/2m} - \cos \left( \frac{\sqrt{4m-1}}{2m} t_r \right) \right] + (1-3m) \sin \left( \frac{\sqrt{4m-1}}{2m} t_r \right)$$

and

$$B_0 = (1-3m) \left[ e^{t_r/2m} - \cos \left( \frac{\sqrt{4m-1}}{2m} t_r \right) \right] - (1-m) \sqrt{4m-1} \sin \left( \frac{\sqrt{4m-1}}{2m} t_r \right)$$

The expressions of  $e_0(t)$  for the other two cases, viz. (i)  $m = \frac{1}{4}$  and (ii)  $m < \frac{1}{4}$ , will not be considered here. With the aid of equations (48) and (49) the response characteristics in the case of a saw-tooth input have been plotted in figures 16-20. It is observed from the figures that the maximum amplitude occurs at a time  $t = t_f$  and this assumes a much greater magnitude when shunt-compensation is used in an RC-coupled amplifier.

## CONCLUSION

This investigation of the effect of ramp function input on the response characteristics of shunt-compensated pulse amplifiers leads us to some interesting conclusions.

First of all, when the input pulse is not very sharp, the magnitude of peak overshoots may be made negligible for many practical applications by a suitable choice of  $m$ . For example, let us consider the case of  $t_1 = 3.5 RC$ , i.e.,  $t_r = 3.5$  and  $m = 0.5$ . Then the overshoot reaches its peak value .030854 (3 percent of the normalized value) at the time  $t_{0.1} = 5.060497$ .



Secondly, the contribution of the pulse amplifier to the rise time of the output is not at all appreciable when the build-up time of the input is not very short. If we consider the previous case, we find that  $(t_u - t_i - 0.8t_r)$  is only  $-0.008097$ . We, therefore, find that when the amplifier RC constant is several times smaller than the input pulse rise time, the transmission of the leading edge of the pulse through the amplifier may be made very faithful.

An unexpected result of this analysis is the finding that when the rise time of the input pulse becomes greater by several times the RC constant of the plate circuit, the output pulse may be sharper compared to the input for values of  $m$  higher than a lower limit which is determined by the rise time of the incoming wavefront. In the case of pulses with linear rise and fall, it has been noticed that the maximum amplitude of the output pulse and the time that corresponds to this maximum, depend very much upon times of both rise and fall of the input. The maximum amplitude of the output increases noticeably when shunt-compensation is used in an RC-coupled amplifier.

This study of pulse amplifiers using shunt compensation gives us important design information which cannot be obtained from the step-function response characteristics (Valley and Wallman, 1948). It was, therefore, felt necessary to derive the response functions of pulse amplifiers with the assumption of an input waveform the shape of which is the best approximation to that of the actual input.

#### ACKNOWLEDGMENTS

It is a pleasure to record grateful thanks to Prof. M. N. Saha, D. Sc., F.R.S., and to Prof. B. D. Nag, Ph. D., for their kind interest in the work. The author is also indebted to Mr. B. M. Banerjee for his valuable suggestions and advice during the progress of the work.

#### REFERENCES

- Bhattacharyya, B. K., 1954, *Ind. J. Phys.*, **28**, 31.
- Gardner, M. F. and Barnes, J. L., 1948 *Transients in Linear Systems*, Vol. I, Wiley, New York.
- Goldman, S., 1949, *Transformation Calculus and Electrical Transients*, Prentice-Hall Inc., New York.
- Scarborough, J. B., 1950, *Numerical Mathematical Analysis*, The Johns Hopkins Press, Baltimore.
- Valley, G. B. and Wallman, H., 1948, *Vacuum Tube Amplifiers*, McGraw Hill Book Co., Inc., New York.

# RELATIVE CROSS-SECTION OF (n, p)-REACTION IN $\text{Al}^{27}$ AND $\text{Mg}^{24}$

BY S. K. NANDI AND N. K. SAHA  
PHYSICS DEPARTMENT, UNIVERSITY OF DELHI, DELHI

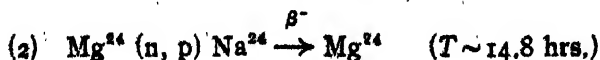
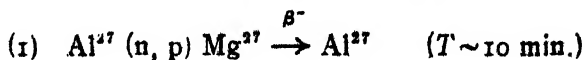
(Received for publication, June 17, 1954)

**ABSTRACT.** Using fast neutrons from a 100 mgm ( $\text{Ra}\alpha + \text{Be}$ )-source the relative cross-section of the (n, p)-reactions in  $\text{Al}^{27}$  and  $\text{Mg}^{24}$  are determined by the method of 'threshold detector' following a previous work on  $\text{S}^{32}$  and  $\text{P}^{31}$ . Rates of  $\beta$ -disintegrations from  $\text{Mg}^{27}$  ( $T=10$  min) and  $\text{Na}^{24}$  ( $T=14.8$  hrs) formed in the reactions are measured under identical geometry. Methods for applying corrections for self absorption of the  $\beta$ -rays in the active sample and due to other causes are discussed. The relative cross-sections with respect of  $\text{S}^{32}$  (n, p)-reaction are obtained as 0.11 for  $\text{Al}^{27}$  and 0.14 for  $\text{Mg}^{24}$ , showing a reasonably good agreement with the values obtained by Cohen. The importance of these results in interpreting the nuclear level-structure is discussed.

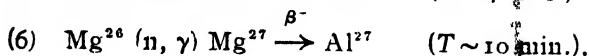
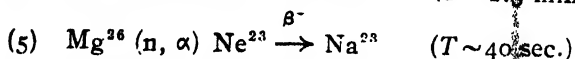
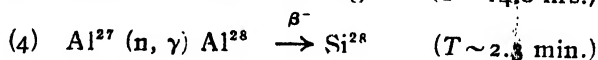
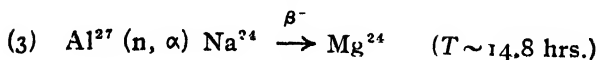
## 1. INTRODUCTION—PROPOSED WORK

It is well-known that a study of the nuclear reactions with neutrons have contributed a great deal to an understanding of the complexities of nuclear structure. Valuable informations regarding the width and spacing of energy levels of heavy nuclei in the region of about 8 MeV excitation energy have been obtained by a study of the cross-section of nuclear reactions with slow neutrons. With fast neutrons endothermic reactions of the type (n, p), (n,  $\alpha$ ), (n, 2n), etc. are possible, the (n, p) type of reaction being fairly common when the neutron energy is well above the threshold energy of the reaction. Following a previous work, by Saha and Choudhuri (1953), the method of the "threshold detector" has been employed to determine the relative cross-section of the (n, p) reactions in target nuclei which give radioactive end products of reaction. The rates of  $\beta$ -ray disintegration of two radioactive end products produced under a constant fast neutron-flux and identical geometry of irradiation of the target and also measured under identical geometry, give directly the relative cross-sections of the processes leading to the formation of those products. The results of such measurements on  $\text{Al}^{27}$  and  $\text{Mg}^{24}$  using a 100 mg ( $\text{Ra}\alpha + \text{Be}$ ) source are reported below.

The (n, p) reactions in  $\text{Al}^{27}$  and  $\text{Mg}^{24}$  consist of the following :



The other reactions which may occur in  $_{13}Al$  and  $_{12}Mg$  consist of



The product of the (n, p) reaction in  $Al^{27}$  is radio-magnesium,  $Mg^{27}$ , with mean half life  $\sim 10$  min. and that in  $Mg^{24}$  is radio-sodium,  $Na^{24}$ , of mean half-life  $\sim 14.8$  hrs. Besides these products a number of other activities are likely to develop with much less intensities due to the reactions shown under (3) to (6). Some of these activities which actually appear to develop feebly under our experimental conditions have been carefully taken into account in computing decay curves of  $Mg^{27}$  and  $Na^{24}$ , as explained later.

The saturation mass and the saturation thickness of the material to be exposed to fast neutrons are determined, these being necessary in the final measurement of the activity of the end product. Corrections are applied for (1) self absorption of  $\beta$ -rays in the active layer, (2) unsaturated period of exposure to neutron source and (3) for the isotopic composition (*i.e.*, relative abundance of the nuclear species to be activated) of the irradiated substances.

## 2. EXPERIMENTAL DETAILS

A thin-walled  $\beta$ -ray G-M tube counter mounted in a fixed position was used and the activated substance was thoroughly mixed and placed in thin co-axial cylinders just outside the counter. The radio-active end product  $Mg^{27}$  in reaction (1) above was produced by exposing pure aluminium powder to fast neutrons from the 100 mg (Ra+Be) source filtered through 1 mm cadmium. It has a half life of  $\sim 10$  min. as seen from the decay curve in figure 1. Due to (n,  $\gamma$ ) reactions and (n,  $\alpha$ ) reactions in  $Al^{27}$  a short period activity ( $T \sim 2.3$  min.) and a long period activity ( $T \sim 14.8$  hrs.) also appeared to develop with small intensities (reactions (4) and (3) above). The short period activity raised the few initial points in the decay curve and became practically negligible after a decay time of  $\sim 20$  min. The long period activity gave a residual effect of  $\sim 6$  c.p.m. appearing as a tail. These were carefully eliminated from the observed decay curve and the initial intensity of the 10 min. activity determined.

By exposing  $Mg^{24}$  to fast neutrons radio-sodium  $Na^{24}$  was formed according to the reaction (2) above. This decays with a half life of  $\sim 14.8$  hrs. as given by the decay curve in figure 2. The (n,  $\alpha$ ) reaction in  $Mg^{26}$  would give radio-neon  $Ne^{23}$  of about 40 sec. half-life and the (n,  $\gamma$ ) process in the same would give radio-magnesium  $Mg^{27}$  with a half life of  $\sim 10$  min. But since the relative abundance of  $Mg^{26}$  is only  $\sim 11\%$ , under the

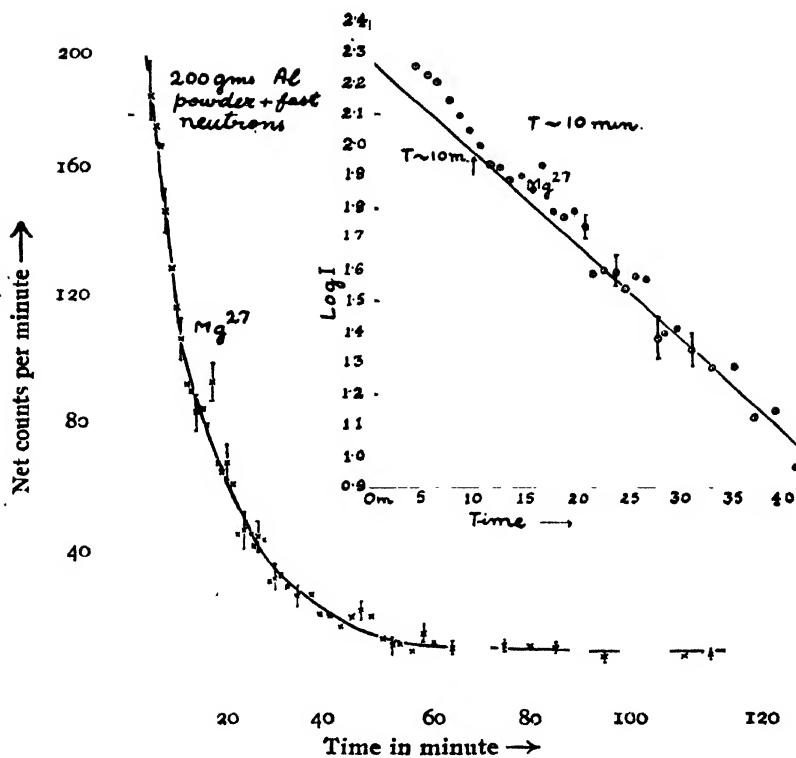


Fig. 1

Decay curve of radio-magnesium  $Mg^{27}$  showing a half life of  $\sim 10$  minutes.

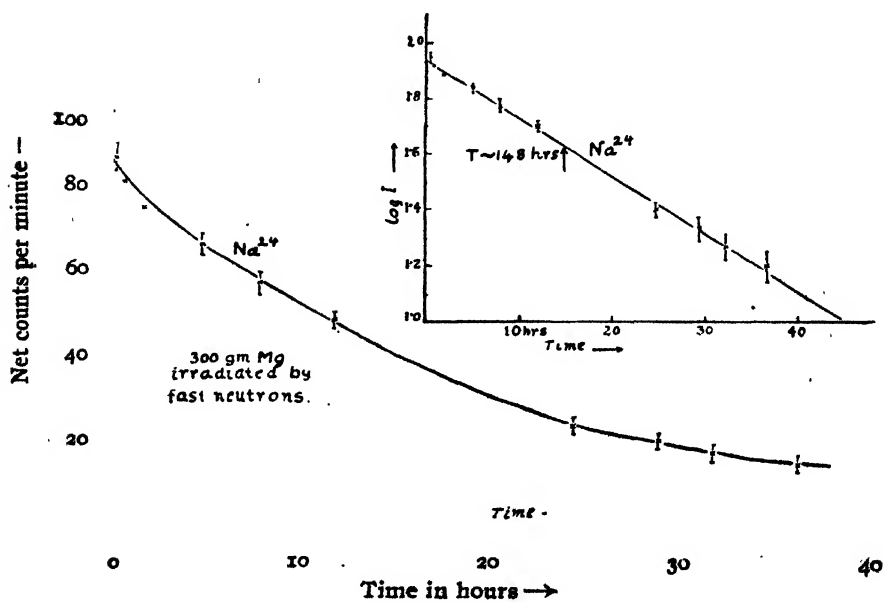


Fig. 2

Decay curve of radio-sodium  $Na^{24}$  showing a half life of  $\sim 14.8$  hrs.

condition of our fast neutron exposure there is little possibility of radio-magnesium to develop. This is proved by the fact that the observed points in figure 2 fit quite well with the 14.8 hr. slope of the decay curve almost from the beginning. Further any feeble intensity of radio-neon that might be developing completely dies out before measurements are commenced.

The saturation mass and the saturation thickness of the material to be exposed to fast neutrons ( $Al^{27}$  and  $Mg^{24}$ ) were investigated separately, this being done by identical methods used for sulphur and phosphorus (Saha and Choudhuri, 1953). The results indicate a saturation mass occurring at about 550 gms for Al and 750 gms for Mg. The thickness of the saturation layer comes out to be  $0.8 \text{ gm/cm}^2$  and  $1.27 \text{ gm/cm}^2$  in the two cases respectively.

The final measurements of the activity of radio-magnesium ( $Mg^{27}$ ) produced from  $Al^{27}$  and radio-sodium ( $Na^{24}$ ) produced from  $Mg^{24}$  by the (n, p)-reaction were carried out carefully under identical geometry as used before. The saturation mass of the substance was activated, thoroughly mixed up, and the decay curve of the well mixed active powder in a cell of saturation thickness was obtained. From the curves the initial activity comes out to be 120.2 counts/min. in  $Al^{27}$  (n, p)  $Mg^{27}$  and 73 counts/min. for  $Mg^{24}$  (n, p)  $Na^{24}$  after subtracting background.

### 3. CORRECTIONS

The following corrections were obtained :

(a) Correction for self-absorption in the thick layers of the active substance used in the final measurement was obtained by the method given by Aten (1950). If we consider an infinitesimal layer of thickness  $dx \text{ gm/cm}^2$  of the active substance with a true activity at a depth  $x$  below the surface,  $dA_t = \alpha \cdot \Omega \cdot dx$ , then the measured activity of this layer as transmitted through it becomes

$$dA_m = e^{-x/\xi} \cdot dA_t = \alpha \cdot \Omega \cdot e^{-x/\xi} \cdot dx,$$

where  $\Omega$  is the surface area of the layer and  $\alpha$ , the true activity of the sample per gm and  $\xi$  the reciprocal absorption coefficient in  $\text{gm/cm}^2$ . On integration we obtain the measured activity

$$A_m = \int_0^x \alpha \cdot \Omega \cdot e^{-x/\xi} \cdot dx = \alpha \cdot \xi \cdot \Omega \cdot (1 - e^{-x/\xi}).$$

Also  $A_t = \alpha \cdot \Omega \cdot x$ , giving finally

$$\frac{A_m}{A_t} = \frac{1 - e^{-x/\xi}}{x/\xi} \tag{1}$$

At  $x$  very large, the activity for the infinite layer becomes

$$A_{ms} = \alpha \cdot \Omega \cdot \xi, \text{ giving } \frac{A_m}{A_{ms}} = 1 - e^{-x/\xi}.$$

A plot of  $\log (1 - A_m/A_{m\infty})$  against  $x$  gives the slope of the curve as  $-1/\xi$ . In figure 3, curve (a), this plot for aluminium is shown, from which we obtain the slope  $-1/\xi = -2.3 \times 2.43 = -5.6$  and  $A_m/A_t \approx 22.3\%$  from relation (1), for a sample thickness  $x_0 = 0.8 \text{ gm/cm}^2$ . Likewise for magnesium the slope  $-1/\xi \approx -4.6$  and  $A_m/A_t = 17\%$  for a sample thickness  $1.27 \text{ gm/cm}^2$ .

The results obtained were checked by an independent method given by Metzger, Alder and Huber (1948) in which the true activities of the samples of different thicknesses converted to the activities per gm of the material are plotted as a function of the sample thickness in  $\text{gm/cm}^2$  and the corrected activity per gm extrapolated to zero thickness is determined. A plot for aluminium is shown in figure 3, curve (b), which

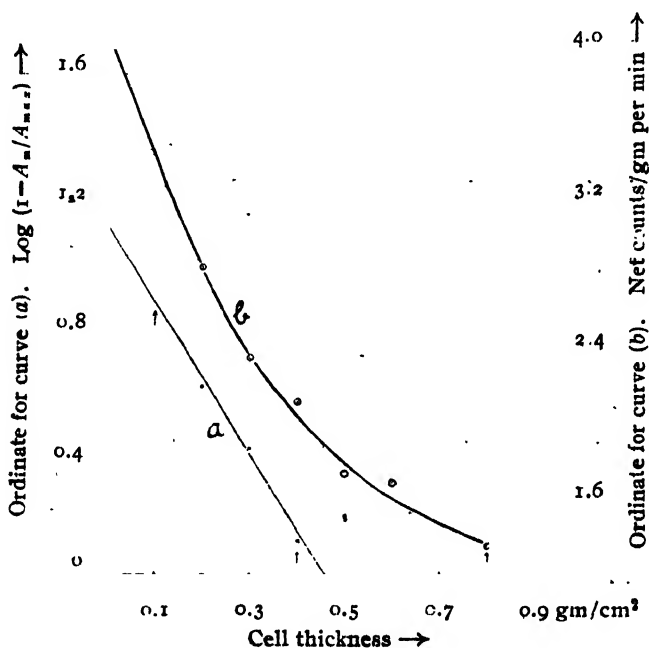


Fig. 3

Correction for self-absorption in Al.

Curve (a): The logarithmic plot for obtaining the coefficient of absorption.

Curve (b): Direct plot of activity per gm obtained at various layer thicknesses used for extrapolation to zero thickness.

gives  $A_m/A_t = 1.0/4.3 = 23\%$ . The Mg-curve (not shown) likewise gives  $A_m/A_t \approx 0.3/1.95 = 15\%$ . These results agree well with those obtained by the earlier method.

(b) Correction for isotopic composition of the activated substance was necessary for  $\text{Mg}^{24}$ . The relative abundance for  $\text{Mg}^{24}$  being 77.4%, a correction factor of  $100/77.4$  is therefore necessary to convert to the 100% pure isotope. For  $\text{Al}^{27}$  no correction is necessary.

(c) Correction for the non-saturation time of irradiation to the fast neutron source was applied to the observed activity for  $\text{Mg}^{24}$ . The

multiplication factor for converting the observed activity to that at infinite exposure is  $(1 - e^{-\lambda t})^{-1} = (1 - e^{-\frac{0.693t}{T}})^{-1}$ ;  $t$  being the time of exposure and  $T$  the mean half life)  $\approx 1.05$ .

The sample of  $Al^{27}$  was always irradiated for 6 times the decay period and hence practically no correction is necessary on this account.

## RESULTS

The initial activity for aluminium reaction for the saturation sample of Al after applying the above corrections comes out to be

$$A_{\infty} = \frac{120 \text{ counts/min}}{60 \text{ sec}} \times \frac{1}{0.23} \approx 8.7 \text{ counts/sec.}$$

For the saturation sample of Mg, the corresponding initial activity is

$$A_{\infty} = \frac{73 \text{ counts/min}}{60 \text{ sec}} \times 1.05 \times \frac{100}{77.4} \times \frac{1}{0.15} \approx 11.2 \text{ counts/sec.}$$

Using the measured initial activity from the  $S^{32}$  (n,p)-reaction to be 79 cps (Saha and Choudhury, 1953), we obtain the relative cross-sections :

$$\frac{\sigma(n, p)Al^{27}}{\sigma(n, p)S^{32}} \approx 0.11 ; \quad \frac{\sigma(n, p)Mg^{24}}{\sigma(n, p)S^{32}} \approx 0.14$$

with a probable error of  $\pm 10$  to 15%.

## DISCUSSION

Similar measurements of cross-section of (n, p)-reactions in Al and Mg have been made by Cohen (1951) by using  $d^2-d^2$  neutron source upto 18 MeV who has obtained the values 25 mb for  $Al^{27}$  and 39 mb for the  $Mg^{24}$  reaction. The ratio of the two cross-sections comes out to be 1.56 which compares favourably with our result obtained at a much lower neutron energy. Forbes (1952) has determined the reaction cross-section for  $Al^{27}$  to be 79 mb at a maximum neutron energy of  $\sim 14$  MeV. There seems to be considerable divergence of values obtained by these authors.

It is known from theoretical formulae (Feschbach, Peaslee and Weisskopf, 1947) that for a given fast neutron energy in this region, any variation in the cross-section from isotope to isotope reflects mainly the variation in the level spacing  $D$  of nuclei. It would therefore be expected that at neutron energy above the reaction threshold, the cross-section would increase with the nuclear mass, quite rapidly at first, as  $D$  decreases with increasing complexity of the nucleus and then for heavy nuclei would change only slowly. The cases of  $Mg^{24}$  and  $Al^{27}$ , however, do not appear to fit in this scheme. It is, therefore, important that the average level behaviour of the nuclei, particularly the level spacing  $D$ , would be obtained from a measurement of the absolute cross sections at a suitable neutron energy. Any unusual behaviour of a nucleus observed in this respect should be

correlated to an unusual binding energy of the neutron in the nucleus. The study of fast neutron reaction cross-section for the even-even and even-odd isotopes is important in this respect. With a view to verifying these theoretical conclusions, similar measurements of  $(n, p)$ -reaction cross-sections have been made in  $S^{32}$ ,  $P^{31}$  and  $Fe^{56}$ , besides the present cases, and a few more measurements have been taken in hand. A consolidated account will be presented when the present series of measurements are complete.

#### ACKNOWLEDGMENTS

In conclusion we wish to express our sincere thanks to Prof. D. S. Kothari and to Prof. R. C. Majumdar of this department for allowing us facilities for doing this work. The present work forms part of a research scheme under the auspices of the Atomic Energy Commission, Government of India, whose financial support we gratefully acknowledge.

#### REFERENCES

- Aten, A. H. W. 1950, *Nucleonics* VI, 1, 68  
Cohen, B. L., 1951, *Phys. Rev.*, **81**, 184  
Feschbach, Peaslee and Wesiskopf, 1947, *Phys. Rev.*, **71**, 145.  
Forbes, S. G., 1952, *Phys. Rev.*, **88**, 1309.  
Metzger, F., Alder, F., and Huber, P., 1948, *Helv. Phys. Acta*, **21**, 278.  
Saha N. K. and Choudhuri M., 1953, *Ind. J. Phys.*, **27**, 244.



# ANALYSIS OF THE ULTRAVIOLET FLUORESCENCE SPECTRA OF $I_2$ MOLECULE

By C. V. NARAYANA RAO AND V. RAMAKRISHNA RAO

DEPARTMENT OF PHYSICS, ANDHRA UNIVERSITY, WALT AIR

(Received for publication, July 16, 1954)

## Plates XVA-D

**ABSTRACT.** New and improved wavelength data on the fluorescence bands of iodine vapour excited by mercury lines is given. Wavelength data on McLennan bands is obtained from thallium spark excitation for the first time. A complete analysis of these fluorescence bands in the region  $\lambda\lambda$  4738—1959 Å. U. is presented for the first time. Four new electronic states in Mulliken's term scheme for  $I_2$  molecule are identified. It is suggested that no resonance series are obtained in ultraviolet on excitation with mercury arc lines.

## INTRODUCTION

The fluorescence spectrum of iodine vapour is one of the most extensively studied topics. All the important results have been summarised by Pringsheim in his masterly treatise on "Fluorescence and Phosphorescence" (1949). Dealing with the ultraviolet band systems in fluorescence he says that their analysis is by far less complete than that of the visible bands. Almost all data referring to the upper states are missing. Iodine is one of the few molecules in which we get information about the upper states from fluorescence data, on account of the rich fluorescence spectrum it gives in the ultraviolet. In the absence of a satisfactory analysis of all these bands it is felt worth while to take up an exhaustive investigation of these ultraviolet fluorescence bands.

Oldenberg (1923) discovered this ultraviolet fluorescence giving the resonance spectra on irradiating the vapour with mercury lines 1849 and 1942 Å, the bismuth line 1903 Å and the zinc line 1900 Å. For only the last of these spectra, the wavelengths of the individual members have been published. They were interpreted as forming the resonance series from 5th anti-Stokes member to the 35th Stokes member. The data on the resonance spectrum excited by mercury lines is not available in literature. While no bands were recorded below 2100 Å by Oldenberg on excitation with mercury radiations, he claims that the other bands measured by him form two resonance series. He also mentions that some bands in the region below 2310 Å, are of a doublet or a triplet character with a separation of 7 Å. U. He further observes two pairs of bands at 1887 and 1910 Å, which have a splitting of 0.9 and 1.1 Å. U. respectively. The explanation of the splitting is not clear. In the visible

resonance series the splitting was observed to be about 0.2 A.U. representing the rotational splitting. The splitting observed by Oldenberg is by far greater than the above rotational splitting and so cannot be assigned to the rotational level separations in the vibrational states of the ground state of  $I_2$  molecule. In such a case the nature of the splitting requires close investigation.

The most interesting and complicated bands appear to be those discovered by McLennan and named after him. They extend from 4600 to 2100 Å and were obtained on irradiating the vapour with mercury lines 1849 and 1942 Å, and Al, Zn, Cd, Mg sparks. Experimentally it was established that these bands were excited only by wavelengths less than 2100 Å. They were recorded by him on a low dispersion instrument. They were diffuse and spread out into various groups, the one between 3300 and 3100 Å being most conspicuous. McLennan observed that for most of these bands the wavelengths are independent of the exciting radiation. Though qualitative groupings of these bands have been made by Duschinsky and Pringsheim, they admit that they are not of any special significance. An analysis of these bands has not been made till now perhaps due to lack of a complete understanding of the possible electronic states of  $I_2$  molecule.

Mulliken (1935) worked out the complete term scheme in iodine with possible locations of the various configurations with respect to one another. There has been a considerable progress recently on the analysis of the emission and absorption bands of iodine. Venkateswarlu (1946, 1947) analysed the emission bands of iodine and identified a number of electronic states in the scheme given by Mulliken. He observed some coincidences between these Mc bands and those obtained by him and others (Curtis and Evans, 1933) in emission. He suggested therefore that these Mc bands could be explained on the same basis as his interpretation for the emission bands. It was felt that a thorough investigation of this casual suggestion is desirable.

Pringsheim points out a long regular sequence of fluctuations in the region below 2500 Å, with a spacing of  $\Delta\nu \sim 380 \text{ cm}^{-1}$  appearing simultaneously with the resonance progression. This  $\Delta\nu$  of  $380 \text{ cm}^{-1}$  is claimed to be about twice the ground state frequency (215) and does not find an easy explanation. These points needed clarification. It was also necessary to pick out the resonance series excited by mercury radiation, if any, and separate their wavelength data which do not exist in literature, from that of the Mc bands. Then we might be able to understand the nature of the so called splitting observed by Oldenberg in some bands. Also the various casual suggestions regarding the origin of the Mc bands had to be thoroughly examined and the exact states involved in the emission of these bands are to be identified. Their nature, whether repulsive or non-repulsive has also to be determined.

## EXPERIMENTAL

A pyrex glass tube of the special form suggested by Wood, with a strain-free bulb at one end and a Wood's horn at the other has been prepared and used for work in the visible region. Instead of the bulb, a quartz-to-pyrex graded seal tube with a fused-in quartz window is attached to the above tube for work in ultraviolet. A side tube is provided with a constriction to evacuate and seal off with iodine crystals in it. Under such conditions the fluorescence tube contains only iodine crystals and its vapour at a pressure corresponding to the saturated vapour pressure of the substance at a given temperature. For the work in visible region a Fuess spectrograph which has a dispersion of 16Å/mm at 4200 Å has been used. Hilger small quartz spectrograph having a dispersion of 19Å/mm at 2500 Å and medium quartz spectrograph having a dispersion of 10Å/mm at 2700 Å and 5Å/mm at 2200 Å, are used for investigations in ultraviolet. Spectra in visible region have been recorded on HP3 and Ilford panchromatic plates, whereas Ilford Selochrome, Special Rapid, Q2 and Q3 plates have been employed in ultraviolet region. A quartz mercury arc run on 220 D. C. at 3.5 amps. and a thallium spark run on a 20,000 volts transformer are the sources of excitation. With thallium spark an exposure of 120 hrs. in ultraviolet region and 150 hrs. in visible region are required with a slit width of about 400 microns, whereas with the mercury arc 48 hrs. in ultraviolet and 24 hrs. in visible were sufficient with a slit width of 230 microns. In the case of the mercury arc special precautions are taken to avoid all extraneous radiation.

## RESULTS

With mercury arc excitation the Mc bands could be obtained in the region 4569 to 1942 Å and with thallium spark in the region 4738 to 2035 Å (figures 1, 4 and 5 in Plates XVA and XVC). As seen from Table I, there is a close agreement between our data and these of McLennan's in the region 2800 to 2100 Å, whereas there is a considerable deviation in the region 4600 to 2800 Å. A close band to band examination reveals that our data is more accurate. McLennan bands in the visible region excited by mercury arc and recorded on a Fuess spectrograph (which has a higher dispersion in this region than the medium quartz spectrograph) gave more accurate data and revealed four discrete bands instead of the continuum at 4130 to 4015 Å, as reported by McLennan. The other data are also claimed to be accurate within an error of 1 to 2 Å.U. as a result of the higher dispersion we could use than McLennan.

## ANALYSIS

The starting point of our analysis of the Mc bands was the analysis of the emission bands of iodine in that region by Vankateswarlu. Of all the terms given in Mulliken's term scheme, Venkateswarlu was able to identify fifteen terms and attribute various band groups to transitions between those

terms. The diffuse nature of the bands and the absence of a development as a whole of any system was explained by his suggestion that most of the transitions involved are between a stable state and various repulsive states. His work and that of Mulliken established the fact that in  $I_2$  molecule case  $c$  type coupling holds good rather than cases  $a$  and  $b$ .

TABLE I

McLennan's data $\lambda$ (A.U.)	Present measurements			
	Mercury arc		Thallium spark	
	Intensity	$\lambda$ (A.U.)	Intensity	$\lambda$ (A.U.)
			8	4738
			6	4703
			6	4641
			6	4605
4608				
4550	1	4569	1	4570
			2	4532
4505	0	4512		
4452	1	4458	4	4454
	1	4408		
			2	4358
			1	4339
4290			2	4303
	1	4269		
4250	2	4238	2	4246
4210	2	4196	2	4200
4170	1	4152	4	4156
4130	0	4118	4	4130
	2	4090	4	4099
			3	4055
4015	2	4005		
			2	3979
3925	3	3926	2	3922
3870	4	3857	2	3852

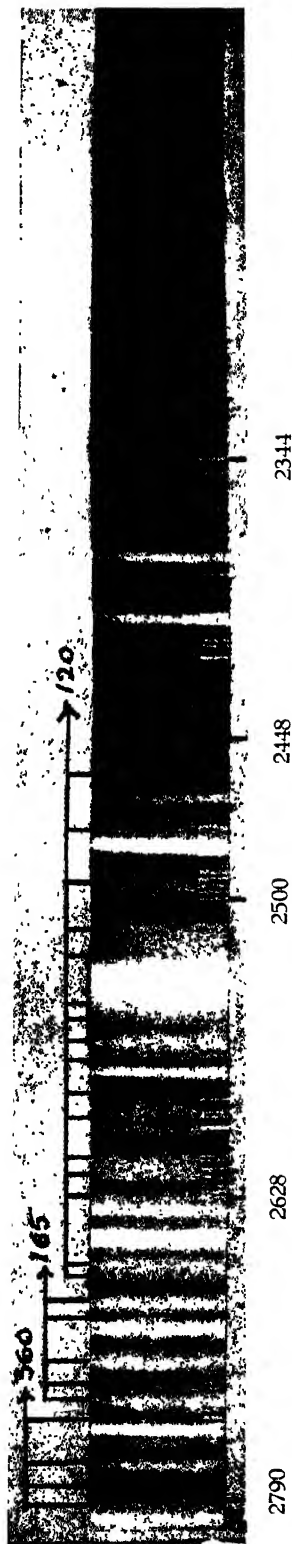
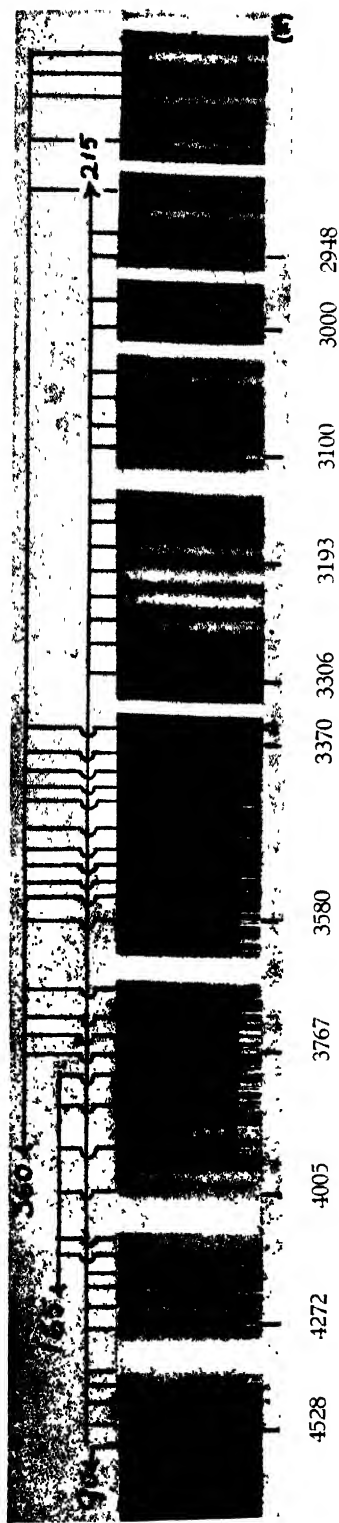


Fig. 1. McLennan bands of I<sub>2</sub> vapour excited by Hg arc, on medium quartz spectrograph. They are marked as different groups, into which they have been analysed. The numbers 90, 120 etc. are the values of  $\omega_e$ , in units of  $\text{cm}^{-1}$ , of the upper states from which the groups arise, due to transitions to lower repulsive states. The wavelengths of standard iron lines are marked in Å U.

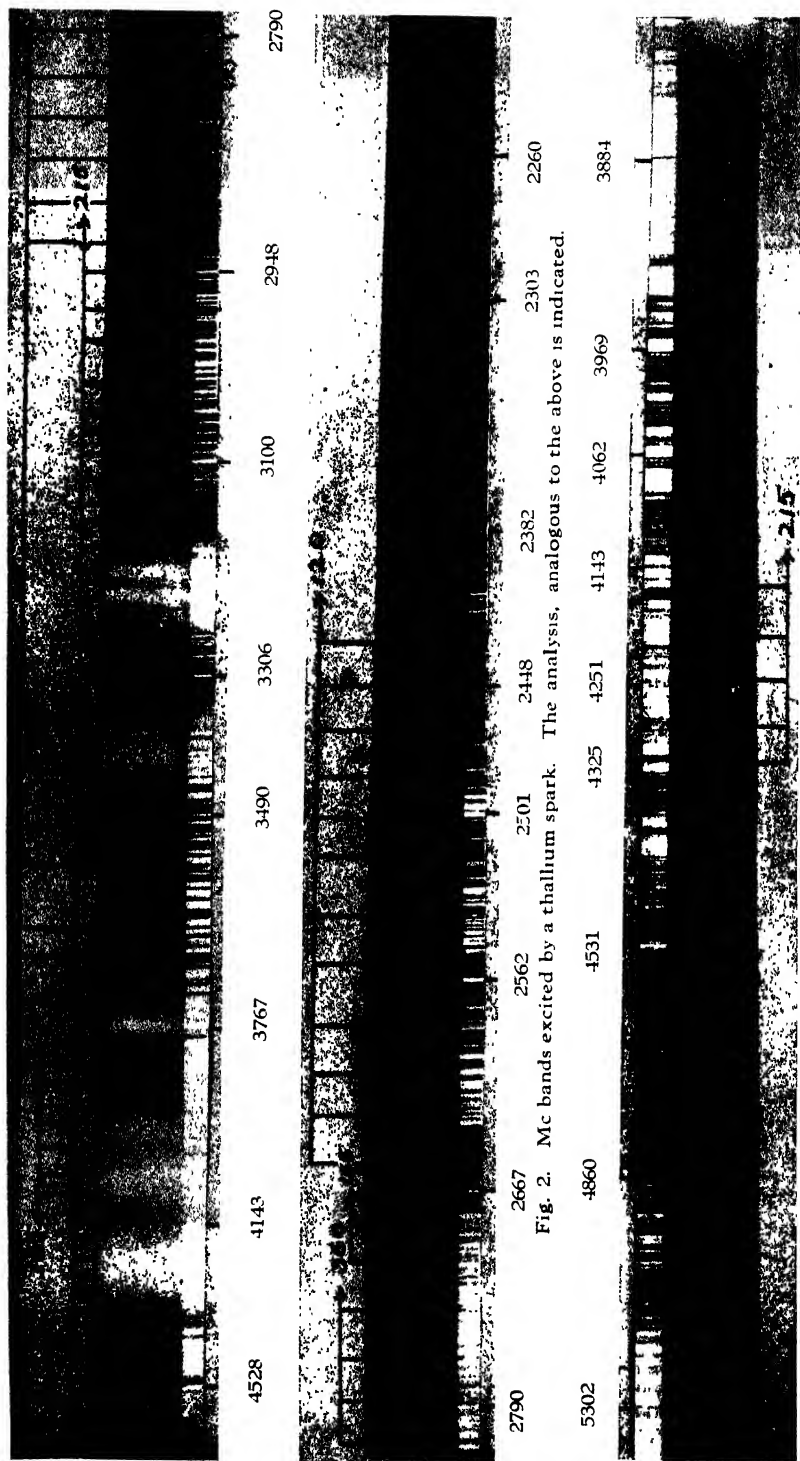


Fig. 3. Mc bands in visible excited by thallium spark and recorded on Fuess spectrograph.

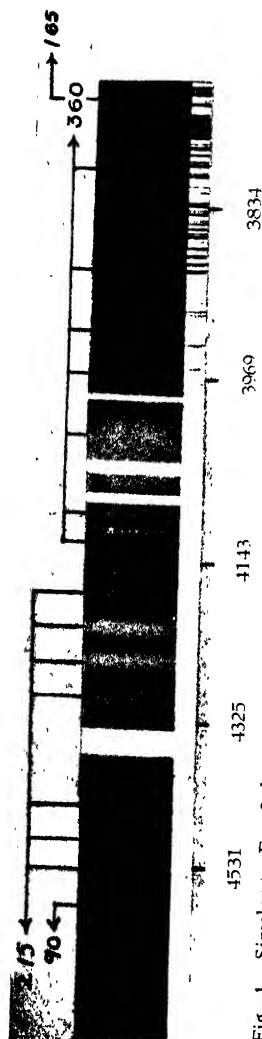


Fig. 4. Similar to Fig. 3, but excited by a mercury arc and reveal greater number of bands. On analysis they are grouped as indicated

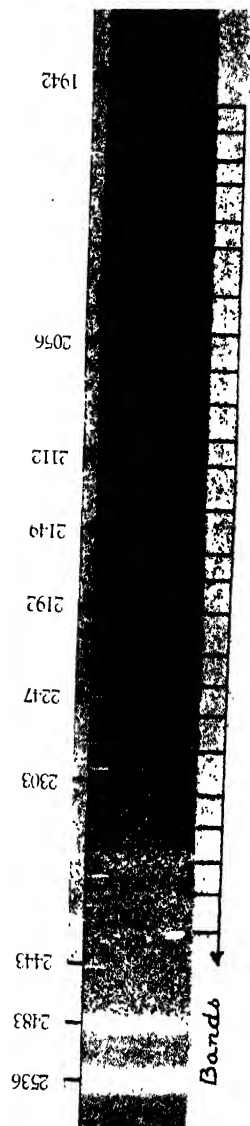


Fig. 5. Hg bands below 2500 Å.U. recorded on a small quartz spectrograph, showing the extension upto 1942 Å.U., the exciting mercury line

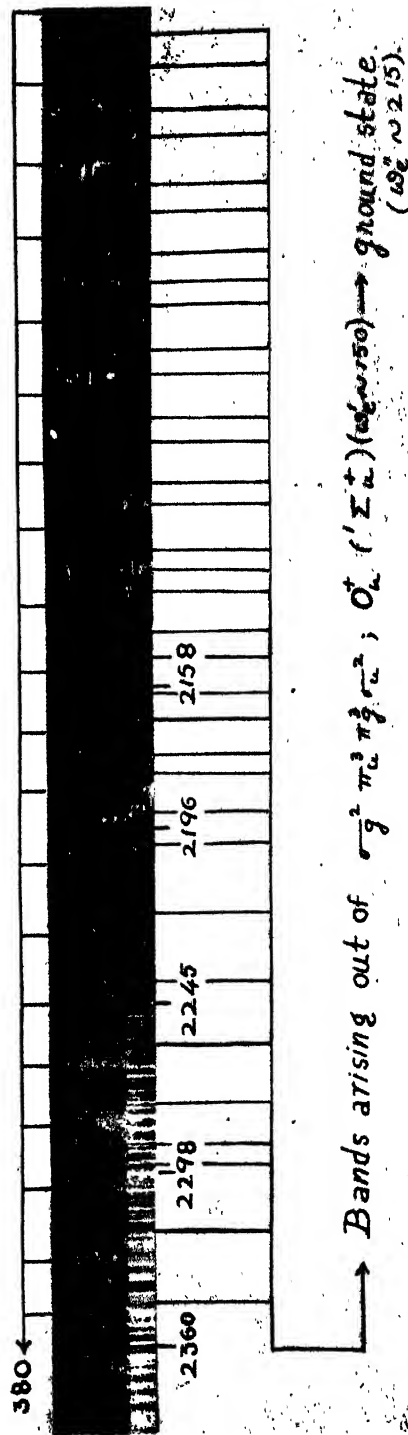


Fig. 6

Fig. 6. Bands below 2400 Å U. recorded on Ilford Q3 plate with a medium quartz spectrograph, excited by mercury lines. Bands with  $380 \text{ cm}^{-1}$  successive differences arise out of a transition from an upper repulsive state to a lower state ( $\omega_e = 380$ ). Other bands represent a system involving the ground state ( $\omega_e = 215$ ) and a stable upper state ( $\omega_e = 150$ ).



TABLE I (contd.).

McLennan's data $\lambda$ (A U.)	Present measurements			
	Mercury arc		Thallium spark	
	Intensity	$\lambda$ (A.U.)	Intensity	$\lambda$ (A U.)
3800	2	3805	2	3795
	2	3777		
	0	3750		
3725	0	3730	3	3732
	1	3699		
	2	3673	2	3668
3525			2	3640
			2	3607
3585	4	3585		
3555	1	3554		
	1	3539	2	3543
3520	1	3512		
	0	3504	2	3495
3475	2	3468	3	3475
3445	1	3436	2	3446
3420	1	3414	4	3415
3395	3	3383	4	3392
3365	0	3355	4	3364
			4	3353
			3	3318
3315				
3290	4	3301	3	3302
3266	8	3276	3	3282
3245	10	3252	4	3253
3220	10	3229	6	3230
3195	10	3205	3	3202
3175	9	3182	4	3178
	4	3162	4	3157
	3	3135	4	3141
	3	3123	4	3121

TABLE I (contd.)

McLennan's data $\lambda$ (A.U.)	Present measurements			
	Mercury arc		Thallium spark	
	Intensity	$\lambda$ (A.U.)	Intensity	$\lambda$ (A.U.)
3107				
3090	6	3097	4	3096
3065	1	3077	2	3076
	6	3057	4	3058
3047	6	3038	4	3038
3009	4	3000	3	3003
2993	5	2984	4	2984
2960				
2946	4	2951	2	2951
2930	3	2935	3	2929
2915				
2900	5	2904	2	2899
2883	6	2874	3	2871
2853	6	2845	3	2857
2825	1	2832		
	4	2819	2	2815
2799	4	2793	2	2790
	1	2780		
2774	4	2771	2	2766
2760	2	2745	2	2740
2737	4	2735		
2727	2	2725	4	2725
2715	6	2714	4	2709
2697	4	2701		
2685	8	2683	4	2684
	4	2671		
2667	6	2662	4	2656
2638				

TABLE I (contd.)

McLen. an's data $\lambda$ (A U)	Present measurements			
	Mercury arc		Thallium sparks	
	Intensity	$\lambda$ (A.U.)	Intensity	$\lambda$ (A.U.)
2628	4	2629	3	2632
2622	4	2621		
2617				
2612	1	2612	2	2610
2594	3	2591		
2580	2	2582	2	2581
	2	2568		
2560	6	2561	2	2556
	1	2552		
2545	2	2545		
			2	2534
	1	2520		
2515	1	2516		
	2	2512	2	2512
2495	8	2495	2	2491
2476	6	2470	2	2474
2450	6	2453	2	2458
			2	2444
2426	8	2427	2	2425
2408	8	2408	2	2407
2382	8	2386	2	2381
2360	7	2363	2	2361
2340	6	2345	2	2340
	4	2329		
2320	6	2322	2	2322
	2	2308		
2300	5	2300		
	3	2287	2	2292

TABLE I (contd.)

McLennan's data $\lambda$ (A.U.)	Present measurements			
	Mercury arc		Thallium spark	
	Intensity	$\lambda$ (A.U.)	Intensity	$\lambda$ (A.U.)
2277	5	2279		
	4	2263	2	2266
2254	4	2257		
2237	3	2246	2	2239
2218	3	2226	2	2220
2195	3	2205	1	2196
2170	2	2182	1	2176
2162	2	2161		
2148	2	2142	1	2148
2129	1	2122	1	2121
	1	2103	1	2103
	1	2084	1	2081
	1	2066	1	2066
	1	2052	1	2057
			1	2047
	1	2034	1	2035
	1	2020		
	1	2005		
	1	1989		
	1	1971		
	1	1959		
	2	1942		

Tables II, III, IV, V, VI include all Mc bands extending from the visible region down to  $40754\text{ cm}^{-1}$ . Table II contains five groups of bands arising out of a transition from the stable state  $\sigma_g\pi^4u\pi^3g\sigma^2u$ .  $1g(^3\Pi_{1g})$  with  $\omega \sim 215$  to various repulsive states as identified by Venkateswarlu. A few bands excited by mercury arc radiations do not appear among those excited by thallium spark and vice versa. The bands given in our data do not always agree with those in the data due to Venkateswarlu. But the differences of the order of  $215\text{ cm}^{-1}$  appear to be genuine. The transition being between a

TABLE II

Bands arising out of transition from a stable state  $\sigma_g\pi^4u\pi^3\sigma^2u$ .  $I_0(^3\Pi_{1g})$  with  $\omega \sim 215$  to various repulsive states (figures 1 and 2).

Mercury arc		Transition	Thallium spark	
$\nu(\text{cm}^{-1})$	$\Delta\nu$		$\nu(\text{cm}^{-1})$	$\Delta\nu$
22157	268	$I_0 \rightarrow \sigma_g^2\pi_u^3\pi_g^3\sigma_u^2$ . $I_u(^3\Sigma_u^+)$	22445	$3 \times 198$
22425			23040	
22680	255		23233	193
23418	171	$I_0 \rightarrow \sigma_g^2\pi_u^3\pi_g^3\sigma_u^2$ . $O_u(^3\Sigma_u^+)$	22940	$3 \times 198$
23589			23545	
23826	237		23803	258
24078	252		24055	252
30285	231	$I_0 \rightarrow \sigma_g^2\pi_u^3\pi_g^3\sigma_u^2$ . $I_u(^3\Delta_{1u})$	30281	179
30516			30460	
30741	225		30732	272
30960	219		30951	219
31192	232		31221	270
31418	198	$I_0 \rightarrow \sigma_g^2\pi_u^3\pi_g^3\sigma_u^2$ . $I_u(^3\Delta_{1u})$	31457	210
31616			31667	
31889	$2 \times 196$	$I_0 \rightarrow \sigma_g^2\pi_u^3\pi_g^3\sigma_u^2$ . $2_u(^3\Delta_{2u})$	31828	204
32280			32032	
32490	210		32292	258
32702	205	$I_0 \rightarrow \sigma_g^2\pi_u^3\pi_g^3\sigma_u^2$ . $I_u(^3\Pi_u)$	32500	210
32907			32692	
33324	$2 \times 209$		32907	215
33502	178		33290	$2 \times 192$
33877	$2 \times 178$		33502	212
34062	185		34131	$3 \times 210$

TABLE III.

Bands arising out of transition from a stable state  $\sigma_g\pi_u^4\pi_g^4\sigma_u$   $O^+(^1\Sigma^+u)$  with  $m \sim 165$  to various repulsive states (figures 1 and 2).

Mercury arc		Transition	Thallium spark	
$\nu(\text{cm}^{-1})$	$\Delta\nu$		$\nu(\text{cm}^{-1})$	$\Delta\nu$
24277	166 3 × 173	$O_u^+ \rightarrow \sigma_g^2\pi_u^4\pi_g^3\sigma_u^2$ $O_g^+(^1\Sigma_g^+)$	24055	151 183 2 × 133 3 × 157
24443			24206	
24962			24389	
			24654	
			25125	
25464		$O_u^+ \rightarrow \sigma_g^2\pi_u^4\pi_g^3\sigma_u^2$ $O_g^+(^3\Sigma_g^-)$	25490	
25920		$O_u^+ \rightarrow \sigma_g^2\pi_u^4\pi_g^2\sigma_u^2$ $I_g(^3\Sigma_g^-)$	25953	
26274		$O_u^+ \rightarrow \sigma_g^2\pi_u^3\pi_g^4\sigma_u$ $I_g(^1\Pi_u)$	26343	
36552	134 149 177 2 × 130	$O_u^+ \rightarrow \sigma_g^2\pi_u^3\pi_g^4\sigma_u$ $O_g^+(^3\Pi_{ug})$	36903	2 × 172
36686			37247	
36835				
37012				
37261				

stable upper state and a repulsive lower state, the band system corresponds only to a single progression containing the upper state frequencies. If different sets of vibrational levels in this state are responsible for the emission and fluorescence bands, then the wavelength positions need not be the same in both cases. This might possibly explain any discrepancy between the emission and fluorescence data. For instance, two progressions excited by mercury arc start at 23418 and 30285  $\text{cm}^{-1}$ , whereas 22948 and 30006  $\text{cm}^{-1}$  are the starting points for similar progressions in emission data. These transitions given in Table II from  $I_u$  to five repulsive lower states are able to account for 23 bands (figures 1 and 2).

The upper state  $I_u$  ( $^3\Pi_{1g}$ ) is located at 51528  $\text{cm}^{-1}$  by Venkateswarlu from the data on the dissociation limits and products and the first bands of three of the groups given by him. The first bands in our groupings are systematically of a higher frequency than those given by Venkateswarlu to a maximum of 500  $\text{cm}^{-1}$ . In the light of the above explanation we can consider that at least two higher vibrational quanta are involved in the transition giving rise to fluorescence spectrum. If this interpretation is valid

then the approximate value of the height of the  $1_g$  state may be confirmed to be  $51528 \text{ cm}^{-1}$ . The five lower states  $1_u(^3\Sigma^+_u)$ ,  $0_u(^3\Sigma^+_u)$ ,  $1_u(^3\Delta_{1u})$ ,  $2_u(^3\Delta_{2u})$ ,  $1_u(^1\Pi_u)$  may be confirmed at 29399, 28580, 21522, 19712,  $18878 \text{ cm}^{-1}$  respectively as located by Venkateswarlu.

A similar procedure and explanation led us to the identification of five groups of bands arising out of transitions from a stable upper state  $\sigma_g\pi^4_u\pi^4_g\sigma_u 0^+_u(^1\Sigma^+_u)$  with  $\omega \sim 165$  to various repulsive states. The groups and transitions are set out in Table III. In three transitions  $0^+_u \rightarrow ^3\Sigma^-_g$ ,  $1_g(^3\Sigma^-_g)$ ,  $^1\Pi_g$  we find only one band each. The assignment of these single bands has been made possible by comparison with the emission data. Venkateswarlu obtained only pairs of bands with separation of about  $165 \text{ cm}^{-1}$  and assigned these transitions. We obtained one component each in these pairs and hence the assignment. 11 bands excited by mercury lines and 10 bands excited by thallium lines are assigned to these transitions.

The determination of the heights of these levels is more reliable than in the earlier case. The upper state  $0^+_u(^1\Sigma^+_u)$  was located at  $51683 \text{ cm}^{-1}$  from an analysis of the Cordes bands in the region 1950 to 1794 Å. The lower states  $0^+_g(^1\Sigma^+_g)$ ,  $0^+_g(^3\Sigma^-_g)$ ,  $1_g(^3\Sigma^-_g)$ ,  $1_g(^1\Pi_g)$ ,  $0^+_g(^3\Pi_g)$  may be considered to be at 27619, 26345, 25916, 25525,  $14821 \text{ cm}^{-1}$  respectively.

There are three groups of bands with separations of the order of  $120 \text{ cm}^{-1}$  assigned to three transitions from a stable upper state  $1_g(^1\Pi_g)$  with the configuration  $\sigma_g\pi^4_u\pi^3_g\sigma^2_u$  to three repulsive states (Table IV) (figures 1 and 2). In the first two transitions more bands are obtained in the mercury source while there is an equal number of bands in mercury and thallium sources in the third group. A maximum number of 17 bands are assigned to these transitions. The state  $1_g(^1\Pi_g)$  is fixed up at  $58572 \text{ cm}^{-1}$  and the lower states  $1_u(^3\Delta_{1u})$ ,  $2_u(^3\Delta_{2u})$ ,  $1_u(^1\Pi_u)$  at 21522, 19712,  $18878 \text{ cm}^{-1}$ . The process of identification of these states was the same as that adopted in the case of the states giving rise to the bands with separations of  $215 \text{ cm}^{-1}$  (Table II).

Table V contains five groups of bands with separations of about  $360 \text{ cm}^{-1}$ . The transitions were suggested to be from the stable state  $\{\sigma^2_g\pi^4_u\pi^3_g; ^3\Pi_{g,1/2}\sigma^2_g\}^3\Pi_{2,1g}$  to five different repulsive states. As could be seen from the table there is better consistency in the values of  $\Delta\nu$  in these transitions than in previous cases. The progression with  $34062 \text{ cm}^{-1}$  as its first band started with  $34432 \text{ cm}^{-1}$  in case of emission bands. But this agrees with the second band  $34425 \text{ cm}^{-1}$  in our data. So the actual location of the repulsive state  $1_u(^3\Delta_{1u})$  has to be fixed at  $21892 \text{ cm}^{-1}$  instead of at  $21522 \text{ cm}^{-1}$  as given by Venkateswarlu. The stable state  $^3\Pi_{2,1g}$  has been identified at  $56000 \text{ cm}^{-1}$ , and the other repulsive states  $1_u(^3\Sigma^+_u)$ ,  $0_u(^3\Sigma^+_u)$ ,  $2_u(^3\Delta_{2u})$ ,  $1_u(^1\Pi_u)$  may be identified at 29399, 28580, 19712,  $18878 \text{ cm}^{-1}$  respectively.

There are about 6 bands (in mercury arc source) and 3 bands (in thallium source) in the region 3750 to 3383 Å not fitting into any one of these transitions. They have a mean separation of about  $360 \text{ cm}^{-1}$ . These bands are not contained in the list of emission bands given by Venkateswarlu. They

could not be connected with any of the bands given in the earlier tables. The value of the separations is the same as that to be found in Table V. This suggests that these bands may arise out of the same upper state as those contained in Table V. The lower state may be likewise identified as a repulsive state  $\sigma_g^2 \pi_u^3 \pi_g^3 \sigma_u^2$ ;  $o_u^- (^1\Sigma_u^-)$ . This newly identified transition is tabulated as a continuation of Table V because of the common upper state. It is interesting to note that this transition occurs only in fluorescence but not in emission. It may be added, however, that the lower state  $o_u^- (^1\Sigma_u^-)$  was suggested to be involved in another transition with  $\sigma_g \pi_u^4 \pi_g^3 \sigma_u^2; 1_g (^3\Pi_g)$  resulting in a continuum at 3416 Å. The height of the state  $o_u^- (^1\Sigma_u^-)$  is located by us at  $29341 \text{ cm}^{-1}$ .

TABLE IV

Bands arising out of transition from a stable state  $\sigma_g \pi_u^4 \pi_g^3 \sigma_u^2$ ;  $1_g (^3\Pi_g)$  with  $\omega \sim 120$  to various repulsive states (figures 1 and 2).

Mercury arc		Transition	Thallium spark	
$\nu(\text{cm}^{-1})$	$\Delta\nu$		$\nu(\text{cm}^{-1})$	$\Delta\nu$
37428	127	$1_g \rightarrow \sigma_g^2 \pi_u^3 \pi_g^3 \sigma_u^2$ . $1_u (^2\Delta_{1u})$	37639	
37555	$4 \times 118$		37983	$3 \times 115$
38026	176		38303	$3 \times 107$
38142	131			
38273				
38584	134	$1_g \rightarrow \sigma_g^2 \pi_u^3 \pi_g^3 \sigma_u^2$ . $2_u (^3\Delta_{7u})$	38738	$3 \times 126$
38718	$2 \times 106$		39112	$3 \times 113$
38929	107			
39036	134		39451	
39170	111			
39281	$4 \times 113$			
39734				
39671	126	$1_g \rightarrow \sigma_g^2 \pi_u^4 \pi_g^3 \sigma_u^2$ . $1_u (^1\Pi_u)$	39797	$3 \times 112$
39797	$2 \times 135$		40132	$2 \times 138$
40068	$3 \times 135$		40408	$2 \times 131$
40474	$2 \times 140$		40671	$2 \times 116$
40754			40904	



TABLE V

Bands arising out of transition from a stable state  $\{(\sigma_g^2 \pi_u^4 \pi_g^3, {}^2\Pi_{g1/2} \sigma_g^2)\}$   
 ${}^3\Pi_{2, 1g}$  with  $\omega \sim 160$  to various repulsive states.

Mercury arc		Transition	Thallium spark	
$\nu$	$\Delta\nu$		$\nu$	$\Delta\nu$
26469			27259	
	$2 \times 374$			$4 \times 379$
27218			28777	
	$2 \times 334$			$2 \times 348$
27886			29473	
	363	${}^3\Pi_{2, 1g} \rightarrow \sigma_g^2, \pi_u^3, \pi_g^3, \sigma_u^2, 1_u^- ({}^3\Sigma_u^+)$		338
28249			29811	
	306			
28555				
	$2 \times 362$			
29283				
26738			26798	
	$3 \times 383$			$2 \times 334$
27886			27465	
	363	${}^3\Pi_{2, 1g} \rightarrow \sigma_g^2, \pi_u^3, \pi_g^3, \sigma_u^2, \sigma_u^- ({}^3\Sigma_u^+)$		$2 \times 376$
28249			28217	
	...			387
29095			28604	
	$2 \times 352$			$2 \times 335$
29798			29274	
34062			34485	
	363			336
34425			34821	
	360			
34785				
	354			
35139				
	324	${}^3\Pi_{2, 1g} \rightarrow \sigma_g^2, \pi_u^3, \pi_g^3, \sigma_u^2, 1_u ({}^3\Delta_{1u})$		
35463				
	330			
35793				
	...			
36077				
	342			
36419				
35300			35514	
	$2 \times 331$	${}^3\Pi_{2, 1g} \rightarrow \sigma_g^2, \pi_u^3, \pi_g^3, \sigma_u^2, 2_u ({}^3\Delta_{2u})$		318
35961			35832	
				311
			36143	
				343
			36486	
...	...	${}^3\Pi_{2, 1g} \rightarrow \sigma_g^2, \pi_u^4, \pi_g^3, \sigma_u^2, 1_u ({}^1\Pi_u)$	36686	...
26659			27716	
	368			$4 \times 324$
27027			29011	
	$3 \times 367$			$2 \times 356$
28129			29722	
	337	${}^3\Pi_{2, 1g} \rightarrow \sigma_g^2, \pi_u^3, \pi_g^3, \sigma_u^2, \sigma_u^- ({}^1\Sigma_u^-)$		
28466				
	361			
28827				
	$2 \times 362$	(This transition is newly identified).		
29551				

TABLE VI

Bands arising out of transition from a stable state  $\sigma_g \pi_u^4 \pi_g^4 \sigma_u$ .  $1_u (^3\Sigma_u^+)$  with  $\omega \sim 90$  go to various repulsive states.

$\nu(\text{cm}^{-1})$	Mercury arc $\Delta\nu$	Transition	$\nu(\text{cm}^{-1})$	Thallium spark $\Delta\nu$
...	...	$1_u (^3\Sigma_u^+) \rightarrow \sigma_g^2 \pi_u^4 \pi_g^2 \sigma_g^2$ . $0_g^+ (^3\Sigma_g^-)$	21100	$2 \times 79$
			21257	
...	...	$1_u (^3\Sigma_u^+) \rightarrow \sigma_g^2 \pi_u^4 \pi_g^2 \sigma_g^2$ . $1_g (^3\Sigma_g^-)$	21541	$2 \times 84$
			21709	
21881	...	$1_u (^3\Sigma_u^+) \rightarrow \sigma_g^2 \pi_u^3 \pi_g^4 \sigma_u$ . $1_g (^1\Pi_g)$	21876	$2 \times 91$
			22059	

Another set of transitions where we can give better information than available from earlier work is the pairs of bands with a separation of  $90 \text{ cm}^{-1}$  (Table VI). Venkateswarlu identified three bands at 4747.2, 4662.1 and 4575.2 Å as due to the three transitions given in Table VI. As remarked by us earlier the data of Mc bands in this region as given by Mc Lennan are not quite reliable. In the excitation by mercury lines we obtain only one band 4569 Å corresponding to 4575.2 Å in emission. We, however, obtain six bands with the thallium spark source which could be easily paired off with separations of  $2 \times 84 \text{ cm}^{-1}$  (figures 1 and 2). The upper state  $1_u (^3\Sigma_u^+)$  at  $44900 \text{ cm}^{-1}$  is also involved in the transition resulting in Pringsheim-Rosen, Kimura-Miyaniishi (P.R. K.M.) bands in the region 2700 to 2000 Å. It has an  $\omega$ -value =  $90 \text{ cm}^{-1}$  obtained from the analysis of the above bands. This could be identified with the mean value  $84 \text{ cm}^{-1}$  suggested above by us. This observation confirms with definite evidence the identification of the above transitions,  $1_u (^3\Sigma_u^+)$  to the repulsive states  $0_g^+ (^3\Sigma_g^-)$ ,  $1_g (^3\Sigma_g^-)$ ,  $1_g (^1\Pi_g)$ . The heights of these repulsive states are 26345, 25916,  $25525 \text{ cm}^{-1}$ .

The band 2444 Å is the least wavelength involved in all the above tables. Below this wavelength there are in all 64 bands in the region. 2427 to 1959 Å recorded on Ilford Q3 plates. This whole region was obtained by excitation with mercury lines. Excitation with thallium spark gave bands upto 2035 Å only (Table I). The original data of Mc Lennan extends upto 2129 Å (Table I). Venkateswarlu published no emission bands in this region. The P.R. K.M. bands extend from 2700 to 2000 Å. There is a close agreement between some of these fluorescence bands and the P.R.K.M. bands in this region.

According to earlier workers some of these bands may form the resonance series excited to vibrational quanta of large values. As already pointed out the successive difference of  $380 \text{ cm}^{-1}$  in some bands is difficult to explain as

two times the ground state difference. Also the magnitude of the splitting of some bands into doublets is not of the proper value corresponding to the rotational separation in the resonance series. Besides some bands show actually a triplet structure with peculiar intensity distribution. A close examination of the bands and their successive differences led us to doubt whether there is any genuineness about the so called doublet and triplet structure. We are more inclined to consider these doublets and triplets as accidental groupings of two and three bands. The higher dispersion used by us led to a more reliable data both on the magnitude of the separations and the relative intensities of the bands under consideration.

We ultimately rejected the theory of attributing the doublet structure to the resonance series. If we accept the existing suggestion that some of these bands form the resonance series the following peculiarities are conspicuous. Low values of the vibrational quanta are not evidently excited. Only high values of the vibrational quanta appear in the analysis. If we accept  $380\text{ cm}^{-1}$  as  $2 \times 215$  (which is in itself a questionable approximation) only alternate vibrational quanta seem to be excited. While the presence or absence of some bands in a resonance progression is not in itself a serious draw back on the analysis (for instance, the 2nd, 5th etc., members in the visible resonance series are recorded as missing), it must be noted that these missing bands are too regular to believe. It appeared plausible to us that the systematic difference of  $380\text{ cm}^{-1}$  covering the whole region 2427 to 1959 Å may be a genuine difference not connected with 215 in the ground state. The bands involved in these differences are marked in figures 5 and 6. It is evident from these two that there is a gradual decrease in intensity as we go down to the short wavelength side of this progression. This series of bands includes besides others some components of the so called doublets and triplets. It appears reasonable to consider that these bands result out of a transition between two states neither of which is the ground state. Considering the diffuse nature of the bands we can conclude that one of the two states is a repulsive state while the other one is a stable state with  $\omega \sim 380\text{ cm}^{-1}$ . These two states have to be identified in the term scheme given by Mulliken. The upper state may be reasonably identified with the repulsive state proposed by Pringsheim (1949) at an approximate height of 55000 to 60000  $\text{cm}^{-1}$ . In the term scheme due to Mulliken there is one state  $2_g (^3\Pi_{2g})$  in the configuration  $\sigma_g \pi_u^4 \pi_g^3 \sigma_u^2$ . The overall height of this configuration was suggested by him to be 8.1 e.v. In the same configuration two other states  $1_g (^3\Pi_{1g})$  and  $1_g (^1\Pi_g)$  with  $\omega \sim 215$  and  $120\text{ cm}^{-1}$  respectively were identified earlier, at heights of 6.39 and 7.26 e.v. If we consider this new state  $2_g (^3\Pi_{2g})$  to be at about 7.5 e.v. the lower state may be fixed up at about 1.0 to 1.5 e.v. The right type of state can be identified as  $2_u (^3\Pi_{2u})$  in the configuration  $\sigma_g^2 \pi_u^4 \pi_g^3 \sigma_u$ .

TABLE VII

Bands arising out of transition from a repulsive state  $\sigma_g\pi_u^4\pi_g^3\sigma_u^2$ ;  $2_g(^3\Pi_{2g})$  to a stable state  $\sigma_g^2\pi_u^4\pi_g^3\sigma_u$ ;  $2_u(^3\Pi_{2u})$  with  $\omega \sim 380$  (figures 5 and 6).

(These two states are newly identified.)

Intensity	$\lambda(\text{\AA}, \text{U})$	$\nu(\text{cm}^{-1})$	$\Delta\nu$
8	2427	41191	325
8	2408	41516	382
8	2386	41898	408
7	2363	42306	345
4	2344	42651	389
6	2323	43040	400
4	2301	43440	377
6	2282	43817	335
6	2264	44152	386
4	2245	44538	388
6	2225	44926	387
4	2206	45313	418
6	2186	45731	310
4	2171	46041	357
3	2155	46398	360
4	2138	46758	426
3	2119	47184	384
3	2102	47568	328
4	2087	47896	388
4	2070	48284	433
2	2052	48717	383
5	2036	49100	389
4	2020	49489	385
2	2004	49874	377
1	1989	50251	382
1	1974	50633	387
1	1959	51020	

This state is a stable state with  $\omega \sim 380 \text{ cm}^{-1}$ . In the same configuration two other states  $1_u(^3\Pi_{1u})$  and  $0_u(^3\Pi_{0u})$  which are also stable,





were identified from an analysis of the near infrared and visible bands. There is also one repulsive state ( $1_u$  ( $^1\Pi_u$ ), involved in a transition giving rise to the Mc bands with  $120\text{ cm}^{-1}$  separation (Table IV). The upper state for these  $120\text{ cm}^{-1}$  bands results out of the same configuration as the repulsive state  $2_g$  ( $^3\Pi_{2g}$ ) suggested by us for the  $380\text{ cm}^{-1}$  bands. As case *c* type of coupling holds good in  $I_2$  molecule both repulsive and stable states can occur in the same configuration. It appears therefore plausible that the above group of bands may arise out of a transition between a repulsive upper state  $\sigma_g^2\pi_u^4\pi_g^3\sigma_u^2$ ;  $2_g$  ( $^3\Pi_{2g}$ ) and a stable lower state  $\sigma_g^2\pi_u^4\pi_g^3\sigma_u$ ;  $2_u$  ( $^1\Pi_{2u}$ ). (Table VII).

We are finally left with 38 bands in the region 2353 to 2010 Å. The most intense bands appear to be in the region below 2150 Å. In general these bands are more intense than the earlier group of  $380\text{ cm}^{-1}$  separation. It can be seen from Table IX that the successive differences of these bands alternate between 150 and  $215\text{ cm}^{-1}$  (average values) systematically. There appeared no other way of connecting these bands with other groups or treating them as two independent groups. They could be arranged into a Deslander's scheme as given in Table VIII. The scheme is built up starting with the highest frequency band and treating  $150\text{ cm}^{-1}$  as the upper state vibrational frequency. Then  $215\text{ cm}^{-1}$  will readily fit in as the lower state frequency developing a peculiar Deslander's scheme. Each band can be seen to be characterised by a ( $v'$ ,  $v''$ ) value. The exact numbering of these  $v'$ ,  $v''$  values is however not possible as no band could be definitely ascribed to a particular ( $v'$ ,  $v''$ ) value. So an arbitrary start with  $v'$  and  $v''$  is made and successive positions are marked as  $v' + 1$ ,  $v' + 2$ ,  $v' + 3$ , ...etc., 24 successive  $v'$  levels and 19 successive  $v''$  levels could definitely be identified. No bands corresponding to low  $v'$ ,  $v''$  values are obtained. From Table VIII it appears again that only bands corresponding to high  $v'$  and  $v''$  values are observed. This is rather peculiar, but yet consistent with the systems discussed earlier. In the band system with  $380\text{ cm}^{-1}$  it was pointed out how the intensity of bands was observed to increase with the higher  $v''$  values. Likewise it may be possible that in the present system bands with low ( $v'$ ,  $v''$ ) values may altogether vanish.

Of the two states the one with a mean separation of  $215\text{ cm}^{-1}$  may be identified with the ground state itself. The upper state is also a stable state with a number of quantized vibrational levels. Its exact height cannot be fixed up as the exact ( $v'$ ,  $v''$ ) numbering is not known for this system. However, from the region of bands it may be fixed up at about  $45000$  to  $50000\text{ cm}^{-1}$  above the ground state  $o_u^+$  ( $^1\Sigma_u^+$ ). A suitable state at about this height and satisfying all the requirements of the selection rules may be found in the configuration  $\sigma_g^2\pi_u^3\pi_g^3\sigma_u^2$  and designated as  $o_u^+$  ( $^1\Sigma_u^+$ ). The fact that it is a  $^1\Sigma_u^+$  may support the idea of a stable state. This interpretation of these bands as a transition between two stable states one of which is the ground level will explain (1) the difficulties about the doublet and triplet

TABLE IX

Bands arising out of transition from a stable state  $\sigma^2_g \pi^3_u \pi^3_g \sigma^2_u$ .  $\sigma^+_{u}(^1\Sigma^+_u)$  with  $\omega \sim 150$  to the ground state  $\sigma^2_g \pi^4_u \pi^4_g$ .  $\sigma^+_{g}(^1\Sigma^+_g)$  with  $\omega \sim 215$   
(The first stable state is newly identified).

Intensity	$\lambda$ (A.U.)	$\nu$ (cm <sup>-1</sup> )	$\Delta\nu$
2	2353	42491	422
2	2330	42913	386
2	2309	43299	240
2	2296	43539	148
4	2288	43687	236
3	2276	43926	134
4	2269	44057	203
2	2259	44260	155
3	2251	44415	240
3	2239	44655	174
4	2230	44829	222
2	2219	45051	178
3	2210	45229	207
4	2200	45436	164
3	2192	45600	278
3	2179	45878	297
6	2165	46175	139
4	2159	46314	179
4	2150	46493	149
8	2143	46642	204
6	2134	46846	127
8	2128	46973	325
6	2114	47298	145
4	2107	47443	211
4	2098	47654	123
8	2092	47777	220
4	2083	47997	139
12	2077	48136	



TABLE IX (contd.)

Intensity	$\lambda$ (Å U.)	$\nu$ (cm <sup>-1</sup> )	$\Delta\nu$
12	2077	48136	
4	2066	48382	246
10	2062	48486	104
6	2055	48641	155
8	2046	48870	229
8	2040	49011	141
6	2031	49223	212
8	2025	49372	149
3	2016	49594	222
8	2010	49741	147

structure, (2) the reason why the resonance series are not obtained even though a transition to the ground state is obtained, and (3) the relative intensity anomalies of the doublets and triplets.

(Our final conclusion is that when iodine vapour is excited by mercury lines below 2000Å, no resonance series in the rigorous sense of the word is obtained. All the bands form one system or another of the McLennan type of bands. A transition to the ground state is involved in some bands but only from various vibrational levels of a stable upper state, resulting in the development of a band system involving the vibrational differences in both the states.

With this interpretation we are able to explain all the bands obtained in fluorescence spectrum of iodine excited by mercury and thallium lines. Finally we may add the explanation given by Pringsheim as to how a molecule in the ground state could be raised to a level possibly higher than the exciting radiation. It was suggested that the exciting radiation might take up the molecule to a stable state, lower than the exciting radiation, from which it is transferred to any higher state possibly by some process of collisions (Pringsheim, 1949).

#### ACKNOWLEDGMENT

Our thanks are due to Prof. K. R. Rao for his kind interest in the work.

#### REFERENCES

- Curtis, W. E. and Evans S. F., 1933, *Proc. Roy. Soc.*, **141A**, 603.  
 Duschinsky, F., Hirschlaiff E. and Pringsheim P., 1935, *Physica*, **2**, 439

- Duschinsky, T. and Pringsheim P., 1935, *Ibid.*, **2**, 633 and 923.  
 Hirschlaff, E., 1932, *Z. f. Physik.* **75**, 325.  
 Loomis, F. W., 1926, *Phys. Rev.*, **27**, 802,  
 „ 1927, *Ibid.*, **29**, 112, 355.  
 McLennan, J. C., 1913, *Proc. Roy. Soc.* **88A**, 289.  
 „ 1915, *Ibid.* **91A**, 23.  
 Mulliken, R. S., 1934, *Phys. Rev.*, **46**, 549.  
 Oldenberg, O., 1923, *Z. f. Physik.* **18**, 1.  
 „ 1924, *Ibid.*, **25**, 136.  
 Pringsheim, P., 1921, *Ibid.* **8**, 126.  
 „ 1921, *Ibid.*, **8**, 130.  
 „ 1949, "Fluorescence and Phosphorescence" p. 162, 165,  
 Venkateswarlu, P., 1946, *Proc. Ind. Acad. Sci.*, **24A**, 473, 480.  
 „ 1947, *Ibid.* **25A**, 119, 133.

# RAMAN AND FLUORESCENCE SPECTRA OF ORTHO- AND PARA BROMOTOLUENE IN THE SOLID STATE AT LOW TEMPERATURES \*

BY D. C. BISWAS

OPTICS DEPARTMENT, INDIAN ASSOCIATION FOR THE CULTIVATION OF SCIENCE, CALCUTTA-32

(Received for publication, July 24, 1954)

## Plates XVI A—C

**ABSTRACT.** The Raman spectra of ortho- and para bromotoluene in the solid state at different low temperatures were recorded. With solidification one line due to C=C vibration of both the compounds diminishes in intensity. It is suggested that this fact indicates the association of some of the molecules in the solid state at the expense of the C=C bond as in the case of polymerisation of styrene.

Only one new line at  $94\text{ cm}^{-1}$  appears in the low-frequency region when ortho bromotoluene is solidified and cooled down to  $-60^{\circ}\text{C}$ . With lowering of temperature of the solid to  $-180^{\circ}\text{C}$ , another line is observed at  $36\text{ cm}^{-1}$ . In the case of para compound in the solid state at  $-20^{\circ}\text{C}$ , two lines are observed in low-frequency region. With lowering of temperature of the solid to  $-180^{\circ}\text{C}$  the intense line at  $33\text{ cm}^{-1}$  disappears but three more extra lines appear in the low-frequency region. All these irregular changes have been critically discussed.

In the solid state at  $-180^{\circ}\text{C}$  either of the substances exhibits two fluorescence bands in the visible region, the frequency difference between the bands being about  $1600\text{ cm}^{-1}$ . It is suggested from the evidences available that the fluorescence of bromotoluenes in the solid state at  $-180^{\circ}\text{C}$  is a property of the groups of molecules of the substances.

## INTRODUCTION

It was shown in previous papers (Biswas, 1954a, 1954b) that the intensities, positions and sometimes the number of the low-frequency Raman lines due to organic crystals change irregularly with the change of temperature of the crystals. The data reported so far indicate that these lines are produced by some oscillations in the lattice in which the restoring force is much larger than the Van der Waals force in the liquid, and that some of the lines are definitely not due to the angular oscillation of the molecule, postulated by some previous workers (Kastler and Rousset, 1941; Bhagavatam, 1941). It has not yet been possible, however, to interpret quantitatively the results observed in individual cases. For instance, the increase in the number of low-frequency Raman lines with lowering of temperature of the crystal observed in several cases was explained

\* Communicated by Prof. S. C. Sirkar

by assuming that association of molecules with next neighbours takes place at lower temperatures, but this is only a qualitative hypothesis. The quantitative explanation on this hypothesis is possible only in those cases in which the crystal structure is definitely known at different low temperatures, so that we can find out the changes in intermolecular distances taking place with change of temperature. Also the results of investigation of the ultraviolet absorption spectra of these substances at low temperatures may throw some light on the influence of lowering of temperature of the crystals on the oscillation of the molecules in the lattice, as pointed out by Sirkar and Swamy (1952). For this reason it was thought worthwhile to study the Raman spectra of a few more isomeric disubstituted benzenes of which the results of investigation of the ultraviolet absorption spectra at different temperatures are known. The present paper deals with the Raman spectra of ortho- and para bromotoluene in the solid state at different temperatures.

#### EXPERIMENTAL

The liquids used in the present investigation were supplied by the Eastman Kodak Co., U. S. A., and were of chemically pure quality. The experimental procedure and the technique employed to record the Raman spectra in different states are exactly similar to those described earlier (Biswas, 1954a). The Raman spectra of these substances in the liquid state were also investigated and the results were compared with those reported by previous workers in order to check the purity of the sample used. A Fuess glass spectrograph with a dispersion of about  $11\text{\AA}$  per mm in the  $4046\text{\AA}$  region was used for photographing the Raman spectra of these substances in the solid state, while the spectrograms of the substances in the liquid state were obtained with the help of a spectrograph of dispersion about  $14\text{\AA}$  per mm in the  $4046\text{\AA}$  region. Microphotometric records of some of the Raman lines were taken with a Kipp and Zonen type Moll microphotometer.

#### RESULTS AND DISCUSSIONS

##### 1. Raman Spectra :

The calculated Raman shifts of the substances in the liquid state and in the solid state at different low temperatures are given in Tables I and II. The tables also include for comparison the results of investigation by some previous workers in the liquid state of these substances. The spectrograms are reproduced in figures 1 and 2, Plate XVII. Microphotometric records showing the relative intensities of some of the Raman lines due to intramolecular oscillations as well as the intensities of the low-frequency lines of the crystals at different temperatures relative to some other line due to molecular vibration are reproduced in figures 3, 4, and 5 in Plates XVII-B—C.

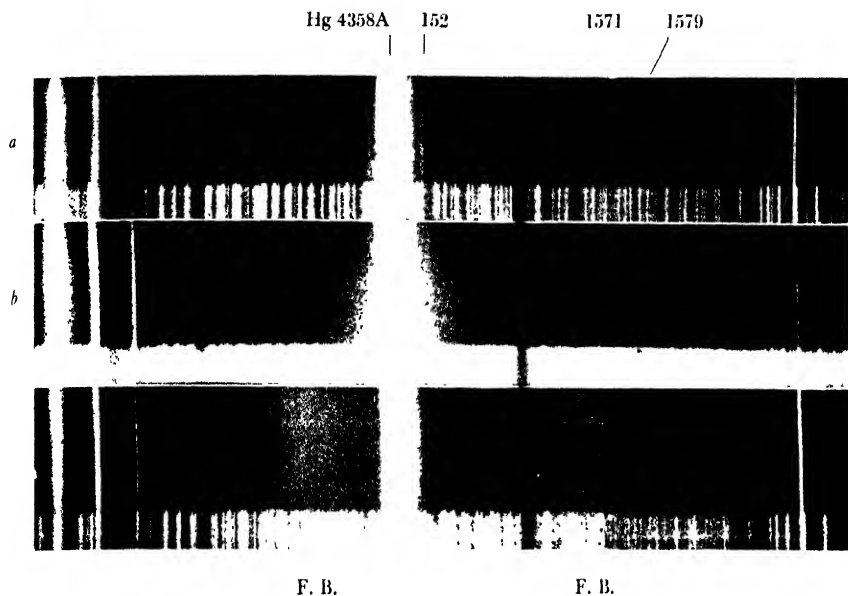


Fig. 1

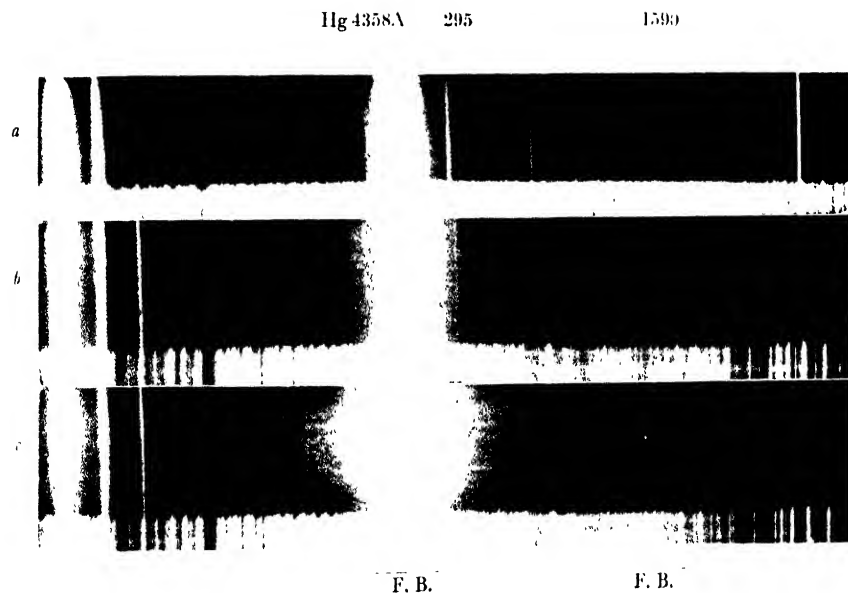


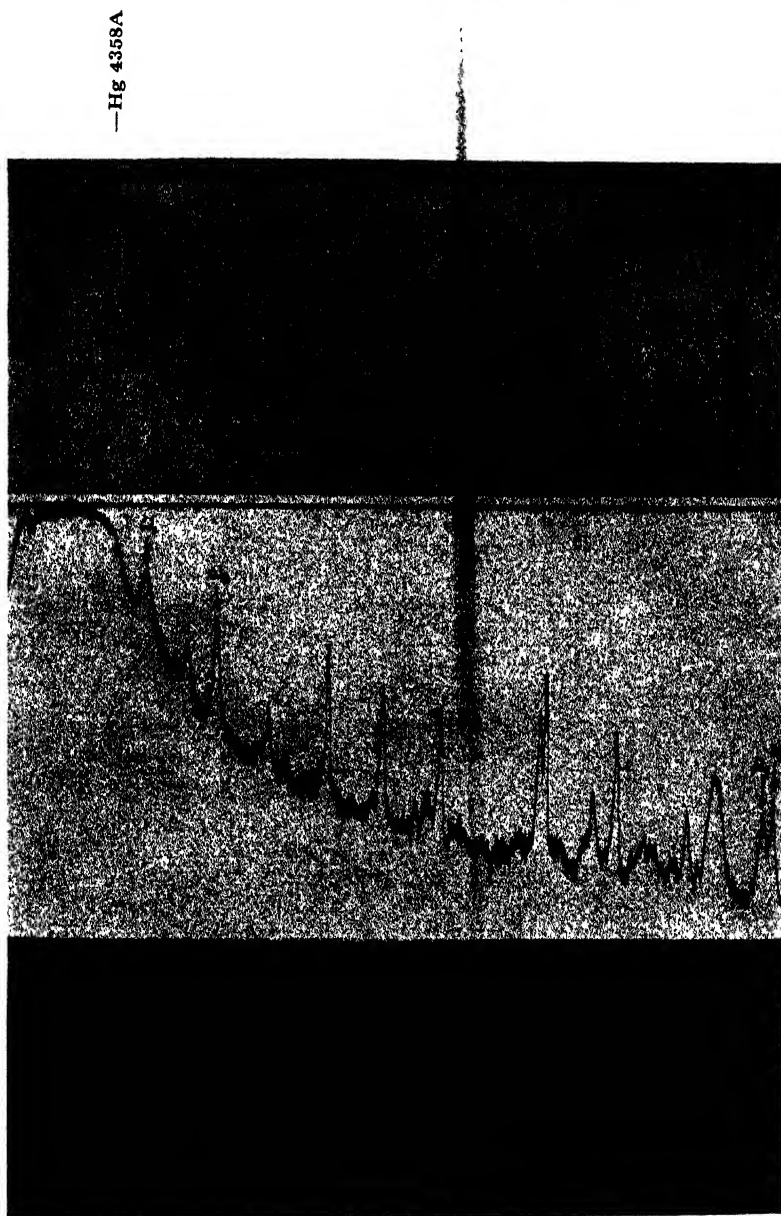
Fig. 2

Fig. 1. Ortho bromotoluene  
 (a) Liquid at 30°C  
 (b) Solid at about -60°C  
 (c) Solid at -180°C

Fig. 2. Para bromotoluene  
 (a) Liquid at 30°C  
 (b) Solid at about -20°C  
 (c) Solid at -180°C

F. B.—Fluorescence band



Microphotometric records of Raman spectra of *o*-bromotoluene

F. B.

Fig. 3

Fig. 3 (a) Liquid at 32°C

,, (b) 40% solution in *n*-heptane

,, (c) Solid at -180°C

(  $\omega_1 = 152 \text{ cm}^{-1}$  ,  $\omega_2 = 297 \text{ cm}^{-1}$  ,  $\omega_3 = 1571 \text{ cm}^{-1}$  ,  $\omega_4 = 1597 \text{ cm}^{-1}$  )

(Dispersion in (a) is about 14A per mm and in (b) and (c) about 11A per mm in the region of 4047A)

Microphotometric records of Raman spectra of *p*-bromotoluene

Hg 4358A

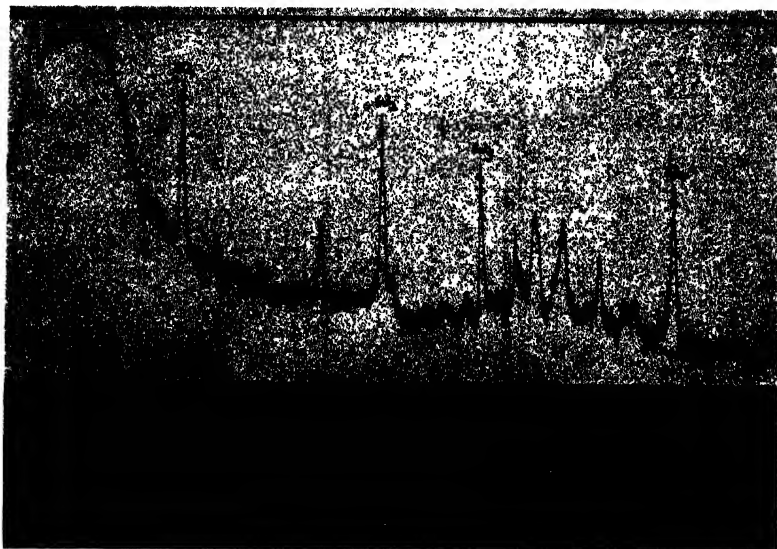


Fig. 4

6A

Hg  
33 118

295

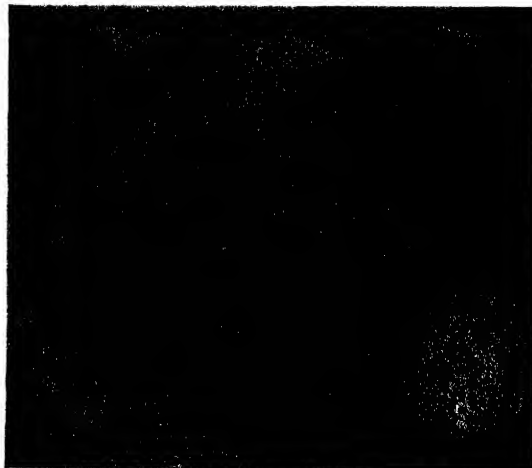


Fig. 5

Fig. 4 (a) Liquid at 32°C  
 " (b) Solid at -180°C

( $w_1 = 295 \text{ cm}^{-1}$ ,  $w_2 = 794 \text{ cm}^{-1}$ ,  $w_3 = 1061 \text{ cm}^{-1}$ ,  $w_4 = 1592 \text{ cm}^{-1}$ )  
 Fig. 5 (a) Solid at -20°C  
 (b) Solid at -180°C

( $w_1 = 52 \text{ cm}^{-1}$ ,  $w_2 = 94 \text{ cm}^{-1}$ ,  $w_3 = 133 \text{ cm}^{-1}$ ,  $w_4 = 162 \text{ cm}^{-1}$ )

(Dispersion in (a) of Fig. 4 is 14A per mm and in (b) of  
 Fig. 4 is about 11A per mm)



TABLE I  
o-Bromotoluene;  $\text{BrC}_6\text{H}_4\text{CH}_3$   
 $\bar{\nu}$  in  $\text{cm}^{-1}$

Liquid		Solid (present author)	
Magat (1936)	Present author	At about $-60^\circ\text{C}$	At $-180^\circ\text{C}$
			36 (2) k
		94 (5b) e, k	107 (4b) e, k
154 (10b)	152 (8b) $\pm$ e, $\pm$ k, i	168 (4b) e	172 (5) e
217 (0.5)	221 (1) e		
236 (4)	239 (4) $\pm$ e, $\pm$ k	247 (0) e, k	247 (1) e, k
296 (8)	297 (10) $\pm$ e, $\pm$ k, i	297 (3) e, k	297 (4) e, k
411 (2)	414 (3) e, k	414 (0) e, k	413 (0) e, k
544 (7)	544 (10) $\pm$ e, k, i	544 (3) e, k	546 (4) e, k
656 (6)	655 (8) $\pm$ e, k, i	660 (3) e, k	660 (4) e, k
	737 (1) e, k		
796	799 (9) e, k, i	799 (3) e, k	799 (4) e, k
852 (0)	863 (0) e		
	947 (0) e		
986 (1b)	996 (1b) e		
1030 (4)	1028 (5) e, k	1028 (2) e, k	1028 (2) e, k
1043 (6)	1046 (10) e, k, i	1046 (4) e, k	1046 (4) e, k
1156 (4)	1162 (4) e, k	1162 (1) e	1162 (1) e
1204 (5)	1216 (9) e, k	1216 (4) e, k	1216 (4) e, k
	1250 (1b) e		
1274 (2)	1280 (2b) k		
1378 (3)	1383 (5) e, k	1383 (1) e, k	1383 (2) e, k
	1431 (1b) e		
1456 (0)			
1567 (3)	1571 (6) e, k	1571 (0) e, k	1568 (2) e, k
1593 (3)	1597 (7) e, k	1597 (0) e, k	1597 (1) e, k
2875 (0)			
2927 (1)	2928 (2) e, k	2926 (1) k	2926 (1) e, k
		2944 (0) k	2944 (0) e, k
3061 (3b)	3063 (5b) e, k, i	3063 (5) e, k	3063 (5) e, k

TABLE II  
*p*-Bromotoluene ;  $\text{BrC}_6\text{H}_4\text{CH}_3$   
 $\nu$  in  $\text{cm}^{-1}$

Liquid		Solid (present author)	
Magat (1936)	Present author	At about $-20^\circ\text{C}$	At $-180^\circ\text{C}$
		33 (4) k	52 (1) k
		118 (1b) k	94 (3b) e, k
			133 (4) e, k, i
			162 (1) e, k
	242 (o) e		
291 (10)	295 (10) $\pm$ e, k, i	295 (4) e, k	295 (5) e, k
363 (o)	366 (o) e		
	418 (o) e		
462 (o)	488 (ob) e		
631 (4)	634 (4) $\pm$ e, k, i	634 (1) e, k	634 (2) e, k
702 (0.5)	698 (o) e		
792 (9)	794 (9) e, k, i	791 (5) e, k	791 (7) e, k
819 (o)	822 (1) e, k		
840 (0.5)			
	1005 (1) e, k		
1069 (7)	1061 (8) e, k, i	1051 (4) e, k	1061 (5) e, k
	1102 (o) e		
1170 (2)	1177 (1) e, k		
1209 (5)	1214 (6) e, k	1214 (2) e, k	1214 (3) e, k
	1279 (1b) e, k		
1300 (0.5)			
1374 (3)	1383 (3) e, k	1378 (o) e, k	1377 (1) e, k
	1406 (o) e		
1436 (oo)	1452 (1b) e		
	1539 (o) e		
1588 (5)	1592 (6) e, k	1590 (o) e, k	1590 (2) e, k
2870 (2)			
2920 (2)	2925 (4) e, k	2915 (4) e, k	2915 (4) e, k
2972 (2)		2942 (1) e	2942 (2) e
3028 (0.5)			
3056 (4)	3063 (6b) e, k, i	3063 (5) e, k	3063 (5) e, k

## (a) Low-frequency lines :

Ortho-bromotoluene yields one intense and broad Raman line at  $94\text{ cm}^{-1}$  in the low-frequency region when the substance is solidified and cooled down to  $-60^{\circ}\text{C}$ . With lowering of temperature of the solidified mass to  $-180^{\circ}\text{C}$ , this line shifts to  $100\text{ cm}^{-1}$  and another new line appears at  $36\text{ cm}^{-1}$ . It can be seen from the microphotometric records reproduced in figure 4 that in the case of solid *p*-bromotoluene at  $-20^{\circ}\text{C}$  only two low-frequency lines at  $33$  and  $118\text{ cm}^{-1}$  respectively are observed. The first line at  $33\text{ cm}^{-1}$  is intense and sharp while that at  $118\text{ cm}^{-1}$  is weak and diffuse. When the temperature of the solidified mass is lowered to  $-180^{\circ}\text{C}$ , the intense line at  $33\text{ cm}^{-1}$  disappears, the line  $118\text{ cm}^{-1}$  shifts to  $133\text{ cm}^{-1}$  and becomes stronger and three other lines appear at  $52$ ,  $94$  and  $162\text{ cm}^{-1}$  respectively. Of these four lines observed at  $-180^{\circ}\text{C}$  those at  $94$  and  $133\text{ cm}^{-1}$  are very intense.

These data indicate that the line  $36\text{ cm}^{-1}$  observed in the case of *o*-bromotoluene at  $-180^{\circ}\text{C}$  cannot be due to any angular oscillation, because there is no such line in the crystal at  $-60^{\circ}\text{C}$  and an angular oscillation is expected to have a larger amplitude at  $-60^{\circ}\text{C}$  than at  $-180^{\circ}\text{C}$ . Also, in the case of *p*-bromotoluene the spectrum in the low-frequency region undergoes thorough change with the lowering of the temperature of the crystal from  $-20^{\circ}\text{C}$  to  $-180^{\circ}\text{C}$ . The appearance of the new lines  $133\text{ cm}^{-1}$  and  $162\text{ cm}^{-1}$  at  $-180^{\circ}\text{C}$  clearly indicates that some virtual bonds are formed at this temperature between neighbouring molecules, because such large frequencies cannot be explained by Van der Waals forces, especially, in a molecule containing bromine atom. It is not possible, however, to draw from these results any definite conclusion regarding the changes which take place in the arrangement of the molecules with lowering of temperature of the crystal and it would be interesting to study the crystal structure of this substance at  $-20^{\circ}\text{C}$ . In the case of *o*-bromotoluene the changes are less remarkable, probably because the molecule being more asymmetric than the molecule of the para compound, lowering of temperature does not increase the asymmetry to a much greater extent. The appearance of the new line at  $36\text{ cm}^{-1}$  at  $-180^{\circ}\text{C}$ , indicates that the virtual bond between the neighbouring molecules formed in the case of the para compound at  $-20^{\circ}\text{C}$  appears in this case at  $-180^{\circ}\text{C}$ . Hence it would be highly interesting to compare the crystal structures of these two isomers at different temperatures.

## (b) Intramolecular vibrations :

It can be seen from the microphotometric records that in case of both *o*- and *p*-bromotoluene the intensity of the line at about  $1592\text{ cm}^{-1}$  due to  $\text{C}=\text{C}$  oscillation diminishes when the substances are solidified and cooled to  $-180^{\circ}\text{C}$ . It has been shown by previous workers (Hibben, 1937 ; Roy, 1953) that when polymerisation takes place in the case of methylmethacrylate,

the line due to C=C vibration of the single molecule disappears completely. In the present case, therefore, the appreciable diminution of the intensity of the line due to C=C vibration in the solid state at  $-180^{\circ}\text{C}$  may indicate that some of the molecules of *o*- and *p*-bromotoluene in the solid state at  $-180^{\circ}\text{C}$  form associated groups at the expense of some of the C=C bonds. Similarity between the present case with another case of polymerisation has been dealt with in a subsequent paragraph.

As regards the changes in the other molecular lines with solidification of the substances, it can be pointed out that the line at  $295\text{ cm}^{-1}$  of para bromotoluene undergoes a diminution in intensity when the substance is solidified and cooled down to  $-180^{\circ}\text{C}$ . This line corresponds probably to some deformation oscillation of the C-Br group. In the solid state the amplitude of this oscillation has been probably restricted by the presence of neighbouring molecules. It is also observed that in both the cases the C-H valence oscillation undergoes changes with solidification and in place of a line at about  $2928\text{ cm}^{-1}$  at room temperature two lines are observed. The distance between these two lines is larger in the case of the para compound than in the case of the ortho compound. It may be mentioned in this connection that even when the molecules of either methylmethacrylate or styrene are polymerised, only a few lines due to the molecule undergo changes in intensity and position. So, in the case of association of molecules postulated in the present case much change in the intensities and positions of the lines due to the single molecule is not expected.

It is further seen from Table I that the line  $152\text{ cm}^{-1}$  of *o*-bromotoluene shifts to  $172\text{ cm}^{-1}$  and its intensity increases with solidification and cooling down to  $-180^{\circ}\text{C}$ . In the case of *o*-chlorotoluene also such a change was observed by Sanyal (1953). He suggested that that the line might be due to a dimer. To test the correctness of this hypothesis the Raman spectrum of solution of *o*-bromotoluene in heptane was studied in the present investigation. It was observed that the intensity of the line  $152\text{ cm}^{-1}$  relative to that of other lines is less in the case of the solution than in the case of the pure liquid. So, if this line be due to a dimer, the bond between the two molecules must be quite strong. No definite conclusion can, however, be drawn without studying Raman spectrum of the substance in the vapour state.

## 2. Fluorescence Spectra:

It is seen in the spectrograms reproduced in Plate XVIIA that both the substances in the solid state at  $-180^{\circ}\text{C}$  exhibit two broad fluorescence bands in the visible region. The centres of the bands as well as their approximate widths and visually estimated intensities are given in Table III.

TABLE III  
Fluorescence bands

<i>o</i> -Bromotoluene at $-180^{\circ}\text{C}$				<i>p</i> -Bromotoluene at $-180^{\circ}\text{C}$			
Position of band in $\text{cm}^{-1}$	Interval in $\text{cm}^{-1}$	Width in $\text{cm}^{-1}$	Relative intensity	Position of band in $\text{cm}^{-1}$	Interval in $\text{cm}^{-1}$	Width in $\text{cm}^{-1}$	Relative intensity
23456	1638	515	5	22955	1599	330	4
21818		535	4	21356		370	4

The spectrograms due to *o*- and *p*-bromotoluene in the solid state at  $-60^{\circ}\text{C}$  and  $-20^{\circ}\text{C}$  respectively do not show any trace of fluorescence. This fact suggests that in this particular case close proximity of the molecules in the crystal lattice is absolutely necessary for the excitation of fluorescence. It is interesting to compare these results with those observed by Roy (1954) in the case polystyrene at  $-180^{\circ}\text{C}$ . When styrene molecules form polymerised groups, the line due to  $\text{C}=\text{C}$  vibration of a single molecule disappears and when the solidified mass of polystyrene is cooled down to  $-180^{\circ}\text{C}$ , the substance produces two fluorescence bands at  $4260 \text{ \AA}$  and  $4655 \text{ \AA}$  respectively. In the present investigation both the ortho - and para bromotoluene in the solid state at  $-180^{\circ}\text{C}$  show an appreciable diminution in the intensity of the line due to  $\text{C}=\text{C}$  vibration and both exhibit broad fluorescence bands in the visible region. This striking similarity between spectra of *o*- and *p*-bromotoluene in the solid state at  $-180^{\circ}\text{C}$  and the spectrum of polystyrene at  $-180^{\circ}\text{C}$  is quite significant. The molecules of polystyrene exist as large polymerised groups without definite lattice structure. The excitation of fluorescence in polystyrene at  $-180^{\circ}\text{C}$  is therefore, a property of the molecules in the polymerised groups. Similar fluorescence exhibited by bromotoluenes in the solid state at  $-180^{\circ}\text{C}$  then probably indicates the fact that in this particular case it is the molecules of the substances and not the lattice, that is responsible for the appearance of fluorescence at  $-180^{\circ}\text{C}$ . With solidification, the molecules of bromotoluenes are believed to form associated groups and with lowering of temperature to  $-180^{\circ}\text{C}$ , these groups undergo contraction and are subjected to uneven stresses from different sides. This, of course, introduces some inhomogeneity in the groups and causes the substance to fluoresce. Further, it is seen from Table III, that the frequency-difference between the successive fluorescence bands approximates to the frequency of the  $\text{C}=\text{C}$  vibration of the molecules. It is therefore, quite likely that when the molecules in the solid state get associated at the expense of  $\text{C}=\text{C}$  bonds, this disturbed oscillation is coupled with the electronic state of the associated molecules and gives rise to a second fluorescence band with the observed frequency shift.

## ACKNOWLEDGMENT

The author is indebted to Prof. S. C. Sirkar, D. Sc., F.N.I. for his kind interest and helpful guidance throughout the progress of the work.

## REFERENCES

- Bhagavantam, S., 1941, *Proc. Ind. Acad. Sc.*, **13A**, 543.  
Biswas, D. C., 1954a, *Ind. J. Phys.*, **28**, 85.  
Biswas, D. C., 1954b, *Ind. J. Phys.*, **28**, 303.  
Hibben, J. H., 1937, *J. Chem. Phys.*, **5**, 704.  
Kastler, A., and Rousset, A., 1941, *Comptes Rendus*, **218**, 998.  
Magat, M., 1936, Annual Table of Constants, p 26—77.  
Roy, N. K., 1953, *Ind. J. Phys.*, **27**, 167.  
Roy, N. K., 1954, *Ind. J. Phys.*, **28**, 365.  
Sanyal, S. B., 1953, *Ind. J. Phys.*, **27**, 447.  
Sirkar, S. C. and Swamy, H. N., 1952, *J. Chem. Phys.*, **21**, 1177.

# MEAN LIFE OF DECAY OF MUONS IN THE ABSENCE OF MATTER \*

BY N. N. BISWAS  
BOSE INSTITUTE CALCUTTA-9

(Received for publication, July 5, 1954)

**ABSTRACT** The possibility of a slow decrease of the mean life of the positive muons with the decrease of  $Z$ , as seen from some accurate experiments of recent times has been utilised to infer that the mean life of free decay of the negatives (in the absence of matter) is about  $2.35 \mu$  secs., which is higher than the mean life of the positives ( $2.22 \mu$ sec), if the positives are assumed to undergo free decay in the presence of matter.

It is argued that the variation of  $\tau_+$  with  $Z$ , if true, may either be due to the deceleration of the positives by the Coulomb field or the capture of the positives as the Coulomb barrier decreases. The latter process is thought to be more likely

The mean lives of free decay of both positive and negative  $\mu$ -mesons are generally believed to be the same (Krausher, 1948). Recently, however, some accurate experiments on the determination of the mean life of the positive mesons in different elements have given rise to some complications. Bell and Hincks (1951), and Morewitz and Shamos (1953) evaluated  $\tau_+$  in iron ( $Z=26$ ) and sulphur ( $Z=16$ ) absorbers respectively by the method of delayed coincidence. Alvarez, et al (1950) determined  $\tau_+$  in carbon using artificially produced mesons of high intensity. All these data led Morewitz and Shamos (1953) to suggest the possibility of the dependence of  $\tau_+$  on the atomic number of the absorbing element such that

$$\tau_+ = 2.22 \pm 0.02 \mu\text{secs} \quad (\text{Bell and Hincks}) \text{ for } Z \geq 26$$

$$\tau_+ = 2.09 \pm 0.03 \mu\text{secs} \quad (\text{Morewitz and Shamos}) \text{ for } Z \leq 16.$$

Thus a slow decrease of  $\tau_+$  with the decrease of  $Z$ , as shown above, indicates a low but finite amount of capture probability ( $\sim 10^4$  per sec.) of the positives as the Coulomb field decreases ( $Z \leq 6$ ).

Assuming the values of the mean lives of a composite beam of mesons as obtained by Bell and Hincks (1952a) at sea level in elements of  $Z=6, 4$  and  $3$  to be respectively  $2.12 \pm 0.02$ ,  $2.15 \pm 0.02$  and  $2.20 \pm 0.02 \mu$ secs as correct, the values of  $\tau_-$  in these elements can be determined assuming a fixed mean life of  $2.09 \mu$ secs for the positive mesons.

In figure 1 is shown how one can evaluate  $\tau_-$  from the decay curve of the composite beam of mesons at sea level. The line labelled  $2.20 \mu$ secs represents the composite decay curve of a meson mixture in Li, such that altogether 200 particles (arbitrary unit) are available for decay, out of which 103 particles are positive (assuming  $\mu^+/\mu^- = 1.06$ , from the experiments of

\* Communicated by Dr. D. M. Bose.

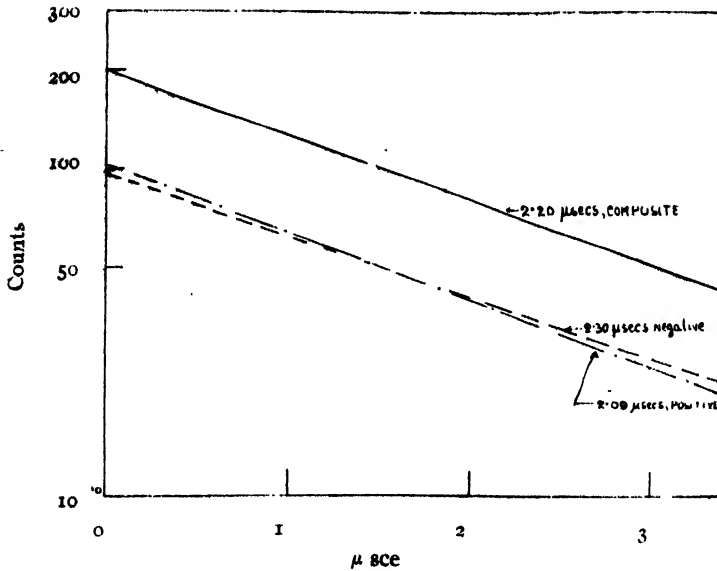


Fig. 1. Decay curve of a composite, positive and negative meson beam in lithium.

Morewitz and Shamos  $\mu^+/\mu^- = 1.06 \pm 0.03$ ). Assuming these positive particles to have a mean life of  $2.09 \mu\text{secs}$  in Li, a decay curve (line labelled  $2.09 \mu\text{secs}$ ) has been drawn. By subtraction, one gets the decay curve of the negatives alone, yielding a mean life of  $2.30 \mu\text{secs}$  in Li.

The values of  $\tau_-$  evaluated in this way are shown in Table I.

TABLE I

Values of  $\tau_-$  for  $\mu^+/\mu^- = 1.06$ ,  $\tau_+ = 2.09 \pm 0.03 \mu\text{secs}$

Element	Z	$Z_{eff}$	$\tau_-$ in $\mu\text{secs}$
C	6	5.78	$2.16 \pm 0.06$
Be	4	3.93	$2.23 \pm 0.06$
Li	3	3	$2.30 \pm 0.06$

It is thus seen from the above table that if the slow decrease of  $\tau_+$  with the decrease of  $Z$  be real, a higher value of the apparent mean life of the negative mesons than that of the positives in the cases of  $Z \leq 4$  is clearly seen. The accuracy of the experiments of Morewitz and Shamos (1953), Bell and Hincks (1951) and Alvarez et al (1950), as shown above, is quite high and the above considerations have led us to the value of  $\tau_{-Li} = 2.30 \mu\text{secs}$ . Hence a slightly higher value, say  $2.35 \mu\text{secs}$  has to be taken for the mean life of free decay of negative mesons in the absence of matter in order to have a finite capture probability of the negative muons for the Li nucleus. In other words,



we are led to believe that  $\tau_{-}^{free}$  is probably higher than that of the positives, if  $\tau_{+}$  in elements of  $Z \geq 26$  is taken to be equal to  $2.22 \pm 0.02$   $\mu$ secs.

It is worth mentioning in this connection that Dallaporta (1952) attempted, though in a somewhat different manner, to show that the value of  $\tau_{-}^{free}$  is about 2.50  $\mu$ secs in the absence matter. He extrapolated Wheeler's (1949)  $\log \Lambda$  versus  $\log Z_{eff}$  curve obtained from the experimental points corresponding to  $10 \leq Z \leq 29$ , to lower values of  $Z$ , assuming the validity of the law for  $Z < 10$ .

Now, the capture probabilities of the negatives in various elements have been calculated (Table II) from the relation,

$$\Lambda = 1/\tau_{-} - 1/\tau_{-}^{free}$$

taking  $\tau_{-}^{free} = 2.35$   $\mu$ secs, and the values of  $\tau_{-}$  for  $Z \leq 6$  from Table I.

TABLE II  
Values of  $\Lambda$  for  $\tau_{-}^{free} = 2.35$   $\mu$ secs

Z	$Z_{eff}$	$\tau_{-}$ in $\mu$ secs	Author	$\Lambda$ per sec.
29	20.6	$0.116 \pm 0.009$	Kenuff et al (1952)	$8.20 \pm 0.67 \times 10^6$
26	19.5	$0.163 \pm 0.027$	" "	$5.71 \pm 1.02 \times 10^6$
16	13.7	$0.54 \pm 0.12$	Ticho (1948)	$1.43 \pm 0.41 \times 10^6$
14	12.33	$0.60 \pm 0.09$	Cathey (1952)	$1.24 \pm 0.25 \times 10^6$
13	11.58	$0.75 \pm 0.07$	Ticho (1948)	$9.08 \pm 0.93 \times 10^5$
12	10.83	$0.95 \pm 0.06$	" "	$6.20 \pm 0.65 \times 10^5$
10	9.25	$1.28 \pm 0.12$	" "	$3.56 \pm 0.73 \times 10^5$
8	7.56	$1.89 \pm 0.15$	" "	$1.04 \pm 0.42 \times 10^5$
6	5.78	$2.16 \pm 0.06$	See Table I	$3.8 \pm 1.3 \times 10^4$
4	3.93	$2.23 \pm 0.06$		$2.3 \pm 1.2 \times 10^4$
3	3	$2.30 \pm 0.06$		$9.2 \pm 1.2 \times 10^3$

In figure 2 is plotted  $\Lambda$  versus  $Z_{eff}$  curve on a double logarithmic scale and a straight line is fitted following a  $Z_{eff}^2$  law in the range  $3 \leq Z \leq 29$ . The Wheeler law of  $Z_{eff}^2$  does not hold good for  $Z > 29$  due to the "shell structure" of the nucleus as shown by Kennedy (1952), but there seems to be no reason to doubt its validity for low values of  $Z$  ( $Z < 8$ ), and the points discussed above regarding the increase of  $\tau_{-}$  and the decrease of  $\tau_{+}$  with the decrease of  $Z$  are found to be supported by the close fit of the values of  $\Lambda$  for  $Z=6, 4$  and  $3$  in the Wheeler's diagram.

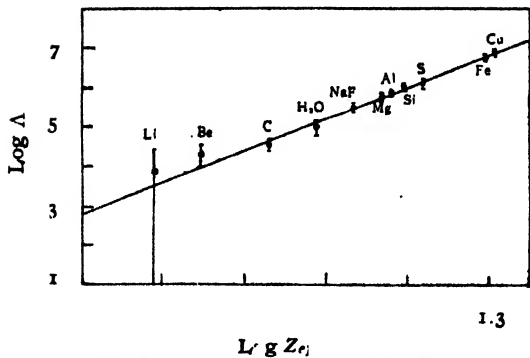


Fig. 2. Plot of Wheeler's curve with the values shown in Table II.

The dependence of  $\tau_-$  and  $\tau_+$  on the atomic number of the absorbing element is shown in figures 3 and 4 respectively. Figure 3 shows that  $\tau_-$  increases with the decrease of  $Z$  tending to attain a value of about  $2.35 \mu\text{secs}$  for  $Z=0$  (absence of matter). The value of  $\tau_+$  (figure 4), on the other hand, shows a slow increase with  $Z$ , tending to reach a saturated limit. This figure has, however, been drawn tentatively and with the accumulation of sufficient data in future, the values of  $\tau_+$  for other values of  $Z$  may not fit the curve closely.

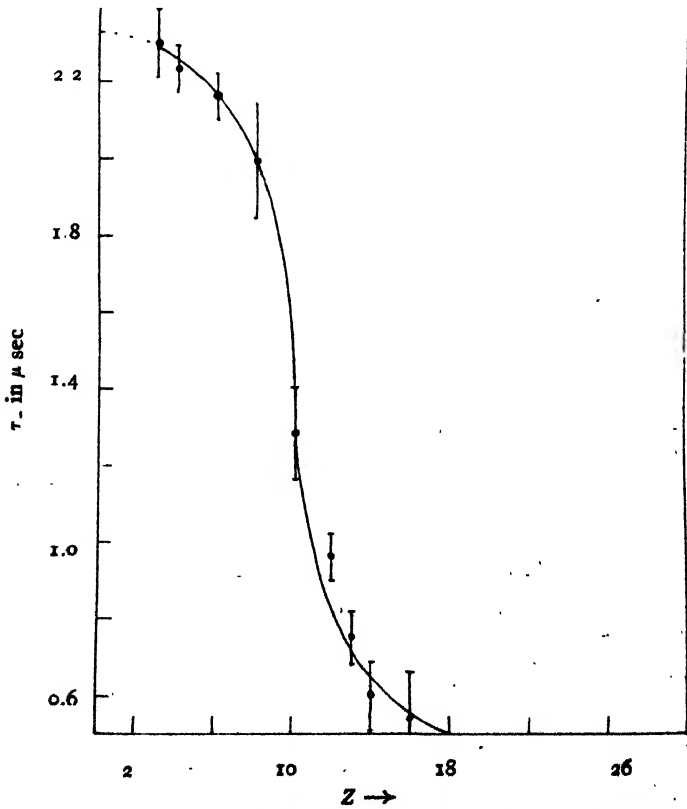


Fig. 3. Plot of  $\tau_-$  against  $Z$ , with the values shown in Table II.

The variation of  $\tau_+$  with  $Z$  requires some explanation and the effect may be accounted for in either of the following ways :

(a) The value of  $\tau_+$  tends to a value of about 2.05  $\mu$ secs as  $Z$  tends to zero, as seen from figure 4. Now, if one assumes that the value of  $\tau_+$  for lower values of  $Z$  ( $Z$  tending to zero) corresponds to the mean life of free decay of the positive muons, then the increase of  $\tau_+$  with the increase of  $Z$  may be explained to be due to the effect of a deceleration of the mu-positive decay by the Coulomb field. The effect of the Coulomb field on the capture of mesons was first pointed out by Tomonaga and Araki (1940). That the Coulomb field may

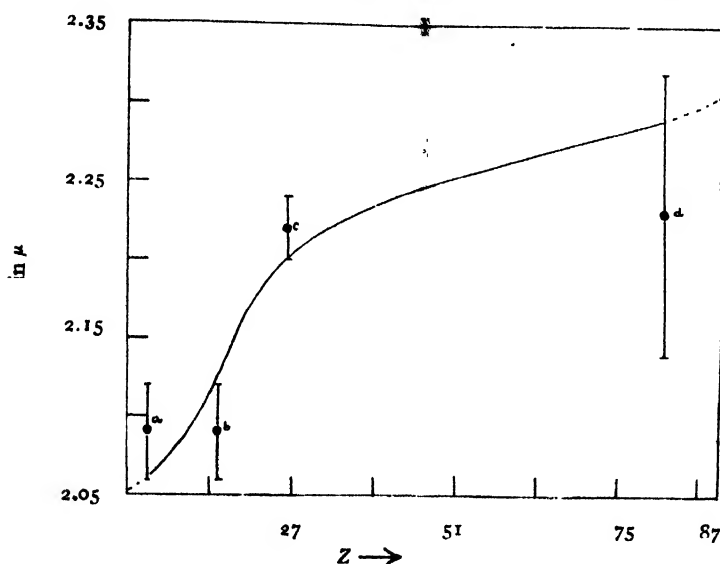


Fig. 4. Plot of  $\tau_+$  against  $Z$ . The points correspond to (a) Alvarez et al, 1950, (b) Morewitz and Shamos 1953, (c) Bell and Hinks, 1951, (d) Biswas and Sinha, 1954.

accelerate the decay of mu-negatives and that the competition of radiationless decay increases as  $Z^3$ , have been theoretically shown by Epstein, Finkelstein and Oppenheimer (1948).

(b) If, on the other hand, one assumes that  $\tau_+^{free}$  is the same as  $\tau_-^{free}$  both being equal to 2.35  $\mu$ secs, then the saturation limit of  $\tau_+$  in figure 4 should be 2.35  $\mu$ secs and the positives show a low value of capture probability ( $\sim 10^4$  per sec) as the value of  $Z$  decreases. This means that there is a very low but finite amount of probability for the positive muons to penetrate into the nucleus when the potential barrier due to the Coulomb field is small and this may be significant for lower values of  $Z$  ( $Z < 6$ ).

Of the two possibilities, the latter seems to be more plausible. In the case of negative muons, the acceleration effect on account of the Coulomb field has been found to be absent from the experimental evidence and hence its effect on the positives may not also be present.

## ACKNOWLEDGMENTS

In conclusion, the author wishes to thank Professor D. M. Bose, Director Bose Institute and Dr. M. S. Sinha for some critical discussions, encouragement and advice. The work was done under a scheme supported by the Atomic Energy Commission, Government of India.

## REFERENCES

- Alvarez, Longacre, Orgen and Thomas 1950, *Phys. Rev.*, **77**, 752.  
Bell and Hincks, 1951, *Phys. Rev.*, **84**, 1243.  
,, 1952, *Phys. Rev.*, **88**, 1424.  
Biswas and Sinha, 1954, *Phys. Rev.*, in press.  
Cathey, 1952, *Phys. Rev.*, **87**, 162.  
Dallaporta, 1952, *Nuovo Cimento*, **9**, 449.  
Epstein, Finkelstein and Oppenheimer, 1948, *Phys. Rev.*, **73**, 1140.  
Krausher, 1948, *Phys. Rev.*, **73**, 1408.  
Kennedy, 1952, *Phys. Rev.*, **87**, 953.  
Keuffel, Harrison, Godfrey and Reynolds, 1952, *Phys. Rev.*, **87**, 942.  
Morewitz and Shamos, 1953, *Phys. Rev.*, **92**, 136.  
Ticho, 1948, *Phys. Rev.*, **74**, 1337.  
Tomonaga and Araki, 1940, *Phys. Rev.*, **58**, 90.  
Wheeler, 1949, *Rev. Mod. Phys.* **21**, 133.

# ON DEPENDENCE OF RESOLVING POWER OF PRISM, GRATING AND REFLECTING ECHELON ON STAGE OF RESOLUTION AND DETECTING INSTRUMENT

BY OM PRAKASH SHARMA AND MAHENDRA SINGH SODHA\*

DEPARTMENT OF PHYSICS, ALLAHABAD UNIVERSITY, ALLAHABAD

(Received for publication, March 20, 1954)

**ABSTRACT.** The authors have discussed the variation of resolving power of prism, grating and reflecting echelon with the value chosen for  $I_{\min}/I_{\max}$  at limiting resolution, which is characteristic of the stage of resolution desired and the detecting instrument.

## INTRODUCTION

Ditchburn (1930) has pointed out that the resolving power of an instrument depends upon the stage of resolution desired and the detecting instrument. The stage of resolution and the detecting instrument are characterised by the value of  $C = I_{\min}/I_{\max}$  at limiting resolution, where  $I_{\min}$  and  $I_{\max}$  are the central minimum and maxima of the resultant intensity pattern of two lines to be resolved.

The values of  $C$  for three important stages of resolution, distinguished by Ditchburn, when the spectrogram is examined by a microphotometer are as follows :

Stage of resolution	...	$C$
Detection of inhomogeneity in radiation	...	0.98
Partial resolution (approximate incasement of wavelength separation)	...	0.8
Complete measurement (measurement of wavelength separation and relative intensities)	...	0.4

This communication discusses the dependence of resolving power of prism, grating and reflecting echelon, which is characteristic of the stage of resolution desired and the detecting instrument.

## VARIATION OF RESOLVING POWER WITH $C$

The intensity pattern of a spectral line after diffraction by a grating is given by

$$I' = B \frac{\sin^2 N\beta}{\sin^2 \beta} \quad (1)$$

\*Now at Defence Science Laboratory, New Delhi.

where  $N$  is the number of lines in the grating and  $2\beta = 2\pi\nu e'(\sin i - \sin \theta)$  is the phase difference between the rays diffracted by two adjacent elements of grating, where the symbols have usual meanings.

The maximum intensity, say  $I_0$ , is given by

$$I_0 = BN^2$$

and hence equation (1) may be expressed as

$$\frac{I'}{I_0} = \frac{\sin^2 NB}{N^2 \sin^2 \beta} = \frac{\sin^2 x}{x^2} \quad (2)$$

where  $x = N\beta$  and  $\beta \ll 1$ .

Equation (2) also represents the intensity pattern in case of a prism if  $x = \pi/\nu \sin \theta$ , the symbols having usual meanings.

The quantity  $\Delta x$  is proportional to the angle between two close spectral lines and therefore we shall use  $\Delta x$  instead of  $\Delta \theta$  to represent the latter in this investigation.

The intensity distribution of another spectral line separated by an angle  $\Delta x = a$  is given by

$$\frac{I''}{I_0} = \frac{\sin^2(x-a)}{(x-a)^2} \quad (3)$$

The resulting intensity pattern is given by

$$\frac{I}{I_0} = \frac{\sin^2 x}{x^2} + \frac{\sin^2(x-a)}{(x-a)^2} \quad (4)$$

The central maxima ( $x \approx 0$ ) and minimum ( $x \approx a/2$ ) are given by

$$I_{max} = 1 + \frac{\sin^2 a}{a^2} \quad (5)$$

$$\text{and} \quad \frac{I_{min}}{I_0} = \frac{2 \sin^2(a/2)}{(a/2)^2} \quad (6)$$

For limiting resolution

$$C = I_{min}/I_{max} \quad \dots (7)$$

$$= \frac{2 \sin^2(a/2)}{(a/2)^2} \bigg/ \left( 1 + \frac{\sin^2 a}{a^2} \right) \quad \dots (8)$$

If the separation of two lines at limiting resolution is  $a$  it can be shown that the resolving power  $R$  is given by

$$R = k \lambda \frac{d\mu}{d\lambda} \quad \text{for a prism} \quad \dots (9a)$$

$$\text{and} \quad R = kNn \quad \text{for a grating and for a reflecting echelon,} \quad \dots (9b)$$

$$\text{where} \quad k = \pi/a \quad \dots (9c)$$

Table I gives the variation of  $k$  with  $C$  obtained by calculating both  $C$  and  $k$  for some values of  $a$ .

TABLE I  
Variation of  $k$  with  $C$

Serial no.	$a$		$C$	$k$
	in degrees	in radians		
1	150	$\frac{5}{6}\pi$	1.051	1.2
2	160	$\frac{8}{9}\pi$	.98	1.125
3	165	$\frac{11}{12}\pi$	.9401	1.091
4	170	$\frac{17}{18}\pi$	.8982	1.059
5	175	$\frac{35}{36}\pi$	.8553	1.028
6	180	$\pi$	.8106	1.00
7	185	$\frac{37}{36}\pi$	.7647	.973
8	190	$\frac{19}{18}\pi$	.7199	.947
9	195	$\frac{13}{12}\pi$	.6747	.923
10	200	$\frac{10}{9}\pi$	.6306	.900
11	205	$\frac{41}{36}\pi$	.5866	.878
12	210	$\frac{7}{6}\pi$	.5451	.857
13	220	$\frac{43}{36}\pi$	.473	.837
14	225	$\frac{5}{4}\pi$	.4640	.800
15	230	$\frac{23}{18}\pi$	.3931	.770

The variation of  $k$  with  $C$  is illustrated by the graph below :

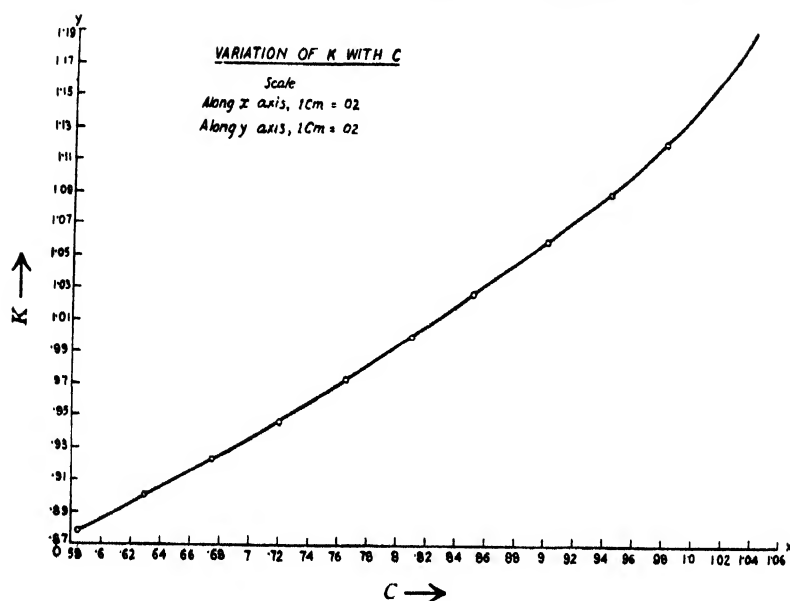


FIG. 1 Variation of  $k$  with  $C$

The treatment for grating equation (9b) is also applicable to reflecting echelon for both have the similar intensity pattern.

#### ACKNOWLEDGMENTS

The authors are grateful to Prof. K. Banerjee, Dr. K. Majumdar and Shri Keshto Chandra Banerji for their kind interest in the investigation.

#### REFERENCE

Ditchburn, 1930, *Proc. Roy. Irish Acad.*, **39**, 58.



# A STUDY OF AIR ABSORPTION OF SOME LIQUIDS

By G. L. DE AND P. MAHANTI

DIELECTRIC RESEARCH LABORATORY, DEPARTMENT OF APPLIED PHYSICS,  
CALCUTTA UNIVERSITY.

(Received for publication, July 24, 1954)

**ABSTRACT.** A study of the air absorption characteristics of some liquids gives an idea of the stability, degree of polarity and the quality of the liquids under investigation. An empirical relation is also attributed.

## INTRODUCTION

It is well known that the gas absorption of insulating liquids is one of their important physical properties and it plays a very important role so far as their electrical properties are concerned. In fact, an ordinary non-degassed liquid suffers a huge change in its physical, chemical and in electrical properties when it is subjected to the process of degassing. The gas absorption of a particular insulating liquid is an effective agent in determining its dielectric strength. Clark (1935) observed that the relation with temperature for both air absorption and dielectric strength of an insulating oil were similar in nature. He also found that the effect of temperature and pressure on the dielectric strength of an insulating liquid is a logarithmic function of the relative density of the dissolved gas. In fact the absorbed air within an insulating liquid forms gas-pockets; due to insipient discharges during an increased voltage stress they form easy seats for ionising centres, thus leading to a heavier conduction current and a premature break-down of the liquid. The oxygen in the dissolved air has a deleterious effect on the chemical structure of the liquid and consequently is responsible for an increased polarization and power-factor. The electrical conduction in a highly refined liquid may be taken as obeying the corresponding laws for gases, and Nikuradse (1932) showed that the behaviour of such a liquid in the current voltage relation corresponds to that of a gas. Organic liquids have a tendency to acquire an increased dielectric constant when bubbled with air, due to the polarization of the carbon molecules by oxydation. Sisskind and Kasarnovsky (1937) examined a most interesting relation between electric polarizability, dipole moment and solvent power. In fact insulating oils are graded according to their gas absorptive power for their relative suitability as insulants in different service requirements.

In view of the importance of gas absorption in liquid dielectrics, investigation of this property was undertaken with special reference to insulating oils, vegetable oils being the centres of interest. When specially refined

and processed, vegetable oils are expected to work as good substitute for their mineral and synthetic relatives. Properties of some of the vegetable oils in raw and unprocessed condition were studied previously by Bhattacharya (1936, 1937) and Ghosh (1940). The works of several other investigators viz., Paranjpe and Deshpande (1934-35), Mahanti and Chakrabarty (1942) can be mentioned in this connection. Attempt was here made to study the nature of absorption of a few vegetable oils in their refined stages. Distilled water and transformer oil were also included in the list for investigation, as standards for comparison. The following liquids were used for investigation purposes: (1) Distilled water, (2) transformer oil, (3) linseed oil, (4) groundnut oil and (5) sesame oil.

#### EXPERIMENTAL

##### (a) Preparation of sample:

Redistilled conductivity water was used in the present investigation. The oils were carefully refined in the laboratory. Firstly a specimen of the oil was washed with a definite strength of lye solution and after separating the soap it was washed again with a lye of higher strength and the process repeated till the acid number was as low as possible. Finally the oil obtained was treated with 5% of its weight with Fuller's earth and sufficient quantity of silica gel. All such treatments and washing were performed at an elevated temperature of about 50°—60°C. The oil was then filtered under fine filter paper and its acid number tested as usual with standard KOH solution. The sample was then ready for absorption measurement.

##### (b) Measurement technique:

The measuring apparatus was the same as used by Bhattacharya (1936, 1937) but the technique of measurement was a little modified. The liquid under investigation was degassed for four to five hours and as the temperature of the liquid was lowered due to degassing, it was kept at rest for some time to attain temperature equilibrium. Air was let in and the absorption process commenced when the flask was shaken. Throughout the absorption process the mercury menisci were always kept to the same level in the manometer limbs, so that the pressure of air inside the flask was always constant. The experiment was continued for sufficient time so that equilibrium conditions were attained regarding absorption.

#### RESULTS

The experimental data are given in Tables I—V. For a comparative study absorption of air per c.c. of the liquid was considered and the experimental temperature and pressure were reduced to N.T.P. Volume per cm. of the manometer tube was found to be 0.162861 c.c. and the samples having acid number greater than 0.17 mgm. of KOH/gm. of oil, were rejected.

TABLE I. Distilled water

Experimental conditions: Volume taken—70 c.c, temperature  $-32.8^{\circ}\text{C}$ ,  
initial level  $-6.0$  cm, degassed for 4 hours.

$$\alpha_0 = 0.02202.$$

$$\lambda = 0.3.$$

Time interval minutes	Mercury level in manometer cm.	Length of mercury column cm	Absorption per c.c. $\alpha_{\text{obs. c.c.}}$	Absorption per c.c. $\alpha_{\text{cal. (c.c.)}}$
1	17.5	11.5	0.02389	0.02121
3	17.5	11.5	0.02389	0.02202
8	16.6	10.6	0.02202	0.02202
12	16.6	10.6	0.02202	0.02202
17	16.55	10.55	0.02192	0.02202
22	16.55	10.55	0.02192	0.02202
27	16.35	10.35	0.02149	0.02202
47	16.35	10.35	0.02149	0.02202

TABLE II. Transformer oil.

Experimental conditions: Volume taken—49.95 c.c, temperature  $-25.1^{\circ}\text{C}$ .  
initial level  $-4.65$  cm. degassed for 4 hours.

$$\alpha_0 = 0.09428.$$

$$\lambda = 0.87.$$

Time interval. mins.	Mercury level in manometer cm.	Length of mercury column cm.	Absorption per c.c. $\alpha_{\text{obs. (c.c.)}}$	Absorption per c.c. $\alpha_{\text{cal. (c.c.)}}$
2.10 sec	33.7	29.05	0.08678	0.08654
3.30 "	35.9	31.25	0.09335	0.09255
4.40 "	36.0	31.25	0.09364	0.09386
7.30 "	36.0	31.35	0.09364	0.09426
10.0	36.0	31.35	0.09364	0.09428
15.0	36.2	31.55	0.09426	0.09428
20	36.2	31.55	0.09426	0.09428
25	36.8	32.15	0.09602	0.09428
30	36.8	32.15	0.09602	0.09428
35	37.3	32.65	0.09754	0.09428
38	37.8	33.15	0.09904	0.09428
41	38.0	33.35	0.09963	0.09428
50	38.9	34.25	0.10231	0.09428
60	38.9	34.25	0.10231	0.09428
65	39.9	35.25	0.10529	0.09428
75	39.9	35.25	0.10529	0.09428
80	39.9	35.25	0.10529	0.09428

TABLE III. Sesame oil

Experimental conditions: Volume taken—35.5 c.c, temperature—30.35°C,  
initial level—3.4cm, degassed for 3 hours 30 mins.

$$\alpha_0 = 0.12833.$$

$$\lambda = 0.96.$$

Time interval	Mercury level in manometer	Length of mercury column	Absorption per c.c.	Absorption per c.c.
mins.	cm.	cm.	$\alpha_{obs}$ C.C.	$\alpha_{cal}$ C.C.
2	30.8	27.4	0.11319	0.11319
5	34.7	31.3	0.1293	0.12829
13	34.7	31.3	0.1293	0.12899
23	34.3	30.9	0.1276	0.12899
33	34.3	30.9	0.1276	0.12899
43	34.3	30.9	0.1276	0.12899
53	34.3	30.9	0.1276	0.12899
60	34.3	30.9	0.1276	0.12892
73	34.9	31.5	0.1301	0.12899
83	34.4	31.0	0.1280	0.12899
93	34.3	30.9	0.1276	0.12899
108	33.8	30.4	0.1256	0.12899

TABLE IV. Linseed oil

Experimental conditions: Volume taken—36.7c.c, temperature—31.0°C,  
initial level—4.0 cm, degassed for 5 hours.

$$\alpha_0 = 0.11740$$

$$\lambda = 1.0$$

Time interval	Mercury level in manometer	Length of mercury column	Absorption per c.c.	Absorption per c.c.
minutes	cm.	cm	$\alpha_{obs}$ C.C.	$\alpha_{cal}$ C.C.
2	29.5	25.5	0.10260	0.10151
5	33.4	29.4	0.11740	0.11661
12	33.4	29.4	0.11740	0.11740
17	33.4	29.4	0.11740	0.11740
21	33.4	29.4	0.11740	0.11740
41	33.4	29.4	0.11740	0.11740
56	33.4	29.4	0.11740	0.11740

TABLE V. Groundnut oil

Experimental Conditions: Volume taken—49.1 c.c, temperature—25.4°C.  
 initial level—4.0 cm, degassed for 4 hours.  
 $\alpha_0 = 0.08524$ .  $\lambda = 1.52$ .

Time interval	Mercury level in manometer	Length of mercury column	Absorption per c.c.	Absorption per c.c.
minutes	cm.	cm.	$\alpha_{obs}$ c.c	$\alpha_{cal}$ c.c.
5	31.0	27.0	0.08196	0.08209
10	32.0	28.0	0.08500	0.08512
15	32.0	28.0	0.08500	0.08524
20	32.0	28.0	0.08500	0.08524
25	32.0	28.0	0.08500	0.08524
35	32.4	28.4	0.08620	0.08524
40	32.4	28.4	0.08620	0.08524
45	32.4	28.4	0.08620	0.08524

## DISCUSSIONS

All the liquids under investigation showed a high rate of absorption within a period of 2-7 minutes from the beginning and then the rate slowed down. Over a long period of air absorption some of the characteristic curves show steady conditions for sometime while some others show variations. The variation of absorption within the period of observation can be accounted for by the fact that the net absorption processes, is the result of two different absorption factors *viz.*, the absorption of gas by the liquid and the evolution of gas from the liquid.

Now the association of gas and liquid molecules in the absorption process is maximum under a favourable condition when the liquid is said to be in equilibrium. But the absorption of gas is dependent on several factors, *viz.*, depth of liquid, free surface exposed to the gaseous medium, catalyst, if any, and the temperature. Since the process is a dynamic one and the temperature over a long period is difficult to control, the condition for a steady state is not easy to approach. Further there is the chance for the formation of volatile gases due to oxidation causing evolution of gas from the liquid. The electrostatic forces of attraction to form association of molecules in the absorption mechanism is sensitive to temperature variation of the system and consequently difficulty may arise for the accuracy of attaining an equilibrium condition. The identical nature of the curves indicate that the liquids under investigation are stable in character having high ordinates at the beginning. But if high ordinate is reached after sometime, *i.e.*, if the rate of absorption is slow at the

beginning, the liquid can be said to be unstable, for the slow process of attaining the high ordinate indicates that both the absorption and evolution of gas are going on simultaneously and the more gas is evolved the liquid becomes less stable.

From a study of the nature of the characteristic curves, it can well be represented empirically by an equation of the form

$$\alpha = \alpha_0 (1 - e^{-t/\lambda})$$

where

$\alpha$  = absorption per c.c. in time  $t$ .

$\alpha_0$  = maximum absorption.

$t$  = time in minutes.

$\lambda$  = a coefficient, characteristic for a particular liquid.

For certain experimental conditions  $\alpha_0$  is constant for a particular liquid, while  $\lambda$ , determining the quality of the liquid, is also a constant under that specified condition. The slope of the characteristic curves for a particular liquid is determined by the value of  $\lambda$  which indicates the chemical condition of the liquid. So values of  $\lambda$  for a liquid give information of the chemistry and degree of purification of the liquid under investigation. Solution of the above equation yields values of  $\lambda$  and  $\alpha_0$  for a particular liquid and the calculated values of  $\alpha$  are in close agreement with the observed values as shown in the tables. The full line curve and the dotted one indicate the experimental and theoretical curves respectively (see figure 1). The discrepancy between the theoretical and

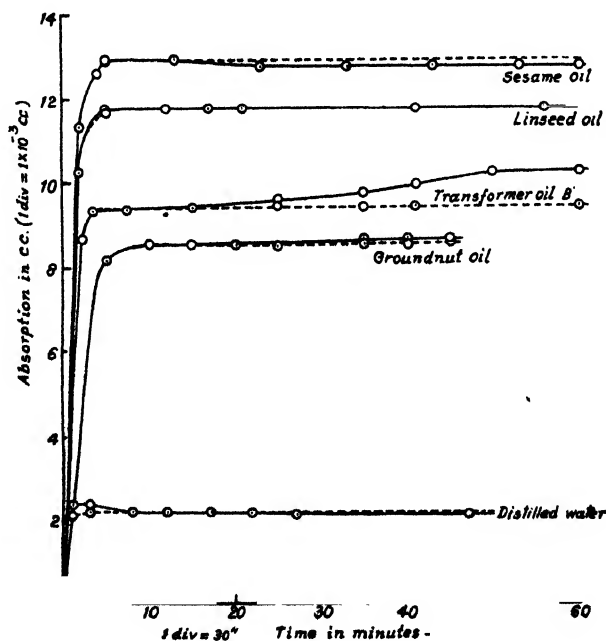


FIG. 1

experimental curves is attributable to varying experimental conditions within the period of observation, the rate of absorption is an exponential function of time. One notices from the graph that the absorption of dry air is low for distilled water while it is comparatively high for the oils. From the nature of the liquids it is evident that water is highly polar, while the oils being highly refined, the degree of polarity of the molecules is much low and dry air is non-polar in character. Since in the absorption mechanism some types of electrostatic forces come into play to form an association of molecules, the degree of polarity of the molecules in the two phases influences the absorption process. So the nature of the absorption characteristic gives an idea of the degree of polarity of the molecules in the gas and also in the liquid and thus speaks in a qualitative way about the conditions of the liquid and the gas.

#### REFERENCES

- Bhattacharya, G. N., 1936a, *Ind. J. Phys.*, **10**, 209.  
 „ 1936b, „ **10**, 281.  
 „ 1936c, „ **10**, 403.  
 „ 1937, „ **11**, 65.  
 Clark, F. M., 1935, *Trans. A. I. E. E.*, **54**, 52.  
 Ghosh, C. S., 1940, *Ind. J. Phys.*, **14**, 153.  
 Mahanti, P. C., and Chakrabarty, S., 1942, *Ind. J. Phys.*, **16**, 81.  
 Nikuradse, A., 1932, *Physik. Z.*, **13**, 553.  
 Paranjpe and Deshpande 1934-35, *Proc. Ind. Acad. Sc.* 1A, 880, 1934-35.  
 Sisskind and Kasarnovsky, 1937, *Trans. Farad. Soc.*, **33**, Pt. I.





# PROCEEDINGS OF THE INDIAN ASSOCIATION FOR THE CULTIVATION OF SCIENCE

*(Proceedings of the High Polymer Symposium held in the  
Association in March 1954)*



## SYMPOSIUM ON HIGH POLYMERS

(including rubbers, resins, plastics and fibres.)

A symposium on High Polymers including rubbers, resins, plastics and fibres, organised by the Physical Chemistry Department of the Indian Association for the Cultivation of Science was held at the Association Hall on the 29th and 30th March, 1954, which was followed by a three days summer course on the same subject. Dr. S. S. Bhatnagar had kindly consented to inaugurate the symposium but for unavoidable reasons he could not be present on the occasion. Scientists from different parts of India including Poona, Bombay, Kanpur, Digboi (Assam), Delhi and Madras and also from various Industrial firms and research institutes including the Imperial Chemical Industries, I.J.M.A.R.I., National Rubber Works, Jardine Henderson Research Laboratory, Bengal Immunity Research Institute, Bengal Tanning Institute, Bengal Chemical and Pharmaceutical Works, Shalimar Paints Co. Ltd., Burma Shell Oil Co., Science College, College of Engineering & Technology, Jadavpur, Bengal Engineering College, Shibpur, National Chemical Laboratory, Poona, Central Leather Research Institute, Madras, Assam Oil Co., Digboi, Fuel Research Institute, Dhanbad, Indian Standards Institution, Delhi, Tata Oil Mills Co., Bombay, All India Plastics Mfg. Association, Institute of Sugar Technology, Kanpur, Institute of Rubber Industry, Paint Mfg. Association and Central Glass & Ceramic Research Institute, attended the symposium to make it a success.

### Inauguration

Prof. Santi R. Palit welcomed the delegates from different parts of India and others present, and Dr. M. N. Saha, F.R.S., inaugurated the symposium. Messages of goodwill from Dr. S. S. Bhatnagar and Dr. J. C. Ghosh were also presented by Dr. Saha in course of his inaugural address. He referred to the sad demise while working in

the Laboratory of Sri Nanigopal Saha, Senior Scholar of the department, on the 20th March, 1954. Dr. Saha stressed on the necessity of such symposia being held periodically to promote the healthy growth of science in our country. A group photograph of the members attending the symposium was then taken.

**29th March, 1954**

**Morning Session**

The morning session under the chairmanship of Prof. Santi R. Palit was then opened with a lecture on **"Polymeric Constitution of Coal"** by **Dr. A. Lahiri, Director, Fuel Research Institute, Dhanbad.** Dr. Lahiri said that scientific investigations for the last half century has shown that coal is a naturally occurring polymer, with structure similar to that of cellulose or rubber, the repeat unit tending to be in one plane only. He stressed the necessity of investigating coal, particularly its solutions by the established techniques of high polymer chemistry. Reaction and properties are markedly influenced by their colloid structure and cross linking may take place in high oxygen containing non-coking coals. Study of the adsorption isotherm of water vapour on coal indicates the presence of a pronounced hysteresis loop between sorption-desorption cycles which is an indication of a micro-capillary structure of coal. The surface area values lie in the range of 20—200 sq. m. per gm. of coal, depending on rank. X-ray diffraction studies indicate the presence of incipient layer plane structure present in coal. With bituminous coal pyrolysis in molecular still, action of solvents, mild hydrogenation and mild oxidation have been carried out which leads to the conclusion that the nucleus of this coal is a condensed  $C_6$  ring structure with occasional heterocyclic rings containing oxygen and sulphur. Infra red spectroscopy shows that coal is a gel and that in the course of metamorphosis from the stage of peat to high rank coal with 90% carbon, the change is from a lyophilic to a lyophobic colloid.

Following this, **Dr. D. Banerjee, National Rubber Works, delivered a lecture on "The Rubber Manufacturing Industry in India".**

He said that Rubber Manufacturing industry in India is just over 20 years old and has developed and expanded considerably to which much impetus was given by the war. Imports of rubber goods have dwindled and export has gone up.

The industry requires about 22,000 tons of raw rubber annually. The main source is Indian plantations whose annual output is approximately 20,000 tons, the balance being imported. Other raw materials are textiles, carbon-black, sulphur, chemicals, etc. Textiles are available from indigenous sources while the rest are chiefly imported.

India manufactures various rubber goods, of which tyres are most important and account for nearly 67% of the total raw rubber consumption. Recently, rubber manufacturers have embarked on the production of a number of new lines which were hitherto imported.

Dr. Banerjee then referred to the research facilities available at the Industrial and Government laboratories and gave an account of the problems under investigations at present. He also recommended various problems of direct benefit to the Industry and made a plea for these being investigated at the National Laboratories.

**29th March, 1954**

**Afternoon Session**

Under the chairmanship of Dr. S. L. Bafna (N.C.L., Poona), the afternoon session started with a lecture on "**Fibre Science**" by **Dr. D. B. Das (Jardine Henderson Research Laboratories)**. Dr. Das gave a detailed account of the formation and various modern uses of fibres. He showed that the properties of fibres are dependent on the length of the chain, and the molecular weight should be at least 10,000 for making fibres. Attention was given to problems related to cotton cellulose, jute fibres, etc., and the structure of fibres was discussed.

The session was then devoted to six papers on plastics. The first paper on "**Future Possibilities for the Plastic Industry in India**" was read by **Sri T. V. Subba Rao (Tata Oil Mills Co. Ltd., Bombay)**, who stressed on the need for the expansion of the plastics industry in India. Though it is well recognized, the limitations in the way of

this expansion are not so well appreciated. Emphasis has been hitherto laid more on the slow progress of the Indian Chemical Industry as the main limiting factor in the expansion of the Indian Plastics Industry. While this is no doubt true, the very slow progress and in some cases, no progress made by way of development of the many mechanical and electrical industries that are very closely interlinked with the plastics industry for the offtake of the plastics products cannot be ignored. The present position of some of these industries and the need for synchronising the development of these chemical, mechanical and electrical industries that are interlinked with the plastics and allied industries are discussed.

The second paper on **‘Plastics from Mollasses’** was read by **Dr. S. Mukherjee (Indian Institute of Sugar Technology, Kanpur)** who said that sugarcane molasses, containing about 50% of sugars on condensation with phenol, creosote and wood tar phenol gives a resin which is insoluble in water. This, on mixing with requisite quantities of filler, hardening agent and lubricant and on compression moulding gives insoluble and infusible thermo setting plastic. The physical and electrical properties of the finished products compare favourably with those of phenol-formaldehyde plastics. Of the various compositions tried, molasses and phenol give the best results. The cheapest product was from molasses and wood tar phenol.

**Sri T. V. Subba Rao** again read a paper on **‘A Review on Plastics from Proteins and Lignin’**, when he told that the present limitations in the development of the synthetic plastics in India for want of some of the essential raw materials required for their manufacture, necessitates a serious consideration of utilisation of some of the indigenous natural products for making plastic compositions of practical utility. Proteins and lignin are two natural products that are available in plenty. Several attempts have been made to make plastic compositions from these materials only with a limited success. A brief review of the present position of our understanding about proteins and lignin with special reference to the various processes suggested for their utilisation as plastic compositions was given.

**Dr. P. K. Chaudhuri** then presented his paper on **"Thermosetting Moulding Powder from Agricultural Wastes"**, wherein he described preparation of a plastic from groundnut shell and sawdust by a very simple method. No formaldehyde is required and only a small percentage of outside phenolic body will convert the shell or the sawdust into the moulding powder. No special equipment is necessary for the reaction. The method of fabrication is also very similar to that of phenolic resin. The moulding conditions, the curing time, temperature etc., are also practically the same. The cured product is unaffected by water and acetone and has a high resistance to temperature standing up to a continuous temperature of 230°C without any sign of distortion or decomposition.

The chairman then read out a paper communicated to the symposium, entitled **"Plastics Industry in India"** by **N. Srinivasan** and the session closed with the last paper on **"Standardisation in the field of Plastics"** read by **Sri V. B. Mainkar** (Indian Standards Institute Delhi). Sri Mainkar discussed the present state of the Plastics industry in India and the causes and necessity for their standardization. He referred to the various methods for testing to evolve suitable standards not only for plastics, but also for other commodities and to the work done in the Indian Standards Institution for their acceptance throughout India.

**30th March, 1954**

**Morning Session**

The morning session on 30th March, 1954 was devoted to the reading of papers on Fundamentals of Polymerization. Dr. S. Mukherjee (I.S.T., Kanpur) was in the chair and **Sri K. O. Majumdar** opened the session with a paper on **"Distribution of Molecular Weight of High Polymers"**. He gave new equations for the distribution of molecular weight of High Polymers as affected by chain transfer. He has deduced a number of relationships which are now being subjected to direct experimental test.

The second paper on **"Determination of Kinetic Constants of Polymerization of vinyl monomers using various Peroxides and**

**Azobisnitriles'** by Late Nani Gopal Saha, (I.A.O.S., Calcutta 32) was read by Sri U. S. Nandi. Two minutes' silence was observed in honour of late Nani Gopal Saha before reading his paper. The paper consists of a thorough study on the kinetics of addition polymerization with nine substituted peroxides and seven azobis nitriles both in bulk and in solution of solvents. Most of the catalysts were found to be ideal in behaviour and follow the square root law. Substituents were found to have marked effect on the initiation and transfer reactions. The nitro substituted dibenzoyl peroxides were found to behave abnormally in this connection.

Prof. Santi R. Palit then read out the last two papers "**Studies on Chain Transfer**" by R. N. Chada and G. S. Misra (Lucknow University, Lucknow) and "**Studies on Macromolecules**" by N. H. Shivarmakrishnan and M. R. A. Rao (Indian Institute of Science, Bangalore), sent to be presented at the Symposium. The first paper consists of a study on the chain transfer reaction between growing styrene (M) polymer radical and toluene (S), when catalysed by phenylazotriphenyl methane (B). It has been shown that the transfer constant from the slope of  $1/P$  against  $S/M$  plots at constant  $B/M$  values is not appreciably affected by the presence of low concentrations of the catalyst and initiation reaction was found to be bimolecular.

The other paper consists of a study of spreading properties of rubber and its derivatives. Effect of protein content and solvent towards the spreading of rubber was studied and it was found that the double bond of the isoprene group was responsible for the spreading property of rubber. Attention was given to the rate of oxidation of rubber films as influenced by the pH and halogens in the aqueous substrate. Moreover, the spreading and other physico-chemical properties of chlorinated rubber samples were compared.

#### Afternoon Session

With Sri K. V. Gopalan (Assam Oil Co., Digboi) in the chair the afternoon session was devoted to papers on Ion-exchange Resins and miscellaneous subjects. The session was opened with the paper



on **"High Polymer in Therapy"** by **Mr. S. K. Ganguly (Bengal Immunity Research Institute, Calcutta)**, the paper describes some preliminary experiments on the use of polyvinyl pyrrolidone as plasma expander and its examination both chemically and biologically. The purity of the high polymer and the molecular weight as also the viscosity, surface tension, specific gravity, of the aqueous solution of polyvinyl pyrrolidone for therapeutic use were considered in respect of the suitability for intravenous transfusion. The product was made isotonic with blood with the addition of electrolytes and tested biologically for maintenance of blood pressure by intravenous transfusion in artificially bled experimental animals.

**Dr. S. Mukherjee (Institute of Sugar Technology, Kanpur)** then read his paper on **"Ion exchange Resins from Sugars"**. He said that a number of cation exchange resins from sugars using different proportions of sucrose and phenolsulphonic acids at different temperatures of condensation was prepared and their properties studied. The capacities of the resins were measured by four different methods.

**Dr. S. L. Bafna (N.C.L., Poona)** then gave a lecture on **"Ion exchange Resins"**, in which a comprehensive survey was given of the various modern uses of both anion and cation exchanges. A short history of the phenomenon of ion-exchange in natural earths was discussed leading to the discovery of ion-exchange resins. Attention was drawn as to how the basic principles for the synthesis of cross linked polymers are utilized for the synthesis of ion-exchanges. The exchanging groups are either already present in the simple molecules which are polymerized or are introduced after crossed linked polymer is formed by standard methods of organic chemistry.

Next **Dr. S. K. Mukherjee (Science College, Calcutta)** presented a paper on the use of ion exchange membranes as electrodes in the determination of the activities of alkali metals. This is an improvement on the old clay membranes in which Dr. Mukherjee substituted ion exchange clay by synthetic resins thereby improving the accuracy and sensitivity of the method considerably. He also suggested some possible developments on the preparation of these membranes in which mixture of ions could be determined by proper choice of some

fixing components on the resin molecule itself. He reported some preliminary results on the determination of sodium in presence of calcium.

The concluding paper on "Gums as Polyelectrolytes" was read by Dr. Sadhan Basu (I.A.C.S., Calcutta-32). He said that natural gum acid salts like sodium arabate and sodium salt of agar acid have been found to behave like synthetic polyelectrolytes like poly vinyl pyridinium methyl bromide. These assumptions have been corroborated by viscometric and osmometric methods. This was assumed to mean, indirectly, that gum acids are linear chain polymers with some branching.

Dr. P. Dutt, Head of the Organic Chemistry department, I.A.C.S., thanked the delegates and others present for taking part in the Symposium on behalf of the Association. Sri T. V. Subba Rao and Dr. S. L. Bafna on behalf of the delegates thanked in return.

### Entertainments

The Director invited all delegates to an "At home" held at the I.A.C.S. lawn on the 29th March and Prof. Santi R. Palit entertained the out-of station delegates and many outstanding local Scientists including Dr. J. C. Ghosh, Dr. J. N. Mukherjee, Dr. Ashima Chatterjee, Prof. Baradananda Chatterjee (Bengal Engineering College, Shibpur), Dr. P. B. Sarkar (Director, Central Jute Laboratory), Dr. S. Chanda (I.C.I.) and others at a dinner party in his house.

### Summer Course

A three-day summer course for senior workers was availed of by five senior men from different laboratories. The latter were given the opportunity of preparing a few polymers for themselves and studying their properties. Special emphasis was given towards imparting them an experimental acquaintance with the existing methods of determination of molecular weight of high polymers.

**Sadhan Basu**  
Convenor.

# PULSE SLOPE MODULATION—A NEW METHOD OF MODULATING VIDEO PULSES AND ITS POSSIBLE APPLICATION ON LINE CIRCUITS

By JAJNESWAR DAS

INDIAN INSTITUTE OF TECHNOLOGY, KHARAGPUR

(Received for publication, April 28, 1954)

## Plate XVII

**ABSTRACT.** Pulse slope modulation, a new method of modulating video pulses has been realised by using a rectangular gating pulse feeding an integrating circuit. The charging current to the integrating capacity has been made to vary according as the signal voltage. Demodulation is performed by differentiating the slope-modulated pulses and by passing the resultant modulated pulses through memory circuit and low-pass filter.

Possible applications of these pulses on line circuits have been studied, and successful transmission of these through a 100 mile long open wire circuit has been shown.

Signal/noise ratio and linearity of modulation have been found to be very satisfactory and possibility of a more advantageous time-division multiplex system is indicated.

## 1. INTRODUCTION

The development of the different types of pulse modulation (Flood, 1953) like P.A.M., P.D.M., P.P.M., and P. F. M. has been based on the variation of particular characteristics of the generated pulses. The rise-time of the pulses is one of the important characteristics and an attempt has been made to utilise this rise-time characteristic in developing a new method of pulse modulation.

It is known that on integration of a step function, the slope of the ideally integrated function is dependent on the amplitude of the step function and the constants of the integrating circuit. Further, on differentiation of a linear ramp function, the magnitude of the step function, thus generated, is dependent on the slope of the original function. The above facts have been utilised in modulating and demodulating the sampling pulses. A rectangular pulse is used as a gating pulse to a constant current charging circuit. Ideally the output pulse will have its front edge inclined—the slope depending on the value of  $R$  and  $C$  of the charging circuit. The modulating signal is made to vary the value of  $R$  and hence the slope of the output pulse.

Demodulation is carried out by differentiating the variable-sloped pulses and the resulting variable amplitude pulses are passed through a memory circuit and a low-pass filter to give the original signal voltage.

Possible application of the slope-modulated video pulses to the line circuit

has been studied and it is found that with simple R-C semi-differentiating network, good equalisation of loss-frequency distortion produced in the line, is possible. Due to the restricted frequency band-width in lines, trapezoidal pulses are used instead of rectangular pulses.

By using slicing process and narrow gate pulses for the differentiated amplitude modulated pulses, very high degree of 'noise and interference' reduction is attainable by the method.

## 2. THEORY OF MODULATION AND DEMODULATION

A. *Modulation*: It has been shown that (figure 1) when switch opens at time  $t=0$ , the current  $i$  is given by (Chance et al, 1949)

$$i = I_0 e^{-t/RC} \quad (t \geq 0)$$

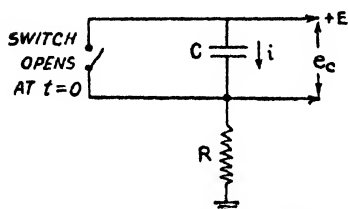


FIG 1. CHARGING CIRCUIT

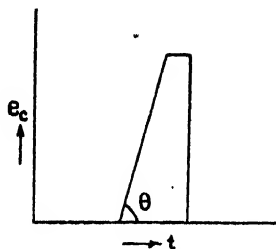


FIG 2 SLOPE-MODULATED PULSE

and the voltage across the condenser is given by,

$$e_c = E (1 - e^{-t/RC}),$$

and the slope 
$$\frac{de_c}{dt} = \frac{I_0}{C} e^{-t/RC} \quad \dots (1)$$

and expressed in power series form

$$e_c = E \left[ t/RC - \frac{(t/RC)^2}{2!} + \frac{(t/RC)^3}{3!} - \dots \right]$$

If the time for which the switch remains open is small compared to  $RC$ , then the charging current will be nearly constant during the charging period, and the voltage

$$e_c = (E/RC)t$$

By using a constant current pentode in place of  $R$ , the condenser is charged at constant current and hence the equation

$$e_c = \frac{1}{C} \int_0^t i dt$$

is modified in the form  $e_c = I_0 t/C$  when  $I_0 =$  constant current through pentode. This is the equation applicable to the modulating circuit used in this system.

If the modulating voltage  $A \sin \phi$  is made to vary the pentode current  $I_0$  in such a way that

$I_0 = I_m (1 + KA \sin \varphi)$  when  $I_m$  = pentode current with no modulation,

then, 
$$e_c = \frac{I_m}{C} (1 + KA \sin \varphi) t \quad \dots (2)$$

and the slope 
$$\frac{de_c}{dt} = \frac{I_m}{C} (1 + KA \sin \varphi) \quad \dots (3)$$
  

$$= \tan \theta. \quad [\text{figure 2.}]$$

In equations (2) and (3), although the modulating voltage  $A \sin \varphi$  is a time-function of the nature of  $e^{j\omega t}$ , the time  $t$  for which the switch remains open (i.e., the duration of the sampling pulse) is very small compared to the time period of the modulating signal. Hence  $A \sin \varphi$  is taken as constant during time  $t$  for the definite integral  $\int_0^t idt$  and the differentiation of the resulting sloped edge of the pulse given by equation (3).

### B. Demodulation.

On differentiation of the voltage  $e_c$ , we have the amplitude of the output pulse,

$$\begin{aligned} \frac{de_c}{dt} &= \tan \theta \\ &= \frac{I_m}{C} (1 + KA \sin \varphi) \\ &= B + K' \sin \phi, \text{ when } B \text{ and } K' \text{ are constants.} \end{aligned}$$

Therefore, the output pulse has an amplitude variation proportional to the modulating signal voltage.

In the case of R-C differentiation (figure 3)

$$e_o/e_c = j\omega RC / (1 + j\omega RC) \quad \dots (4)$$

whereas, the ideal differentiator should have

$$\frac{e_o}{e_c} = \frac{\frac{d}{dt}(e^{j\omega t})}{e^{j\omega t}} = j\omega \quad \dots (5)$$

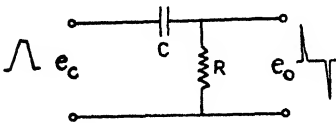


FIG.3. R-C DIFFERENTIATING CIRCUIT.

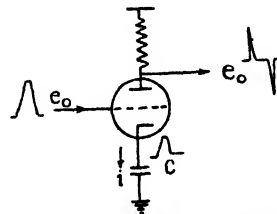


FIG.4 CATHODE FOLLOWER TYPE DIFFERENTIATOR

when  $e^{j\omega t}$  represents the complex input waveform. Hence it is necessary to use small values of  $\omega RC (\ll 1)$  to make

$$e_o/e_c \approx j\omega RC.$$

In the case of cathode follower type of differentiator, (figure 4) when the grid voltage rises, the cathode also follows the grid voltage in the same phase and hence

$$e_c = \frac{M}{C} \int i dt, \text{ where } M \text{ is a constant.}$$

$$de_c/dt = Mi/C \quad \dots (6)$$

This charging current produces a voltage drop at the anode given by,

$$e_o = Ri = \frac{RC}{M} \frac{de_c}{dt}$$

Hence, the output is proportional to the slope of the input pulses.

### 3. CIRCUIT TECHNIQUE

A. *Modulation*: As the sampling frequency has to be at least twice the highest modulating frequency, the pulse repetition frequency is chosen to be 10 kc/s. By the use of square wave generator, differentiating amplifier and limiting wave-shaper, a variable width pulse train is generated. The width of the pulses is variable from 2 microseconds to 20 microseconds. In the particular experiment with the artificial line, 10 microseconds wide pulses are used. Figure 5 shows the block schematic of the pulse generator and modulator. The conventional circuits have not been described (Chance et al, 1949).

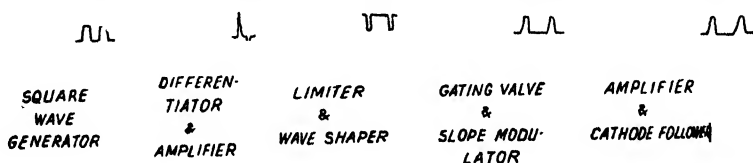


FIG. 5. BLOCK SCHEMATIC OF PULSE GENERATOR & MODULATOR.

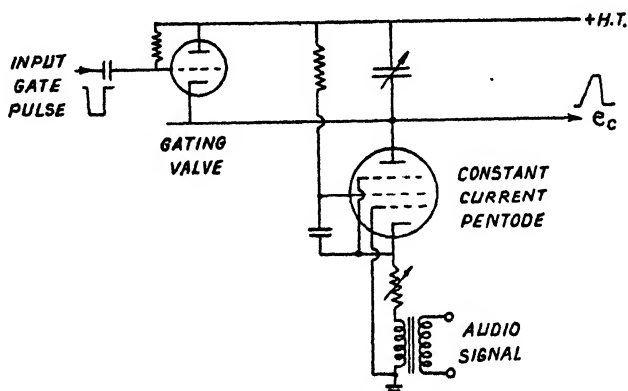


FIG. 6. SLOPE MODULATOR

The slope modulator (figure 6) consists of a gating valve and a charging circuit with a constant current pentode. A negative gating pulse is applied to the switching valve, which, on being cut off, allows the condenser to be

charged through the constant current pentode. A cathode degenerative resistance is used to make the charging more linear and to control the value of the effective  $R$  of the charging circuit.

The modulating signal is fed through an audio transformer in the cathode circuit and the effective variation of the cathode potential (with respect to the grounded grid) changes the value of the charging current and hence the slope of the leading edge of the output pulse varies accordingly. The production of slope modulation is also possible with the variation of screen potential or grid potential. But the variation of screen potential requires much higher modulating voltage and the variation of grid potential produces slight curvature of the slope of the leading edge of the pulse.

The slope modulated pulse is further amplified and passed through a cathode follower to produce a low impedance output of the order of 1–50 volts



FIG. 7(a) UNMODULATED PULSES

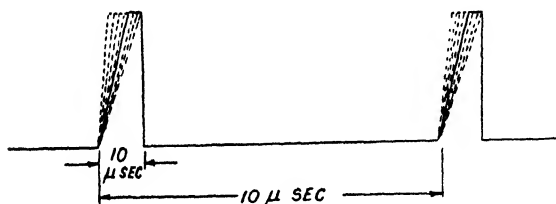


FIG. 7(b) MODULATED PULSES

peak. Figure 7(a) shows the nature of the unmodulated pulses with the leading edges inclined approximately half-way between extreme possible positions. Figure 7(b) shows the nature of the modulated pulses and the dotted sloping edges show the different positions of the leading edge with different modulating voltages.

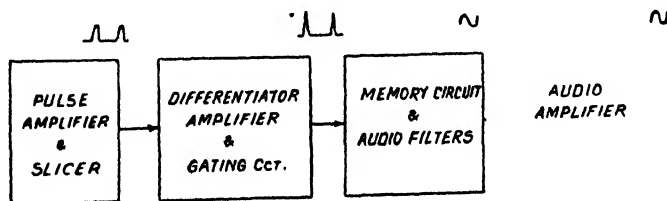


FIG. 8. BLOCK SCHEMATIC OF RECEIVER FOR SLOPE MODULATION.

**B. Demodulation:** Figure 8 shows the block schematic of the receiver used in the system. Amplified slope modulated pulses are passed through the slicer circuit for noise reduction and then differentiated to produce amplitude modulated pulses. A very narrow gate is used after the A.M. pulse amplifier

to effect further noise reduction. Finally A.M. pulses are detected in the memory circuit and then passed through the necessary low-pass audio filters and audio amplifiers.

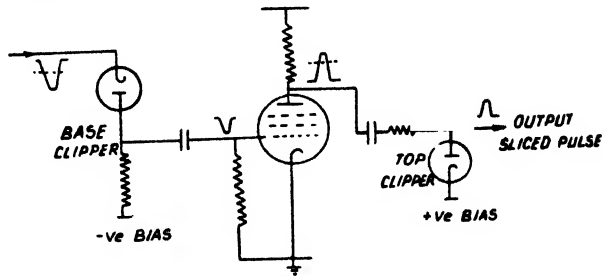


FIG.9 SLICER CIRCUIT

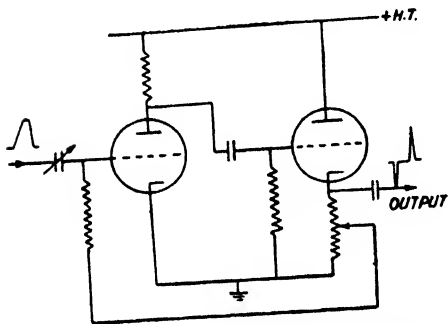


FIG 10 (a). RC DIFFERENTIATING AMPLIFIER.

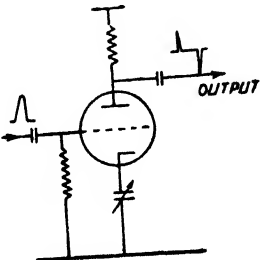


FIG.10 (b) CATHODE FOLLOWER TYPE DIFFERENTIATOR.



FIG 11 (a) AMPLIFIED MODULATED PULSES.

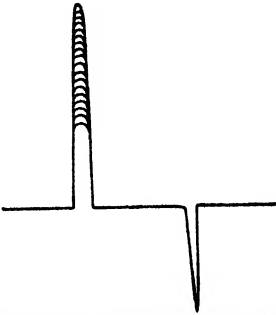


FIG.11 (b). DIFFERENTIATED AMPLITUDE-MODULATED PULSES. SHOWING AMPLITUDE-VARIATION CORRESPONDING TO THE SLOPE VARIATION OF FIG.11 (a)

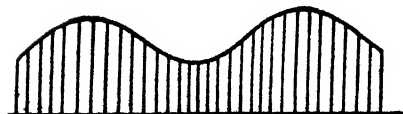


FIG.11 (c) SHOWING A.M. PULSES ON SLOW TIME BASE.



FIG.11 (d) DEMODULATED AND DETECTED AUDIO SIGNAL BEFORE THE FINAL FILTER CIRCUIT.



Many slicer circuits are in vogue. A simple circuit is shown in figure 9. Negative and positive bias on the clipper diodes are adjusted depending upon the noise level in the circuit. The simple differentiator may be either a R-C differentiating amplifier or a cathode follower type differentiator as shown in figure 10. In both the cases the product  $RC$  is very small, as explained in the theory (Section 2).

The gate-pulse can be applied to the next amplifier to select only the A.M. pulses and stop the spurious noise in between the pulses. Nature of the differentiated pulses and the audio output from the memory circuit are shown in figure 11. The process of the complete detection of the information signal is evident and the reproduction is seen to be fairly faithful.

#### 4. APPLICATION ON LINE CIRCUITS

A. *Fourier analysis and frequency bandwidth* : The generated pulses with considerable rise-time may be considered as trapezoidal pulses and their amplitude spectrum can be calculated by Fourier analysis. Figure 12 shows a

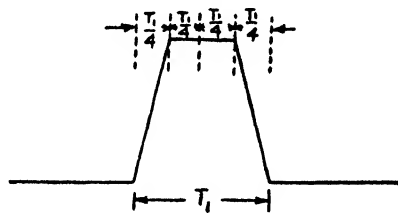


FIG. 12 TRAPEZOIDAL PULSES.

symmetrical trapezoidal pulse with repetition frequency  $= 1/T_0$ , pulse duration  $= T_1$ , rise-time  $= T_1/4$ , and peak voltage  $= E$ .

The amplitude of the  $n$ th harmonic is given by Cherry (1949)

$$a_n = \frac{4ET_0}{\pi^2 n^2 T_1} \left( \cos \frac{\pi n T_1}{T_0} - \cos \frac{\pi n T_1}{2T_0} \right)$$

$$= \frac{40E}{\pi^2} \left[ \frac{\cos \pi n / 10 - \cos \pi n / 20}{n^2} \right]$$

where  $T_0/T_1 = 10$ , repetition frequency  $= 10$  kc/s, pulse duration  $= 10 \mu$  sec.

The energy of the  $n$ th harmonic is given by

$$E_n = a_n^2 = \left[ \frac{40E}{\pi^2 n^2} (\cos \pi n / 10 - \cos \pi n / 20) \right]^2$$

Table I gives the values of  $[(\cos \pi n / 10) - (\cos \pi n / 20)]/n^2$  proportional to  $a_n$  and the values of  $\{[(\cos \pi n / 10) - (\cos \pi n / 20)]/n^2\}^2$  proportional to the energy of the  $n$ th harmonic.

TABLE I

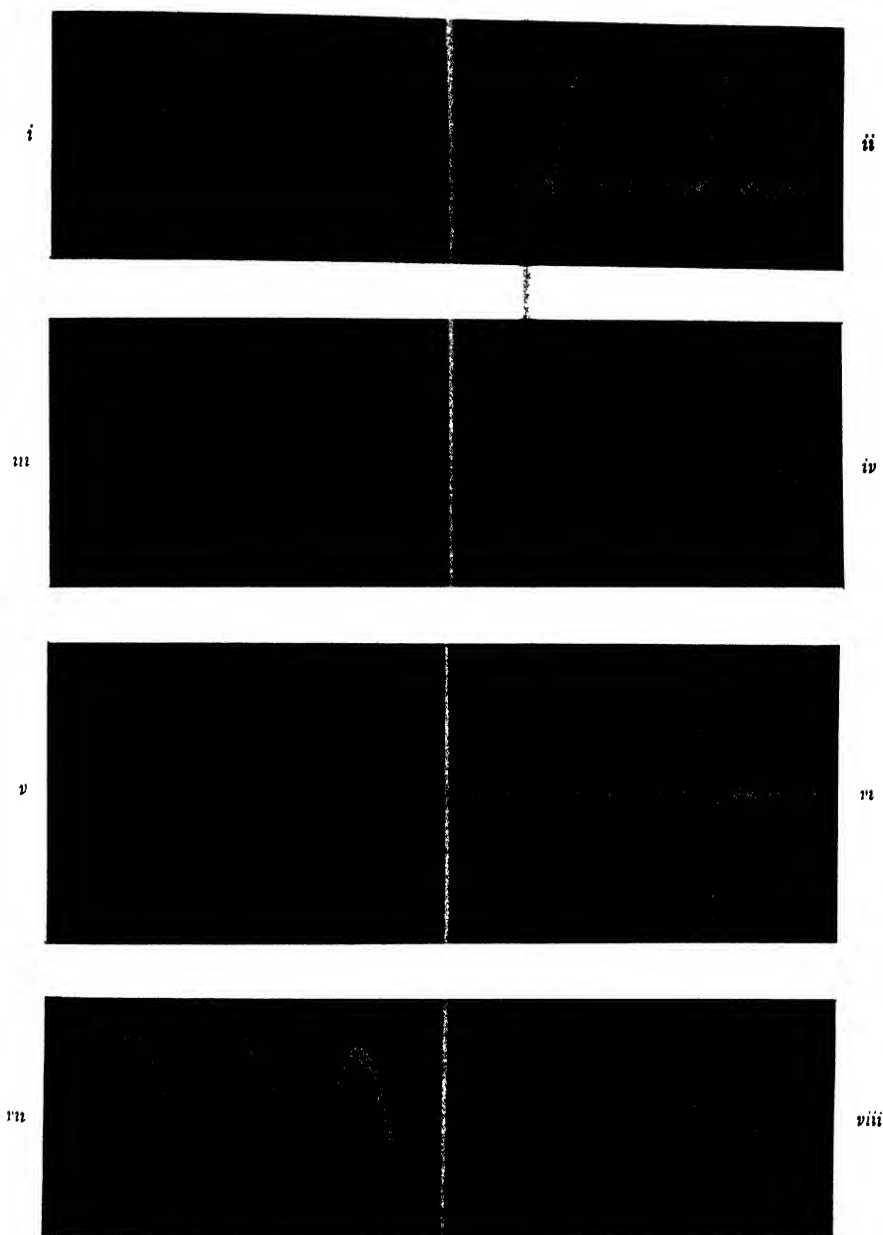
No. of the harmonics	Amplitude of the $n$ th harmonic $\propto \left( \frac{\cos \pi n/10 - \cos \pi n/20}{n^2} \right)$	Energy of the $n$ th harmonic $\propto \left( \frac{\cos \pi n/10 - \cos \pi n/20}{n^2} \right)^2$
1st	- 0366	.001340
2nd	-.0355	.00126
3rd	- 0337	.001136
4th	-.03125	.0009765
5th	- 0283	.0008009
6th	-.0249	.00062
7th	-.021125	.0004515
8th	- 0175	.0003065
9th	-.0133	.0001769
10th	-.01	.0001
11th	-.00657	.00004316
12th	-.00347	.00001204
13th	-.00079	.0000006241
14th	-.0014	.00000196
15th	+ .0034	.00001156
16th	+ .0044	.00001936
17th	+ 0051	.00002601
18th	+ 0054	.00002916
19th	+ .0054	.00002916
20th	+ .0052	.00000675

Figure 13 shows the graphical relation between the  $n$ th harmonics and their energy content.

It is seen that the energy of the 12th harmonic (equal to 120 kc/s) is less than 1% of that of the fundamental and the energy of the 18th and 19th harmonics (corresponding to 180 kc/s and 190 kc/s) is about 2% of that of the fundamental. It is clear that the band width required for these pulses is only 120 kc/s for average transmission and 200 kc/s for faithful transmission.

The characteristics of an open-wire line are such that their loss-frequency relation is parabolic in nature between 10 kc/s and 300 kc/s., the loss being given by,

$$\alpha = A + \left( \frac{k}{276} \cdot \frac{\sqrt{f}}{b} \cdot \frac{b/a}{\log b/a} \right)$$



(i) Unmodulated transmitted pulses. (ii) Modulated transmitted pulses. The thickness of the starting edges is due to modulation. (iii) Unmodulated received amplified pulses after passage through the artificial line. (iv) Received modulated pulses. Thickness of the starting edge is due to modulation. (v) Differentiated pulses on a slow time-base showing the amplitude modulation. (vi) Differentiated pulses. Thickness of the positive pulses is due to the variation of the pulse amplitudes due to modulation. (vii) Demodulated audio signal before the final filter circuit. (viii) Modulating audio signal (1 kc/s).



and is proportional to  $\sqrt{f}$ , where  $k$ =constant,  $f$ =frequency,  $b/a$ =ratio of diameter and spacing of wires, and  $A$ =constant.

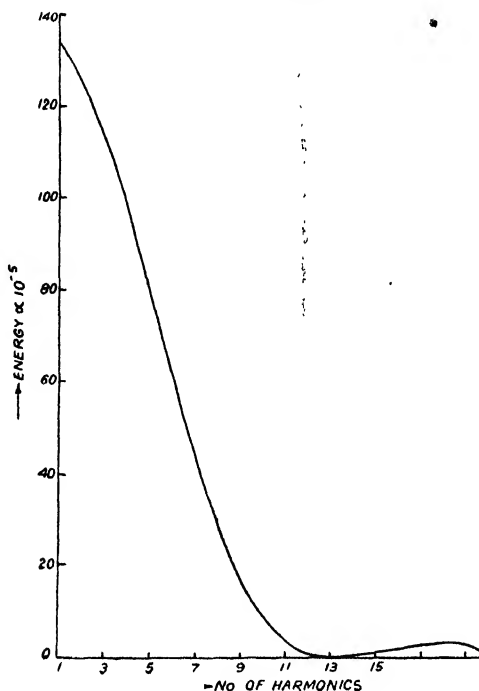


FIG. 13. Energy spectrum of trapezoidal pulses

It is easy to construct a compensating network for losses of this nature and the line equipments working at frequencies upto 140 kc/s are in use. It is, therefore, reasonable to expect that transmission of 10 microseconds video pulses in open-wire line circuit will be possible and the distortion in the frequency band 10 kc/s to 120 kc/s, as required by the system, can easily be compensated by suitable networks.

#### B. Tests with Artificial Line

Pulse communication systems are now well established in the U. H. F. and microwave bands. But very little work (Moss and Park, 1947) has been done to find out the possibilities of pulse applications on line circuits. As seen from the Fourier analysis, a comparatively wide pulse of trapezoidal shape requires much lesser band-width than the rectangular pulses usually used in the microwave pulse communication system. It is expected that even with greater bandwidth requirements than the current carrier equipments, more efficient system of 'line communication equipment' can be devised on the principles stated in this paper.

In order to study experimentally the response of the video pulses in lines, a number of constant resistance L-type net-works with inverse arms were constructed and connected in tandem to simulate the loss characteristics of a

100-mile long open-wire line (of 12 in. spacing 300 lb. copper-wire). The actual characteristic as measured, is shown in figure 14. The curve represents

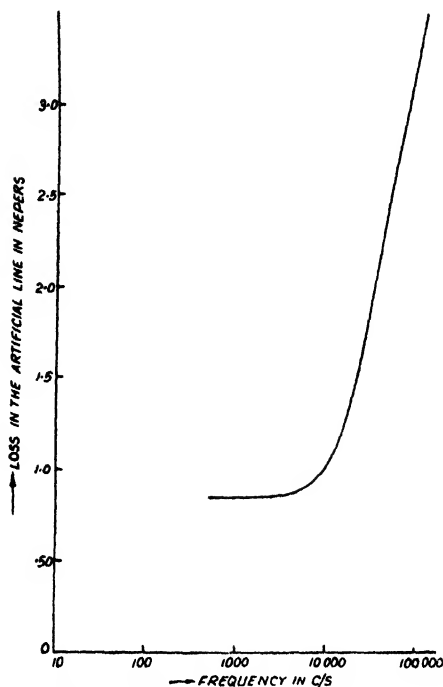


FIG. 14. Characteristics of the artificial line  $Z_0 = 600 \Omega$

the loss characteristic of an actual line very fairly. The impedance of the artificial line varied between 500 and 600 ohms within the measured frequency band.

The nature of the received pulses are shown in figure 15(a). It is apparent that the line has a sort of integrating effect on the shape of the



FIG. 15(a). NATURE OF THE RECEIVED PULSES (UNEQUALISED)



FIG 15(b). EQUALISED RECEIVED PULSES.

pulses and they are slightly widened. But the pulses are not beyond recognition and the slope characteristic persists without any evident distortion.

The problem of equalisation has been successfully dealt with much simpler networks than are used in the current line communication equipments. It is only necessary to use a simple R-C semi-differentiating network to re-shape the partially integrated pulses (figure 15(b)).

The circuit arrangement for equalisation is shown in figure 16. The value of  $RC$  is dependent on the amount of distortion produced in the line. To compensate for the seasonal and climatic variation of line characteristics,

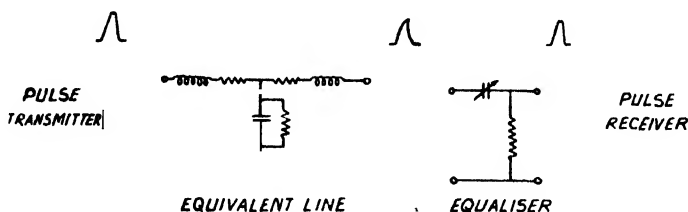


FIG 16. EQUALISER CIRCUIT

a bias-controlled pentode can be used as the resistance component of the R-C equalising network. The grid-bias of the pentode may be varied automatically in synchronism with the variable line loss and hence the effective resistance will vary synchronously.

A time division multiplex system suitable for the line circuits can be evolved on the basis of this promising result and our existing knowledge of similar systems. The work is in progress to produce a specific equipment which can replace some of the present carrier current equipment with better advantage. The long distance signalling can be accomplished either by suppressing the pulses during ringing or usual tone signalling can be utilized.

The loss in average signal level, as measured by a wide-band average detector type levelmeter, is 19.5 db. This is the approximate loss of 100 kc/s signals on a similar 100-mile open-wire circuit.

#### 4. PERFORMANCE

A. *Interference and Noise*: Types of interference and noise in a pulse communication system may be classified as below:

- (a) Amplitude modulation of the base line and the top line of the pulse train by the interfering signal (A. M. or F. M. or P. M.).
- (b) Partial cancellation of the pulses due to overlapping interfering pulses received in phase opposition.
- (c) Spurious time-shifts of the pulse edges due to the overlapping pulse envelope of an interfering station.
- (d) Random fluctuation noise, generally in the nature of random pulses on the base and top line of the signal pulses.

Analysis of the effects of the above in the slope modulated system is similar to the analysis of P. D. M. and P. P. M. as done by Kretzmer, (1950), except in the case of time-shift effect.

The main key to the noise reducing property of pulse modulation is the slicing process. Both theory and experiments show that the optimum value

of the slicing level is half the peak signal voltage, taking all types of interference and noise into consideration. Further, for maximum signal/noise ratio in the output, the thickness of the slice of the pulse should not exceed a few per cent of the pulse height and the width of the gating pulse should be as small as possible. The resultant ideal signal level is 6 db above the noise level for perfect noise-free reception.

In case of slope modulation, this ideal cannot be reached even theoretically. To obtain the information back, an appreciable percentage of the pulse height is to be sliced as the leading edge of the pulse slice has to be differentiated. It is found that the thickness of the slice should be about

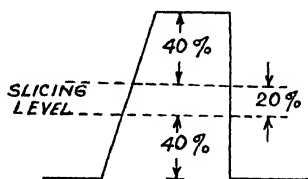


FIG. 17. SLICING LEVEL.

20 % of the pulse height for efficient differentiation (figure 17). Hence the slicing level is at 40 % of the pulse height and the allowable signal/noise ratio = 8 db for noise-free reception.

With respect to the time-shift effect it is seen that the resultant noise should be very small as the output information is dependent not on the

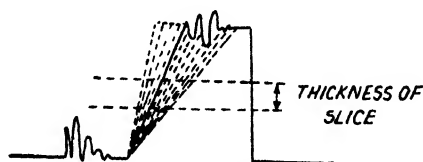


FIG. 18 (a)

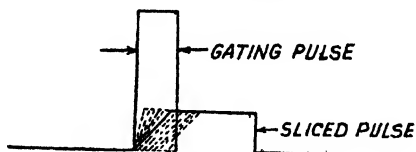


FIG. 18 (b)

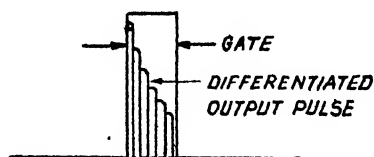


FIG. 18 (c)

FIG. 18. REDUCTION OF NOISE BY SLICING & GATING.



position of the leading edge of the pulses as in P. D. M., but on the slope.

All the other three types of interference have to be dealt with by efficient slicing and faithful differentiation of the slope.

Production of spurious signal (pulses) at the output of the slicer; when the noise level is above the slicing level, can be nullified by using a narrow gating pulse in the amplifier after the differentiator, so that only the information carrying differentiated narrow pulses corresponding to the leading edge of the transmitted pulses are selected and further amplified and demodulated (figure 18). This process will effectively bring the performance of the system similar to those using narrow pulses, although here considerably wider pulses are transmitted.

### B. Modulation Characteristics.

Linearity of modulation with different input levels has been studied and it is found that the input/output characteristic is linear over a range of 35 db as shown in figure 19. The level of audio input at the modulator and the level of audio output at the demodulated audio amplifier have been

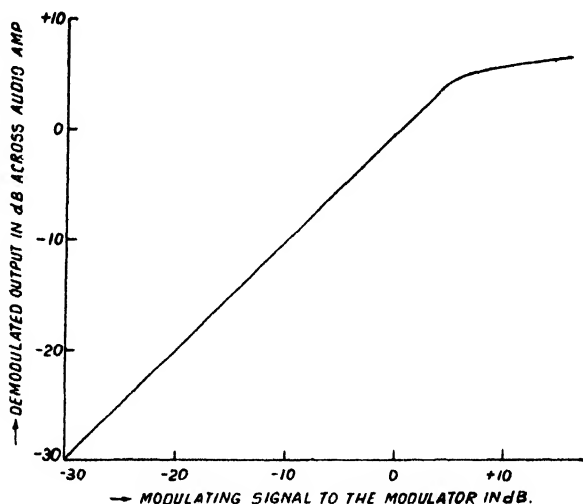


FIG 19 INPUT/OUTPUT CHARACTERISTIC OF MODULATION

measured. The curve shows saturation after +5 db input and this is the point where further slope variation of the trapezoidal pulse decreases the amplitude of the triangular pulse formed on maximum positive modulation. However, the linearity seen in the graph is enough to accommodate the level variation in average audio channels of a telephone circuit (approximately 30 db).

## 5. DISCUSSION

Although the performance of this slope modulation is similar to that of P. D. M. and P. P. M. (Kretzmer, 1950 and Earp, 1948) and much better

than P. A. M., the space occupied by each channel pulses on a time division multiplex scheme remains the same with and without modulation. Using pulses of equal duration, slope modulated system will provide more channels than P. D. M. and P. P. M. Conversely, for the same number of required channels wider pulses can be used in slope modulation and hence lesser band-width is required for faithful transmission. It may become difficult in producing slope modulation in extremely narrow pulses, but slope modulation of pulses of the order of two microseconds and above, as used in microwave pulse communication equipment, is easily done with simple circuit technique.

Considering the overall circuit technique involved in transmission and reception of slope modulated signals, it is seen to be simpler than P. P. M. and is equally simple as P. D. M. and P. A. M. In its application in line circuits, equalisation is very simple and the conversion of four-wire circuit to two-wire working may be easily done by adequate gate pulses incorporated in the receiver.

The system has further advantage that due to its complexity in demodulation, it will maintain more secrecy than P. D. M. and P. A. M. and offers a suitable application as mobile sets behind the front line for defence purposes.

It is further estimated that a slope modulated time-division multiplex system providing two or four channels will compare very favourably with the existing carrier equipments in respect of performance, simplicity, maintenance and cost.

#### ACKNOWLEDGMENTS

The author records his grateful thanks to Dr. J. C. Ghosh, Director, Indian Institute of Technology, Kharagpur. He is grateful to Dr. K. K. Bose of the same Institute for helpful discussions. The author wishes to thank Sri B. M. Banerjee of the Institute of Nuclear Physics, Calcutta, for going through the manuscripts and for very helpful discussions.

#### REFERENCES

- Chance, B., et al, 1949, "Wave forms" McGraw Hill.
- Cherry, C., 1949, Pulses and transients in communication circuits-Chapman and Hall
- Earp, C. W., 1948, *Elec Communication*, **25**, 178.
- Flood, J. E., 1953, *Electronic Engineering*, **25**, p. 2, 58, 101 and 146.
- Kretzmer, E. R., 1950, *Proc. I. R. E.*, **38**, 252.
- Meacham, L. A. and Peterson, R., 1948, *Bell Sys. Tech. Jour.* **27**, 1.
- Moss, S. H. and Parks, G. H., 1947, *J. I. E. E.* **94**, Part III A, 503.

# FORCE CONSTANTS FOR METHYL CYANIDE AND METHYL ISOCYANIDE \*

BY S. L. N. G. KRISHNAMACHARI

DEPARTMENT OF PHYSICS, ANDHRA UNIVERSITY, WALT AIR

(Received for publication, April 15, 1954)

**ABSTRACT.** Force constants have been determined for methyl cyanide and methyl isocyanide using the Wilson F-G matrix method. The CN stretching force constant changes from 17.98 for  $\text{CH}_3\text{CN}$  to 16.13 for  $\text{CH}_3\text{NC}$ , the CC stretching force constant changes from 5.131 for  $\text{CH}_3\text{CN}$  to 5.322 for  $\text{CN}_3\text{NC}$ , the CCN bending force constant changes from 0.1237 for  $\text{CH}_3\text{CN}$  to 0.07731 for  $\text{CH}_3\text{NC}$  while the force constants of the methyl group remain very nearly the same for the two molecules.

## INTRODUCTION

The infrared spectra of methyl cyanide and methyl isocyanide in the vapour state have been recently investigated and accurate values of the fundamental frequencies are reported by Thompson and Williams (1952). The sets of force constants determined by Linnett (1940) and Crawford and Brinkley (1941) using a valency type force field, reproduce the frequencies which are only in rough agreement with the recent values, although they compare well with the earlier values of the liquid state. So it was thought desirable to redetermine the force constants. Further, more accurate data about the bond-lengths and interbond angles are now available from the work of Kessler and others (1950) who have investigated the microwave spectra of  $\text{CH}_3\text{CN}$ ,  $\text{CH}_3\text{NC}$  and their isotopic species. These are employed in the calculations and new sets of force constants are obtained which reproduce the observed frequencies accurately.

## NORMAL COORDINATE TREATMENT

A normal coordinate treatment is carried out using the F-G matrix method developed by Wilson (1939, 1941). The two molecules belong to the  $C_{3v}$  point group. Of the twelve fundamentals of each of the molecules, four belong to the totally symmetric  $A_1$  type and four belong to the doubly degenerate  $E$  type vibrations.

The internal coordinates are represented in figure 1 where 1, 2 represent N and C atoms in the case of  $\text{CH}_3\text{CN}$ , and C and N atoms in the case of

\* Communicated by Prof K. R. Rao

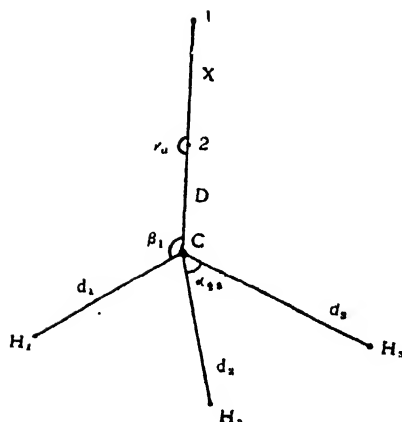


FIG. 1

$\text{CH}_3\text{NC}$ . From these internal coordinates, the following ortho-normal symmetry coordinates are formed for the two molecules :

For the  $A_1$  type vibrations,

$$R_1 = \Delta X, \quad R_2 = \Delta D, \quad R_3 = (\Delta d_1 + \Delta d_2 + \Delta d_3) / \sqrt{3}$$

$$R_4 = (\Delta\alpha_{12} + \Delta\alpha_{13} + \Delta\alpha_{23} - \Delta\beta_1 - \Delta\beta_2 - \Delta\beta_3) / \sqrt{6}$$

For the  $E$  type vibrations,

$$R_{1a} = (2\Delta d_1 - \Delta d_2 - \Delta d_3) / \sqrt{6}$$

$$R_{1b} = (\Delta d_2 - \Delta d_3) / \sqrt{2}$$

$$R_{2a} = (2\Delta\beta_1 - \Delta\beta_2 - \Delta\beta_3) / \sqrt{6}$$

$$R_{2b} = (\Delta\beta_2 - \Delta\beta_3) / \sqrt{2}$$

$$R_{3a} = (2\Delta\alpha_{23} - \Delta\alpha_{12} - \Delta\alpha_{13}) / \sqrt{6}$$

$$R_{3b} = (\Delta\alpha_{13} - \Delta\alpha_{12}) / \sqrt{2}$$

$$R_{4a} = \Delta\gamma_a$$

$$R_{4b} = \Delta\gamma_b$$

The following potential energy function has been used in the calculations :

$$\begin{aligned} 2V = & f_X (\Delta X)^2 + f_D (\Delta D)^2 + f_d \{ (\Delta d_1)^2 + (\Delta d_2)^2 + (\Delta d_3)^2 \} \\ & + 2f_{XD} (\Delta X)(\Delta D) + 2f_{dd} \{ \Delta d_1 \cdot \Delta d_2 + \Delta d_1 \cdot \Delta d_3 + \Delta d_2 \cdot \Delta d_3 \} \\ & + d^2 f_\alpha \{ (\Delta\alpha_{12})^2 + (\Delta\alpha_{13})^2 + (\Delta\alpha_{23})^2 \} + d^2 f_\beta \{ (\Delta\beta_1)^2 + (\Delta\beta_2)^2 + (\Delta\beta_3)^2 \} \\ & + D^2 f_\gamma \{ (\Delta\gamma_a)^2 + (\Delta\gamma_b)^2 \} + 2f_{Dd} \{ \Delta D (\Delta d_1 + \Delta d_2 + \Delta d_3) \} \\ & + 2f_{d\beta} d^2 \{ \Delta\beta_1 (\Delta\alpha_{12} + \Delta\alpha_{13}) + \Delta\beta_2 (\Delta\alpha_{21} + \Delta\alpha_{23}) + \Delta\beta_3 (\Delta\alpha_{13} + \Delta\alpha_{23}) \} \\ & + 2f_{D\beta} d \{ \Delta D (\Delta\beta_1 + \Delta\beta_2 + \Delta\beta_3) \} \end{aligned}$$

From the potential energy matrix and the matrix formed from the coefficients of the internal coordinates as obtained from the symmetry coordinates, the following  $F$  matrices are obtained for the two molecules.

$A_1$			
	$f_X$	$f_{XD}$	$0$
		$f_D$	$0$
$F_{\alpha\alpha}$			$f_d + 2f_{dd}$
	$F_{ji} = F_{ij}$		$(f_{D\alpha} - f_{D\beta})$
			$f_\alpha + f_\beta - 4f_{\alpha\beta}$
$E$			
	$f_d - f_{dd}$	$0$	$0$
$F =$		$d^2 f_\beta$	$-d^2 f_{\alpha\beta}$
	$F_{ij} = F_{ji}$		$d^2 f_\alpha$
			$D^2 f_\gamma$

The  $G$  matrices are obtained from the relations given by Wilson.

$A_1$			
	$\mu_O + \mu_N$	$-\mu_C$	$0$
		$[-\mu_N]_*$	$0$
		$2\mu_O$	$-\mu_C / \sqrt{3}$
$G =$		$[\mu_C + \mu_N]$	$\frac{4}{\sqrt{3}} c$
	$G_{ij} = G_{ji}$		$\mu_H + \mu_C / 3$
			$-\frac{4}{3} a \mu_O$
			$2a^2(\mu_H + 8/3\mu_O)$
$E$			
	$\mu_H + \frac{4}{8}\mu_O$	$-\sqrt{2}\mu_C\left(b + \frac{a}{3}\right)$	$\frac{1}{3}\sqrt{2} a \mu_C$
			$\frac{-b}{\sqrt{3}}\mu_C$
$G =$	$a^2\mu_H + \frac{3}{2}\mu_C \left\{ b^2 + \left(b + \frac{a}{3}\right)^2 \right\}$		
	$\left[ a^2\mu_H + \frac{3}{2}b^2\mu_N + \left(b + \frac{a}{3}\right)^2\mu_C \right] \frac{a}{2}\mu_H - 2a\mu_C\left(b + \frac{a}{3}\right)$	$\frac{\sqrt{6}}{4} b \mu_C \left( 2b + c + \frac{a}{3} \right)$	
		$\frac{5}{2}a^2\mu_H + \frac{8}{3} a^2\mu_O$	$-ab \sqrt{\frac{2}{3}}\mu_O$
			$\mu_N c^2 + \mu_C (2b^2 + c^2 + 2bc)$
			$[\mu_O (b^2 + c^2) + \mu_N (b + c)]$
	$G_{ij} = G_{ji}$		

Here  $a = 1/d$ ,  $b = 1/D$  and  $c = 1/X$ .

The bond distances (Kessler and others) and the reciprocals of masses used in the calculations are

$\text{CH}_3\text{CN}$	$\text{CH}_3\text{NC}$	
$d = 1.092 \text{ A.U.}$	$1.074 \text{ A.U.}$	$\mu_H = 59.75 \times 10^{23} \text{ gm.}^{-1}$
$D = 1.460 \text{ ,,}$	$1.427 \text{ ,,}$	$\mu_C = 5.0148 \times 10^{23} \text{ gm.}^{-1}$
$X = 1.158 \text{ ,,}$	$1.167 \text{ ,,}$	$\mu_N = 4.3005 \times 10^{23} \text{ gm.}^{-1}$

\* For those elements which differ for the two molecules, the two values are given; the unbracketed ones corresponding to  $\text{CH}_3\text{CN}$  and the bracketed ones to  $\text{CH}_3\text{NC}$ . The other elements are common for the two molecules.)

With these and the force constants given in the fourth column of Table I the following secular equations are obtained.

$\text{CH}_3\text{CN}$

$A_1$  type vibrations.

$$\lambda^4 - 5.9405 \times 10^{29} \text{ sec}^{-2} \cdot \lambda^3 + 1.0815 \times 10^{59} \text{ sec}^{-4} \cdot \lambda^2 - 6.6920 \times 10^{47} \text{ sec}^{-6} \cdot \lambda + 1.1870 \times 10^{118} \text{ sec}^{-8} = 0.$$

$E$  type vibrations.

$$\lambda^4 - 4.4055 \times 10^{29} \text{ sec}^{-2} \cdot \lambda^3 + 4.1519 \times 10^{59} \text{ sec}^{-4} \cdot \lambda^2 - 1.1112 \times 10^{67} \text{ sec}^{-6} \cdot \lambda + 4.2990 \times 10^{114} \text{ sec}^{-8} = 0.$$

$\text{CH}_3\text{NC}$

$A_1$  type vibrations.

$$\lambda^4 - 5.8093 \times 10^{29} \text{ sec}^{-2} \cdot \lambda^3 + 1.0306 \times 10^{59} \text{ sec}^{-4} \cdot \lambda^2 - 6.3761 \times 10^{47} \text{ sec}^{-6} \cdot \lambda + 1.1625 \times 10^{118} \text{ sec}^{-8} = 0$$

$E$  type vibrations.

$$\lambda^4 - 4.3980 \times 10^{29} \text{ sec}^{-2} \cdot \lambda^3 + 4.0793 \times 10^{59} \text{ sec}^{-4} \cdot \lambda^2 - 1.0380 \times 10^{67} \text{ sec}^{-6} \cdot \lambda + 2.4180 \times 10^{114} \text{ sec}^{-8} = 0$$

The roots of these secular equations are obtained by Dandelin's root squaring method (Whittaker, 1948). The frequencies that are obtained from the roots of these equations are given in the fourth column of Table II. All the force constants derived by Linnett, Crawford and Brinkley are also given in the Table for the sake of comparison.

TABLE I  
Force constants. ( $10^8$  dynes/cm.)

Force constant	Crawford's values $\text{CH}_3\text{CN}$	Linnett's values		Present values	
		$\text{CH}_3\text{CN}$	$\text{CH}_3\text{NC}$	$\text{CH}_3\text{CN}$	$\text{CH}_3\text{NC}$
$f_X$	17.727	17.50	16.30	17.98	15.43
$f_D$	4.94	5.30	5.45	5.131	5.322
$D$	0.22	...	...	0.4706	0.4706*
$f_a$	4.79	5.0	5.0	4.937	4.958
$f_{aa}$	...	...	...	0.105	0.110
$f_a$	0.46	0.487	0.522	0.454	0.461
$f_\beta$	0.55	0.685	0.681	0.5705	0.5705
$f_{a\beta}$	0.01	...	...	0.0129	0.0129*
$f_{D_a} - f_{D_\beta}$	-0.24	$f_{D_a} = -0.51$	-0.34	-0.2619	-0.2619
$f_\gamma$	0.155	0.32	0.205	0.1237	0.07731

\* Taken from methyl acetylene (Meister, 1948)

TABLE II  
Frequencies ( $\text{cm}^{-1}$ )

	Crawford's values $\text{CH}_3\text{CN}$	Linnett's values		Present calculations		Observed frequencies	
		$\text{CH}_3\text{CN}$	$\text{CH}_3\text{NC}$	$\text{CH}_3\text{CN}$	$\text{CH}_3\text{NC}$	$\text{CH}_3\text{CN}$	$\text{CH}_3\text{NC}$
$A_1$	902	918	928	920	947	920	945
	1396	1370	1413	1407	1409	1400	1410
	2251	2259	2167	2262	2163	2267	2166
	2905	2949	2948	2970	2970	2965	2966
$E$	378	376	292	361	270	361	270
	1036	1040	1042	1037	1041	1041	1041
	1475	1417	1435	1458	1456	1454	1459
	3022	3076	3077	3014	3020	3009	3014

## DISCUSSION

As is seen from the last column of Table I the CN stretching force constant changes from 17.98 for  $\text{CH}_3\text{CN}$  to 16.43 for  $\text{CH}_3\text{NC}$  which is in conformity with the increase of the bond distance from 1.158 A.U. for  $\text{CH}_3\text{CN}$  to 1.167 A.U. for  $\text{CH}_3\text{NC}$ . Also the CCN bending force constant changes from 0.1237 for  $\text{CH}_3\text{CN}$  to 0.07731 for  $\text{CH}_3\text{NC}$ . When the calculations are made for  $\text{CH}_3\text{NC}$  using the same force constants for the methyl group as those determined for  $\text{CH}_3\text{CN}$ , slight discrepancies were observed, so the transferred force constants of the methyl group are slightly altered so as to get the best possible agreement between the calculated and observed frequencies. The calculations also revealed that such a high value as  $1130 \text{ cm}^{-1}$  for  $\nu_7$  for  $\text{CH}_3\text{NC}$  as reported by Thompson and Williams could not be obtained without highly distorting the force constants of the methyl group. These calculations favour a value of  $1041 \text{ cm}^{-1}$  for  $\nu_7$ . It is interesting to note that for methyl isocyanate (Eyster and Gillette, 1940) there are two bands in the region  $1100\text{--}1195 \text{ cm}^{-1}$ . These bands correspond to the rocking frequencies of the methyl group and so would have a fine structure similar to that of  $\nu_7$  of  $\text{CH}_3\text{NC}$ .

## ACKNOWLEDGMENTS

The author wishes to express his deep indebtedness to Prof. K. R. Rao for his kind and valuable guidance throughout the work. The author is grateful to the Government of India for the award of a Senior Research Scholarship.

## REFERENCES

- Crawford, B.L., and Brinkley S.A., 1941, *J. Chem. Phys.* **9**, 69.  
Eyster, E.H. and Gillette, R.H., 1940, *J. Chem. Phys.* **8**, 369.  
Kessler, M., Ring, H., Trambarulo, R., and Gordy, W., 1950, *Phys. Rev.*, **79**, 54.  
Linnette, J. W., 1940, *J. Chem. Phys.*, **8**, 91.  
Meister, A.G., 1948, *J. Chem. Phys.*, **16**, 950.  
Thompson, H. W. and Williams, R. L., 1952, *Trans. Far. Soc.*, **48**, 502.  
Whittaker, E , 1948, ' The Calculus of observations ' p. 106, 4th Ed..  
Wilson, Jr. E. B , 1941, *J. Chem. Phys.* **9**, 76.  
., 1939, *ibid*, **7**, 1047.



# STUDY OF HULBERT-HIRSCHFELDER $U(r)$ FUNCTION IN $C_2$ (SWAN) SYSTEM\*

By N. R. TAWDE

DEPARTMENT OF PHYSICS, KARNATAK UNIVERSITY, DHARWAR

AND

K. GOPALKRISHNAN

UNIVERSITY OF DELHI

(Received for publication, July 31, 1954)

**ABSTRACT.** The rôle of Hulbert-Hirschfelder potential energy expression to predict the most probable transitions in vibrational levels has been examined in relation to the expressions of Morse and Rydberg. These predictions have been critically discussed in the light of the results of the theoretical treatments of Hutchisson, Pillow, Bates and Wyller and results of precise experimental observations.

Of the various expressions available for representing the potential energy of a diatomic molecule, perhaps the Hulbert-Hirschfelder function (1941) is the one which has been rarely used. Though Morse's (1929) expression is, by far, the most commonly employed, Gaydon (1947) has indicated some superior properties of Hulbert-Hirschfelder's expression while discussing critically the subject of potential energy curves of diatomic molecules. This point has been examined in this paper with the help of accurate data of the transition probabilities obtained in our experiments on  $C_2$ (Swan) bands in under-glycerine spark and the calculated theoretical data of exact mathematical treatments.

The Hulbert-Hirschfelder (H-H) expression  $U(r) = D_e[(1 - e^{-x})^2 + cx^3e^{2\alpha}(1 + bx)]$  uses the five experimentally determined constants  $B_e$ ,  $\omega_e$ ,  $D_e$ ,  $x_e\omega_e$  and  $\alpha$  in the quantities  $x$ ,  $c$ ,  $b$  for evaluation of the potential energy. The constants are readily obtainable from band analysis. By the use of them in the above expression, potential energy curves have been derived for  $C_2$  (Swan) system and they have been studied side by side with those of Morse (1929) and Rydberg (1931). The expected parabolic distribution obtained from all these by graphical method is recorded in Table I in terms of the bands occurring at the locus of the maxima and it is shown along with the similar calculated distribution, resulting from the more rigorous wave mechanical treatments of Hutchisson (1930), Pillow (1953), Bates (1949) and Wyller as quoted by McKellar and Climenhaga (1952).

\* The experimental work on this problem was carried out and completed at the Spectroscopic Laboratories of the Institute of Science, Bombay, during the years 1947-49.

TABLE I  
Bands on parabolic locus

$$r_{max} \rightarrow r_{max}$$

Graphical method			Exact mathematical treatments				Experimental
Morse	Rydberg	H-H	Hutchisson	Pillow	Wyller	Bates	Author
1,0	1,0	1,0	1,1	1,1	1,1	1,1	1,0
2,1	2,1	2,0	2,1	2,1	2,1	2,1	2,1
		3,1					
3,2	3,1	3,1	3,2	3,2	3,2	3,2	3,2

TABLE I (continued)

$$r_{min} \rightarrow r_{min}$$

Graphical method			Exact mathematical treatment				Experimental
Morse	Rydberg	H-H	Hutchisson	Pillow	Wyller	Bates	Author
0,1	0,1	0,1	...	...	..	...	0,1
1,3	1,2	1,3	1,2	1,1	1,1	1,1	1,2
		1,4					
2,5	2,3	2,5	2,3	2,3	2,3	...	2,3
3,6	3,4	3,7	3,4	3,4	3,4	3,3	3,4
						3,4	

The quantitative intensity data on  $C_2$  (Swan) bands as obtained from our experiments on under-glycerine spark has been brought to bear on the results of (1) purely graphical and of (2) exact mathematical derivations to study the limits of applicability of Hulbert-Hirschfelder expression. The comparison shows that experimental distribution is more in accord with exact mathematical derivations than with graphical distributions in both the branches of the curves. Among the latter distributions, the one resulting from Hulbert-Hirschfelder expression shows comparatively inferior agreement to that given by Morse's or Rydberg's, the last showing comparatively the best performance of the three. There is, however, very little to choose

between Morse's and Hulbert-Hirschfelder's expressions, the former being only about a shade better than the other, even though the Hulbert-Hirschfelder expression is supposed to be an improvement over Morse's. The disparity noticed is in the transitions belonging to  $r_{min} \rightarrow r_{min}$  branch, the  $r_{max} \rightarrow r_{max}$  side being more or less in close fit with experimental as well as exact mathematical deductions. It has thus been concluded from the present results that the applicability of the Hulbert-Hirschfelder expression is limited to the region of the internuclear distances  $r > r_e$  i.e. for positive values of  $\xi [(r - r_e)/r_e]$ . Recent experimental results of Tawde and Laud (1954) also confirm this aspect.

The relatively poorer performance of Hulbert-Hirschfelder expression on the whole, may probably be traced to the fact that this expression is actually a correction of three-parameter Morse function by the use of two more constants. The greater flexibility and accuracy sought to be achieved by the introduction of these constants seems to be vitiated by the use of the same quantities  $a_0$ ,  $a_1$  and  $a_2$  in the expression as those of Dunham (1932). These are only approximate owing to the W. K. B. method used for solution of the wave equation. As a result of these approximations, the Hulbert-Hirschfelder expression probably inherits some of the defects of Dunham's function. One such defect is the occurrence of appreciable errors in the case of molecules, having nearly equal atomic masses i.e., symmetric molecules like  $H_2$ ,  $C_2$ ,  $N_2$ , etc. It is likely that such molecules show increasing errors with increasing masses of constituent atoms. For, it has been shown already that small correcting terms are necessary in Dunham's constants for  $H_2$  molecule, whereas, only a negligible correction is required for hydrides in which there is larger mass asymmetry in the component atoms.

The  $C_2$  molecule examined here occurs next to  $H_2$  in the above series, and the disparities noticed in the Swan system of it due to working of Hulbert-Hirschfelder expression, appear to be a consequence of the above reasoning. This point needs further confirmation by studying the case of  $N_2$  in the light of this expression.

What seems to be actually effective, however, in the Hulbert-Hirschfelder expression is the introduction and use of anharmonic quantity, which, by properly correcting the errors expected at large values of internuclear distance ( $r > r_e$ ), explains the comparatively superior agreement in transitions of  $r_{max} \rightarrow r_{max}$  branch. Probably the relatively greater disparity seen in the range of negative values, of  $(r - r_e)$  i.e. for  $r_{min} \rightarrow r_{min}$  branch is the result of exaggerated correction brought about by the combined effect of convergent power series and the anharmonic constant  $x_e \omega_e$ .

In view of these findings on the study of Hulbert-Hirschfelder expression, it will be interesting to see how far the different potential energy expressions which have been proposed but not given adequate trial, come up to

expectation of even semi-quantitative approximations of theories and with more exact intensity data of experiments, so as to be a useful guide in the band spectrum analysis.

#### REFERENCES

- Bates, D. R., 1949, *Proc. Roy. Soc.*, **196A**, 217.  
Dunham, J. L., 1932, *Phys. Rev.*, **41**, 713 and 721.  
Gaydon, A. G., 1947, "Dissociation Energies and Spectra of Diatomic Molecules", pp. 52-37, Chapman & Hall Ltd.  
Hulbert, H. M. and Hirschfelder, J. O., 1941, *J. Chem. Phys.*, **9**, 61.  
Hutchisson, E., 1930, *Phys. Rev.*, **36**, 410.  
McKellar, A. and Climenhaga, J. L., 1952, *Dom. Astrophys. Obs. Canada*, contribution No. 28, p. 156.  
Morse, P. M., 1929, *Phys. Rev.*, **34**, 57.  
Pillow, M. E., 1953, *Mem. de Soc. Roy. Sci. de Liege*, **13**, 145.  
Rydberg, R., 1932, *Zeit. f. Phys.*, **73**, 376.  
Tawde, N. R. and Laud, B. B. 1954, *Proc. Nat. Inst. Sci. Ind.*, **20**, 259.

# SYNTHESIS OF A NETWORK FOR A PRESCRIBED TIME FUNCTION\*

By NIRMAL BARAN CHAKRABARTY

INSTITUTE OF RADIO PHYSICS AND ELECTRONICS, CALCUTTA UNIVERSITY.

(Received for publication, July 51 1954)

**ABSTRACT.** The paper discusses the problem of the synthesis of a linear network for a specified time response. Two methods, the moment generating function method and the time series method, are presented. In the former, the generating function of the transfer immittance is found on the basis of moment approximation, and in the latter, the free modes of the system are determined from the spectrum or from the regressive equation of the time series of the waveform. It is shown that the methods presented give physically realisable network structures under quite general conditions. Three examples are considered to illustrate the procedure.

## INTRODUCTION

A linear network can be specified either by its frequency response or by its waveform response to any standard input. In the past one was generally concerned with the frequency response of a network, and as such, one's task was to design the network for a prescribed frequency response. Modern communication techniques, e.g. radar, servo-mechanisms, pulse modulation system etc., are, however, concerned more directly with the waveform response. Further, one is also required to generate special waveforms, for example, the normal error pulse shape which is known to be the best pulse shape for detection of weak signals. Such demands have caused the attention to be directed to the problem of synthesis of networks with a prescribed waveform or time response.

The problem of synthesizing a network having a specified time response involves, firstly, the choice of a proper basis of approximation and, secondly, obtaining the approximate network function in a physically realisable form. For the former some criterion of goodness of approximation has to be applied and those generally used are the least square deviation and the Tschobycheff approximation.

Several methods of synthesizing a network for a specified time response are reported in the literature on the subject. Much work, however, still remains to be done before a general solution of the problem is obtained. The present paper aims at making some contributions to the solution of the problem by suggesting extensions of and possible alternatives to the existing methods of attack. The methods that will be described here are, (a) the

\* Communicated by Prof. S. K. Mitra.

moment generating function method and (b) the time series method. In the first method one identifies the coefficients of the power series of the transfer immittance with the moments of the time function. The power series is assumed to be a recurrent one and its generating function is then found. A simple algebraic procedure is then shown to give the network function. The application of the method is, however, restricted to cases where the time function is monotonic. In the second method the free modes of the network are determined from the characteristics of the time series. For this purpose one forms the periodogram or the correlogram, or constructs the autoregression equation. Then, with the estimates of the location of the poles of the network, one selects the zeros for least square approximation to the given time function.

Before going into the suggested methods we give a brief summary of the principal works in the field.

#### SUMMARY OF PREVIOUS WORK

As usual, we define the transfer immittance  $g(p)$  as

$$g(p) = \frac{Lf(t)}{LS(t)} \quad (1)$$

where  $LS(t)$  and  $Lf(t)$  are Laplace transforms of the input  $S(t)$  and output  $f(t)$  respectively. In what follows  $S(t)$ , unless otherwise stated, will denote Dirac's  $\delta$  function, so that  $f(t)$  becomes the weighting function  $W(t)$  specifying  $g(p)$ . The practical problem now is to find a physically realisable network function  $\Phi(p)$  which approximates so closely to  $g(p)$  as to render

$$U = \int_0^\infty \{L^{-1}(\Phi(p)) - g(p)\}^2 dt \quad \dots (2)$$

a minimum,  $L^{-1}$  meaning the inverse Laplace transform.

Now, in order that  $\Phi(p)$  be the transfer immittance of a finite network with lumped constants it must be of the form

$$\Phi(p) = \frac{\sum_{r=0}^m a_r p^r}{\sum_{r=0}^n b_r p^r} = \frac{N(p)}{D(p)} \quad \dots (3)$$

where  $N(p)$  and  $D(p)$  are rational polynomials in  $p$  satisfying the following conditions:

- (a) the coefficients of  $N(p)$  and  $D(p)$  are all real,
- (b) the zeros of  $D(p)$  cannot lie in the right half  $p$ -plane,
- (c) degree of  $N(p)$  cannot be higher than that of  $D(p)$ .

Airgrain and Williams (1949a) have suggested a method resting on the minimisation of the integral (2). Writing  $\Phi(p) = \sum_{p+a_s} \frac{A_s''}{p+a_s}$  one forms the system of equations

$$\frac{\partial U}{\partial a_s} = 0, \quad \frac{\partial U}{\partial A_s''} = 0 \quad (s=1, 2, \dots, n)$$

solutions of which give  $as$  and  $As$ . Airgrain and Williams, (1949a) have also extended the method by employing the Laguerre series expansion of any time function.

Thomson (1952) has adopted the method of moments for finding the approximate network function. He takes a special Hurwitz polynomial as the denominator and then finds the numerator polynomial.

Another method (Nadler, 1949), useful for realising the input impedance function employs the continued fraction expansion of the Poisson-Stieltjes integral,

$$g(p) = pC + \int_0^{\infty} \frac{d\psi(x)}{p^2 + x}, \text{ where } d\psi(x) = \operatorname{Re} \frac{g(i\sqrt{x})}{\pi\sqrt{x}} dx,$$

and

$$C = \lim_{p \rightarrow \infty} \frac{g(p)}{p}.$$

The Fourier series representation of  $f(t)$  may also be used for obtaining the transfer immittance. More generally, the output time function may be represented by means of any orthogonal complete set having rational Fourier transform, so that

$$f(t) = \sum \beta_n \psi_n(t) \text{ and } g(p) = \sum \beta_n \chi_n(p) \quad \dots (3a)$$

where  $\chi_n(p)$  is the Fourier transform of  $\psi_n(t)$ . The coefficients  $\beta_n$  are

$$\text{obtainable from } \beta_n = \frac{\int f(t) \psi_n(t) dt}{\int [\psi_n(t)]^2 dt}.$$

It should be noted that Fourier series representation implies choice of commensurate complex poles while Laguerre series representation implies selection of  $n$ th order real pole.

#### THE MOMENT GENERATING FUNCTION METHOD

If in the fundamental relation  $g(p) = \int_0^{\infty} e^{-pt} f(t) dt$ ,  $f(t)$  is normalised, that is,

if  $\int_0^{\infty} f(t) dt = 1$ , then on expanding  $e^{-pt}$  we have

$$\begin{aligned} g(p) &= \int_0^{\infty} f(t) dt - p \int_0^{\infty} t f(t) dt + \dots + \frac{(-p)^r}{(r)!} \int_0^{\infty} t^r f(t) dt + \dots \\ &= 1 - \mu_1' p + \mu_2' \frac{p^2}{2!} + \dots + \frac{(-p)^r}{r!} \mu_r' + \dots \end{aligned} \quad \dots (4)$$

where  $\mu_r'$  denotes the  $r$ th order moment about the origin. Differentiating  $g(p)$   $r$  times one obtains

$$\frac{\partial^r}{\partial p^r} g(p) = \int_0^{\infty} (-t)^r f(t) e^{-pt} dt. \quad \dots (4a)$$

Thus the coefficients of the power series expansion of  $g(p)$  are obtainable from the transform of  $(-t)^r f(t)$ .

The moments can be related to the real and imaginary parts,  $A(\omega)$  and  $B(\omega)$  respectively, of the transfer function  $g(j\omega)$ . From

$$\mu'_r = (-1)^r \left[ \frac{\partial^r}{\partial p^r} g(p) \right]_{p=0}$$

we note

$$A(0) = 1, B'(0) = \mu'_1, A''(0) = \mu'_2, \dots A^{2n}(0) = (-1)^n \mu'_{2n} \dots \quad (5)$$

The moments can also be related to the delay time and rise time thus :  
Delay time can be defined as

$$t_d = \int_0^\infty t f(t) dt = \mu'_1 \quad \dots \quad (6a)$$

$$\text{and the rise time as } t_r = \left[ 2\pi \int_0^\infty (t - t_d)^2 f(t) dt \right]^{\frac{1}{2}} = \left[ 2\pi \mu'_2 \right]^{\frac{1}{2}} \quad \dots \quad (6b)$$

It will be seen that  $g(p)$  determines the moments (when these exist) and hence the distribution function. It should, however, be observed that a set of moments determines the distribution uniquely only under certain restrictions. A criterion of unique determination is that  $\overline{\lim} \frac{\mu_n^{1/n}}{n!}$

is finite. This criterion is derived from the condition of convergence of the power series of  $g(p)$ . It is worth noting here that two distributions having identical moments up to the  $n$ th order are equal in the sense of least square approximation. It is also to be noted that the method of moments is applicable only if the time response is monotonic.

As already stated,  $\Phi(p)$ , in order to be realisable in the form of a network, must be of the form  $\Phi(p) = \sum_0^m a_r p^r / \sum_0^n b_r p^r$ . Here,  $n > m$ , for  $n = m$  implies an impulse at  $t = 0$  and such cases are outside our purview. Also, it has been mentioned that for realising  $\Phi(p)$  one may choose a rational Hurwitz polynomial for the denominator and then adjust the numerator to approximate to  $g(p)$ . The alternative suggested here is to consider instead the power series of  $g(p)$  as a recurring series of order  $n$  and then find the coefficients of the generating function, i.e., the denominator polynomial  $D(p)$ , from the set of recurrent relations

$$\frac{b_n \mu'_k}{k!} - \frac{b_{n-1} \mu'_{k+1}}{(k+1)!} + \dots + (-1)^n \frac{\mu'_{k+n}}{(k+n)!} \quad \dots \quad (7)$$

Equation (7) will be recognised as an  $n$ th order difference equation with constant coefficients. If the roots of the characteristic equation

$$x^n - b_1 x^{n-1} + \dots + (-1)^n b_n = 0 \quad \dots \quad (8)$$



are  $C_1, C_2, \dots, C_n$ , then  $\frac{\mu_r}{r!} = A_1 C_1^r + A_2 C_2^r + \dots + A_n C_n^r$ . An evident

constraint on the roots is that  $\frac{\mu_r}{r!} \rightarrow 0$  as  $r \rightarrow \infty$ . Hence  $0 < |C_K| < 1$ .

Now the solution of  $D(p)$  from the set of relations (7) and  $D(p) = \sum_0^n b_r p^r$  can be presented in the form

$$D(p) = \frac{C}{\Delta_{n-1}} \frac{1}{p^{v_1} p^{v_2} \dots p^{v_n}} \quad , \text{ where } v_n = (-1)^n \frac{\mu_n}{n!} \quad (9)$$

$v_{n-1} \quad v_n \quad \dots v_{2n-1}$

and

$$\Delta_n = \begin{vmatrix} 1 & & & \\ & \ddots & & \\ & & 1 & \\ & & & v_n \end{vmatrix}$$

and  $C$  is a constant.

The numerator polynomial will then be

$$N(p) = 1 + (\mu_1' - b_1)p + \left( \frac{\mu_2'}{2} - b_1\mu_1' + b_2 \right) p^2 + \dots$$

$$+ (-p)^{n-1} \left[ \frac{\mu_{n-1}'}{(n-1)!} - \frac{b_1\mu_{n-2}'}{(n-2)!} + \dots + (-1)^n b_{n-1} \right] \quad (10)$$

Equations (9) and (10) determine the network function completely. We may now write  $\Phi(p)$  as

$$\Phi(p) = \frac{N(p)}{D(p)} \text{ or as } \sum \frac{A_K}{p + \gamma_K}$$

or as

$$\frac{1}{\alpha_0 p + \alpha_1} + \frac{1}{\alpha_2 p + \alpha_3} + \frac{1}{\alpha_4 p + \alpha_5} + \dots \quad (11a)$$

From the theory of linear simultaneous equations, it is known that for the parameters  $b_1, b_2, \dots, b_n$  to be independent, it is necessary that the rank of the matrix of the system be equal to the order. This sets the upper limit to the order of the polynomial. We have now to ensure that the  $b_r$ 's are all positive and that  $D(p)$  is Hurwitz. It should be observed that if the power series of  $g(p)$  converges, so will the continued fraction and the rational fraction associated with it; further that for boundedness of  $f(t)$ , it is required that  $g(p)$ , and hence  $D(p)$ , be regular when  $\text{Re } p > 0$ . It is easy to prove that in the continued fraction

$$\Phi(p) = \frac{1}{\alpha_0 p + \beta_1} + \frac{1}{\alpha_1 p + \beta_2} + \frac{1}{\alpha_2 p + \beta_3} + \dots \quad (11b)$$

if  $\alpha_r$ 's and  $\beta_r$ 's are all positive, the roots of  $D(p)$  are simple, real and negative. For this we consider the sequence  $q_{r+1}, q_n, \dots, q_1, q_0$  as Sturm functions where  $q_{r+1} = (\alpha_r p + \beta_r) q_r + q_{r-1}$ , where  $p_r/q_r$  is the  $r$ th convergent.

It is evident that none of the Sturm functions can pass through zero in the interval 0 to  $\infty$  on the axis of reals and that  $n$  changes of sign will be lost in the sequence of Sturm functions as  $p$  passes from  $\infty$  to  $-\infty$ .

It can easily be demonstrated that if  $dF(t)$  has not less than  $n+1$  points of increase one must have  $\Delta_1 > 0$ ,  $\Delta_2 > 0$ , ...  $\Delta_n > 0$ , and conversely if the inequalities are satisfied,  $dF(t)$  has at least  $n+1$  points of increase, where

$$\Delta = \begin{vmatrix} \mu_0' & \dots & \mu_n' \\ \vdots & \ddots & \vdots \\ \mu_n' & \dots & \mu_{2n}' \end{vmatrix}, \quad \mu_r' \text{ meaning the } r \text{th moment.}$$

For this we easily see that the quadratic form

$$\theta = \int_{-\infty}^{\infty} (U_0 + U_1 t + \dots + U_n t^n)^2 dF(t) = \sum \mu_{i+K}' U_i U_K$$

is definitely positive, for, by hypothesis  $dF(t)$  has at least  $(n+1)$  points of increase and at least one of these must be different from all the zeros of

$$U_0 + U_1 t + \dots + U_n t^n$$

so that the integral is always positive so long as  $U_i$ 's are not all zero. This positive definite character ensures the determination of  $dF(t)$  with a set of moments  $\mu_r'$ .

This result may profitably be used in realising a minimum phase shift type transfer function when its real part is non-negative. Consider the Poisson line integral

$$\begin{aligned} g(p) &= \frac{2p}{\pi} \cdot \int_{-\infty}^{\infty} \frac{\operatorname{Re} g(j\omega)}{p^2 + \omega^2} d\omega = \frac{2p}{\pi} \int_0^{\infty} \frac{\operatorname{Re} g(j\omega)}{p^2 + \omega^2} d\omega \cdot \left[ 1 - \frac{\omega^2}{p^2} + \frac{\omega^4}{p^4} - \dots \right] \\ &= \frac{2}{\pi p} \cdot \left[ m_0 - \frac{m_2}{p^2} + \frac{m_4}{p^4} - \dots \right] \end{aligned}$$

where  $m_s$  is the  $s$ th moment and  $\operatorname{Re} g(j\omega)$  is the real part of  $g(j\omega)$ .

Stipulating that on expanding  $\int_{-\infty}^{\infty} \frac{\operatorname{Re} g(j\omega)}{p^2 + \omega^2} d\omega = \frac{N(p^2)}{D(p^2)}$  into a power series of

$\frac{1}{p^2}$ , terms involving  $\frac{1}{p^2}$  to  $\frac{1}{p^{4n}}$  are absent, we obtain

$$\int_{-\infty}^{\infty} \theta(\omega) D(\omega) \operatorname{Re} g(j\omega) d\omega = 0 \quad (12b)$$

for an arbitrary polynomial  $\theta$  of degree  $S$ ,  $S \leq n$ . It is easy to show that the roots of  $N(p^2)$  and  $D(p^2)$  are real, simple and contained within the interval 0 to  $-\infty$ . Equations (12) thus completely determine the network function.

We may add in conclusion that it sometimes saves labour and yields more accurate result if orthogonal series expansion of  $g(p)$  instead of the

actual power series is taken. This procedure is particularly preferable when the form of the transfer immittance is readily obtainable. As the orthogonal series we may take the Laguerre series in the interval 0 to  $\infty$ , or the Tschebycheff or the Legendre series in the reduced interval  $-1$  to  $+1$ .

#### TIME SERIES METHOD

A time series of a wave form  $f(t)$  is a sequence of its values at equal intervals of time, i.e., the sequence

$$(f_0, 0), (f_1, \alpha), \dots, (f_K, K\alpha)$$

where  $f_r$  is the value of  $f(t)$  at  $r\alpha$ ,  $\alpha$  being the spacing. It is well known that if  $\omega_0$  is the highest frequency of interest in the spectrum of a band-limited function  $f(t)$  then it can be represented as

$$f(t) = \sum_0^{2\omega_0 T} f\left(\frac{r}{2\omega_0}\right) \frac{\sin \pi(2\omega_0 t - r)}{\pi(2\omega_0 t - r)}, \quad T \text{ being the total interval} \quad (13)$$

The importance of the relation is that it enables one to specify a continuous function of time in terms of its values at intervals of  $1/2\omega_0$  apart. For example, the response of a low pass filter with frequency response, uniform up to a frequency  $f_c$  and zero for all other frequencies can be represented by a time series of interval  $1/2f_c$ .

The time series, it will be understood, describes completely the characteristic of a linear network. If the response of the linear network to an input  $S(t)$  be  $f(t)$ , then  $f(t) = \int_0^\infty S(\tau)W(t-\tau)d\tau$  where  $W(t)$  is the weighting function. The time series of  $f(t)$  and  $S(t)$  can be used to determine  $W(t)$  completely. The problem now is to realise the transform of  $W(t)$ . For this, we shall describe two alternative methods for finding out the poles of the approximate network: (a) the spectrum method and (b) the regressive equation method.

##### (a) Spectrum Method.

The relation

$$g(p) = \int_0^\infty W(t)e^{-pt}dt = \alpha \sum W(r\alpha)e^{-pr\alpha} \quad (14)$$

for the transfer function is satisfied by

$$g(p) = \sum_1^P \frac{1}{p + \alpha_r} + \sum_1^Q \frac{b_r \omega_r}{p^2 + \omega_r^2} + \sum_1^Q \frac{c_r}{p^2 + \omega_r^2} \quad (14a)$$

if, at discrete points  $t = r\alpha$ ,

$$W(r) = \sum a_r e^{-\alpha_r r} + \sum b_r \sin \omega_r r + \sum c_r \cos \omega_r r \quad (15)$$

where  $\alpha_r$ 's denote the real poles and  $\omega_r$ 's the imaginary poles. One has now to find the poles  $\alpha_r$  and  $\omega_r$  and the coefficients  $a_r$ ,  $b_r$ ,  $c_r$ . For this one first

forms the correlogram or the periodogram] or constructs the spectrum by conventional methods. To form the correlogram we first write

$$r_K = T \rightarrow \infty \frac{1}{T} \int_0^T f(t)f(t+k)dt \quad (16)$$

and then form 
$$e(\omega) = \int_{-\infty}^{\infty} r_K \cos \omega k dk.$$

To construct the periodogram, we write,

$$A = \int_0^{\infty} f(t) \cos \omega t dt, B = \int_0^{\infty} f(t) \sin \omega t dt$$

and then form 
$$S^2 = A^2 + B^2 \quad \dots (17)$$

When the spectrum is such that the number and the locations of the poles cannot be accurately ascertained, reasonable assumptions regarding the same have to be made. One has then to select the unknown  $a_r$ ,  $b_r$ , and  $c_r$  for least square approximation to the given time function. For the purpose one forms

$$U = \sum_r \left[ f(\tau) - \{ \sum a_r e^{-a_r \tau} + \sum b_r \sin \omega_r \tau + \sum c_r \cos \omega_r \tau \} \right]^2 \quad \dots (18)$$

and minimises it with respect to  $a_r$ ,  $b_r$  and  $c_r$ , i. e. equate  $\frac{\partial U}{\partial a_r}$ ,  $\frac{\partial U}{\partial b_r}$  and  $\frac{\partial U}{\partial c_r}$

separately to zero. Now  $\frac{\partial U}{\partial a_1} = 0$  gives

$$a_1 \sum x_{1m}^2 + \sum a_K \sum x_{Km} x_{1m} + \sum b_K \sum x_{1m} y_{Km} + \sum c_K \sum x_{1m} z_{Km} = \sum f_m x_{1m} \quad (18a)$$

where  $x_{rm}$ ,  $y_{rm}$ ,  $z_{rm}$  and  $f_m$  denote the values respectively of  $e^{-a_r \tau}$ ,  $\sin \omega_r \tau$ ,  $\cos \omega_r \tau$ ,  $f(\tau)$  at the  $n$ th sampling point.

From the set of linear equations (18a) one solves  $a_r$ ,  $b_r$  and  $c_r$ .  $g(p)$  is then in the network realisable form (14a).

It is necessary to note that only if the time function is the response of a linear network with finite elements it is possible to find out  $a_r$  and  $\omega_r$  with reasonable accuracy from the correlogram or the periodogram. In the general case of an arbitrary time function, the representation (3a), in terms of a complete orthogonal set, has the advantage over the representation (14a) that the coefficients  $\beta_n$  are more easily found.

(b) *Regressive Equation Method.* The time response of a linear system is known to possess the useful property, namely, that its time series is linear auto-regressive. The basis of linear auto-regression is the fact that an  $n$ th order linear differential equation may be regarded as the limiting case of  $m$  linear algebraic equations when in the limit  $m$  tends to infinity. If we consider the second order differential equation

$$p\ddot{x} + q\dot{x} + rx = \psi(t)$$

where  $p, q, r$  are continuous in the interval  $0 \leq t \leq T$ , the difference equation from

$$p(t_v) \frac{\Delta^2 x_v}{\Delta t^2} + q(t_v) \frac{\Delta x_v}{\Delta t} + r(t_v) x_v = \psi(t_v),$$

where  $\Delta x_v = x_{v+1} - x_v$ ,  $\Delta^2 x_v = x_{v+2} - 2x_{v+1} + x_v$ ;  $v = 0, 1, 2, \dots, \frac{T}{\alpha} - 1$

and where  $\alpha$  is the spacing, will be

$$P_v x_v + Q_v x_{v+1} + R_v x_{v+2} = \psi_v$$

Proceeding similarly the  $n$ th order difference equation is

$$P_0 x_v + P_1 x_{v+1} + \dots + P_n x_{v+n} = \psi_v \quad v = 0, 1, 2, \dots, \frac{T}{\alpha} - n$$

In the application we have in mind, the coefficients  $P_r$ 's will be constants. Then the  $n$ th order difference equation for the time series, that is the linear auto-regressive equation with constant coefficients  $a_1, a_2, \dots, a_n$ , is

$$f_{t+n} + a_1 f_{t+n-1} + \dots + a_n f_t = 0 \quad \dots (19)$$

Here  $\psi$  is zero, since we are considering free modes.

There will be  $N - n$  such equations. It may be observed that the auto-correlation coefficients are related by the equation

$$r_{m+n} + a_1 r_{m+n-1} + \dots + a_n r_m = 0 \quad \dots (20)$$

The solution of (19) is  $f(t) = \sum_1^n A_k Z_k^t$  ... (21)

where  $Z_k$  are the roots of the equation

$$Z^n + a_1 Z^{n-1} + \dots + a_n = 0 \quad \dots (22)$$

Now, it will be noted from the differential equation of the output time function  $D(p)f(t) = N(p)S(t)$  that the poles, i.e., the roots of  $D(p)$  are related to the  $Z_k$  by  $\gamma_k = \log Z_k$ . For boundedness of  $f(t)$ ,  $0 < \text{mod } Z_k < 1$ .

The order of the system is to be chosen with reference to the complexity of the network and the rank of the linear equations (19). It is thus seen that the equations (19), through (22), contain all the informations about the locations and the nature of the poles. When the time series shows irregular feature, in setting up the equation (22), we choose instead of (19), the derived

equation (20). The transfer function now becomes  $g(p) = \sum \frac{A_k}{p + \gamma_k}$ . To deter-

mine the  $A_k$ , we may employ the method of the previous section, i.e., minimise  $U$  with respect to  $A_k$ , where

$$U = \sum_0^N [f(\tau) - \sum_1^n A_k Z_k^t]^2.$$

The methods discussed in this section can be used for obtaining waveform correcting network. If, for example, the impulse response of a networks is  $f_1(t)$ , and the desired waveform is  $f_s(t)$ , then, from the convolution integral

$$f_3(t) = \int_0^{\infty} f_2(u) f_1(t-u) du.$$

one can find by serial division the time series of the corrector,  $f_2(t)$ . The correcting network can then be designed by the methods of this section.

#### ILLUSTRATIVE EXAMPLES

(1) To realise the square wave time response defined by  $f(t) = k$ ,  $0 < t < T$ , and  $f(t) = 0$ , elsewhere.

Its transform cannot be realised with a finite network, for as is well known, the spectrum of a pulse having steep edges decays as  $\frac{1}{p}$  and that of one having corners decays as  $\frac{1}{p^2}$ . This property is reflected in the fact that the moments of transform form a very slowly convergent sequence. The recurrent series obtained is

$$1 + \frac{x}{2} + \frac{3}{28}x^2 + \frac{x^3}{84} + \frac{x^4}{24 \times 70}; (x = pT)$$

$g(p)$  is then

$$\frac{1 + x^2/42}{1 + \frac{x}{2} + \frac{3}{28}x^2 + \frac{x^2}{84} + \frac{x^4}{24 \times 70}}$$

The network response calculated is observed to improve with the addition of two real poles at  $10^6 \text{ sec}^{-1}$  and  $\frac{1}{2} 10^6 \text{ sec}^{-1}$  of strength 2. The resultant waveform is shown in figure 1. The network configuration corresponding to  $g(p)$  can be found following Cauer.

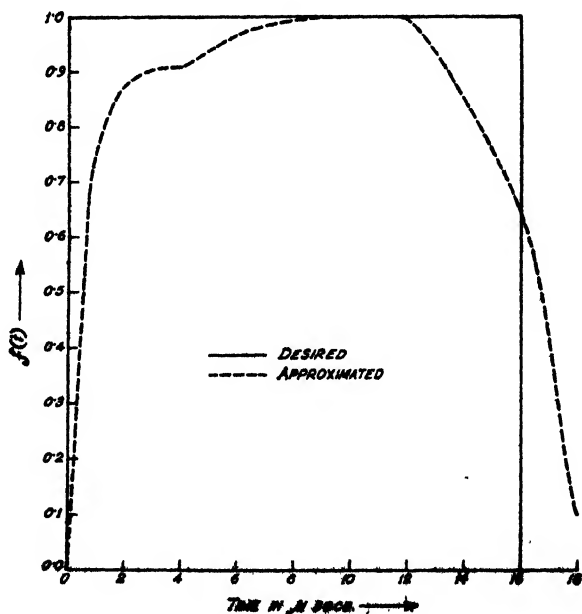


FIG. 1

(2) To synthesize the network for generating a trapezium (figure 2).

The time function has obviously no oscillatory components, i.e., the poles are real ones. Instead of going through the whole procedure, we

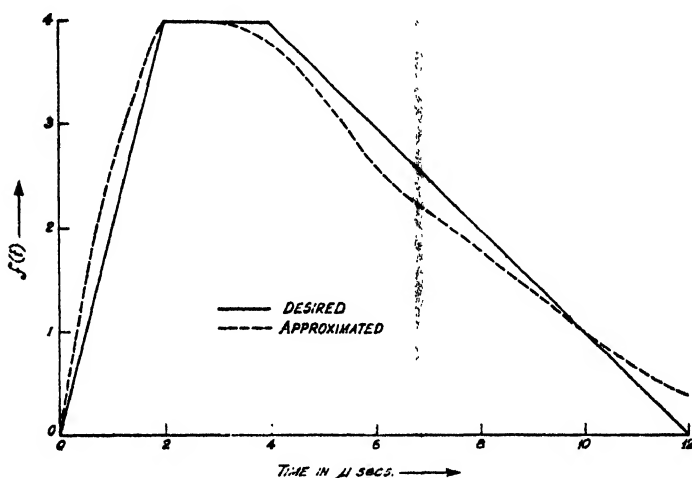


FIG. 2

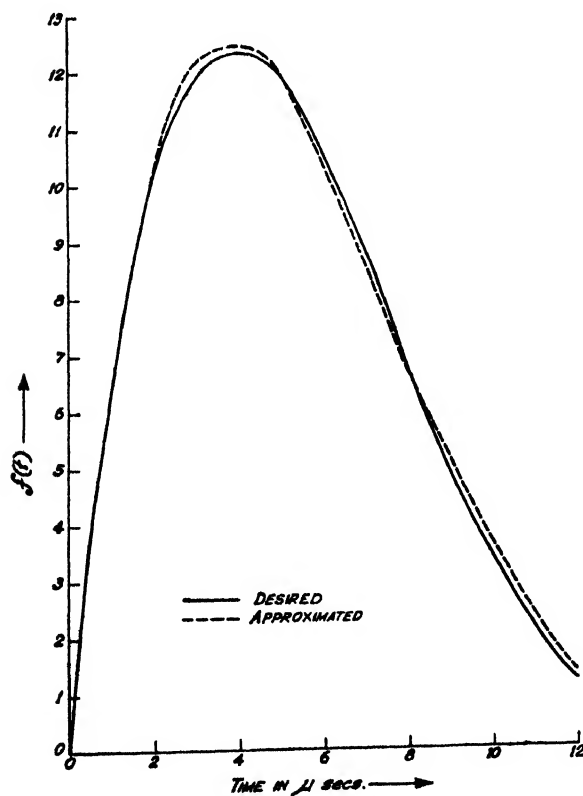


FIG. 3

select, on a preliminary study of the time response,  $0.3 \times 10^6$ ,  $0.4 \times 10^6$ ,  $0.5 \times 10^6$ ,  $0.6 \times 10^6$ , as the locations of the poles.

The transfer function is then

$$\frac{a_1}{p + 0.3 \times 10^6} + \frac{a_2}{p + 0.4 \times 10^6} + \frac{a_3}{p + 0.5 \times 10^6} + \frac{a_4}{p + 0.6 \times 10^6}.$$

The linear algebraic equations referred to in (18a) are solved and the constants found are  $a_1 = 38$ ,  $a_2 = -52$ ,  $a_3 = 44$ ,  $a_4 = -20$ .  $g(p)$  is then

$$g(p) = \frac{1.4x^3 + 7.7x + 1.18}{x^4 + 1.8x^3 + 1.19x^2 + 0.342x + .036}.$$

(3) To realise the network for the time response shown in figure 3.

The auto-regression equation of the third order formed is

$$U_{t+3} - 2.2145U_{t+2} - 1.682U_{t+1} + 0.440U_t = 0$$

The roots are  $\alpha_1 = 0.8025$ ,  $\beta_1$ ,  $\beta_2 = 0.706 \pm 0.31i$ . The constants  $A_k$  are now chosen for best fit. The solution is

$$f(t) = 25.8e^{-0.22t} + 15.4e^{-0.70t} \sin 0.31t - 25.8e^{-0.70t} \cos 0.31t, t \text{ being in } \mu \text{ secs.}$$

The network response is found to agree well with the specified time function.

#### ACKNOWLEDGMENTS

It is a great pleasure to record my indebtedness to Professor S. K. Mitra for his guidance and interest. I am also thankful to Mr. A. K. Chowdhury for his aid and encouragement and to Mr. D. Gupta Sarma for some helpful discussions.

#### REFERENCES

- Airgrain, P. R., and Williams, F. M., 1949a, *Jour. Appl. Phys.*, **20**, 597
- Airgrain, P. R. and Williams, F. M., 1949b, *Proc. I. R. E.*, **37**, 866.
- Nadler, M., 1949, *Proc. I. R. E.*, **37**, 627.
- Pulse Generators, R. L. Series No. 5. p.189.
- Thomson, W. E., 1952, *Jour. I. E. E.*, **99**, 379.



# ABSORPTION OF 3.18 CM MICROWAVES IN SOME AROMATIC AND ALIPHATIC COMPOUNDS IN THE LIQUID STATE\*

By DILIP KUMAR GHOSH

OPTICS DEPARTMENT, INDIAN ASSOCIATION FOR THE CULTIVATION OF SCIENCE, CALCUTTA 32.

(Received for publication, August 6, 1954)

**ABSTRACT.** The absorption of 3.18 cm microwaves in *o*-cresol, *m*-cresol and 3-chloropropene has been studied by the direct optical method avoiding formation of stationary waves. Maximum absorption of 3.18 cm microwaves has been exhibited by *o*-cresol, *m*-cresol and 3-chloropropene at temperatures 50°C, 80°C and -80°C respectively. In the case of cresols these are assumed to be due to rotation of the OH group about the diameters of the molecule passing through the carbon atoms to which the OH group is attached. In the case of 3-chloropropene probably the rotor is rotating around the length of the molecule. It has been observed that toluene, *o*-bromotoluene and xylenes do not exhibit any absorption in the 3.18 cm microwave region which corroborates views expressed in the previous papers of the author that the absorption in the microwave region is due to the rotational freedom of the group containing permanent electric moment about an axis of the molecule. Toluene and *o*-bromotoluene also do not exhibit any absorption in the U.H.F. region 250-900 Mc/sec. This may be due to the fact that the permanent electric moment in the case of toluene is very small and that the moment of inertia of *o*-bromotoluene is very high.

## INTRODUCTION

It has been reported recently (Ghosh, 1954) that some substituted benzenes exhibit absorption maxima at the 3.18 cm microwave region and that the radii of the rotors calculated from Debye's theory are found to be too small to be that of the molecule and they are equal to the projections of the lengths of the substituent groups on a diameter of the benzene ring passing through the point of substitution. This shows that in the case of these substituted benzenes the time of relaxation has different discrete values in each case and the occurrence of "effective time of relaxation" owing to freedom of rotation of the substituent group about a diameter of the molecules postulated by Fischer (1949) is corroborated by these results. The presence of rotational freedom of some groups in substituted benzenes was inferred by Fischer (1949) from the values of dielectric loss observed in the solution of some substituted benzenes in the metre wavelength region. In the method employed by the present author, the frequencies of absorption peak are actually observed in the case of pure liquids for wavelengths shorter than 1 metre and the radius of the rotor is calculated from Debye's theory.

\* Communicated by Prof. S. C. Sirkar.

It was observed that the pure liquids such as benzyl alcohol, benzyl chloride, benzyl amine, ethylene chloride, ethylene bromide and chloroform exhibit maximum absorption of 3.18 cm microwaves at suitable temperatures. In the case of the substituted benzenes mentioned above the substituent groups were assumed to have rotational freedom in explaining the observed absorption. It would be interesting, however, to find out whether substituted benzenes in which there is no such group with rotational freedom also exhibit absorption in the 3.18 cm microwave region. In the present investigation the absorption of 3.18 cm microwave as well as of U.H.F. radiowaves of frequency ranging from 250 Mc/sec to 900 Mc/sec in a few more liquids has, therefore, been studied for different temperatures of the liquids and attempts have been made to calculate the radii of the rotors from Debye's theory.

#### EXPERIMENTAL

The liquids studied in the present investigation are toluene, *o*-bromotoluene, *o*-xylene, *m*-xylene, *o*-cresol, *m*-cresol and 3-chloropropene. The experimental arrangement used in the present investigation was the same as that reported previously (Ghosh, 1953a, 1953b, 1954). The liquids studied were of chemically pure quality. They were all distilled in vacuum after proper dehydration. The liquids were supplied by Fisher Scientific Company, New York. Ortho and meta cresol were supplied by B.D.H.

#### RESULTS

The values of  $a^3$  and  $\tau$  calculated from Debye's theory and the different constants involved in this calculation are shown in Table I.

TABLE I  
 $\omega/2\pi = 9415$  Mc/sec.

Liquid	T°K for max. abs.	$\epsilon_0$	$\epsilon_1$	$\eta \times 100$	$\tau \times 10^{11}$	$a \times 10^8$ c.c.
<i>o</i> -Cresol	323	2.393	6.3	2.5	1.518	1.28
<i>m</i> -Cresol	353	2.372	5.5	1.8	1.458	1.46
3-Chloropropene	193	2	10.6	75	1.235	1.51

Toluene and *o*-bromotoluene showed no absorption at all in the range 250-900 Mc/sec and also in the 3.18 cm microwave region when the liquid was heated nearly up to the boiling point and cooled up to the freezing point.

Ortho-xylene and *m*-xylene showed no absorption in the 3.18 cm microwave region. Absorption by *o*-xylene and *m*-xylene in the U.H.F. region was reported by Ghosh (1953a). Absorption by *o*-cresol and *m*-cresol in the U.H.F. region was studied by Kastha (1952) and the absorption in the microwave region has been plotted in figures 1 and 2 respectively.

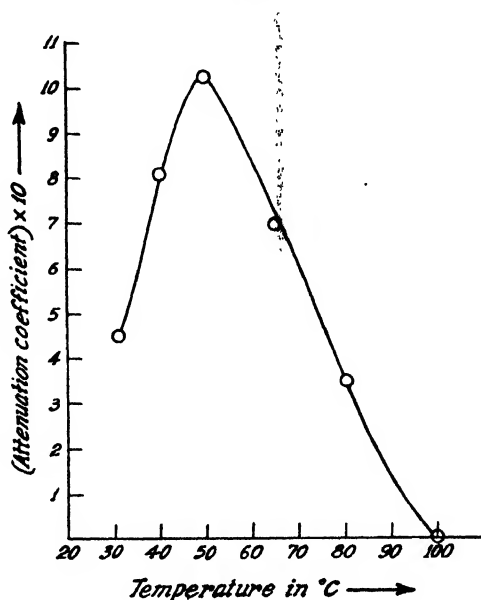


FIG. 1. *o*-Cresol  
 $f=9.115$  Mc/sec thickness of liquid=1cm.

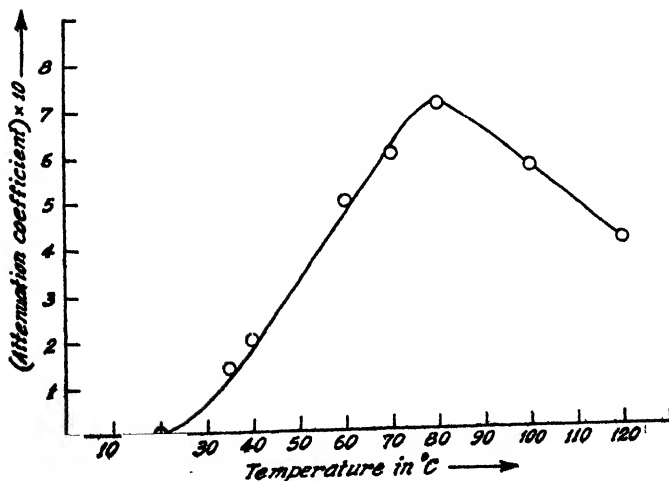


FIG. 2. *m*-Cresol.  
 $f=9.115$  Mc/sec, thickness of the liquid=1 cm.

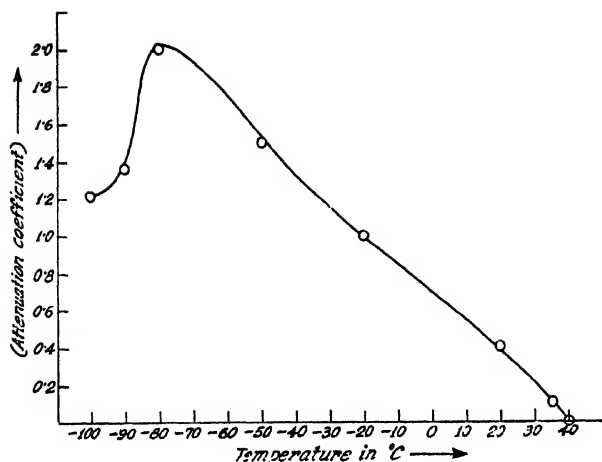


FIG. 3. 3-Chloropropene

$f=9415$  Mc/sec, thickness of the liquid = 1.5 cm

It has been observed that 3-chloropropene shows no absorption in the U.H.F. region in the range 250-900 Mc/sec even when cooled upto the freezing point of the liquid. The absorption in the microwave region has been plotted in figure 3.

The values of  $\eta$  are obtained from the results reported in the International Critical Tables. The values of  $\epsilon_1$  have been obtained from the table of dielectric constants of pure liquids published by National Bureau of Standards, United States Department of Commerce and also from the International Critical Tables. The results at very low and high temperatures have been obtained by extrapolation. The values of  $\epsilon_0$  have been assumed to be equal to square of  $n$ , the refractive index at 20°C for sodium D-line.

## DISCUSSION

It can be seen from the Table I that the radii of the rotor in all the three liquids are much smaller than that of the single molecule. So, in the case of cresols probably the OH group rotates about the diameter of the molecule passing through the carbon atoms to which the OH group is attached. Since the values of viscosity were obtained from the International Critical Table, they are quite reliable. Therefore, the difference in the values of  $a$  for the *m*-cresol molecule and that for the *o*-cresol molecule may not be due to any uncertainty regarding the accuracy of the data used in the calculation, but it may be a genuine difference. If that be the case, it can be inferred that the angle COH between C and OH bonds is smaller in the case of *o*-cresol than in the case of *m*-cresol. This may be due to the proximity of the CH<sub>3</sub> group in the case of *o*-cresol.

In the case of 3-chloropropene the rotation of the molecules about an axis perpendicular to the length of the molecule would require a large volume and the radii also would be much larger than  $1.51 \text{ \AA}$  calculated from observed absorption. Probably, in the particular case the rotor is rotating around the length of the molecule. In that case the projection of the radius of the rotor would be of the order of  $1.51 \text{ \AA}$  shown in the Table I. Such a value was also observed in the case of ethylene chloride and ethylene bromide. Now the absence of absorption in the region 250 - 900 Mc/sec indicates that the frequency of absorption corresponding to the rotation of the molecule about an axis at right angles to the length of the molecule is much lower than the lowest frequency used in the present investigation.

It is well known that in the case of toluene, *o*-bromotoluene and xylenes the rotational group does not change the orientation of the permanent electric moment and it is not surprising that these liquids do not exhibit any absorption in the 3.18 cm microwaves region. Toluene and bromotoluene do not show any absorption also in the range 250 - 900 Mc/sec. This may be due to the fact that in the case of toluene the permanent electric moment is much smaller. In the case of bromotoluene the moment of inertia is very high and the absorption may be in a region of much lower frequency. The results thus fully corroborate the views expressed in the previous papers (Ghosh, 1954) that the absorption in the microwave region is due to the rotational freedom of the group containing permanent electric moment about an axis of the molecule. These results also demonstrate the fact that the molecules in the liquid state of these type exhibit more than one absorption maximum due to the orientation of the whole molecule as well as of part of it as postulated by previous workers.

#### ACKNOWLEDGMENT

Author's grateful thanks are due to Prof. S. C. Sirkar, D.Sc., F.N.I., for his kindly suggesting the problem and for his constant guidance during the progress of the work.

#### REFERENCES

- Fischer, Von. E., 1949, *Z Naturforsch.*, **4a**, 707.  
Ghosh, D. K., 1953a, *Ind. J. Phys.*, **27**, 285.  
Ghosh, D. K., 1953b, *ibid*, **27**, 511.  
Ghosh, D. K., 1954, *ibid*, **28**, 191.  
Kastha, G. S., 1952, *Ind. J. Phys.*, **26**, 103.  
Sirkar, S. C., and Ghosh, D. K., 1953, *J. Chem. Phys*, **21**, 1614.



# INTERPRETATION OF THE NEAR ULTRAVIOLET ABSORPTION SPECTRUM OF ACETALDEHYDE MOLECULE AS DUE TO A SINGLE ELECTRONIC TRANSITION

By V. RAMAKRISHNA RAO

AND

I. ACHYUTA RAO

PHYSICS DEPARTMENT, ANDHRA UNIVERSITY, WALTAIR

(Received for publication, July 16, 1954)

## Plates XVIII A-B

**ABSTRACT.** A complete analysis of the near ultraviolet absorption spectrum of acetaldehyde molecule based on a single electronic transition is obtained.

About 113 bands are measured in the region  $\lambda\lambda$  3485—2610 A.U. The band at 3204.1 A.U. is chosen as the 0,0 band. The C=O frequency is established to be  $1125\text{ cm}^{-1}$  in the upper state instead of  $1053\text{ cm}^{-1}$  as given by Eastwood and Snow (1935).

The following six pairs of fundamentals explained the whole spectrum.

Upper state	Lower state	Assignment
1125	1730	C=O valence
1205	1222	C—H wagging
975	1363	CH <sub>3</sub> sym. bending
666	1066	C—C valence
547	562	C—C=O bending
390	449	Torsion

The analysis shows the characteristics of an allowed transition.

## INTRODUCTION

The ultraviolet absorption spectra of the aliphatic aldehydes do not seem to have been interpreted to the same extent of thoroughness as those of the aromatic compounds. The above aldehydes containing a C=O, generally give a weak absorption spectrum in the near ultraviolet. In acetaldehyde for instance, the band spectrum in the region  $\lambda\lambda$  3480—2300 A.U. is known for a long time without any satisfactory analysis. A thorough investigation of this appears desirable. Earlier work on the near and far ultraviolet absorption spectrum of this molecule may be summarised as follows:

Henri and Schou (H & S, 1928) were the first to study the near ultraviolet absorption spectrum of acetaldehyde. They measured 60 bands

and interpreted them assuming a doublet excited state. This interpretation is of no fundamental significance. Leighton and Blacet (L & B, 1933) reinvestigated the spectrum during their study of photo-decomposition of acetaldehyde and found the diffuse bands extending upto 2740 A. U. (against 2820 A.U. as given by Schou, 1929) with a trace of band structure appearing down to 2660 A.U. They found fluorescence extending throughout the region of distinct and diffuse bands. Pringsheim (1949) notes that the fluorescence bands are due to biacetyl.

Eastwood and Snow (1935) studied the  $C=O$  frequency in the upper state in various aldehydes and ketones. In acetaldehyde, they gave 9 bands with separations averaging about  $1053\text{ cm}^{-1}$  and assigned this as the  $C=O$  frequency in the upper state.

Walsh (1953) analysed a few bands in the near ultraviolet spectrum taking the data from Schou (1929). Assuming the spectrum as involving more than one transition he found it difficult to perform a rigorous vibrational analysis. He considered the transition as of a forbidden type.

Walsh (1946) found the far ultraviolet absorption spectrum consisting of two systems: (i) 1820—1650 A. U., (ii) below 1650 A. U. and attributed them to two allowed transitions. He felt that both the far ultraviolet systems were complicated and so could not obtain a full analysis.

It is clear from the earlier work that a complete analysis of the band system or systems in the near ultraviolet was not achieved. While the bands were complicated in their appearance, it occurred to us that there may possibly be only one system due to a single electronic transition. A thorough and independent attempt at the analysis was found desirable. So fresh experimental investigations were taken up under various conditions. Unbiased attempts at analysis were also made. The results of the above investigations are reported in the following pages. Preliminary results were reported by us earlier (Rao and Rao 1954).

## EXPERIMENTAL

Pure acetaldehyde supplied by Merck and Company is used for the experimental work. All-quartz absorption tubes of lengths varying between 5 cm. to 50 cm. are used. The container is kept at temperatures varying between  $-15^{\circ}\text{C}$  and  $60^{\circ}\text{C}$  thus regulating the vapour pressure inside. The tubes and windows are always kept at a temperature, higher, at least by  $10^{\circ}\text{C}$ , than that, at which the container is kept, to avoid condensation of vapour on the sides and windows of the tube.

Adam Hilger hydrogen arc lamp operating on their FI-16 stabilised power unit is used as the source of continuum. The Hilger medium quartz spectrograph having a dispersion of 17 A. U./mm at 3200 A. U., 8 A.U./mm at 2650 A.U. and 5 A.U./mm at 2000 A.U. was used to photograph the spectra with Ilford Special Rapid plates.



# DESCRIPTION OF THE SPECTRUM

The region of absorption extends from 3485 A. U. to 2350 A. U. in the case of maximum path length (50 cm) used by us. The distinct bands appear in the long wavelength end of the spectrum and the bands are underlaid by continuous absorption which predominates at higher pressures and with larger path lengths. With 5 cm path length, the container being kept at 0°C, the region  $\lambda\lambda 3400-2600$  A.U. shows bands, no continuous absorption being perceivable. The bands on the short wavelength end are superposed by continuum. Measurements are made on this plate giving relative intensities to all band, in the scale 1 to 10. The most distinct bands appear in the region 3400 to 3250 A. U. the distinct bands in the region 3250 to 2970 A. U., the diffuse bands in the region 2970 A. U. to 2800 A.U. and the very diffuse bands in the region 2800-2610 A.U. The region below 2610 A. U. is superposed by continuum.

The bands in the region 2780-2610 A.U. are not measurable on the plates and so measurements are made on the positives taken on Kodak 4-S high contrast photographic paper, exclusively for that region. Intensities are also given relatively among themselves. For measurement of bands in the region 3485-3250 A. U. the plate corresponding to 50 cm path length and container at room temperature (28°C) is used.

Plates are taken varying the path length or the vapour pressure (container temperature). Increase of path length and increase of vapour pressure are found to increase the region of absorption with the appearance of additional bands on the red side more distinctly, while the bands on the short wavelength side merge more and more into continuous absorption. The mean values of measurements on six plates are recorded in the present work.

A few pictures were also taken on  $E_1$  quartz Littrow spectrograph. High dispersion is a disadvantage for bands of this type without sharp edges. Further, partial resolution of rotational structure is an additional draw-back.

## ANALYSIS

The development of the spectra under various experimental conditions suggested that the 0,0 band should be near about the region 3204 A. U. On account of the low symmetry of the molecule ( $C_2$ ) the transition could be of an allowed type. So the 0,0 band can be expected to be one of the stronger bands, though not necessarily the strongest. In the earlier work of Eastwood and Snow (E & S, 1935) a progression of bands with a mean separation of  $1053\text{ cm}^{-1}$  was observed. In Table I the bands observed by them are given with the separations. Our observed values for these are also given in column 3. One of the bands included in our list is at  $31201\text{ cm}^{-1}$ . This was chosen as the 0,0 band and the separations of all other bands from this are given in column 4 of Table II. Walsh (1953) analysed about 12 bands ( $28711$  to  $30499\text{ cm}^{-1}$ ) choosing the band at  $29490\text{ cm}^{-1}$  as the 0,0 band. He assumed the data as given by Schou (1929). He has not given

any reason in support of his choice of the o,o band. To the short wavelength side of  $30499\text{ cm}^{-1}$  there are at least 86 bands which he considers as belonging to different transitions and impossible for vibrational analysis. His analysis is conspicuous by the absence of the  $\text{C}=\text{O}$  frequency in upper state which may be reasonably expected to be strong and responsible for the occurrence of the band system itself in the near ultraviolet region. For these reasons we do not feel inclined to agree with his identification of the o,o band. A discussion of the frequencies, as identified by him, will be taken up later. Besides, as already pointed out, we are not completely convinced that the bands should arise out of more than one transition. Serious attempts were made by us to fit all the bands reasonably into one system and after various trials we chose the band at  $31201\text{ cm}^{-1}$  as the o,o band.

When once this choice is made, our attempt has been to identify the  $\text{C}=\text{O}$  frequency in the upper state, in the region  $1053\text{ cm}^{-1}$  as observed by E & S (Loc. cit). This led us nowhere with the analysis of the system. A close examination of their value  $1053\text{ cm}^{-1}$  revealed that the above authors have taken the mean of 8 values ranging between 1150 and  $989\text{ cm}^{-1}$  with very wide deviation from the

TABLE I

$\nu\text{ cm}^{-1}$ (E & S.)	Separation	$\nu\text{ cm}^{-1}$ (our value)
31182	...	31201
32332	1150	32326
33413	1081	33385
34508	1095	34510
35539	1031	35544
36566	1027	36583
37555	989	37550
38509	1044	...
39608	1009	...
mean $1053\text{ cm}^{-1}$		...

mean value  $1053\text{ cm}^{-1}$  (see Table I). This does not appear to be reasonable. So we made an independent attempt to identify this frequency. The band at  $32259\text{ cm}^{-1}$  (Int. 3) is at a distance of  $1058\text{ cm}^{-1}$  from the o,o band and the next one at  $32326\text{ cm}^{-1}$  (Int. 5) is at a distance of  $1125\text{ cm}^{-1}$ . This frequency of  $1125\text{ cm}^{-1}$  was quickly observed to be repeating itself with good accuracy up to 6 (1125) at  $37948\text{ cm}^{-1}$  with a fall in intensity from 5 to 1\*. The bands already get diffuse at this stage and merge into a continuum and this can easily explain any deviation of the calculated values from the observed values. The value  $1125\text{ cm}^{-1}$  for  $\text{C}=\text{O}$  upper state frequency is just what one would expect on comparison with allied

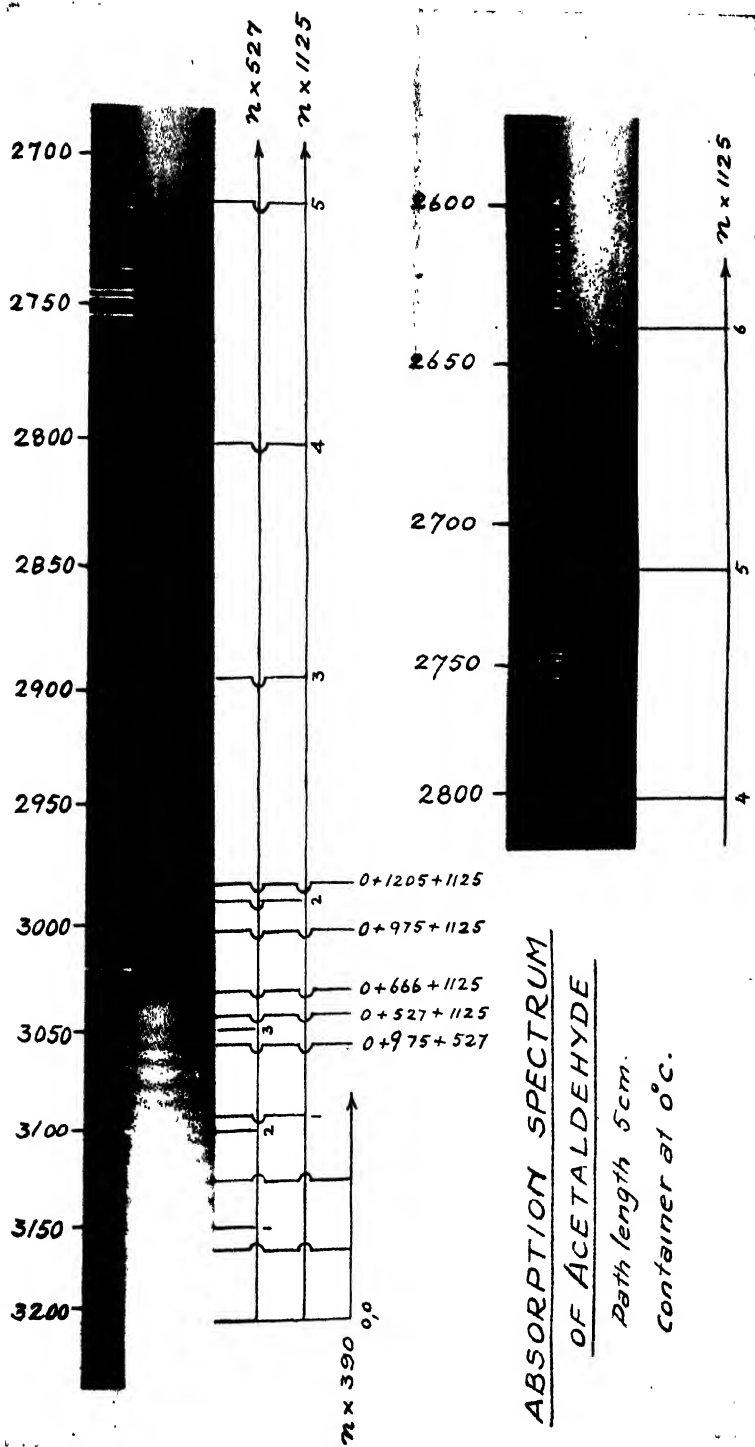


Fig. 1

Fundamental frequencies of acetaldehyde

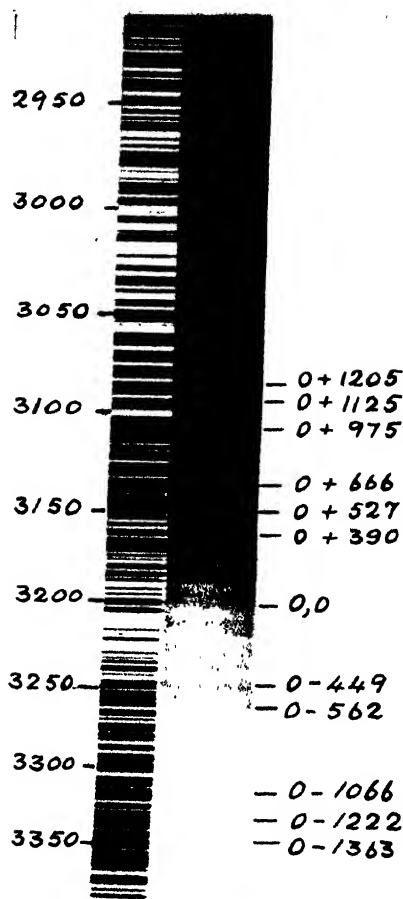


Fig. iii  
Container at 0°C  
Path length 10 cm

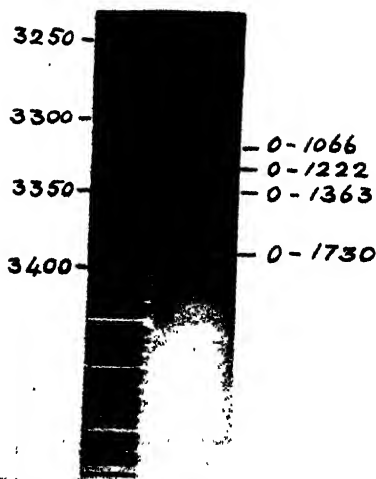


Fig. ii  
Container at 28°C  
Path length 50 cm.

molecules. So this was chosen as the starting point of the analysis.

As already pointed out, these spectra present no regular patterns like those of aromatic substances which will be a guide to the analysis. An intrinsic pattern which we could easily demonstrate in column 5, in Table II and in figure 1, was obtained as follows. Starting from the band at  $32376\text{ cm}^{-1}$

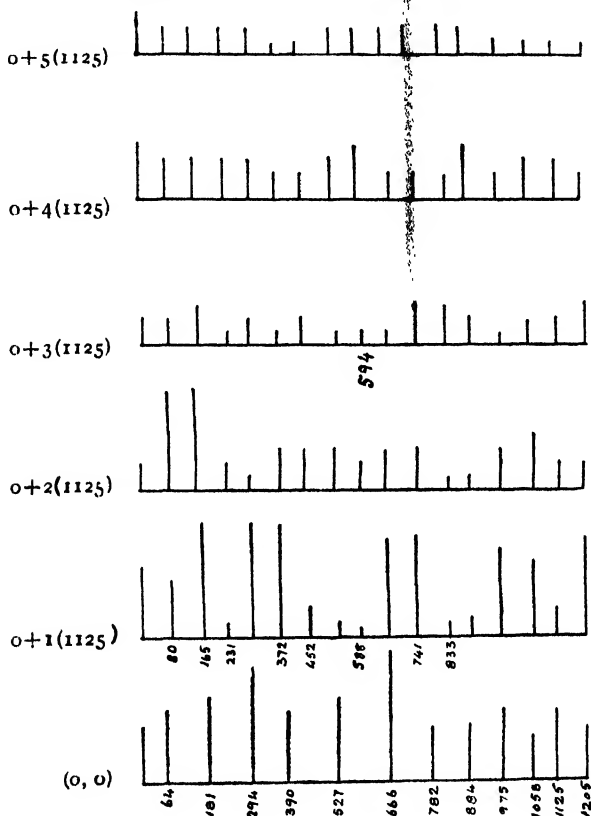


FIG. 1 Band repetition pattern

Intensities for bands next to  $0+4(1125)$  are given from positives taken exclusively for that region but not from the plate as given for the rest of the bands.

$(0,0+1125)$  we obtain the shifts of all the bands from this upto  $33447\text{ cm}^{-1}$   $(0,0+2 \times 1125)$ . We repeat this process for other limits  $2(1125)$  to  $3(1125)$ ,  $3(1125)$  to  $4(1125)$ ,  $4(1125)$  to  $5(1125)$ ,  $5(1125)$  to  $6(1125)$  and  $6(1125)$  to  $7(1125)$  (Plate XVIII A). It was at once apparent that there is a regular repetition of frequencies which is interesting and instructive. For instance, frequencies like 527, 532, 517 and 525 may be considered as repetitions within permissible tolerance of measurements (particularly for headless bands of this type). Most of the bands between  $0,0$  and  $0,0+1125$  repeat themselves in other intervals. In the intervals between higher overtones of  $1125$ , there are 4 to 6 bands more which may be expected as some higher combinations. They also, when once they appear, repeat themselves. For instance, the band with a shift of  $231\text{ cm}^{-1}$

TABLE II

$\lambda$	Int	$\nu$ $\text{cm}^{-1}$	Separation from 0,0 $\Delta\nu$	Separation from $n(1125)$	Assignment	Calc $\Delta\nu$	Obs. —Calc.
Path length 5 cm, container tube at 28°C							
3483.3	1	28701	-2500		0-2(1730)-1222+1125+2(527)	-2503	-3
3463.8	1	28862	-2339		0-2(1730)+1125	-2335	+4
3444.1	1	29027	-2174		0-2(1363)-562+1125	-2163	+11
3424.3	1	29195	-2006		0-1730-562-1363+1125+527	-2003	+3
3406.2	1	29350	-1851		0-2(1363)-1222+1125+975	-1848	+3
3396.5	4	29433	-1768		0-2(1363)-1730+2(527)+666+975	-1761	+7
3392.2	3	29471	-1730		0-1730	...	...
3385.7	6	29527	-1674		0-2(1363)+2(527)	-1672	+2
3383.0	6	29551	-1650		0-1730-1222-562+527+2(666)	-1655	-5
3374.6	4	29625	-1576		0-1730-1066-562+666+1126	-1567	+9
3369.5	4	29670	-1531		0-2(1363)+527+666	-1533	-2
3364.3	4	29716	-1485		0-1730-2(1363-1066+3(1125)+666	-1481	+4
3358.2	4	29770	-1431		0-2(1363)-562+527+2(666)	-1429	+2
Path length 5 cm, container tube at 0°C							
3395.6	1	29441	-1760		0-2(1363)-1730+2(527)+666+975	-1761	-1
3392.2	1	29471	-1730		0-1730	...	...
3384.3	2	29540	-1661		0-2(1363)+2(527) or	-1672	-11
...	...	...	...		0-1730+1125-1066	-1671	-10
3369.5	1	29670	-1531		0-2(1363)+527+666	-1533	-2
3350.5	4	29838	-1363		0-1363	...	...
3334.7	5	29979	-1222		0-1222	...	...
3317.5	5	30135	-1066		0-1066	...	...
3309.5	3	30208	-993		0-1730-1363+4(527)	-985	+8
3302.6	4	30270	-931		0-2(1363)+666+1125	-935	-4
3292.4	5	30364	-837		0-1363+527	-836	+1
3277.6	5	30501	-700		0-1363+666	-697	+3
3262.9	7	30639	-562		0-562	...	...
3250.9	7	30752	-449		0-449	...	...
3237.3	2	30881	-320		0-1730-1363+527+2(1125)	-316	+4
3227.5	2	30975	-226		0-1730+975+527	-228	-2

TABLE II (contd)

$\lambda$ A. U.	Int	$\nu$ $\text{cm}^{-1}$	Sepn. from 0,0 $\Delta\nu$	Sepn. from $n(1125)$	Assignment	Calc $\Delta\nu$	Obs -Calc
3219.7	2	31050	-151		$0-1730+3(527)$	-149	+2
3212.4	4	31120	-81		$0-1730+527+1125$	-78	+3
3204.1	4	31201	0		(0,0)		
3197.5	5	31265	+64	64	$0+1125-1066$	+59	+5
3185.6	6	31382	+181	181	$0+2(1125)+666-2(1363)$	+190	-9
3174.2	8	31495	+294	294	$0+527+1125-1363$	+289	+5
3164.5	5	31591	+390	393	$0+390$		
3150.9	6	31728	+527	527	$0+527$		
3137.1	9	31867	+666	666	$0+666$		
3125.8	4	31983	+782	782	$0+2(390)$	+780	+2
3115.8	4	32085	+884	884	$0+2(1125)-1363$	+887	-3
3107.0	5	32176	+975	975	$0+975$		
3099.0	3	32259	+1058	1058	$0+2(527)$	+1054	+4
3092.6	5	32326	+1125	1125	$0+1125$		
3085.0	4	32406	+1205	80	$0+1205$		
3076.9	8	32491	+1290	165	$0+527+2(666)-62$	+1297	-7
3071.0	1	32557	+1356	231	$0+527+2(666)-562-1066+1125$	+1356	0
3064.5	8	32622	+1421	296	$0+527+2(1125)-1363$	+1414	+7
3057.4	8	32698	+1497	372	$0+975+527$	+1502	-5
3049.9	2	32778	+1577	452	$0+3(527)$	+1581	-4
3042.5	1	32858	+1657	532	$0+527+1125$	+1652	+5
3037.3	1	32914	+1713	588	$0+527+2(1125)-1066$	+1711	+2
3030.4	7	32989	+1788	663	$0+666+1125$	+1791	-3
3023.3	7	33067	+1866	741	$0+2(666)+527$	+1959	+7
3014.2	1	33159	+1958	833	$0+975+1125+3(527)-1730$	+1951	+7
3009.8	1	33215	+2014	889	$0+3(1125)-1363$	+2012	+2
3002.4	6	33297	+2096	971	$0+975+1125$	+2100	-4
2994.5	5	33385	+2184	1059	$0+2(527)+1125$	+2179	+5
2988.9	2	33447	+2246	1121	$0+2(1125)$	+2250	-4
2981.8	7	33527	+2326	76	$0+1125+1205$	+2330	-4
2975.3	7	33600	+2399	149	$0+975+527+2(1125)-1363$	+2389	+10
2968.1	2	33682	+2481	231	$0+527+2(666)+2(1125)-562-1066$	+2481	0

TABLE II (contd)

$\lambda$ Å. U.	Int	$\nu$ cm <sup>-1</sup>	Sepn. from 0,0 $\Delta\nu$	Sepn from n(1125)	Assignment	Calc $\Delta\nu$	Obs -Calc
2962.6	1	33744	+2543	293	0+527+3(1125)-1363	+2539	+4
2955.6	3	33824	+2623	373	0+527+975+1125	+2627	-4
2949.8	3	33891	+2690	440	0+975+527+2(1125)-1066	+2686	+4
2943.1	3	33968	+2767	517	0+527+2(1125)	+2777	-10
2937.3	2	34035	+2834	584	0+527+3(1125)-1066	+2836	-2
2931.0	3	34109	+2908	658	0+666+2(1125)	+2916	-8
2923.6	3	34195	+2994	744	0+2(666)+527+1125	+2984	+10
2916.0	1	34284	+3083	833	0+3(527)+975+2(1125)-1730	+3076	+7
2911.2	1	34340	+3139	889	0+4(1125)-1363	+3137	+2
2904.2	3	34423	+3222	972	0+975+2(1125)	+3225	-3
2897.8	4	34510	+3309	1059	0+2(527)+2(1125)	+3304	+5
2891.0	2	34580	+3379	1129	0+3(1125)	+3375	+4
2885.5	2	34646	+3445	70	0+1205+2(1125)	+3455	-10
2878.9	3	34725	+3524	149	0+975+527+3(1125)-1363	+3514	+10
2872.3	1	34805	+3604	229	0+527+2(666)+3(1125)-562-1066	+3606	-2
2867.0	2	34869	+3668	293	0+527+4(1125)-1363	+3664	+4
2860.9	1	34944	+3743	368	0+975+527+2(1125)	+3752	-9
2855.7	2	35007	+3806	431	0+527+975+3(1125)-1066	+3811	-5
2848.1	1	35101	+3900	525	0+527+3(1125)	+3902	-2
2842.5	1	35170	+3969	594	0+527+4(1125)-1066	+3961	+8
2837.2	1	35236	+4035	660	0+666+3(1125)	+4041	-6
2830.7	3	35317	+4116	741	0+2(666)+527+2(1125)	+4109	+7
2824.2	3	35395	+4194	819	0+3(527)+975+3(1125)-1730	+4201	-7
2818.9	2	35464	+4263	888	0+5(1125)-1363	+4262	+1
2812.6	1	35544	+4343	968	0+975+3(1125)	+4350	-7
2806.2	2	35624	+4423	1048	0+2(527)+3(1125)	+4429	-6
2800.4	2	35699	+4498	1123	0+4(1125)	+4500	-2
2794.7	1	35772	+4571	71	0+1205+3(1125)	+4580	-9
2788.8	3*1	35847	+4646	146	0+975+527-1363+4(1125)	+4639	+7
2782.6	3*1	35927	+4726	226	0+527+2(666)+4(1125)-562-1066	+4731	-5
2777.4	3*1	35994	+4793	293	0+527+5(1125)-1363	+4789	+4



TABLE II (contd.)

$\lambda$ A.U.	Int.	$\nu$ $\text{cm}^{-1}$	Sepn. from $\nu_0$ $\Delta\nu$	Sepn. from $n(1125)$	Assignment	Calc $\Delta\nu$	Obs —Calc
2771.7	2*	36068	+4867	367	$0+975+527+3(1125)$	+4877	-10
2766.3	2*	36139	+4938	438	$0+527+975+4(1125)-1066$	+4936	+2
2760.3	3*	36217	+5016	516	$0+527+4(1125)$	+5027	-11
2754.9	4*	36288	+5087	587	$0+527+5(1125)-1066$	+5086	+1
2748.3	2*	36375	+5174	674	$0+666+4(1125)$	+5166	+8
2743.1	2*	36444	+5243	743	$0+2(666)+527+3(1125)$	+5234	+9
2737.1	2*	36524	+5323	823	$0+3(527)+975+4(1125)-1363$	+5326	-3
2732.7	4*	36583	+5382	882	$0+6(1125)-1363$	+5387	-5
2726.3	2*	36668	+5467	967	$0+975+4(1125)$	+5475	-8
2720.4	3*	36748	+5547	1047	$0+2(527)+4(1125)$	+5554	-7
2714.8	3*	36824	+5623	1123	$0+5(1125)$	+5625	-2
2709.6	2*	36895	+5694	69	$0+1205+4(1125)$	+5705	-11
2704.4	2*	36966	+5765	140	$0+975+527+5(1125)-1363$	+5764	+1
2698.3	2*	37049	+5848	223	$0+527+2(666)-562-1066+5(1125)$	+5856	-8
2692.8	2*	37125	+5924	299	$0+527+6(1125)-1363$	+5914	+10
2688.0	1*	37192	+5991	366	$0+527+975+4(1125)$	+6002	-11
2683.8	1*	37250	+6049	424	$0+527+975+5(1125)-1066$	+6061	-12
2677.2	2*	37341	+6140	515	$0+527+5(1125)$	+6152	-21
2672.4	2*	37408	+6207	582	$0+527+6(1125)-1066$	+6211	-4
2667.2	2*	37481	+6280	655	$0+666+5(1125)$	+6291	-11
2662.3	2*	37550	+6349	724	$0+2(666)+527+4(1125)$	+6359	-10
2655.9	2*	37641	+6440	815	$0+3(527)+975+5(1125)-1730$	+6451	-11
2652.0	2*	37696	+6495	870	$0+7(1125)-1363$	+6512	-71
2645.3	1*	37792	+6591	966	$0+570+5(1125)$	+6600	-9
2639.3	1*	37878	+6677	1052	$0+2(527)+5(1125)$	+6679	-2
2634.4	1*	37948	+6747	1122	$0+6(1125)$	+6750	-3
2628.8	1*	38029	+6828	78	$0+1205+5(1125)$	+6830	-2
2623.3	1*	38109	+6908	158	$0+975+527+6(1125)-1363$	+6880	+19
2614.1	1*	38243	+7042	292	$0+527+7(1125)-1363$	+7039	+3
2610.0	1*	38303	+7102	352	$0+975+527+5(1125)$	+7127	-25

The bands whose intensities are marked (\*) are measured from the positive taken exclusively for the region below 2800 A.U. (corresponding to a pathlength of 5 cm, the container being at 0°C).

from  $0,0 + 1125$ . The results of this observation are two-fold. Most of the fundamentals excited in the upper state may be expected to be within  $1125 \text{ cm}^{-1}$ . It is adequate to interpret the bands between  $0,0$  and  $1125$ , for, the others can be easily interpreted by combining the original assignment with the proper overtone of  $1125$ . Our attempts are hereafter directed on these lines, leading to the identification of some other fundamentals in the upper state.

On the long wavelength side of the  $0,0$  band there is no such pattern. The number of bands is small, being only 27 in all. It is obvious that the region could possibly contain the ground state fundamentals and some combinations. At this state we made one more attempt to see if the  $0,0$  band could be shifted further to the long wavelength side, retaining our observed pattern. As there is no band corresponding to  $-1125 \text{ cm}^{-1}$  shift such an attempt is not necessary in an allowed transition. But yet the shifts with respect to such an absent band are obtained upto the band at  $31201 \text{ cm}^{-1}$  (the present  $0,0$  band) which showed no pattern at all. We are inclined to take this as further confirmation of our identification of the  $0,0$  band and the genuineness of the observed pattern. Also this is one of the reasons why the notion of a forbidden transition is not favoured by us.

Of the 113 bands measured by us, more than 105 could be definitely analysed. Six fundamentals, are observed in both ground state and upper state. The others are assigned as overtones and combinations of these 12 fundamentals. The difference between the observed and calculated values is given in the last column of Table II. Of them, 54 bands show agreement within 0 to  $5 \text{ cm}^{-1}$ , 35 bands agree within 5 to  $10 \text{ cm}^{-1}$  and about 12 bands show a deviation of more than  $10 \text{ cm}^{-1}$ .

For bands of this type having no sharp edge for measurement, and under the comparatively low dispersion we are forced to use, agreement within  $10 \text{ cm}^{-1}$  between observed and calculated values may be considered satisfactory. Larger deviations which occur on the shorter wavelength side of the spectrum may be partly due to the anharmonicity factors in overtones. In Table III are given the fundamentals observed in both states with their corresponding values in Raman and infrared spectra (vide Table III).

#### DISCUSSION AND ASSIGNMENT OF FUNDAMENTALS

The acetaldehyde molecule,  $\text{CH}_3\text{CHO}$ , can have a maximum symmetry corresponding to  $C_s$  point group. The plane is one containing one C—H bond of the methyl group, C—C bond and C—H bond of the aldehyde group. With such a low symmetry the electronic transition can be an allowed type, possibly between two singlet terms. From our analysis, the  $0,0$  band and the totally symmetric vibrations are able to account for most of the strong bands of the spectrum. Non-totally symmetric vibrations are not observed.

The molecule has seven atoms and so 15 normal modes of vibrations, 10 of  $A'$  (totally symmetric species) and 5 of  $A''$  species. Both types are

active in Raman and infrared spectra of which 10 ( $A'$  type) will be polarised in Raman spectra. There will be six essentially valency type vibrations corresponding to the four C—H bonds, one C—C bond and one C=O bond. There will also be the torsional oscillation about C—C bond (which belongs to the  $A''$  species) and the remaining eight modes correspond to the deformation types. The more important modes of this type are a parallel deformation of methyl group, one deformation of COH group in its own plane and one deformation of the C—C=O chain in its own plane. The other five are the bending and rocking motions of the methyl and COH groups with respect to each other.

TABLE III  
Assignment of frequencies

Raman*	Infrared†	Lower state	Upper state	Assignment.
1724	1736 } 1758 }	1730	1125	C=O valence ( $A'$ )
1351	1345 } 1372 }	1363	975	CH <sub>3</sub> sym. bending ( $A'$ )
1127	1118	1066	666	C—C valence ( $A'$ )
511 } or 661 }	517 } or 625 }	562	527	C—C=O bending ( $A'$ )
	426 } 1/2 (852) }	449	390	Torsion ( $A''$ )
1238	1222	1222	1205	C—H wagging ( $A'$ )

\* The mean values of the Raman lines observed by various authors (as given by T & H, 1942) are taken as the most probable Raman frequencies.

† The mean values of the observed infrared frequencies from Morris's work are taken.

The presence of the band at  $426\text{ cm}^{-1}$  is doubted by some authors. But its overtone  $852\text{ cm}^{-1}$  is found by all workers.

Not all these vibrations can be expected in electronic vibrational spectra. The C—H valence vibrations lying in the region  $2700\text{--}3000\text{ cm}^{-1}$  are never obtained probably because of their very low Boltzmann factors. As already pointed out, in this case the non-totally symmetric vibration may be reasonably ruled out. Thus we are left with only a few fundamentals of mainly  $A'$  species for identification in our analysis. Such frequencies and their assignments in the light of Raman and infrared data are discussed below. Reference may be made to Table III for assignments.

Complete data on Raman frequencies obtained by (1) Petrikaln and Hochberg (P & H, 1939), (2) Dadiou and Kohlrausch (D & K, 1929), (3)

Venkateswaran and Bhagavantam (V & B 1930), (4) Kohlrausch and Koppl (K & K 1934), (5) Canals and Gstaad (C & G 1937) and by Gerding and Rjinders (G & R 1939) were collected by Thompson and Horris (T & H 1942). The values given in Table III are the mean values of those observed by various authors.

The infrared absorption spectrum of acetaldehyde vapour was studied by Gerding and Lecomte (G & L 1939), T & H (1942) and Morris (1943). The latter authors gave their assignments of vibration frequencies. Pitzer and Weltner (P & W 1949), during their study of the thermodynamic properties of acetaldehyde reinvestigated the assignments of vibrational frequencies. For the assignment of frequencies reference may be made to Table IV which is an extract taken from P & W. The values for propylene ( $\text{CH}_3\text{.HC:CH}_2$ ) (which is an allied molecule) were also given for purposes of comparison.

TABLE IV  
Vibration frequencies of acetaldehyde

Sym	Motion	Morris	T & H	P & W	Propylene
A'	C-C-O bending	426	525	525	417
	CH <sub>3</sub> rocking	890	883	918	1042
	C-C stretching	917	918	1114	920
	CH wagging	1121	1114	1350	2297
	CH <sub>3</sub> sym. bending	1370	1355	1370	1370
	CH <sub>3</sub> unsym. bending	1414	1405	1414	1444
	C=O stretching	1740	1720	1740	...

T & H = Thompson and Harris (1942)    P & W = Pitzer and Weltner, (1949)

In our analysis, the C=O vibration in the upper state is the most important one and is observed to be  $1125\text{ cm}^{-1}$ . It is recorded accurately upto six overtones and the seventh overtone is also probably identified in combination with another fundamental  $975\text{ cm}^{-1}$ . About 70 bands to the short wavelength side of 0,0 band could be interpreted as one or other combination of some fundamental with 1125 or its overtones. It and its overtones combine with almost all the upper state frequencies like 527, 666 and  $975\text{ cm}^{-1}$ , and some of their overtones. It also occurs in combination with ground state frequencies like  $1363\text{ cm}^{-1}$ . On the long wavelength side of 0,0 it occurs in combination with 1363, 2 (1363),  $1730\text{ cm}^{-1}$  and other frequencies. Thus it might justly be considered as pivot of the whole band system. If we consider the acetaldehyde molecule as a combination of HC=O with methyl group ( $\text{CH}_3$ ), then we might claim

C=H as being entirely responsible for this transition occurring in near ultraviolet, for, it is well known that all methyl group electronic transitions are in far ultraviolet. (This empirical observation is fully justified by the theoretical works of Mulliken (1935) discussed later). If so, it is not surprising that it should be the outstanding vibration in the spectrum. The intensities fall off regularly from 5 for  $\nu_{125}$  to  $\nu_{125}^*$  for  $\nu_{125}$  while the 7th overtone is not observed. This might even explain the region of continuous absorption below 2610 Å.U. with considerable pathlengths, as simply due to the dissociation of the C=O bond as a result of excitation into higher vibrational states.

The C=O frequency is identified in the upper state in formaldehyde ( $H_2CO$ ) to be  $1187\text{ cm}^{-1}$  (Sponer and Teller, 1941). It is quite normal that in the heavier molecule  $CH_3CHO$  this frequency should fall to  $1125\text{ cm}^{-1}$ .

It appears quite certain that C=O frequency in the upper state for acetaldehyde molecule is  $1125\text{ cm}^{-1}$ . It is not  $1053\text{ cm}^{-1}$  as given by E & S (1935).

In the ground state, the weak but sharp band at  $29470\text{ cm}^{-1}$  separated by  $-1730$  from the o,o band can be definitely assigned to the C=O frequency in the ground state. This band was incidentally taken by Walsh (1953) as the o,o band in his analysis of the 12 bands. As per Schou's (1929) measurements given by Walsh this is a medium strong band at  $29490\text{ cm}^{-1}$ . We recorded two bands at  $29441$  and  $29540\text{ cm}^{-1}$  (corresponding to 5 cm pathlength and  $0^\circ\text{C}$ ) on either side of this band, of which the mean value is  $29400\text{ cm}^{-1}$ . The two bands were not recorded separately by Schou and he obviously obtained the reading to the mean position. In fact the band at  $29540\text{ cm}^{-1}$  is the stronger of the three. This accounts for the comparatively high intensity observed by him. The low intensity observed by us may be easily explained on the basis of very low Boltzmann factors corresponding to that comparatively high frequency.

Various authors observed in Raman spectra a strong and polarised line at  $1715$  (K & K),  $1716$  (P & H),  $1721$  (G and R),  $1727$  (V & B) and  $1739\text{ cm}^{-1}$  (C and G). In infrared spectra this is located at  $1720\text{ cm}^{-1}$  by T & H (1942), at  $1732$  by Morris and at  $1740$  by P and W (1949). There is unanimity in the assignment of this frequency to the C=O ground state vibration. In our work this is established to have a value of  $1730\text{ cm}^{-1}$  corresponding to the upper state frequency of  $1125\text{ cm}^{-1}$ . There is another band at  $-1760$  in our data ( $29441\text{ cm}^{-1}$ ) which agrees with the  $1755$  (Morris) and  $1760$  (T & H) in infrared. T & H assign this frequency as an overtone of  $883\text{ cm}^{-1}$  but it appears more correct to consider this as a rotational head of  $1720$  (Morris).

The next important ground state frequency is  $1363\text{ cm}^{-1}$ . About 32 bands could be explained as combinations with this, with a number of

other fundamentals in both states. Of the 27 bands to the long wavelength side of 0,0 band, 13 are accounted for with the help of this frequency. This band is not included in Schou's list but is quite distinct on our plates. Probably in his plates it merged with the stronger band at  $29974\text{ cm}^{-1}$  (our value  $29979$ ). We identify the corresponding upper state frequency to be  $975\text{ cm}^{-1}$ , a band of medium intensity. This frequency occurs particularly in combination with the  $1125$  and its overtones. This pair of frequencies  $1363$  and  $975\text{ cm}^{-1}$  may be assigned for the  $\text{CH}_3$  symmetrical bending vibration in ground and upper states. T and H record two bands of medium intensity at  $1348\text{ cm}^{-1}$  and  $1370\text{ cm}^{-1}$  in infrared and correlate the former with  $1351$  (G & R) or  $1352$  (K & K) in Raman data. They assign the frequency to the  $\text{CH}_3$  symmetrical bending vibration. There is no polarisation data available for this frequency. Morris (1943) records these two bands at  $1342$  and  $1373\text{ cm}^{-1}$  and considers them very strong. He assigns the  $1373$  band as due to  $\text{CH}_3$  symmetric bending vibration. P & W support this assignment. The band at  $1348\text{ cm}^{-1}$  (T & H) may be considered as the rotational head of the same band  $1370\text{ cm}^{-1}$ . In such a case our value of  $1363\text{ cm}^{-1}$  is just less than the fundamental observed in infrared data, as can be expected. Thus we may conclude that the  $1363$  and  $975\text{ cm}^{-1}$  frequencies may be identified with the  $\text{CH}_3$  symmetrical bending in the lower and upper states respectively.

We identified another pair of fundamentals in lower and upper states at the  $1066$  and  $666\text{ cm}^{-1}$  respectively. There is no frequency in the limits  $1000$  and  $1100\text{ cm}^{-1}$  recorded either in Raman or infrared spectra. The upper state frequency  $666\text{ cm}^{-1}$  is probably the strongest band in the spectrum. About 12 important bands could be analysed with the help of this frequency. The overtone of  $666\text{ cm}^{-1}$  was not identified but there are 13 combinations with other fundamentals  $527$ ,  $1125$ ,  $-562$  and  $-1066$ . In the lower state also the corresponding frequency  $1066\text{ cm}^{-1}$  is equally prominent accounting for 15 bands in the spectrum. The C—C totally symmetric valency vibration should be a prominent one in the spectrum and the frequency should lie in the region of  $1000\text{ cm}^{-1}$ . T and H identify this frequency at  $918\text{ cm}^{-1}$  and Morris at  $917\text{ cm}^{-1}$ . This is a strong absorption band in infrared with the corresponding Raman value at  $905$  (V & B),  $932$  (C & G),  $914$  (K & K) and  $923\text{ cm}^{-1}$  (G & R). The line is very weak and noted polarised by T & H and the value of depolarisation factor was given as  $0.73$  (G and R). This assignment was disputed by P & W (1949) who assigned the frequency  $1114\text{ cm}^{-1}$  to the C—C stretching vibration. They justify the assignment by comparing it with the value in propylene ( $920\text{ cm}^{-1}$ ) (see Table IV). The increase in value in the case of acetaldehyde was consistent with the shorter C—C distance  $1.50\text{ A.U.}$  in acetaldehyde as compared with  $1.53\text{ A.U.}$  in propylene. With this change in assignment (among a few more changes) they find a much better agreement with observed thermody-

namic properties as also with the product rule (Redlich-Teller) between  $\text{CH}_3\text{CHO}$  and  $\text{CD}_3\text{CDO}$ . The line  $1114\text{ cm}^{-1}$  in Raman effect was given various values like 1111 (K & K), 1118 (G & R), 1136 (C & G) and 1137 (V & B) by different authors and it is weak (but stronger than 918 (T and H) and partially polarised with the depolarising factor 0.52 from Morris's paper, less than that for  $918\text{ cm}^{-1}$ . The evidence thus appears to be more in favour of the  $1114\text{ cm}^{-1}$  being the C—C valence vibrational frequency and it is adopted by us as corresponding to 1066 and  $666\text{ cm}^{-1}$ . Besides, if we adopt the assignment of  $918\text{ cm}^{-1}$ , we cannot explain the increase in its value to  $1066\text{ cm}^{-1}$ . So if our assignment is correct, it confirms the assignment as given by P and W. However, it may be pointed out that there is a considerable discrepancy of  $48\text{ cm}^{-1}$  between the values of P & W and ours. One possible explanation is that the different rotational heads may be excited to considerably different intensities in infrared and ultraviolet absorption. Probably we recorded one rotational head and the other was recorded in infrared work. This view may be supported by the fact that in the infrared measurements of Morris we have bands bracketted together like 1342 and 1373, 1732 and 1755, etc., separated by a distance of  $30\text{ cm}^{-1}$ . Hence we feel it reasonable to assign 1066 and  $666\text{ cm}^{-1}$  frequencies to the C—C symmetric stretching frequency fixed up at  $1114\text{ cm}^{-1}$  by P & W.

The frequencies 562 in lower state and 527 in the upper state may be assigned to the symmetric C—C=O bending vibration. The order of magnitude for this is generally 500 to  $600\text{ cm}^{-1}$ . In Raman spectra frequencies are found at 502 (P and H), 521 (V & B), 505 (C & G) and 516 (G & R) with medium intensity and 688 (V & B) and 634 (C & G) with very weak intensity. Both the lines represented by the above two sets of observations are partially polarised. The corresponding infrared band was located at 525 and  $625\text{ cm}^{-1}$  (weak) by T & H, 509 by Morris and also by P & W. The latter authors do not agree with the observation of 625 band at all. T & H assign the  $525\text{ cm}^{-1}$  frequency to the C—C=O symmetric bending vibration. Morris, however, considers the  $426\text{ cm}^{-1}$  band should be assigned to this vibration on the ground that this vibration should have the lowest frequency in the molecule. The reason, however, is not correct for it is the torsional frequency corresponding to the internal rotation of C—H bond about C—C bond that should be the lowest. Besides, P & W find the experimental behaviour of  $426\text{ cm}^{-1}$  peculiar (they claim that it was absent as checked by the staff of Shell Development Co.) and also that the higher value  $525\text{ cm}^{-1}$  should be preferred for calculations of heat capacity. This assignment satisfied the product rule also on comparison with the acetaldehyde- $d_4$ . T and H do not find the  $426\text{ cm}^{-1}$  band at all. In fact, suggestions in this line will be taken up presently. Thus the evidence

seems to be in favour of  $525\text{ cm}^{-1}$ . However, there are no suggestions about the infrared band at  $625\text{ cm}^{-1}$  (T & H) and the Raman lines at 688 (V & B) and 634 (C & G). T & H consider 625 infrared and  $650\text{ ? }p^p$  (Raman) as some kind of bending vibration. Both the frequencies  $562$  and  $527\text{ cm}^{-1}$  observed by us are very strong and conspicuous. If we associate this pair with  $525\text{ cm}^{-1}$  (as C—C=O bending vibration) then there is an unusual rise in the value of ground state frequencies. The difference is  $37\text{ cm}^{-1}$ . One way of explaining this discrepancy is to consider  $525$  and  $562\text{ cm}^{-1}$  as two rotational heads of the same band the former being outstanding in infrared and Raman spectra and the latter in ultraviolet. Another possibility is to consider the weak bands at 625 in infrared and 634 in Raman as the C—C=O bending frequencies. This assignment may not materially alter the consideration presented by P & W and others. However, this possibility is limited by the consideration that there is no unanimity about the existence of the band among various authors. We can only say that the  $562$  and  $527\text{ cm}^{-1}$  frequencies observed by us can be reasonably assigned to the C—C=O symmetric bending vibration with their infrared counterpart being either  $525$  or  $625\text{ cm}^{-1}$ .

We now take up the pair of frequencies  $449\text{ cm}^{-1}$  (lower state) and  $390\text{ cm}^{-1}$  (upper state). Both the bands are comparatively strong in the spectrum. No overtones could be found for 449; only one overtone at  $782\text{ cm}^{-1}$  was found for  $390\text{ cm}^{-1}$ . The shifts of 390 and  $782\text{ cm}^{-1}$  are not to be found repeating from successive 1125's thus justifying a relationship between themselves and a lack of connection with others. We are therefore inclined to consider the pair of 449 and  $390\text{ cm}^{-1}$  as the lower and upper state frequencies corresponding to the torsional mode of vibration. This vibration is due to hindered rotation of the non-methyl C—H bond about the C—C bond and belongs to the species  $A''$ . Such a vibration is generally found to have the lowest value of all the fundamentals. T & H were the only investigators who suggested that this frequency may be identified in its overtone at  $852\text{ (}2 \times 426\text{) cm}^{-1}$  the fundamental itself not being observed either in Raman or in infrared spectra. They suggest that the torsional character may be responsible for the more complex rotational structure of the band at  $852\text{ cm}^{-1}$ . Morris's measurement of a strong band is disputed by P & W. Further, his assignment of this  $426\text{ cm}^{-1}$  band as due to C—C=O bending vibration has been shown earlier to be possibly wrong. In any case, we are inclined to confirm the suggestion of T & H that the torsional mode of vibration should lie in the region  $\frac{1}{2}(852)$ . In the low pressure vapour condition in which the ultraviolet spectra have to be studied, the tendency for the torsional mode of vibration may be expected to increase considerably, thus accounting for the intensity of the band. Besides, for such a low frequency the Boltzmann factor would be high even at room temperatures and enhance the intensity of absorption. If our assignment of 449 and



390  $\text{cm}^{-1}$  is as the lower and upper state frequencies of the torsional mode of vibration, then our work is the only source of information about that frequency in the acetaldehyde molecule.

Lastly we take up the assignment of the pair of fundamentals 1222  $\text{cm}^{-1}$  (lower) and 1205  $\text{cm}^{-1}$  (upper) as it appears to be the least certain in our work. The main reasons for our treating them as fundamentals are the intensity of the bands and our inability to explain them otherwise. The frequency of the C—H wagging motion was fixed up at 1350  $\text{cm}^{-1}$  by P & W and at 1121  $\text{cm}^{-1}$  by Morris and 1114  $\text{cm}^{-1}$  by T & H. In the analogous molecule propylene the value is 1297  $\text{cm}^{-1}$  and P & W consider their assignment as higher than what is to be expected from comparison with propylene. But they chose 1350  $\text{cm}^{-1}$  because it was nearer to 1114 as identified by T & H and Morris. (P & W assign 1114 to C—C stretching frequency). Now the C—H wagging frequency in acetaldehyde can be comparable in magnitude with that in propylene and the weak band at 1222  $\text{cm}^{-1}$  (T & H) in infrared and 1270 (V & B) and 1207 (?) (G & R) in Raman effect may be probably assigned to this vibrational mode. If we take the value to be 1222  $\text{cm}^{-1}$  as given by T & H, then it will be much nearer the value to be expected from propylene and within the reasonable order of magnitude. Hence we suggest that 1222  $\text{cm}^{-1}$  and 1205  $\text{cm}^{-1}$  may be treated as the lower and upper state frequencies of the C—H wagging mode.

*Remarks on the work of Walsh.*

Throughout the above discussion we did not make any mention of the work by Walsh on the near ultraviolet spectrum. The reason is that our approach to the problem is fundamentally different from his. His analysis is based on the assumption that the system involves more than one transition and only a few bands could be analysed. From the outset our efforts are directed towards interpreting this system as due to one transition and it is clear from our analysis that we succeeded. Our choice of the 0,0 band differs from his. The nature of the fundamentals as, observed by us, appears more meaningful.

He claims to have identified four frequencies 630, 779, 475  $\text{cm}^{-1}$  in the ground state and 320  $\text{cm}^{-1}$  in the upper state. The first two ground state frequencies are claimed to confirm the two fundamentals 625 and 764  $\text{cm}^{-1}$  suggested by T & H. Both these are bending vibrations, 625 of C—H rocking ( $A'$ ) and 764 of  $\text{CH}_3$  rocking ( $A''$ ). No corresponding upper state frequencies were suggested. From the discussion given by Walsh himself on the basis of the work of Morris and others we are inclined to consider these frequencies as accidental approximations to infrared frequencies of controversial assignment. The other frequency 475  $\text{cm}^{-1}$  was supposed to repeat itself in the far ultraviolet spectrum with the value 481  $\text{cm}^{-1}$ . He associates it with the 525  $\text{cm}^{-1}$  in infrared and considers it as being possibly due to in-plane C—C=O bending. He also considers

it significant that in the acetaldehyde spectrum a progression is found in a frequency other than that of  $C=O$  stretching. This is contrary to the expectation that the near ultraviolet spectrum in acetaldehyde should owe its origin entirely to the  $C=O$ . Our analysis is in complete conformity with this expectation. The outstanding frequencies in our analysis are  $1730\text{ cm}^{-1}$  in ground state and  $1125\text{ cm}^{-1}$  in the upper state definitely attributable to the  $C=O$  vibration. We may conclude by observing that the frequencies suggested by Walsh may be accidental numerical coincidences arising out of an improbable choice of the  $0,0$  band.

In his work on the far ultraviolet spectrum Walsh observed two regions  $1820-1650\text{ A.U.}$  and below  $1350\text{ A.U.}$ , he did not give complete data of the measured bands. He considered the two regions as due to two transitions. In the first region he observed three frequencies  $1200\text{ cm}^{-1}$  (mean value of  $1178$  and  $1221\text{ cm}^{-1}$ ),  $750\text{ cm}^{-1}$  and  $350\text{ cm}^{-1}$ . He found the vibrational structure complicated and difficult to interpret. Similar complications were found by him in the second region as well. He however, used his data primarily to obtain the ionisation potential as  $10.1811 \pm 0.0007\text{ e.v.}$

The only frequency he discussed was the  $1200\text{ cm}^{-1}$  in the region  $1820-1650\text{ A.U.}$  which he assigned to  $C=O$  frequency. There appears to be another view of this frequency, that it might be the  $C-H$  bending in the methyl group (Lawson and Duncan, 1944). An additional support for this latter view is the observation in  $CH_3I$  (Sponer and Teller, 1941). It was found that  $CH_3$  vibration is more conspicuous in far ultraviolet spectrum than  $CI$  frequency. The position is far from clear.

On the other hand, we are not sure that on an independent and fresh approach to the problem, the far ultraviolet bands cannot be interpreted as a single system. A careful analysis of the vibrational structure may possibly lead us to this. It would be extremely profitable to make such an attempt. It is reasonable to expect the vibrational frequencies of the methyl group to predominate in such a scheme.

#### ELECTRONIC STATES

Pending a reinvestigation of the far ultraviolet bands it is not easy to comprehend the nature of the electronic states. However, a few remarks may find a place here.

Mulliken (1935), McMurray and Mulliken (1940) and McMurray (1941) have discussed the electronic structures of aldehydes and ketones in the light of which Walsh attempted an assignment of transitions. They designate a normal state,  $N$ , with the relevant electronic structure of the  $C=O$  group as



It is the  $\gamma_o$  and  $\pi$  electrons that are responsible for the long-wavelength spectrum.

The three lowest possible excited states of the  $C=O$  may be represented as

$$A : (zt)^2 \quad (\psi\psi)^2 \quad y_0 \quad (\psi\bar{\psi})$$

$$B : (zt)^2 \quad (\psi\psi)^2 \quad y_0 \quad (z\bar{t})$$

$$\text{and } V : (zt)^2 \quad (\psi\psi) \quad (\psi\bar{\psi}) \quad y_0^2$$

The transitions were supposed to be thus  $N \rightarrow A$ ,  $N \rightarrow B$  and  $N \rightarrow V$  of which  $N \rightarrow A$  is forbidden by electronic selection rules.  $N \rightarrow B$  and  $N \rightarrow V$  are allowed and so are more intense than  $N \rightarrow A$ .  $N \rightarrow V$  is more intense than  $N \rightarrow B$ .

Walsh attributes the comparatively weaker near ultraviolet spectrum to  $N \rightarrow A$  and his vacuum ultraviolet spectra to  $N \rightarrow B$  (1800 A.U.) and  $N \rightarrow V$  (below 1650 A.U.). As expressed by Walsh himself the only system in acetaldehyde that agrees at all well with the predictions of McMurray and Mulliken as regards the intensity and position of the  $N \rightarrow V$  transition is that at 1650 A.U. So, while there is a possibility that  $N \rightarrow V$  transition might be located correctly we are doubtful about the location of the  $N \rightarrow B$  and  $N \rightarrow A$ . The assignment of the near ultraviolet spectrum to a forbidden transition does not appear to be quite satisfactory for the following reasons. It is granted the absorption strength in this region does not appear to be large. However, the analysis of the bands shows all characteristics of an allowed transition. Thus, in our analysis, the 0,0 band is one with medium intensity and only totally symmetric vibrations are identified as fundamentals, overtones and combinations. The only exception is the torsional frequency belonging to the  $A''$  species the reasons for which are already given. Even in the analysis of Walsh the 0,0 band does exist : in fact it is very strong according to his notation. Besides he thinks that the near ultraviolet spectrum consists of multiple transitions. If so, what are the states connected with those different systems in that region ? He already attributes the spectrum in the 1800 A.U. region to  $N \rightarrow B$  transition. One possible explanation may be that state  $A$  is possibly a triplet. Apart from our work which establishes that it is not so, the approximate identification of  $C=O$  frequency by Eastwood and Snow does not support such a view. For these reasons we are inclined to suggest that the present system in the near ultraviolet may be due to a single transition.

In this connection, it is worthwhile quoting from Mulliken (1935). He discusses the various possibilities of the near ultraviolet spectra in aldehydes and ketones corresponding to an allowed or forbidden type of transition. The main reason for suggesting the forbidden transition was that these near ultraviolet systems are considerably weaker than their counterparts in the far ultraviolet. The ratio is suggested to be 1 : 300 by Snow. Mulliken opines that the ratio is actually not so very large. Cases are not lacking both in "diatomic and polyatomic molecules

where long wavelength bands are very much weaker than shorter wavelength bands even when there is no reason to believe that the electronic transition is barred by a selection rule. Hence the low intensity of the bands is not at all a conclusive evidence of a forbidden electronic transition ; if anything, the observed intensity is surprisingly high for such." We may, however, add that in the later work by Mulliken and McMurray (1940) the idea of the forbidden transition is very much favoured. We wish to point out that the strongest bands in the system and long series of strong bands conform to the Franck-Condon principle and belong to the totally symmetric vibrations. This points to an allowed type of transition.

In view of the above considerations it may be possible that the near ultraviolet spectrum may be due to an allowed type of transition.

Any way, the question of electronic transition can be decided only after a fresh attempt at an analysis of the far ultraviolet bands is made.

#### ACKNOWLEDGMENTS

This work was taken up under the Research Scheme "Fluorescence and Absorption Spectra of Organic molecules" granted by the Council of Scientific and Industrial Research to one of us (V. R. Rao). Our thanks are due to Prof. K. R. Rao for his kind interest in the work.

#### REFERENCES

- Canals, E. and Gastaud, J., 1937, *Bull. Soc. Chim.*, **4**, 2042.  
 Dadieu, A. and Kohlrausch, K. W. F., 1929, *Wien. Ber*, **138**, 607.  
 Eastwood, E. and Snow, C. P., 1935, *Proc. Roy. Soc.*, **A149A**, 434.  
 Gerding, H. and Rjinders, G. W. A., 1939, *Rec. Trav. Chim.*, **58**, 603.  
 Gerding, H. and Lecomte, J., 1939, *Rec. Trav. Chim.*, **58**, 614.  
 Henri, V. and Schou, S. A., 1928, *Z. f. Phys*, **49**, 774.  
 Kohlrausch, K. W. F. and Koppl., F., 1934, *Z. f. Phys. Chem*, **24**, 370.  
 Lawson, M. and Duncan, A. B. F., 1944, *J. Che. Phy.* **12**, 329.  
 Leighton, P. A. and Blacet, F. E., 1933, *J. Am. Chem. Soc.*, **55**, 1766.  
 McMurray, H. L., 1941, *J. Chem. Phy.*, **9**, 231.  
 Morris, J. C., 1943, *J. Chem. Phy.*, **11**, 230.  
 Mulliken, R. S., 1935, *J. Chem. Phy.*, **3**, 564.  
 Mulliken, R. S. and McMurray, H. L., 1940, *Proc. Nat. Ac. Sci.*, **26**, 312.  
 Petrikaln and Hochberg, S., 1939, *Z. Phy. Chem.*, **4**, 299.  
 Pitzer, K. S. and Weltner, W(Jr) 1949, *J. Am. Chem. Soc.*, **71**, 2842.  
 Pringsheim, P., 1949, *Fluorescence and Phosphorescence* 258.  
 Rao, I. A. and V. Ramakrishna Rao, 1954, *J. Sci. Ind. Res.*, **13**, 371.  
 Schou, S. A., 1929, *J. Chl. Phy*, **28**, 1.  
 „ 1928, *J. Chl. Phy*, **28**, 669.  
 Sponer, H. and Teller, H., 1941, *Rev. Mod. Phy.*, **13**, 113.  
 Thompson, H. W. and Harris, G. P, 1942, *Trans. Far Soc.*, **38**, 37.  
 Venkateswaran, S. and Bhagavantam, S. 1930, *Proc. Roy. Soc.*, **A128**, 252.  
 Walsh, A. D., 1946, *Proc. Roy. Soc.*, **A188**, 176.  
 Walsh, A. D., 1953, *J. Chem. Soc.*, **7**, 2318.

# MOLECULAR ORBITAL CALCULATION ON PHTHALOCYANINE

BY SADHAN BASU

INDIAN ASSOCIATION FOR THE CULTIVATION OF SCIENCE, CALCUTTA-32

(Received for publication, July 20, 1954)

**ABSTRACTS** MO calculations have been made on phthalocyanine and the permanent charge distribution has been correlated with the chemical reactivity of the different positions of the molecule. A prediction of the allowed spectral transition has also been made from the calculated energy levels of the  $\pi$ -electrons

## INTRODUCTION

In the recent years phthalocyanine has assumed great importance to the theoretical scientists. The molecule has been made visible under field emission electron microscope and its work function and ionization potential have been calculated (Gomer, 1952). In solid state this compound shows intrinsic semi-conductivity and is the first organic compound in which band structure of the electronic energy levels have been established almost conclusively (Vartanyan, 1949; Eley *et al*, 1953).

In the present paper we shall investigate the electronic structure of phthalocyanine using molecular orbital theory in its simplest form (Wheland, 1945; Coulson, 1947). We shall attempt to interpret certain interesting features of this compound and correlate its chemical reactivity with the calculated  $\pi$ -electron densities and permanent charge distribution in the molecule. In addition, the present paper shows how quantum mechanical calculations can be extended to as complex a molecule as phthalocyanine (figure 1). Similar calculations have also been made by Longuet-Higgins *et al* (1950) for porphine and tetrahydro porphine.

## THEORY

The quantal treatment of conjugated molecules depends upon the classification of the valency electrons. Carbon in its quadavalent state has the structure  $1s^2 2s^2 2p^2$ . The  $2s$ ,  $2p_x$  and  $2p_y$  orbitals are hybridised to form so called trigonal or  $\sigma$ -orbitals, while  $2p_z$  or  $\pi$ -orbitals retain their individuality. The  $\sigma$ -orbitals are used to form the frame work C-C and C-H bonds, and the  $\pi$ -orbitals, one for each carbon atom, give the conjugated property. The usual quantal approximation to conjugated system is to treat the  $\pi$ -electrons only. For a molecule containing

$n$   $\pi$ -electrons moving in the field of a core, the Hamiltonian operator will be expressed in the form

$$H = H_{\text{core}} + \frac{1}{2} \sum_{ij} (e^2/r_{ij}) \quad \dots (1)$$

where  $(e^2/r_{ij})$  is the electrostatic repulsion between  $\pi$ -electron  $i$  and  $j$ , and

$$H_{\text{core}} = \sum_i H_{\text{core}}(i) \quad \dots (2)$$

where  $H_{\text{core}}(i)$  is the kinetic energy operator for electron  $i$  plus its potential energy operator in the field of the core

$$H_{\text{core}}(i) = T(i) + U_{\text{core}}(i) \quad \dots (3)$$

Other than  $\pi$ -electrons are evinced only through the term  $U_{\text{core}}(i)$ . This is the so called  $\pi$ -electron approximation.

We approximate the individual one electron wavefunctions  $\phi_j$  by means of linear combination of the orbitals  $\psi_k$  belonging to the different atoms

$$\phi_j = \sum_k c_{jk} \psi_k \quad \dots (4)$$

The variation method shows that the best values of the coefficients  $c_{jk}$ 's are those which satisfy the equations

$$\sum_{k=1}^l c_{jk} (H_{mk} - \Delta_{mk} E_j) = 0 \quad j, m = 1, 2, \dots, l \quad \dots (5)$$

where  $l$  is the number of  $\pi$ -electrons and

$$H_{mk} = \int \psi_m^* H \psi_k d\tau, \quad \Delta_{mk} = \int \psi_m^* \psi_k d\tau$$

and  $E_j$  is the energy of the  $\pi$ -electron occupying the molecular orbital  $\phi_j$ . The condition for the solution of this set of equations is that their determinants vanish. The  $l$  roots of this secular equation,  $E = E_j(1, 2, \dots, l)$  gives the energies of the  $l$  molecular orbitals.

$$|H_{mk} - \Delta_{mk} E| = \begin{vmatrix} H_{11} - \Delta_{11} E & H_{12} - \Delta_{12} E & \dots & H_{1l} - \Delta_{1l} E \\ H_{21} - \Delta_{21} E & H_{22} - \Delta_{22} E & \dots & H_{2l} - \Delta_{2l} E \\ \dots & \dots & \dots & \dots \\ \dots & \dots & \dots & \dots \\ H_{l1} - \Delta_{l1} E & H_{l2} - \Delta_{l2} E & \dots & H_{ll} - \Delta_{ll} E \end{vmatrix} = 0 \quad \dots (6)$$

The values of  $E_j$  thus found are then substituted back into equation (5), from which the ratios of the values of the coefficients  $c_{jk}$ 's can be derived. The absolute magnitudes of the coefficients can be determined by the normalization condition  $\int \phi_j^* \phi_j d\tau = 1$ . An electron occupying the molecular orbital  $\phi_j$  will spend a fraction of its time given by the expression  $|c_{jk}|^2$  in the atomic orbital  $\psi_k$ . Consequently, the total average charge on the atom  $k$  will be

$$c_k = 2e \sum |c_{jk}|^2 \quad \dots (7)$$

where the summation is extended over all the occupied  $\phi_j$ 's and  $e$  represents the charge of the electron.

As usual in these calculations, we make the following assumptions with regard to the magnitudes of the various integrals involved :

$H_{kk} = E_0$  = Coulomb integral for carbon.

$H_{mk}$  = exchange integral =  $\beta$ , if  $\psi_m$  and  $\psi_k$  are on adjacent atoms.  
= 0, otherwise.

$\Delta_{kk} = 1$ , from normalizing condition.

$\Delta_{mk} = 0$ , for  $m \neq k$  = overlap integral.

With these assumptions the secular equations take the form

$$(E_0 - E)c_r + \sum_{\text{all bonded}} \beta c_s = 0 \quad (8)$$

or more briefly

$$xc_r + \sum c_s = 0 \quad \dots (9)$$

where  $x = (E_0 - E)/\beta$  (an energy parameter).

We make the additional assumptions that  $\beta$  is same for all CC and CN bonds, and the Coulomb integral  $E_0$  is same for all atoms. Second assumption is not true; nitrogen is more electronegative than carbon and will certainly have a higher value for Coulomb integral. However, it is most convenient to begin by assuming all the  $E_0$  values equal and correct the resulting energy values later on. There are forty atoms constituting the conjugated system in phthalocyanine, so we get 40 secular equations like (9), solution of which will give 40 roots for  $x$ . It is evident what a formidable task it will be to solve an equation of order forty.

#### APPLICATION OF GROUP THEORY

High symmetry of phthalocyanine, however, enables us to break down the 40th order equation into a number of smaller order equations by the application of group theory. The symmetry group of phthalocyanine is  $D_{4h}$ . The  $\pi$ -electron MO's are by definition all antisymmetric with respect

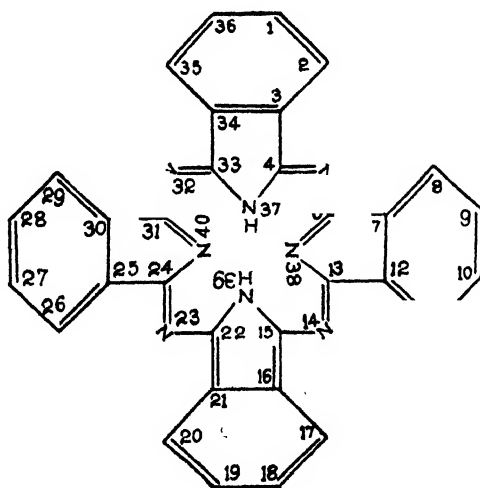


FIG. 1

Molecular structure of phthalocyanine

to molecular plane, and therefore belong to the species  $A_{2u}$ ,  $B_{2u}$ ,  $A_{1u}$ ,  $B_{1u}$ , and  $E_g$ . MO species are shown diagrammatically in figure 2.

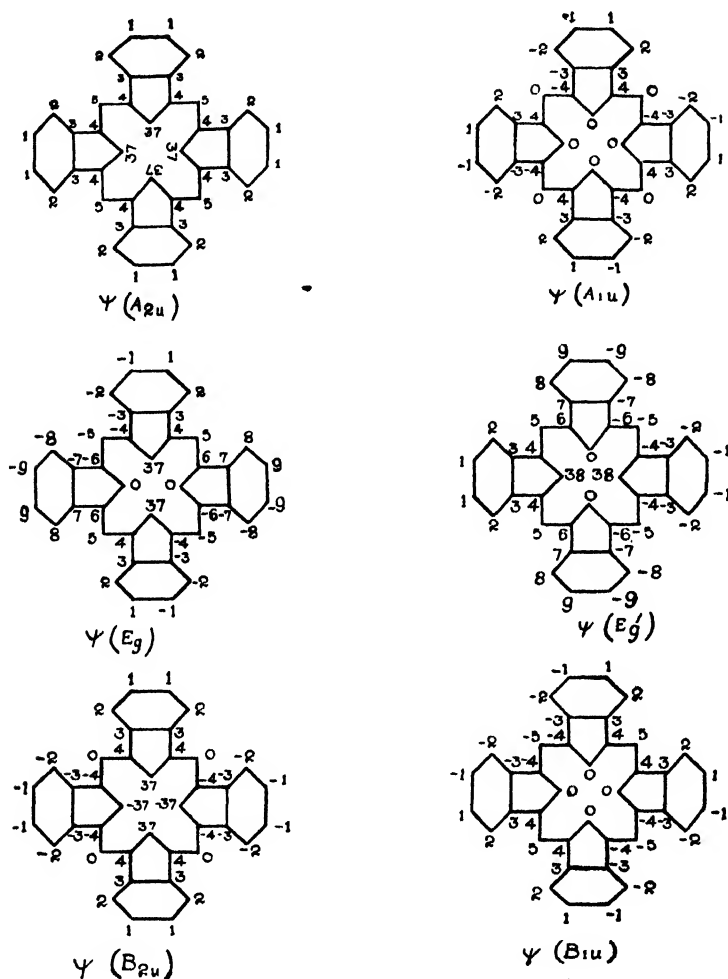


FIG. 2

### Species $A_{2u}$

The secular equations for this species are

- (i)  $(x+1)c_1+c_2=0$
- (ii)  $xc_2+c_1+c_3=0$
- (iii)  $(x+1)c_3+c_2+c_4=0$
- (iv)  $xc_4+c_3+c_5+c_{37}=0$
- (v)  $xc_5+2c_4=0$
- (vi)  $xc_{37}+2c_4=0$

from which we get the secular determinant



$$\begin{array}{cccccc}
 x+1 & 1 & 0 & 0 & 0 & 0 \\
 1 & x & 1 & 0 & 0 & 1 \\
 0 & 1 & x+1 & 1 & 0 & 0 \\
 0 & 0 & 1 & x & 1 & 0 \\
 0 & 0 & 0 & 2 & x & 0 \\
 0 & 0 & 0 & 2 & 0 & x
 \end{array} = 0 = x^6 + 2x^5 - 6x^4 - 11x^3 + 5x^2 + 8x$$

This equation has six real roots, so there are 6 MO of species  $A_{2u}$  with energies  $E = E_0 + x\beta$ . The equation was solved by 'Pinch' method correct upto first decimal place. The values of  $x$  are given in Table I. The ratios of the coefficients  $c_r$  for each of these are obtained by substituting the appropriate values of  $x$  back into the equations; and their absolute values are fixed by the condition that the MO be normalized, viz.

$$8c_1^2 + 8c_2^2 + 8c_3^2 + 8c_4^2 + 4c_5^2 + 4c_{37}^2 = 1.$$

#### Species $B_{2u}$

Secular equations for this species are

- (i)  $(x+1)c_1 + c_2 = 0$
- (ii)  $xc_2 + c_1 + c_3 = 0$
- (iii)  $(x+1)c_3 + c_2 + c_4 = 0$
- (iv)  $xc_4 + c_3 + c_{37} = 0$
- (v)  $xc_{37} + 2c_4 = 0$

from which we get the fifth order equation

$$x^5 + 2x^4 - 4x^3 - 7x^2 + 3x + 4 = 0$$

which gives five real roots for  $x$  as given in Table I. The fact that  $c_5$ , etc., are zero means that the species satisfies the secular equations for an isolated phthalimide molecule.

#### Species $A_{1u}$

Secular equations for this species are

- (i)  $(x-1)c_1 + c_2 = 0$
- (ii)  $xc_2 + c_3 + c_1 = 0$
- (iii)  $(x-1)c_3 + c_2 + c_4 = 0$
- (iv)  $xc_4 + c_3 = 0$

from which we get the fourth order equation

$$x^4 - 2x^3 - 2x^2 + 3x - 1 = 0$$

in which  $x$  has four real roots given in the Table I.

#### Species $B_{1u}$

Secular equations for this species are

- (i)  $(x-1)c_1 + c_2 = 0$
- (ii)  $xc_2 + c_1 + c_3 = 0$
- (iii)  $(x-1)c_3 + c_2 + c_4 = 0$
- (iv)  $xc_4 + c_3 + c_5 = 0$
- (v)  $xc_5 + 2c_4 = 0$

from which we get the fifth order equation

$$x^5 - 2x^4 - 5x^3 + 6x^2 + 4x - 4 = 0$$

in which  $x$  has five real roots as given in Table I. Since this species has nodal planes through the pyrrole nitrogen atoms, they satisfy the secular equations for a twenty membered ring with symmetrically fused four phenyl nucleus

*Species  $E_g$*

The MO species  $E_g$  occurs in degenerate pairs and though the energy of each pair is determinate, there is certain freedom of choice in the forms of the MO. We use the forms shown in figure 2. The secular equation for this species are

$$\begin{array}{ll}
 (i) & (x+1)c_1 + c_2 = 0 \\
 (ii) & xc_2 + c_1 + c_3 = 0 \\
 (iii) & (x+1)c_3 + c_2 + c_4 = 0 \\
 (iv) & xc_4 + c_3 + c_5 + c_{37} = 0 \\
 (v) & xc_5 + c_4 + c_6 = 0 \\
 (vi) & xc_6 + c_5 + c_7 = 0 \\
 (vii) & (x-1)c_7 + c_6 + c_8 = 0 \\
 (viii) & xc_8 + c_7 + c_9 = 0 \\
 (ix) & (x-1)c_9 + c_8 = 0 \\
 (x) & xc_{37} + 2c_8 = 0
 \end{array}$$

from which we get the tenth order equation

$$x^{10} - 2x^9 - 7x^8 - 13x^7 + 14x^6 + 27x^5 - 19x^3 - 17x^2 + 3x + 8 = 0$$

which gives 10 real roots for  $x$  as shown in Table I.

TABLE I  
Group species and energy parameters ( $x$ ).

$A_{2u}$	$B_{2u}$	$A_{1u}$	$B_{1u}$	$E_u$	
0.00	-0.70	-0.29	+1.00	+0.58	-0.50
+0.97	+0.90	+1.95	-1.00	-0.50	-1.50
-0.97	-0.26	-1.23	+2.90	+1.00	-2.62
+2.20	-3.02	+1.47	-1.65	-1.00	+1.82
-2.40	+1.28		+0.75	-1.20	
-1.80				-1.00	

It must be re-emphasised that the above values of the energy parameter have been calculated on the assumption that the nitrogen atoms and the carbon atoms all have the same Coulomb integral ( $E_0$ ). With this assumption in mind, let us calculate the electron densities at different positions of the molecule in its ground state. We have already defined this quantity as

$$c_k = 2e \sum |c_k|^2$$

summation being taken over 21 MO's of lowest energies, since this molecule has altogether 42  $\pi$ -electrons and each energy states will be occupied by two electrons. Summing over these orbitals we get for electron densities the values given in Table II. In addition to electron densities there is another quantity used in determining the electronic structure of the molecule called mobile order of the bond (Coulson, 1947b) and defined as  $p_{rs} = 2 \sum c_r c_s$

(mobile order of the bond  $\pi$ s). As a result of conjugation the bonds in the aromatic molecules become intermediate between pure single and double bond. They may be described in terms of their mobile order  $p$ . The word 'mobile' denotes that the electrons responsible for unsaturation are free to move over the whole nuclear frame work. In the case of carbon-carbon bonds and other similar non-polar bonds,  $p=1$  denotes a pure double and  $p=0$  denotes a pure single bond. If for any particular bond  $p$  lies in the range 0.3 to 0.7 the bond is neither single nor double and it will be expected to have properties similar, to a more or less extent, to those of the aromatic compounds. The calculated values for the mobile bond orders for the various bonds in phthalocyanine are also shown in Table II.

TABLE II  
Electron densities and mobile bond orders

$c_A$	$p$
1 = 1.006	1,36 = 0.60
2 = 0.946	1,2 = 0.46
3 = 0.954	2,3 = 0.36
4 = 0.864	3,4 = 0.38
5 = 0.756	3,34 = 0.43
37 = 1.210	1,5 = 0.36
	4,37 = 0.55

It may be noted from the Table II that all the bonds have got bond orders intermediate between single and double bond, consequently there is extensive delocalization and the molecule is highly stabilized by resonance.

It is interesting to note that the  $\pi$ -electron density comes out highest on atoms 37, 38, 39 and 40, (figure 1) although no allowance has been made for the greater electronegativity of nitrogen compared to carbon. This suggests two things. First, that greater stability of phthalocyanine is largely due to the presence of nitrogen atoms at points in the skeleton, where for purely geometrical reason, the  $\pi$ -electrons tend to congregate. Secondly, this piling up of the electrons may reduce the electron affinity of nitrogen atoms to a value not very far from that of the carbon atoms, so it is not a bad approximation to set the Coulomb integral of the nitrogen atoms equal to that of carbon. It may, however, be observed that the  $\pi$ -electron density is lowest at 5, 14, 23 and 32 (figure 1) positions. Introduction of nitrogen atoms at these positions will tend to draw electrons away from other parts of the molecule. Consequently it is expected that

although in porphine neglect of nitrogen electronegativity is permissible, for phthalocyanine this is rather a drastic approximation.

#### CORRECTION FOR ELECTRONEGATIVITY

For this purpose we set Coulomb integral for nitrogen equal to  $E_0 + \delta\beta$ , where  $\delta$  is a small positive number. Next we start with the parent hydrocarbon and find its electron densities and energy states as has been done. Replacement of CH by N or C by N<sup>+</sup> will alter some of the energy parameters upon which electron density depends. If the alteration of Coulomb integral be not large, we can use perturbation method, in which we expand both the energy  $E$  and the wavefunctions in rising power of  $\delta$  (Wheland, 1935; Coulson, 1947). If we carry the procedure only as far as the first order, we obtain linear expressions which represent approximately the variations of the different quantities in question for small values of  $\delta$ . The familiar equation of the first order perturbation theory shows that the corresponding perturbed quantities are

$$E' = \int \phi_j^* H \phi_j d\tau = E + \int \phi_i^* H' \phi_j d\tau$$

and

$$\phi_j' = \phi_j + \sum' \frac{\int \phi_k^* H' \phi_j d\tau}{E_j - E_k} \phi_k \quad (10)$$

where  $H'$  is the part of the Hamiltonian operator which refers to the perturbation, such that

$$\begin{aligned} \int \psi_k^* H' \psi_l d\tau &= \delta\beta \text{ if } k=i=37, 38, 39, 40, 5, 14, 23 \text{ and } 32 \\ &= 0, \text{ otherwise} \end{aligned}$$

and the prime on the summation sign indicates that the term  $k=j$  is omitted. This procedure gives us for perturbed energy parameter ( $x'$ )

$$x' = x + \delta(c_{37}^2 + c_{38}^2 + c_{39}^2 + c_{40}^2) + \delta(c_5^2 + c_{14}^2 + c_{23}^2 + c_{32}^2) \quad \dots \quad (11)$$

for each perturbed MO. Now it has been shown by Wheland (1935) and Coulson (1947) that best value for  $\delta$  in the case of nitrogen is 2, which gives good agreement between the calculated electron density and chemical reactivity of the different positions of a nitrogen-containing system. When the energy parameters are thus corrected the new values obtained are given in Table III.

Of these states 21 lowest ones will be occupied. When electron densities are calculated with these new energy values we get the results shown in Table IV.

The calculated electron densities can be correlated very well with the chemical reactivity of the compound. High electron densities at the carbon atoms (1) make the outside hydrogens easily replaceable by halogens, sulfonic acid, phenyl, nitro and azo groups. Two inner hydrogens attached

TABLE III  
Energy parameter.

Group species	Uncorrected	Corrected for electronegativity	Corrected for overlap
$B_{2u}$	-3.02	-3.00	-12.00
$E_u$	-2.62	-1.45	-2.26
$A_{2u}$	-2.40	-2.08	-4.10
$A_{2u}$	-1.80	-1.16	-1.63
$B_{1u}$	-1.65	-1.33	-2.80
$E_u$	-1.50	-0.90	-1.15
$A_{1u}$	-1.23	-1.23	-1.77
$E_u$	-1.20	-1.12	-1.55
$E_u$	-1.00	-1.00	-1.33
$E_g$	-1.00	-1.00	-1.33
$B_{1g}$	-1.00	-1.00	-1.33
$A_{2u}$	-0.97	-0.97	-1.27
$B_{2u}$	-0.70	-0.69	-0.84
$E_g$	-0.59	-0.77	-0.56
$E_g$	-0.50	-0.75	-0.64
$A_{1g}$	0.00	0.00	0.00
$B_{2u}$	+0.29	+0.29	+0.31
$B_{1u}$	+0.75	+1.17	+0.90
	+0.90	+0.93	+1.70

(All the  $E_u$  states are doubly degenerate).TABLE IV  
Corrected electrons densities and bond orders

$c_k$	$p$
1=1.074	1, 36=0.46
2=0.990	1, 2 =0.36
3=0.962	2, 3 =0.38
4=0.922	3, 4 =0.36
5=0.778	4, 5 =0.48
37=1.136	4, 37=0.09

to nitrogen are replaceable by such metals like Na, Mg, Ca, Cu, Cr, Fe, etc. Electron density is lowest at position 5, so the oxidative degradation proceeds through this point with the production of p' thalimide and ammonium salt.

#### CORRECTION FOR OVERLAP

In the above deduction for the permissible energy levels we have set  $\Delta_{mk}$  (overlap integral) equal to zero. Wheland (1941) has shown that this has a value of about 0.25. Although introduction of this value makes very little difference in the permanent charge distribution, energy values are appreciably altered which introduces quite high error in the calculated frequency of absorption. It is, however, possible to introduce correction for overlap at this stage using the equation deduced by Wheland

$$E = E_0 + m\beta$$

where

$$m = \frac{v'}{(1 + \Delta_{mk}v')}$$

corrected energies are given in the column 4 of Table III.

#### *Prediction of $\pi$ -electron transition spectra :*

LCAO MO calculations have been commonly used to predict the one or two longest wave length transition either in the visible or in the near ultraviolet region. The predictions have all been made by the following prescription :

- (1) Compute the roots,  $x$ , of the simple LCAO secular equation, neglecting overlap, and setting all  $E_0$ 's equal and all  $\beta$ 's equal.
- (2) Set  $\beta = 32,000 \text{ cm}^{-1}$  for short polyenes,  $\beta = 23,000 \text{ cm}^{-1}$  for ring system.
- (3) Lowest transition frequencies are then given approximately by  $[x (\text{low empty orbital}) - x (\text{high filled orbital})]\beta$ , which is the energy of a one-electron jump. The polarizations will be determined by the symmetries of the initial and final orbitals.

This procedure neglects 'electron interactions' or 'configuration interaction'. Analogy with the benzene spectrum and its interpretation shows that such interactions must be important. This interaction is one which changes the energies and wavefunctions of two neighbouring molecular states which have the same parity and symmetry. The familiar quantum mechanical result is that the total wavefunction of such states mix, so that such a state becomes a hybrid, the lower state has its energy lowered further and the upper state has its energy raised. These effects are stronger the closer the two states are together. If they have the same energy and mutually degenerate, in one electron approximation, as in benzene, the interaction removes the degeneracy and has an especially large effect. It is convenient to call spectra exhibiting strong configuration

interaction 'round field' spectra and those showing little interaction 'long field' spectra.

A look at the table shows that there is very little energy difference between the states 19, 20, 21 and 22. So there will be strong configurational interaction between the highest filled level and lowest empty level so the molecule will give a 'round field' type of spectrum, and it is rather difficult to predict the frequency of absorption for the transition between these states. Transition between  $E_g$  and  $B_{2u}$  and  $B_{1u}$  state is, however, associated with appreciable energy change so these transitions are allowed and will be fairly strong. The values are listed in Table V, along with their degeneracy

TABLE V

Transition	Degeneracy	Calculated frequency	
		uncorrected $\text{cm}^{-1}$	corrected $\text{cm}^{-1}$
$B_{2u} - E_g$	double	20,470 (89 $\beta$ )	21,620 (94 $\beta$ )
$B_{1u} - E_g$	double	13,570 (59 $\beta$ )	14,720 (64 $\beta$ )

There is no recorded data in literature for the absorption spectra of free phthalocyanine. The present calculations are just predictions.  $B_{2u} - E_g$  band will be polarized parallel and perpendicular to the long axis of the molecule.

## REFERENCES

- Coulson, C. A. and Longuet-Higgins, H. C., 1947a, *Proc. Roy. Soc.*, **A191**, 39.  
 Coulson, C. A., and Longuet-Higgins, H. C., 1947b, *Trans. Farad. Soc.*, **43**, 87.  
 Elev. Parfitt, Perry and Taysum, 1953, *Trans. Farad. Soc.*, **49**, 79.  
 Gombel, R., 1952, *J. Chem. Phys.*, **20**, 1772.  
 Longuet-Higgins, H. C., Rector, C. W., and Platt, J. R., 1952, *J. Chem. Phys.* **18** 1174.  
 Vartanyan, 1949, *Chem. Abstr.*, **43**, 1272g.  
 Wheland, G. W. and Pauling, L., 1935, *J. Amer. Chem. Soc.*, **57**, 2086.  
 Wheland, G. W., 1941, *J. Amer. Chem. Soc.*, **63**, 2025.

# ON THE RESOLVING POWER OF COMPOUND FABRY-PEROT ETALON

By MADHUKAR KASHINATH MACHWE

DELHI UNIVERSITY, DELHI, 1

AND

MAHENDRA SINGH SODHA

DEFENCE SCIENCE LABORATORY, NEW DELHI, 12.

(Received for publication, August 9 1954)

**ABSTRACT.** The authors have calculated the resolving power of compound Fabry-perot etalon on both Rayleigh and Abbe criteria, taking into account the contribution of the tails of the individual intensity patterns of the two lines to the maxima of resultant intensity pattern

## INTRODUCTION

Meissner (1942), in his calculation of the resolving power of the compound Fabry-Perot etalon on the Rayleigh criterion has neglected the contribution of the tails of individual intensity patterns of the two components to the central maxima of the resultant intensity pattern. Taking this into account the authors have calculated the resolving power of compound Fabry etalon on Rayleigh as well as Abbe criterion in this communication.

## INTENSITY CONSIDERATIONS

Consider two etalons of lengths  $D'$  and  $D''$  where  $D' = pD''$  and  $p$  is an integer. The intensities due to the two etalons separately at a point whose order in the longer etalon is  $n_0 + n$ , and the smaller one  $(n_0/p) + (n/p)$ , where  $n_0/p$  is an integer and  $n$  is small, is given by

$$I_1' = \frac{I_0'}{1 + F' \sin^2 \pi(n_0 + n)} = \frac{I_0'}{1 + x^2}$$

$$I_1'' = \frac{I_0''}{1 + F'' \sin^2 \pi(n_0 + n - \Delta n)/p} = \frac{I_0''}{1 + bx^2}$$

where  $x = \pi F'^{1/2} n$  and  $b = F''/4F'p^2$ .

The intensity distribution due to the two etalons in tandem (Meissner 1942) is

$$I_1 = I_0 / (1 + x^2)(1 + bx^2) \quad \dots (1)$$

The intensity distribution of another line, separated by an order  $\Delta n$  is given by



$$I_2 = I_0 / \{1 + (x-a)^2\} \{1 + b(x-a)^2\} \quad \dots (2)$$

Hence the resultant intensity pattern is given by

$$\frac{I}{I_0} = \frac{I_1 + I_2}{I_0} = \frac{1}{(1+a^2)(1+bx^2)} + \frac{1}{\{1+(x-a)^2\}\{1+b(x-a)^2\}} \quad \dots (3)$$

Neglecting shrinkage effect of close components the intensity maxima ( $x \approx 0$  or  $a$ ) and minimum ( $x = a/2$ ) are given by

$$\frac{I_{max}}{I_0} = 1 + 1 / \{ (1+a^2)(1+ba^2) \} \quad (4)$$

and

$$\frac{I_{min}}{I_0} = 2 / \{ (1+a^2/4)(1+ba^2/4) \} \quad (5)$$

#### CALCULATION OF RESOLVING POWER

For limiting resolution

$$I_{min} = c I_{max} \quad (6)$$

where  $c = 0.8$  and  $0.981$  for Rayleigh and Abbe criteria respectively.

The resolving power is given by

$$\frac{\lambda}{d\lambda} = \frac{n_0}{\Delta n} = \frac{\pi}{a} n_0 F'^{\frac{1}{2}} = \pi n_0 F'^{\frac{1}{2}} \quad (7)$$

In his solution of Eqn. (6) for  $c = 0.8$ , Meissner has neglected the term  $1/(1+a^2)(1+ba^2)$  and he finally obtains

$$\alpha = \frac{\pi}{\sqrt{12}} \left\{ 1 + b + \sqrt{1 + 8b + b^2} \right\}^{\frac{1}{2}} \quad \dots (8)$$

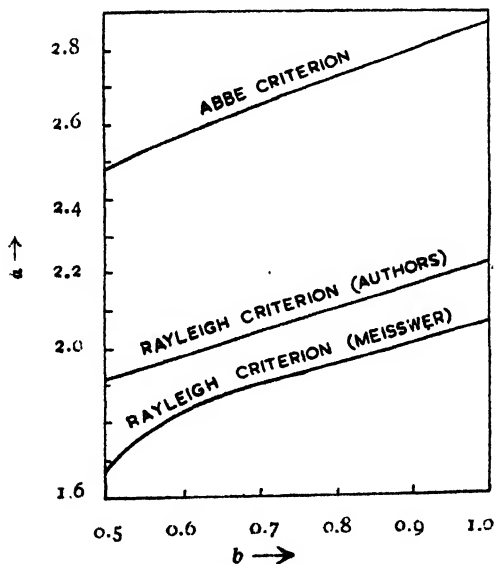


Fig. 1 Variation of  $\alpha$  with  $b$

The authors have solved Eqn. (6) for particular values of  $b$  (1.0, 0.9, 0.8, 0.7, 0.6 and 0.5) and  $c=0.8$  and 0.981 by the method of successive approximations. The high accuracy of the results obtained is evident from Tables I and II, which give the variation of  $\alpha$  with  $b$  according to Rayleigh and Abbe criteria respectively. Table I also includes values of  $\alpha$  calculated by Eqn. (6) due to Meissner, for comparison. The tables are illustrated by figure 1.

TABLE I  
Variation of  $\alpha$  with  $b$  on the Rayleigh criterion.

$b$	$a^2$	$I_{\max}$	$I_{\min}$	$I_{\min}/I_{\max}$	$\alpha$ (authors)	$\alpha$ (Meissner)
1.0	2.0	10/9	8/9	0.8000	2.222	2.061
0.9	2.12	1.1066	0.8850	0.7998	2.159	2.009
0.8	2.24	1.1055	0.8851	0.8000	2.100	1.954
0.7	2.36	1.1122	0.8904	0.8003	2.046	1.895
0.6	2.52	1.1131	0.8974	0.7999	1.980	1.833
0.5	2.70	1.1150	0.8925	0.8005	1.913	1.766

TABLE II  
Variation of  $\alpha$  with  $b$  on the Abbe criterion.

$b$	$a^2$	$I_{\min}$	$I_{\max}$	$I_{\min}/I_{\max}$	$\alpha$
1.0	1.20	1.1834	1.2066	0.9807	2.860
0.9	1.26	1.1850	1.2073	0.9815	2.800
0.8	1.332	1.1848	1.2076	0.9811	2.724
0.7	1.41	1.1861	1.2088	0.9812	2.646
0.6	1.5	1.1874	1.2105	0.9809	2.566
0.5	1.6	1.1905	1.2137	0.9809	2.484

#### ACKNOWLEDGMENT

The authors are grateful to Dr. D. S. Kothari for his interest in the investigation.

#### REFERENCE

Meissner, (1942). *Jour. Opt. Soc. Amer.*, **32**, 185.

## BAND SPECTRUM OF CrF MOLECULE

BY MRS. B. KANAKA DURGAVATHI AND V. RAMAKRISHNA RAO

PHYSICS DEPARTMENT, ANDHRA UNIVERSITY, WALTAIR.

(Received for publication, July, 16, 1951)

Plates : XIX A-B

**ABSTRACT.** Two band systems (I and II) attributable to CrF molecule were obtained in emission in a heavy current discharge in the regions  $\lambda\lambda$  4230–4470 A.U. and  $\lambda\lambda$  3830–4050 A.U. respectively. System I was interpreted as due to the electronic transition  ${}^6\Pi \rightarrow {}^6\Sigma$  and System II as due to a transition  ${}^6\Sigma \rightarrow {}^6\Sigma$  with a common lower state. The  $\omega_e$  value is observed to be approximately  $520\text{ cm}^{-1}$ .

## INTRODUCTION

The band spectrum of CrCl molecule was studied by one of us (V. R. Rao) and K. R. Rao (1949) and shown to be due to a transition  ${}^6\Pi \rightarrow {}^6\Sigma$ . The spectrum of CrBr was also investigated by V. R. Rao (1949). It was felt that if the spectrum of CrF molecule is also studied, a comparison between the characteristics of the spectra of different halides of chromium can be made. The transitions might be expected to be similar to that in CrCl. The results of our study of the CrF spectra are described below.

## EXPERIMENTAL

The substance chromium fluoride supplied by Thomas Tyrer and Co. London, was used in these investigations. The experimental technique was the same as used in the investigations on CrCl and CrBr (Loc. cit.). A characteristic discharge of bright yellow colour is obtained at 2000 V. and 0.8 amperes. Photographs are taken on Ilford Selochrome plates on Fuess instrument with a dispersion of 20 A/mm. in the region  $\lambda$  4400 A.U. Exposures of about half an hour were required to record the spectrum. As the intensity of the bands is very low, they could not be obtained on a higher dispersion instrument.

## DESCRIPTION OF THE SPECTRUM

When the vapour of CrF was excited by the generator discharge bands were obtained in the region  $\lambda\lambda$  4573–3800 A.U. The region is also overlaid with strong atomic lines. They appear in two different groups. One of them, i.e. the stronger one lies in the region  $\lambda\lambda$  4230–4470 A.U. The second group

(see figure 2 in Plate XIX B) which consists of four weak groups, lies in the region  $\lambda\lambda$  3830—4050 A.U. This appears to have a less complicated structure than the first group.

#### ANALYSIS

From the intensity distribution of the band groups and a comparison with allied halides, the bands could be divided into two system: (1) in the region  $\lambda\lambda$  4467—4198 A.U. and (2) in the region  $\lambda\lambda$  3993—3840 A.U. The long wavelength system, hereafter referred to as System I, is of a very complex structure as in TiCl, MnCl and CrCl, etc. Possibly this is due to the transition  ${}^{\circ}\Pi \rightarrow {}^{\circ}\Sigma$ . System II, the one on the shorter wavelength side appears comparatively simpler and may be due to the transition  ${}^{\circ}\Sigma \rightarrow {}^{\circ}\Sigma$ . The lower  $\Sigma$  state is possibly common to both,

The three states  ${}^{\circ}\Sigma$ ,  ${}^{\circ}\Pi$  and  ${}^{\circ}\Sigma$  may be derived as follows. The chromium atom with 6 effective electrons and the fluorine atom with 5 effective electrons have the following electron configurations.

Cr:  $1s^2 2s^2 2p^6 3s^2 3p^2 3d^5$  4 giving a as ground term,

F:  $1s^2 2s^2 2p^5$  giving a as ground term.

In the molecule CrF the configuration

$$\sigma^2 \pi^4, \sigma \pi^2 \delta^2$$

gives a  ${}^{\circ}\Sigma$  term as in CrCl. The following configurations

$$\sigma^2 \pi^4, \pi^2 \delta^2 \pi \rightarrow {}^{\circ}\Pi \quad \text{and}$$

$$\sigma \pi^4 \pi, \pi^2 \delta^2 \pi \rightarrow {}^{\circ}\Sigma$$

involving single and double electron excitation, give the two upper states noted against them. Transitions from these to the lower state  ${}^{\circ}\Sigma$  give two band systems with  ${}^{\circ}\Sigma \rightarrow {}^{\circ}\Sigma$  lying to the short wavelength side of  ${}^{\circ}\Pi \rightarrow {}^{\circ}\Sigma$ . The former has a simple structure as both states are  $\Sigma$ 's. The latter has a more complicated structure involving six multiplets of  ${}^{\circ}\Pi$  state and some rotational branches (vide CrCl).

It is necessary now to determine the forms of rotational heads to be expected in these bands. The formulae for individual forms of rotational heads are given in the paper on CrCl (Loc. cit). Following the steps given there, we find in red-degraded bands in which  $B'' > B'$ , we can expect only the R, S, T and Q forms to form the heads. The  $K_h$  values are as follows.

Form	Q	R	S	T
$K_h$	0	$\frac{3B' - B''}{2(B - B'')}$	$\frac{5B' - B''}{2(B' - B'')}$	$\frac{7B' - B''}{2(B' - B'')}$

The possible theoretical transitions for this type of red-degraded bands have not been worked out earlier (the CrCl bands are violet degraded). The list of theoretical transitions is given below. Each of the letters A to U represents

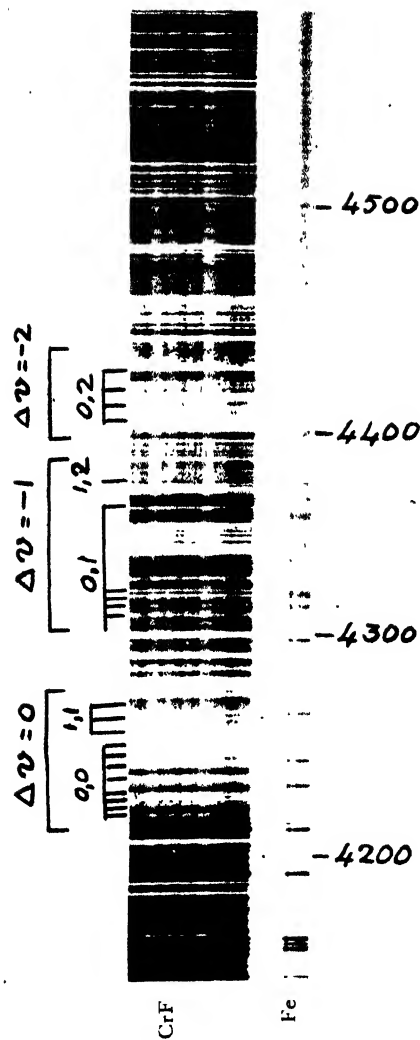


Fig. 1  
Band spectrum of CrF System I

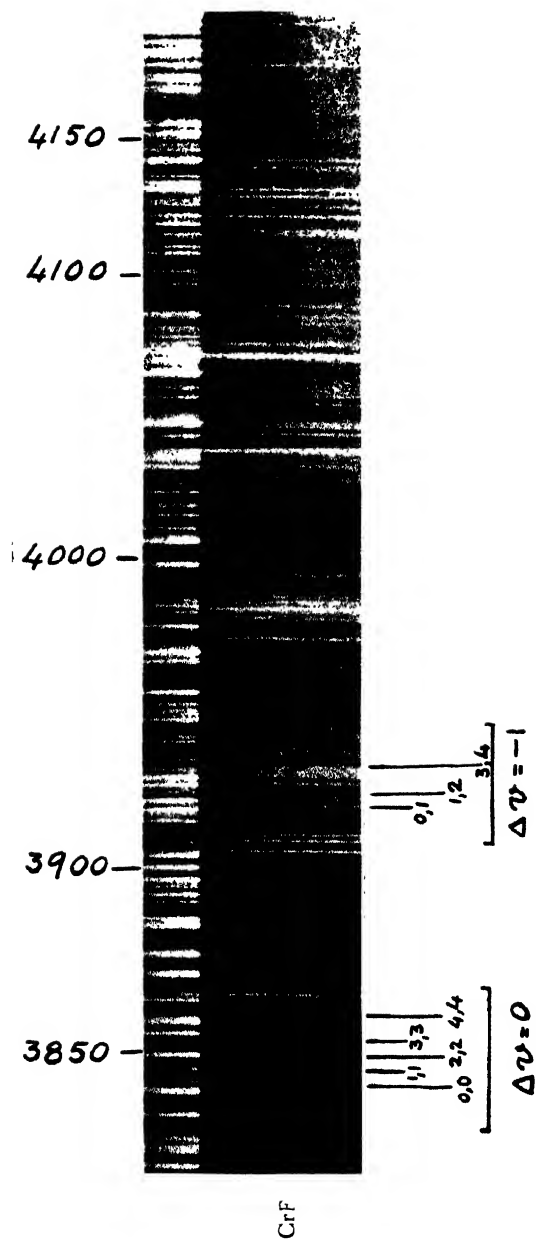


Fig. 2  
Band spectrum of  $\text{CrF}$ , system II

the various bands that are not resolved and so found as one band. Thus corresponding to each  $v' v''$  transition we can expect 21 bands, some of them being multiplet components, and the others various forms of the rotational heads. Table I gives for any particular  $v' v''$  transition the positions of the various bands in terms of the symbols A to U. A structure like this can be held responsible for the very complicated appearance of the band system. The direction of the arrow (Table II) indicates the increasing frequency.

TABLE I  
List of theoretical transitions

$\Delta J =$	1	0	-1	Symbol
	$TR_{12}$	$TQ_1$		U
	$SR_{13}$	$SQ_{12}$	$SP_1$	T
	$R_{14}$	$RQ_{13}$	$RP_{12}$	S
	$QR_{15}$	$Q_{14}$	$QP_{13}$	R
	$TR_{23}$	$TQ_2$	$TP_{21}$	Q
	$SR_{24}$	$SQ_{23}$	$SP_2$	P
	$R_{25}$	$RQ_{24}$	$RP_{22}$	O
	$QR_{26}$	$Q_{25}$	$QP_{21}$	N
	$TR_{34}$	$TQ_3$	$TP_{32}$	M
	$SR_{35}$	$SQ_{34}$	$SP_3$	L
	$R_{36}$	$RQ_{35}$	$RP_{34}$	K
		$Q_{36}$	$QP_{35}$	J
	$TR_{45}$	$TQ_4$	$TP_{43}$	I
	$SR_{46}$	$SQ_{45}$	$SP_4$	H
		$RQ_{46}$	$RP_{45}$	G
			$QP_{46}$	F
	$TR_{56}$	$TQ_5$	$TP_{54}$	E
		$SQ_{56}$	$SP_5$	D
			$RP_{56}$	C
		$TQ_6$	$TP_{65}$	B
			$SP_6$	A

TABLE II  
Multiplets

Form	$F_6$		$F_4$			$F_1$	
$T$	$\uparrow$	B	E	$\rightarrow$ I	M	Q	U
$S$		A	D	II	L	P	T
$R$		—	C	G	K	O	S
$Q$		—	—	F	J	N	R

For an analysis of this type of bands we should have an approximate idea of the lower state vibrational frequencies and the multiplet separation factors. Table III gives a collection of the  $\omega_e''$  values for allied halides.

TABLE III  
Lower state frequencies,  $\omega_e''$  in some halides of the transition group of elements.

	Ti	Cr	Mn	Fe	Co	Ni
Fluoride	—	510	612	—	—	740
Chl ride	455	292	385	405	401	416
Bromide	—	—	290	—	305	312

It would be seen that the chlorides of the various elements have their  $\omega_e''$  values ranging between  $300\text{ cm}^{-1}$  and  $450\text{ cm}^{-1}$  increasing from chromium to nickel. Similar features exist in fluorides and bromides as well, as far as they are investigated. We can therefore expect that in chromium fluoride the  $\omega_e''$  may lie in the region  $500\text{--}600\text{ cm}^{-1}$ . The multiplet separation factor ( $A$ ) in chromium chloride was found to be nearly  $46\text{ cm}^{-1}$  while in chromium bromide it was suggested that it might be about  $52\text{ cm}^{-1}$ . It is known that this  $A$  factor should decrease from a bromide to a chloride. So in chromium fluoride it might be between  $30\text{ cm}^{-1}$  and  $40\text{ cm}^{-1}$ . We expect six multiplet components in chromium fluoride corresponding to the  $^4\text{II}$  level. If the above orders of magnitude are correct then  $6 \times 35 = 210\text{ cm}^{-1}$  or a maximum of  $300\text{ cm}^{-1}$  appears to be the spread of the multiplet. This is less than the value of  $\omega_e''$  predicted earlier. So an overlap of the vibrational structure and multiplet structure need not be expected.

During our attempts of analysis the presence of strong lines in the whole region of the spectrum proved a great handicap. They appear to have obscured quite a few important bands. Besides, their presence in the immediate proximity of a band gives anomalous impressions about relative



intensities. Under the circumstances the assignments given in Table IV for System I and Table IV for System II appear to be reasonable. The features of this analysis are described below.

## SYSTEM II

In Table IV about 19 bands that could be definitely distinguished from lines are given. 8 bands could be analysed as forming two sequences ( $\Delta v = 0$  and  $-1$ ) as shown in the Deslander's scheme (Table V). The  $\Delta v = +1$  sequence was in the region below 3840 A.U. and the appearance of the bands in this region is not very definite. Hence we might conclude that the sequence is very weak in intensity and does not manifest itself. This feature seems to be shared by System I as well as will be pointed out later. The ground state differences are of the order of  $525 \text{ cm}^{-1}$  while the upper state differences

TABLE IV  
Catalogue of CrF band-heads. System II

Wavelength A.U.	Wavenumber $\text{cm}^{-1}$	Intensity	$v' v''$
3993.5	25034	1	
3987.4	25072	2	
3984.4	25091	7	
3978.8	25126	1	
3975.4	25148	2	
3969.8	25183	1	
3959.5	25249	0	
3938.5	25383	3	
3933.8	25414	6	3,4
3925.3	25469	0	1,2
3921.6	25493	5	0,1
3899.2	25639	2	
3895.8	25661	1	
3882.3	25751	1	
3876.9	25787	1	
3860.2	25898	3	4,4
3854.4	25937	2	3,3
3850.2	25965	3	2,2
3846.6	25990	2	1,1
3841.7	26023	6	0,0

TABLE V

Deslander's scheme

$v''$	0		1		2	3		4
0	26023 (5)	530	25493 (5) 497					
1			25990 (2)	521	25469 (1) 496			
2					25965 (3)			
3						25937 (2)	523	25414 (6) 484
4								25898 (3)

appear to be about  $490\text{ cm}^{-1}$ . The development of the sequences instead of progressions is a comparison to the similar case in the corresponding system in TiCl (Rao, 1949)

From the spectrogram (figure 2) it appears that  $\Delta v = -1$  sequence looks stronger than the  $\Delta v = 0$  sequence. Part of this intensity may be attributed to the strong atomic lines present in this region. Besides, no progress could be achieved with our attempts to locate at the (0,0) band in this apparently more intense group; a  $\Delta v = -1$  sequence could not be located consistent with the red-degradation of the bands ( $\omega_e' < \omega_e''$ ). The analysis presented here is the only one that satisfied all the above requirements, besides those demanded by an analysis of System I as well.

This following approximate values may be assigned to the various vibrational constants and  $\nu_e$  for this system.

$$\begin{aligned} \nu_e &= 26041\text{ cm}^{-1} & \omega_e' &= 499.9\text{ cm}^{-1} & x_e' \omega_e' &= 1.9\text{ cm}^{-1} \\ \omega_e'' &= 535.6\text{ cm}^{-1} & x_e'' \omega_e'' &= 2.78\text{ cm}^{-1} \end{aligned}$$

This simple band system may be attributed to the transition  ${}^6\Sigma \rightarrow {}^6\Sigma$ .

#### SYSTEM I

This system occurs in three groups in the region  $\lambda\lambda\ 4199\text{--}4467\text{ A.U.}$  of which the one on the short wavelength side is the strongest. As a starting point in the analysis regularities in these band groups of the order of  $35\text{ cm}^{-1}$  (as predicted earlier) have been attempted and sorted out in each of these groups. The frequency shifts vary between  $27\text{ cm}^{-1}$  and  $37\text{ cm}^{-1}$  and may be considered as the multiplet separations with a mean value of  $32\text{ cm}^{-1}$ . Connected with the above bands are also some additional bands

with frequency shifts of about  $18 \text{ cm}^{-1}$ . This may be considered as the shift between the various rotational forms of the same multiplet component. The corresponding value in CrCl varies between 5 and  $17 \text{ cm}^{-1}$  with increasing shifts from *Q* to *P*, *P* to *O* and *O* to *N* forms. If we expect in CrF a similar increasing tendency with higher forms (*Q* to *T*), we might consider the comparatively high value of  $18 \text{ cm}^{-1}$  as the separation between *S* and *T* forms. Bands with smaller separations have not been found. They are either submerged by atomic lines or not resolved.

TABLE VI  
Catalogue of CrF band-heads. System I

Wavelength A.U.	Wavenumber $\text{cm}^{-1}$	Intensity	$v' v''$	Symbol
4467.2	22379	3		
4462.7	22402	3		
4459.6	22417	2		
4455.3	22439	2		
4453.2	22450	2		
4431.1	22561	5	0,2	E
4423.1	22602	1	0,2	I
4411.3	22563	1	0,2	Q
4404.5	22698	1	0,2	U
4401.0	22716	5		
4398.5	22729	1		
4388.5	22781	1		
4379.1	22829	1		
4373.1	22861	0		
4368.5	22885	4	1,2	E
4340.3	23033	2	0,1	B
4323.0	23126	1	0,1	M
4316.0	23163	1	0,1	Q
4313.6	23176	1	0,1	T
4309.8	23196	1	0,1	U
4305.1	23222	1		
4272.2	23401	2	1,1	F
4264.0	23446	3	1,1	I
4258.2	23478	2	1,1	M
4251.6	23514	1	0,0	A
4244.6	23553	1	0,0	D
4241.5	23570	0	0,0	E
4235.3	23605	8	0,0	I
4229.6	23636	6	0,0	M
4227.4	23649	2	0,0	P
4224.3	23666	2	0,0	Q
4219.4	23693	2	0,0	U
4178.8	23810	1		

Accepting these groups and taking the differences between corresponding bands in the groups  $\lambda\lambda$  4219–4305 A.U. and  $\lambda\lambda$  4309–4373 A.U., we obtain an average shift of  $500 \text{ cm}^{-1}$ . This is of the same order of magnitude as the value we obtain for the first lower state difference in System II. Thus our expectation that both the systems must have a common lower state is justified. The first group therefore is the  $\Delta v=0$  group and the second one is the  $\Delta v=-1$  group. In the third group between

$\lambda$  4400 A.U. and  $\lambda$  4467 A.U., a few more bands could be indentified as belonging to  $\Delta v = -2$  group. Table VI contains all these bands with their assignments. For the meaning of the symbols E, I, Q, U etc. reference may be made to Table II. It would be seen from this table that only a few bands could be identified as belonging to (1,1) group in the  $\Delta v = 0$  group. Such fragmentary identifications for higher members of the sequence are not uncommon in these complex spectra. The  $\Delta v = +1$  group is not definitely observed in the spectrum. The nature of a few very weak bands in the possible region is doubtful. This feature is shared by System II as well. The upper state vibrational frequency could therefore be fixed up at about  $338 \text{ cm}^{-1}$ . This is smaller than the lower state frequency and consistent with the red-degradation of the bands. The Deslander scheme of intervals in (0,0) group is given in Table VII

TABLE VII  
Intervals in the (0,0) group

$v''$											
	$\Delta K$	${}^6\Pi$		${}^6\Pi$		${}^6\Pi$		${}^6\Pi$		${}^6\Pi$	
$v'$	T	B	39	E 17	35	I 31	M 17	30	Q	27	U
	S	A		D	H	L	P	T			
	R	—		C	G	K	O	S			
	Q	—		—	F	J	N	R			

This analysis may be considered to satisfy the requirements of the transition  ${}^6\Pi \rightarrow {}^6\Sigma$ . The coupling constant has a value of about  $35 \text{ cm}^{-1}$ , with  $\omega_e' \simeq 338 \text{ cm}^{-1}$  and  $\omega_e'' \simeq 510 \text{ cm}^{-1}$ .

#### ACKNOWLEDGMENTS

Our thanks are due to Prof. K. R. Rao, for his kind interest in the work.

#### REFERENCES

- Rao, V. R. and Rao, K. R., 1949, *Ind. J. Phys.*, **23**, 508.  
 Rao, V. R., 1949, *Curr. Sci.*, **18**, 338.  
 „ „ , 1949, *Ind. J. Phys.*, **25**, 535.

# ANALYSIS OF THE RELAXATION PERIOD OF A MULTIVIBRATOR

BY D. C. SARKAR AND RAIS AHMED

DEPARTMENT OF PHYSICS, MUSLIM UNIVERSITY, ALIGARH

(Received for publication, July 25, 1952, received after revision October 20, 1954)

**ABSTRACT.** An improved mathematical analysis of the relaxation periods of a free running symmetrical multivibrator has been made showing expressions for different electrode potentials and time periods. The theoretical values obtained have been compared with experimental data, part of which is also presented here.

## INTRODUCTION

As a result of the many common as well as specialized applications of the multivibrator circuits and their derivatives, a large number of papers have appeared on the subject in recent years. The analyses made generally pertain either to the relaxation periods (e.g. Kiebert and English, 1945) or to the switching periods between two states of passive relaxation (e.g. Williams et al, 1950; Rais Ahmed, 1950). However, it is noticed that although the voltages obtained in the relaxation period are used as boundary conditions in the switching period, it is not always possible to carry over the assumptions implicit in one analysis into the other. For example, with reference to the waveforms shown in figure 2, the maximum negative grid voltage appearing at the grid has to be computed without ignoring the positive drive of the other grid, and the voltage division between the shunting and coupling capacitances. A common relaxation analysis assuming no positive grid swing and negligible shunting capacitance will lead not only to erroneous values of the relaxation period but also to unreliable boundary conditions for the switching period, especially for high frequency multivibrators.

In the present analysis both these shortcomings of the older discussions have been removed so that the results can be safely applied to the more minute observations of the switching period.

## THE ANALYSIS

$e_0$  = positive swing of the grid voltage,

$E_{c0}$  = static cut-off grid voltage for supply potential  $E_b$ ,

$E_b$  = the plate supply potential.

$E_0$  = voltage drop across the load resistance  $R_L$  when the grid voltage of the same tube is zero with coupling condenser removed,

$E_1$  = voltage drop across  $R_L$  when the grid voltage of the same tube is  $e_c$ ,

$C_1$  and  $C_2$  are shunting capacitances from plate to cathode and grid to cathode respectively of each tube,

$e_{gm}$  = maximum negative grid voltage,

$r_p$  = plate resistance of the tube, and

$k$  = non-linearity factor of the tube characteristic.

With the notations indicated in figures 1 and 2,  $E_o$  and the current through the load resistance  $R_L$ , namely  $i_{bo}$  will be :

$$i_{bo} = \frac{E_b - K}{r_p + R_L}; \quad E_o = \left( \frac{E_b - K}{r_p + R_L} \right) R_L \quad (1)$$

The voltage  $E_1$  is greater than  $E_o$  because of the fact that a greater current  $i_{b1}$  flows through  $R_L$  when the grid of the tube is positive. The current in the tube is then

$$i_{b1} = \frac{\mu e_c + E_b - K}{r_p + R_L}$$

and

$$E_1 = \left( \frac{\mu e_c + E_b - K}{r_p + R_L} \right) R_L \quad (2)$$

where  $\mu$  stands for  $g_m r_p$ , both the latter factors having a value different from the normal value of the tube transconductance and plate resistance when taken in the region of positive grid drive. Since the difference in the value of  $\mu$  is usually not more than 15 % of the normal mean value, this difference may be ignored (when  $e_c$  is large  $\mu$  decreases sharply). The grid voltage  $e_c$  can be found from the equivalent circuit of figure 3 which represents the conditions just at the instant when the grid voltage jumps from  $-E_{o0}$  to  $e_c$ , the positive value.

At the instant  $\tau_1$  (figure 2), the tube  $V_2$  begins to conduct and  $V_1$  is suddenly cut off. Just before  $\tau_1$ ,  $V_1$  was conducting and its plate voltage was  $E_b - E_o$ , so that the condenser was charged to  $E_b - E_o$  at the plate side of the tube  $V_1$ , and to  $-E_{o0}$  at the grid side of  $V_2$ , because  $V_2$  just reaches cut-off at that instant, so that the condenser was charged to  $(E_b - E_o + E_{o0})$  volts.

From a consideration of the total driving voltage and the potential drop in the parallel combination of  $r_g$  and  $R_g$  of figure 3, we get

$$e_c = \frac{[E_b - (E_b - E_o + E_{o0})] r'_g}{R_L + r'_g}$$

where  $r_g$  = grid cathode resistance of  $V_2$  when it is conducting

$$\text{and} \quad \frac{r_g R_g}{r_g + R_g} \quad \text{or} \quad e_c = \frac{(E_o - E_{o0}) r'_g}{R_L + r'_g} \quad \dots \quad (3)$$

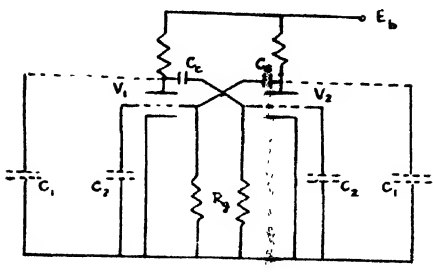


FIG. 1. A symmetrical multivibrator

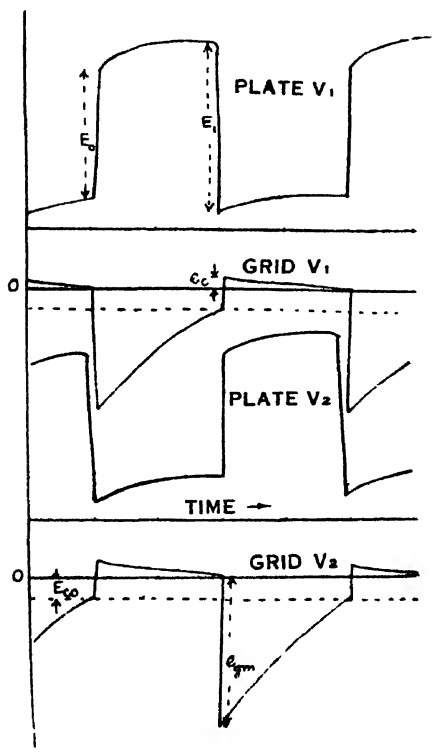


FIG. 2. The voltage waveform of a symmetrical multivibrator

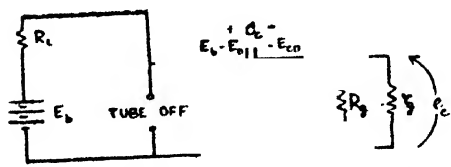


FIG. 3. Equivalent circuit for the calculation of the positive grid drive

If  $E_o$  is substituted in (3) from (1), we obtain

$$e_o = \frac{\left[ \frac{R_L(E_b - K)}{r_p + R_L} - E_{eo} \right] r'_g}{R_L + r'_g}$$

or 
$$e_o = \frac{[R_L(E_b - K) - (R_L + r_p)E_{eo}]r'_g}{(R_L + r'_g)(R_L + r_p)} \quad \dots (4)$$

On substitution of (4) in (2), we find

$$E_1 = \frac{R_L \left[ \mu \left\{ \frac{R_L(E_b - K)}{(R_L + r'_g) R_L + r_p} \right\} r'_g + E_b - K \right]}{R_L + r_p}$$

or 
$$E_1 = \frac{R_L [\mu r'_g \{ (E_b - K) R_L - (R_L + r_p) E_{eo} \} + (E_b - K) (r_p + R_L) (R_L + r'_g)]}{(R_L + r_p)^2 (R_L + r'_g)} \dots (5)$$

It is obvious that when the shunting capacitance  $C_2$  is small compared to the coupling capacitance  $C_c$ , the voltage  $E_1$  is also equal to  $e_{gm}$ . At higher frequencies, where  $C_2$  is not negligible, the maximum negative grid voltage is given by

$$e_{gm} = \frac{C_c}{C_c + C_2} E_1 \quad \dots (6)$$

The above equation will give an idea of the maximum possible frequency attainable by the multivibrator. So long as  $e_{gm} = \frac{C_c}{C_c + C_2} E_1 > E_{eo}$  the multivibrator will oscillate. When  $C_2$  is so large compared with  $C_c$  that  $e_{gm}$  is less than  $E_{eo}$ , the multivibrator will stop oscillating.

Once the maximum negative grid voltage is known accurately, the period of relaxation can be calculated from the equivalent circuit of figure 4.

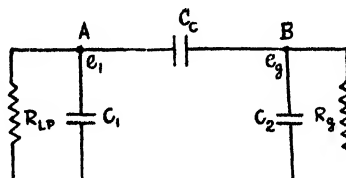


FIG. 4. Equivalent circuit for the calculation of relaxation time.

The equations for the circuit are :



$$R_{Lp} = \frac{r_p R_L}{r_p + R_L} = \frac{1}{G_1} ; \quad R_g = \frac{1}{G_2}$$

at the junction A,

$$C_e \frac{d(e_1 - e_g)}{dt} = -C_1 \frac{de_1}{dt} - \frac{e_1}{R_{Lp}} = -C_1 \frac{de_1}{dt} + \frac{e_1}{R_{Tp}}$$

or

$$C_e \frac{de_1}{dt} + C_1 \frac{de_1}{dt} + \frac{e_1}{R_{Tp}} = C_e \frac{de_g}{dt} \quad \dots (7)$$

and at the junction B,

$$C_e \frac{d(e_1 - e_g)}{dt} = C_2 \frac{de_g}{dt} + \frac{e_g}{R_g}$$

or

$$C_e \frac{de_1}{dt} = C_e \frac{de_g}{dt} + C_2 \frac{de_g}{dt} + \frac{e_g}{R_g} \quad \dots (8)$$

Denoting  $d/dt$  by  $p$ , (7) and (8) become

$$C_e p e_1 + C_1 p e_1 + e_1 G_1 = C_e p e_g$$

$$C_e p e_1 = C_e p e_g + C_2 p e_g + e_g G_2$$

or

$$(p C_e + p C_1 + G_1) e_1 - p C_e e_g = 0 \quad \dots (9)$$

$$C_e p e_1 - (p C_e + p C_2 + G_2) e_g = 0 \quad \dots (10)$$

From (9) and (10) we get  $(p C_{e1} + G_1)(p C_{e2} + G_2) - p^2 C_e^2 = 0$

where

$$C_{e1} = C_e + C_1 \text{ and } C_{e2} = C_e + C_2$$

or

$$p^2 (C_{e1} C_{e2} - C_e^2) + p (C_{e1} G_2 + C_{e2} G_1) + G_1 G_2 = 0 \quad \dots (11)$$

$$\text{so } p = \frac{-(C_{e1} G_2 + C_{e2} G_1) \pm [(C_{e1} G_2 + C_{e2} G_1)^2 - 4(C_{e1} C_{e2} - C_e^2) G_1 G_2]^{1/2}}{2(C_{e1} C_{e2} - C_e^2)}$$

The above two values of  $p$  may be denoted by  $-\alpha$  and  $-\beta$ . The grid voltage during the relaxation period may now be written as :

$$e_g = A e^{-\alpha t} + B e^{-\beta t} \quad \dots (12)$$

where  $A$  and  $B$  are the constants which are to be determined by the boundary conditions that :

$$(i) \quad e_g = e_{gm} \text{ at } t=0,$$

and

$$(ii) \quad \frac{de_g}{dt} = 0 \text{ at } t=0.$$

Thus at  $t=0$

$$e_{gm} = A + B$$

$$\frac{de_g}{dt} = 0 = A\alpha + B\beta$$

The above equations give  $A = \frac{-\beta e_{gm}}{\alpha - \beta}$ ,  $B = \frac{\alpha e_{gm}}{\alpha - \beta}$ .

After substituting the values  $A$  and  $B$  in (12), we obtain

$$e_g = \frac{e_{gm}}{\alpha - \beta} [\alpha e^{-\beta t} - \beta e^{-\alpha t}] \quad \dots (13)$$

By putting  $e_g = E_{eo}$  in this expression, the time required by the grid voltage to go from its most negative value to the tube current cut-off voltage  $E_{eo}$  can be found. In this way the relaxation time is found with positive grid drive as well as shunting capacitances taken into account.

There are two special cases of interest.

Case I. When  $C_1 = C_2 = 0$  and  $C_{e1} = C_e = C_{e2}$ , Eqn. (11) becomes

$$pC_e(G_1 + G_2) + G_1G_2 = 0$$

$$\text{or} \quad p = \frac{-G_1G_2}{(G_1 + G_2)C_e} = \frac{-1}{(R_{Lp} + R_g)C_e}$$

$$\text{or} \quad e_g = A e^{-t/(R_{Lp} + R_g)C_e}$$

In this case from (6),  $e_{gm} = E_o$ ; and at  $t = 0$ ,  $e_g = e_{gm} = E_o$ ,

$$\text{so that} \quad e_g = E_o e^{-t/(R_{Lp} + R_g)C_e}$$

$$\text{and} \quad \text{relaxation time} = \left( \frac{R_L r_p}{R_L + r_p} + R_g \right) C_e \ln \frac{E_o}{E_{eo}}$$

This is the conventional formula.

Case II. When  $C_1 = 0$ ,  $R_{Lp} = 0$ ; Eqn. (11) becomes

$$p(C_e + C_2)R_g + 1 = 0, \quad \text{or} \quad p = \frac{-1}{(C_e + C_2)R_g}$$

$$e_g = A e^{-t/(C_e + C_2)R_g}$$

$$\text{when} \quad t = 0, \quad e_g = e_{gm} = A = \frac{C_e}{C_e + C_2} E_1$$

$$\text{or} \quad e_g = \frac{C_e}{C_e + C_2} E_1 e^{-t/(C_e + C_2)R_g}$$

$$\text{In this case the relaxation time} = (C_e + C_2)R_g \ln \frac{C_e}{C_e + C_2} \cdot \frac{E_1}{E_{eo}}$$

This is the formula given by Puckles (1951).

The practical method of calculating the relaxation time is given below.

Suppose in a particular case  $C_e = 200$  mmf,  $C_1 = 50$  mmf,  $C_2 = 50$  mmf.;  $C_{e1} = C_{e2} = 250$  mmf.;  $R_L = 100 \text{ K}\Omega$ ;  $R_g = 1 \text{ M}\Omega$ ;  $r_p = 8 \text{ K}\Omega$ ;  $R_{Lp} = 7 \times 10^{-7} = 1/G_1$ ;  $e_{gm} = 96v$ . (measured);  $E_{eo} = 9.5v$ .

$$C_{e1}C_{e2} - C_e^2 = 22.5 \times 10^{-21}; \quad C_{e1}G_2 + C_{e2}G_1 = 35.96 \times 10^{-15};$$

$$\text{and } G_1G_2 = 1.43 \times 10^{-10}$$

$$\text{Equation (11) becomes } 22.5 \times 10^{-21}p^2 + 35.96 \times 10^{-15}p + 1.43 \times 10^{-10} = 0$$

$$\text{or} \quad p = \frac{-35.96 \pm 35.78}{45 \times 10^{-8}}$$

which gives  $\alpha = -4 \times 10^3$  and  $\beta = -1.594 \times 10^6$

Since  $|\alpha| \ll |\beta|$ ;  $\frac{\beta}{\alpha - \beta} e^{-\alpha t} \gg \frac{\alpha}{\alpha - \beta} e^{-\beta t}$  and  $\frac{-\beta}{\alpha - \beta} = 1$

so  $= e_{gm}^{-\alpha t} = 96e^{-4 \times 10^3 t}$ ;

$$\text{Relaxation time} = \frac{1}{4 \times 10^3} \ln \frac{96}{9.5} = 575 \text{ microseconds}$$

The time period will be twice the relaxation time and so is 1150 microseconds. An experimental value in this case was found to be 1020 microseconds.

#### EXPERIMENTAL RESULTS

A double beam Cossor oscillograph was used to measure the different electrode potentials and time periods. The measurement of time was checked by means of a standard oscillator.

TABLE I

$E_b = 110V$ ,  $R_L = 100K\Omega$ ;  $R_g = 1 M\Omega$ ; tube 6C5;  $C_1 = 0$ ;  $C_2 = 46 \text{ mmf.}$

$C_c$ in mmf	$E_0$ in volts	$E_1$ in volts	$e_{gm}$ in volts	$e_{gm}$ in volts (cal)
1000	84	94	90	90.0
500	86	94	87	86.1
250	85	94	80	79.3
100	84	94	68	64.3
50	86	94	44	48.9
25	86	94	30	33.0

By applying formula (6) in the first observation the value of  $C_2$  was found to be 46 mmf. This value of  $C_2$  was used in the calculation of  $e_{gm}$  for different values of the coupling condenser.

Equation (6) was further verified by taking a fixed value of  $C_c$  and observing the variation of  $e_{gm}$  with  $C_2$ .

TABLE II

$C_2$ in mmf.	$E_1$ in volts	$E_0$ in volts	$e_{gm}$ in volts	$e_{gm}$ calc
550	120	111	33	32.0
350	120	111	45	43.6
250	120	111	57	53.4
150	120	111	70	68.5
50	120	111	96	96.0

The constants for this set of observations were  $E_b=150$  v., tube 6C5;  $R_g=1$  megohm.,  $R_L=100\text{ K}\Omega$  and  $C_o=200$  mmf. The value of  $C_2$  inherent in the circuit was estimated from the last reading when no external shunting capacitance was used, and  $e_{gm}$  was calculated on the basis of equation (6).

TABLE III

$E_b=150$ v., tube 6C5;  $R_L=100\text{ K}\Omega$ ;  $R_g=1$  megohm.,  $r_p=8\text{ K}\Omega$ ;  $C_o=200$  mmf.  $C_1=50$  mmf. (assumed);  $\tau$  stands for time period in microseconds.

$C_2$ in mmf.	$e_{gm}$ in volts	$E_{c.}$ in volts	$\tau$ obs.	$\tau$ cal
550	33	9.5	1750	1880
350	45	9.5	1500	1620
250	57	9.5	1450	1508
150	70	9.5	1200	1280
50	96	9.5	1020	1150

TABLE IV

$E_b=130$  v.; tube 6SN7;  $R_L=20\text{ K}\Omega$ ;  $R_g=1$  megohm;  $r_p=8\text{ K}\Omega$ ;  $C_2=80$  mmf;  $C_1=50$  mmf (assumed);  $\tau/2$  measured in microseconds = relaxation period.

$C_2$ in mmf.	$E_1$ in volts	$e_{gm}$ in volts	$E_{c.}$ in volts	$\tau/2$ obs.	$\tau/2$ cal.
1000	92	85	8	2500	2510
500	92	80	8	1350	1298
250	92	68	8	550	611
100	92	56	8	340	328
50	90	37	8	130	137
25	90	21	8	70	86

TABLE V

$E_b=125$  v.; tube 6C5;  $R_g=1$  megohm;  $r'_g=1000$  ohm;  $r_p=10\text{ K}\Omega$ ;  $E_{c0}=6$  v.;  $k=15$  v.;  $C_o=500$  mmf.;  $\mu$  nearly 10.

$R_L$ in $\text{K}\Omega$	$E_0$ obs in volts	$E_0$ cal. in volts	$E_1$ obs. in volts	$E_1$ cal in volts	$e$ , obs.	$e$ , cal.
100	83	100	94	109	1.5	1.5
30	70	82	92	100	3.0	2.4
10	50	55	78	77	5.0	4.5
5	30	36	58	54	5.0	5.1
2	18	18	38	28	3.0	4.0

## CONCLUSION

It can be concluded from these tables that the set of equations derived here gives a reliable manner of calculating the relaxation period and the various electrode voltages of a multivibrator running at fairly high frequencies. These equations, therefore, can be safely taken to yield the boundary conditions for an accurate determination of the switching periods in a multivibrator.

## ACKNOWLEDGMENTS

The authors are very grateful to Dr. H. Rakshit for his going through the manuscript and making valuable suggestions. They are also thankful to Professor P. S. Gill for given facilities for this work in the Department of Physics.

## REFERENCES

- Ahmed, Rais 1950, *Ind. Jour. Phys.*, **24**, 281.  
Kiebert, M. V., and Inglis A. F., 1945, *Proc I R E*, **33**, 534.  
M. I. T. Staff 1946, *Principles of Radar*, McGraw Hill  
Puckle, O. S., 1951, *Time Bases*, Chapman and Hall  
Williams, E. M., Aldrich, D. F., and Woodford, J. B., 1950, *Proc. I. E. E.*, **38**, 65.



# ON DEPENDENCE OF RESOLVING POWER OF FABRY-PÉROT ETALON, LUMMER-GEHRCKE PLATE AND TRANSMISSION ECHELON ON STAGE OF RESOLUTION\*

By SHASHANKA SHEKHAR MITRA  
DEPARTMENT OF PHYSICS, ALLAHABAD UNIVERSITY, ALLAHABAD

(Received for publication, July 31, 1954)

**ABSTRACT.** The dependence of the resolving power on the stage of resolution desired and the detecting instrument available has been studied for the case of Fabry-Perot etalon, Lummer-Gehrcke plate and transmission echelon including the absorption by the material of the last two instruments. Tables and graphs have been given to show the dependence.

## INTRODUCTION

Ditchburn (1930) has pointed out that the value of  $I_{\min.}/I_{\max.}$  ( $=c$ ) of a spectral pattern at limiting resolution chosen for the calculation of resolving power of an optical instrument decides the stage of resolution desired by a detecting instrument. Using a microphotometer he was able to distinguish between three important stages of resolution :

Stage of resolution	$c = I_{\min.}/I_{\max.}$
(i) Detection of inhomogeneity in radiation	0.98
(ii) Approximate measurement of wavelength and relative intensities	0.8
(iii) Accurate measurement of wavelength and relative intensities	0.4

Sharma and Sodha (1954) have studied the variation of resolving power of grating, prism and reflecting echelon with  $c$ , which is characteristic of the stage of the resolution desired and the detecting instrument used. This paper presents a similar study for Fabry-Perot etalon, Lummer-Gehrcke plate and transmission echelon.

## FABRY-PÉROT ETALON

The intensity pattern in Fabry-Perot etalon is given by

$$I_1 = \frac{I_0}{1 + F \sin^2 \pi (n_0 + n)} = \frac{I_0}{1 + X^2}$$

where,  $F$  is the coefficient of fineness,  $n_0 + n$  is the order,  $n_0$  being an integer and  $n$  a fraction and  $X = \pi n F^{\frac{1}{2}}$ .

The intensity pattern of another line separated by a small order  $\Delta n$  is given by

\* Communicated by Dr. K. Majumdar

$$I_0 = \frac{I_a}{1 + F \sin^2 \pi(n_0 + n - \Delta n)} = \frac{I_a}{1 + (X - a)^2}$$

where  $a = \pi \Delta n F^{1/2}$ . The resultant intensity pattern is given by

$$I = I_1 + I_2 = I_0 \left\{ \frac{1}{1 + X^2} + \frac{1}{1 + (X - a)^2} \right\} \quad \dots (1)$$

The maxima ( $X \approx 0$  or  $a$ ) and minimum ( $X = a/2$ ) of the resultant intensity pattern are given by

$$\frac{I_{\max}}{I_0} = 1 + \frac{1}{1 + a^2} = \frac{2 + a^2}{1 + a^2} \quad \dots (2)$$

and

$$\frac{I_{\min}}{I_0} = \frac{2}{1 + a^2/4} = \frac{8}{4 + a^2} \quad \dots (3)$$

Putting the criterion

$$I_{\min}/I_{\max} = c \quad \dots (4)$$

for limiting resolution we get,

$$8(1 + a^2) = c(4 + a^2)(2 + a^2) \quad \dots (5)$$

Considering only the positive root of the above equation one gets

$$a = \left\{ \frac{(4 - 3c) + \sqrt{(4 - 3c)^2 + 8c(1 - c)}}{c} \right\}^{1/2} \quad \dots (6)$$

The resolving power is given by :

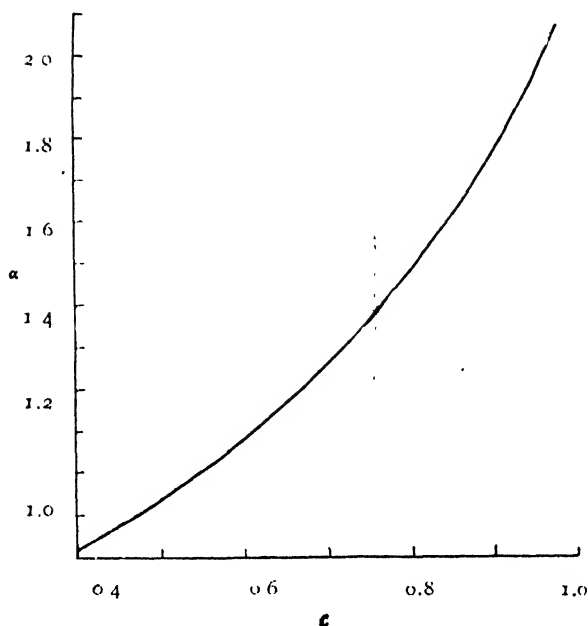
$$\frac{\lambda}{d\lambda} = \frac{n_0}{\Delta n} = \frac{\pi}{a} n_0 F^{1/2} = \alpha n_0 F^{1/2} \quad \dots (7)$$

Table I and figure 1 illustrate the variation of  $\alpha$  with  $c$ . The values of  $\alpha$  for  $c = .8$  and  $.981$  corresponding to Rayleigh and Abbe criteria are the same as given by Meissner (1941) and Sodha (1953a).

TABLE I

$c$	$a^2$	$\alpha$
.40	14.815	.816
.45	12.556	.887
.50	10.745	.958
.55	9.253	1.033
.60	7.999	1.111
.65	6.929	1.193
.70	6.000	1.282
.75	5.182	1.380
.80	4.449	1.490
.85	3.785	1.614
.90	3.169	1.764
.95	2.584	1.954
.981	2.260	2.085




 FIG. 1. Dependence of  $\alpha$  on  $C$ 

## LUMMER-GEHRCKE PLATE

The expression for intensity of an emerging beam system of a Lummer-Gehrcke plate is given by (Gehrcke, 1906 and Candler, 1951).

$$I = I_0 \frac{\{(1 - R^N)^2 + 4R^N \sin^2 N\varphi/2\}(1 - R)}{(1 - R)^2 + 4R \sin^2 \varphi/2} \quad \dots (8)$$

symbols having their usual meanings. Putting  $F = 4R/(1 - R)^2$  and  $F_N = 4R^N/(1 - R^N)^2$ , equation (8) is simplified to

$$\frac{I}{I_0} = \frac{(1 - R^N)^2}{(1 - R)} \cdot \frac{1 + F_N \sin^2 N\varphi/2}{1 + F \sin^2 \varphi/2} \quad \dots (8a)$$

The intensity  $I_c$  at the centre of the fringe ( $\varphi = 0$ ) is given by

$$I_c = I_0 \frac{(1 - R^N)^2}{1 - R} \quad \dots (9)$$

If  $I_1$  and  $I_2$  represent the intensities at  $\varphi$  and  $2\varphi$  then the ratio  $I_{\min.}/I_{\max.}$  is given by

$$I_{\min.}/I_{\max.} = \frac{2I_1}{I_c + I_2} \quad \dots (10)$$

Combining equations (10), (9), (8a) and (4) we get

$$1 + \frac{1 + F_N \sin^2 N\varphi}{1 + F \sin^2 \varphi} = \frac{2}{c} \cdot \frac{1 + F_N \sin^2 N\varphi/2}{1 + F \sin^2 \varphi/2}$$

or

$$c = \frac{2(1 + F_N \sin^2 N\varphi/2)(1 + F \sin^2 \varphi)}{(1 + F \sin^2 \varphi/2)(2 + F_N \sin^2 N\varphi + F \sin^2 \varphi)} \quad \dots (11)$$

This equation may be solved by giving particular values to  $R$  and  $N$  and the general solution can be written as

$$\varphi = \frac{\pi}{N_e} \quad \dots (12)$$

$N_e$  being the effective number of beams.

The resolving power is given by the expression (Williams, 1950):

$$\frac{\lambda}{d\lambda} = N_e \left( n - \frac{2t}{\cos \tau} \frac{d\mu}{d\lambda} \right) \quad \dots (13)$$

Tables II and III record the values of  $c$  for different values of  $N_e$ , for a particular  $N$  value ( $=50$ ), for  $R=.9$  and  $.8$  respectively. When  $N=50$ ,  $R=.9$ , the value of  $F_N=.021$  and  $F=360$  and when  $R=.8$ ,  $F_N=.0001$  and  $F=80$ .

TABLE II

$R=.9, N=50$

$N_e$	40	35	30	25	20	15	10
$\varphi$	$4^\circ 30'$	$5^\circ 8' 34''$	$6^\circ$	$7^\circ 12'$	$9^\circ$	$12^\circ$	$18^\circ$
$c$	.9961	.9315	.8392	.7188	.5693	.3880	.2025

TABLE III

$R=.8, N=50$

$N_e$	20	18	15	12	10	8	5
$\varphi$	$9^\circ$	$10^\circ$	$12^\circ$	$15^\circ$	$18^\circ$	$22^\circ 30'$	$36^\circ$
$c$	1.0	.9623	.8718	.7313	.6063	.4583	.3237

In figure 2-  $N_e$  has been plotted against  $c$ , similar other graphs and tables can be prepared for different  $N$  and  $R$  values.

Considering the absorption by the material of the Lummer-Gehrcke plate the intensity expression becomes (Sodha, 1952)

$$I = I_0 \frac{[\{1 - (RM)^N\}^2 + 4(RM)^N \sin^2 N\varphi/2](1 - RM)}{(1 - RM)^2 + 4RM \sin^2 \varphi/2} \quad (14)$$

where  $M = e^{-k/l \sec r}$ ,  $k$  being intensity absorption coefficient. In Sodha's original note there was no  $(1 - RM)$  term in the numerator since he neglected the initial reflection. This expression differs from (8) only in having  $(RM)$  instead of  $R$  and hence assigning particular values also for  $M$ ,  $N$ - $c$  graphs can be drawn.

#### TRANSMISSION ECHOLON

The expression for intensity in case of the Michelson echelon is given by (Sodha, 1953b)

$$I = I_0 \frac{(1 - M^N)^2 + 4M^N \sin^2 N\varphi/2}{(1 - M)^2 + 4M \sin^2 \varphi/2} \quad (15)$$

The expression (15) differs from (8) only in having  $M$  instead of  $R$ , hence Tables II and III and figure 2 may be used in this case also by replacing  $R$  by  $M$ .

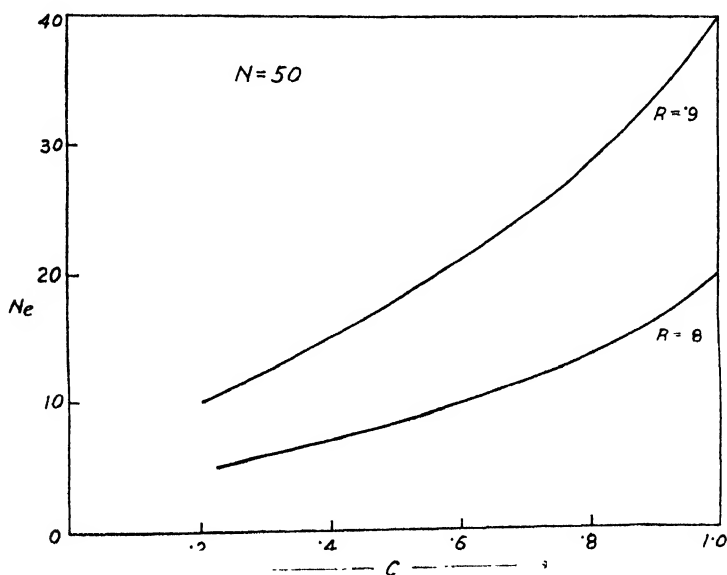


FIG. 2. Dependence of  $N$ , on  $c$

#### ACKNOWLEDGMENT

The author is grateful to Dr. K. Majumdar for his guidance in the work. He also thanks Dr. D. Sharma and Mr. M.S. Sodha for helpful discussions.

## REFERENCES

- Candler, 1951, *Modern Interferometers*, Hilger and Watts, p. 335  
Ditchburn, 1930, *Proc. Roy. Irish Acad. Sci.*, **39**, 58  
Gehrcke, 1906, *Interferenzen*, 39.  
Meissner, 1941, *Jour. Opt. Soc. Amer.*, **31**, 401  
Sharma, O. P., and Sodha, M.S., 1954, *Ind. J. Phys.* **23**, 437.  
Sodha, M.S., 1952, *J. Sci. Ind. Res.*, **11B**, 395  
Sodha, M.S., 1953a, *Curr. Sci.*, **22**, 139  
Sodha, M.S., 1953b, *Sci. and Cult.*, **18**, 480.  
Williams, 1950, *Applications of Interferometry* (Methuen, London) p 98-99

# THE BAND SPECTRUM OF TELLURIUM IN THE VISIBLE

By N. DURGA PRASAD AND P. TIRUVENGANNA RAO

PHYSICS DEPARTMENT, ANDHRA UNIVERSITY, WALT AIR

(Received for publication, August, 16, 1954)

Plates XXA-B

**ABSTRACT.** The band spectrum of tellurium in the visible region was reinvestigated. The well-resolved fluctuation bands, analysed by Desirant and Minne (1936) into two separate systems have been found to belong to the principal system. The following vibrational constants were derived for the principal system.

$$\omega_e'' = 251.0 \quad x_e'' \omega_e'' = 0.56$$

$$\nu_e = 22709$$

$$\omega_e' = 163.0 \quad x_e' \omega_e' = 0.96$$

The analysis is confirmed from considerations of isotope effect.

## INTRODUCTION

Preliminary investigations on the molecular spectra of sixth group elements, sulphur, selenium and tellurium were confined to fluorescence and absorption. Rosen (1927) was the first to propose the vibrational analyses for the spectra of these molecules, studied by him in resonance, fluorescence and absorption. Each one of these was found to give rise to an extensive system described as the principal system.

Of these three molecules the spectrum of selenium was most extensively studied. In the near ultraviolet and visible regions, this spectrum was found to consist of a large number of bands obtained both in emission and in absorption. Prior to 1937, these bands have been arranged into seven different systems. The system of fluctuations extending from  $\lambda 4900 - \lambda 5950$ , according to Rosen and Montfort (1936) is represented by the formula

$$\nu = 19891 + 50n' - 0.1n'^2 - 362n'' + 1.8n''^2 \quad \dots (1)$$

A definite advance of our knowledge of the spectrum of selenium was made by Asundi and Parti (1937) who arranged these bands into two separate systems. All the bands except those found in absorption by Moraczewska (1930) and by Rosen and Montfort (1936) in emission were arranged into one single system. The system of fluctuations of Rosen and Montfort is included as a part of this system, which is analogous to the extensive main system of sulphur. Thus according to him only two systems of  $\text{Se}_2$  exist; one; the principal system observed in emission and absorption and the other, the new emission system of Rosen and Montfort ( $\lambda 6000 - \lambda 6600$ ).

Rosen, in 1939, reinvestigated the spectrum of selenium in emission, absorption and fluorescence and taking into account of the selenium isotope effect found that the well-resolved bands in the fluctuation groups ( $\lambda 5250$ – $\lambda 5900$ ) could be assigned to  $v''$  ground state progressions (with  $v'=7, 8, 9$ , and  $10$ ) of the main system. He, however, maintained that the unresolved patches in the fluctuation groups arise in a different electronic transition.

The spectrum of tellurium bears a striking resemblance to that of selenium but was not so extensively studied. The spectrum, as reported by Rosen and others, in fluorescence and absorption consists of bands extending from  $\lambda 3800$ – $\lambda 5660$  comprising of one single system and is represented by the formula

$$v = 22714 + 164 (v' + \frac{1}{2}) - 1.0 (v' + \frac{1}{2})^2 - 251 (v'' + \frac{1}{2}) + 0.53 (v'' + \frac{1}{2})^2 \quad \dots (2)$$

Some broad diffuse bands were recorded on the red side of  $\lambda 5660$ , in fluorescence and in absorption (at higher temperatures) and were found to be resolved into fine narrow bands under higher dispersion instruments.

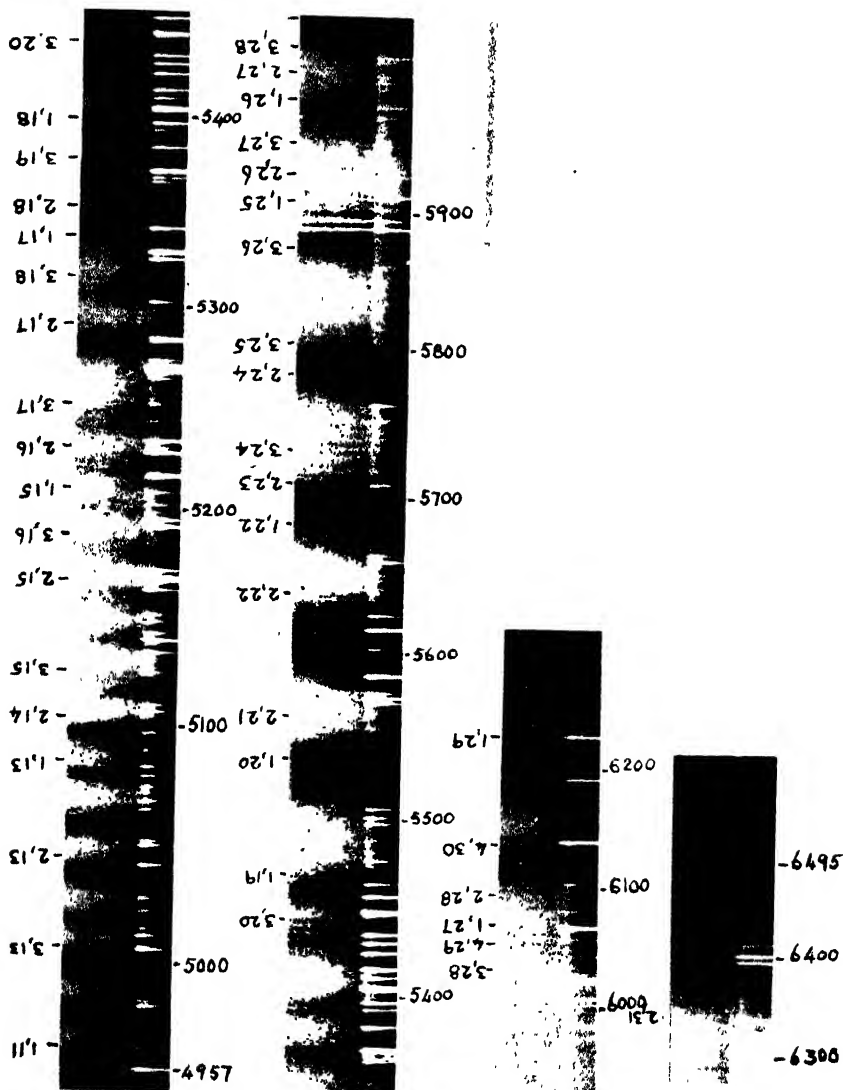
Olsson (1935) in an investigation of the emission spectrum of tellurium in the region  $\lambda 3900$ – $\lambda 4900$  in an ordinary electric discharge found that the diffuse bands occurring on the violet side of the system were well resolved into fine components under a dispersion of  $1\text{A/mm}$ . This well resolved structure has been attributed by him as due to the tellurium isotope effect. A detailed study of the isotope effect for 1 of the bands ( $\lambda 3900$ – $\lambda 4150$ ) has resulted in a change of the vibrational numbering of the bands. According to him the following vibrational formula represents the band system

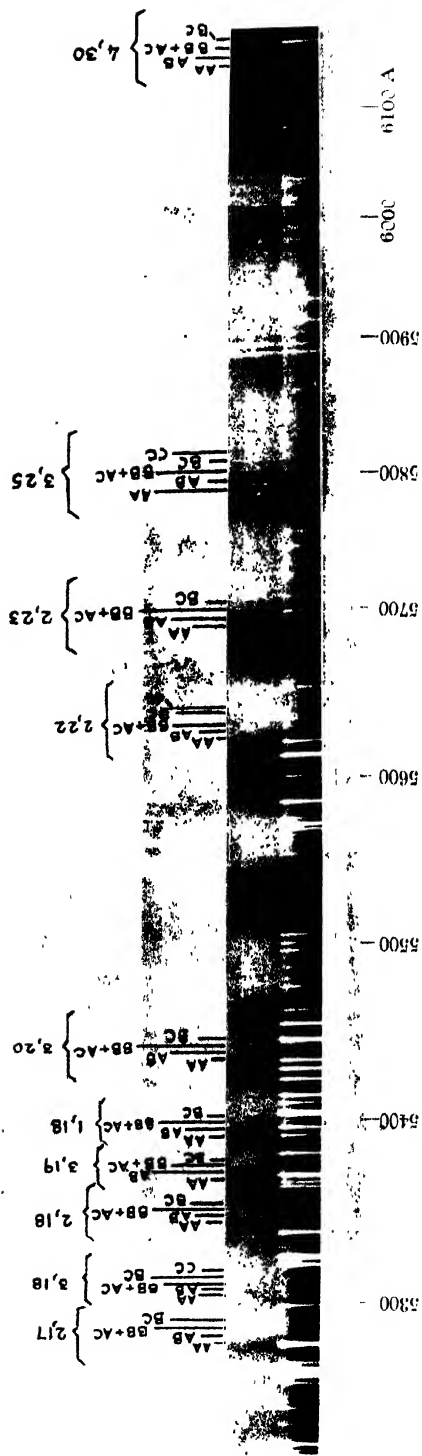
$$v = 22189 + 169.2(v' + \frac{1}{2}) - 0.92(v' + \frac{1}{2})^2 - 251.5(v'' + \frac{1}{2}) + 1.0 (v'' + \frac{1}{2})^2 \quad \dots (3)$$

Thus two formulæ are in vogue for the main system of tellurium. R. Migeotte (1942) from a study of resonance and isotope series of the bands redetermined the anharmonic constant  $x_e''\omega_e''$  to be  $0.55 \pm 0.05$  and concluded that the older formula (2) given by Rosen gives a better representation of the bands of the system.

The spectrum of tellurium in the visible region was reinvestigated by Desirant and Minne (1936) in a high frequency discharge through tellurium vapour under a dispersion of  $10\text{A/mm}$  at  $\lambda 5700$ . The fluctuation groups of bands beyond  $\lambda 5250$ , which are very similar to those observed in selenium, were found to be well resolved by them. On the analogy of the interpretation of the fluctuation bands in selenium given by Rosen and Montfort these authors have ascribed these bands as belonging to two separate systems. The lower state of these two systems, as in selenium, is common and the same as the ground state of the molecule and the upper state frequencies were of the order of  $25\text{ cm}^{-1}$  and  $20\text{ cm}^{-1}$ . But as has already been mentioned, the well resolved fluctuation bands in selenium have been found to belong to the main system by Asundi and Parti and later also by Rosen with a different analysis (1933). In the light of this recent interpretation of the

Band spectrum of tellurium





Isotope effect in tellurium



resolved fluctuation bands in selenium, it is thought desirable to reinvestigate the spectrum of tellurium in emission in the visible region. The results obtained by the authors in this reinvestigation are described in the present paper.

#### EXPERIMENTAL

The spectrum was excited by a high power oscillator (100 watts) employing a Hartley series feed circuit. The discharge tube was made of pyrex glass and the substance, a pure E.D.H. sample, was spread in the tube. Intermittent heating of the tube by an Etna burner was found necessary to maintain the discharge. The colour of the discharge was bluish white and was maintained throughout the experiment.

Using Special Rapid Panchromatic plates, exposures varying from 15 to 45 minutes were found necessary on the glass Littrow instrument. For work in the extreme red, the plates were sensitized with 1:5000 stock solution Rubrocyanine. The exposures on the sensitized plates could be reduced to 20 to 30 minutes duration, owing to the general increase in sensitivity of the plate.

#### DESCRIPTION OF PLATES

Plate XXA shown in strips *a*, *b*, *c* and *d* gives the appearance of the  $\text{Te}_2$  spectrum in the region  $\lambda 4900$ – $\lambda 6400$ . The classification of some of the bands of the principal system is shown. Plate XXB gives the detailed isotopic classification of some of the bands from  $\lambda 5300$  where the resolution is suitable for measurement.

#### VIBRATIONAL ANALYSIS

In attempting the vibrational analysis of the bands from  $\lambda 4900$ – $6400$ , we have at the outset compared our band head data with those of the absorption data given by Rosen. A comparison of these wavenumber data shown in the first and the fourth columns of Table I clearly shows that the emission bands are identical with those observed in absorption. Each band measured by Rosen under low dispersion appears now well resolved under high dispersion of the three-prism glass Littrow. Further a comparison of data shown in columns (3) and (4) shows that the resolved fluctuation bands reported by Desirant and Minne are identical with the emission bands obtained in the present work. On the analogy of the interpretation given by Rosen and Montfort for similar bands in selenium, these emission bands between  $\lambda 5250$  and  $\lambda 6400$  have been interpreted by Desirant and Minne as arising due to the transitions between the vibrational levels of two different quasi-stable excited states (situated very near the upper state of the main system) and the high vibrational levels of the ground state. Consequently, these bands were arranged by them into two systems with  $\nu_{0,0} = 18900$  and

$16370\text{ cm}^{-1}$ , where the lower level  $n''=0$  corresponds to a high vibrational level  $v''$  (in between 12 and 15 for system *A* and in between 15 and 20 for system *B*) of the ground state. The vibrational frequencies of the upper state were of the order of  $25\text{ cm}^{-1}$  and  $20\text{ cm}^{-1}$ . Such an analysis is contradicted here and all the bands between  $\lambda_{4900}-\lambda_{6350}$  are regarded as belonging to the principal system from the following considerations.

(1) The resolved fluctuation bands observed in the spectrum of selenium have been first interpreted by Asundi and Parti as belonging to the main system, in contradiction to the analysis proposed by Rosen and Montfort (1936) on the basis of an independent system. The explanation of these resolved bands in the fluctuation groups as a part of the main system was later maintained by Rosen (1939) with a different analysis). The interpretation of the fluctuation bands in  $\text{Te}_2$  should also be similar.

(2) These bands are observed in absorption at high temperatures by Rosen, Desirant and Nevin (1939) which indicates definitely that higher vibrational levels of the ground state are involved in the system. Moreover, Rosen has arranged these absorption bands between  $\lambda_{4900}-\lambda_{5660}$  into the main system.

(3) In their vibrational analysis of the fluctuation bands, Desirant and Minne have not taken into account the tellurium isotope effect, which would certainly be noticeable, if  $\omega_e'$  and  $\omega_e''$  are of the order of  $25\text{ cm}^{-1}$  and  $251\text{ cm}^{-1}$  and if  $v''$  also takes large values (15 to 20). Consequently, the view that the bands belong to two independent systems, as reported by these authors, has to be abandoned.

(4) The separations between successive members in each group increases from  $\lambda_{5000}$  to higher wavelengths which is to be expected as is shown later, from considerations of isotope effect, if the bands belong to the main system. These are as follows.

As has already been mentioned two formulæ (2) and (3) are in vogue for the bands of the main system. Migeotte (1942) from a study of resonance and isotope series has determined accurately the value of the anharmonic constant  $x_e'' \omega_e''$  to be  $0.55 \pm 0.05$  in contrast to 1.0 as obtained by Olsson and concluded that Rosen's formula gives a correct representation of the bands. Moreover, the anharmonic constant  $x_e'' \omega_e''$  as determined by him is in keeping with the values for the related molecules sulphur and selenium. These are :

Sulphur  $2.75\text{ cm}^{-1}$

Selenium  $1.06\text{ cm}^{-1}$

Tellurium  $0.55\text{ cm}^{-1}$

The above considerations have led the authors to adopt the vibrational scheme as given by Rosen. In the scheme proposed in Table III the band head data from  $\lambda_{3900}-\lambda_{4900}$  are taken from Olsson's measurements because of the higher dispersion used by him. From  $\lambda_{4900}$  Rosen's data were

TABLE I

Rosen		Desirant and Minne, Emission	Author, Emission	Calculated $\nu$	Assignment
Absorption	Fluorescence				
20545	20534		20544 20536 20530	20537	2,10
20454	20456		20470 20464 20456 20450 20443	20455	3,11
20379	20378		20384 20379 20373	20378	1,10
20300	20300		20309 20302 20295	20298	2,11
20223	20221		20234 20226 20215	20218	3,12
20148	20140		20158 20148 20140 20133	20130	1,11
20058	20061		20073 20063 20056 20050	20061	2,12
19973	19987		19999 19989 19981 19973 19964 19958 19938	19982	3,13
19918	19905		19916 19908 19899 19893 19879	19901	1,12
19812	19826		19845 19837 19828 19818 19810	19824	2,13
19760	19749		19760 19752 19745 19732	19746	3,14

TABLE I (contd.)

Rosen		Desirant and Minne, Emission	Author, Emission	Calculated ν	Assignment
Absorption	Fluorescence				
19682	19666		19688 19578 19663 19646 19631	19665	1,13
19588	19590		19606 19596 19586 19578 19569*	19589	2,14
19510	19505		19539 19529 19518 19507 19495*	19511	3,15
19430	19428		19453 19446* 19436 19427	19430	1,14
19355	19360		19370 19349 19339* 19329*	19355	2,15
19277	19281		19297 19290 19279 19270 19260	19279	3,16
19178			19235 19223 19213 19201 19188	19195	1,15
19121	19121		19153 19143 19128 19122* 19105 19194	19121	2,16
19041	19041		19080 19066 19056 19044 1,032	19047	3,17
		19017	19024 19012		

TABLE I (contd.)

Rosen		Desirant and Minne, Emission	Author, Emission	Calculated ν	Assignment	
Absorption	Fluorescence					
18965	18907	19002	18996	18962	1,16	
		18988	18986			
			18976			
		18967	18965			
18892			18949		18890	2,17
			18949			
			18939			
			18908			
18787			18831	18818	18816	3,18
			18820	18825		
			18794	18813		
			18794	18801		
18749			18775	18788	18730	1,17
			18775	18775		
			18765	18765*		
			18746	18745		
18651			18733	18732	18659	2,18
			18720	18719		
			18706	18706		
			18692	18693		
18584			18677	18680	18585	3,19
				18666		
				18632		
				18620		
18512				18606	18500	1,18
				18593		
				18581		
			18561	18553		
18422			18551	18538	18358	3,20
			18537	18525		
			18522	18512		
			18509	18497		
18362			18501		18270	1,10
				18431*		
				18409*		
				18395		
18251				18380		
				18366		
			18344	18352		
			18330	18335		
				18325*		
			18318			
			18303	18312*		
			18292	18298		
			18277	18284*		
				18270		
			18262	18257		

TABLE I (contd.)

Rosen		Desirant and Minne, Emission	Author, Emission	Calculated "	Assignment
Absorption	Fluorescence				
18215		18230	18244* 18229* 18220*	18200	2,20
		18211			
		18105			
		18181			
		18165			
		18149			
18121			18116	18041	1,20
			18102		
			18089		
		18077	18070		
		18060	18058		
		18043	18044		
			18028		
		18013	18019*		
		18007	18003		
		17977	17978		
		17961	17962	17973	2,21
17889			17932		
17806		17834			
		17814	17811		
		17795	17796		
		17779	17780		
17759		17761	17767		
		17745	17751		
		17731	17735	17747	2,22
		17713	17716		
		17696	17701		
			17686		
			17678		
17649			17606	17587	1,22
			17587		
			17573		
			17556		
		17538	17541		
	17528	17523	17525		
	17504	17505	17507		
	17482	17489	17490		
			17472		
	17460	17460	17461		
	17442		17442	17454	3,24
	17420		17424		
	17408		17405		
			17392*		
			17377*		
			17333*		
		17322	17322		
		17304	17302		
		17284	17284	17297	2,24
		17254	17255		
		17240	17238		

TABLE I (contd.)

Rosen		Desirant and Minne, Emission	Author, Emission	Calculated ν	Assignment
Absorption	Fluorescence				
		17222	17221	17231	3,25
		17204	17202		
		17194	17184		
		17176	17174		
		17146	17155		
		17130	17134	17138	1,24
			17118		
			17098*		
			17056*		
		17041	17037*		
		17021	17017	17010	3,26
		16999	16998		
		16985	16981*		
	16976	16960			
	16959	16937	16936		
	16938	16915	16919	16915	1,25
	16916	16896	16899		
		16870	16874		
		16851	16854	16852	2,26
		16825	16835		
			16815		
			16792*	16789	3,27
		16777	16776		
		16757	16755		
		16739	16735		
		16714	16713		
		16690	16691	16693	1,26
		16671	16673		
		16646	16654		
			16640	16632	2,27
		16621	16622		
			16617?		
		16600	16596		
		16576	16576	16568	3,28
		16553	16556		
		16530	16533		
		16509	16511	16506	4,29
		16490	16492		
		16472	16476	16472	1,27
		16451	16453		
		16428	16433		
		16414	16418	16412	2,28
			16396		
			16376*		
		16358			
		16335	16339		
		16316	16318		
		16295	16298	16288	4,30
		16276	16276		
		16255	16257		
		16176	16182		
		16159	16159		
		16133	16142*	16133	3,30
		16119	16123*		
		16097	16099		
		16082	16089		

TABLE I (contd.)

Rosen		Desirant and Minne, Emission	Author, Emission	Calculated ν	Assignment
Absorption	Fluorescence				
		16060 16043	16064 16046 16025 16003	16034	1,29
		15932 15918 15897 15864 15842	15968 15941 15929 15909 15887 15864* 15851* 15829	15917	3,31
		15800 15783 15763 15745 15722	15795 15774 15755 15732*  15697 15673 15638 15614	15817  15760	1,30  2,31

\* Bands not clear, hence measurement uncertain.

TABLE II

Assignment	ν	Isotope separation		Interpretation
		observed	calculated	
(2,17)	18919	11		AA
	18908	12	13.5	AB
	18896		14.3	BB+AC
	18884	12	14.6	BC
(3,18)	18838			AA
	18825	13	13.7	AB
	18813	12	14.5	BB+AC
	18801	13	14.9	BC
	18788	13	14.5	CC
	18775			?
(2,18)	18706			AA
	18693	13	14.3	AB
	18680	13	15.1	BB+AC
	18666	14	15.5	BC



TABLE II (contd.)

Assignment	$\nu$	Isotope separation		Interpretation.
		observed	calculated	
(3,19)	18625	14	14.5	AA
	18606	14	15.3	AB
	18593	12	15.7	BB+AC
	18581			BC
(1,18)	18538	13	14.9	AA
	18525	13	15.7	AB
	18512	15	16.1	BB+AC
	18497			BC
(3,21)	18395	15	15.3	AA
	18380	14	16.1	AB
	18366	14	16.5	BB+AC
	18352	17	16.1	BC
	18335			CC
(2,22)	17767	16	17.3	AA
	17751	16	18.3	AB
	17735	19	18.7	BB+AC
	17716	15	18.3	BC
	17701			CC
(2,23)	17541	16	18.1	AA
	17525	18	19.0	AB
	17507	17	19.5	BB+AC
	17490			BC
(3,25)	17255	17	19.0	AA
	17238	17	20.0	AB
	17221	19	20.5	BB+AC
	17202	18	20.0	BC
	17184			CC
(4,30)	16339	21	21.9	AA
	16318	20	23.1	AB
	16298	22	23.7	BB+AC
	16276	19	23.1	BC
	16257			CC

replaced by the band head measurements of the authors, each band observed by Rosen being well resolved into isotopic components under the high dispersion employed. The assignment in Table III refers to the most abundant molecule ( $BB+AC$ ) i.e.  $\text{Te}^{128} \text{Te}^{127} + \text{Te}^{130} \text{Te}^{126}$ . The scheme could be extended above  $\lambda 5660$  to include all the bands upto  $\lambda 6400$ . All the bands observed by Desirant and Minne have been interpreted as forming part of this system. As indicated in Table III, the  $v''$  progressions with  $v' = 1, 2$  and  $3$  are extended upto high values of  $v''$  (about  $30$ ). The peculiarities of the appearance of the fluctuation groups from about  $\lambda 5500$  exhibited in Plate XXA is due to the overlapping of the progressions with  $v' = 1, 2$  and  $3$ . The classification of some of the bands is shown in Plate XXA. The  $\Delta G(v)$  differences shown in the scheme were believed to be more accurate than those obtained by Rosen. The following vibrational constants were deduced by drawing the usual  $\Delta G(v) - v$  curves. (figure 1).

$$\begin{aligned} \omega_e' &= 163.0 & x_e' \omega_e' &= 0.96 \\ \nu_e &= 22709 \\ \omega_e'' &= 251.0 & x_e'' \omega_e'' &= 0.56 \end{aligned}$$

#### ISOTOPE EFFECT

Further confirmation of the analysis has been obtained by an extensive study of the tellurium isotope effect. As is well known, tellurium has several isotopes which, following Olsson, may be designated as  $A, B, C, D, E, F$

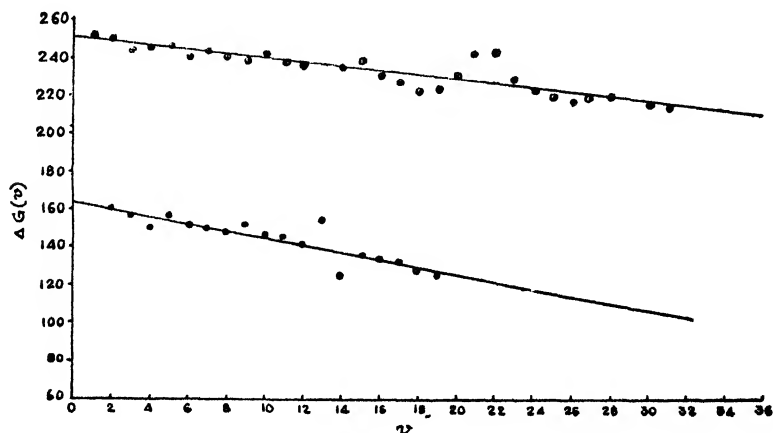


FIG. 1  
 $\Delta G(v)$  vs.  $v$  curves

and  $G$ . The masses of the various isotopes and their relative abundance ratios are given in Olsson's paper (1935). Reference can also be made to this paper for a determination of  $\rho$  factors and the percentage abundance

v' \

$\Delta G(v')$

	22839 155		160.0
	22994 145		155.4
	23139 143	259 22 14	150.0
	23282 158	251 230 15	155.5
	23440 149	258 231 15	150.5
	23589 147	256 233 15	150.0
	23736 148.6	2 234 14	147.2
	23884.6 149.4	251.6 231 14	151.3
	24034.0 145.8	247.9 231 14	145.5
	24179.8 144.4	248.6 231 14	144.7
	24324.2 142.0	248.0 241 14	141.3
12	24466.2 154.0	249.2 241 14	153.9
13	24620.2 124.1	249.7 241 14	124.1
14	24741.3 135.1		135.1
15	24879.4 133.7		133.7
16	25013.1 130.9		130.9
17	25144.0 126.9		126.9
18	25270.9 124.6		124.6
19	25395.5		$\Delta G(v')$

$\Delta G(v'')$

$\Delta G(v'')$



for the various molecules formed from different combinations namely  $AA, AB, BB, AC, \dots$ . Out of these only five heads with detectable intensity may be expected for each band and these arise from molecules with relative abundance ratios 3:5:6:4:2. These are  $AA, AB, (BB+AC), BC$  and  $CC$ .

The separation factors  $(\rho-1)$  for  $BB$  and  $AC$  being almost equal, the isotopic separation between these molecules is of a very small order of magnitude (below  $1 \text{ cm}^{-1}$ ) which cannot be resolved with the glass Littrow instrument employed. The bands whose classification is shown in Table III refer to the molecules  $BB+AC$ .

The relative dispositions of these five isotopic heads is shown in figure 2. For bands on the violet side of the spectrum, i.e., with  $\nu > \nu_e$  the disposition is as shown in (b), while for those on the red end with  $\nu < \nu_e$  it is as shown

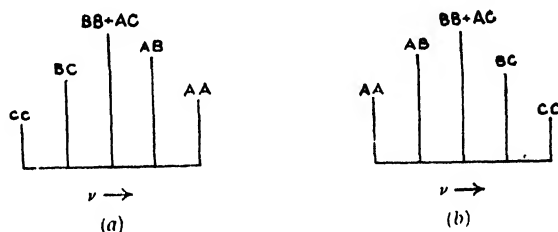


FIG. 2

in (a). The bands analysed in the present work lie on the red side of the system origin and hence the relative positions of the isotopic heads are given by figure 2(a).

Starting from the bands at  $\lambda 5200$  the separations between successive bands in each group gradually increase towards the red. That is to be theoretically expected as the  $\nu''$  values for the bands increase towards the red. This fact itself lends support to the view that these bands belong to the main system. Even on the basis of a separate system for these bands, as reported by Desirant and Minne with the vibrational constants about  $25 \text{ cm}^{-1}$  and  $251 \text{ cm}^{-1}$ , the expected isotopic separations are of the order of 10 to  $15 \text{ cm}^{-1}$ . This aspect of isotopic effect was completely ignored by Desirant and Minne.

The isotopic separations  $\Delta\nu$ , with respect to the most abundant molecule, are calculated according to the formula

$$\Delta\nu = (\rho-1)\omega_e'(v'+\frac{1}{2}) - (\rho^2-1)x_e'\omega_e'(v'+\frac{1}{2})^2 - (\rho-1)\omega_e''(v''+\frac{1}{2})^2 + (\rho^2-1)x_e''\omega_e''(v''+\frac{1}{2})^2$$

The calculated values for these isotopic separations are, shown in column 4 of Table II. The agreement between these and observed values is found to be quite satisfactory within the limits of dispersion of the instrument employed.

## ACKNOWLEDGMENT

The authors desire to express their grateful thanks to Prof. K. R. Rao for his interest in the work.

## REFERENCES

- Asundi, and Parti, 1937, *Proc. Ind. Acad. Sci.*, **6A**, 207.  
Desirant and Minne, 1936, *Comptes Rendus*, **202**, 1272.  
do 1936, *Bull. Sci. Acad. Roy. Belg.*, **22**, 646.  
Migeotte, 1942, *Bull. Sci. Roy. Soc. Liege.*, **11**, 48.  
Moraczewska, 1930, *Zell. fur. Physik*, **62**, 270.  
Olsson, 1935, do **95**, 215.  
Rosen, 1927, do **43**, 69.  
do 1939, *Physica*, **6**, 205.  
Rosen and Montfort, 1936, *Physica*, **3**, 257.  
do 1936, *Bull. Sci. Acad. Roy. Belg.*, **22**, 215.  
Rosen, Desirant and Nevin, 1936, *Nature*, **137**, 498.

# EFFECT OF SOLAR ACTIVITY ON IONOSPHERE AND EARTH'S MAGNETIC FIELD \*

By S. N. MITRA AND S. C. MAZUMDAR

RESEARCH DEPARTMENT, ALL INDIA RADIO, NEW DELHI

(Received for publication, October 21, 1954)

**ABSTRACT:**—The paper deals with an analysis of radio fade-outs and magnetic storms with a view to correlating them with solar flares and sun-spot numbers. Data for the years 1946-1949 have been analysed. Dellinger fade-outs have been observed to be well correlated with solar flares. Based on the theory of corpuscular emission from solar disturbances, delayed types of fade-outs and magnetic storms have been observed to go together and the delay time gives an approximate measure of the speed of the corpuscles. Occurrence of a solar flare has also been found to agree with that of high sunspot number. The analysis of the magnetic character figure indicates that it has no regular relationship with sunspot numbers. However, the central meridian passage of large sunspot groups is often found to be associated with flares, fade-outs and magnetic storms. Various correlations have been represented in the form of graphs and tables. A very high percentage of radio fade-outs has been found uncorrelated with solar flares and sunspot numbers. It has been postulated that such radio fade-outs may be caused by M-region activity

## 1. INTRODUCTION

It is known for a long time that certain disturbances happening in the sun produce significant changes in the ionosphere and in the earth's magnetic field. Solar disturbances are in the form of sunspots, bright chromospheric eruptions and very high frequency radio noise. In the ionosphere we have radio fade-outs, ionospheric storms, sudden phase anomaly on very long waves and fading of ionospheric signals. The magnetic disturbances are usually in the form of sudden variations in the horizontal intensity of the earth's magnetic field and the production of "Crotchets" in the magnetograms. Attempts have been made in the past to correlate the ionospheric and magnetic disturbances with solar flares and sunspot numbers but no regular relationship has yet been established. It has, however, been observed that certain brilliant solar flares have produced simultaneous radio fade-outs and magnetic storms. But when one attempts to analyse statistically the solar, ionospheric and magnetic data, any generalisation regarding the "cause and effect" relationship cannot be obtained. The object of this paper is to present one

\* This paper was read before the Indian Science Congress held in January 1951 at Bangalore and was later revised and extended.

such statistical analysis of the data for radio fade-outs, magnetic storms, solar flares and sunspot numbers covering the period 1946 to 1949. For the purpose of clarity, we have divided the data in discrete groups and individual analysis has been presented. The data are considered not sufficient and as such the analyses might not yield highly satisfactory conclusions. Nevertheless, they may show some useful correlations.

In the present paper we have analysed the data for radio fade-outs as recorded at the receiving station of All India Radio in Delhi (latitude  $28^{\circ} 35'N$ , longitude  $77^{\circ} 5'E$ ). These fade-out data are not based on any continuous records of signal strength. But as the reception conditions of regional and foreign stations are regularly checked round the clock throughout the year, the data may be considered to be fairly comprehensive. The data for solar flares and individual sunspot groups have been taken from Kodaikanal (latitude  $10^{\circ} 14'N$ , longitude  $77^{\circ} 28'E$ ) observatory. A few flare data have also been noted from published reports of the observatories. The magnetic data are mainly the geomagnetic character figures as supplied by Greenwich (latitude  $=50^{\circ} N$ , longitude  $=0^{\circ}$ ). The data for great magnetic storm have been taken from records at Alibag (latitude  $=18^{\circ} 45'N$ , longitude  $=73^{\circ} E$ ) magnetic observatory. The sunspot numbers have been taken from the data published by Zurich Observatory in the *Journal of Geophysical Research* (previously named *Terrestrial Magnetism and Atmospheric Electricity*). The period under consideration is 1946 to 1949.

## 2. EFFECT OF SOLAR FLARE

In this section we shall summarise the more recent work on the correlation of ionospheric and magnetic effects supposed to be due to solar flares. It is known that certain types of solar flares give rise to a train of terrestrial effects including radio fade-outs. Different aspects of these effects have been discussed by Ellison (1949), Rydbeck and Stranz (1949). Some effects are simultaneous which are supposed to be caused by wave radiations (mainly ultraviolet). Almost simultaneously with the occurrence of a flare, a newly ionised layer is formed at a height of 70-90 km. This layer affects the sky-wave radio transmission in a profound manner. Depending upon the amount of ionisation, short wave transmissions are completely or partially interrupted. We shall describe this type of fade-outs in more detail in Section 3.

On very long waves the effect of this newly formed layer is completely different. These waves suffer almost mirror-like reflection from the edge of the layer and reflection is very much improved. Due to this reason, increase in low frequency atmospherics is also noticed. Bracewell and Straker (1949) have shown that on very long waves (16 kc/s) the phase difference between the ground wave and the reflected wave shows sudden change with the occurrence of solar flares. The nature of the sudden phase



anomaly is such that it indicates sudden lowering of the reflecting layer and they are always observed whenever there is a flare even though the ionisation in the layer may not be sufficient to produce any noticeable fade-out in the high-frequency sky-wave transmissions. The correlation between the incidence of solar flare and the occurrence of sudden phase anomalies on very long waves is so satisfactory that the observation of the phase of the down-coming waves on very low frequencies provides a powerful tool unhampered by conditions of visibility for investigating the solar flares.

Another direct effect is the formation of geomagnetic 'Crotchet'. Fleming (1936) and McNish (1937) have pointed out that the magnetic effect is an augmentation of the normal daily variation over the sunlit hemisphere, probably due to increase in ionisation of the atmosphere, by ultraviolet light from the solar eruption, at the bottom of or below the E-layer.

After the discovery of the emission of solar radio noise, attempts have been made from time to time to correlate the emission of solar noise with radio fade-outs and happenings on the sun. It has been observed that variations in noise intensity are closely linked with sunspot activity. Allen (1947) has shown that the average intensity of solar noise at 1.5m wavelength follows the variation of the integrated projected area of sunspots. Better correlation has, however, been observed between noise intensity and the central meridian passage of large sunspots. This has been explained by directive emission of noise when sunspots are near the central meridian.

Allen (*loc. cit*) has analysed the records of short period increases in noise intensity over a year at 1.5m wavelength with a view to correlating them with visual phenomena. He remarks, "We could find no chromospheric or photospheric features which appeared to have an invariable physical connection, or high short period correlation, with the solar radio noise". Appleton and Hey (1946), on the other hand, have reported instances when large increases in solar noise at 4.7m wavelength were associated with solar flares. Covington (1948) has also observed substantial increase in noise intensity at 10 cm accompanied by sudden ionospheric disturbances which are usually attributable to solar flares.

Attempt has also been made to correlate the occurrence of radio fade-outs with the emission of noise-bursts at various wavelengths (Payne-Scott, Yabsley and Bolton, 1947). No conclusion has yet been arrived at. Considerable amount of data spread over a large number of years is needed before any correlation can be established.

Some effects of solar flare are delayed. These are considered to be due to corpuscular emissions. Magnetic storms and auroræ are the most conspicuous phenomena amongst the delayed effects. The time-delay depends upon the travel-time of the particles from the sun to the earth. F<sub>2</sub>-layer ionisation and layer-height show abnormal variations during and after a magnetic storm, thereby, adversely affecting radio transmissions on high frequencies.

Considerable attempt is now being made to correlate cosmic ray bursts with solar flares and sunspot activity. But no conclusive evidence regarding the increase in cosmic ray intensity after an intense solar flare (after a few minutes to an hour or so, depending on whether the constituent of the ray is high speed electron or proton) is yet available.

### 3. RADIO FADE-OUTS AND SOLAR FLARES

In this section we shall consider the radio fade-outs that may or may not have been caused by solar flares. Now, it is known that there are two types of fade-outs usually observed. In one type, suddenly within the space of a minute or so, short-wave (10-50 metres) channels of communication suffer a partial or complete interruption, at least if any part of them happens to lie in the sunlit hemisphere of the earth. These are termed Dellinger type, named after their discovery by Dellinger in 1935. In the other type, however, the process of interruption to communication service is rather slow and gradual. We shall first describe the Dellinger type.

Since in the Dellinger fade-outs, the propagation through sunlit hemisphere is affected, it can be deduced that the cause is a wave and not a particle effect. Some such fade-outs have been found to be synchronous with certain solar flares and their duration comparable with the visibility of the flare in  $H\alpha$  light. The immediate cause of the fade-out is the formation of a newly ionised non-reflecting layer at a height of 70-90 km, the cause of which is usually ascribed to the resonance line of hydrogen, Lyman $\alpha$ . This emission line ( $1215.7 \text{ \AA}$ ) in a flare must have an intensity and a line width far exceeding those recorded in the visible spectrum for  $H\alpha$ . This in itself would not give rise to atmospheric ionisation; but it so happens, as first noted by Chapman and Price (1937), that the resonance line of atomic oxygen has a wavelength of  $1217.6 \text{ \AA}$ . The wide wings of  $L\alpha$  will certainly overlap this oxygen line for the greater part of the lifetime of a flare. The oxygen in the atmosphere will therefore be excited and in the denser part of the atmosphere (70-90 km) collisions will be sufficiently frequent to prevent re-radiation. Extra ionisation will therefore take place and as soon as the ionising agency is removed, the disappearance of the ionised layer takes place. As the cause of the fade-out is absorption by the newly formed layer, lower frequencies are more affected and in the case of a complete fade-out, higher frequencies are the first to recover.

#### 3(a) ANALYSIS OF DATA

In this section we describe the analysis of the data for Dellinger fade-outs with a view to ascertaining their cause.

From the list of fade-outs, recorded in the Receiving Station (Todapur) at Delhi for the years 1946-1949, 41 fade-outs are found to have clear Dellinger characteristics. Of these 12 were recorded during the forenoon period

and 29 in the afternoon. Five forenoon fade-outs are found to coincide unmistakably with solar flares observed at Kodaikanal. Whereas, in the remaining seven, there is some uncertainty since the observations of solar flares are limited due to weather condition. For the afternoon period there is no coincidence since practically no solar flare data are available from Kodaikanal during this period. It is, however, observed that some of the outstanding flares recorded elsewhere and occurring during Indian day-light hours have not been reported from Kodaikanal Observatory, probably due to poor visibility. Unfortunately all such flare data cannot be utilised for our purpose as sometimes only the dates of occurrence are given. Even then eight of the twenty-nine afternoon fade-outs were found to coincide with flares.

The simultaneous occurrence of 13 fade-outs with solar flares is indicated in figure 1. In this figure time is reckoned from the start of the fade-out which is known correct to within a few minutes. Whereas, in the case of solar flare, time of start is not very often known. In some cases, only the time of peak intensity of the flare is given. If these uncertainty factors are taken into account, figure 1 clearly brings out the simultaneity of the

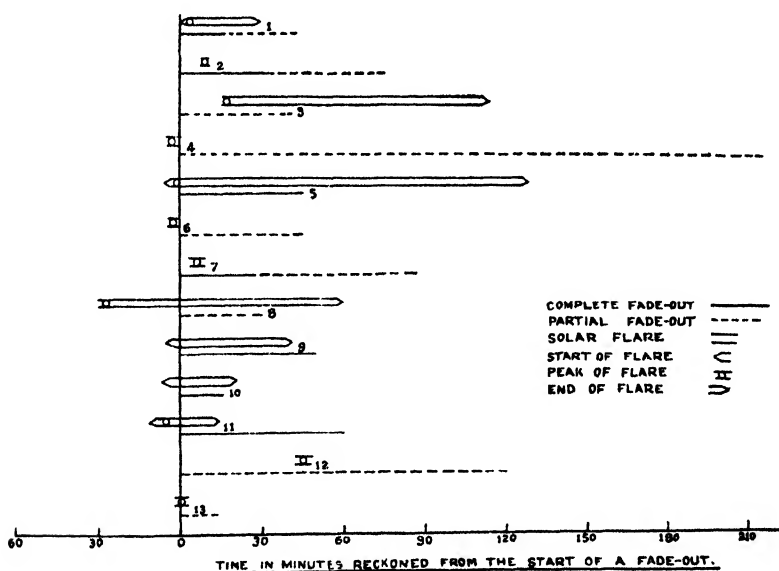


FIG. 1  
Correspondence of flares with Dellinger fade-outs

occurrence of Dellinger fade-outs with corresponding solar flares. Since the fade-out data are not based on any continuous record of signal strength, variation with time of intensity in the received radio wave cannot be compared with the variation of  $H\alpha$  line-width of the solar flare. Attempts have been made by Bracewell and Straker (1949) to compare the amount of "Sudden phase anomaly" (in degrees) with the line-width of  $H\alpha$  emission during

the solar flare of June 7, 1948. Ellison (1949) has shown graphically the correspondence between the intensity of solar radio noise and the line-width of  $H\alpha$  emission line during flares.

### 3. (b) OTHER FADE-OUTS

In the previous section we have seen the correspondence between Dellinger fade-outs and solar flares. In this section we shall analyse all the fade-outs, and attempt to find out how many of them may be ascribed to be due to ultraviolet emission from solar flares and how many due to corpuscular emission from them.

As many as 122 fade-outs were recorded during the years 1946-1949. These fade-outs were of various intensities and durations. The frequency ranges affected and the geographical locations of the transmitters so affected are also different in different cases.

Table I gives the number and duration of the following three classes of fade-outs:

- (1) Fade-outs which more or less coincided with an observed solar flare (ultraviolet effect);
- (2) Fade-outs which were observed 20 to 40 hours after an observed solar flare (corpuscular effect);
- (3) Fade-outs unassociated with any observed solar flare. In considering solar flares, lower intensity flares were not discriminated against.

TABLE I.

Group No.	Nature	No.	Relative abundance	Total duration Hrs. Mins.	Average duration Hrs. Mins.
1.	Fade-outs which more or less coincided with an observed flare (Kodaikanal data).	11	9%	44 45	4 4
2.	Fade-outs which were observed 20 to 40 hrs. after an observed flare.	12	9.8%	39 54	3 19
3.	Fade-outs unassociated with any observed flare.	99	81.2%	269 48	2 43
	Total	122			

It will be seen from Table I that about 20% of the total number of fade-outs have either direct or delayed correlation with a solar flare. Such a low percentage of correlation does not necessarily prove that most fade-outs are unassociated with solar flares.

The observation of flares is highly dependent upon weather conditions and for a better correlation, if any, one needs observing flares in any climatic condition. For this purpose the sensitive method of detecting a flare by

sudden phase anomalies on very long waves may prove useful and when systematic data are available over a large number of years, better correlation between radio fade-outs and solar flares may be obtained. Furthermore, on a very long distance circuit, the receiving point lying in the dark hemisphere may report a fade-out when a flare has actually affected the propagation condition in that part of the ionosphere lying on the sunlit side. In this case the flare data may not be ordinarily available. Again, for the delayed type of radio fade-out, the corresponding solar flare may not necessarily be observable at the receiving point. All these factors indicate a poor correlation between radio fade-outs and solar flares. A world-wide coordination of fade-out and flare data is therefore necessary for the purpose of a more effective correlation between the two data.

Table II shows the correlation between flares of different intensities and the radio fade-outs associated with them. It will be observed from the table that relatively small number of flares of intensity 3 has been effective in producing larger number of fade-outs, simultaneous or delayed.

TABLE II

Flare type (intensity)	Number observed	Relative abundance	Simultaneous fade-outs	Relative abundance	Delayed fade-outs (20-40 hrs)	Relative abundance	Percentage correlation
1	141	79.7%	6	54.5%	7	58.3%	10%
2	23	13.0%	1	9.1%	2	16.7%	13%
3 and 3+	13	7.3%	4	36.4%	3	25.0%	54%
Total	177		11		12		

The last column in the Table II shows the percentage of solar flares (out of the total number of each individual type observed) effective in producing a corresponding fade-out. Here again it will be seen that in 54% of intensity 3 flares a corresponding fade-out is observed. It must, however, be remembered that the classification of flare types in different intensity groups is purely arbitrary and the same flare, while being observed at the same time, has been classified differently by different astronomers. Continuous photography of H $\alpha$  line-width during a flare has been attempted in a few exceptional cases and the intensity of a flare has not yet been given a quantitative basis. It may, however, be noted from the above analysis, that although type 1 flares are not usually associated with a corresponding fade-out, type 3 flares are fairly well correlated.

## 4. SUNSPOT NUMBERS AND SOLAR FLARES

In previous sections we have discussed the correlation between the occurrence of solar flare and a corresponding radio fade-out. It may be of interest to see whether the probability of occurrence of a flare can be foreseen. As it is also known that these flares usually occur in the vicinity of active sunspot groups (particularly of bipolar groups) it will be worth investigating how the number of flares of differing intensity varies with the sunspot number. (The mechanism of formation of such flares and the probable mechanism of emission of ultraviolet and corpuscular radiations are outside the scope of the present paper).

Figures for Provisional Zurich Sunspot number and Kodaikanal solar flares have been grouped (1946-1949). Table III shows the number of flares of different types against days on which sunspot number was lying between certain limits (*i.e.* 0-50, 50-100 etc.,). Figure 2 shows a plot of total number of flares against sunspot numbers. The number of days on which the sunspot number was lying within those limits is also shown in the same figure by the dotted curve. The dashed curve indicates the number of radio fade-outs.

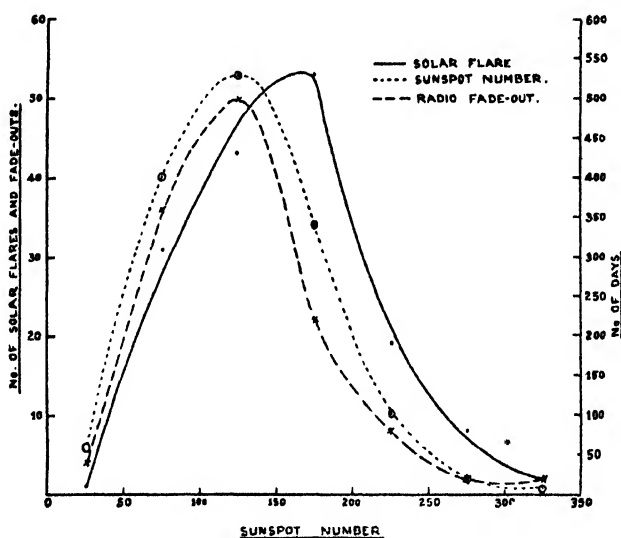


FIG. 2

Dependence of flares and fade-outs on sunspot number

It will be seen from figure 2 that the largest number of flares was observed on those days when the sunspot number was lying between 150 and 200, whereas, the largest number of days were found to indicate a sunspot number lying between 100 and 150. The correlation between the fade-out curve and the sunspot number curve is not very significant since it is quite probable that large number of days will produce larger number of fade-outs. To further clarify this point, Table III shows the percentage of days having

certain sunspot number effective in producing a flare or a fade-out. It will be seen from this table that the days having higher sunspot numbers are more effective in producing relatively higher number of flares. But for radio fade-outs no such generalisation can be made. It should, of course, be remembered that the occurrence of flares is dependent more on the activity of sunspots than on the number of spots. In a later section we have shown the correspondence of the central meridian passage of large sunspot groups with radio fade-outs, solar flares and magnetic storms.

TABLE III

Sunspot No. lying between	No. of days	No. of solar flares	% of days	No. of fade-outs	% of days
0-50	59	1	1.7	4	6.8
50-100	402	31	7.7	36	9
100-150	529	43	8	50	9.4
150-200	341	53	16	22	6.5
200-250	101	19	19	8	8
250-300	19	8	42	2	10
300-350	8	2	25	2	25

#### 5. CHARACTER OF GEOMAGNETIC FIELD AND RADIO FADE-OUTS.

There is another class of fade-outs which do not possess the Dellinger characteristic and is generally attributed to the F<sub>2</sub>-layer. There is no sudden onset and reception generally starts becoming poorer gradually and sometimes signals disappear altogether. Very often reception conditions remain subnormal for a considerable length of time, higher frequencies being affected more than the lower frequencies. Magnetic and ionospheric disturbances producing this type of fade-outs often go together, the ionospheric disturbances sometimes continuing for a considerable length of time after the magnetic disturbances have subsided. This point will be further discussed in the next section.

#### ANALYSIS OF DATA

Fade-outs other than those of Dellinger type recorded during the years 1947-49 were considered. Table IV gives the number of fade-outs taking place on days, the geomagnetic character figure for which or for the previous day (whichever value is higher) lies between certain limits (*i.e.* 0-0.5, 0.5-1.0 etc.). It will be seen from this table that the fade-out is more frequent on those days having higher character figure. Though the number of days

having a character figure lying between 0.5 and 1 greatly outnumbers that having higher character figure, the largest number of fade-outs is observed on the days having character figure lying between 1 and 1.5. Furthermore, the number of days having character figure between 2.0 and 2.5 is very small, still the number of fade-outs observed during these small number of days is quite high. This trend both in respect of complete and partial fade-outs shows that magnetic storms and radio fade-outs could have the same origin.

TABLE IV

Character figure	Number of fade-outs		Total	No. of days	% of days
	Complete	Partial			
0-0.5	0	0	0	237	0
0.5-1.0	1	9	10	568	1.6%
1.0-1.5	2	9	11	248	5%
1.5-2.0	3	7	10	38	26.3%
2.0-2.5	1	6	7	7	100%

N.B. Character figure 2.5 is regarded as indicative of the most disturbed condition of the earth's magnetic field.

#### 6. MAGNETIC STORM, RADIO FADE-OUT AND SOLAR FLARE

In this section we shall describe radio fade-outs during and after great magnetic storms. These storms disturb the geomagnetic field throughout the world including the dark hemisphere and sometimes continue for days. Chapman and Ferraro (1931-1933) have suggested that the corpuscles emitted from a disturbance in the sun cannot penetrate into the earth's atmosphere and these form a current ring round the earth. These corpuscles ultimately drift towards the polar regions following the magnetic lines of force. During the formation of the current ring and the drift of the stream of corpuscles, the magnetic field of the earth is disturbed and a magnetic storm is in progress. It is, therefore, seen that a magnetic storm which is being caused by the incidence of corpuscular radiation is a delayed process since the particles take considerable time to reach the earth from the sun. The ionospheric storms that generally accompany magnetic storms are also possibly caused by the incidence of these charged corpuscles. Now, these storms which are characterised by lowering of the F<sub>2</sub>-layer critical penetration frequency and increase in the layer height, are naturally expected to be more severe at higher latitudes and particularly in the auroral zones. During worst disturbances stratification of the F<sub>2</sub>-layer has been known to occur. Table V gives a number of magnetic storms recorded at Alibag Magnetic



TABLE V

Sl. No.	Magnetic storm		Radio fade-outs			Remarks
	Date and time of start	Date and time of end	Intensity	Date and time of start	Time of end	Nature
1.	7.2.46 15-48 IST	8.2.46 22-30 IST	Great	8.2.46 11-00 IST	12-30 IST	Partial
2.	22.3.46 11-08	25.3.46 07-30	"	25.3.46 09-30	12-30	No trace of B. B. C.
3.	28.3.46 12-05	29.3.46 22-30	Severe	28.3.46 16-00	21-00	Complete
4.	22.4.46 12-28	24.4.46 17-00	Moderate	24.4.46 08-30	20-30	Partial B. B. C. poor.
5.	6.5.46 09-00	8.5.46 01-30	"	6.5.46 11-40	12-05	Partial, all S. W. Sts. subnormal
6.	27.7.46 00-15	27.7.46 18-00	Strong	27.7.46 04-15	07-45	Complete fade-out of B. B. C. H. F. affected
				15-00	21-00	All stations poor.
				28.7.46 06-00	13-00	Complete fade-out

Flare observed on 27.3.46 at 09.10. Time difference between start of flare and start of storm = 26 hours 25 minutes.

Ionospheric conditions remaining disturbed till about 17 hrs. after the end of the storm.

Flare observed on 25.7.46 at 21.45 IST. Time difference between start of flare and start of storm = 26 hours 30 minutes.

Ionospheric condition remaining disturbed till about 19 hrs. after the end of the storm.

TABLE V (contd.)

Sl. No.	Magnetic storm		Radio fade-outs			Remarks
	Date and time of start	Date and time of end	Intensity	Date and time of start	Time of end	Nature
7.	18.9.46 05-18	19.9.46 22-30	Moderate	18.9.46 08-00	17-00	9 hours Partial B. B. C. SEAC Moscow poor
8.	21.9.46 22-41	23.9.46 24-00	"	22.9.46 23.9.46 24.9.46	Throughout till 11-00 on 24.9.46	Flare observed on 16.9.46 at 08.15. Time difference between start of flare and start of storm = 45 hrs. 3 mins. Ionospheric conditions remaining disturbed till about 164 hrs. after the end of the storm.
9.	2.3.47 09-29	4.3.47 15-00	"	3.5.47 11-30	13-00	1½ hours B. B. C. poor. Ionospheric conditions remaining disturbed till about 11 hrs. after the end of the storm.
				4.3.47 09-00	16-30	7½ hours Complete. H. F. more affected. Ionospheric conditions remaining disturbed till about 44 hours after the end of the storm.
				5.3.47 06-30	13-20	7 hours B. B. C. poor complete between 11.30 & 13.30
				6.3.47 07-30	13-00	5½ hours B. B. C. poor
10.	8.3.47 11-30	9.3.47 03-30	"	10.3.47 09-00	13-00	4 hours Partial

TABLE V (contd.)

Sl. No.	Magnetic storm		Radio fade-outs			Remarks
	Date and time of start	Date and time of end	Intensity	Date and time of start	Time of end	
11.	15.3.47 14-12	16.3.47 22-00	Moderate	No	fade out	Flare observed on 14.3.47 at 08.50. Time difference between the peak of the flare and start of the storm = 29 hours 22 minutes.
12.	17.4.47 17-54	19.4.47 04-00	Great	18.4.47 04-30	6 hours 10-30	R. B. C. nil till 09.30
13.	14.6.47 01-20	14.6.47 13-30	Moderate	14.6.47 13-30	3½ hours 16-45	Partial till 16.00 H. F. more affected. Complete after 16.30
14.	17.7.47 23-18	19.7.47 01-30	Great	17.7.47 11-00	1 hour 12-30	Partial. All foreign stations. H. F. more affected
15.	22.8.47 14-40	24.8.47 01-00	"	25.8.47 08-00	5½ hours 13-30	Partial. All foreign stations
16.	30.9.47 23-40	3.10.47 10-00	Moderate	No	fade out	Flare observed on 16.7.47 at 07.45. Time difference between start of the flare and start of the storm = 39 hours 24 min. Radio fade-out was observed 10 hrs. 30 min. after the end of the storm.
17.	9.11.47 14-26	10.11.47 00-30	"	No	fade out	Flare observed on 2.10.47 at 09.30.  Flare observed on 8.11.47 at 08.08. Time difference between start of the flare and start of the storm = 30 hrs. 18 minutes.

TABLE V (contd.)

Sl. No.	Magnetic storm			Radio fade-outs			Remarks
	Date and time of start	Date and time of end	Intensity	Date and time of start	Time of end	Duration	
18.	12.3.48 02-08	15.3.48 02-00	Moderate	13.3.48 15-30	18-30	3 hours	Partial. B. B. C. affected.
19.	15.3.48 09-04	15.3.48 24-00	Fairly strong	15.3.48 10-30	19-30	9 hours	Partial. H. F. on W. stations more affected
20.	21.4.48 04-36	22.4.48 20-30	Moderate	21.4.48 13-30	15-00	1½ hours	Partial; all frequencies affected
21.	24.1.49 23-58	27.1.49 05-30	Moderately strong	25.1.49 08-00	14-00	6 hours	Partial; all S. W. stations affected.
22.	11.5.49 07-34	11.5.49 17-30	Moderate	no	fade	out	Flare observed on 23.1.49 at 08.00. Dclinger fade-out on 23.1.49. Time difference between start of flare and start of storm = 39 hrs. 58 minutes.
23.	12.5.49 12-10	13.5.49 21-30	Strong	13.5.49 09-30	10-15	43 mins.	Flare observed on 10.5.49 at 09.00. Time difference between start of flare and start of the storm = 12 hrs. 34 mins.
24.	4.6.49 03-22	6.6.49 07-30	Moderate	5.5.49 14-25 16-20 17-25	14-30 16-45 17-35	5 mins. 25 " 10 "	All stations subnormal; B. B. C. 15 Mc/s nil. 21 Mc/s affected

Observatory during the years 1946-1949 which were accompanied by fade-outs. Details of these fade-outs show that most of them were of considerable duration and in large number of cases transmissions originating from places at higher latitudes were only affected. Radio reception at higher frequencies was more disturbed and in a number of instances higher frequencies originating at higher latitudes were the only transmission circuits to be affected. In some cases, the ionospheric disturbances, as evidenced by radio fade-outs, continued quite often for some 10 to 20 hours after the end of magnetic storms. In one instance it was found to continue for as long as 44 hours.

In the Table V, any solar flare corresponding to an observed magnetic storm has been noted. The time difference between the start of the flare and the start of the storm has also been indicated in individual cases. The average time interval appears to be 30 hours. The average speed of the particles is therefore about 1400 km/sec. An interesting feature in the above analysis is the fact that almost all the flares thus correlated with magnetic storms and radio fade-outs were situated within  $45^\circ$  of the central meridian thus confirming the hypothesis that corpuscular emission from a flare is confined to a narrow cone normal to the solar surface at the point of emission.

Corpuscular emission from the sun has been extensively studied during auroral displays. Recently, during the intense auroral storm of 18-20 August, 1950, Dr. Meincl of Verkes Observatory has observed the spectral region of the  $H\alpha$  line with a high resolution spectrograph, both with the spectrograph pointed towards the magnetic zenith and also towards the magnetic horizon. He found that the  $H\alpha$  line photographed along the magnetic zenith was very unsymmetrical, the maximum being displaced by  $10\text{\AA}$  and the violet wing was shifted  $71\text{\AA}$ . This is attributed to the Doppler shift due to the motion of protons. The velocity of the protons entering the earth's atmosphere was thus found to be 3200 km/sec. These observations gave direct support to the corpuscular emission from the sun during aurorae and magnetic storms (Chapman, 1950).

## 7. SUNSPOT NUMBER AND CHARACTER OF THE GEOMAGNETIC FIELD

In the previous section we have seen that solar flares may be regarded as responsible for producing a very few geomagnetic storms. But it has been fairly well established that whatever cause produces the geomagnetic storm, the same could be responsible for the type of fade-outs described in the previous section since almost all the fade-outs occurred nearly at the same time as the magnetic storms (Table V). In this and the following sections we shall enquire whether sunspots have any influence on the occurrence of storms.

It has been experimentally observed in the past that active spot groups, generally of bi-polar type and of relatively bigger dimensions affect the geomagnetic field rather profoundly during certain period of the life of the spot-group. In the following section we have considered separately the effect of the central meridian passage of large sunspot groups. However, an analysis for all the days in the year 1948 of the relative sunspot numbers and magnetic character figures indicates that there is no regular relationship between sunspot numbers and magnetic index. This is in good agreement with the observed events since only the centrally situated active spot-groups are known to affect the geomagnetic field whereas, the daily sunspot numbers take into account all the spots, big or small, situated anywhere on the visible solar hemisphere. Moreover, there are too many minor disturbances in the magnetic activity. Hence a correlation between magnetic character figure and daily average sunspot number cannot be expected. But during long periods of greater sunspot activity, the geomagnetic field may be expected to be more disturbed. This has been dealt with in the next section.

#### 8. EFFECT OF CENTRAL MERIDIAN PASSAGE OF LARGE SUNSPOTS

In the previous sections, while discussing the effect of sunspot numbers, we have considered only the relative number of spots. We have also seen that there is no close relationship between the daily sunspot number and the values of the magnetic activity. Intense magnetic storms are, on the contrary, decidedly correlated with individual large sunspots and vice versa.

Exhaustive analysis of large sunspot numbers and magnetic storms has been made by Greeves and Newton (1928) and Maunder (1904 etc.). The analysis reveals the interesting fact that the occurrence of large magnetic storms is associated with the presence of large spots in a sector between  $26^{\circ}\text{E}$  and  $53^{\circ}\text{W}$ . The average position is a meridian which at the time of commencement of the storm had passed the central meridian about one day before. It has further been observed that storms with sudden commencements are more closely correlated with sunspots than storms without this character.

In this section we present an analysis of the effects of the central meridian passage (CMP) of large sunspot groups. The data for sunspot activity have been mostly collected from the reports of Kodaikanal Observatory. Figure 3 shows the correspondence between the CMP of large spot-groups with radio fade-outs, solar flares and magnetic storms. The areas (in millionths of sun's visible hemisphere) for individual spot-groups are known in very few cases which have been indicated along the line showing the CMP. We have considered three days on either side of the CMP of a spot-group and any flare, fade-out and magnetic storm occurring

within these seven days has been shown in the figure. We have no quantitative basis for indicating the flare since the  $H\alpha$  line-width has not been plotted in most of the flares. Only types 2 and 3 flares have been

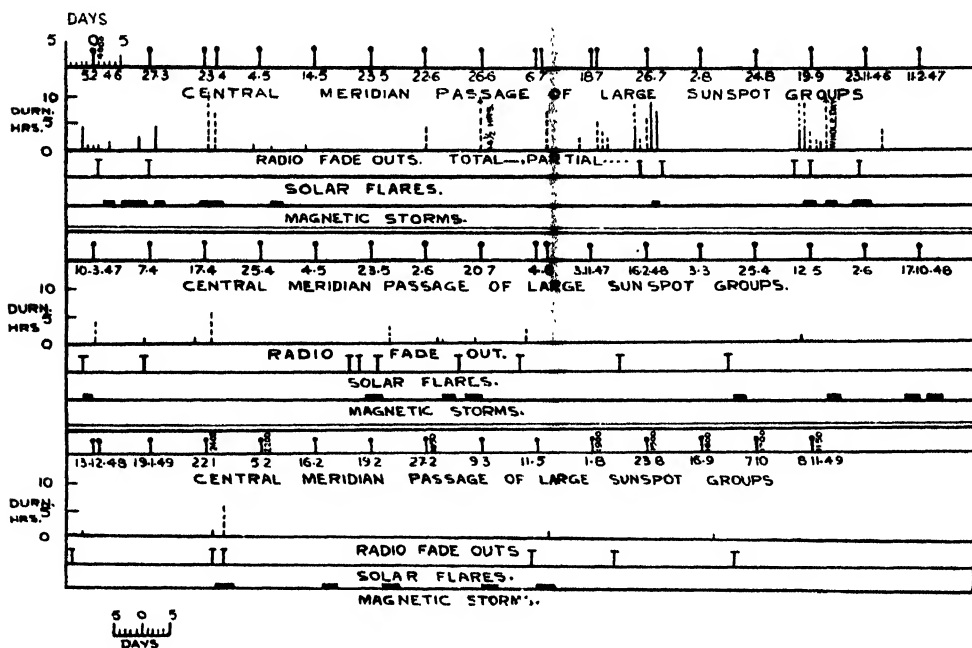


FIG. 3

Effect of central meridian passage of large sunspot groups

included. For the case of the magnetic storms, we have indicated the number of days through which the storms lasted; their intensity has not been taken into account.

It will be evident from figure 3 that, considering the very meagre data at our disposal (four years), the central meridian passage of large spot-groups is often found to be associated with flares, fade-outs and magnetic storms. We refrain from making any statistical analysis since the data are considered to be very limited.

#### CONCLUSION

Our analysis indicates that a large number of the radio fade-outs are usually not correlated with solar flares and sunspot numbers although they appear to be well correlated with magnetic storms. Out of 122 fade-outs, 99 are unassociated with a solar flare and out of 177 flares, 154 do not produce either a simultaneous or a delayed fade-out. The correspondence between the radio fade-outs and magnetic storms is understandable since they are supposed to be caused by the same mechanism.

The high percentage of fade-outs unassociated with flares is suggestive of a new source of solar origin for the fade-outs. It seems plausible to

attribute the occurrence of a fade-out (except those very few associated with flares) to the M-region activity. Recent experimental evidence indicates that the M-regions on the sun are likely to emit corpuscular radiation (Sengupta and Mitra, 1954). The speed of these corpuscles may vary within wide limits. We wish to point out that there are a number of observations on record where the effect of M-region activity upon the F<sub>2</sub>-layer has been observed. The possibility of the M-region emitting ultraviolet radiation cannot also be excluded. Detailed investigation regarding a possible correlation between the M-region activity and radio fade-outs is in progress.

#### ACKNOWLEDGMENTS

The work described in this paper formed a part of ionospheric research programme of All India Radio. The authors are grateful to the Directors, Kodaikanal Solar Observatory and Alibag Magnetic Observatory for kindly supplying the solar and magnetic data, and to the Astronomer Royal, Greenwich Observatory for kindly supplying the magnetic character figures. The authors are thankful to Mr. A. C. Ramchandani, Chief Engineer, All India Radio, for permission to publish this paper.

#### REFERENCES

- Allen, C. W. 1947, *M. N. R. A. S.*, **107**, 386.  
 Appleton, E. V. and Hey, J. S., 1946, *Phil. Mag.*, **37**, 73.  
 Bracewell, R. N. and Straker, T. W., 1949, *M. N. R. A. S.*, **109**, 28.  
 Chapman, S., 1950, *J. Geophys. Res.*, **55**, 361.  
 Chapman, S. and Ferraro, V. A., 1931-33, *Terr. Mag.*, **36**, 38.  
 Chapman, S. and Price, N. C., 1937, *Phys. Soc. Rep. Prog. Phys.*, **3**, 61.  
 Covington, A. E., 1948, *Proc. I. R. E.*, **36**, 454.  
 Dellinger, J. H., 1937, *Proc. I. R. E.*, **25**, 1253.  
 Ellison, M. A., 1949, *Nature*, **163**, 749.  
 Greaves, W. M. H. and Newton, H. W., 1928, *M. N. R. A. S.*, **88**, 556.  
     do                      1928, *M. N. R. A. S.*, **89**, 84.  
 Fleming, J. A., 1936, *Terr. Mag.*, **41**, 104.  
 McNish, A. G., 1937, *Terr. Mag.*, **42**, 109.  
 Maunder, E. W., 1904, *M. N. R. A. S.*, **64**, 205.  
     do                      1905, *M. N. R. A. S.*, **65**, 2, 538, 665.  
     do                      1916, *M. N. R. A. S.*, **76**, 63.  
 Meinel, A. B., 1950, *Science*, **112**, 590.  
 Payne Scot, R., Yabsley, D. B. and Bolton, J. G., 1917, *Nature*, **160**, 256.  
 Rydbeck, O. B. H. and Stranz, D., 1919, *Transactions of Chalmers University, Gothenburg, Rep. No. 1*.  
 Sengupta, P. K. and Mitra, S. N. *Nature*, 1954, **173**, 814.



# CALCULATION OF PERTURBATIONS IN CERTAIN MOLECULAR ELECTRONIC TERMS. PART II. ${}^2\Pi - {}^4\Sigma$ , ${}^2\Pi - {}^4\Pi$ , ${}^4\Sigma - {}^4\Pi$ AND ${}^4\Pi - {}^4\Pi$ PERTURBATIONS\*

By D. PREMASWARUP

DEPARTMENT OF PHYSICS, ANDHRA UNIVERSITY, WALTAIR

(Received for publication, September 16, 1954)

**ABSTRACT.** In this paper theoretical expressions for the course of the perturbed energy values in the perturbation cases  ${}^2\Pi - {}^4\Sigma$ ,  ${}^2\Pi - {}^4\Pi$ ,  ${}^4\Sigma - {}^4\Pi$  and  ${}^4\Pi - {}^4\Pi$  are evaluated. Graphical representations of these perturbation schemes are also given.

In this paper the perturbation calculations explained in Part I (Premaswarup, 1954) are applied to the perturbation types  ${}^2\Pi - {}^4\Sigma$ ,  ${}^2\Pi - {}^4\Pi$ ,  ${}^4\Sigma - {}^4\Pi$  and  ${}^4\Pi - {}^4\Pi$ . As the method has been explained in detail in the previous paper only the main results are given in all these cases.

**${}^2\Pi - {}^4\Sigma$  Perturbations.** The different states that have to be considered here are  ${}^2\Pi_{3/2}$ ,  ${}^2\Pi_{1/2}$ ,  ${}^2\Pi'_{-3/2}$ ,  ${}^2\Pi'_{-1/2}$ ,  ${}^4\Sigma_{3/2}$ ,  ${}^4\Sigma_{1/2}$ ,  ${}^4\Sigma_{-3/2}$  and  ${}^4\Sigma_{-1/2}$ .

The matrix elements  $H^\circ$  are given by the following :

$$\left. \begin{aligned} W_1^\circ = W_3^\circ = B_{11} [J(J+1) - \frac{7}{4}] + \frac{1}{2}A & \quad W_2^\circ = W_4^\circ = B_{11} [J(J+1) + \frac{1}{4}] - \frac{1}{2}A \\ W_5^\circ = W_7^\circ = hv + B_2 (J + \frac{3}{2})(J - \frac{1}{2}) + 3c & \quad W_6^\circ = W_8^\circ = hv + B_2 [(J - \frac{1}{2})^2 + 2] - 3c \\ H_{12}^\circ = H_{31}^\circ = 2B_{11} \sqrt{(J + \frac{3}{2})(J - \frac{1}{2})} & \quad H_{56}^\circ = H_{78}^\circ = B_2 \sqrt{3(J + \frac{3}{2})(J - \frac{1}{2})} \\ H_{15}^\circ = H_{27}^\circ & \quad H_{16}^\circ = H_{38}^\circ \\ H_{17}^\circ = H_{35}^\circ & \quad H_{18}^\circ = H_{36}^\circ \\ H_{26}^\circ & \quad H_{48}^\circ \\ H_{46}^\circ & \quad H_{28}^\circ \\ H_{68}^\circ = 0 & \quad \text{and} \quad H_{ik}^\circ = H_{ki}^{\circ*}, \end{aligned} \right\} \quad (1)$$

where  $hv$  stands for the interval between the null positions of the  $\Pi$  and  $\Sigma$  states. Here two cases arise according as the  $\Sigma$  state is positive or negative.

**Case (a).  ${}^2\Pi - {}^4\Sigma^+$  Perturbations.** Here the eighth order determinant breaks into two fourth order determinants according to the following scheme.

$$\begin{aligned} {}^2\Pi & \left\{ \begin{array}{cccc|cccc} W_1^\circ - W & H_{12}^\circ & H_{15}^\circ & H_{16}^\circ & W_3^\circ - W & H_{34}^\circ & H_{37}^\circ & H_{38}^\circ \\ H_{21}^\circ & W_2^\circ - W & & H_{26}^\circ & H_{43}^\circ & W_4^\circ & W & 0 \\ H_{31}^\circ & & W_5^\circ - W & H_{56}^\circ & H_{73}^\circ & & & \\ H_6 & H_6 & H_{65}^\circ & W_6^\circ - W & H_{83}^\circ & H_8 & H_{87}^\circ & W_8^\circ - W \end{array} \right\} \quad (2) \\ {}^4\Sigma & \left\{ \begin{array}{cccc|cccc} & & & & & & & \\ & & & & & & & \\ & & & & & & & \\ & & & & & & & \end{array} \right\} \end{aligned}$$

\* Communicated by Prof. K. R. Rao.

As a next step each of these determinants is transformed with unitary matrices  $S$ , so that in the transformed matrices the portions completely belonging to the  ${}^2\Pi$  and  ${}^4\Sigma$  states (i.e. the dotted portions) become diagonal. The elements of the transformation matrices are given by

$$S_{ii} = S_{kk} = \sqrt{\frac{1}{2} \left[ 1 + \sqrt{1 - \left| \frac{H_{ik}^{\circ}}{\Delta_{ik}} \right|^2} \right]} \quad \dots (3)$$

$$S_{ik} = S_{ki} = \sqrt{\frac{1}{2} \left[ 1 - \sqrt{1 - \left| \frac{H_{ik}^{\circ}}{\Delta_{ik}} \right|^2} \right]} \quad \dots (4)$$

$$\text{where} \quad \Delta_{ik} = \sqrt{\left( \frac{W_i^{\circ} - W_k^{\circ}}{2} \right)^2 + |H_{ik}^{\circ}|^2} \quad \dots (5)$$

and  $i, k = 1, 2$  or  $5, 6$  for the first determinant and  $3, 4$  or  $7, 8$  for the second determinant. The remaining elements of  $S$ , not included in the above are equal to zero.

After the transformation the matrix elements are given by

$$H_{ik} = S_{ii}(S_{kk}^* H_{15}^{\circ} + S_{k6}^* H_{16}^{\circ}) + S_{i2} S_{k6}^* H_{26}^{\circ} \text{ and } H_{ik} = H_{ki}^* \quad \dots (6)$$

with  $i, k = 1, 2; 5, 6$  or  $3, 4; 7, 8$  respectively.

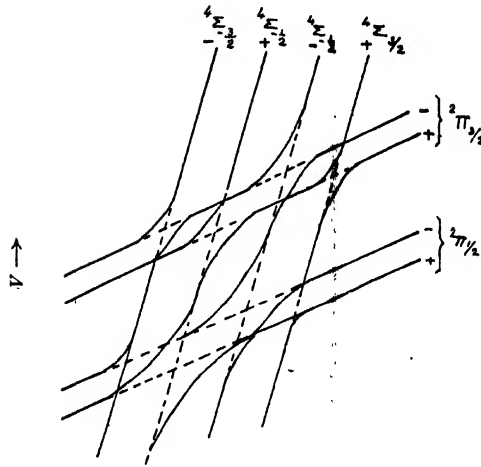
The values of the perturbed energies at the crossing point of any two levels are now given with these matrix elements from the equation

$$\left. \begin{matrix} W_i' \\ W_k' \end{matrix} \right\} = \frac{W_i + W_k}{2} \pm \sqrt{\left( \frac{W_i - W_k}{2} \right)^2 + |H_{ik}|^2} \quad \dots (7)$$

where  $(W_i - W)$  etc., represent the diagonal terms in the transformed matrices. Thus we see that in this case the levels  $W_1$  and  $W_2$  of the  $\Pi$  state are perturbed only by the components  ${}^4\Sigma_{3/2}(W_5)$  and  ${}^4\Sigma_{-1/2}(W_6)$  while the levels  $W_3$  and  $W_4$  are perturbed by the components  ${}^4\Sigma_{1/2}(W_7)$  and  ${}^4\Sigma_{-3/2}(W_8)$  and vice versa. A diagrammatic representation of this case is given in figure 1. Although this and the other diagrams are not drawn to scale, a qualitative picture of the relative magnitudes of perturbations in each case is given therein.

*Case (b).  ${}^2\Pi - {}^4\Sigma^-$  Perturbations.* This case will be exactly similar to the previous case, except that in the splitting of the eighth order determinant the levels 1, 2 and 7, 8 go over into one determinant while the other contains the levels 3, 4 and 5, 6. Therefore in this case the components  $W_1$  and  $W_2$  of the  ${}^2\Pi$  state are perturbed by  ${}^4\Sigma_{1/2}(W_7)$  and  ${}^4\Sigma_{-3/2}(W_8)$  while the levels  $W_3$  and  $W_4$  are perturbed by the components  ${}^4\Sigma_{3/2}(W_5)$  and  ${}^4\Sigma_{-1/2}(W_6)$  and vice versa.

*${}^2\Pi - {}^4\Pi$  Perturbations.* Here the states are  ${}^2\Pi_{3/2}$ ,  ${}^2\Pi_{1/2}$ ,  ${}^2\Pi'_{-3/2}$ ,  ${}^2\Pi'_{-1/2}$ ,  ${}^4\Pi_{5/2}$ ,  ${}^4\Pi_{3/2}$ ,  ${}^4\Pi_{1/2}$ ,  ${}^4\Pi'_{-1/2}$ ,  ${}^4\Pi'_{-3/2}$ ,  ${}^4\Pi'_{-5/2}$ ,  ${}^4\Pi'_{-3/2}$ ,  ${}^4\Pi'_{-1/2}$  and  ${}^4\Pi'_{1/2}$ . The different matrix elements between these states are given by



$J(J+1) \rightarrow$   
FIG. 1  
 ${}^2\Pi - {}^4\Sigma^+$  perturbation

$$\begin{aligned}
 W_1^\circ &= W_3^\circ = B[J(J+1) - \frac{7}{4}] + A/2 & W_2^\circ &= W_4^\circ = B[J(J+1) + \frac{1}{4}] - A/2 \\
 W_5^\circ &= W_9^\circ = h\nu + B^*[J(J+1) - \frac{1}{4}] + \frac{3}{2}A^* & W_6^\circ &= W_{10}^\circ = h\nu + B^*[J(J+1) + \frac{5}{4}] + \frac{1}{2}A^* \\
 W_7^\circ &= W_{11}^\circ = h\nu + B^*[J(J+1) - \frac{1}{4}] - \frac{1}{2}A^* & W_8^\circ &= W_{12}^\circ = h\nu + B^*[J(J+1) + \frac{5}{4}] - \frac{3}{2}A^* \\
 H_{13}^\circ &= H_{34} = 2B \sqrt{(J+\frac{3}{2})(J-\frac{1}{2})} & H_{36}^\circ &= H_{9,10} = B^* \sqrt{(J+\frac{3}{2})(J-\frac{3}{2})} \\
 H_{67}^\circ &= H_{10,11} = 2B^* \sqrt{(J+\frac{3}{2})(J-\frac{1}{2})} & H_{78}^\circ &= H_{11,12} = \sqrt{3} B^*(J+\frac{1}{2}) \\
 H_{15}^\circ &= H_{39} = \phi_1 \sqrt{(J+\frac{3}{2})(J-\frac{3}{2})} & H_{16}^\circ &= H_{3,10} = \mu_1 \\
 H_{17}^\circ &= H_{3,11} = \phi_2 \sqrt{(J+\frac{3}{2})(J-\frac{1}{2})} & H_{26}^\circ &= H_{4,10} = \chi_1 \sqrt{(J+\frac{3}{2})(J-\frac{1}{2})} \\
 H_{27}^\circ &= H_{4,11} = \mu_2 & H_{28}^\circ &= H_{4,12} = \chi_2 (J+\frac{1}{2}) \\
 & & H_{ik}^\circ &= H_{ki}^{*}
 \end{aligned} \tag{8}$$

Here  $h\nu$  is the wavenumber interval between the two  $\Pi$  states and the starred quantities refer to the  ${}^4\Pi$  term while the unstarred ones belong to the  ${}^2\Pi$  term. With these matrix elements the original secular determinant breaks into two determinants of sixth order, one of which contains only one set of the  $\Lambda$ -doublets while the other contains the other  $\Lambda$ -components. The transformation matrix which transforms the  ${}^2\Pi$  and  ${}^4\Pi$  portions of these determinants into diagonal form is given partly by the equations (3) to (5) above and partly by the equations (13) of Part I. After the transformation the matrix elements  $H$  are given by

$$H_{ik} = S_{i1}(S_{k5}^* H_{15}^\circ + S_{k6}^* H_{16}^\circ + S_{k7}^* H_{17}^\circ) + S_{i2}(S_{k6}^* H_{26}^\circ + S_{k7}^* H_{27}^\circ + S_{k8}^* H_{28}^\circ) \dots \tag{9}$$

and

$$H_{ik} = H_{ki}^*$$

where  $i=1,2$  and  $k=5,6,7,8$ . The perturbed energy values at the point of intersection of two levels are now given by equation (7) using these matrix elements.

Figure 2 gives the perturbation scheme for the  ${}^3\Pi-{}^4\Pi$  perturbation. Only one set of the  $\Lambda$ -doublets are shown in this figure. Since the positive levels of the  $\Lambda$ -doublets of the  ${}^3\Pi$  state perturb only the positive levels of the  $\Lambda$ -components of the  ${}^4\Pi$  term while the negative levels of the  ${}^4\Pi$  term are perturbed only by the negative components of the  ${}^3\Pi$  state and vice versa, it has not been necessary to draw the second  $\Lambda$ -doublets in the diagram as their perturbations will be exactly similar.

**${}^4\Sigma-{}^4\Pi$  Perturbations.** The states to be considered here are  ${}^4\Sigma_{3/2}$ ,  ${}^4\Sigma_{1/2}$ ,  ${}^4\Sigma_{-3/2}$ ,  ${}^4\Sigma_{-1/2}$ ;  ${}^4\Pi_{5/2}$ ,  ${}^4\Pi_{3/2}$ ,  ${}^4\Pi_{1/2}$ ,  ${}^4\Pi_{-1/2}$ ,  ${}^4\Pi'_{-5/2}$ ,  ${}^4\Pi'_{-3/2}$ ,  ${}^4\Pi'_{-1/2}$ ,  ${}^4\Pi'_{1/2}$ . The matrix elements connecting these different states are

$$W_1^\circ = W_3^\circ = B_2(J + \frac{3}{2})(J - \frac{1}{2}) + 3\epsilon$$

$$W_2^\circ = B_2[J(J + \frac{3}{2})^2 + 2] - 3\epsilon \quad W_4^\circ = B_2[(J - \frac{1}{2})^2 + 2] - 3\epsilon$$

$$W_5^\circ = W_9^\circ = h\nu + B\pi[J(J + 1) - \frac{1}{2}] + \frac{3}{2}A \quad W_6^\circ = W_{10}^\circ = h\nu + B\pi[J(J + 1) + \frac{3}{2}] + \frac{1}{2}A$$

$$W_7^\circ = W_{11}^\circ = h\nu + B\pi[J(J + 1) + \frac{1}{2}] - \frac{1}{2}A \quad W_8^\circ = W_{12}^\circ = h\nu + B\pi[J(J + 1) + \frac{3}{2}] - \frac{3}{2}A$$

$$H_{12}^\circ = H_{34}^\circ = B_2\sqrt{3(J + \frac{3}{2})(J - \frac{1}{2})} \quad H_{56}^\circ = H_{9,10}^\circ = B\pi\sqrt{3(J + \frac{3}{2})(J - \frac{3}{2})}$$

$$H_{67}^\circ = H_{10,11}^\circ = B\pi\sqrt{2(J + \frac{3}{2})(J - \frac{1}{2})} \quad H_{78}^\circ = H_{11,12}^\circ = B\pi\sqrt{3(J + \frac{1}{2})}$$

$$\left. \begin{aligned} H_{15}^\circ &= H_{39}^\circ \\ H_{19}^\circ &= H_{35}^\circ \end{aligned} \right\} = [1 \pm (-1)^{\Sigma}] 2\eta\sqrt{(J + \frac{3}{2})(J - \frac{3}{2})} \quad \left. \begin{aligned} H_{16} &= H_8 \\ H_{1,10} &= H_{38}^\circ \end{aligned} \right\} = [1 \pm (-1)^{\Sigma}](\xi + 2\eta)\sqrt{3} \quad (1c)$$

$$H_{18}^\circ = -H_{3,12}^\circ = [1 \pm (-1)^{\Sigma}] 2\eta\sqrt{(J + \frac{3}{2})(J - \frac{1}{2})}$$

$$H_{1,12}^\circ = -H_{38}^\circ$$

$$\left. \begin{aligned} H_2 &= H_{4,1}^\circ \\ H_{2,10}^\circ &= H_4 \end{aligned} \right\} = [1 \pm (-1)^{\Sigma}] 2\eta\sqrt{(J + \frac{3}{2})(J - \frac{1}{2})} \quad \left. \begin{aligned} H_2 &= -H_{4,12}^\circ \\ H_{2,12}^\circ &= -H_{48}^\circ \end{aligned} \right\} = [1 \pm (-1)^{\Sigma}](\xi + 2\eta)\sqrt{3}$$

$$\left. \begin{aligned} H_{27}^\circ \\ H_{2,11}^\circ \end{aligned} \right\} = [1 \pm (-1)^{\Sigma}]\{2(\xi + 2\eta) + 2\eta(J + \frac{1}{2})\} \quad \left. \begin{aligned} H_{4,1}^\circ \\ H_{4,7}^\circ \end{aligned} \right\} = [1 \pm (-1)^{\Sigma}]\{2(\xi + 2\eta) - 2\eta(J + \frac{1}{2})\}$$

$$H_{ik}^\circ = H_{ki}^{\circ*}$$

with the notation similar to the previous cases. Here, again two cases arise according as the  $\Sigma$  state is positive or negative. Considering the  $\Sigma$  state to be positive, the secular determinant breaks into two sixth order determinants one of which contains only the states 1, 2; 5, 6, 7, 8 and the other contains the remaining states. This determinant when transformed by an  $S$  matrix such that the  $\Sigma$  and the  $\Pi$  state portions become diagonal, has its matrix elements given by the relation

$$H_{ik} = S_{i1}(S_{k5}^*H_{15}^\circ + S_{k6}^*H_{16}^\circ + S_{k8}^*H_{18}^\circ) + S_{i2}(S_{k6}^*H_{26}^\circ + S_{k7}^*H_{27}^\circ + S_{k8}^*H_{28}^\circ) \quad \dots (1x)$$

with  $i, k = 1, 2; 5, 6, 7, 8$  and  $H_{ik} = H_{ki}^*$ .





**PROCEEDINGS  
OF THE  
INDIAN ASSOCIATION FOR THE  
CULTIVATION OF SCIENCE**





# STUDIES IN CHAIN-TRANSFER. PHENYLAZOTRIPHENYL METHANE CATALYSED POLYMERISATION OF STYRENE IN TOLUENE\*

By R. N. CHADHA AND G. S. MISRA

DEPARTMENT OF CHEMISTRY, UNIVERSITY OF LUCKNOW, LUCKNOW

(Received for publication, June, 17, 1951)

**ABSTRACT.** The present paper consists of a study on the chain transfer reaction between growing styrene ( $M$ ) polymer radical and toluene ( $S$ ), when catalysed by phenylazotriphenyl methane ( $B$ ). It has been shown that the transfer constant from the slope of  $1/\bar{P}$  against  $S/M$  plots at constant  $B/M$  values is not appreciably affected by the presence of low concentrations of the catalyst and initiation reaction was found to be bimolecular.

It was found by Suess and his co-workers, that addition of small amounts of benzene to pure styrene hardly affects the degree of polymerisation of the polymer formed at  $100^\circ\text{C}$ , while small amounts of carbon tetrachloride depresses the molecular weights very markedly. These results as well as those of Schulz et al, were explained very satisfactorily by Mayo, (1943) and Eyring et al (1943) by making use of the concept of chain-transfer. Mayo (*loc. cit.*) showed that for an uncatalysed polymerisation

$$\frac{1}{\bar{P}} = \frac{1}{\bar{P}_0} + \frac{k_{tr}'}{k_p} \cdot \frac{S}{M} \quad \dots (1)$$

where  $\bar{P}, \bar{P}_0$  are the number average degrees of polymerisation in solution and in pure monomer respectively,  $k_{tr}'$  and  $k_p$  are the velocity constants for chain-transfer with solvent and propagation and  $S/M$  is the mole ratio solvent/monomer. The ratio  $k_{tr}'/k_p$  is called the chain-transfer constant and is usually designated by  $C$ .

Mayo and others calculated the chain-transfer constants for the polymerisation of styrene in a number of solvents from the work of Suess and Schulz (*loc. cit.*), as well as from the data subsequently collected by Gregg and Mayo (1947).

For a catalysed reaction, the following relationship has been established, on the basis of a bimolecular initiation :

$$\frac{1}{\bar{P}} = \frac{(k_i k_t)^{1/2}}{k_p} \sqrt{\frac{B}{M}} + \frac{k_{tr}}{k_p} + \frac{k_{tr}'}{k_p} \cdot \frac{S}{M} \quad \dots (2)$$

where  $k_i, k_t$ , and  $k_{tr}$  are the velocity constants for initiation, termination and chain-transfer with monomer respectively and  $B$  is the concentration of the catalyst.

\* Presented at the High Polymer Symposium held at the Indian Association for the Cultivation of Science Calcutta in March 1954.

If, however, the initiation reaction is unimolecular with respect to the catalyst, a slightly different equation is obtained :

$$\frac{1}{P} = \frac{(k_i k_t)^{1/2}}{k_p} \cdot \frac{\sqrt{B}}{M} + \frac{k_{tr}}{k_p} + \frac{k_{tr}'}{k_p} \cdot \frac{S}{M} \quad \dots (3)$$

As will be seen, equation (2) can also be used for the determination of chain-transfer constant. Gregg and Mayo (1948) found that the value of the chain-transfer constant in the benzoyl peroxide catalysed polymerisation of styrene in carbon tetrachloride was in good accord with the value of this constant for the uncatalysed reaction. Valuable results in the evaluation of this method have been obtained by Palit and his co-workers (1952), who have studied the benzoyl peroxide catalysed polymerisation of methyl methacrylate in toluene.

#### EXPERIMENTAL

Mixtures of redistilled styrene, toluene and the catalyst, phenylazotriphenyl methane were taken in pyrex tubes, degassed and sealed under vacuum. They were heated in a thermostat at 80°C, until about

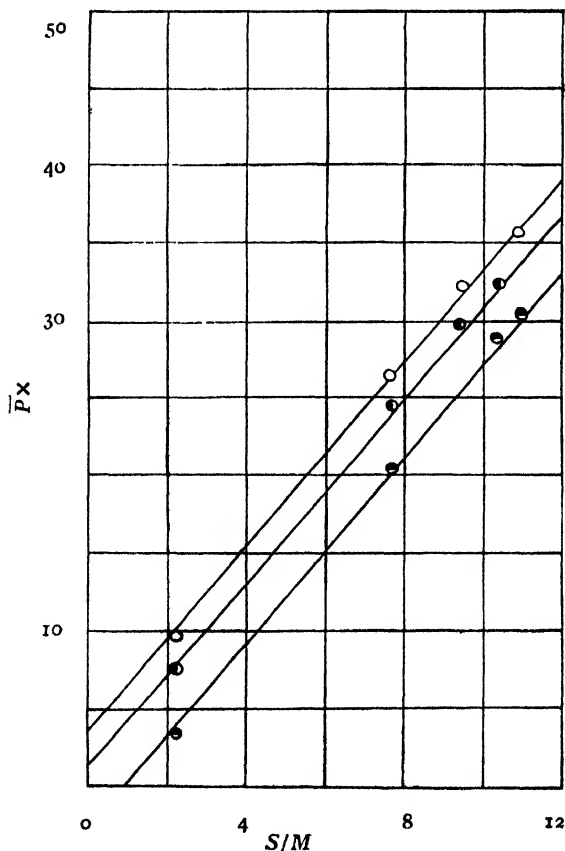


FIG. 1. Temp. 80°C.

$\sqrt{(B/M)}$  values : Lower curve,  $7.941 \times 10^{-3}$  ; Middle curve,  $3.213 \times 10^{-3}$  ; Upper curve, nil. C (chain-transfer constant) 3.10 ; 3.13 ; 3.10.

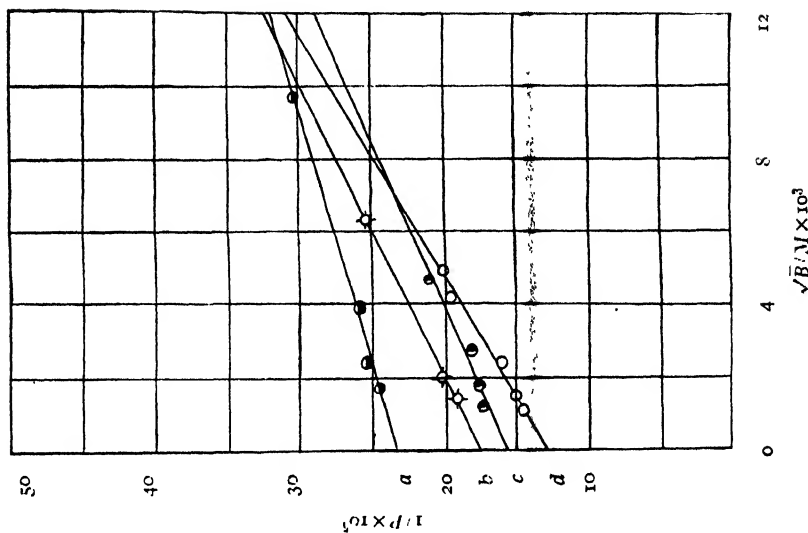


FIG. 2.—Temp. 80°C.

S/M values : Upper curve, 9.711 ; middle curve, 4.316 ; lower curve, 1.079.

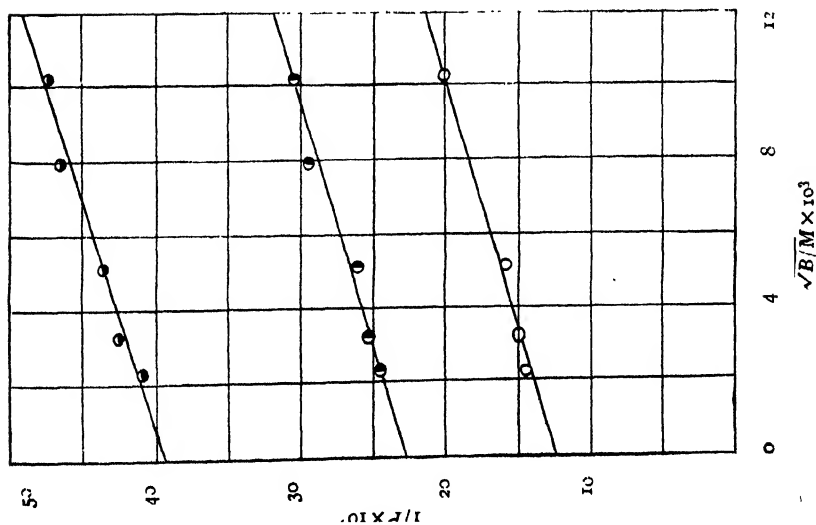


FIG. 3 Temp. 80°C.

S/M values : a. 4.316 ; b. 2.519 ; c. 1.619 ; d. 1.079.

10% polymerisation had occurred. The polymers were isolated by precipitation with a large excess of methanol.

Intrinsic viscosities of the polymers were determined in benzene at 25°C using an Ostwald No. 1 viscometer, and extrapolated to zero concentration using the formula of Schulz and Blaschke (1941). Molecular weights were found out by using the formula

$$[\eta] = K \cdot M^{\alpha} \quad \dots (4)$$

The values of  $K$  and  $\alpha$  were those determined by Bawn and his co-workers (1950).

## RESULTS AND DISCUSSION

In figure 1, values of  $1/\bar{P}$  are plotted against  $S/M$  for styrene toluene mixtures at 80°C; at constant  $\sqrt{(\bar{B}/\bar{M})}$  values. It would be seen that the slope of the plots remains practically the same as in the case of the uncatalysed reaction.

The chain-transfer constant calculated from the slopes are found to have the values of 3.10, 3.13 and 3.10 respectively. These are in good agreement with the value of this constant (3.13) calculated by Nozaki, (1947), from the data of Mayo (*loc. cit.*) for the uncatalysed polymerisation of styrene in toluene.

Phenylazotriphenyl methane on heating can give rise to two free radicals, which can act as initiators in addition to polymerisation :



This has been demonstrated by Hey and Misra, (1949), who using marked arylazotriaryl methanes, proved that under appropriate conditions both types of freeradicals can get incorporated into the polymer molecule.

According to Schulz, (1939), for low concentrations of the azo compound, the initiation reaction in the bulk polymerisation of styrene is monomolecular with respect to the catalyst concentration. A test has been made as to whether the initiation reaction is monomolecular or bimolecular. In figure 2

$1/\bar{P}$  has been plotted against  $\sqrt{(\bar{B}/\bar{M})}$  for a series of constant  $S/M$  values. The plots are found to be linear and parallel to each other. On the other

hand, as would be seen from figure 3, the plots of  $1/\bar{P}$  against  $\sqrt{\bar{B}/\bar{M}}$ , for a series of constant  $S/M$  values, though linear, have different slopes. This shows that equation (2) and not (3) is applicable in the present case. The evidence is thus in favour of a bimolecular initiation.

## REFERENCES

- Bawn *et al*, 1950, *Trans. Farad. Soc.*, **46**, 1107.  
 Pyring *et al*, 1943 *Ann. N. Y. Acad. Sci.*, **44**, 371.  
 Gregg and Mayo, 1947, *Farad. Soc. Disc.*, **2**, 328.  
 " " 1948, *Jour. Amer. Chem. Soc.*, **70**, 2373.  
 Hey and Misra, 1949, *Jour. Chem. Soc.*, 1807  
 Mayo, 1943, *J. Amer. Chem. Soc.*, **65**, 2324.  
 Nozaki, 1947, *Farad. Soc. Disc.*, **2**, 340.  
 Palit, S. R. *et al*, 1952 *Proc. Roy. Soc. A*, **214**, 247.  
 Schulz, *et al* 1939, *Z. Phys. chem.*, **B43**, 47; 385.  
 Schulz and Blaschke, 1941, *J. Prac. Chem.*, **155**, 130.  
 Schulz, 1939, *Naturwiss.*, **27**, 659.  
 Suess, *et al*, 1937, *Z. Phys. Chem.*, **A179**, 361.  
 " " 1937, *ibid.*, **A181**, 81.

# STUDIES ON MACROMOLECULES. THE SPREADING PROPERTIES OF RUBBER AND ITS DERIVATIVES\*

BY N. H. SIVARAMAKRISHNAN

AND M. R. A. RAO

DEPARTMENT OF GENERAL CHEMISTRY, INDIAN INSTITUTE OF SCIENCE, BANGALORE

(Received for publication, June, 17, 1954)

**ABSTRACT.** The spreading properties of rubber and its derivatives have been studied in detail. The effect of protein content and solvent towards the spreading of rubber has been investigated and it was found that the double bond of the isoprene was responsible for the spreading property of rubber. Attention has been given to the rate of oxidation of rubber films as influenced by the pH and halogens of the aqueous substrate. Moreover, the spreading and other physico-chemical properties of chlorinated rubber samples have been compared.

## INTRODUCTION

In the solid condition each crystallite of rubber consists of about 80,000–150,000 isoprene molecules and the length of this unit being 300–600 Å, width and thickness being 500 Å and 150 Å respectively (Hangstenberg and Mark, 1929). In the case of solutions, however, there are varying values for the molecular weights depending upon the method employed.

Method	Molecular weight
Light scattering (Dogadkin and Soboleva, 1949) and diffusion methods (Passynsky, 1946)	700,000–900,000
Ultra centrifuge method (Kraemer and Nicholas, 1940)	400,000–435,000
Viscosity (Carter et al 1946) and Osmometry (Gee, 1940, 1942)	100,000–400,000

The molecular weight depends on the nature of the solvent employed and also on the concentration of the solution.

Regarding the size and the shape of the molecules in the solid condition, X-ray (Hangstenberg, *loc. cit.*) and birefringence methods (Treloar, 1941) indicate that the macromolecule of rubber is an elongated bundle of long chain molecules with comparatively small diameter. Even in the case of solutions, experiments on scattering of light and diffusion have indicated that the micelles of rubber in solutions are elongated. The thickness and the width obtained by the X-ray method are of the order of 150 Å and of 500 Å, but in the case of solution, these diameters vary from 30 to 60 or 70 Å. Thus, there has been a considerable diversity of opinion regarding the size and shape of the micelles of rubber when it is dissolved in organic solvents.

\* Presented at the High Polymer Symposium held at the Indian Association for the Cultivation of Science, Calcutta in March, 1954.

Crisp, (1946), Moss (1934) and Harkins *et al* (1935) have studied in detail the spreading property of high polymers, in which the monomer, of each of one of these polymers, has a hydrophilic group. They have observed that the specific area of these polymer films is independent of the molecular weight. In general, the thickness of the film is found to be between 30 and 50 Å.

The spreading properties of rubber hydrocarbon have not been investigated so far. This might be perhaps due to the idea [Crisp (1942), Wall and Murry Zelikoff (1946) and Suzuki (1949)] that rubber is a pure hydrocarbon and cannot therefore spread over the water surface to give a stable film. Nevertheless, it was found by the present authors that rubber hydrocarbon could be spread over water surface to give rise to stable films. The hydrophilic group, that is responsible for the film-forming behaviour, is the double bonds of the molecule or the proteins (an impurity present in rubber). It has been recognised by the researches of Adam (1922), Langmuir (1917) and Mittelman and Palmer (1942), that organic compounds having double bonds are partly hydrophilic. So, it can be expected that rubber can be spread to a reasonable extent over water surface. In the present paper, the nature of the spreading property of rubber, depending on the nature of the solvent concentration of the solution and also the substitution of the double bond by other groups, is completely described.

#### EXPERIMENTAL

The rubber latex was subjected to various methods of purification to get rid of the inorganic and organic impurities. The inorganic impurities were removed by dialysis. The resins were removed by hot acetone by means of a soxhlet. For the removal of proteins, the following purification methods were used :

1. Alkali purification (Memler, 1934)
2. Autoclave purification (Mc Pherson, 1932)
3. Fractional precipitation (Midgley, 1931) and
4. Trypsin digestion (Freundlich *et al*, 1925)

The purified samples of rubber obtained by all these methods were preserved in organic solvents in an atmosphere of carbon dioxide to prevent the rubber getting oxidised by the atmospheric oxygen. The nitrogen estimation of the rubbers were conducted by the microkjeldahl method (Ma *et al*, 1942). The unsaturation value was obtained by the iodine number method (Kemp, 1943). It was found that in all these cases, the nitrogen values varied from 0.15 to 0.008% and the iodine values obtained were between 99.6 to 99.8% of the theoretical value.

Having obtained such pure rubber hydrocarbon, the spreading property of the rubber was conducted on a Langmuir-Adam surface pressure balance.

## RESULTS

The thickness of rubber films at "zero pressure" when spread on water at various dilutions of the rubber solutions in benzene and chloroform are given in Table I.

TABLE I

Weight of rubber spread	Benzene		Chloroform	
	Area/mg. in sq. cms.	Thickness in Å	Area/mg. in sq. cms.	Thickness in Å
<i>Alkali purified rubber</i>				
2.445 mg.	141.2	769.8	180.6	601.9
1.630 mg.	159.6	681.0	245.9	442.1
1.360 mg.	190.1	571.8	284.2	382.4
1.080 mg.	181.5	598.8	407.1	266.8
Extrapolated value for zero concentration	207.0	525.0	400.0	271.7
<i>Autoclave purified rubber</i>				
4.200 mg.	79.8	1362.0	89.8	1211.0
2.800 mg.	104.0	1045.0	135.6	801.7
2.330 mg.	113.8	955.2	143.3	758.6
1.870 mg.	120.0	905.7	198.9	546.4
Extrapolated value for zero concentration	153.0	710.1	213.0	510.2
<i>Fractionally precipitated rubber</i>				
4.635 mg.	114.3	951.0	105.7	1028.0
3.090 mg.	147.2	738.4	148.2	733.1
2.580 mg.	166.1	654.3	198.1	548.7
2.060 mg.	159.7	680.5	312.9	347.5
Extrapolated value for zero concentration	214.0	507.9	202.0	372.2
<i>Trypsin digested rubber</i>				
3.000 mg.	138.7	844.5	140.0	776.4
2.000 mg.	136.0	790.3	154.0	705.8
1.500 mg.	146.7	740.8	174.0	624.7
1.000 mg.	151.0	719.7	190.0	572.0
Extrapolated value for zero concentration	163.0	666.8	214.0	507.9

The results indicate that rubber hydrocarbon is capable of spreading on water surface, a result which was not anticipated by previous workers.

In the case of benzene solutions, the thickness of the film diminishes with progressive dilution and a constant value for thickness is obtained at sufficiently high dilution. In the case of chloroform, however, a constant value is not obtained even when the solution is diluted considerably. It is also observed that different methods of purification give different values for thickness indicating the extent of degradation of the molecule by the various methods of purification.

TABLE II

Effect of protein content on the spreading of rubber hydrocarbon.  
Solvent—Benzene. Quantity of rubber used for spreading = 1.5 mg.

Pressure in dynes/cm.	Amount of nitrogen in the sample		
	0.050%	0.017%	0.008%
	Area of the film in sq. cms.		
1	367.0	326.0	323.0
2	343.0	298.0	293.0
3	322.0	273.0	268.4
4	298.0	256.0	243.0
5	278.0	238.0	223.0
6	257.4	226.0	205.0
7	239.0	211.0	189.0
8	223.0 (214.0)	201.0 (195.0)	174.5 (171.0)
Extrapolated value at zero dyne/cm.	373.3	316.6	311.7
Area/mg.	248.9	211.1	207.8
Thickness of the film in Å	436.6	514.8	523.0

The results indicate that though there is a wide variation of nitrogen content of the three fractions, the thickness of the film is not considerably altered which clearly indicates that the spreading of rubber is not due to the protein content but an inherent quality of the rubber hydrocarbon itself.

TABLE III

Effect of solvents on the spreading property of rubber hydrocarbon.

Sample number	Toluene solutions				Benzene solutions		Benzene-methyl alcohol mixture		Benzene-acetone mixture	
	Intrinsic viscosity	Molecular weight	Area/mg sq. cms.	Thickness in Å	Area/mg sq. cms.	Thickness in Å	Area/mg sq. cms	Thickness in Å	Area/mg sq. cms.	Thickness in Å
1	1.79	211,300	278.0	391.0	308.7	352.2	244.6	444.2	218.0	498.6
2	2.17	282,500	260.7	417.0	302.0	360.0	234.0	464.5	206.6	526.0
3	2.35	318,400	233.3	465.8	243.3	446.7	206.6	526.0	206.0	527.5
4	2.90	436,500	206.0	527.5	208.0	522.5	170.3	638.4	170.1	639.2



The molecular weights of these samples (vide Table III) were determined by the viscosity method using the well known Mark's formula  $[\eta] = KM^a$  where  $K$  and  $a$  are constants. The values for  $K$  and  $a$  were taken to be  $5.02 \times 10^{-4}$  and 0.667 respectively for toluene at  $25^\circ\text{C}$  (Carter et al, 1946).

It is found from the results in Table III that the thickness of the film goes on increasing with an increase in the molecular weight. It is also observed that the thickness of the film is slightly greater with toluene than with benzene and when benzene has a precipitating agent like acetone or alcohol, the thickness is further enhanced.

In the case of carbon disulphide and carbon tetrachloride stable films could not be obtained.

In all these above studies, it was found that the double bond of the isoprene group was responsible for the spreading property of the rubber. In the following work, the oxidation of rubber film by means of potassium permanganate and hydrogen peroxide solutions was conducted. It was observed that the rate of oxidation of rubber film was enhanced by the increase in concentration of potassium permanganate. In all these cases, the pressure was kept constant at 2 dynes/sq.cm and the amount of rubber allowed to spread was also kept constant at 0.02 mgm. The rate of oxidation was measured by the increase in area of the film at different intervals. In the case of potassium permanganate solutions, the rate of oxidation of rubber was studied with different pH values of the solutions. Similar studies were conducted on hydrogen peroxide solutions and these values are reported in Table IV (a) and (b).

TABLE IV (a)

Effect of pH on the rate of oxidation of rubber films.

Concentration of potassium permanganate solution =  $M/500$ .

Quantity of rubber spread = 0.02 mg.

Time in minutes	Area of the film in sq. cms. at a pH of						
	2.00	3.00	3.96	5.80	7.00	8.00	10.00
1	528.0	506.0	492.0	396.0	320.0	170.0	130.0
2	480.0	426.0	468.0	468.0	350.0	218.0	192.0
3	432.0	396.0	426.0	438.0	372.0	283.0	252.0
4	414.0	384.0	372.0	420.0	394.0	348.0	312.0
5	408.0	360.0	360.0	400.0	349.0	360.0	360.0
6	360.0	348.0	350.0	366.0	330.0	332.0	336.0
8	354.0	330.0	330.0	354.0	228.0	282.0	276.0
10	300.0	318.0	312.0	351.0	246.0	264.0	276.0

TABLE IV (b)

Effect of pH on the rate of oxidation of rubber films.

Concentration of hydrogen peroxide solution =  $M/500$ .

Quantity of rubber spread = 0.02 mg.

Time in minutes	Area of the film in sq. cms. at a pH of		
	4.0	7.0	10.1
2	48.0	132.0	192.0
5	72.0	192.0	336.0
10	126.0	312.0	408.0
15	144.0	384.0	444.0
20	144.0	342.0	480.0
30	144.0	384.0	564.9

The results indicate that the rate of oxidation of rubber increases rapidly with an increase in the pH of the solution in the case of hydrogen peroxide solutions and the opposite effect is observed in the case of potassium permanganate solutions.

In all these cases the C=C group of the isoprene unit gets oxidised and the OH groups, that get linked up, are highly hydrophilic and they are responsible for the stability of the films. Hence, it was thought that instead of OH groups if certain halogens are added to these carbon atoms then the hydrophilic nature of these films cannot be enhanced and the area measurement would give us some different result. Hence a study of the rate of oxidation of rubber over aqueous solutions of halogens in the substrate was undertaken.

TABLE V

Effect of halogens in the aqueous substrate ( $M/200$ ) on the oxidation of rubber film. Quantity of rubber spread = 0.02 mg.

Time in minutes	Area of the film in sq. cms. on		
	Chlorine	Bromine	Iodine
2	216.0	384.0	42.0
5	264.0	396.0	66.0
10	264.0	418.0	60.0
15	276.0	396.0	84.0
20	300.0	396.0	96.0
30	246.0	396.0	96.0

The film obtained in the case of bromine water is far more stable than that in the case of chlorine water, the area of the film diminishes slowly with progress of time. In the case of iodine solution, it is highly surprising to notice that the area of the film obtained is comparatively smaller.

Thus, it is noticed that when rubber film was spread over aqueous chlorine or bromine, the stability of the film increased due to the formation of less soluble halogenated compounds. But, in these cases only addition reaction takes place. Hence when a solution of chlorinated rubber, a product prepared by passing chlorine through an emulsion of rubber in carbon tetrachloride, where addition and substitution of chlorine takes place, is spread over water surface the thickness of the chlorinated rubber films would indicate the extent of disaggregation of the original rubber hydrocarbon. The thickness obtained in these cases is of the order of 46–62 Å. Table VI gives the comparison of spreading properties of chlorinated rubber with its other physico-chemical properties.

TABLE VI

Comparison of the spreading and other physico chemical properties of chlorinated rubber samples.

Sample	Chlorine content %	Viscosity C P.	Density	Molecular weight	Area per mg in sq. cms.	Thickness in Å
A (1)	57.0	14.9	1.552	1927	1035	62.27
A (2)	61.5	19.5	1.591	2520	1165	53.95
A (3)	62.5	23.2	1.581	2219	1087	58.16
B (1)	63.6	24.8	1.582	4437	1060	59.61
C (1)	62.0	2.3	1.485	1512	1120	60.10
C (2)	66.0	6.2	1.580	1886	1257	50.32
C (3)	68.5	1.7	1.563	1300	1192	53.68
C (4)	68.0	12.6	1.687	2503	1230	48.19
C (5)	56.5	9.2	1.598	2453	1351	46.33
C (6)	69.0	7.3	1.605	2246	1229	50.71
C (7)	65.0	14.3	1.639	3613	1520	40.15
C (8)	67.5	16.8	1.633	2693	1253	48.88

## DISCUSSION AND CONCLUSION

The purity of the rubber sample prepared by the various methods described is in general agreement with the usual standards described in literature. The molecular weights obtained by the viscosity method are also of the same order as noticed by previous workers. The iodine value obtained is 99.6 to 99.8% of the theoretical value. This shows that the oxygenated impurities, which may aid the spreading of rubber, are not present in the samples. It can also be concluded that the use of carbon dioxide as an inert atmosphere during the purification process is quite effective. The second group of polar substances that may aid spreading consists of resins, esters and organic fatty acids. The soxhlet treatment with acetone has effectively removed these impurities. The proteins of the rubber can be considered to form the next group to influence its spreading. In spite of the best efforts, it has only been possible to reduce the nitrogen content

of the sample to 0.008%. But, it is gratifying to note that the samples of rubber having varying amounts of nitrogen (0.05 to 0.008%) give practically similar results for the specific area of the rubber films. This indicates that the small percentage of nitrogenous matter present after purification does not effectively contribute to the spreading property of rubber. The inability of the nitrogenous matter to influence the spreading property may be due to the denaturation of the protein during the purification. The small nitrogen content may be due to the non-protein and non-polar organic substances, which cannot contribute to spreading. On account of these reasons, it can be concluded that the spreading of rubber hydrocarbon is an inherent property of the rubber and not due to the impurities present in the rubber. The spreading property has been attributed to the presence of double bond of the isoprene units of rubber.

The rubber samples when spread over water give stable condensed films. The films are stable up to pressures of 8 to 9 dynes per cm., after which there is a gradual collapse. With the increase in dilution of the spreading solution, the limiting value for the thickness of the film is generally obtained with each solvent. The limiting value, however, is also dependent on the nature of the solvent. The limiting value for the film thickness obtained for the various rubber samples, in the same solvent, varies from 300 to 600 Å. This indicates that the rubbers purified by the different methods are liable to have different structural properties. The high value obtained for the thickness of the rubber film is due to the comparatively poor hydrophilic nature of the double bond and the high cohesive forces of the rubber which tend to minimise the spreading area. The thickness of the film also indicates that only 1% of the double bonds in rubber is in actual contact with water, while the remaining double bonds are present in the rubber medium. This further confirms the coiled and network structure of the rubber hydrocarbon indicated by optical methods.

The solvents have a profound influence on the nature of the spreading. The maximum and minimum for the spreading are noticed with solutions of chloroform and toluene respectively. This confirms that the degree of coiling is quite different in different solvents. When a precipitant, like acetone or methyl alcohol, is added to the benzene solution of rubber, the spreading property of rubber is further reduced, indicating thereby, that the precipitant increases the degree of coiling of rubber.

When carbon tetrachloride is used as a solvent for rubber, the stability of the film is greatly reduced, even at a pressure of one dyne per cm. Carbon disulphide could not be employed as a spreading agent, since the rubber got coagulated due to the poor spreading property and rapid evaporation of the solvent. This indicates that the choice of the solvent is very important in the study of the spreading property of rubber.

Although in the solid condition crepe rubber is only slowly oxidised, yet as a film, the rate of oxidation is extremely rapid even in the presence

of air. When the aqueous phase has an oxidising agent like potassium permanganate or hydrogen peroxide, the rate of oxidation is considerably enhanced and the oxidised films become unstable and finally dissolve in water. In the case of oxidising agents like chlorine and bromine, the film is stabilized over the surface of water, on account of the formation of insoluble halogenated compounds. The rate of expansion of the film is very slow with iodine solutions. This may perhaps be due to the weak oxidising nature of iodine. Chlorinated rubbers give stable condensed films. The molecular weight and the chlorine content do not affect the specific area of these films to any large extent.

Regarding the size and shape of the molecules, the present studies have indicated that in the case of pure rubber hydrocarbon, the diameter of the micelles is greater than what has been found by the light scattering and diffusion coefficient experiments. These values are more in agreement with the dimensions of the crystallites investigated by the X-ray method. In the case of chlorinated rubber, however, the molecular weight and the thickness of the film are considerably reduced due to the breakdown of the rubber molecule during chlorination.

## REFERENCES

- Adam, N.K., 1922, *Proc. Roy. Soc.*, **101A**, 516.  
 Adam, N.K., and Dyer, J.W.W. 1924, *Ibid.*, **106A**, 694.  
 Adam, N.K., and Jessop, G., 1926, *Ibid.*, **112A**, 362  
 Carter, W. C., Scott, R. L., and Magat, T., 1946, *J. Amer. Chem. Soc.*, **68**, 1480  
 Crisp, D.J., 1942, *Trans. Faraday Soc.*, **38**, 320  
 Crisp, D.J., 1946, *I. Colloid Sci.*, **1**, 49, 161  
 Dogadkin, B., Soboleva, I. and Arkhangel'skaya, M., 1949, *Kolloid Zhur*, **11**, 143;  
 1949, *C.A.*, **43**, 7742  
 Freundlich H. and Hauser, E.A. 1925, *Kolloid Z.*, **36**, 15  
 Gee, G., 1940, *Trans. Faraday Soc.*, **36**, 1171; 1942, **38**, 108  
 Harkins, W.D., Carman, E.F. and Ries, H.E. 1935, *J. Chem. Phys.*, **3**, 692  
 Hengstenberg, J. and Mark, H., 1929, *Z. Krist.*, **69**, 271  
 Kemp, A.R., and Peters, H., 1943, *Ind. Eng. Chem., Anal. Edn.*, **15**, 453  
 Kraemer, E.O., and Nicholas, J.B., 1940, "The Ultra Centrifuge" Svedberg and Pedersen (Oxford), page 423  
 Langmuir, I., 1917, *J. Amer. Chem. Soc.*, **39**, 1848  
 Ma, T.S. and Zuazaga G., 1942, *Ind. Eng. Chem., Anal. Edn.*, **14**, 280  
 McPherson, A.T., 1932, *J. Res. Bur. Standards.*, **8**, 751  
 Memier, 1934, "Science of Rubber", p. 172  
 Midgley, T., Henne, A.L. and Renoll, M.W., 1931, *J. Amer. Chem. Soc.*, **53**, 2733  
 Mittelman, R. and Palmer, R.C. 1942, *Trans. Faraday Soc.*, **38**, 506  
 Moss, S.A., 1934, *J. Amer. Chem. Soc.*, **56**, 41  
 Passynsky, A. and Gatovaskaya, T., 1946, *Acta. Phy. Chm.*, **21**, 1055  
 Suzuki, K., 1949, *Bull. Chem. Soc., Japan*, **22**, 165  
 Treloar, L.R.G., 1941, *Trans. Faraday Soc.*, **37**, 84; 1947, **43**, 284  
 Wall, F.T. and Murry Zelikoff, M., 1946, *J. Amer. Chem. Soc.*, **68**, 726

"

"

# AUTHOR INDEX

Author	Subject	Page
Ahmed, Rais	See Sarkar, D. C. and	533
Banerjee, B. M.	A reactance tube controlled oscillator of unusually wide frequency sweep	67
Banerjee, C. C.	Proton-proton scattering at 340 Mc	221
Banerjee, Sukhendu Bikash	On the Raman spectra of ethylene dichloride in solutions of different strengths	205
Basu, D.	Pseudoscalar interaction and proton-proton scattering	201
Basu, Sadhan	Molecular orbital theory and the reactivity of polyphenyls	319
Do	Molecular orbital calculations on phthalocyanine	511
Bhattacharyya, Bimal Krishna	The effect of steepness of rise and fall of the input pulse on the response of pulse amplifiers. Part I.	31
Do	Do Part II.	371
Bhattacharya, J. C.	An instrument for direct measurements of capacitance and power factor	75
Biswas, D. C.	Raman spectra of ortho and para chlorophenol in the solid state at low temperatures	85
Do	The Raman spectra of <i>m</i> - and <i>p</i> -xylene in the solid state at different low temperatures	303
Do	Raman and fluorescence spectra of ortho and para bromolouene in the solid state at low temperatures	423
Biswas, N. N.	Mean life of decay of muons in the absence of matter	431
Biswas, S. N.	On Born's approximation and its connection with covariant perturbation theory	119
Chakrabarty, Nirmal Baran	Synthesis of a network for a prescribed time-function	473

Author	Subject	Page
Chakraborty, D. M.	An X-ray study of <i>o</i> -phthalic acid	129
Chakrabarty, R.	See Roy, S. B. and	167
Chatterjee, B.	Ionization distribution in the F-region	53
Chatterjee, G. P.	Hardness of metals and alloys	9
Chowdhury, Amalendu	See Dutta, Ajit Kumar and	312
Das, Jajneswar	Pulse slope modulation—A new method of modulating video pulses and its possible application on line circuits	449
Datta, Sunil Kumar	Accurate determination of the magnetic anisotropies of the hydrated salts of some elements of the iron group	239
De, G. L. and Mahanti, P. C.	A study of air absorption of some liquids	441
De, M. L. and Saha, D. K.	Distortion in electron lens	263
Deb, A. R.	The ultraviolet absorption spectra of $\alpha$ -chloronaphthalene and $\alpha$ -bromonaphthalene in different states	21
Deb, S.	Electron optical treatment of current division in radio valves	349
Dube, G. P. and Lal Saheb Singh	On the validity of semi-empirical atomic mass formula in the region of rare earth nuclides	177
Do Do	On the kinetic energy of fission-fragments from $U^{235}$	227
Durgavathi, B. Kanaka and Rao, V. Ramakrishna	Band spectrum of $CrF$ molecule	525
Dutt, P. K.	A demountable all-metal hot cathode vacuum ionisation gauge	1
Dutta, Ajit Kumar and Chowdhury, Amalendu	Electrical conductivity of single crystals of graphite along the basal plane and a new and simple method of measuring electrical conductivities	312
Dutta Roy, S. K.	A new electrodynamic method of measuring magnetic fields	183
Ghosh, Dilip Kumar	On the time of relaxation of some organic molecules in pure liquid state	191



Author	Subject	Page
Ghosh, Dilip Kumar	Absorption of 3.18 cm microwaves in some aromatic and aliphatic compounds in the liquid state	485
Gill, P. S.	The lead absorption of cosmic rays	335
Gopalakrishnan, K.	See Tawde, N. R. and	469
Hans, H. S.	An instrument for measuring decay of $\mu$ -mesons	93
Iyengar, V. C.	See Mitra, S. N. and	147
Karunes, B.	A rigid bivilinear polygonal core in an infinite plate under tension at infinity and shear	133
Kastha, G. S.	On the intensity-distribution in the wing of the Rayleigh line due to liquid oxygen	329
Krishnamachari, S. L. N. G.	Force constants for methyl cyanide and methyl isocyanide	463
Machwe, Madhukar Kashinath and Sodha, Mahendra Sirgh	On resolving power of compound Fabry-Perot etalon	522
Mahanti, P. C.	See G. L. De and	441
Majumdar, K. and Varshni, Y. P.	Spectroscopic constants of molecules. I. On the ground state frequencies of diatoms of the type XX	103
Do	Spectroscopic constants of molecules. II. On the vibration frequency of diatoms of the type XX	209
Mazumdar, S. C.	See Mitra, S. N. and	563
Mazumdar, Monomohan	On the Raman spectra of acetyl chloride and chloroacetyl chloride in the vapour state	297
Mazumder, S. C. and Mitra, S. N.	Peak amplitude recorder for investigation on fading	251
Mitra, A. P.	Atomic nitrogen as a constituent for region $F_1$	269
Mitra, S. N. and Iyengar, V. C.	Observation of scatter echoes on high power pulsed transmissions	147
Mitra, S. N.	See Mazumder, S. C. and	251
Mitra, S. N. and Mazumdar, S. C.	Effect of solar activity on ionosphere and earth's magnetic field	563

Author	Subject	Page
Misra, G. S.	See Chadha, R. N.	37
Palit, Santi R. and Majumdar, Kesab Chandra	The effect of chain transfer on the distribution of molecular weights in high polymers. Part I. Combination	1
Palit, Santi R.	See Mazumder, Kesab Chandra and	19
Rao, M. R. A.	See Sivaramkrishnan, H. N. and	41
Sivaramakrishnan, H. N. and Rao, M. R. A.	Studies on macromolecules. The spreading properties of rubber and its derivatives	41

# SUBJECT INDEX

Subject	Author	Page
Absorption of 3.18 cm microwaves in some aromatic and aliphatic compounds in the liquid state.	Dilip Kumar Ghosh	485
Air absorption of some liquids. A study of	G. L. De and P. C. Mahanti	441
Atomic mass formula in the region of rare-earth nuclides. On the Validity of semi empirical	G. P. Dube and Lal Saheb Singh	177
Atomic nitrogen as a constituent for region $F_1$	A. P. Mitra	269
Background intensity on resolution. Effect of	Mahendra Singh Sodha	141
Bands involving high multiplicity terms. Intensity formulae for. Part III. ${}^6II - {}^6\Sigma$ and ${}^6II - {}^6II$ transitions.	D. Premaswarup	48
Band spectrum of CrF molecule	B. Kanaka Durgavathi and V. Ramakrishna Rao	525
Band spectrum of tellurium in the visible. The	N. Durga Prasad and P. Tiruvenganna Rao	549
Born's approximation and its connection with covariant perturbation theory. On	S. N. Biswas	119
Capacitance and power factor. An instrument for direct measurement of	J. C. Bhattacharya	75
Charged meson pairs by neutral particles in cosmic rays. On the production of	S. B. Roy and R. Chakravarti	167
Cosmic rays. Lead absorption of	P. S. Gill	335
Decay of Mu-mesons. An instrument for measuring	H. S. Hans	93
Decay of muons in the absence of matter. Mean life of	N. N. Biswas	431
Distortion in electron lens	M. L. De and D. K. Saha	263
Electrical conductivity of single crystals of graphite along the basal plane and a new and simple method of measuring electrical conductivities.	Ajit Kumar Dutta and Amalendu Roy Choudhury	312
Electrodynamic method of measuring magnetic fields. A new	S. K. Dutta Roy	183

Subject	Author	Page
Electron capture by ions passing through gases	N. C. Sil	232
Electron optical treatment of current division in radio valves	S. Deb	349
Fission fragments from $U^{235}$ . On the kinetic energy of	G. P. Dube and Lal Sahab Singh	227
Force constants and Thermodynamic properties of $TiCl_4$	D. Tirumalesa and V. Ramakrishna Rao	216
Force constants for methyl cyanide and methyl isocynide	S. L. N. G. Krishnamachari	463
Hardness of metals and alloys	G. P. Chatterjee	9
Hulbert-Hirschfelder $U(r)$ function in $C_2$ (Swan) system. Study of	N. R. Tawde and K. Gopala-krishnan	469
Ionization distribution in the E-region	B. Chatterjee	53
Ionosphere and nature of fading patterns of received radio signals	R. N. Singh	109
Magnetic anisotropies of the hydrated salts of some elements of the iron group. Accurate determination of	Sumil Kumar Datta	239
Molecular orbital calculation on phthalocyanine	Sadhan Basu	511
Molecular orbital theory and the reactivity of polyphenyls	Sadhan Basu	319
Multiplet separation factors in the spectrum of chromium II.	V. Suryanarayana and V. Ramakrishna Rao	285
Net-work for a prescribed time-function. Synthesis of a	Nirmal Baran Chakrabarty	473
Peak amplitude recorder for investigation of fading	S. C. Mazumder and S. N. Mitra	251
Perturbation in certain molecular electronic terms. Calculation of. Part I.	D. Premaswarup	256
Perturbation in certain molecular electronic terms. Calculation of. Part II. $^2\Pi - ^4\Sigma$ , $^2\Pi - ^4\Pi$ , $^1\Sigma - ^4\Pi$ and $^4\Pi - ^4\Pi$ perturbations.	D. Premaswarup	581
Proton-proton scattering at 340 Mev	C. C. Banerjee	221
Pseudoscalar interaction and proton-proton scattering	D. Basu	261
Pulse slope modulation—A new method of modulating video pulses and its possible application on line circuits	Jajneswar Das	449

Subject	Author	Page
Raman spectra of acetyl chloride and chloroacetyl chloride in the vapour state. On the	Monomohan Mazumder	297
Raman and fluorescence spectra of ortho and para bromotoluene in the solid state at low temperatures	D. C. Biswas	423
Raman spectra of ethylene dichloride in solutions of different strengths. On the	Sukhendu Bikash Banerjee	205
Raman spectra of <i>m</i> - and <i>p</i> -xylene in the solid state at different low temperatures. The	D. C. Biswas	303
Raman spectra of ortho and para chlorophenol in the solid state at low temperatures	D. C. Biswas	85
Raman spectra of styrene and polystyrene at $-180^{\circ}\text{C}$ . On the	N. K. Roy	365
Reactance tube controlled oscillator of unusually wide frequency sweep. A	B. M. Banerjee	67
Relative cross-section of (n-p) reactions in $\text{Al}^{27}$ and $\text{Mg}^{24}$	S. K. Nandi and N. K. Saha	396
Relaxation period of a multivibrator. Analysis of the	D. C. Sarkar and Rais Ahmed	533
Response of pulse amplifiers. Effect of steepness of rise and fall of the input pulse on the. Part I	Bimal Krishna Bhattacharyya	31
Do	Part II	Do
Resolving power of compound Fabry-Perot etalon. On	Madhukar Kashinath Machwe and Mahendra Singh Sodha	522
Resolving power of Fabry-Perot etalon, Lummer-Gehrcke plate and transmission echelon on stage of resolution. On dependence of	Shashanka Shekhar Mitra	543
Resolving power of prism, grating and reflecting echelon on stage of resolution and detecting instrument. On dependence of	Om Prakash Sharma and Mahendra Singh Sodha	437
Rigid curvilinear polygonal core in an infinite plate under tension at infinity and shear. A	B. Karunes	133

Subject	Author	Page
Scatter echoes on high power pulsed transmissions. Observation of	S. N. Mitra and V. C. Iyengar	147
Shifts in substituted benzenes. Theoretical calculation of	S. Ramamurty	325
Spectroscopic constants of molecules. I. On the ground state frequencies of diatoms of the type XX.	K. Majumdar and Y. P. Varshni	103
Spectroscopic constants of molecules. II. On the vibration frequency of diatoms of the type XX	K. Majumdar and Y. P. Varshni	209
Solar activity on ionosphere and earth's magnetic field. Effect of	S. N. Mitra and S. C. Mazumdar	563
Surface tension from measurements of sessile drops. A table for the calculation of	N. R. Tawde and K. G. Parvatikar	345
Time of relaxation of some organic molecules in pure liquid state. On the	Dilip Kumar Ghosh	191
Ultraviolet absorption spectra of $\alpha$ -chloronaphthalene and $\alpha$ -bromonaphthalene in different states. The	A. R. Deb	
Ultraviolet absorption spectrum of acetaldehyde molecule as due to a single electronic transition. Interpretation of the near	V. Ramakrishna Rao and I. Achyuta Rao	491
Ultraviolet fluorescence spectra of $I_2$ molecule. Analysis of the	C. V. Narayana Rao and V. Ramakrishna Rao	403
Vacuum ionisation gauge A demountable all-metal hot-cathode	P. K. Dutt	1
Wing of the Rayleigh line due to liquid oxygen. On the intensity distribution in the	G. S. Kastha	329
X-ray study of <i>o</i> -phthalic acid. An	D. M. Chakraborty	129
<i>Proceedings of the Indian Association for the Cultivation of Science.</i>		
Chain-transfer. Studies on, Phenylazo, triphenyl methane catalysed polymerisation of styrene in toluene*	R. N. Chadha and G. S. Misra	37
Distribution of molecular weights in high polymers. The effect of chain transfer on the. Part I. Combination	Santi R. Palit and Kesab Chandra Majumdar	1

## *Subject Index*

599

Subject	Author	Page
Distribution of molecular weights in high polymers. The effect of chain transfer on the. Part II. Termination by disproportionation	Kesab Chandra Majumdar and Santi R. Palit	19
High polymer Symposium held in the Association in March 1954. Proceedings of the		29
Macromolecules. Studies on. The spreading properties of rubber and its derivatives	H. N. Sivaramakrishnan and M. R. A. Rao	41